

University of Southampton Research Repository ePrints Soton

Copyright © and Moral Rights for this thesis are retained by the author and/or other copyright owners. A copy can be downloaded for personal non-commercial research or study, without prior permission or charge. This thesis cannot be reproduced or quoted extensively from without first obtaining permission in writing from the copyright holder/s. The content must not be changed in any way or sold commercially in any format or medium without the formal permission of the copyright holders.

When referring to this work, full bibliographic details including the author, title, awarding institution and date of the thesis must be given e.g.

AUTHOR (year of submission) "Full thesis title", University of Southampton, name of the University School or Department, PhD Thesis, pagination

UNIVERSITY OF SOUTHAMPTON

FACULTY OF NATURAL AND ENVIRONMENTAL SCIENCES

Chemistry

A Crystal Engineering Study of Molecular Electronic Behaviour in TCNQ Salts

By

BINGJIA YAN

Thesis for the degree of Doctor of Philosophy

February 2016

UNIVERSITY OF SOUTHAMPTON

ABSTRACT

FACULTY OF NATURAL AND ENVIRONMENTAL SCIENCES

Chemistry

Doctor of Philosophy

A CRYSTAL ENGINEERING STUDY OF MOLECULAR ELECTRONIC BEHAVIOUR IN TCNQ SALTS

By

Bingjia Yan

This thesis explores the “crystal engineering” of the solid-state behaviour of a series of alkali metal TCNQ salts. This can exhibit a variety of electronic and magnetic properties, depending on the solid-state architecture. TCNQ is a good one-electron acceptor and the resulting radical anion salt is quite stable. The architectural behaviour of TCNQ salts is very dependent on the nature of the counter-cation and the stoichiometry of the material. In the present study, the effect of ionophore-encapsulation of the cation ($M = \text{Li, Na, K, Rb and Cs}$) has been explored using single crystal X-ray diffraction, IR, Raman, EPR and pressed discs conductivity measurements. In addition, the effect of changing the ionophore:metal cation ratio and the presence of additional TCNQ^0 has been investigated. 25 new crystal structures have been obtained and analysed in detail and this has grown new insight into the impact of the effect of controlling ion pair interactions through ionophore complexation and of steric factors on the nature of TCNQ assemblies adopted. A range of solid-state motifs have been observed including some novel solid-state behaviour. In addition, the solid-state behaviour of two hydrated lanthanide TCNQ salts has been investigated.

Contents

| | |
|--|---------------|
| ABSTRACT | i |
| Contents | i |
| List of tables..... | ix |
| List of figures..... | xv |
| List of schemes..... | xxix |
| DECLARATION OF AUTHORSHIP | xxxi |
| Acknowledgements..... | xxxiii |
| Definitions and Abbreviations | xxxv |
| 1. Introduction | 1 |
| 1.1 Molecular electronics | 1 |
| 1.2 Electronically active organic materials | 2 |
| 1.2.1 Main structural types of conducting materials | 2 |
| 1.2.1.1 Metal-complex stacks..... | 2 |
| 1.2.1.2 Polymer chains | 3 |
| 1.2.1.3 Molecular stacks..... | 5 |
| 1.2.2 Molecular-based organic conducting materials..... | 8 |
| 1.3 TCNQ ^{•-} anion and its compounds, derivatives and analogues..... | 10 |
| 1.3.1 Phenothiazine-TCNQ complex | 10 |
| 1.3.2 Naphthalene-TCNQ complex..... | 11 |
| 1.4 The physical and chemical behaviour of TCNQ | 12 |
| 1.4.1 The reactions of TCNQ | 13 |
| 1.4.2 An introduction to TCNQ ²⁻ salts | 15 |
| 1.4.3 An introduction to TCNQ ²⁻ salts of organic cations..... | 16 |
| 1.5 Solid state behaviour of TCNQ ^{•-} salts..... | 18 |
| 1.6 Radical ion TCNQ salts..... | 19 |
| 1.6.1 Donor acceptor complexes with Tetrathiafulvalene (TTF) and its analogues..... | 21 |
| 1.6.1.1 Analysis of TTF-TCNQ salt..... | 21 |
| 1.6.1.2 Analysis of tetramethyltetrathiafulvalenium (TMTTF) TCNQ salt..... | 23 |
| 1.6.1.3 Analysis of dibenzotetrathiafulvalenium (DBTTF) TCNQ salt..... | 24 |
| 1.6.1.4 Comparison between hexamethylenetetrathiafulvalenium (HMTTF) TCNQ and hexamethylenetetraselenafulvalenium (HMTSeF) TCNQ salts..... | 25 |

| | | |
|-----------|--|-----------|
| 1.6.1.5 | The bis(Ethylenedithio)tetrathiafulvalene (BEDTTTF) TCNQ salt | 26 |
| 1.7 | Behaviour of the derivatives of TTF with TCNQ derivatives..... | 28 |
| 1.7.1 | Analysis of tetramethyltetraselenafulvalenium (TMTSeF) – dimethyltetracyanoquinodimethane (DMTCNQ) salt..... | 28 |
| 1.7.2 | Dibenzotetrathiafulvalenium (DBTTF) – 2,5-dichloro-7,7',8,8' - tetracyanodimethanide (TCNQCl ₂)..... | 29 |
| 1.8 | Decamethylferricenium-TCNQ complex | 30 |
| 2. | Applications of Supramolecular Chemistry for Crystal Engineering of the Solid State Behaviour of TCNQ Salts | 32 |
| 2.1 | Supramolecular Chemistry | 32 |
| 2.1.1 | Supramolecular chemistry in the solid state..... | 33 |
| 2.2 | Cation binding hosts | 34 |
| 2.2.1 | Two dimensional hosts | 34 |
| 2.2.2 | Three-dimensional hosts..... | 37 |
| 2.2.3 | Tetrahedral recognition | 39 |
| 2.3 | Self-assembly | 40 |
| 2.3.1 | From pseudorotaxanes to rotaxanes and catenanes | 40 |
| 2.3.2 | Donor-acceptor based pseudorotaxanes | 41 |
| 2.3.3 | Donor-acceptor [2]rotaxanes | 42 |
| 2.3.4 | [2]Catenane synthesis..... | 43 |
| 2.3.5 | Functional [2]catenanes..... | 44 |
| 2.4 | The concept of crystal engineering | 46 |
| 2.4.1 | Intermolecular interactions of crystal engineering..... | 47 |
| 2.4.2 | Hydrogen bond in crystal engineering | 48 |
| 2.4.2.1 | The definition of hydrogen bond..... | 48 |
| 2.4.2.2 | Applications of hydrogen bond in crystal engineering | 48 |
| 2.4.3 | Multiple hydrogen bond arrays and secondary hydrogen bond interactions | 51 |
| 2.5 | Overview of the solid state structures of MTCNQ salts | 53 |
| 2.5.1 | Comparison of Group A and Group B salts in crystal structures..... | 54 |
| 2.6 | An overview of the solid-state behaviour of TCNQ salts | 54 |
| 2.6.1 | Preparation of TCNQ salts | 54 |
| 2.6.2 | Structural investigations of alkali metal TCNQ salts..... | 55 |

| | | |
|-----------|---|-----------|
| 2.6.3 | Ammonium (NH_4^+)TCNQ salt | 60 |
| 2.6.4 | Alkaline earth metal TCNQ salts | 61 |
| 2.6.5 | Transition metal TCNQ salts..... | 62 |
| 2.6.5.1 | Cu(TCNQ) (I/II) | 62 |
| 2.6.5.2 | Ag(TCNQ) (II) | 63 |
| 2.6.6 | Other binary $\text{M}(\text{TCNQ})_2(\text{H}_2\text{O})_2$ family members ($\text{M} = \text{Mn, Fe, Co, Ni}$)..... | 64 |
| 2.6.7 | Lanthanide TCNQ complexes: Its compounds, derivatives and analogues..... | 65 |
| 2.6.8 | Cyanine dye-TCNQ complexes..... | 67 |
| 2.6.9 | TTF-TCNQ..... | 71 |
| 2.6.10 | Electrical behaviour of alkali metal TCNQ salts..... | 72 |
| 2.6.11 | Magnetic properties of TCNQ complexes..... | 76 |
| 2.6.11.1 | Electron spin/paramagnetic resonance | 76 |
| 2.6.11.2 | The Zeeman Effect | 77 |
| 2.6.11.3 | Magnetic properties of TCNQ complexes..... | 78 |
| 2.6.11.4 | ESR spectral characteristics associated with triplet excitons in TCNQ complexes..... | 80 |
| 2.6.12 | Spectroscopic analysis of TCNQ and it corresponding $\text{TCNQ}^{\cdot-}$ salts..... | 80 |
| 2.7 | Discussion of 1:1/1:1:1 versus 2:1/2:1:1 TCNQ complexes | 82 |
| 2.7.1 | Ionophore-complexed MTCNQ salts | 82 |
| 2.7.2 | Ionophore-encapsulated alkali metal TCNQ salts | 87 |
| 3. | Ionophore Encapsulated MTCNQ Salts..... | 90 |
| 3.1 | Summarised crystal structures of TCNQ salts..... | 90 |
| 3.2 | Crystal growth experiments..... | 91 |
| 3.3 | Ionophore encapsulated MTCNQ complexes ($\text{M} = \text{Li, Na, K, Cs}$)..... | 92 |
| 3.3.1 | Preparation of $(12\text{C}_4)_2\text{M}(\text{TCNQ})_n$ complexes ($\text{M} = \text{Li, Na, K}$)..... | 93 |
| 3.3.1.1 | $(12\text{C}_4)_2\text{MTCNQ}$ complexes ($\text{M} = \text{Li, Na}$) | 93 |
| | (a) $(12\text{C}_4)_2\text{LiTCNQ}$ | 93 |
| | (b) $(12\text{C}_4)_2\text{NaTCNQ}$ | 98 |
| 3.3.1.2 | $(12\text{C}_4)_2\text{M}(\text{TCNQ})_2$ ($\text{M} = \text{Li, Na, K}$) | 103 |
| | (a) $(12\text{C}_4)_2\text{Li}(\text{TCNQ})_2$ | 103 |
| | (b) $(12\text{C}_4)_2\text{Na}(\text{TCNQ})_2$ | 107 |
| | (c) $(12\text{C}_4)_2\text{K}(\text{TCNQ})_2$ | 112 |

| | | |
|---------|---|-----|
| 3.3.1.3 | Comparison of $(12C4)_2Li(TCNQ)_2$, $(12C4)_2Na(TCNQ)_2$ and $(12C4)_2K(TCNQ)_2$ structures..... | 116 |
| 3.3.2 | Preparation of $(15C5)M(TCNQ)_n$ complexes ($M = Li, Na$)..... | 119 |
| 3.3.2.1 | $(15C5)MTCNQ$ complexes ($M = Li, Na$) | 119 |
| | (a) $(15C5)LiTCNQ$ | 119 |
| | (b) $(15C5)NaTCNQ$ | 125 |
| 3.3.2.2 | Comparison between $(15C5)LiTCNQ$ and $(15C5)NaTCNQ$ | 131 |
| 3.3.2.3 | $(15C5)M(TCNQ)_2 \cdot H_2O$ complexes ($M = Li, Na$)..... | 132 |
| | (a) $(15C5)Li(TCNQ)_2 \cdot H_2O$ | 132 |
| | (b) $(15C5)Na(TCNQ)_2 \cdot H_2O$ | 139 |
| 3.3.2.4 | Comparison between $(15C5)Li(TCNQ)_2 \cdot H_2O$ and $(15C5)Na(TCNQ)_2 \cdot H_2O$ | 146 |
| 3.3.3 | Preparation of $(18C6)M(TCNQ)_n$ complexes ($M = Na, K, Cs$) | 148 |
| | (a) $(18C6)KTCNQ$ | 148 |
| | (b) $(18C6)Na(TCNQ)_2 \cdot 2H_2O$ | 155 |
| | (c) $(18C6)K(TCNQ)_{2.5}$ | 161 |
| | (d) $(18C6)Cs(TCNQ)_2$ | 167 |
| 3.3.4 | Preparation of $(B15C5)M(TCNQ)_n$ ($M = Li, Cs$)..... | 173 |
| | (a) $(B15C5)LiTCNQ \cdot H_2O$ | 173 |
| | (b) $(B15C5)_2Cs(TCNQ)_3$ | 178 |
| 3.3.5 | Preparation of $(B18C6)K(TCNQ)_2$ | 183 |
| 3.3.6 | Preparation of $(DB18C6)K(TCNQ)_2$ | 188 |
| 3.3.7 | Preparation of $(Dicyc18C6)M(TCNQ)_n$ ($M = K, Cs$) ($n = 2, 3$) | 195 |
| 3.3.7.1 | $(Dicyc18C6)K(TCNQ)_3$ | 195 |
| 3.3.7.2 | $(Dicyc18C6)Cs(TCNQ)_2$ | 202 |
| 3.3.8 | Preparation of $(C222)K(TCNQ)_{2.5}$ | 209 |
| 3.3.9 | Conclusion..... | 215 |
| 3.4 | Ionophore Encapsulated $MTCNQ$ Salts ($M = Rb$)..... | 218 |
| 3.4.1 | Preparation of $(12C4)Rb(TCNQ)_{1.5}$ | 218 |
| 3.4.2 | Preparation of $(15C5)_2RbTCNQ$ | 223 |
| 3.4.3 | Preparation of $(18C6)Rb(TCNQ)_2$ | 229 |
| 3.4.4 | Preparation of $(DB18C6)RbTCNQ$ | 235 |
| 3.4.5 | Preparation of $(Dicyc18C6)Rb(TCNQ)_3$ | 242 |

| | | |
|-----------|---|------------|
| 3.4.6 | Preparation of (C222)Rb(TCNQ) _{2.5} | 249 |
| 3.4.7 | Conclusion | 254 |
| 3.5 | Optical Behaviour of Ionophore-M-TCNQ Salts | 256 |
| 3.5.1 | IR spectra of Ionophore Encapsulated M-TCNQ Salts | 256 |
| 3.5.2 | Raman spectra of Ionophore Encapsulated M-TCNQ Salts | 261 |
| 3.6 | Conductivity of Ionophore Encapsulated M-TCNQ Salts..... | 265 |
| 3.7 | Preliminary Electron Paramagnetic Resonance of Ionophore Encapsulated M-TCNQ Salts | 267 |
| 4. | TCNQ Salts of Some Lanthanide Cations | 275 |
| 4.1 | Crystal structure description of Tb(TCNQ) ₃ (H ₂ O) ₆ ·3H ₂ O | 275 |
| 4.2 | Crystal structure description of Yb(TCNQ) ₃ (H ₂ O) ₆ ·3H ₂ O..... | 281 |
| 4.3 | Comparison between Tb(TCNQ) ₃ (H ₂ O) ₆ ·3H ₂ O and Yb(TCNQ) ₃ (H ₂ O) ₆ ·3H ₂ O complexes | 288 |
| 5. | Conclusions and Further Work..... | 291 |
| 6. | Experimental Details | 293 |
| 6.1 | General Details and Instrumentation | 293 |
| 6.1.1 | Melting Points | 293 |
| 6.1.2 | Elemental Analysis | 293 |
| 6.1.3 | Nuclear Magnetic Resonance Spectra | 293 |
| 6.1.3.1 | Bruker AVII400 FT-NMR Spectrometer (400/1) | 293 |
| 6.1.3.2 | Bruker AVIIIHD400 FT-NMR Spectrometer (400/3) | 293 |
| 6.1.4 | Infra-Red Spectroscopy | 294 |
| 6.1.5 | UV / Vis Spectroscopy | 294 |
| 6.1.6 | Raman Spectroscopy | 294 |
| 6.1.7 | Mass Spectroscopy | 294 |
| 6.1.7.1 | MaXis ELECTROSPRAY IONISATION | 294 |
| 6.1.7.2 | solariX ELECTROSPRAY IONISATION/APPI IONISATION | 294 |
| 6.1.8 | Single Crystal X-ray Diffraction | 295 |
| 6.1.8.1 | Rigaku FR-E+ Ultra High Flux Diffractometer AKA Ros | 295 |
| 6.1.8.2 | Rigaku FR-E+ Very High Flux Diffractometer AKA Kat | 295 |
| 6.1.9 | Electron Paramagnetic Resonance | 296 |
| 6.1.10 | Resistance | 296 |
| 6.2 | Preparation & Purification of Starting Materials, Solvent & Reagents..... | 296 |
| 6.3 | Preparation of TCNQ complexes | 297 |

| | | |
|--------|---|-----|
| 6.3.1 | Purification of TCNQ ²⁸¹ | 297 |
| 6.3.2 | Preparation of NaTCNQ ²⁸¹ | 297 |
| 6.3.3 | Preparation of LiTCNQ ²⁸¹ | 297 |
| 6.3.4 | Preparation of KTCNQ ⁷⁹ | 298 |
| 6.3.5 | Preparation of Rb ₂ (TCNQ) ₃ | 298 |
| 6.3.6 | Preparation of Cs ₂ (TCNQ) ₃ | 298 |
| 6.3.7 | Preparation of (12C4) ₂ LiTCNQ | 299 |
| 6.3.8 | Preparation of (12C4) ₂ NaTCNQ ²⁸¹ | 300 |
| 6.3.9 | Preparation of (12C4) ₂ Li(TCNQ) ₂ | 301 |
| 6.3.10 | Preparation of (12C4) ₂ Na(TCNQ) ₂ | 302 |
| 6.3.11 | Preparation of (12C4) ₂ K(TCNQ) ₂ | 303 |
| 6.3.12 | Preparation of (12C4)Rb(TCNQ) _{1.5} | 304 |
| 6.3.13 | Preparation of (15C5)LiTCNQ | 305 |
| 6.3.14 | Preparation of (15C5)NaTCNQ | 306 |
| 6.3.15 | Preparation of (15C5)Li(TCNQ) ₂ ·H ₂ O | 307 |
| 6.3.16 | Preparation of (15C5)Na(TCNQ) ₂ ·H ₂ O | 308 |
| 6.3.17 | Preparation of (15C5) ₂ RbTCNQ | 309 |
| 6.3.18 | Preparation of (B15C5)LiTCNQ·H ₂ O | 310 |
| 6.3.19 | Preparation of (B15C5) ₂ Cs(TCNQ) ₃ | 311 |
| 6.3.20 | Preparation of (18C6)KTCNQ ²⁸¹ | 312 |
| 6.3.21 | Preparation of (18C6)Na(TCNQ) ₂ ·2H ₂ O | 313 |
| 6.3.22 | Preparation of (18C6)K(TCNQ) _{2.5} | 314 |
| 6.3.23 | Preparation of (18C6)Rb(TCNQ) ₂ | 315 |
| 6.3.24 | Preparation of (18C6)Cs(TCNQ) ₂ | 316 |
| 6.3.25 | Preparation of (B18C6)K(TCNQ) ₂ | 317 |
| 6.3.26 | Preparation of (DB18C6)K(TCNQ) ₂ | 318 |
| 6.3.27 | Preparation of (DB18C6)RbTCNQ | 319 |
| 6.3.28 | Preparation of (DC18C6)K(TCNQ) ₃ | 320 |
| 6.3.29 | Preparation of (DC18C6)Rb(TCNQ) ₃ | 321 |
| 6.3.30 | Preparation of (DC18C6)Cs(TCNQ) ₂ | 322 |
| 6.3.31 | Preparation of (C222)K(TCNQ) _{2.5} | 323 |
| 6.3.32 | Preparation of (C222)Rb(TCNQ) _{2.5} | 324 |
| 6.3.33 | Preparation of Tb(TCNQ) ₃ (H ₂ O) ₆ ·3H ₂ O | 325 |

| | | |
|--------|---|------------|
| 6.3.34 | Preparation of $\text{Yb}(\text{TCNQ})_3(\text{H}_2\text{O})_6 \cdot 3\text{H}_2\text{O}$ | 325 |
| | Appendix 1..... | 327 |
| | Bibliography | 329 |

List of tables

| | |
|---|-----|
| Table 1.1 The conducting polymers ¹⁵ | 4 |
| Table 1.2 The resistivity of MTCNQ salts ⁶⁵ | 19 |
| Table 1.3 Structures of components of some conducting donor-TCNQ complexes ³⁴ | 20 |
| Table 2.1 Comparison of the ionic radii of alkali metal cations with crown ether cavity diameter ¹³⁰ | 36 |
| Table 2.2 Different types of intermolecular interactions ¹⁶⁸ | 47 |
| Table 2.3 Structure features of alkali metal TCNQ salts | 60 |
| Table 2.4 Two typical cyanine dye-TCNQ complexes..... | 69 |
| Table 2.5 Physical properties of TCNQ and its salts at 290±2K ⁶⁵ | 74 |
| Table 2.6 The activation energies of alkali metal TCNQ salts ^{202,203} | 75 |
| Table 2.7 Conductivity and activation energy measurements at room temperature ^{193,202,203} | 75 |
| Table 2.8 IR absorption bands observed of TCNQ and its corresponding TCNQ ^{•-} ^{261,262} | 81 |
| Table 2.9 The characteristics of simple ionophore ammonium/MTCNQ salts ⁶⁴ | 85 |
| Table 2.10 The characteristics of complex ionophore ammonium/MTCNQ salts ⁶⁴ | 86 |
| Table 3.1 Description of key parameters in TCNQ plane..... | 92 |
| Table 3.2 Summary of bond distances (Å) observed of TCNQ ^{•-} in (12C4) ₂ LiTCNQ ... | 95 |
| Table 3.3 Summary of bond lengths (Å) observed of TCNQ ^{•-} in (12C4) ₂ NaTCNQ | 99 |
| Table 3.4 Summary of bond lengths (Å) observed for TCNQ units in (12C4) ₂ Li(TCNQ) ₂ | 104 |
| Table 3.5 Distances (Å) and angles (°) within the TCNQ stacks of (12C4) ₂ Li(TCNQ) ₂ | 106 |
| Table 3.6 Summary of bond lengths (Å) observed for TCNQ units in (12C4) ₂ Na(TCNQ) ₂ | 108 |
| Table 3.7 Distances (Å) and angles (°) within the TCNQ stacks of (12C4) ₂ Na(TCNQ) ₂ | 110 |
| Table 3.8 Summary of bond lengths (Å) observed for TCNQ units in (12C4) ₂ K(TCNQ) ₂ | 113 |
| Table 3.9 Distances (Å) and angles (°) within the TCNQ stacks of (12C4) ₂ K(TCNQ) ₂ | 115 |

| | |
|--|-----|
| Table 3.10 Comparison of key parameters of TCNQ column geometries in (12C4) ₂ Li/Na/K(TCNQ) ₂ | 119 |
| Table 3.11 Summary of bond lengths (Å) observed for TCNQ ^{•-} units in (15C5)LiTCNQ120 | |
| Table 3.12 Distances (Å) and angles (°) within the TCNQ ^{•-} stacks of (15C5)LiTCNQ122 | |
| Table 3.13 Summary of bond lengths (Å) observed for TCNQ ^{•-} units in (15C5)NaTCNQ..... | 126 |
| Table 3.14 Distances (Å) and angles (°) within the TCNQ ^{•-} stacks of (15C5)NaTCNQ128 | |
| Table 3.15 Summary of bond distances (Å) observed for TCNQ units..... | 133 |
| Table 3.16 Distances (Å) and angles (°) within the TCNQ stacks of (15C5)Li(TCNQ) ₂ ·H ₂ O | 136 |
| Table 3.17 Summary of bond distances (Å) observed for TCNQ units in (15C5)Na(TCNQ) ₂ ·H ₂ O | 140 |
| Table 3.18 Distances (Å) and angles (°) within the TCNQ stacks of (15C5)Na(TCNQ) ₂ ·H ₂ O | 143 |
| Table 3.19 Comparison of key parameters of TCNQ column geometries in (15C5)Li ⁺ ·H ₂ O and (15C5)Na ⁺ ·H ₂ O | 147 |
| Table 3.20 Summary of bond lengths (Å) observed for TCNQ ^{•-} units in (18C6)KTCNQ (literature values ³⁶ for comparison are listed in brackets) | 149 |
| Table 3.21 Comparison of key parameters of (18C6)KTCNQ at different data collection temperatures..... | 150 |
| Table 3.22 Distances (Å) and angles (°) within the TCNQ ^{•-} stacks of (18C6)KTCNQ151 | |
| Table 3.23 Summary of bond distances (Å) observed for TCNQ units..... | 156 |
| Table 3.24 Distances (Å) and angles (°) within the TCNQ stacks of (18C6)Na(TCNQ) ₂ ·2H ₂ O | 158 |
| Table 3.25 Summary of bond distances (Å) observed for TCNQ units in (18C6)K(TCNQ) _{2.5} | 162 |
| Table 3.26 Distances (Å) and angles (°) within the TCNQ stacks and between pentamer neighbours of (18C6)K(TCNQ) _{2.5} | 166 |
| Table 3.27 Summary of bond distances (Å) observed for TCNQ units in (18C6)Cs(TCNQ) ₂ | 168 |
| Table 3.28 Distances (Å) and angles (°) within the TCNQ stacks of (18C6)Cs(TCNQ) ₂ 171 | |
| Table 3.29 Summary of bond distances (Å) found for TCNQ ^{•-} in (B15C5)LiTCNQ·H ₂ O174 | |

| | |
|--|-----|
| Table 3.30 Distances (Å) and angles (°) within the TCNQ ^{•-} stacks in (B15C5)LiTCNQ·H ₂ O | 176 |
| Table 3.31 Summary of bond distances (Å) scrutinise for TCNQ units in the cation complex..... | 179 |
| Table 3.32 Distances (Å) and angles (°) within the TCNQ stacks of (B15C5) ₂ Cs(TCNQ) ₃ | 181 |
| Table 3.33 Summary of bond distances (Å) observed for TCNQ units in (B18C6)K(TCNQ) ₂ | 184 |
| Table 3.34 Distances (Å) and angles (°) within the TCNQ stacks of (B18C6)K(TCNQ) ₂ | 187 |
| Table 3.35 Summary of bond distances (Å) observed for TCNQ units in (DB18C6)K(TCNQ) ₂ | 190 |
| Table 3.36 Distances (Å) and angles (°) within the TCNQ stacks of (DB18C6)K(TCNQ) ₂ | 193 |
| Table 3.37 Summary of bond distances (Å) observed for TCNQ units in (Dicyc18C6)K(TCNQ) ₃ | 197 |
| Table 3.38 Distances (Å) and angles (°) within the TCNQ dimer of (Dicyc18C6)K(TCNQ) ₃ | 200 |
| Table 3.39 Summary of bond distances (Å) observed for TCNQ units in (Dicyc18C6)Cs(TCNQ) ₂ | 204 |
| Table 3.40 Distances (Å) and angles (°) within the TCNQ stacks of (Dicyc18C6)Cs(TCNQ) ₂ | 207 |
| Table 3.41 Summary of bond lengths (Å) observed for TCNQ units in (C222)K(TCNQ) _{2.5} | 210 |
| Table 3.42 Distances (Å) and angles (°) within the TCNQ stacks of (C222)K(TCNQ) ₂ | 214 |
| Table 3.43 Summary of bond lengths (Å) observed for TCNQ units in (12C4)Rb(TCNQ) _{1.5} | 219 |
| Table 3.44 Distances (Å) and angles (°) within the TCNQ stacks of (12C4)Rb(TCNQ) _{1.5} | 221 |
| Table 3.45 Summary of bond lengths (Å) observed for TCNQ ^{•-} units in (15C5) ₂ RbTCNQ | 224 |
| Table 3.46 Distances (Å) and angles (°) within the TCNQ ^{•-} stacks of (15C5) ₂ RbTCNQ | 227 |
| Table 3.47 Summary of bond lengths (Å) observed for TCNQ units in (18C6)Rb(TCNQ) ₂ | 230 |
| Table 3.48 Distances (Å) and angles (°) within the TCNQ stacks of (18C6)Rb(TCNQ) ₂ | 233 |

| | |
|---|-----|
| Table 3.49 Summary of bond lengths (Å) observed for TCNQ ^{•-} units in (DB18C6)RbTCNQ | 236 |
| Table 3.50 Distances (Å) and angles (°) within the TCNQ ^{•-} stacks of (DB18C6)RbTCNQ | 240 |
| Table 3.51 Summary of bond lengths (Å) observed for TCNQ units in (Dicyc18C6)Rb(TCNQ) ₃ | 244 |
| Table 3.52 Distances (Å) and angles (°) within the TCNQ stacks of (Dicyc18C6)Rb(TCNQ) ₃ | 247 |
| Table 3.53 Summary of bond lengths (Å) observed for TCNQ units in (C222)Rb(TCNQ) _{2.5} | 250 |
| Table 3.54 Distances (Å) and angles (°) within the TCNQ stacks of (C222)Rb(TCNQ) _{2.5} | 253 |
| Table 3.55 Literature values of MTCNQ and Ionophore-Metal TCNQ salts | 256 |
| Table 3.56 IR spectra of Ionophore Encapsulated M-TCNQ Salts in this study | 257 |
| Table 3.57 Description of cyanide (CN) groups in TCNQ and its five complexes | 260 |
| Table 3.58 Raman spectra of Ionophore Encapsulated M-TCNQ Salts in this study... | 263 |
| Table 3.59 Conductivity of Ionophore Encapsulated M-TCNQ Salts in this study | 265 |
| Table 4.1 Summary of bond lengths (Å) observed for TCNQ units in Tb(TCNQ) ₃ (H ₂ O) ₆ ·3H ₂ O | 276 |
| Table 4.2 Distances (Å) and angles (°) within the TCNQ stacks of Tb(TCNQ) ₃ (H ₂ O) ₆ ·3H ₂ O | 280 |
| Table 4.3 Summary of bond lengths (Å) observed for TCNQ units in Yb(TCNQ) ₃ (H ₂ O) ₆ ·3H ₂ O | 283 |
| Table 4.4 Distances (Å) and angles (°) within the TCNQ stacks of Yb(TCNQ) ₃ (H ₂ O) ₆ ·3H ₂ O | 287 |
| Table 4.5 Significant structural parameters for 1-3 | 289 |
| Table 6.1 Crystal structure information of (12C4) ₂ LiTCNQ in this study | 299 |
| Table 6.2 Crystal structure information of (12C4) ₂ NaTCNQ in this study | 300 |
| Table 6.3 Crystal structure information of (12C4) ₂ Li(TCNQ) ₂ in this study | 301 |
| Table 6.4 Crystal structure information of (12C4) ₂ Na(TCNQ) ₂ in this study | 302 |
| Table 6.5 Crystal structure information of (12C4) ₂ K(TCNQ) ₂ in this study | 303 |
| Table 6.6 Crystal structure information of (12C4)Rb(TCNQ) _{1.5} in this study | 304 |

| | |
|---|-----|
| Table 6.7 Crystal structure information of (15C5)LiTCNQ in this study..... | 305 |
| Table 6.8 Crystal structure information of (15C5)NaTCNQ in this study | 306 |
| Table 6.9 Crystal structure information of (15C5)Li(TCNQ) ₂ ·H ₂ O in this study..... | 307 |
| Table 6.10 Crystal structure information of (15C5)Na(TCNQ) ₂ ·H ₂ O in this study..... | 308 |
| Table 6.11 Crystal structure information of (15C5) ₂ RbTCNQ in this study | 309 |
| Table 6.12 Crystal structure information of (B15C5)LiTCNQ·H ₂ O in this study | 310 |
| Table 6.13 Crystal structure information of (B15C5) ₂ Cs(TCNQ) ₃ in this study | 311 |
| Table 6.14 Crystal structure information of (18C6)KTCNQ in this study | 312 |
| Table 6.15 Crystal structure information of (18C6)Na(TCNQ) ₂ ·2H ₂ O in this study.... | 313 |
| Table 6.16 Crystal structure information of (18C6)K(TCNQ) _{2.5} in this study | 314 |
| Table 6.17 Crystal structure information of (18C6)Rb(TCNQ) ₂ in this study | 315 |
| Table 6.18 Crystal structure of (18C6)Cs(TCNQ) ₂ in this study..... | 316 |
| Table 6.19 Crystal structure information of (B18C6)K(TCNQ) ₂ in this study..... | 317 |
| Table 6.20 Crystal structure information of (DB18C6)K(TCNQ) ₂ in this study..... | 318 |
| Table 6.21 Crystal structure information of (DB18C6)RbTCNQ in this study..... | 319 |
| Table 6.22 Crystal structure information of (DC18C6)K(TCNQ) ₃ in this study..... | 320 |
| Table 6.23 Crystal structure information of (DC18C6)Rb(TCNQ) ₃ in this study | 321 |
| Table 6.24 Crystal structure information of (DC18C6)Cs(TCNQ) ₂ in this study | 322 |
| Table 6.25 Crystal structure information of (C222)K(TCNQ) _{2.5} in this study | 323 |
| Table 6.26 Crystal structure information of (C222)Rb(TCNQ) _{2.5} in this study | 324 |
| Table 6.27 Crystal structure information of Tb(TCNQ) ₃ (H ₂ O) ₆ ·3H ₂ O in this study | 325 |
| Table 6.28 Crystal structure information of Yb(TCNQ) ₃ (H ₂ O) ₆ ·3H ₂ O in this study.... | 326 |

List of figures

| | |
|--|----|
| Figure 1.1 The structure of $K_2Pt(CN)_4$ ¹² | 3 |
| Figure 1.2 The structure of a trans-polyacetylene chain | 3 |
| Figure 1.3 The charge transfer complex of Perylene(D)-TCNQ(A) (ref code: PERTCQ) ¹⁶ | 5 |
| Figure 1.4 The charge transfer complex of Chrysene(D)-Fluoranyl(A) (ref code: CHRFAN) ¹⁷ | 6 |
| Figure 1.5 Principle interactions between π systems | 6 |
| Figure 1.6 The optimum geometry of zinc porphyrin π - π interactions ¹⁸ | 7 |
| Figure 1.7 The geometry of π stacking interactions in [18]annulene ¹⁸ | 7 |
| Figure 1.8 Geometry of π stacking interactions ¹⁸ | 8 |
| Figure 1.9 The packing pattern of PTZ-TCNQ complex (ref code: PTZTCQ and PTZTCQ01) ^{38,39,46,47} | 11 |
| Figure 1.10 The packing pattern of naphthalene-TCNQ complex (ref code: TCQNAP and TCQNAP01) ^{48,50} | 12 |
| Figure 1.11 The 3D structure of $[Mn_2(TCNQ)_3]^{2-}$ coordination networks ⁶² | 16 |
| Figure 1.12 Solid-state behaviour of N,N'-dialkylpyridinium $TCNQ^{2-}$ salts ⁶⁰ | 17 |
| Figure 1.13 Solid-state behaviour of $Pt(bipy)_2^{2+}$ $TCNQ^{2-}$ salts ⁶⁰ | 17 |
| Figure 1.14 Solid-state behaviour of 1,4-bis(N-pyridiummethyl)-benzene $TCNQ^{2-}$ salts ⁶⁰ | 17 |
| Figure 1.15 Solid-state behaviour of 2,5-diaminocyclohexa-2,5-diene-1,4-diiminium $TCNQ^{2-}$ salts ⁶⁰ | 17 |
| Figure 1.16 The formation of $TCNQ^{\bullet-}$ stacks | 18 |
| Figure 1.17 Packing pattern of segregated columns in TTF-TCNQ complex (ref code: TTFTCQ, TTFTCQ01-TTFTCQ06) ⁸⁰⁻⁸³ | 22 |
| Figure 1.18 TMTTF | 23 |
| Figure 1.19 Packing behaviour of TMTTF-TCNQ (ref code: MDTTCQ and THOTCQ) ^{84,85} | 24 |
| Figure 1.20 DBTTF | 24 |

| | |
|--|----|
| Figure 1.21 Packing behaviour of DBTTF-TCNQ (ref code: BALNAD01 and BALNAD10) ^{86,87} | 25 |
| Figure 1.22 The structures of HMTTF and HMTSeF | 25 |
| Figure 1.23 The packing motifs of (ref code: BESPEU) ⁹⁰ and HMTSeF-TCNQ | 26 |
| Figure 1.24 BEDTTTF | 27 |
| Figure 1.25 Packing motifs of one triclinic phase (ref code: FAHLEF02) ⁹⁵ and one monoclinic phase (ref code: FAHLEF01) ⁹⁶ of BEDTTTF-TCNQ | 27 |
| Figure 1.26 The structure of TMTSeF-DMTCNQ | 28 |
| Figure 1.27 The packing motif of TMTSeF-DMTCNQ (ref code: SEFTCQ) ¹⁰³ | 29 |
| Figure 1.28 The structures of DBTTF-TCNQCl ₂ | 29 |
| Figure 1.29 Solid-state behaviour of DBTTF-TCNQCl ₂ (ref code: BABCIQ and BABCIQ 01) ¹⁰⁵ | 30 |
| Figure 1.30 The structure of decamethylferricenium TCNQ ^{•-} | 30 |
| Figure 1.31 Two different phases of decamethylferricenium TCNQ ^{•-} (methyl groups removed for clarity) ^{57,112} | 31 |
| Figure 2.1 The concept of Supramolecular Chemistry ¹¹⁶ | 32 |
| Figure 2.2 Various structures of useful crown ethers | 34 |
| Figure 2.3 The packing motif of (15C5) ₂ KTCNQ ¹⁰⁷ | 35 |
| Figure 2.4 Examples of two-dimensional hosts using other heteroatoms instead of oxygen | 36 |
| Figure 2.5 Some simple cryptands ¹⁵⁴ | 38 |
| Figure 2.6 Spherical recognition in cryptate complexes ^{153,154} | 39 |
| Figure 2.7 Complexation of NH ₄ ⁺ by cryptand (5) ¹⁵³ | 39 |
| Figure 2.8 Formation of a pseudorotaxane to either a [2]rotaxane or [2]catenane ¹⁵⁹ | 40 |
| Figure 2.9 Donor-acceptor based pseudorotaxanes ¹⁵⁹ | 42 |
| Figure 2.10 A graphical representation of three methods of rotaxane formation ¹⁵⁹ | 42 |
| Figure 2.11 The proposed mechanism of switching in a tri-stable [2]catenane working under different voltages ¹⁶³ | 44 |
| Figure 2.12 A proposed general design of the RGB tri-stable [2]catenane ¹⁶³ | 45 |
| Figure 2.13 Common hydrogen bond arrangements ¹⁷² | 48 |

| | |
|---|----|
| Figure 2.14 Hydrogen bonds in forming the dimer of benzoic acid ¹⁷⁹ | 49 |
| Figure 2.15 Catemer hydrogen bond motifs produced by carboxylic acid ¹⁸⁶ | 50 |
| Figure 2.16 Hydrogen bond arrays in DNA ¹⁸⁸ | 51 |
| Figure 2.17 Multiple hydrogen bond arrays ^{189,190} | 52 |
| Figure 2.18 Hydrogen bonds array of 2-butylureido-6-methylpyrimidone ¹⁹¹ | 52 |
| Figure 2.19 A linear chain obtained by the dimerization of the ureidopyrimidone units ¹⁹² | 53 |
| Figure 2.20 Crystal structure of NaTCNQ at room temperature (ref code: NATCNQ) ²⁰⁶ | 56 |
| Figure 2.21 Crystal structure of KTCNQ at room temperature (ref code: KTCYQM01) ²⁰⁸ | 56 |
| Figure 2.22 Typical ring-ring (R-R) overlap of two TCNQ moieties or “short-axis” slipped..... | 57 |
| Figure 2.23 Typical ring-external bond (R-B) overlap of two TCNQ moieties or “long-axis” slipped..... | 57 |
| Figure 2.24 The different packing motifs of RbTCNQ(I) ¹⁹⁵ and RbTCNQ(II) ²¹² | 57 |
| Figure 2.25 A schematic representation of the shallow boat conformation in RbTCNQ(I) | 58 |
| Figure 2.26 Define the bond lengths within TCNQ molecule | 59 |
| Figure 2.27 The average structure of NH ₄ TCNQ ²¹⁵ | 61 |
| Figure 2.28 The different packing motifs of CuTCNQ(I) and CuTCNQ(II) | 62 |
| Figure 2.29 The packing motif of AgTCNQ(II) ²²³ | 64 |
| Figure 2.30 Plots of atomic radii of lanthanides as function of atomic number ²³⁰ | 65 |
| Figure 2.31 Basic skeleton of cyaninium cations used | 67 |
| Figure 2.32 The formation of cyanine dye-TCNQ complexes | 68 |
| Figure 2.33 Cyanine cation absorption data and corresponding complex TCNQ salt ²⁴⁴ | 68 |
| Figure 2.34 A stack of OC7-TCNQ complex (ref code: JEXJEB) ³⁶ | 70 |
| Figure 2.35 Packing pattern of SC7-TCNQ complex (ref code: ECYTCN10) ²⁴⁷ | 70 |
| Figure 2.36 Schematic representation of the TTF-TCNQ structure ²⁴⁹ | 72 |
| Figure 2.37 Electrical resistivity against 1000/T for the alkali metal TCNQ salts ⁶⁵ | 73 |
| Figure 2.38 Explanation the divergence of the energies of an unpaired electron in a magnetic field ²⁵⁴ | 78 |

| | |
|--|-----|
| Figure 2.39 Energy level and ESR transitions as a function of magnetic field for an oriented triplet state molecule ²⁵³ | 79 |
| Figure 2.40 The packing arrangement showing the TCNQ ^{•-} dimer ^{36,107,131} | 87 |
| Figure 2.41 Top (a) and side (b) views of a TCNQ ^{•-} dimer within (15C5) ₂ KTCNQ | 88 |
| Figure 2.42 The C222 complex of K ⁺ DCTC ⁻ as its acetonitrile solvate..... | 88 |
| Figure 2.43 Crystal structure of the C222 complex of K ⁺ DCTC ⁻ as its acetonitrile solvate (ref code: QOBYUB) ⁵⁵ | 89 |
| Figure 3.1: The structure of (a) (18C6)K/Rb/TTCNQ; (b) (15C5) ₂ KTCNQ ^{36,107,131,268} | 91 |
| Figure 3.2 Geometries of adjacent TCNQ ^{•-} units in (12C4) ₂ LiTCNQ (one of the TCNQ ^{•-} units is highlighted as light green and hydrogen atoms are excluded) | 93 |
| Figure 3.3 Top (a) and side (b) views of adjacent TCNQ ^{•-} units in (12C4) ₂ LiTCNQ (one of the TCNQ ^{•-} units is highlighted as light green and hydrogen atoms are excluded) ... | 94 |
| Figure 3.4 Views of the solid state behaviour of (12C4) ₂ LiTCNQ | 96 |
| Figure 3.5 Description of the basic unit in (12C4) ₂ LiTCNQ (carbon and hydrogen atoms are excluded)..... | 97 |
| Figure 3.6 Top (a) and side (b) views of adjacent TCNQ ^{•-} units in (12C4) ₂ NaTCNQ (one of TCNQ ^{•-} units is highlighted as light green and hydrogen atoms are excluded). .. | 98 |
| Figure 3.7 Geometries of adjacent TCNQ ^{•-} units in (12C4) ₂ NaTCNQ (one of TCNQ ^{•-} units is highlighted as light green and hydrogen atoms are excluded) | 99 |
| Figure 3.8 Views of the solid state behaviour of (12C4) ₂ NaTCNQ | 100 |
| Figure 3.9 Description of the basic unit for (12C4) ₂ NaTCNQ (carbon and hydrogen atoms are excluded) | 102 |
| Figure 3.10 Basic structure of (12C4) ₂ Li(TCNQ) ₂ (hydrogen atoms are excluded) | 103 |
| Figure 3.11 Top (a) and side (b) views of TCNQ dimer (AB) in (12C4) ₂ Li(TCNQ) ₂ (hydrogen atoms are excluded) | 104 |
| Figure 3.12 The TCNQ column in (12C4) ₂ Li(TCNQ) ₂ (hydrogen atoms are excluded) | 105 |
| Figure 3.13 Top (a) and side (b) views of TCNQ units (BB'), which is similar as for TCNQ dimer neighbours (AA') in (12C4) ₂ Li(TCNQ) ₂ (hydrogen atoms are excluded) | 105 |
| Figure 3.14 The various contact distances (Å) within the cation complex (carbon and hydrogen atoms are excluded) | 107 |
| Figure 3.15 Basic unit of (12C4) ₂ Na(TCNQ) ₂ (hydrogen atoms are excluded)..... | 108 |
| Figure 3.16 Top (a) and side (b) views of TCNQ dimer (AB) in (12C4) ₂ Na(TCNQ) ₂ (hydrogen atoms are excluded)..... | 109 |

| | |
|--|-----|
| Figure 3.17 The TCNQ column in $(12C4)_2Na(TCNQ)_2$ (hydrogen atoms are excluded) | 109 |
| Figure 3.18 Top (a) and side (b) views of TCNQ units (BB'), which is similar as for TCNQ dimer neighbours (AA') in $(12C4)_2Na(TCNQ)_2$ (hydrogen atoms are excluded) | 110 |
| Figure 3.19 The various contact distances (Å) within the cation complex (carbon and hydrogen atoms are excluded) | 111 |
| Figure 3.20 Core unit of $(12C4)_2K(TCNQ)_2$ (hydrogen atoms are excluded) | 112 |
| Figure 3.21 Top (a) and side (b) views of TCNQ dimer (AB) in $(12C4)_2K(TCNQ)_2$ (hydrogen atoms are excluded) | 113 |
| Figure 3.22 The TCNQ column in $(12C4)_2K(TCNQ)_2$ (hydrogen atoms are excluded) | 114 |
| Figure 3.23 Top (a) and side (b) views of TCNQ dimer units (BB'), which is similar to TCNQ dimer neighbours (AA') in $(12C4)_2K(TCNQ)_2$ (hydrogen atoms are excluded) | 114 |
| Figure 3.24 Summarises the various contact distances (Å) within the cation complex (carbon and hydrogen atoms are excluded) | 116 |
| Figure 3.25 Spacefilled view of $(12C4)_2Li^+$, Na^+ and $K(TCNQ)_2$ (hydrogen atoms are excluded) | 117 |
| Figure 3.26 Tilt angle between TCNQ column and the bottom TCNQ best plane for $(12C4)_2Li^+$, Na^+ and $K(TCNQ)_2$ (hydrogen atoms are excluded) | 118 |
| Figure 3.27 Basic structural unit of $(15C5)LiTCNQ$ (hydrogen atoms are excluded) | 120 |
| Figure 3.28 Top (a) and side (b) views of $TCNQ^{\bullet-}$ dimer and associated counter ions in $(15C5)LiTCNQ$ (hydrogen atoms are excluded) | 121 |
| Figure 3.29 Side (a) and Top (b) views of $TCNQ^{\bullet-}$ dimers in $(15C5)LiTCNQ$ (hydrogen atoms are excluded) | 121 |
| Figure 3.30 Top (a) and side (b) views of $TCNQ^{\bullet-}$ dimer neighbours in $(15C5)LiTCNQ$ (hydrogen atoms are excluded) | 122 |
| Figure 3.31 $TCNQ^{\bullet-}$ dimers geometries in $(15C5)LiTCNQ$ | 123 |
| Figure 3.32 Angular relationships in $(15C5)LiTCNQ$ | 123 |
| Figure 3.33 The various contact distances (Å) within the cation complex (carbon atoms on crown ether unit and hydrogen atoms are excluded) | 124 |
| Figure 3.34 Basic unit of $(15C5)NaTCNQ$ (hydrogen atoms are excluded) | 125 |
| Figure 3.35 Top (a) and side (b) views of $TCNQ^{\bullet-}$ dimer in $(15C5)NaTCNQ$ (hydrogen atoms are excluded) | 126 |
| Figure 3.36 Side (a) and top (b) views of $TCNQ^{\bullet-}$ dimers in $(15C5)NaTCNQ$ (hydrogen atoms are excluded) | 127 |

| | |
|--|-----|
| Figure 3.37 Side (a) and top (b) views of TCNQ ^{•-} dimer neighbours in (15C5)NaTCNQ (hydrogen atoms are excluded) | 128 |
| Figure 3.38 TCNQ ^{•-} dimers geometries in (15C5)NaTCNQ..... | 129 |
| Figure 3.39 Angular relationships within (15C5)NaTCNQ..... | 129 |
| Figure 3.40 The various contact distances (Å) within the cation complex (carbon atoms on crown ether units and hydrogen atoms are excluded)..... | 130 |
| Figure 3.41 Distances to neighbouring dimers in (15C5)Li ⁺ and NaTCNQ compared with (18C6)K ⁺ and RbTCNQ (hydrogen atoms excluded)..... | 132 |
| Figure 3.42 Components present in (15C5)Li(TCNQ) ₂ ·H ₂ O (hydrogen atoms excluded)..... | 133 |
| Figure 3.43 Top (a) and side (b) view of TCNQ dimer (AB) in (15C5)Li(TCNQ) ₂ ·H ₂ O (hydrogen atoms are excluded) | 134 |
| Figure 3.44 Observation of TCNQ repeating units in (15C5)Li(TCNQ) ₂ ·H ₂ O (hydrogen atoms are excluded) | 135 |
| Figure 3.45 Top (a) and side (b) views of dimer neighbours (BB'), which is similar to dimer neighbours (AA') in (15C5)Li(TCNQ) ₂ ·H ₂ O (hydrogen atoms are excluded) .. | 136 |
| Figure 3.46 Angular relationships in (15C5)Li(TCNQ) ₂ ·H ₂ O | 137 |
| Figure 3.47 The various contact distances (Å) within the cation complex (carbon and hydrogen atoms are excluded) | 138 |
| Figure 3.48 Basic structure of (15C5)Na(TCNQ) ₂ ·H ₂ O (hydrogen atoms are excluded)..... | 139 |
| Figure 3.49 Top (a) and side (b) views of TCNQ dimer in (15C5)Na(TCNQ) ₂ ·H ₂ O (hydrogen atoms are excluded)..... | 141 |
| Figure 3.50 Assembly of TCNQ repeating units in (15C5)Na(TCNQ) ₂ ·H ₂ O (hydrogen atoms are excluded) | 142 |
| Figure 3.51 Top (a) and side (b) views of TCNQ dimer neighbours in (15C5)Na(TCNQ) ₂ ·H ₂ O (hydrogen atoms are excluded) | 142 |
| Figure 3.52 Angle descriptions in (15C5)Na(TCNQ) ₂ ·H ₂ O | 144 |
| Figure 3.53 Various contact distances (Å) within the cation complex (carbon and hydrogen atoms excluded) | 145 |
| Figure 3.54 Spacefilled view of cation complex of (15C5)Li ⁺ /Na ⁺ ·H ₂ O (hydrogen atoms are excluded)..... | 146 |
| Figure 3.55 Tilt angle between TCNQ column and the bottom TCNQ best plane for (15C5)Li ⁺ (TCNQ) ₂ ·H ₂ O and (15C5)Na(TCNQ) ₂ ·H ₂ O (hydrogen atoms are excluded)..... | 147 |

| | |
|---|-----|
| Figure 3.56 Basic structure of (18C6)KTCNQ in this study (hydrogen atoms are excluded)..... | 148 |
| Figure 3.57 Top (a) and side (b) views of TCNQ ^{•-} dimer in (18C6)KTCNQ (hydrogen atoms are excluded)..... | 150 |
| Figure 3.58 Top (a) and side (b) views of dimer neighbours in (18C6)KTCNQ (hydrogen atoms are excluded) | 151 |
| Figure 3.59 TCNQ ^{•-} dimer geometries in (18C6)KTCNQ (hydrogen atoms are excluded)..... | 152 |
| Figure 3.60 Side (a) and top (b) views of packing pattern of (18C6)KTCNQ (hydrogen atoms are excluded)..... | 153 |
| Figure 3.61 The various contact distances (Å) within the cation complex of (18C6)KTCNQ (carbon atoms on crown ether unit and hydrogen atoms are excluded)..... | 154 |
| Figure 3.62 Basic unit of (18C6)Na(TCNQ) ₂ ·2H ₂ O (sodium ion is disordered and hydrogen atoms are excluded) | 155 |
| Figure 3.63 Top (a) and side (b) views of TCNQ dimer in (18C6)Na(TCNQ) ₂ ·2H ₂ O (hydrogen atoms are excluded) | 156 |
| Figure 3.64 Views of repeating unit within the complex of (18C6)Na(TCNQ) ₂ ·2H ₂ O (hydrogen atoms are excluded) | 157 |
| Figure 3.65 Top (a) and side (b) views of dimer neighbours, which is similar to dimer neighbours (AA') in (18C6)Na(TCNQ) ₂ ·2H ₂ O (hydrogen atoms are excluded)..... | 158 |
| Figure 3.66 The formation of hydrogen bonding in (18C6)Na(TCNQ) ₂ ·2H ₂ O (hydrogen atoms are excluded)..... | 159 |
| Figure 3.67 The various contact distances (Å) within the cation complex (carbon atoms on crown ether ring and hydrogen atoms are excluded) | 160 |
| Figure 3.68 Core unit of (18C6)K(TCNQ) _{2.5} (hydrogen atoms are excluded) | 161 |
| Figure 3.69 Zigzag conformation of cation complex [(18C6)K ⁺] in (18C6)K(TCNQ) _{2.5} (hydrogen atoms are excluded) | 163 |
| Figure 3.70 Space-fill diagram of TCNQ pentamer stack in (18C6)K(TCNQ) _{2.5} (hydrogen atoms are excluded) | 163 |
| Figure 3.71 Top (a/c/e) and side (b/d/f) views of TCNQ units in (18C6)K(TCNQ) _{2.5} (hydrogen atoms are excluded) | 164 |
| Figure 3.72 Views of pentamers geometry and packing pattern in TCNQ column (hydrogen atoms are excluded) | 165 |

| | |
|---|-----|
| Figure 3.73 Various contact distances (Å) within the cation complex of (18C6)K(TCNQ) _{2.5} (carbon atoms on crown ether unit and hydrogen atoms are excluded)..... | 167 |
| Figure 3.74 Asymmetric unit and basic components of (18C6)Cs(TCNQ) ₂ (hydrogen atoms are excluded) | 168 |
| Figure 3.75 Top (a) and side (b) views of TCNQ trimer in (18C6)Cs(TCNQ) ₂ (hydrogen atoms are excluded) | 169 |
| Figure 3.76 Assembly of the TCNQ repeating units in (18C6)Cs(TCNQ) ₂ (hydrogen atoms are excluded) | 170 |
| Figure 3.77 Top (a) and side (b) views of TCNQ units (AC) in (18C6)Cs(TCNQ) ₂ (hydrogen atoms are excluded) | 171 |
| Figure 3.78 The various contact distances (Å) within the cation complex of (18C6)Cs(TCNQ) ₂ (carbon and hydrogen atoms are excluded) | 172 |
| Figure 3.79 Core unit of (B15C5)LiTCNQ·H ₂ O (hydrogen atoms are excluded) | 173 |
| Figure 3.80 Top (a) and side (b) views of TCNQ ^{•-} dimer in (B15C5)LiTCNQ·H ₂ O (hydrogen atoms are excluded) | 174 |
| Figure 3.81 Top (a) and side (b) views of dimer neighbours in (B15C5)LiTCNQ·H ₂ O (hydrogen atoms are excluded) | 175 |
| Figure 3.82 Side (a) and top (b) views of the packing pattern in (B15C5)LiTCNQ·H ₂ O (hydrogen atoms are excluded) | 175 |
| Figure 3.83 TCNQ ^{•-} dimers geometries in (B15C5)LiTCNQ·H ₂ O (hydrogen atoms are excluded) | 176 |
| Figure 3.84 Hydrogen bonding coordination pattern to TCNQ ^{•-} dimers..... | 177 |
| Figure 3.85 The various contact distances (Å) within the cation complex (carbon, except for benzene ring, and hydrogen atoms are excluded) | 177 |
| Figure 3.86 Core unit of (B15C5) ₂ Cs(TCNQ) ₃ (hydrogen atoms are excluded) | 178 |
| Figure 3.87 Top (a) and side (b) views of TCNQ trimer in (B15C5) ₂ Cs(TCNQ) ₃ (hydrogen atoms are excluded) | 180 |
| Figure 3.88 Side (a) and top (b) views of the packing motif of (B15C5) ₂ Cs(TCNQ) ₃ (hydrogen atoms are excluded) | 180 |
| Figure 3.89 Top (a) and side (b) views of external TCNQ trimer neighbours in (B15C5) ₂ Cs(TCNQ) ₃ (hydrogen atoms are excluded) | 181 |
| Figure 3.90 Tilt angle between two crown ether mean plane (defined by a set of oxygen atoms) (hydrogen atoms are excluded) | 182 |

| | |
|---|-----|
| Figure 3.91 The various contact distances (Å) within the cation complex (carbon, except for benzene ring, and hydrogen atoms are excluded) | 182 |
| Figure 3.92 Basic unit of (B18C6)K(TCNQ) ₂ (hydrogen atoms are excluded) | 183 |
| Figure 3.93 Top (a/c) and side (b/d) views of TCNQ units in (B18C6)K(TCNQ) ₂ (hydrogen atoms are excluded) | 185 |
| Figure 3.94 Observation of TCNQ repeating units in (B18C6)K(TCNQ) ₂ (hydrogen atoms are excluded)..... | 185 |
| Figure 3.95 Side (a) and top (b) views of the packing pattern in (B18C6)K(TCNQ) ₂ , yellow area represents the repeating TCNQ dimer (hydrogen atoms are excluded) | 186 |
| Figure 3.96 Packing pattern of (B18C6)K ⁺ (hydrogen atoms are excluded) | 187 |
| Figure 3.97 Various contact distances (Å) in (B18C6)K(TCNQ) ₂ (carbon, except for benzene ring, and hydrogen atoms are excluded) | 188 |
| Figure 3.98 Basic unit of (DB18C6)K(TCNQ) ₂ (hydrogen atoms are excluded)..... | 189 |
| Figure 3.99 Top (a) and side (b) views of TCNQ dimer (AB) in (DB18C6)K(TCNQ) ₂ (hydrogen atoms are excluded) | 190 |
| Figure 3.100 Observation of TCNQ repeating unit in (DB18C6)K(TCNQ) ₂ (hydrogen atoms are excluded)..... | 191 |
| Figure 3.101 Top (a) and side (b) views of dimer neighbours (BB') of (DB18C6)K(TCNQ) ₂ (hydrogen atoms are excluded) | 191 |
| Figure 3.102 Side (a) and top (b) views of packing pattern within (DB18C6)K(TCNQ) ₂ (hydrogen atoms are excluded) | 192 |
| Figure 3.103 Dimeric structure of cation complex through K ⁺ -π interactions in (DB18C6)K(TCNQ) ₂ (hydrogen atoms are excluded) | 193 |
| Figure 3.104 Various contact distances (Å) within the cation complex (carbon atoms on crown ether ring and hydrogen atoms are excluded) | 194 |
| Figure 3.105 Basic unit of (Dicyc18C6)K(TCNQ) ₃ (hydrogen atoms are excluded)... | 195 |
| Figure 3.106 An “S” formation of cation complex in (Dicyc18C6)K(TCNQ) ₃ (hydrogen atoms are excluded)..... | 196 |
| Figure 3.107 Top (a) and side (b) views of TCNQ dimer in (Dicyc18C6)K(TCNQ) ₃ (hydrogen atoms are excluded) | 198 |
| Figure 3.108 Observation of TCNQ repeating units in (Dicyc18C6)K(TCNQ) ₃ (hydrogen atoms are excluded) | 199 |
| Figure 3.109 Top (a) and side (b) views of external dimer neighbours in (Dicyc18C6)K(TCNQ) ₃ (hydrogen atoms are excluded) | 200 |

| | |
|---|-----|
| Figure 3.110 Various contact distances (Å) within the cation complex (carbon atoms on crown ether ring and hydrogen atoms are excluded) | 201 |
| Figure 3.111 Basic unit of (Dicyc18C6)Cs(TCNQ) ₂ (hydrogen atoms are excluded) . | 202 |
| Figure 3.112 Geometry of cation complex in (Dicyc18C6)Cs(TCNQ) ₂ (hydrogen atoms are excluded)..... | 203 |
| Figure 3.113 Top (a) and side (b) views of TCNQ dimer in (Dicyc18C6)Cs(TCNQ) ₂ (hydrogen atoms are excluded) | 205 |
| Figure 3.114 A wave-like configuration of TCNQ infinite column in (Dicyc18C6)Cs(TCNQ) ₂ (hydrogen atoms are excluded) | 206 |
| Figure 3.115 Observation of TCNQ repeating units in (Dicyc18C6)Cs(TCNQ) ₂ (hydrogen atoms are excluded) | 206 |
| Figure 3.116 Top (a) and side (b) views of dimer neighbours in (Dicyc18C6)Cs(TCNQ) ₂ (hydrogen atoms are excluded) | 207 |
| Figure 3.117 Various contact distances (Å) within the cation complex (carbon, except for the TCNQ and cyclohexane, and hydrogen atoms are excluded) | 208 |
| Figure 3.118 Basic unit of (C222)K(TCNQ) _{2.5} (hydrogen atoms are excluded) | 209 |
| Figure 3.119 Space-fill of TCNQ pentamer stack in (C222)K(TCNQ) _{2.5} (hydrogen atoms are excluded) | 211 |
| Figure 3.120 Top (a/c/e) and side (b/d/f) views of TCNQ units in (C222)K(TCNQ) _{2.5} (hydrogen atoms are excluded) | 212 |
| Figure 3.121 Views of pentamers geometry and packing pattern in TCNQ column (hydrogen atoms are excluded) | 213 |
| Figure 3.122 K ⁺ -N and K ⁺ -O distances (Å) (green labels) in (C222)K(TCNQ) _{2.5} (carbon and hydrogen atoms are excluded)..... | 214 |
| Figure 3.123 Core unit of (12C4)Rb(TCNQ) _{1.5} (hydrogen atoms are excluded) | 218 |
| Figure 3.124 Top (a) and side (b) views of TCNQ dimer in (12C4)Rb(TCNQ) _{1.5} (hydrogen atoms are excluded) | 220 |
| Figure 3.125 TCNQ dimers geometries in (12C4)Rb(TCNQ) _{1.5} (hydrogen atoms are excluded)..... | 220 |
| Figure 3.126 Top (a) and side (b) views of packing pattern of TCNQ ⁻ dimer in (12C4)Rb(TCNQ) _{1.5} (hydrogen atoms are excluded) | 221 |
| Figure 3.127 Various contact distances (Å) within the cation complex of (12C4)Rb(TCNQ) _{1.5} (carbon and hydrogen atoms are excluded) | 222 |
| Figure 3.128 Core unit of (15C5) ₂ RbTCNQ (hydrogen atoms are excluded) | 223 |

| | |
|---|-----|
| Figure 3.129 Top (a) and side (b) views of TCNQ ^{•-} dimer in (15C5) ₂ RbTCNQ (hydrogen atoms are excluded) | 224 |
| Figure 3.130 Side (a), top (b) and end (c) views of the infinite layers of (15C5) ₂ RbTCNQ (hydrogen atoms are excluded) | 226 |
| Figure 3.131 TCNQ ^{•-} dimers geometries in (15C5) ₂ RbTCNQ (hydrogen atoms are excluded)..... | 227 |
| Figure 3.132 Various contact distances (Å) within the cation complex of (15C5) ₂ RbTCNQ (carbon and hydrogen atoms are excluded) | 228 |
| Figure 3.133 Core unit of (18C6)Rb(TCNQ) ₂ (hydrogen atoms are excluded) | 229 |
| Figure 3.134 Top (a/c) and side (b/d) views of TCNQ trimer in (18C6)Rb(TCNQ) ₂ (hydrogen atoms are excluded) | 231 |
| Figure 3.135 Observation of TCNQ repeating units in (18C6)Rb(TCNQ) ₂ (hydrogen atoms are excluded)..... | 232 |
| Figure 3.136 Top (a) and side (b) views of TCNQ units (AC) in (18C6)Rb(TCNQ) ₂ (hydrogen atoms are excluded) | 233 |
| Figure 3.137 TCNQ trimer geometries in (18C6)Rb(TCNQ) ₂ (hydrogen atoms are excluded)..... | 234 |
| Figure 3.138 Various contact distances (Å) within the cation complex of (18C6)Rb(TCNQ) ₂ (carbon and hydrogen atoms are excluded)..... | 235 |
| Figure 3.139 Core unit of (DB18C6)RbTCNQ (hydrogen atoms are excluded)..... | 236 |
| Figure 3.140 Top (a) and side (b) views of TCNQ ^{•-} dimer | 237 |
| Figure 3.141 TCNQ ^{•-} dimer geometries in (DB18C6)RbTCNQ (hydrogen atoms are excluded)..... | 238 |
| Figure 3.142 Side (a) and top (b) views of the packing pattern within (DB18C6)RbTCNQ (hydrogen atoms are excluded)..... | 238 |
| Figure 3.143 Various views of TCNQ column in (DB18C6)RbTCNQ (hydrogen atoms are excluded)..... | 239 |
| Figure 3.144 Angle analysis of (DB18C6)RbTCNQ (hydrogen atoms are excluded) . | 240 |
| Figure 3.145 Various contact distances (Å) within the cation complex of (DB18C6)RbTCNQ (hydrogen atoms are excluded)..... | 241 |
| Figure 3.146 Basic unit of (Dicyc18C6)Rb(TCNQ) ₃ (hydrogen atoms are excluded). | 242 |
| Figure 3.147 A “S”-shaped formation of cation complex in (Dicyc18C6)Rb(TCNQ) ₃ (hydrogen atoms are excluded) | 243 |

| | |
|--|-----|
| Figure 3.148 Top (a) and side (b) views of TCNQ dimer in (Dicyc18C6)Rb(TCNQ) ₃ (hydrogen atoms are excluded) | 245 |
| Figure 3.149 Top (a) and side (b) views of twisted TCNQ units in (Dicyc18C6)Rb(TCNQ) ₃ (hydrogen atoms are excluded)..... | 245 |
| Figure 3.150 Various views of TCNQ column in (Dicyc18C6)Rb(TCNQ) ₃ (hydrogen atoms are excluded) | 246 |
| Figure 3.151 Various contact distances (Å) within the cation complex of (Dicyc18C6)Rb(TCNQ) ₃ (hydrogen atoms are excluded)..... | 248 |
| Figure 3.152 Core unit of (C222)Rb(TCNQ) _{2.5} (hydrogen atoms are excluded) | 249 |
| Figure 3.153 Space-fill of TCNQ pentamer stack in (C222)Rb(TCNQ) _{2.5} (hydrogen atoms are excluded) | 251 |
| Figure 3.154 Top (a/c/e) and side (b/d/f) views of TCNQ units in (C222)Rb(TCNQ) _{2.5} (hydrogen atoms are excluded) | 251 |
| Figure 3.155 Views of pentamers geometry and packing pattern in TCNQ column (hydrogen atoms are excluded) | 252 |
| Figure 3.156 Rb ⁺ -O and Rb ⁺ -N distances in cation complex of (C222)Rb(TCNQ) _{2.5} (carbon and hydrogen atoms are excluded) | 254 |
| Figure 3.157 IR spectra of (12C4) ₂ LiTCNQ in this study | 261 |
| Figure 3.158 Key vibrational motion (black highlighted lines) in the TCNQ molecule | 261 |
| Figure 3.159 A summary of Raman peaks of Ionophore Encapsulated MTCNQ salts | 264 |
| Figure 3.160 Raman spectra sample of (DB18C6)K(TCNQ) ₂ in this study..... | 264 |
| Figure 3.161 The EPR signal intensity as a function of temperature in (15C5)LiTCNQ | 268 |
| Figure 3.162 Roadmap as a function of angular displacement of an (15C5)LiTCNQ crystal at 300K..... | 269 |
| Figure 3.163 Roadmap as a function of angular displacement of an (15C5)NaTCNQ crystal at 315K..... | 270 |
| Figure 3.164 EPR spectra results of (15C5)Li/NaTCNQ·H ₂ O at different temperatures | 271 |
| Figure 3.165 Roadmap as a function of angular displacement of a (18C6)KTCNQ at 380K..... | 272 |
| Figure 3.166 EPR spectra result of (18C6)K(TCNQ) _{2.5} at 380K | 273 |
| Figure 4.1 Basic unit of Tb(TCNQ) ₃ (H ₂ O) ₆ ·3H ₂ O [showing two halves of TCNQ units (C and D)]..... | 275 |

| | |
|---|-----|
| Figure 4.2 Space-fill of TCNQ pentamer stack in $\text{Tb}(\text{TCNQ})_3(\text{H}_2\text{O})_6 \cdot 3\text{H}_2\text{O}$ with Tb^{3+} ions shown in cyan (hydrogen atoms and interstitial solvents are excluded) | 277 |
| Figure 4.3 Top (a/c/e) and side (b/d/f) views of TCNQ units in $\text{Tb}(\text{TCNQ})_3(\text{H}_2\text{O})_6 \cdot 3\text{H}_2\text{O}$ (hydrogen atoms are excluded) | 278 |
| Figure 4.4 Packing diagram of $\text{Tb}(\text{TCNQ})_3(\text{H}_2\text{O})_6 \cdot 3\text{H}_2\text{O}$ viewed along vertical axis (hydrogen atoms and interstitial solvents are excluded) | 279 |
| Figure 4.5 Views of pentamers' geometry and packing pattern in the TCNQ stack with Tb^{3+} cations in cyan (hydrogen atoms are excluded) | 280 |
| Figure 4.6 Perspective view of coordination geometry in $\text{Tb}(\text{TCNQ})_3(\text{H}_2\text{O})_6 \cdot 3\text{H}_2\text{O}$... | 281 |
| Figure 4.7 Cationic structure of $\text{Yb}(\text{TCNQ})_3(\text{H}_2\text{O})_6 \cdot 3\text{H}_2\text{O}$ [showing two halves of TCNQ units (C and D), hydrogen atoms are excluded] | 282 |
| Figure 4.8 Space-fill of TCNQ pentamer stack in $\text{Yb}(\text{TCNQ})_3(\text{H}_2\text{O})_6 \cdot 3\text{H}_2\text{O}$ (Yb^{3+} ions in light green, hydrogen atoms and interstitial solvents are excluded) | 284 |
| Figure 4.9 Top (a/c/e) and side (b/d/f) views of TCNQ units in $\text{Yb}(\text{TCNQ})_3(\text{H}_2\text{O})_6 \cdot 3\text{H}_2\text{O}$ (hydrogen atoms are excluded) | 285 |
| Figure 4.10 Packing diagram of $\text{Yb}(\text{TCNQ})_3(\text{H}_2\text{O})_6 \cdot 3\text{H}_2\text{O}$ viewed along vertical axis (hydrogen atoms and interstitial solvents are excluded) | 286 |
| Figure 4.11 Views of pentamers' geometry and packing pattern in the TCNQ stack (hydrogen atoms are excluded) | 287 |
| Figure 4.12 Perspective view of coordination geometry in $\text{Yb}(\text{TCNQ})_3(\text{H}_2\text{O})_6 \cdot 3\text{H}_2\text{O}$. | 288 |

List of schemes

| | |
|--|-----|
| Scheme 1.1 Structures of TCNQ and TCNQ ^{•-} anion..... | 9 |
| Scheme 1.2 Preparation of TCNQ salt..... | 10 |
| Scheme 1.3 Synthetic route to TCNQ and its radical anion | 13 |
| Scheme 1.4 Mechanism for the formation of DCTC ⁻ ⁵⁸ | 14 |
| Scheme 1.5 Decomposition of TCNQ and its salts to DCTC ⁻ ⁵⁵ | 14 |
| Scheme 1.6 TCNQ process of absorbing free electrons from TCNQ to TCNQ ²⁻ ^{55,63} | 15 |
| Scheme 1.7 Formation of TTF-TCNQ charge-transfer complex ⁷⁹ | 21 |
| Scheme 2.1 The original synthesis route of DB18C6 ¹²⁶ | 33 |
| Scheme 2.2 Equilibrium showing the formation of a cryptate inclusion complex ¹⁵⁴ | 38 |
| Scheme 2.3 The preparation and self-assembly of the [2]catenane ¹⁵⁹ | 43 |
| Scheme 2.4 Hydrogen bonds formation of a dimer of Pyridone ^{180,181} | 49 |
| Scheme 2.5 Standard preparation method of LiTCNQ..... | 54 |
| Scheme 2.6 The Curie Law | 79 |
| Scheme 2.7 Relationship between the peak intensities in ESR spectra | 79 |
| Scheme 2.8 The monomer-dimer equilibrium of TCNQ ^{•-} in aqueous solution..... | 81 |
| Scheme 3.1 Calculation of resistivity (ρ) | 266 |
| Scheme 3.2 The relationship between conductivity (σ) and resistivity (ρ) | 266 |

DECLARATION OF AUTHORSHIP

I, Bingjia Yan declare that the thesis entitled A Crystal Engineering Study of Molecular Electronic Behaviour in TCNQ Salts and the work presented in the thesis are both my own, and have been generated by me as the result of my own original research.

A Crystal Engineering Study of Molecular Electronic Behaviour in TCNQ Salts

I confirm that:

- this work was done wholly or mainly while in candidature for a research degree at this University;
- where any part of this thesis has previously been submitted for a degree or any other qualification at this University or any other institution, this has been clearly stated;
- where I have consulted the published work of others, this is always clearly attributed;
- where I have quoted from the work of others, the source is always given. With the exception of such quotations, this thesis is entirely my own work;
- I have acknowledged all main sources of help;
- where the thesis is based on work done by myself jointly with others, I have made clear exactly what was done by others and what I have contributed myself;
- none of this work has been published before submission.

Signed:

Date:.....

Acknowledgements

I would like to thank everyone who has helped me in the production of this thesis and has made my life in Southampton so enjoyable and peaceful.

Firstly, my Supervisor, Dr. Martin Grossel for his support through the research years and his constant belief the project I was doing would lead somewhere. Thanks to Martin for giving me the freedom to handle day-to-day operation in my own manner. I still remember that Martin demonstrated the skills of recrystallisation to me when I entered the lab and planned to start my work. Because of Martin, he helps me open up horizons in the area of Chemistry, especially in Supramolecular Chemistry and trains me to become a professional chemist. Besides the academic research life in Chemistry, Martin also helps me solve the visa, tuition and accommodation issues. Thanks Martin for doing everything for me. I am really appreciated.

Next, thanks to all members past and present of the Grossel group and assorted hangers-on would have made the 4th floor never a dull place to work. Safety Dom, he taught me the fundamental chemistry knowledge and all the safety information. Thanks Dom for offering me professional opinions and supporting with my project. He helped me adapt to the environments quickly and smoothly. Nick is a very kind person. He introduced lots of engineering friends to me and demonstrated the technique for designing academic poster. It's very enjoyable to talk to him all the time. For Adam, he helped me solve the NMR problems and exhibited lots of interesting video to me. Because of Darren, I have already addicted to Guinness, known lots of funny slang and several communication tools such as Snapchat. Hassan is a very kind hearted person who is willing to help you all the time. We are best friends forever. Gareth, a professional dancing boy, contributed his great passion to the group, who gave everyone endless happiness. Finally, thanks to all the project students over the years that have worked in the lab, who were foolhardy enough to help me.

Then, I would like to thank Dr. Simon Coles for the X-ray Crystallography studies; Dr. John Langley and Ms Julie Herniman for the Mass Spectrometry; Dr. Neil Wells for his help with that many NMR problems; Prof. Andrea Russell for the analysing of IR and Raman spectra; Dr. John Fosbraey and Mr. Colin Flowers for offering the IR equipment in 4th teaching lab; Karl, Keith and Mark for their professional work in store; Ms. Danai

Panagoulia for helping with Raman measurement in a rather short period; Dr. Francesco Cuba for his support and encourage to help me overcome kinds of problems.

Following, I am extremely grateful to Dr. Peter Horton for his outrageous experimental suggestions, patience with my many X-ray Crystallography questions. Thanks Dr. Christopher Wedge for providing EPR equipment and introducing background knowledge of Physical Chemistry. Thanks Dr. Richard Curry for introducing me into the fabulous world of Lanthanide. Thanks Dr. Thomas Logothesis, Miss Nadine Hill and Miss Diana Fernandes for offering me an opportunity to be a demonstrator and technician in 5th teaching lab. Thanks Ms. Carol Marchment provides an opportunity for letting me become an invigilator. I am really appreciated for the precious experience.

Finally, to my girlfriend, Yi Qu, who has encouraged me to go through any difficulties during my life and to my family, Tingwu Yan and Ying Zhang, who have supported me throughout and for providing me with tuition and somewhere to stay in Southampton whenever it was needed.

Definitions and Abbreviations

A: Acceptor

Ad: acridinium

B15C5: Benzo-15-crown-5

B18C6: Benzo-18-crown-6

2-2' BIP: 2-2' Bipyridinium

4-4' BIP: 4-4' Bipyridinium

C222: 2.2.2-Cryptand

CDCl₃: Chloroform

Cryptand: 1,10-diaza-4,7,13,16,21,24-hexaoxabicyclo[8.8.8]hexacosane

Cyclam: 1,4,8,11-tetraazacyclotetradecane

D: Donor

DB18C6: Dibenzo-18-crown-6

Dicyc18C6: Dicyclohexano-18-crown-6

D₂O: Deuterium Oxide

DNA: Deoxyribonucleic acid

DBTTF: Dibenzotetrathiafulvalene

DCM: Dichloromethane

DCTC⁻: α,α -Dicyano-*p*-toluoylcyanide anion

DMSO: Dimethyl sulfoxide

DMTCNQ: Dimethyltetracyanoquinodimethane

DPA: Pyridine-2,6-dicarboxylate (Dipicolinate)

EPR: Electron Paramagnetic Resonance

ES: Electrospray (Mass Spectroscopy)

H₂O: Deionised water

H₂pdC: Pyridine-2,6-dicarboxylic acid

HMTSeF: hexamethylenetetraselenafulvalene

HMTTF: Hexamethylenetetrafulvalene

IR: Infra-red

KCP: K₂Pt(CN)₄Br_{0.30} · 3H₂O

m.p.: Melting point

MeCN: Acetonitrile

Me₁₀Fc: Decamethylferrocene

MeOH: Methanol

NMP: N-methylphenazinium

NMR: Nuclear Magnetic Resonance

Oc7: 3,3'-Diethyloxacyaninium

Paraquat: N,N'-dimethyl-4,4'-bipyridinium dichloride

PTP: 2[5-(2-pyridyl)-1,2,4-triazol-3-yl]phenol

PTZ: Phenothiazine

Qn: Quinolinium

R.T.: Room temperature

TCNE: Tetracyanoethylene

TCNQ: 7,7',8,8'-tetracyanoquinodimethane

TCNQCl₂: 2,5-Dichloro -7,7,8,8-tetracyanoquinodimethanide

TCNQF₄: 2,3,4,5-Tetrafluoro-7,7',8,8'-Tetracyano-*p*-quinodimethane

TCNQH₂: 2,2' - (p-Phenylene)bis(propanedinitrile)

TEA: Triethylamine

TMB: Tri-methyl-bezimidazolium

TMTSeF: Tetramethyltetraselenafulvalene

TMTTF: Tetramethyltetrathiafulvalene

TTF: Tetrathiafulvalinium

TTT: Tetrathiotetracene

UV: Ultra-violet

1. Introduction

1.1 Molecular electronics

Molecular electronics can be regarded as technology utilising single molecules for electronic applications¹. Painstaking attention has been paid to the design of novel functional, inexpensive, high density, nanoelectronic devices, structures and experimental paradigms that share common themes²⁻⁴. Traditional semiconductors suffer from the disadvantages of high heat release, limited electron mobility and connection problems. Consequently, classic semiconductors cannot cope with present needs and will be gradually abandoned. With the progression of technology, new semiconductor devices are becoming associated with quantum phenomena^{2,5}. The concept of a quantum transistor has been applied as one aspect of the design of the new devices^{2,5}. Numerous theoretical and experimental studies have been associated with artificial low-dimensional structures, such as wires and quantum films. The new approach of utilising quantum phenomena is expected to provide a new class of electronic devices^{2,5}.

Molecular electronics involves the replacement of components such as wires, transistors, or other fundamental solid state silicon-based electronic elements¹. These electronic elements are constructed from one or a few molecules^{1,6}. Each molecule is quite minute, approximately one million times smaller than their current microelectronic counterparts. The field of molecular electronics is different from the DNA-based computing where memorising and retrieving of any information is based on the structure of chemical bonds. This is a relatively slow process, which needs solution-based conditions. In addition, molecular electronics can detect unique information, offered by molecules, in order to analyse and generate novel electronic devices⁶. Heath and Ratner⁷ summarised four major advantages for utilising electronics applications, which were: size; assembly and recognition; dynamic stereochemistry; and synthetic tailorability.

One aspect of the area of molecular electronics concerns novel organic materials, particularly organometallic compounds⁷⁻¹⁰. Organic and organometallic compounds can exhibit unique physico-chemical properties, such as high conductivity, magnetic properties, and the potential for energy storage, and they can also be used for homogeneous catalysis⁹⁻¹¹. Furthermore, combining such compounds with other

molecules associated with controlling intermolecular interactions between each molecular unit can lead to useful changes to the structure and physical properties of organic materials. Although the intrinsic characteristic of organometallic compounds is as potentially toxic pollutants, the unique properties of organometallic compounds have been remarkably useful in the field of chemical biology, for example serving as anticancer, antimalarial or antimicrobial agents^{8,9,11}. In addition, organometallic compounds have attracted much attention in the area of medicinal chemistry because of their unique properties, such as multiple structure types, variable ligand bonding modes, different intra/intermolecular interactions and redox characteristics⁸. Therefore, the unique structure and bonding types within organometallic compounds can ameliorate the formulation stages of clinical trials, drug optimisation, and drug design processes⁸.

1.2 Electronically active organic materials

In this section, the content of electronic properties of organic materials will be divided into three separate parts. In the first instance, there will be a discussion about the main structural types of conducting materials. Thereafter, two types of charge transfer complexes will be described as supporting examples in each sub-section. Finally, there will be a short section discussing radical ion salts with corresponding examples.

1.2.1 Main structural types of conducting materials

The main types of molecular conducting materials can be separated into three distinctly different structural classes, namely those of metal-complex stacks, polymer chains and molecular stacks.

1.2.1.1 Metal-complex stacks

Metal complexes such as $\text{Pt}(\text{CN})_4^{2-}$ can form conducting materials. These typically adopt a quasi-one-dimensional structure, which can display one-dimensional electron transfer behaviour. Figure 1.1 shows the spatial distribution¹² of Pt atoms and CN groups in $\text{K}_2\text{Pt}(\text{CN})_4$, a chain or a column of $\text{Pt}(\text{CN})_4^{2-}$ complex anions is formed in a crystal along which the electrons can move through the channel constructed by Pt atoms¹². The electrical conductivity of $\text{K}_2\text{Pt}(\text{CN})_4$ complex is quite high, ca. $300 \text{ (S}\cdot\text{cm}^{-1})$, and anisotropic at room temperature. However, the $\text{K}_2\text{Pt}(\text{CN})_4$ becomes an insulator at low temperatures. If KCP ($\text{K}_2\text{Pt}(\text{CN})_4\text{Br}_{0.30}\cdot 3\text{H}_2\text{O}$) is treated with halogens (Br_2 , Cl_2) as

a doping agent partial oxidation of the platinum centres ($\text{Pt}^{2+} \rightarrow \text{Pt}^{4+}$) occurs resulting in mixed-valence¹². Based on the temperature dependence of the Seeback Effect, Fedutin¹³ would seem to have confirmed the existence of metal-insulator transition in the electron motion along the chains in KCP. According to electrical and optical measurements, at high temperatures and frequencies, KCP behaves as a quasi-one-dimensional metallic system¹².

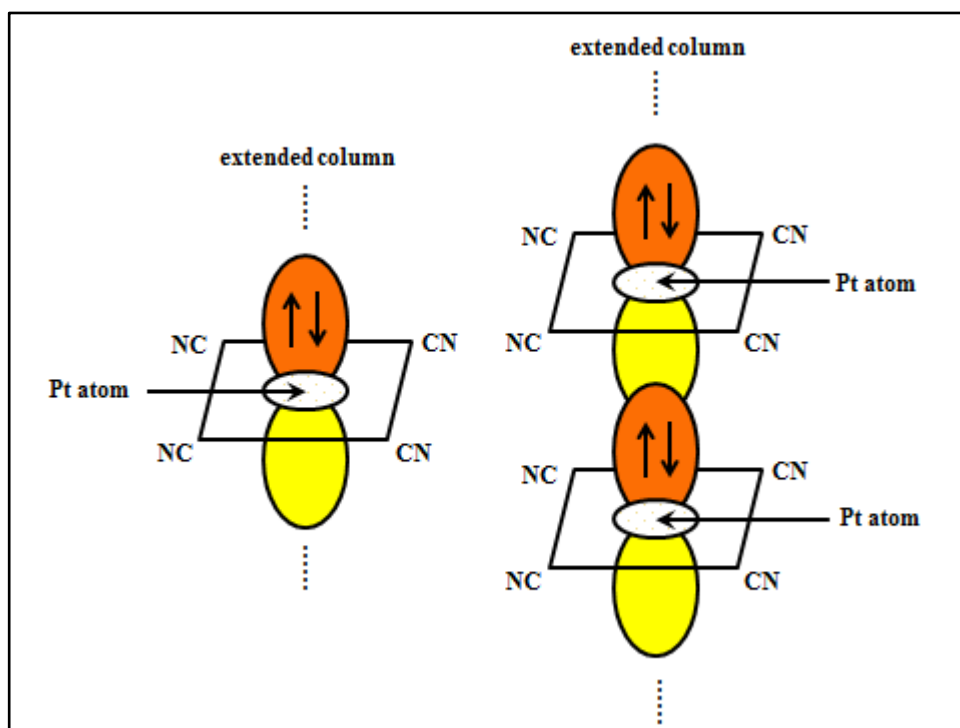


Figure 1.1 The structure of $\text{K}_2\text{Pt}(\text{CN})_4$ ¹²

1.2.1.2 Polymer chains

Polymers based on polyacetylene (Figure 1.2) can become conducting as a result of electron migration along the polymer chain¹⁴.

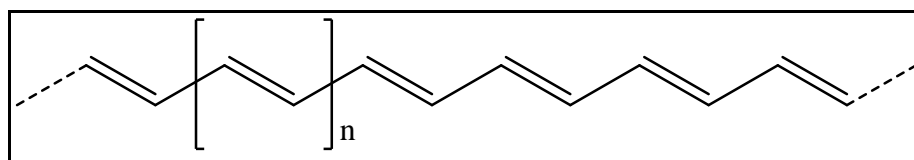


Figure 1.2 The structure of a trans-polyacetylene chain

Table 1.1 displays the structures, maximum conductivities $(\text{S}\cdot\text{cm}^{-1})_{\text{max}}$, and type of doping [negative (n) or positive (p)] for conducting polymers of this type.

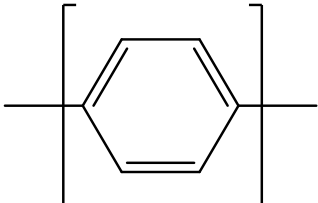
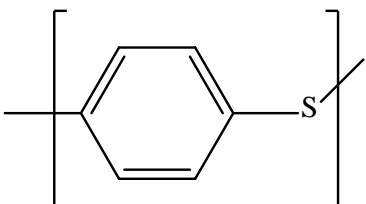
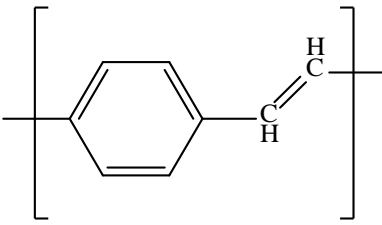
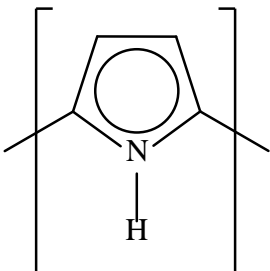
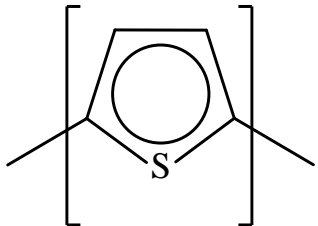
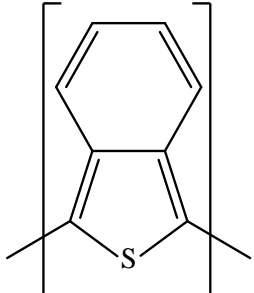
| Polymer | Structure | $(\Omega \cdot \text{cm})^{-1}_{\text{max}}$ | The type of doping |
|---------------------------|---|--|--------------------|
| Polyparaphenylene |  | 500 | n & p |
| Polyparaphenylenesulfide |  | 3-300 | p |
| Polyparaphenylenevinylene |  | 1-1000 | p |
| Polypyrrole |  | 40-200 | p |
| Polythiophene |  | 10-100 | p |
| Polyisothianaphthene |  | 1-50 | p |

Table 1.1 The conducting polymers¹⁵

Undoped polymers are insulators because all electrons are located in discrete π molecular orbitals (a filled valence band), and cannot readily migrate along the unsaturated polymer chain. In order to exhibit high conductivity, electrons must be promoted from a full π orbital into an anti-bonding π^* orbital (conduction band). However, such polymer chains can be doped and then display high conductivity behaviour. For example, when doping polyacetylene, a free electron can either be added to the polymer chain to form a negative chain (n-type) or an electron can be removed to produce a positive chain (p-type). The reagents for producing p-type doping are Br_2 , SbF_5 , HClO_4 . On the other hand, treatment with alkali metals forms n-type semiconducting polymers, in which the polymer acts as an electron acceptor.

1.2.1.3 Molecular stacks

Molecular stacks are constructed of infinite stacks of molecules combined through intermolecular interactions without covalent bonding between the molecules. If the structure consists of one species, then the stacks are insulators. That said, if the system is constructed of two components, it can form alternating stacks associated with π - π interactions, particularly if one component is an electron donor molecule (D), the other is an electron acceptor molecule (A). Examples include perylene(D)-TCNQ(A) and chrysene(D)-fluoranil(A), respectively (see Figure 1.3 and Figure 1.4, respectively).

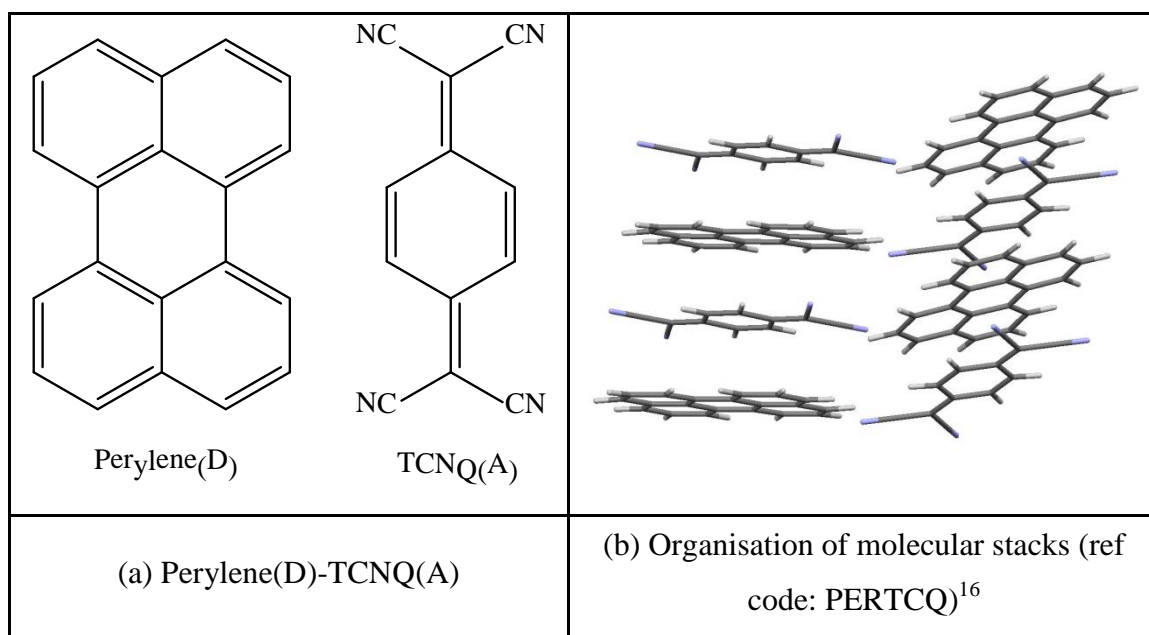


Figure 1.3 The charge transfer complex of Perylene(D)-TCNQ(A) (ref code: PERTCQ)¹⁶

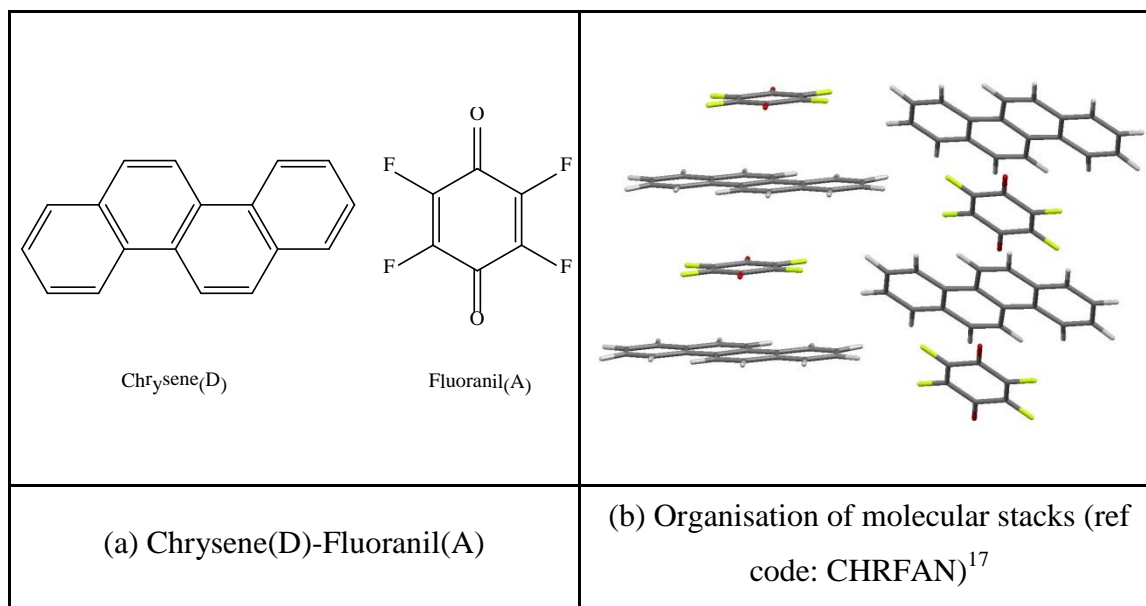


Figure 1.4 The charge transfer complex of Chrysene(D)-Fluoranyl(A) (ref code: CHRFAN)¹⁷

Geometries of such π - π stacks are controlled by electrostatic interactions¹⁸. Hunter and Sanders¹⁸ have summarised the basic principles behind the assembly of non-polarised π -systems, such as simple aromatic molecules. The principle of π - π repulsion, which is dominated in face-to-face π stack packing motif, is displayed in Figure 1.5(b).

Additionally, an edge-on, T-shaped or an offset π stack packing motif Figure 1.5(c) will lead to the π - σ attraction, respectively¹⁸.

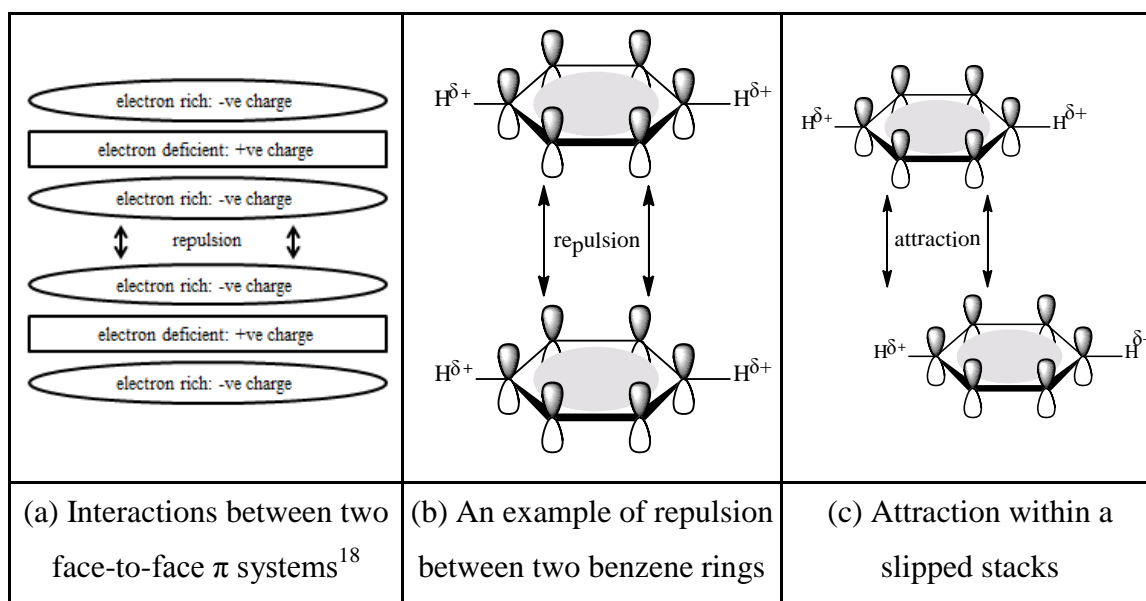


Figure 1.5 Principle interactions between π systems

Systems such as those shown in Figure 1.3 and Figure 1.4, the formation of mixed stacks are, of course, electrostatically favoured. The principle of π - σ attraction predicts a favourable π stacking interaction. Two examples of this behaviour involve the zinc porphyrin (Figure 1.6) and [18]annulene (Figure 1.7), respectively.

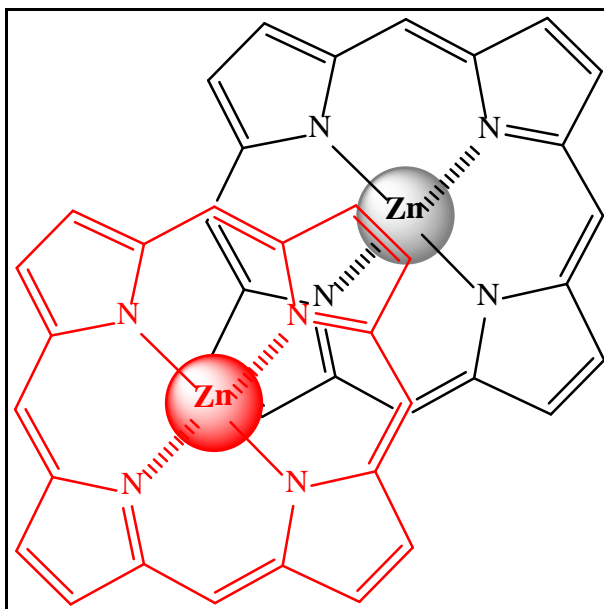


Figure 1.6 The optimum geometry of zinc porphyrin π - π interactions¹⁸

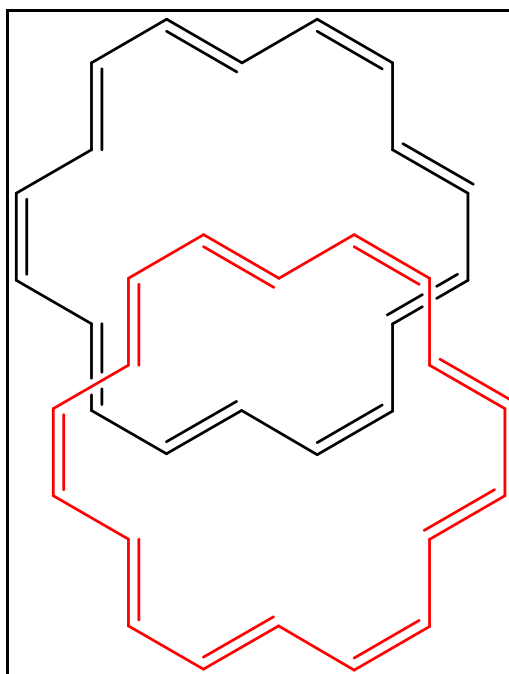


Figure 1.7 The geometry of π stacking interactions in [18]annulene¹⁸

The ideal geometry of the zinc porphyrin minimises π - π repulsion between adjacent molecules and maximises attraction between the inner cavity of one porphyrin and the pyrrole ring from another nearby porphyrin¹⁸. Therefore, porphyrin prefers to form π stack in an offset geometry, which is the same packing functionality as existing π stack in [18]annulene.

In the solid-state structure of benzene, neighbouring molecules are associated via a T-shaped architecture, face-to-face geometry being disfavoured here because of π - π repulsion¹⁸. The geometries of π stacking interactions can be summarised in Figure 1.8. As a function of orientation, the geometry interactions between two π atoms can be ascribed to two attractions and one face-to-face π stack repulsion, respectively¹⁸.

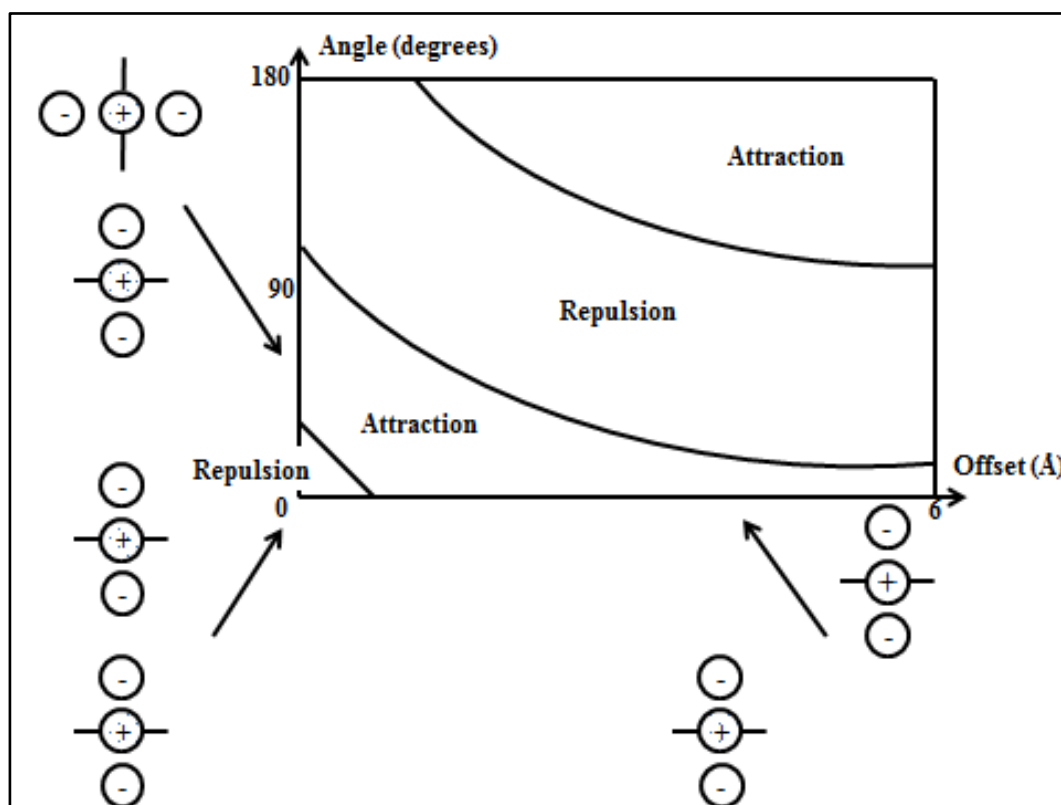


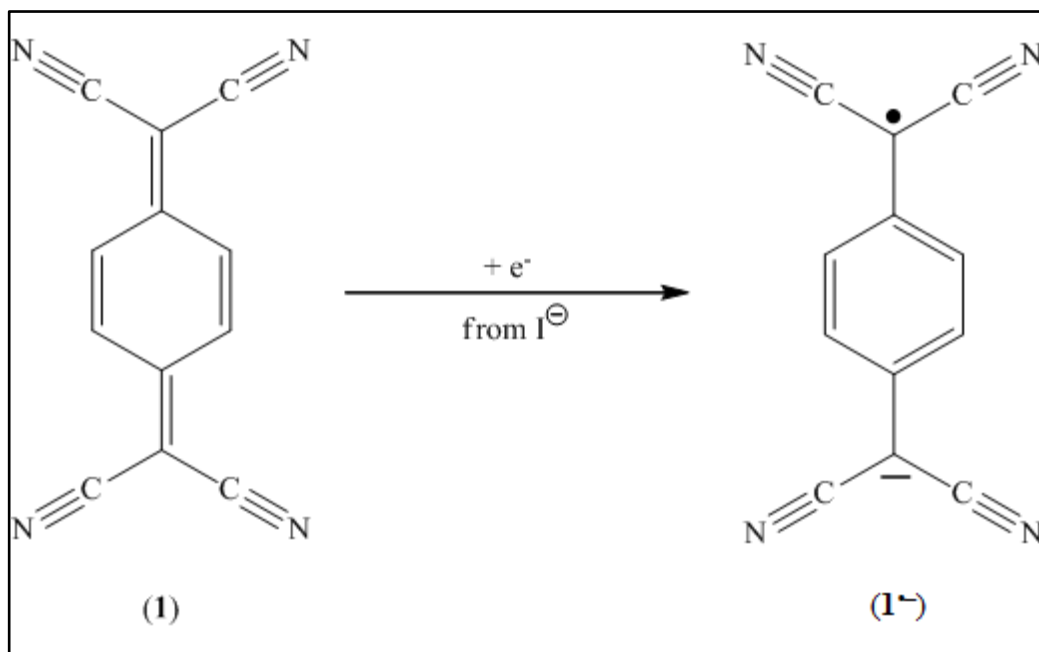
Figure 1.8 Geometry of π stacking interactions¹⁸

1.2.2 Molecular-based organic conducting materials

Simple organic compounds are normally insulators at room temperature. However, a highly conductive organic compound was discovered in 1954 by Akamatu et al.¹⁹. It was observed that organic perylene crystals doped with bromine could exhibit high electrical conductivity, 10^{-1} S·cm⁻¹ compared with 10^{-15} S·cm⁻¹ for pure perylene alone.

This was the first indication that molecular materials could display such physical properties^{19,20}. The next important breakthrough in the area of organic conductors came in 1960, when 7,7',8,8'-tetracyanoquinodimethane (TCNQ) (**1**) (Scheme 1.1) was first prepared by Melby et al.²¹.

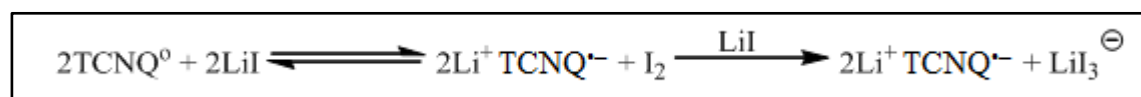
Because of the four peripheral electron-withdrawing cyano groups and the large π -conjugated system in the molecule, TCNQ is a good one electron acceptor with a high electron affinity (2.8 ± 0.1 eV)²²⁻²⁶. TCNQ is easily reduced to its corresponding TCNQ^{•-} radical anion (**1^{•-}**) as viewed in Scheme 1.1 by chemical reduction²¹, photoreduction^{27,28}, or electrochemical methods^{29,30}. The TCNQ^{•-} anion can be stabilised by dimerisation³¹⁻³³, or interaction with various electron-donating compounds^{33,34}, or by forming stable salts, such as M⁺TCNQ^{•-}, where M represents an alkali metal, transition metal, a quaternary ammonium, phosphonium or arsonium counterion³⁵ or an organic dye cation³⁶. The versatile TCNQ and TCNQ^{•-} anion have played an important role in the development of organic semiconducting materials^{22,37}. Scheme 1.1 shows structures of TCNQ and TCNQ^{•-} anion, respectively.



Scheme 1.1 Structures of TCNQ and TCNQ^{•-} anion

1.3 TCNQ^{•-} anion and its compounds, derivatives and analogues

TCNQ is an insulating yellow solid. The reaction of it with excess amount of lithium iodide affords a dark purple solid 1:1 salt, which displays semiconducting behaviour. This is because TCNQ readily accepts one electron upon reaction with iodide salts (e.g. Scheme 1.2)



Scheme 1.2 Preparation of TCNQ salt

In the solid state, these salts adopt structures in which the TCNQ^{•-} anions are face-to-face π stacked²¹. The salts containing TCNQ^{•-} anions exhibit paramagnetic behaviour due to a free single unpaired electron, which can exhibit physical properties such as electronic conductivity, non-linear optical behaviour, and electron paramagnetic resonance behaviour, and are anisotropic as determined by physical measurements along major crystal axes²¹. TCNQ, itself, can also readily form π -donor- π -acceptor 1:1 complexes. For example, phenothiazine, naphthalene and pyrene each form intermolecular electron donor-acceptor π stacked complexes with neutral TCNQ³⁸⁻⁴¹.

1.3.1 Phenothiazine-TCNQ complex

Crystal structures of a number of charge transfer complexes involving TCNQ have been extensively studied⁴²⁻⁴⁵. When TCNQ reacts with planar organic molecules, namely those of phenothiazine and naphthalene, a mixed stacking column of alternating donor and acceptor is obtained. Within the phenothiazine (PTZ)-TCNQ complex, the components form π donor and π acceptor, face-to-face stacked complexes, which are insulators³⁹. In the PTZ-TCNQ complex, the intermolecular distance between TCNQ and an adjacent PTZ unit is 3.44 Å³⁹ and the overlapping pattern of this complex is the ring-external bond type³⁹. The interatomic distance of N-H \cdots N between PTZ and TCNQ in neighbouring columns is 3.37 Å³⁹ and the corresponding angle of N-H \cdots N is 140°³⁹, respectively. Figure 1.9 shows the structures of PTZ and TCNQ and the solid state structure of PTZ-TCNQ complex.

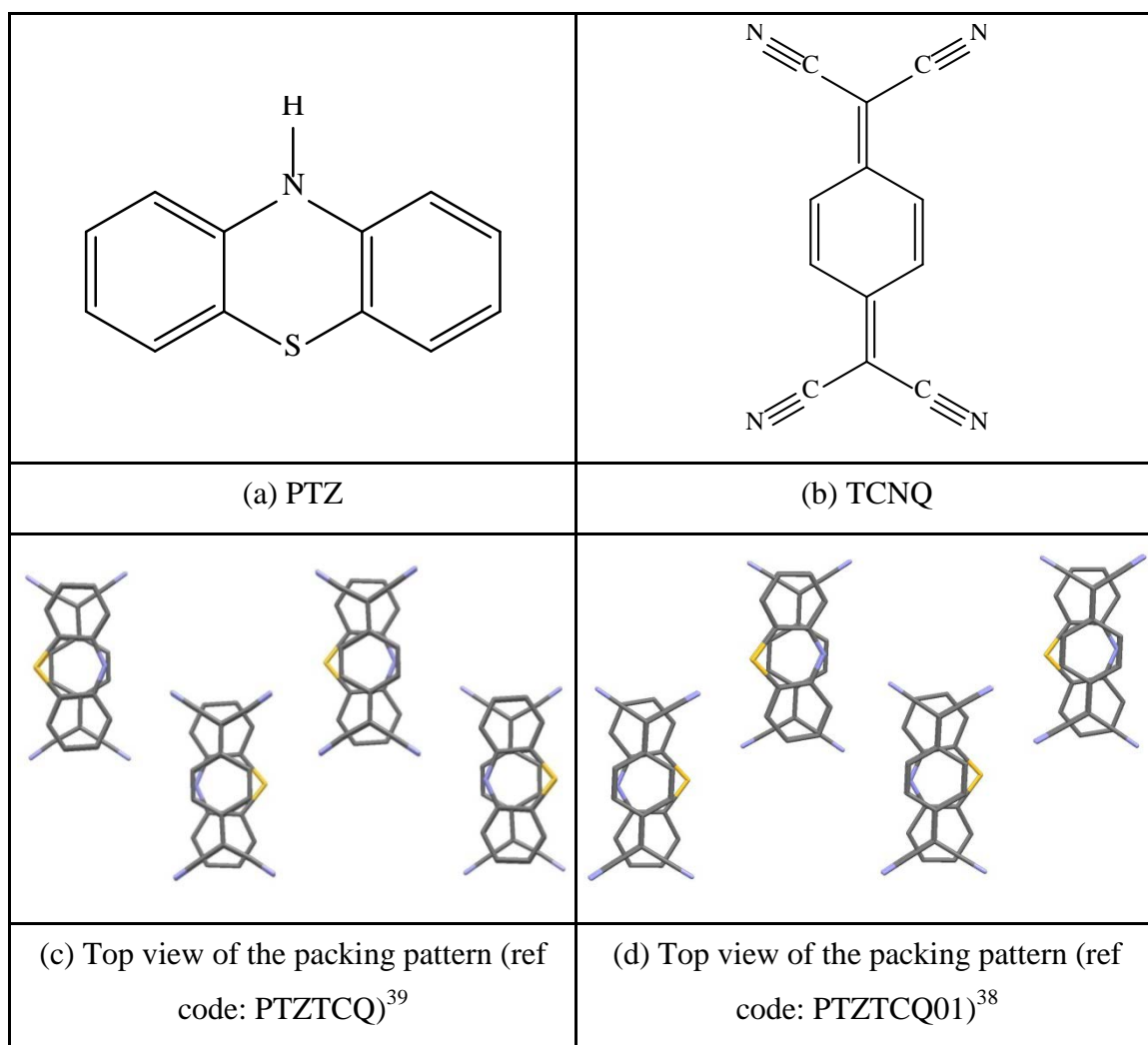


Figure 1.9 The packing pattern of PTZ-TCNQ complex (ref code: PTZTCQ and PTZTCQ01)^{38,39,46,47}

1.3.2 Naphthalene-TCNQ complex

In the case of the naphthalene-TCNQ complex, the electron donor (naphthalene) and the electron acceptor (TCNQ) form alternating stacks as shown in Figure 1.10. The two components are well ordered and the packing arrangements are controlled by dipole-dipole and van der Waal's interactions⁴⁷⁻⁵⁰. Figure 1.10 displays the structure of naphthalene and TCNQ and alternating stacks of the naphthalene-TCNQ complex.

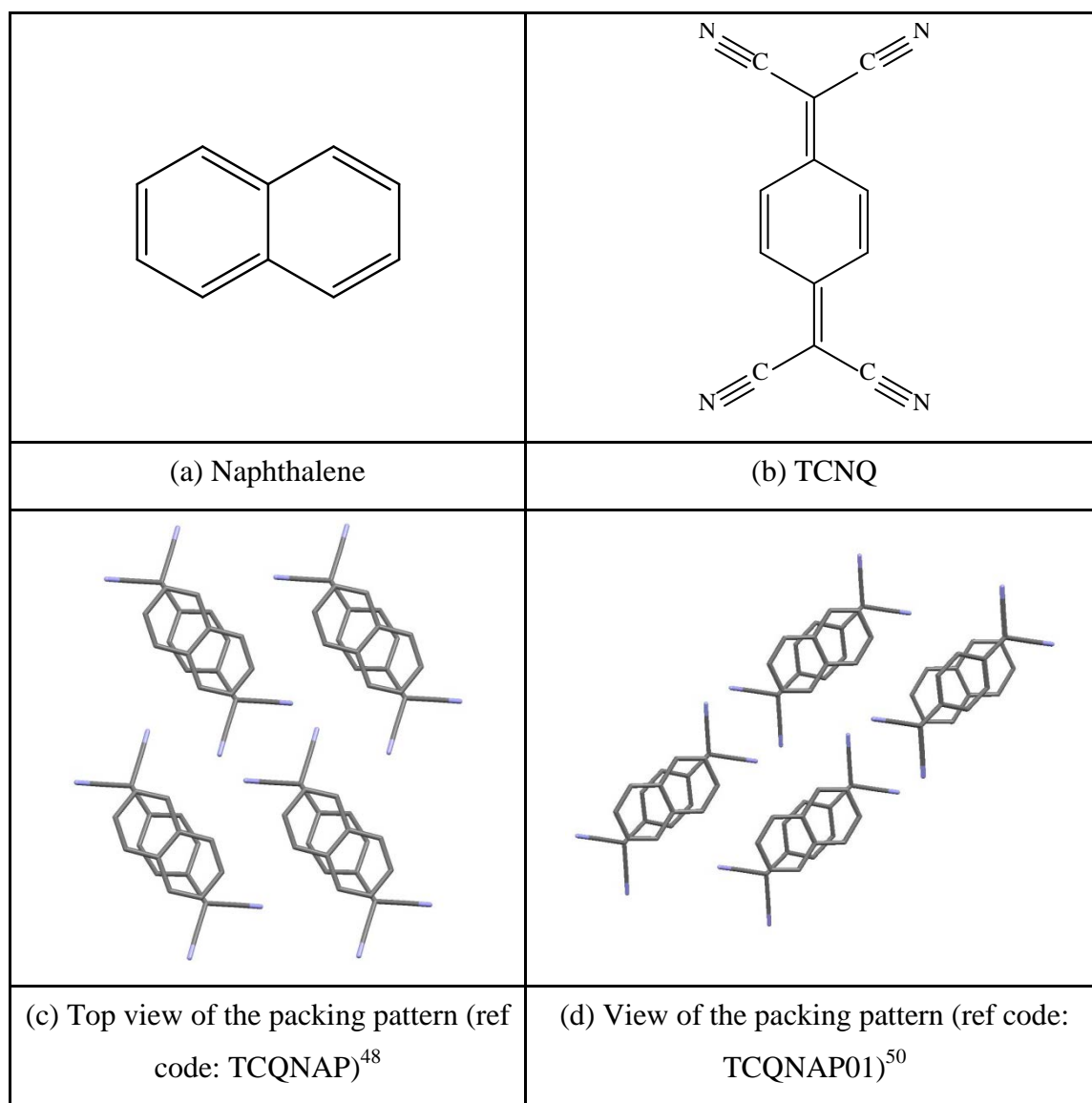


Figure 1.10 The packing pattern of naphthalene-TCNQ complex (ref code: TCQNAP and TCQNAP01)^{48,50}

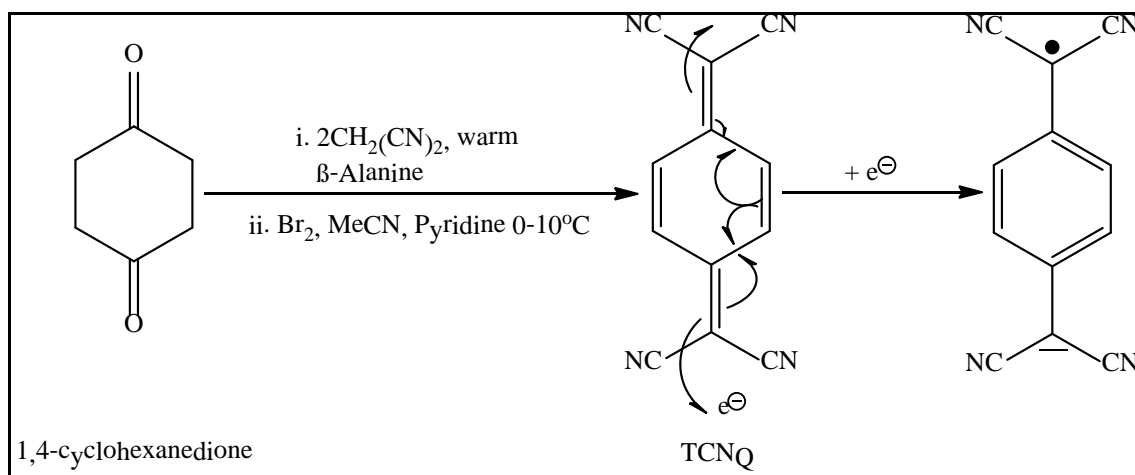
1.4 The physical and chemical behaviour of TCNQ

In this section, the content of the physical and chemical behaviour of TCNQ will be divided into two separate parts. Firstly, the reactions of TCNQ will be discussed. An introduction of TCNQ²⁻ compounds will be presented in the following section.

1.4.1 The reactions of TCNQ

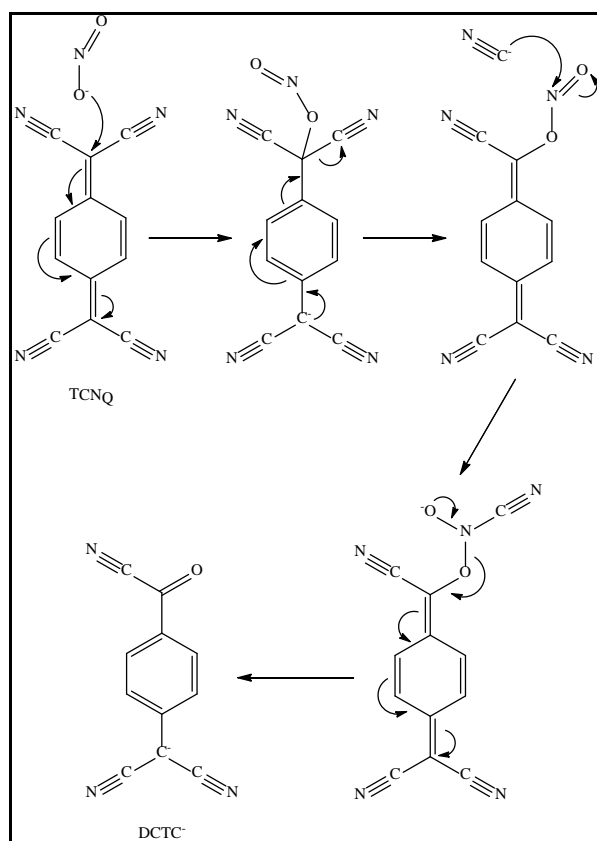
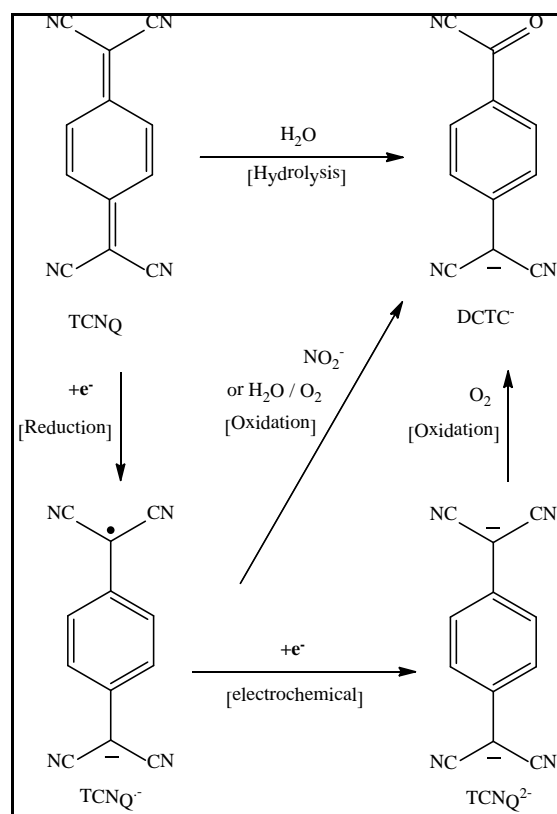
After TCNQ was first synthesised in 1960 by Melby²¹, numerous different compounds containing TCNQ as an electron acceptor have been widely studied^{34,49-52}.

Scheme 1.3 shows the synthetic route of TCNQ and its radical anion, respectively.



Scheme 1.3 Synthetic route to TCNQ and its radical anion

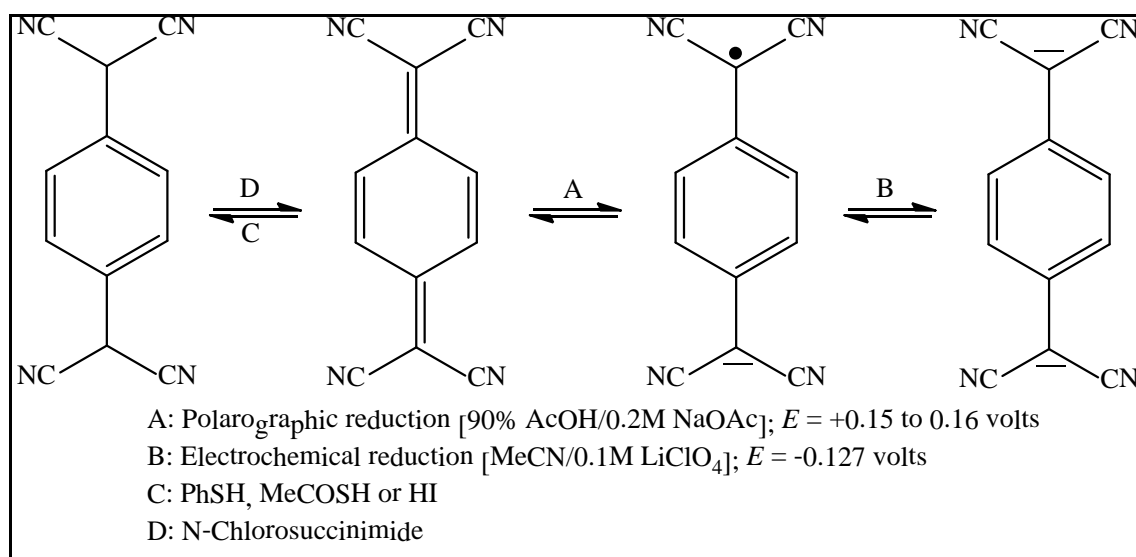
The solid state behaviour of these salts is particularly sensitive to their surroundings, especially to the cation^{53,54}. However, decomposition of TCNQ and its radical anion represents a constraint for the investigation of these electronically active complexes⁵⁵. In the presence of oxygen or nitrite ion, the TCNQ will be converted into DCTC⁻ (α,α -Dicyano-*p*-toluoylcyanide anion). Hertler et al.⁵⁶ were the first to report this process when they separated a salt of DCTC⁻ from reaction of TCNQ with nitrite ion. An X-ray study of the meta-magnetic phase of the decamethylferricenium TCNQ^{•-} complex by Miller et al.⁵⁷ revealed contamination with DCTC⁻ as a result of oxygen reacting with TCNQ^{•-}. Scheme 1.4 shows the mechanism for the formation of DCTC⁻. Scheme 1.5 summarises several of the decomposition routes of TCNQ and its salts to DCTC⁻.

Scheme 1.4 Mechanism for the formation of DCTC⁻ ⁵⁸Scheme 1.5 Decomposition of TCNQ and its salts to DCTC⁻ ⁵⁵

The bond lengths of cyano groups in both of the DCTC⁻ and TCNQ^{•-} are shorter than those found in TCNQ⁵⁵. Grossel et al.⁵⁵ have synthesised and further explored the formation of KDCTC and have isolated and carried out an X-ray structural study of K⁺[2.2.2]DCTC⁻ CH₃CN obtained during an unsuccessful attempt in the preparation of K⁺[2.2.2] TCNQ^{•-}⁵⁵.

1.4.2 An introduction to TCNQ²⁻ salts

TCNQ can also be reduced to its dianion, and because of the double negative charge on this species, it can interact much more strongly with metal cations and more readily forms crystalline networks than do either TCNQ or the TCNQ^{•-} anion⁵⁹⁻⁶². The process of reducing TCNQ to its corresponding TCNQ²⁻ is summarised in Scheme 1.6.



Scheme 1.6 TCNQ process of absorbing free electrons from TCNQ to TCNQ²⁻^{55,63}

In such a situation, the counter-cation determines the structure of the coordination networks and how the choice of cation can afford a way of controlling the structure and function of the anionic network. After reacting with metal cations, the *in-situ* generated TCNQ²⁻ can be coordinated with metal cation at all times, thereby protecting the TCNQ²⁻ from oxidation. Indeed, several complexes have been prepared based on the reaction between TCNQH₂ and metal cations. For example, a hexagonal prismatic crystal which can exhibit an infinite 3D [Mn₂(TCNQ)₃]²⁻ coordination network, can be synthesised in an environment of methanol/DMSO and acetate ion⁵⁹⁻⁶². The resulting crystal structure is shown in Figure 1.11. It forms honeycomb-like 3D coordination

networks [Mn \cdots Mn connections represented as blue rods in Figure 1.11(a)]⁶²; Figure 1.11(b) gives a specific description of a single hexagonal channel⁶²; Figure 1.11(c) shows that one TCNQ²⁻ ligand is coordinated to four metal centres⁶²; Figure 1.11(d) represents the octahedral environment around the metal centre⁶².

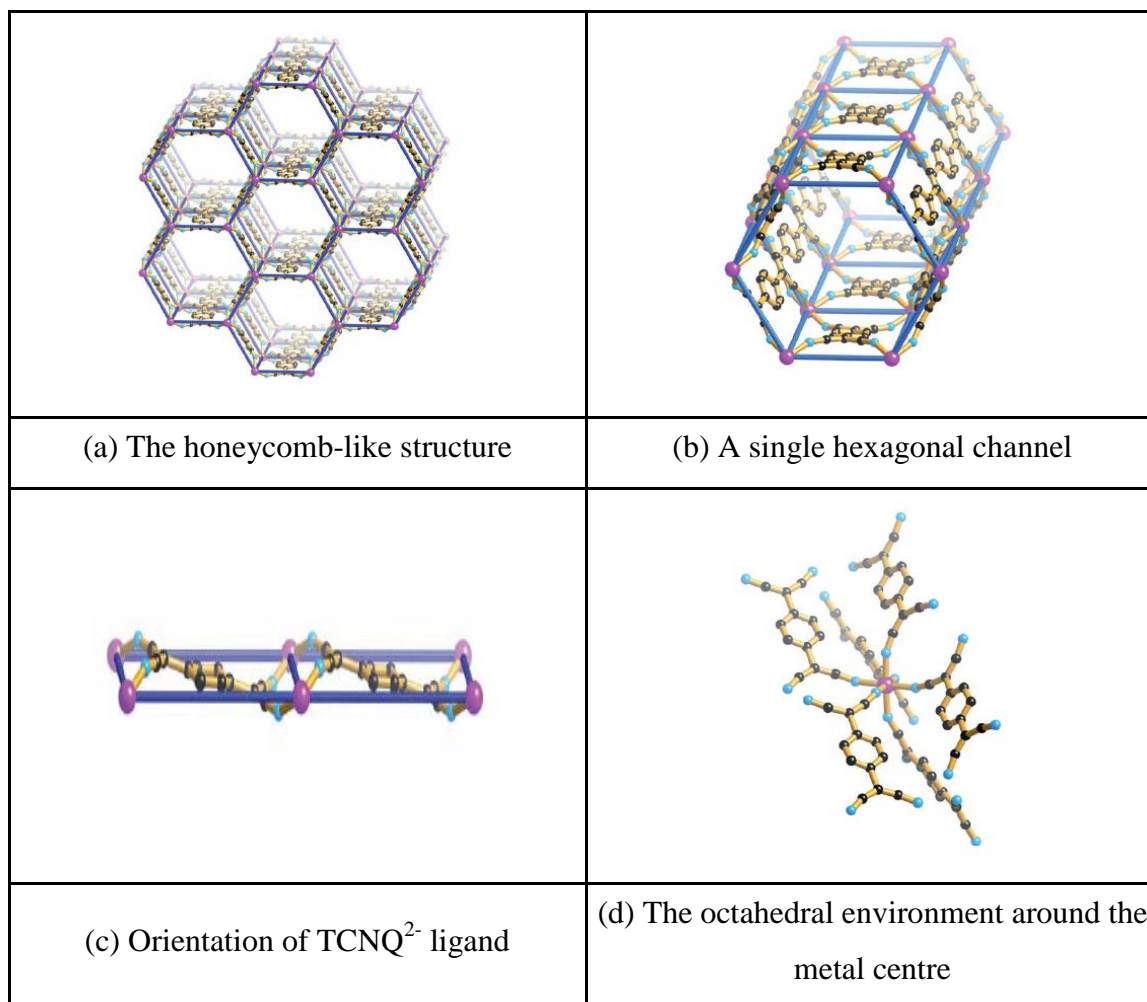
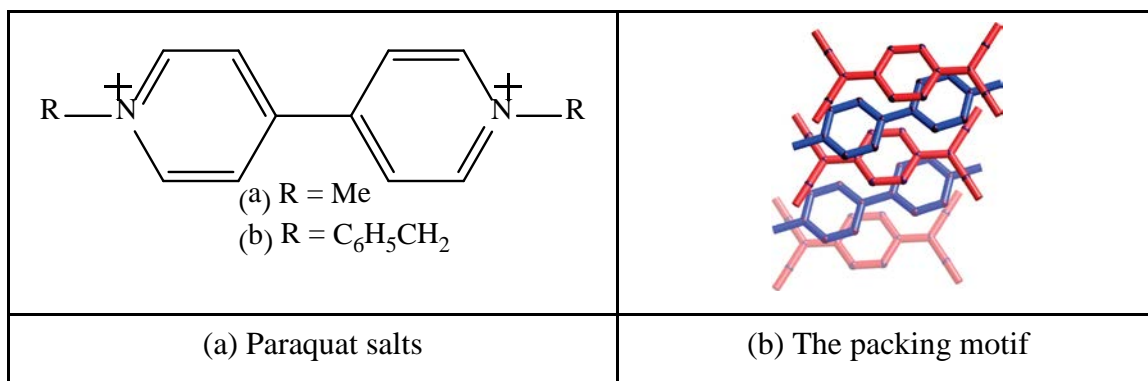
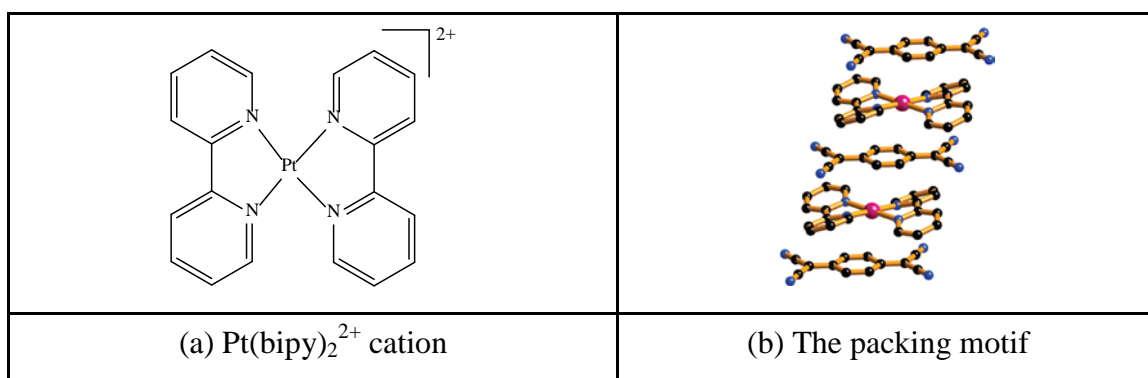
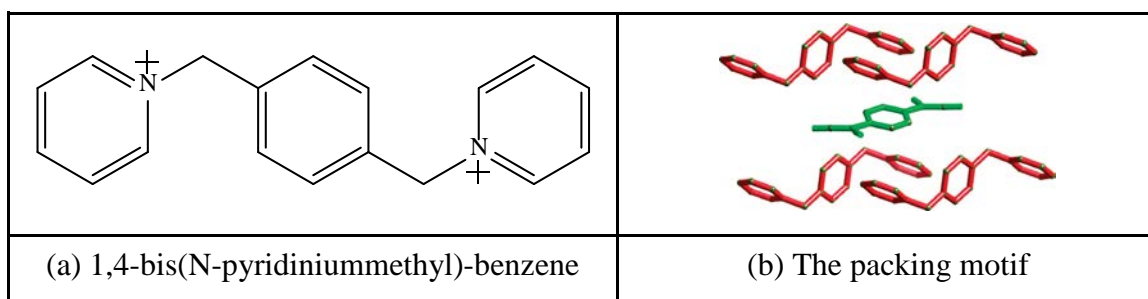
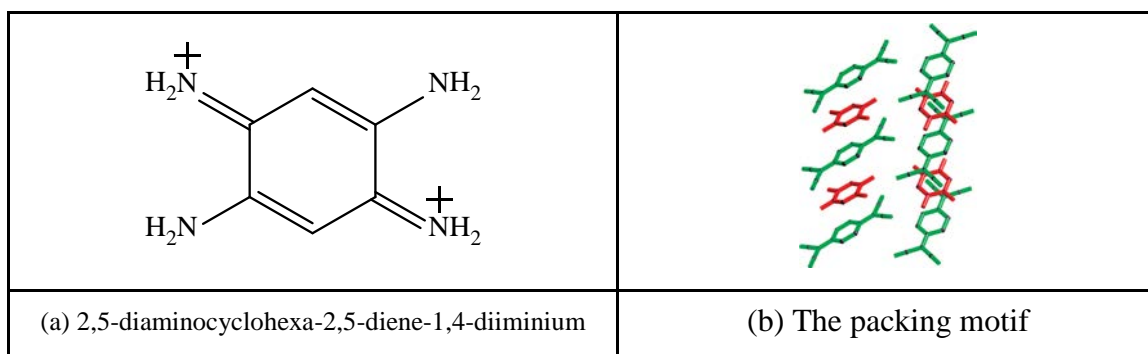


Figure 1.11 The 3D structure of [Mn₂(TCNQ)₃]²⁻ coordination networks⁶²

1.4.3 An introduction to TCNQ²⁻ salts of organic cations

The further reduction of TCNQ into TCNQH₂ may provide a novel way to afford a series of new types of structures based on the TCNQ²⁻ dianion⁵⁹⁻⁶². The solid state behaviour of a number of salts based on TCNQ²⁻ dianion is reported by Hudson and Robson⁶⁰. Figure 1.12 to Figure 1.15 display four different counter cations with the corresponding different packing patterns seen for TCNQ²⁻ dianion salts with four different counter cations.

Figure 1.12 Solid-state behaviour of N,N'-dialkylpyridinium TCNQ²⁻ salts⁶⁰Figure 1.13 Solid-state behaviour of Pt(bipy)₂²⁺ TCNQ²⁻ salts⁶⁰Figure 1.14 Solid-state behaviour of 1,4-bis(N-pyridiniummethyl)-benzene TCNQ²⁻ salts⁶⁰Figure 1.15 Solid-state behaviour of 2,5-diaminocyclohexa-2,5-diene-1,4-diiminium TCNQ²⁻ salts⁶⁰

In the presence of non-coordinative cations, TCNQ^{2-} can form new types of crystalline complexes confirming the presence of the TCNQ^{2-} dianion. In Figure 1.12, the two components of the dimethylpyridinium $^{2+}$ cation $[\text{DM}(\text{bipy})^{2+}]$ and TCNQ^{2-} are not exactly parallel with each other. The distance between adjacent planes varies from 3.27 Å to 3.5 Å. As a result, the TCNQ^{2-} dianion forms face-to-face π -stacks with $\text{DM}(\text{bipy})^{2+}$ to produce infinite stacks constructed by alternating cation and anion. In $\text{Pt}(\text{bipy})_2\text{TCNQ}$, once again alternating $\text{D}^{2+}\text{A}^{2-}$ stacks are formed. The closest distance of $\text{C}\cdots\text{C}$ is 3.28 Å and 3.49 Å for $\text{Pt}\cdots\text{C}$, respectively. The packing motif of this donor-acceptor complex is similar to that seen in $\text{DM}(\text{bipy})(\text{TCNQ})$ and displays alternating stacks of dication and dianion. In both Figure 1.12 and Figure 1.13, the TCNQ^{2-} unit shows π - π interactions with the dication. In Figure 1.14, the TCNQ^{2-} unit sits in a cavity surrounded by four neighbouring cations. In Figure 1.15, all molecular stacks are parallel and equivalent in one discrete column; the orientation of adjacent columns is different from each other. At the same time, $\text{NH}\cdots\text{NC}$ hydrogen bonds are formed between neighbouring stacks⁶⁰.

1.5 Solid state behaviour of $\text{TCNQ}^{\bullet-}$ salts

The architectural motif adopted by the $\text{TCNQ}^{\bullet-}$ units plays an important role in determining whether the crystals obtained show insulating, semiconducting or metallic properties. The $\text{TCNQ}^{\bullet-}$ anion can readily form stable crystals of 1:1 salts and complexes, which are semiconducting. Within these the $\text{TCNQ}^{\bullet-}$ anion can form dimers and extended stacks. Furthermore, a 1:1 mixture of TCNQ^0 and $\text{TCNQ}^{\bullet-}$ can form a mixed stack, which can display high conductivity. Figure 1.16 shows the formation of $\text{TCNQ}^{\bullet-}$ stacks, as a result of face-to-face π stacking of the $\text{TCNQ}^{\bullet-}$ units.

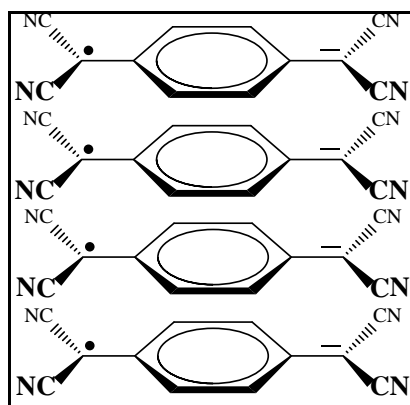


Figure 1.16 The formation of $\text{TCNQ}^{\bullet-}$ stacks

When TCNQ is associated with the donor molecule, in most cases, one of three different types of complexes is formed in the solid state. The first type is a π -associated molecular complex with low conductivity. In the second example, TCNQ forms stable crystalline radical anion salts $[M^{n+}(TCNQ^{\bullet-})_n]$. The M^{n+} here is represented as a metal cation or an organic cation. Thirdly, complex salts can be formed $[M^+(TCNQ^{\bullet-})_p(TCNQ^0)_q]$ involving the presence of neutral additional TCNQ. In this latter type of complex, the electron is considered to be delocalised over both of the TCNQ moieties³⁴. The conductivity behaviour of $[M^+(TCNQ^{\bullet-})_p(TCNQ^0)_q]$ complexes is the highest as a result of forming mixed-valence stacks containing both TCNQ and $TCNQ^{\bullet-}$ units^{34,64}. These complexes can show very high electrical conductivity, exhibiting volume electrical resistivity as low as $0.01 \Omega \cdot \text{cm}$ at room temperature. Some examples of the electrical properties of MTCNQ are listed in Table 1.2. The M^{n+} here is referred to alkali metals (Li^+ , Na^+ and K^+) and transition metals (Mn^{2+} , Fe^{2+} , Co^{2+} , Ni^{2+} , Cu^{2+} and Zn^{2+}).

| Substance | Conductivity at R.T. ($\text{S} \cdot \text{cm}^{-1}$) | Substance | Conductivity at R.T. ($\text{S} \cdot \text{cm}^{-1}$) |
|-----------------|--|----------------------------|--|
| | | $\text{Mn}(\text{TCNQ})_2$ | 2.9×10^{-6} |
| TCNQ | 5.0×10^{-11} | $\text{Fe}(\text{TCNQ})_2$ | 2.9×10^{-6} |
| LiTCNQ | 1.8×10^{-5} | $\text{Co}(\text{TCNQ})_2$ | 1.7×10^{-7} |
| NaTCNQ | 1.1×10^{-6} | $\text{Ni}(\text{TCNQ})_2$ | 2.9×10^{-7} |
| KTCNQ | 5.0×10^{-7} | $\text{Cu}(\text{TCNQ})_2$ | 1.9×10^{-6} |
| | | $\text{Zn}(\text{TCNQ})_2$ | 1.3×10^{-8} |

Table 1.2 The resistivity of MTCNQ salts⁶⁵

1.6 Radical ion TCNQ salts

TCNQ has been widely utilised in fields such as molecular electronics⁶⁶, nonlinear optics^{67,68}, and organic semiconductors⁶⁹. TCNQ can form stable solid state complexes with different kinds of electron donating compounds. Many of its salts and complexes can display significant electrical conductivity³⁴ behaviour as shown in Table 1.3, which illustrates the nature of the donor, the stoichiometry of complex formation, and the electrical conductivity for some of the more highly conducting donor-TCNQ complexes

Chapter 1

at room temperature³⁴. Special structural features in the counterion and varying stoichiometry of the complexes synthesised results in a range of conductivity values which were reported by Jaeger and Bard³⁴ at room temperature.

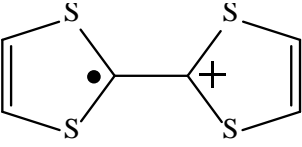
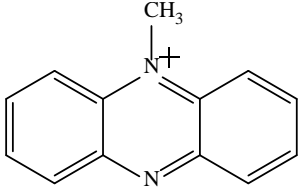
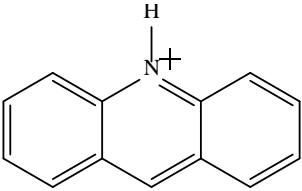
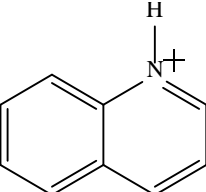
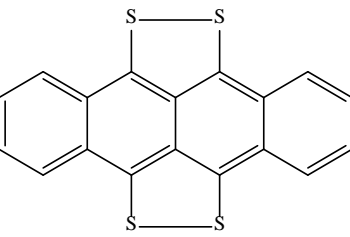
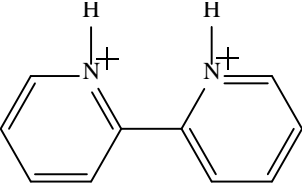
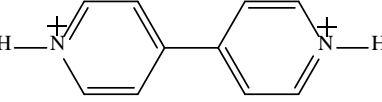
| Donor | Structure | Stoichiometry of complex | σ at R.T. ($S \cdot cm^{-1}$) |
|------------------------------|---|--------------------------|--|
| Tetrathiafulvalinium (TTF) |  | 1:1 | 300 |
| N-methylphenazinium (NMP) |  | 1:1 | 140 |
| Acridinium (Ad) |  | 1:2 | 70 |
| Quinolinium (Qn) |  | 1:2 | 100 |
| Tetrathiotetracene (TTT) |  | 1:1 1:2 | 1 100 |
| 2-2' Bipyridinium (2-2' BIP) |  | 1:2 | 2 |
| 4-4' Bipyridinium (4-4' BIP) |  | 1:1 | -10^{-2} |

Table 1.3 Structures of components of some conducting donor-TCNQ complexes³⁴

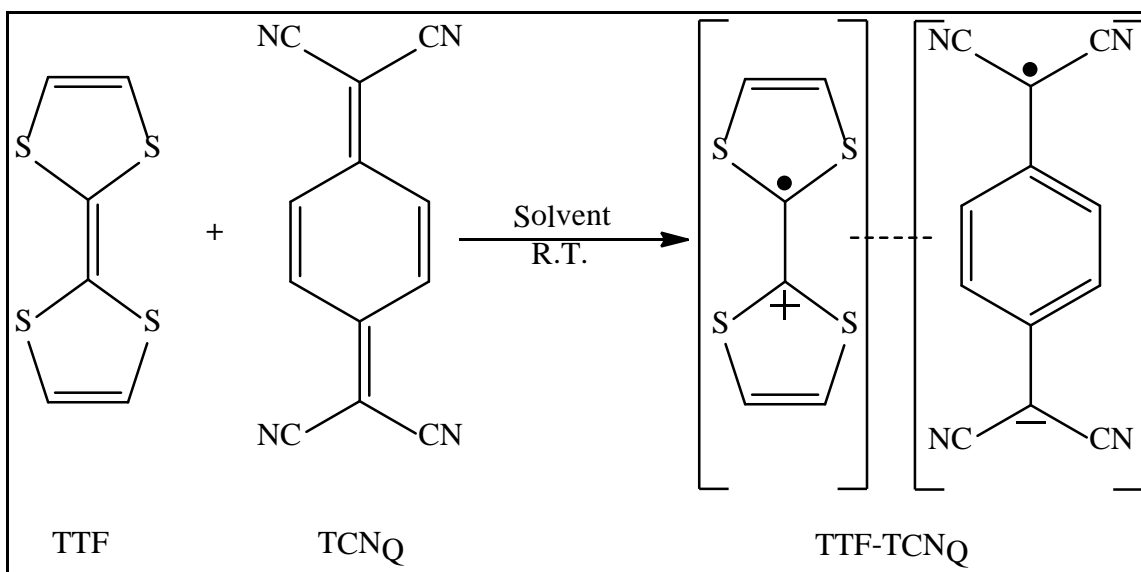
1.6.1 Donor acceptor complexes with Tetrathiafulvalene (TTF) and its analogues

The discovery of TTF⁷⁰ was an important step in the development of interest in TCNQ salts. In this section, the crystallography and physical properties of complexes of TTF and its analogues with TCNQ will be reviewed.

1.6.1.1 Analysis of TTF-TCNQ salt

A particularly interesting example of a donor-acceptor complex is TTF-TCNQ. This is an ionic charge transfer complex, which exhibits metallic conductivity at room temperature along the molecular stacking direction^{26,71-76}. The formation of this black crystalline 1:1 complex is rapid, when their solutions are mixed together^{77,78}, even if the TTF and TCNQ are not presented in equal amounts⁷⁷. TTF-TCNQ was the first organic charge-transfer complex showing metallic properties⁷⁷.

Scheme 1.7 illustrates the formation of TTF-TCNQ charge-transfer complex.



Scheme 1.7 Formation of TTF-TCNQ charge-transfer complex⁷⁹

In this complex, the TTF (D) and TCNQ (A) are stacked separately, making segregated columns "AAA" and "DDD". Both stacks act as a one-dimensional electronic conducting pathway. In TTF-TCNQ, the TTF can readily lose a single electron to form a radical cation and the TCNQ can absorb the corresponding electron to become TCNQ^{•-}. Both types tend to form π stacked columns in the solid state. When crystallised

with TCNQ, the resulting complex contains homoseric stacks, in which the TTF is partially oxidised and the TCNQ is partially reduced. This results in metallic conductivity at room temperature arising from the presence of partially filled valence bands in each component⁷⁶. Odom et al.⁷⁹ commented that single crystal of TTF-TCNQ could display a highly conducting behaviour of ca. $400\text{--}500\text{ S}\cdot\text{cm}^{-1}$, which can be used as electronic devices. Hendon et al.⁷¹ suggested that TTF-TCNQ could exhibit a metallic behaviour above 60K with a maximum of conductivity of $\sigma = 1.5 \times 10^4\text{ S}\cdot\text{cm}^{-1}$, which was the same magnitude observed by Tomkiewicz et al.⁷⁸ However, because of a Peierls distortion, TTF-TCNQ would transform into a semi-conductor below 60K. Goetz et al.⁴⁹ reported that the electrical conductivity of TTF-TCNQ was $7 \times 10^2\text{ S}\cdot\text{cm}^{-1}$ at room temperature. Figure 1.17 displays the packing pattern of segregated columns in TTF-TCNQ complex.

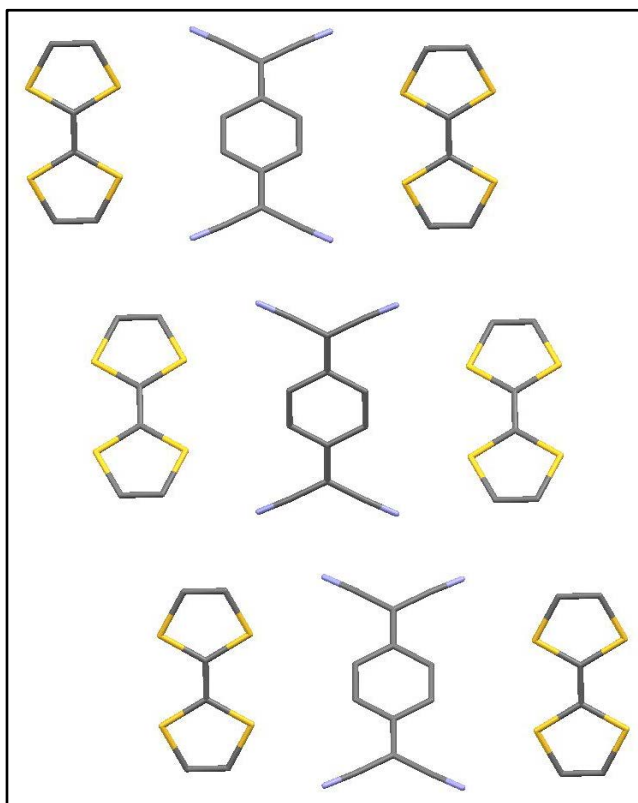


Figure 1.17 Packing pattern of segregated columns in TTF-TCNQ complex (ref code: TTFTCQ, TTFTCQ01-TTFTCQ06)⁸⁰⁻⁸³

1.6.1.2 Analysis of tetramethyltetrathiafulvalenium (TMTTF) TCNQ salt

Figure 1.18 displays the structure of tetramethyltetrathiafulvalene (TMTTF), which can form a charge transfer complex with TCNQ.

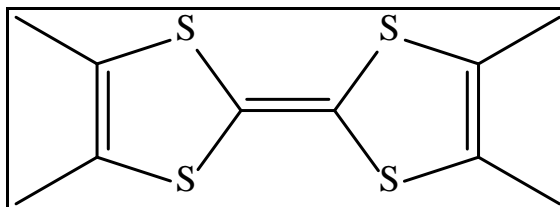


Figure 1.18 TMTTF

In the solid state, TMTTF-TCNQ forms face-to-face π -stacks of infinite segregated columns, i.e. the same packing motif as seen for TTF-TCNQ. At room temperature, the electrical conductivity of TMTTF-TCNQ is $3.5 \times 10^2 \text{ S cm}^{-1}$, would seem to be lower than that observed for TTF-TCNQ⁴⁹. The perpendicular intermolecular distance between adjacent planes of the neighbouring TMTTF units is 3.53 Å, which is greater than that in TTF-TCNQ (3.47 Å), reflecting the need to accommodate the methyl substituents⁸⁴. However, the longer intermolecular distance within TMTTF-TCNQ cannot simply be attributed to the chemical modification of cation component. It is also related to the intercolumn interactions and different degrees of charge transfer⁸⁴. Phillips et al.⁸⁴ also found that the elongated interchain coupling of TMTTF-TCNQ has caused this complex to belong to the most one-dimensional member in the TTF-TCNQ family. Furthermore, the CN \cdots S contact distance in this system is 3.45 Å, which is longer than those found in TTF-TCNQ (3.20 Å and 3.25 Å, respectively). Figure 1.19 displays the packing behaviour of TMTTF-TCNQ from two different structural studies.

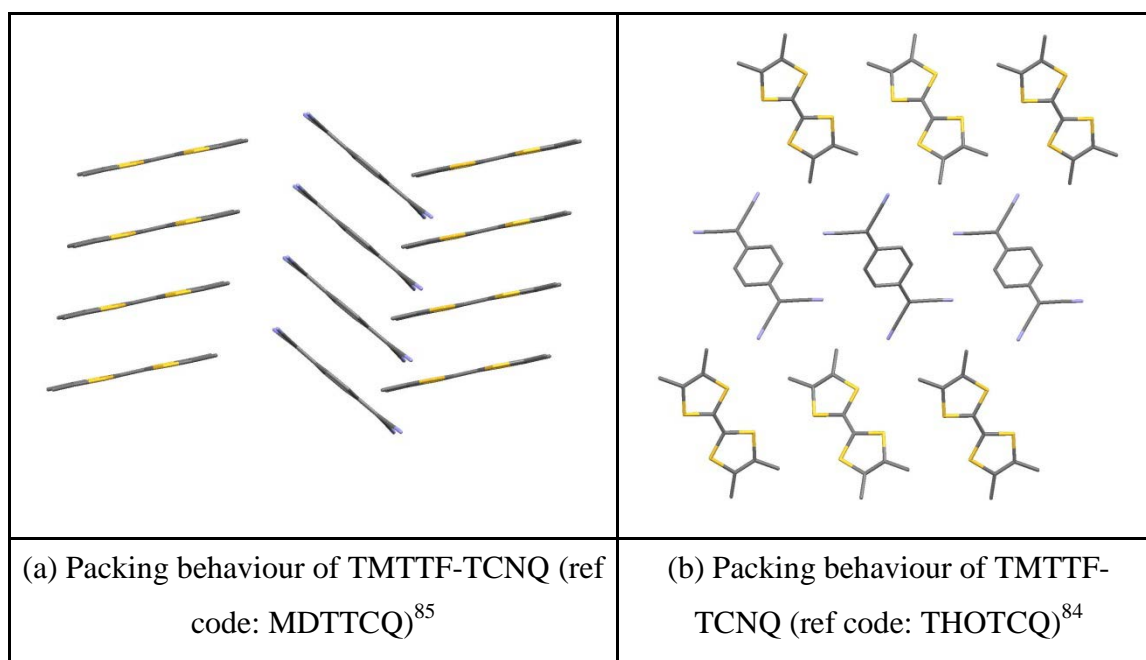


Figure 1.19 Packing behaviour of TMTTF-TCNQ (ref code: MDTTCQ and THOTCQ)^{84,85}

1.6.1.3 Analysis of dibenzotetrathiafulvalene (DBTTF) TCNQ salt

Figure 1.20 exhibits the structure of dibenzotetrathiafulvalene (DBTTF), which can form a charge transfer complex with TCNQ.

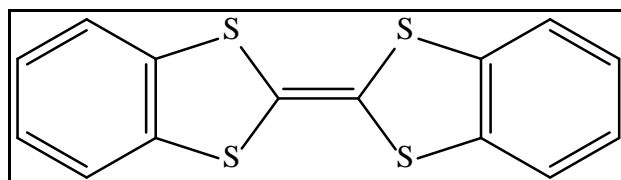


Figure 1.20 DBTTF

The planar π -electron donor DBTTF crystallises with TCNQ to form mixed π -stacked columns, in which the two components alternate. Compared with high conducting complexes of TTF-TCNQ and TMTTF-TCNQ, in which donor and acceptor form segregated columns, the molecular arrangement in DBTTF-TCNQ differs from those highly conductive complexes. The mixed columns within DBTTF-TCNQ result in low electrical conductivity ($10^{-6} \text{ S cm}^{-1}$)^{49,86} at room temperature. The intermolecular face-to-face distance between DBTTF and TCNQ is 3.303 Å, which is shorter than the case in PTZ-TCNQ. Kobayashi and Nakayama⁸⁶ commented that the parameters of short intermolecular distance and the mode of intermolecular overlap would appear to

significantly affect the charge-transfer interaction, which requires a large overlap integral between donor and acceptor. This would seem to be why the complex of DBTTF-TCNQ has low electrical conductivity. Figure 1.21 displays the packing behaviour of DBTTF-TCNQ from two different structural studies.

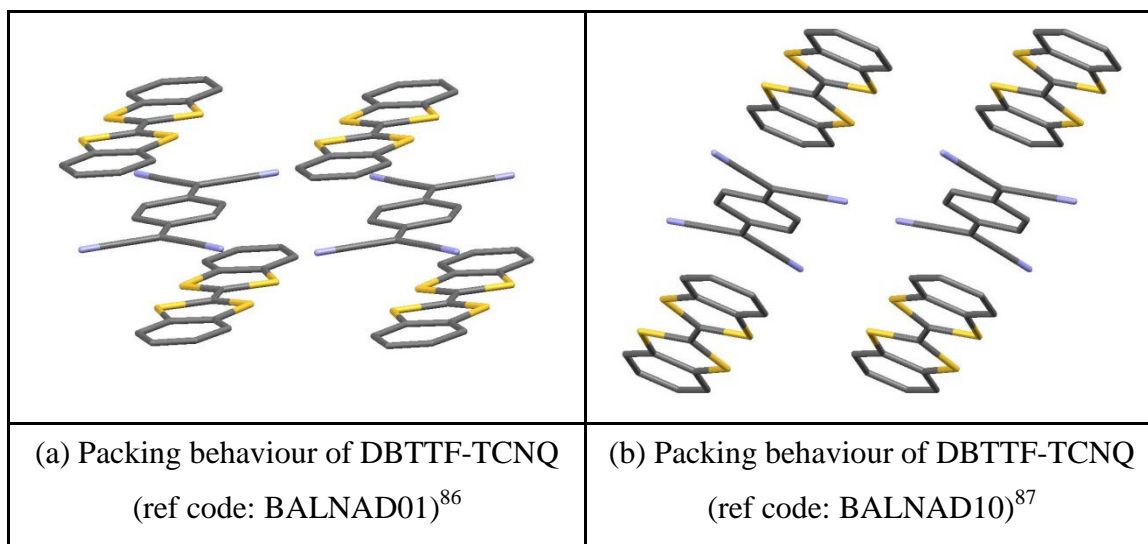


Figure 1.21 Packing behaviour of DBTTF-TCNQ (ref code: BALNAD01 and BALNAD10)^{86,87}

1.6.1.4 Comparison between hexamethylenetetrafulvalenium (HMTTF) TCNQ and hexamethylenetetraselenafulvalenium (HMTSeF) TCNQ salts

Figure 1.22 exhibits the structures of hexamethylenetetrafulvalene (HMTTF), and hexamethylenetetraselenafulvalene (HMTSeF) respectively, which can each form a charge transfer complex with TCNQ.

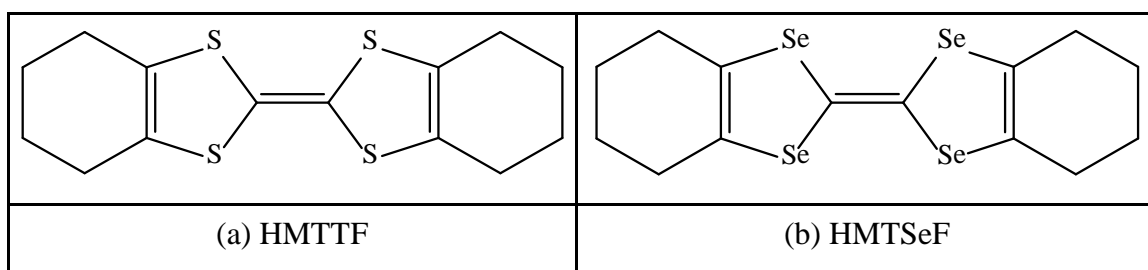


Figure 1.22 The structures of HMTTF and HMTSeF

The complexes of HMTTF-TCNQ and HMTSeF-TCNQ belong to the quasi-one-dimensional conductor family^{88,89}. Tomkiewicz et al.⁸⁸ and Goetz et al.⁴⁹ commented that the electrical conductivity of HMTTF-TCNQ was 400 S cm^{-1} at room temperature.

Meanwhile, Bloch⁸⁹ indicated that the conductivity of HMTSeF-TCNQ ranged from 1391 to 2178 S·cm⁻¹ at room temperature, which was the largest of any known organic substance. The metal-insulator transition temperature for HMTSeF-TCNQ is 50±1K⁸⁸. Comparison of HMTSeF-TCNQ with HMTTF-TCNQ reveals a short selenium-nitrogen distance of 3.1 Å in the former and the larger sulphur-nitrogen distance of 3.25 Å in the latter, which is the major difference between these two complexes⁸⁸. The perpendicular interplanar distance between adjacent TCNQ planes is 3.23 Å in HMTTF-TCNQ in comparison to the distance of 3.17 Å in TTF-TCNQ⁸⁸. Figure 1.23 displays the packing motifs of HMTTF-TCNQ and HMTSeF-TCNQ, respectively.

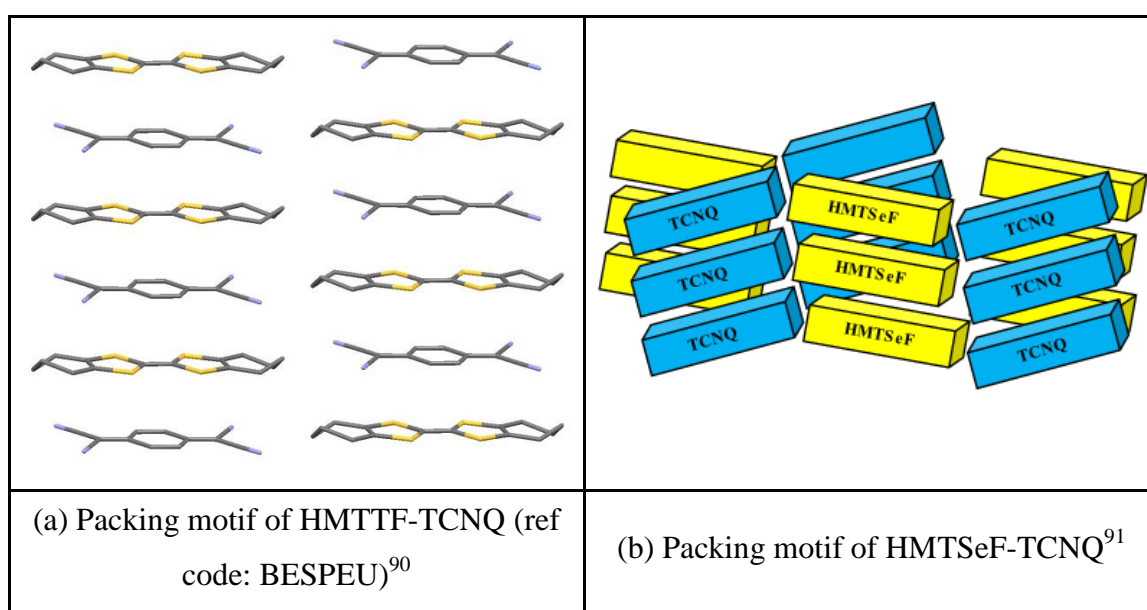


Figure 1.23 The packing motifs of (ref code: BESPEU)⁹⁰ and HMTSeF-TCNQ

1.6.1.5 The bis(ethylenedithio)tetrathiafulvalene (BEDT-TTF) TCNQ salt

Figure 1.24 displays the structure of BEDT-TTF, which can form a charge-transfer complex with TCNQ. Such charge transfer complexes show a highly variable range of electrical behaviour, which include metallic systems, semiconductors and a low-temperature superconductor⁹²⁻⁹⁴. Three different phases of BEDTTF-TCNQ have been published⁹⁵⁻⁹⁸. In monoclinic phase, the complex, which is a semiconductor, is composed of alternating stacks of BEDT-TTF and TCNQ units. The conductivity at room temperature is 10⁻⁶ S·cm⁻¹⁹⁶. Both of the triclinic phases have segregated stacks of BEDTTF and TCNQ molecules^{95,97}. In Figure 1.25(a), separate layers of donor and acceptor molecules are parallel to the *ac* plane⁹⁵. The conductivity of this complex is 10 to 100 S·cm⁻¹ at room temperature and the degree of charge transfer is 74%⁹⁵. A short

H(BEDTTTF)···N(TCNQ) contact (2.57 Å) is recorded between the donor and acceptor molecules.

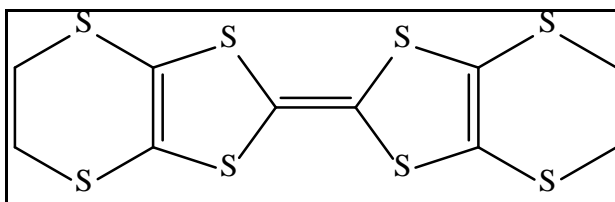


Figure 1.24 BEDTTTF

Figure 1.25 shows the packing motifs of one triclinic phase (ref code: FAHLEF02)⁹⁵ and one monoclinic phase (ref code: FAHLEF01)⁹⁶ of BEDTTTF-TCNQ complex.

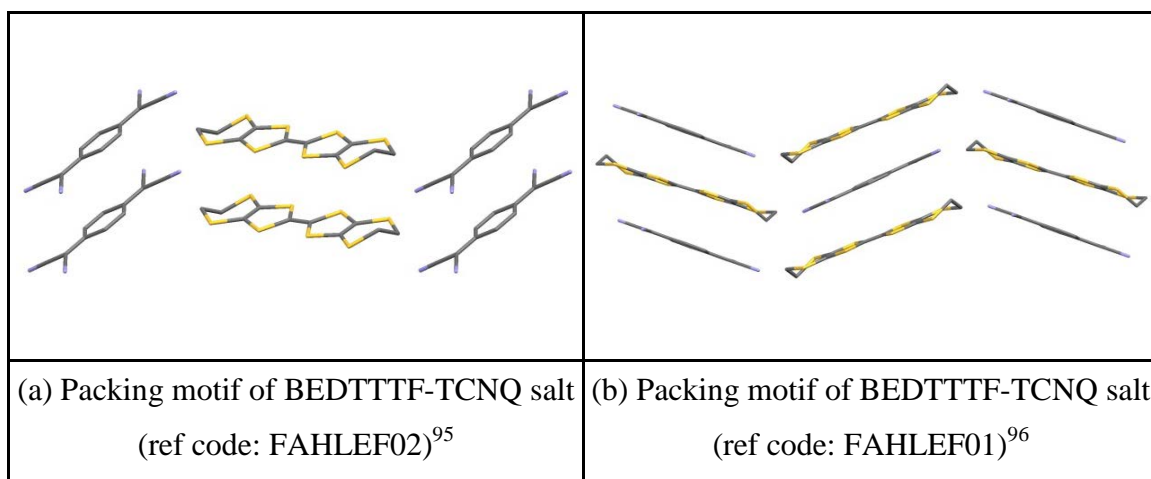


Figure 1.25 Packing motifs of one triclinic phase (ref code: FAHLEF02)⁹⁵ and one monoclinic phase (ref code: FAHLEF01)⁹⁶ of BEDTTTF-TCNQ

Wallis and his co-workers have synthesised several families of chiral TTF derivatives^{92,99-102}. For example, (S,S,S,S)-tetramethyl-BEDT-TTF forms a crystalline 1:1 complex with TCNQ¹⁰², in which the molecules of (S,S,S,S)-tetramethyl-BEDT-TTF and TCNQ can form mix stacks along the *a* axis. They suggest that the use of chiral TTF precursors, and exploiting the combination of chirality and conductivity, can probably offer a method for observing an electrical magneto-chiral anisotropy (eMChA) effect¹⁰², in the presence of an applied external magnetic field. This system can provide a good opportunity to research for this synergistic effect within these materials¹⁰².

1.7 Behaviour of the derivatives of TTF with TCNQ derivatives

A number of TCNQ derivatives have been prepared and the behaviour of their complexes with a number of TTF analogues has been explored. These will be briefly discussed in the following section.

1.7.1 Analysis of tetramethyltetraselenafulvalenium (TMTSeF) – dimethyltetracyanoquinodimethane (DMTCNQ) salt

Figure 1.26 displays the structures of tetramethyltetraselenafulvalene (TMTSeF) and dimethyltetracyanoquinodimethane (DMTCNQ) respectively which can form a charge transfer complex.

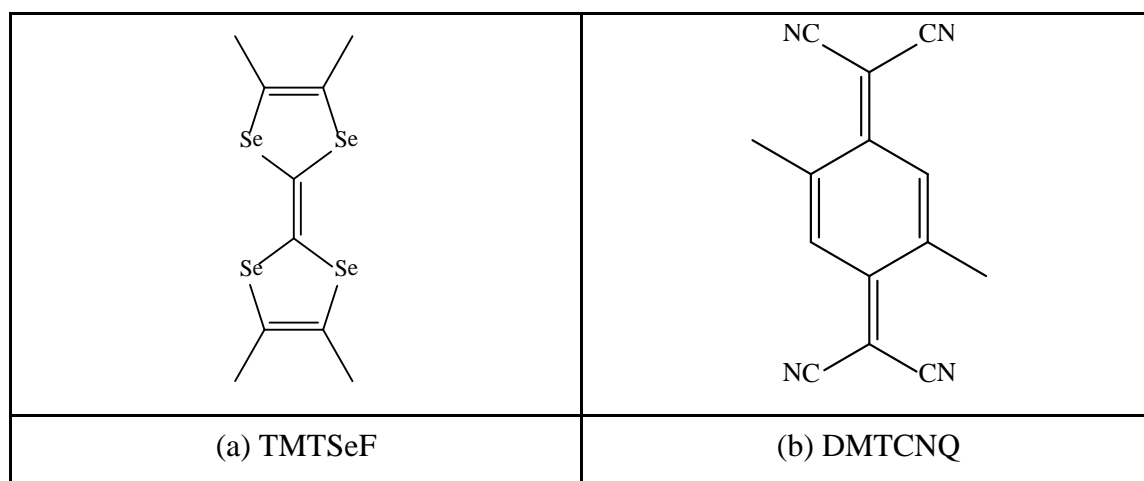


Figure 1.26 The structure of TMTSeF-DMTCNQ

The donor (TMTSeF) and acceptor (DMTCNQ), form a one-dimensional organic conductor of TMTSeF-DMTCNQ. This complex crystallises in segregated, homoseric stacks with 3.64 Å between adjacent TMTSeF planes and 3.31 Å between nearby DMTCNQ planes, respectively¹⁰³. Because of the steric effect of the methyl groups, the intramolecular distance within the DMTCNQ stacks are increased. Additionally, the factors of low symmetry and asymmetric intramolecular overlap of the DMTCNQ stacks reduces the electron mobility in the acceptor stacks, which further affects the electronic properties of this charge transfer complex¹⁰³. Under the high pressure ($P > 10$ kbar) at low temperature, Andrieux et al.¹⁰⁴ demonstrated that the complex of TMTSeF-DMTCNQ has a high conductivity state ($\sigma > 10^5 \text{ S}\cdot\text{cm}^{-1}$). Figure 1.27 displays the packing motif of TMTSeF-DMTCNQ, which is the same as TTF-TCNQ and TMTTF-TCNQ.

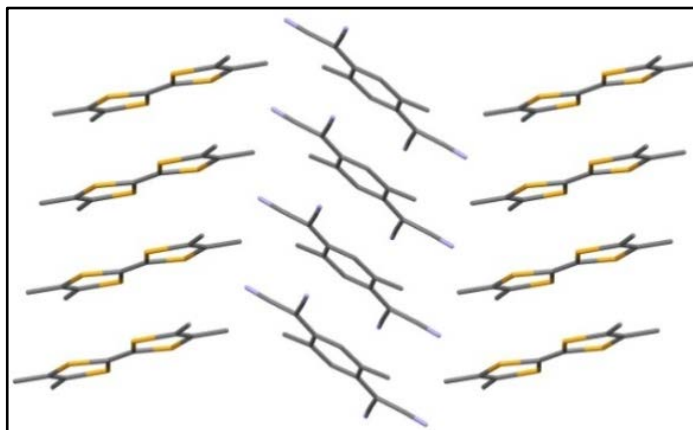


Figure 1.27 The packing motif of TMTSeF-DMTCNQ (ref code: SEFTCQ)¹⁰³

1.7.2 Dibenzotetrathiafulvalenium (DBTTF) - 2,5-dichloro-7,7',8,8'-tetracyanodimethanide (TCNQCl₂)

Figure 1.28 shows the structures of dibenzotetrathiafulvalene (DBTTF) and 2,5-dichloro-7,7',8,8'-tetracyanodimethanide (TCNQCl₂) respectively, which can form a charge transfer complex.

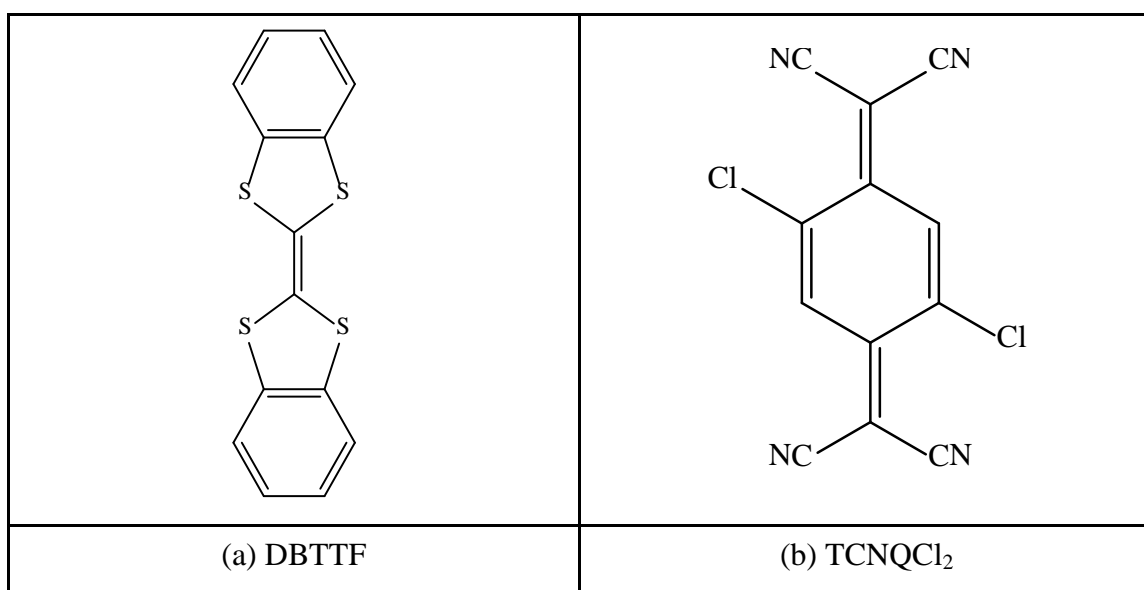


Figure 1.28 The structures of DBTTF-TCNQCl₂

DBTTF is a weaker donor because the presence of the benzene ring tends to reduce the electron density in the TTF unit, whereas TCNQCl₂ is inclined to be a stronger acceptor as a result of the presence of the chlorine atoms¹⁰⁵. The donor (DBTTF) and acceptor (TCNQCl₂) can form separated, homoseric stacks with 3.51 Å between adjacent DBTTF planes and 3.41 Å between neighbouring TCNQCl₂ planes, respectively. The

electrical conductivity is $4000 \text{ S}\cdot\text{cm}^{-1}$ at room temperature but increases slowly with the decreasing temperature¹⁰⁵. Soling et al.¹⁰⁵ also observed that the electrical conductivity would appear to decrease rapidly below 200K. Jacobsen et al.¹⁰⁶ commented that the magnetic susceptibility was $1.5 \times 10^{-8} \text{ m}^3\cdot\text{kg}^{-1}$ at 300K and increased slowly upon cooling. Figure 1.29 displays the packing motif of DBTTF-TCNQCl₂ structural studies.

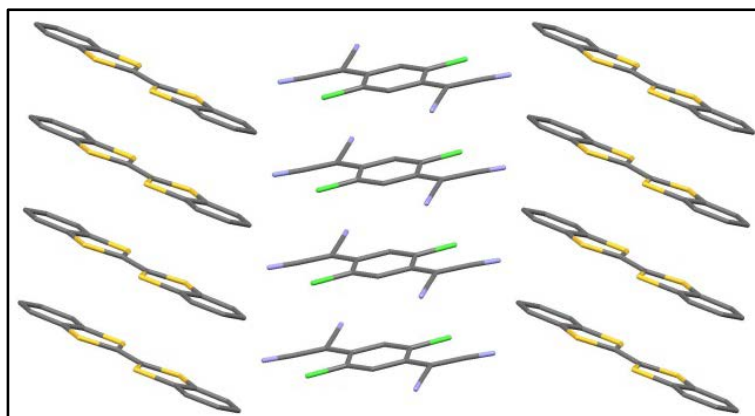


Figure 1.29 Solid-state behaviour of DBTTF-TCNQCl₂ (ref code: BABCIQ and BABCIQ 01)¹⁰⁵

1.8 Decamethylferricenium-TCNQ complex

There has been particular interest in the solid state behaviour of metallocenium salts of TCNQ (and TCNE) because of their potential magnetic properties¹⁰⁷⁻¹¹¹. Figure 1.30 displays the structure of decamethylferricenium TCNQ^{•-}.

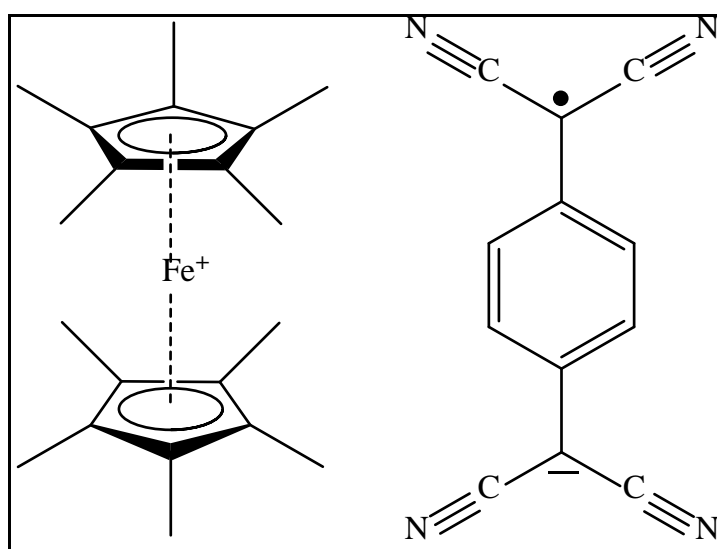


Figure 1.30 The structure of decamethylferricenium TCNQ^{•-}

Decamethylferrocene is well known as an electron donor (D), which reacts with cyano carbon acceptors (A), such as TCNQ, to form charge transfer salts, in which both components are paramagnetic. In the solid state, these charge transfer complexes can form $\cdots D^+ A^- D^+ A^- \cdots$ alternating stacks in the kinetic phase (see Figure 1.31(a))^{57,107,112}. These complexes display interesting bulk magnetic phenomena with different types of ferro-, antiferro-, ferri- and metamagnetism, depending on the stacking arrangement and the intra- or intermolecular interactions in the crystal structure^{57,107,112}. The donor (decamethylferrocenium) and acceptor (TCNQ⁻) form alternate stacks between each other in the kinetic phase.

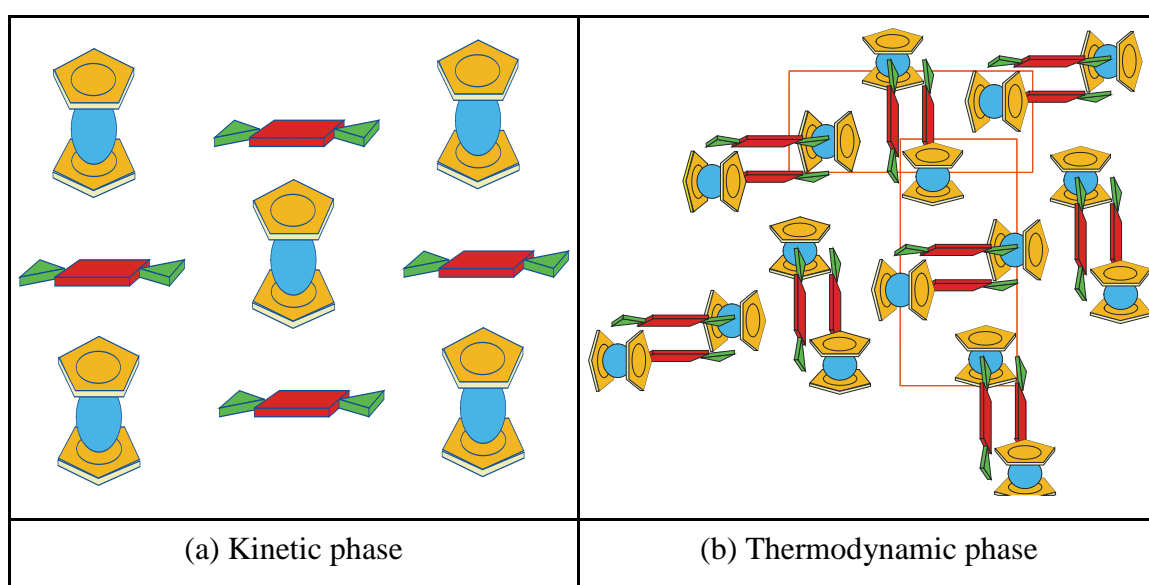


Figure 1.31 Two different phases of decamethylferricenium TCNQ⁻ (methyl groups removed for clarity)^{57,112}

However, a thermodynamic phase has also been prepared in which, the basic structural unit, $\cdots D^+ A^- A^- D^+ \cdots$ is arranged in a herringbone pattern in the solid state^{57,112}.

2. Applications of Supramolecular Chemistry for Crystal Engineering of the Solid State Behaviour of TCNQ Salts

In this chapter, the concept of Supramolecular Chemistry will be discussed firstly and illustrated by relevant examples, such as catenanes and rotaxanes. Supramolecular Chemistry in the solid state will then be considered, together with its applications in the area of crystal engineering.

2.1 Supramolecular Chemistry

The concept of Supramolecular Chemistry, which is described as ‘chemistry beyond the molecule’¹¹³⁻¹¹⁵, is now the subject of a large number of applications in Chemistry, Biology and Materials Science. The definition of Supramolecular Chemistry is that of the noncovalent bond and of molecular assemblies held together by intermolecular forces. In general, Supramolecular Chemistry involves receptors (hosts) and substrates (guests) associating to form more complex assemblies in which individual, covalently bonded molecular units associate through a variety of intermolecular interactions in a controlled manner. Figure 2.1 illustrates the concept of Supramolecular Chemistry.

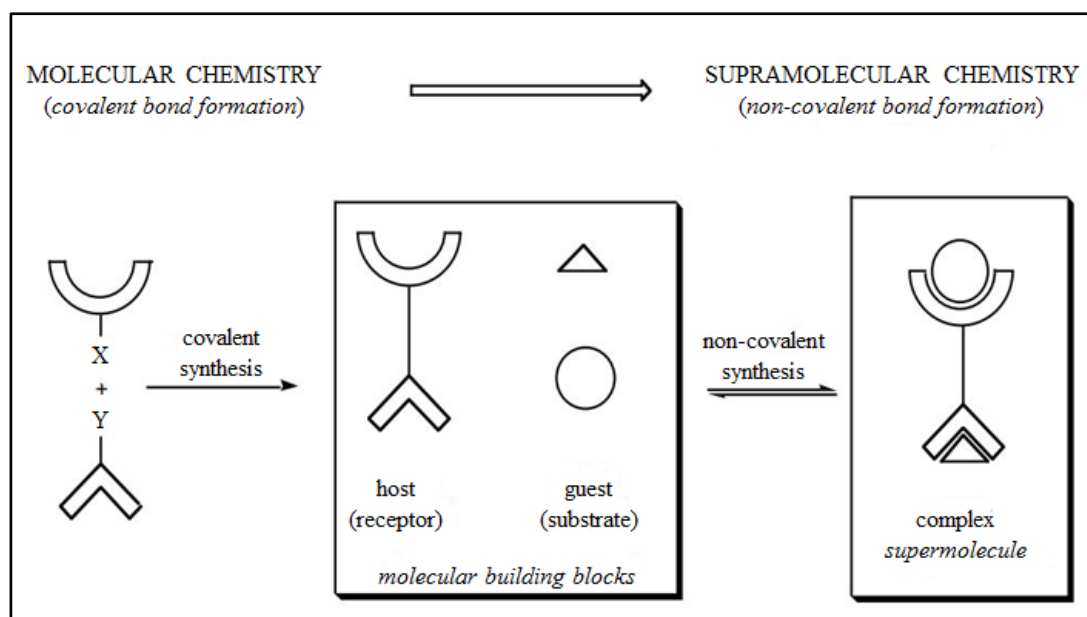
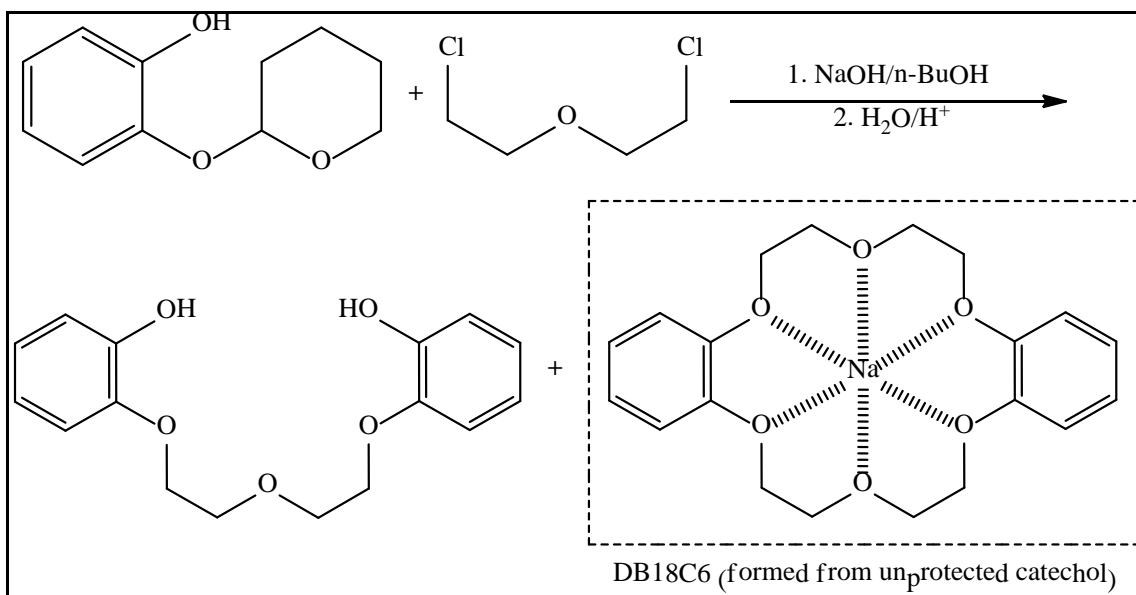


Figure 2.1 The concept of Supramolecular Chemistry¹¹⁶

The field of Supramolecular Chemistry covers a wide range of chemistry, from the designing of receptors based on the knowledge of preorganisation and the effect of hydrogen bonding, such as in a receptor for barbital¹¹⁷⁻¹¹⁹, to the idea of supramolecular approaches to artificial molecular machines^{113,114}, which are based on functional supramolecular assemblies. Examples of artificial molecular machines include rotaxane-based and catenane-based structures synthesised by Hanni and Leigh¹²⁰ and the [2]-catenane-based devices¹²¹⁻¹²³.

2.1.1 Supramolecular chemistry in the solid state

The origins of Supramolecular Chemistry can be traced back to the discovery of dibenzo-18-crown-6 (DB18C6) by Charles Pedersen¹²⁴⁻¹²⁷ on its ability to bind alkali metal cations. The number '18' refers to the number of atoms in the macrocycle and '6' to the number of oxygen atoms in the crown ether ring. Whilst DB18C6 is only slightly soluble in methanol, after adding sodium salts, it dissolves much more easily. DB18C6 was the first synthetic alkali metal cation binder. Strong electrostatic interactions are formed between the oxygen atoms and metal cation. After the discovery of DB18C6, it was discovered that a large number of crown ethers can be synthesised by changing the number and type of donor atoms, the ring size and the molecular flexibility, and that these can be used to complex preferentially with particular cations. The original synthetic route is outlined in Scheme 2.1.



Scheme 2.1 The original synthesis route of DB18C6¹²⁶

2.2 Cation binding hosts

In this section, two dimensional hosts will be discussed with the binding ability with different sizes of metals. Consequently, three dimensional hosts will be illustrated, especially focusing on the utilisation of a group of cryptand complexes with their different tetrahedral recognition.

2.2.1 Two dimensional hosts

Crown ethers are macrocyclic polyether ligands, which are used in Supramolecular Chemistry as hosts for both organic and metallic cations. Pedersen¹²⁴⁻¹²⁶ first discovered DB18C6, many other series of crown ethers with various ring sizes and different numbers and types of heteroatoms and varying flexibility have been prepared. Some examples are shown in Figure 2.2. As the factors such as preorganisation and complementarity¹²⁸, solvation and chelate ring size¹²⁹ are now widely recognised to be the most important factors in deciding the solution selectivity of the macrocycles¹³⁰, the versatile solubility and transport capabilities of the crown ethers lead to applications as, for example, ionophores^{131,132}, sensors for ions, molecular scaffolds for material and biological models¹³³, fluorescent sensors for metal ions¹³⁴, sensors and switches utilised in cation binding affinity¹³⁵ and photoswitches¹³⁶.

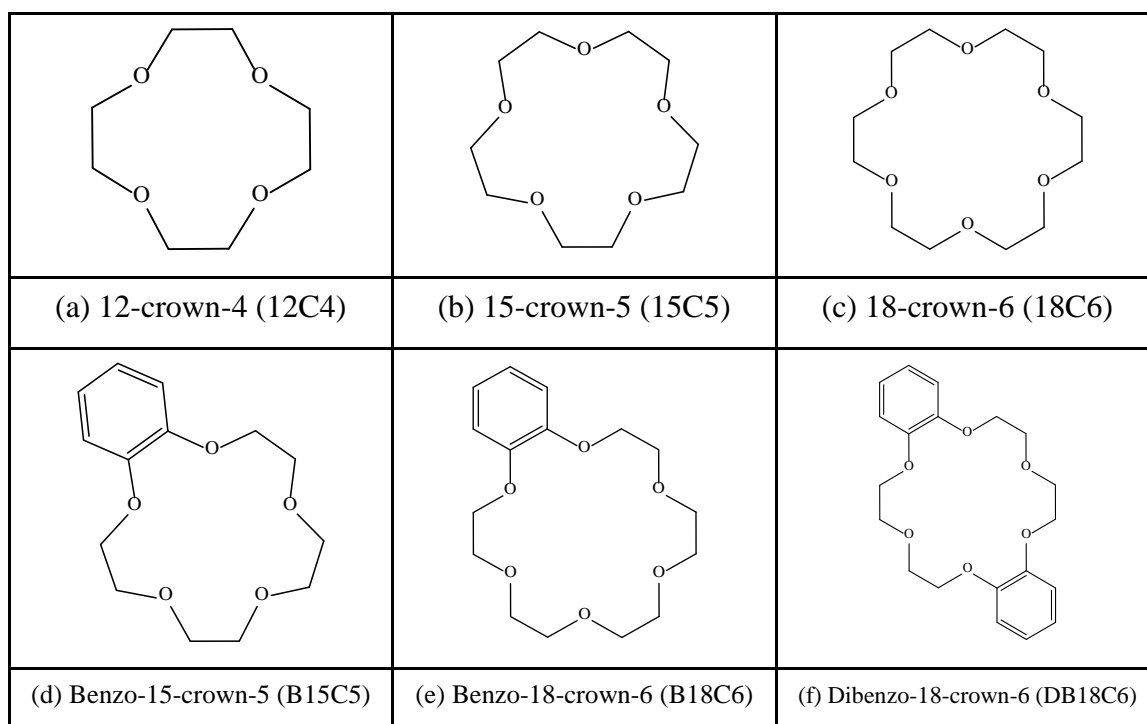


Figure 2.2 Various structures of useful crown ethers

In the field of host-guest chemistry the most stable complexes occur when the macrocyclic cavity of the host matches the size of the guest. If the cation is smaller than the macrocyclic cavity, the host-guest complex will not be formed efficiently. On the other hand, if the cation is bigger than the macrocyclic cavity, a sandwich complex can be formed such as that seen for $(15C5)_2KTCNQ$. This compound has been investigated by the Grossel group (see Figure 2.3)¹⁰⁷.

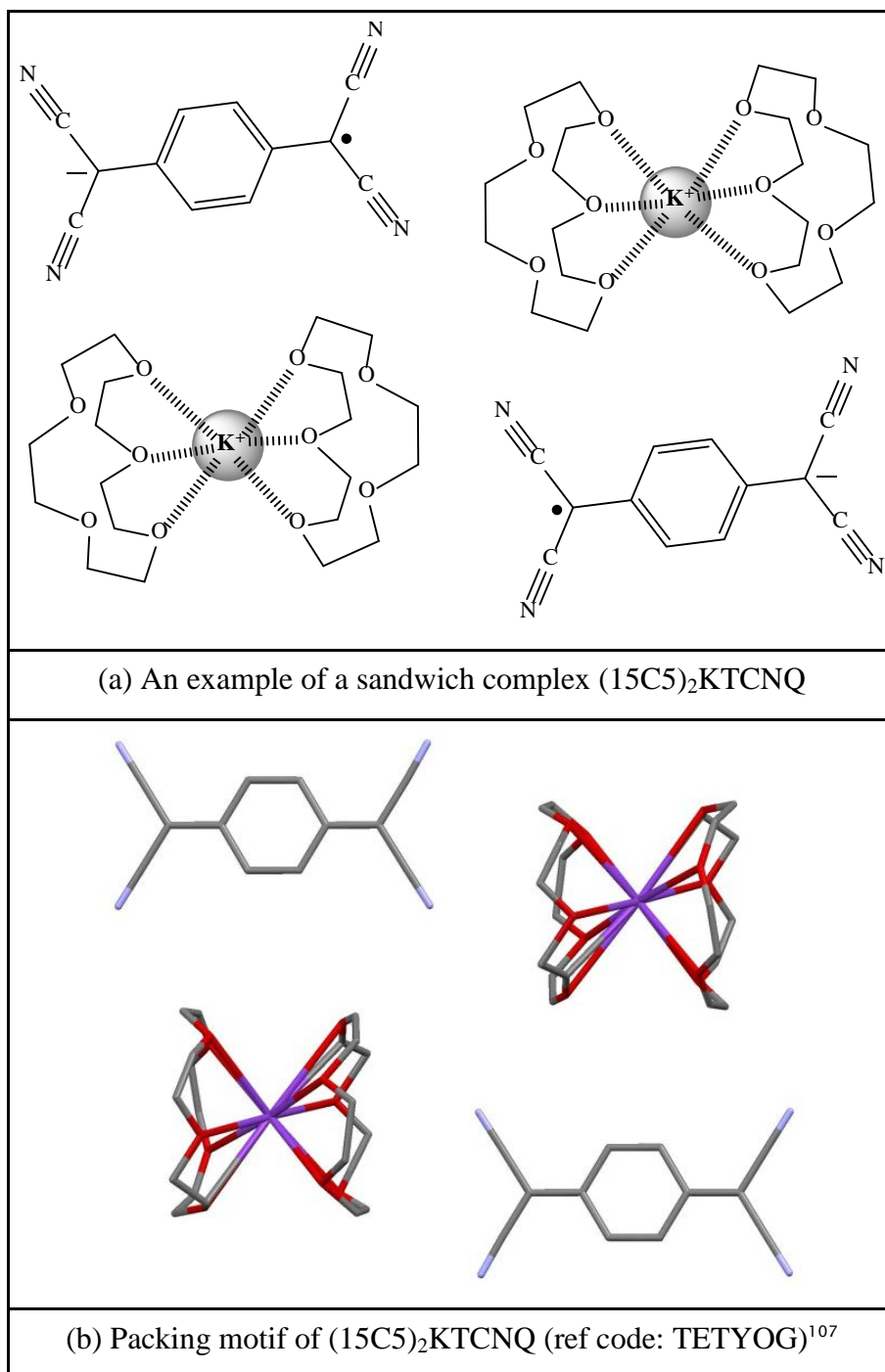


Figure 2.3 The packing motif of $(15C5)_2KTCNQ$ ¹⁰⁷

Table 2.1 summarises a comparison of the ionic radii of alkali metal cations with crown ether cavity diameter¹³⁰.

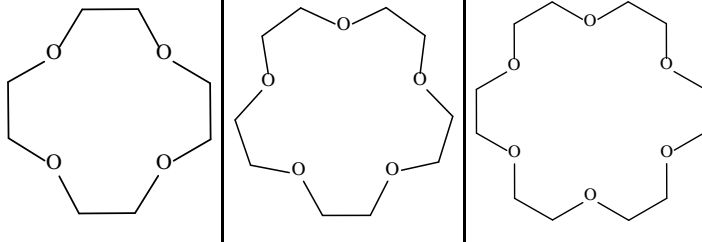
| Metal ions | Li ⁺ | Na ⁺ | K ⁺ | Rb ⁺ | Cs ⁺ |
|--------------------|--|-----------------|----------------|-----------------|-----------------|
| Ionic radius/ Å | 0.78 | 0.97 | 1.33 | 1.48 | 1.67 |
| Crown ethers |  | | | | |
| Cavity diameter/ Å | 1.20-1.50 | | 1.70-2.20 | | 2.60-3.20 |

Table 2.1 Comparison of the ionic radii of alkali metal cations with crown ether cavity diameter¹³⁰

Based on the metal-crown ether oxygen interactions, which are ion-dipole interactions, a variety of novel crystalline geometries are observed^{55,107,131,132,137}. In the field of crystal engineering^{130,138}, such complexation can be used to constrain interactions with counterions and thereby modify the solid-state assemblies formed.

Two dimensional hosts using other heteroatoms as opposed to oxygen have also been synthesised such as diaza-18-crown-6, hexathia-18-crown-6 and cyclam. Figure 2.4 shows three structural examples of these.

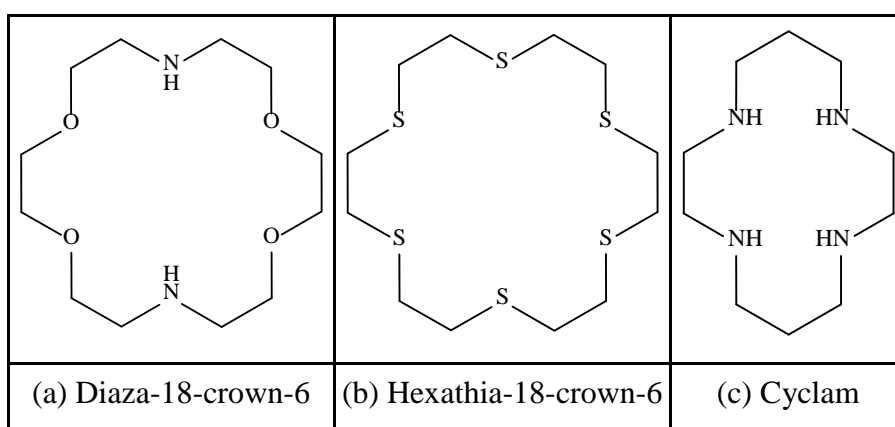


Figure 2.4 Examples of two-dimensional hosts using other heteroatoms instead of oxygen

Crown ethers containing only oxygen binding sites are designed for the complexation of alkali and alkaline earth cations^{124,139}. However, in order to bind transition or heavy metal ions using macrocyclic ligands, a series of substituted crown ethers (aza-, diaza-, tetraaza- and thia-) have been introduced¹⁴⁰⁻¹⁴⁴. For instance, diaza-18-crown-6, which is an ionophore containing amine group, strongly binds alkaline earth and other divalent metal cations, such as Mg^{2+} , Ca^{2+} because these divalent cations have a higher surface charge density¹⁴⁵.

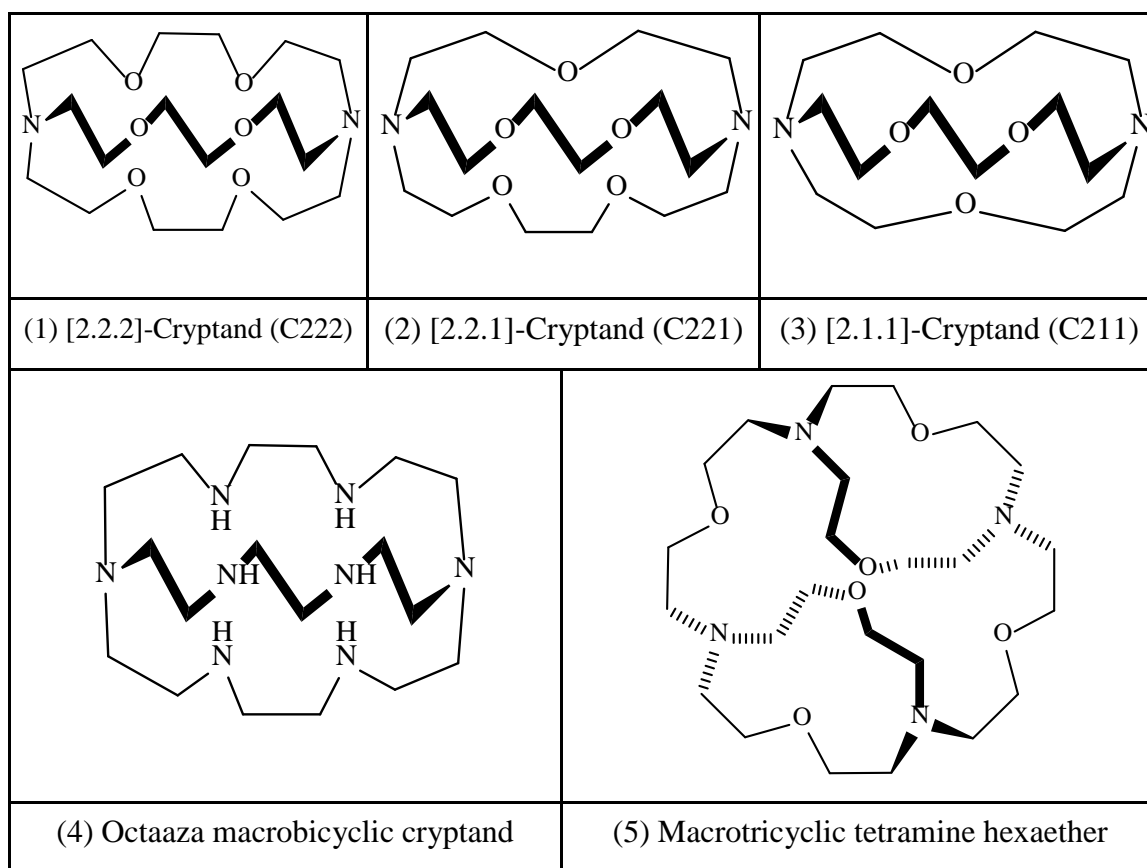
The binding constant for binding alkali and alkaline earth cation decreases dramatically after substitution of some oxygen atoms of crown ether by sulphur atoms^{139,146}.

However, thia-crown ethers can show a significant increase in complexation stability with soft metal ions, namely Hg^{2+} and Ag^{+} ions¹⁴⁷⁻¹⁴⁹.

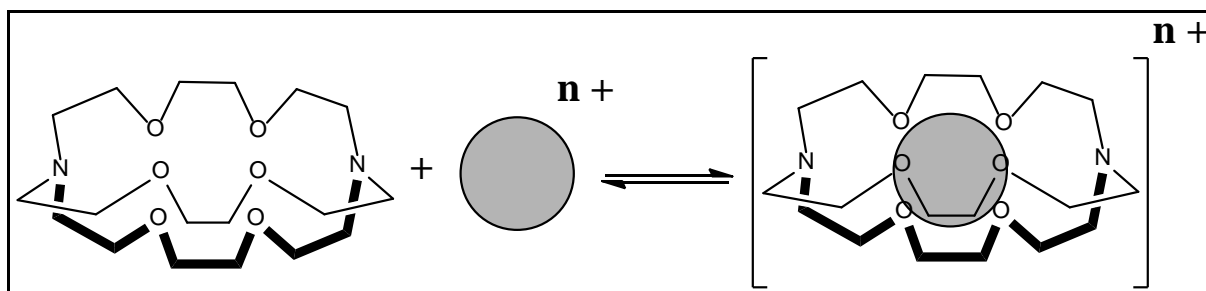
The interesting aspects of using macrocyclic polyamines are focused on their biological properties and importance in coordination chemistry¹⁵⁰. Saturated macrocyclic polyamines can show a pronounced ability to bind a variety of metals¹⁵¹. Cyclam is one of the macrocyclic polyamines which have been used in modern chemistry. It can form complexes with, for example, transition metals with high kinetic and thermodynamic stability based on the chelate effect¹⁵².

2.2.2 Three-dimensional hosts

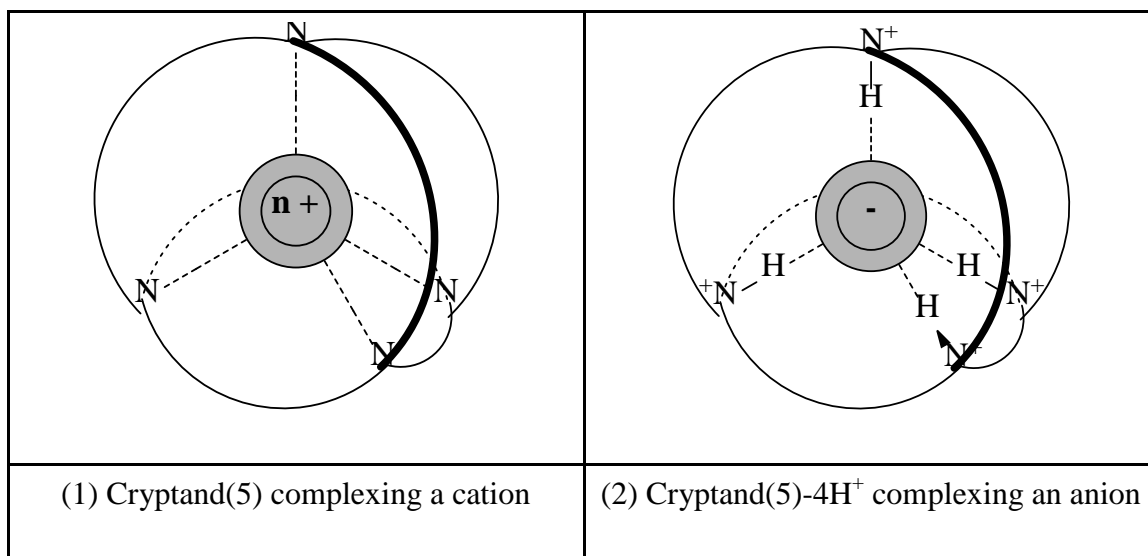
The first polycyclic receptors with three-dimensional cavities which could entirely surround the bound ion were called cryptands. The first of these was C222 [Figure 2.5 (1)] prepared by Lehn¹⁵³. The design, synthesis and properties of this were summarised by Lehn in 1978¹⁵⁴. Compared with crown ethers, cryptands are more rigid and more selective as a result of different cavity and size complementarity, thus C211 (3) binds Li^{+} , C221 (2) binds Na^{+} and C222 (1) binds K^{+} respectively. The macrotricyclic tetramine hexaether (4) can form strong and selective complexes with the large spherical cation Cs^{+} , and the soccer ball cryptand (5) binds tetrahedral cations, such as NH_4^{+} and H_4O^{2+} respectively^{153,154}.

Figure 2.5 Some simple cryptands¹⁵⁴

Scheme 2.2 shows the formation of a cryptate inclusion complex.

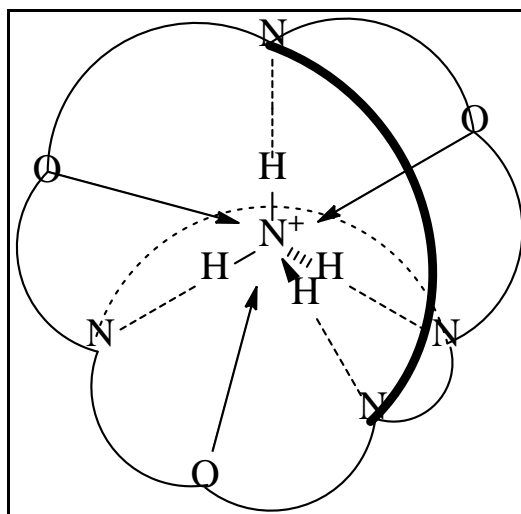
Scheme 2.2 Equilibrium showing the formation of a cryptate inclusion complex¹⁵⁴

Cryptands can also be designed to bind anions. This has been achieved by using protonated polyamines, such as cryptand (5)- $n\text{H}^+$ or cryptand (4), which can bind Cl^- and F^- respectively. Therefore, cryptands can show good spherical recognition under the right circumstances^{153,154}. Figure 2.6 shows cryptand (5) complexing a large spherical cation, such as Cs^+ and cryptand (5)- 4H^+ complexing an anion, such as Cl^- .

Figure 2.6 Spherical recognition in cryptate complexes^{153,154}

2.2.3 Tetrahedral recognition

For binding of a tetrahedral substrate such as NH_4^+ , receptors with a tetrahedral binding site are necessary, as in cryptand (5) which contain four nitrogen atoms and six oxygen binding sites located respectively¹⁵⁵. Indeed, cryptand (5) forms an extremely stable and selective cryptate when combined with NH_4^+ , a consequence of both structural energetic complementarities. The tetrahedral substrate of NH_4^+ has the size and the shape for fitting into the cavity of cryptand (5) with a tetrahedral array of $\text{N}^+ \cdots \text{H} \cdots \text{N}$ hydrogen bonds as viewed in Figure 2.7¹⁵³, which shows the complexation of NH_4^+ by cryptand (5).

Figure 2.7 Complexation of NH_4^+ by cryptand (5)¹⁵³

2.3 Self-assembly

Self-assembly is the process by which specific components spontaneously assemble into a well-defined, discrete supramolecular architecture. Self-assembling processes occur throughout nature and technology. The components are involved from the molecular to the planetary scale and involve various kinds of interactions¹⁵⁶. For example, DNA molecular structures and intermolecular interactions are particularly amenable to the design and synthesis of complex molecular objects¹⁵⁷.

By positive cooperativity, phase change and energy flow, a self-assembling system is driven to completion. It requires binding interactions and implies that information must be stored in the specific components and read out by the following given procedures¹⁵⁸. Firstly, selective binding of complementary components via molecular recognition; secondly, growth through sequential binding of the components in the correct relative orientation; thirdly, termination of the process, requiring a built-in feature, a stop signal, that specifies the end point and signifies that the process has reached completion. This can be a closure relation generating a closed structure. Therefore, such organised supramolecular systems generate well-defined entities following a plan based on molecular recognition events.

2.3.1 From pseudorotaxanes to rotaxanes and catenanes

Figure 2.8 shows a formation of a pseudorotaxane as a precursor to either a [2]rotaxane or [2]catenane.

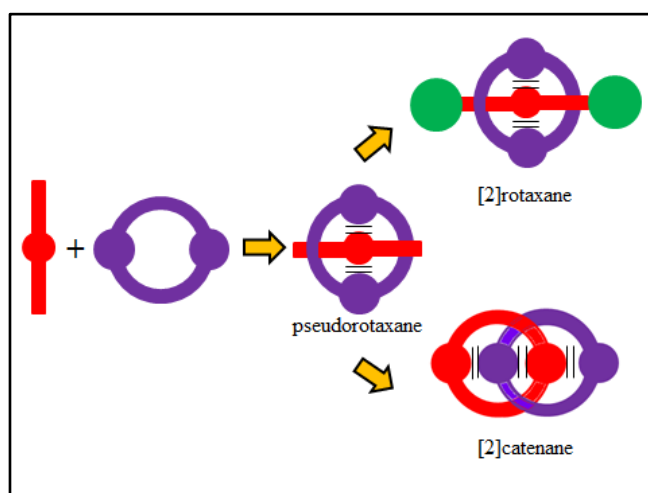


Figure 2.8 Formation of a pseudorotaxane to either a [2]rotaxane or [2]catenane¹⁵⁹

Catenanes and rotaxane can be synthesised from a common intermediate known as a pseudorotaxane, which can be considered as a molecular sibling in Supramolecular Chemistry. The pseudorotaxane here refers to a supramolecular species in which a thread is encircled by one or more macrocycles. The threading of a linear component through the macrocycles is driven by noncovalent bonding interactions to generate the most stable complexes in solution. In particular, noncovalent bonding interactions, which include donor/acceptor forces, metal/ligand coordination, hydrogen bond, π - π stacking, solvophobic repulsion and electrostatic forces, have all been applied to form supramolecular assemblies¹⁵⁹. When subjected to different solvent, temperature, or competitive guests, pseudorotaxane can be decomplexed. However, it is reasonable to fix a pseudorotaxane kinetically, either by adding stoppers on both sides of the chain, or by macrocyclisation to produce a rotaxane or catenane, respectively¹⁶⁰.

Rotaxanes are molecules constituted by a linear dumbbell-shaped component encircled by one or more macrocycles. The stoppers attached to the ends of the dumbbell must be large enough to prevent the macrocycle(s) from dethreading. A standard nomenclature has been established wherein the number of components that constitute the rotaxane appear in square brackets before the term of rotaxane. Therefore, an [n]rotaxane is a molecule constituted by a dumbbell and n-1 macrocyclic components¹⁵⁹.

Catenanes consist of two or more interlocked macrocycles. As described previously, the nomenclature for rotaxanes, the number of macrocycles that form a catenane appears in square brackets before the term. Therefore, an [n]catenane is a molecule constituted of n interlocked macrocycles¹⁵⁹.

2.3.2 Donor-acceptor based pseudorotaxanes

Donor-acceptor based template directed synthesis started with the pairing of π -electron rich macrocycles with π -electron deficient rod-shaped molecules. The rod-shaped molecule would thread through the macrocycle forming a pseudorotaxane^{161,162}. In Figure 2.9, the electron rich macrocyclic polyether host, bis-*p*-phenylene[34]crown-10 (BPP34C10), binds an electron deficient guest, the paraquat dication. This complex is assembled together by π - π stacking interactions between the complementary aromatic units, [C-H \cdots O] interactions between the hydrogen atoms -[CH₃-N] and [CH-N]- in the α -positions in respect to the nitrogen atoms in the bipyridinium unit and the crown ether

oxygen atoms. Based on the assembly of the BPP34C10/paraquat pseudorotaxane, this process can be extrapolated to an inverse recognition system, where the macrocycle is constructed by paraquat units as a host and the guest is a hydroquinone unit carrying ethylene glycol chains¹⁵⁹. Figure 2.9 shows the donor-acceptor based pseudorotaxanes.

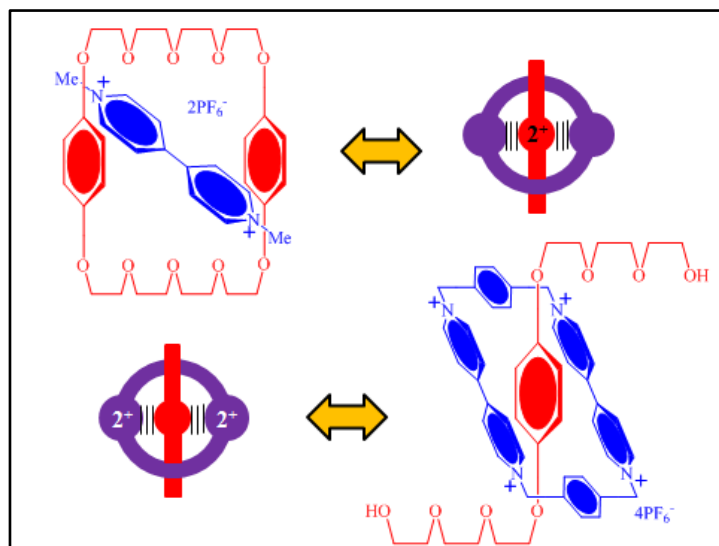


Figure 2.9 Donor-acceptor based pseudorotaxanes¹⁵⁹

2.3.3 Donor-acceptor [2]rotaxanes

Figure 2.10 shows a graphical representation of three methods of rotaxane formation, which are threading followed by stoppering, slippage of the macrocycle over the stoppers at elevated temperatures, and clipping of the macrocycle around the dumbbell.

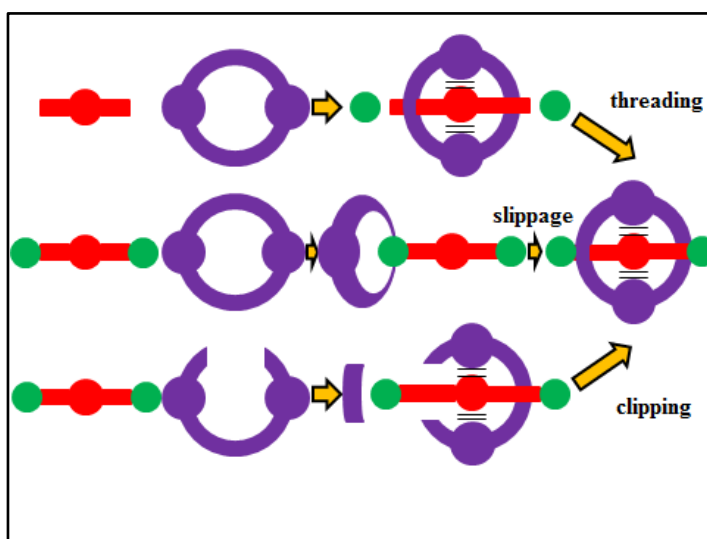
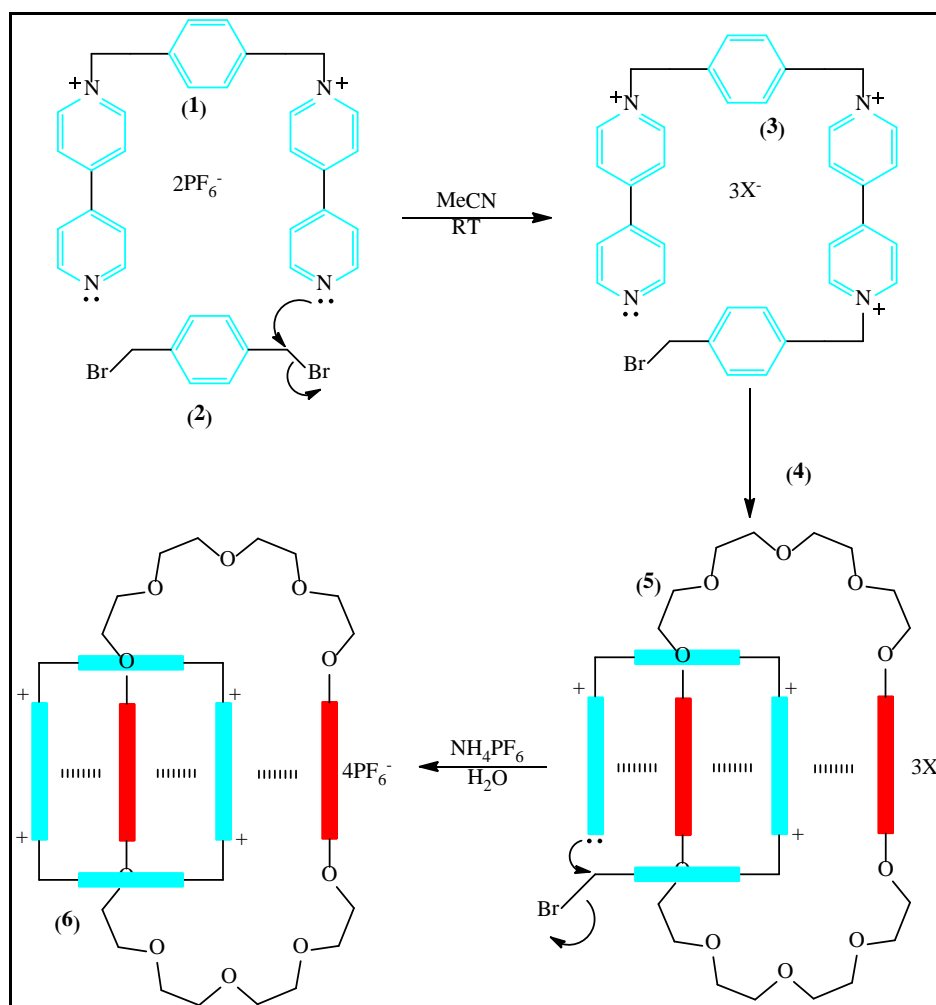


Figure 2.10 A graphical representation of three methods of rotaxane formation¹⁵⁹

The first method, threading, contains the formation of a pseudorotaxane, where the thread is complexed within a macrocycle, and then both ends of the thread are reacted with bulky stoppers to generate the desired [2]rotaxane. In the second method, slippage, the stoppers of a rotaxane are matched closely with the cavity of the macrocycle, when a solution involving both of the dumbbell and macrocycle is heated, the macrocycle has enough energy to pass through the stoppers to form the thermodynamically stable [2]rotaxane. The last method is known as clipping. It contains linear fragment, which will interact noncovalently with a dumbbell, so that the ends of the linear fragment are likely to react while encircling the dumbbell template completely to form the desired [2]rotaxane¹⁵⁹.

2.3.4 [2]Catenane synthesis

Scheme 2.3 shows the preparation and self-assembly of the [2]catenane.



Scheme 2.3 The preparation and self-assembly of the [2]catenane¹⁵⁹

The process of synthesising [2]catenane is believed to proceed in the following way. Firstly, the trication complex (**3**) is formed based on the N-C bond formation between bis-pyridiniumxylyl dication (**1**) and bis-bromomethyl benzene (**2**); Secondly, the trication complex (**3**) threads by itself (**4**) through the neutral macrocycle (**5**) to achieve the next step; Finally, the complex of [2]catenane is formed based on the formation of the second N-C bond. The aromatic interactions of face-to-face π stacking and edge-to-face interactions can be viewed from crystal structure which dominates the way the components assemble in the final product (**6**)¹⁵⁹.

2.3.5 Functional [2]catenanes

Components such as TTF have found applications in switchable catenanes. Figure 2.11 shows the proposed mechanism of switching in a tri-stable [2]catenane working under different voltages. The ring has to switch locations over green ($V=0$), blue ($V=V_1$) and red ($V=V_2$) states, respectively.

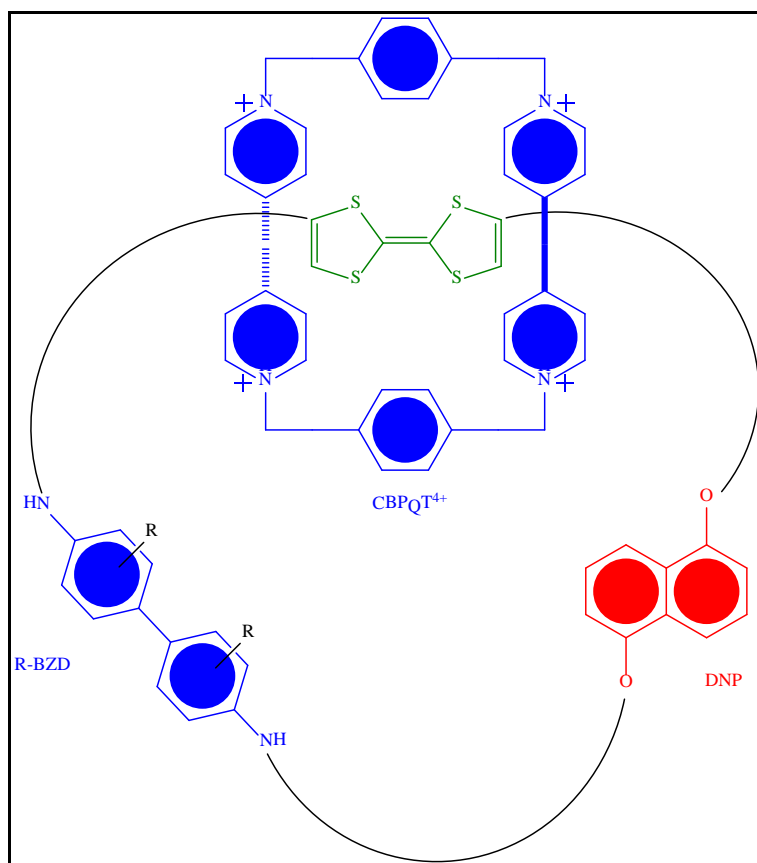


Figure 2.11 The proposed mechanism of switching in a tri-stable [2]catenane working under different voltages¹⁶³

Compared with the old, black/white prototypes of electronic paper display (E-PAD), Deng et al.¹⁶³ proposed a new concept for the pixel component in an E-PAD that consisted of a film of a single switchable 'RGB' (Red-Green-Blue) dye compound, which could exhibit all three different colours depending on the applied voltage. The advantages of using RGB dyes were as follows. Firstly, each pixel unit needed only a single basic cell instead of three to generate red, green, and blue colours. This feature would reduce the complexity dramatically and, therefore, the cost¹⁶³. Secondly, molecular compounds were easily embedded in polymer matrixes and even on paper materials. Hence, simple package processing, such as ink-jet printing technology, could be used to make the displays¹⁶³. Examples of such colour changeable dyes are donor-acceptor catenanes, comprising a ring incorporating TTF, 1,5-dioxynaphthalene (DNP) and a substituted benzidine (R-BZD) donor units, interlocked with the cyclobis(paraquat-*p*-phenylene) (CBPQT⁴⁺) acceptor ring. Figure 2.12 shows a proposed general design of the RGB tri-stable [2]catenane. The coloured units refer to TTF(green), R-BZD(blue) and DNP(red) donors, respectively.

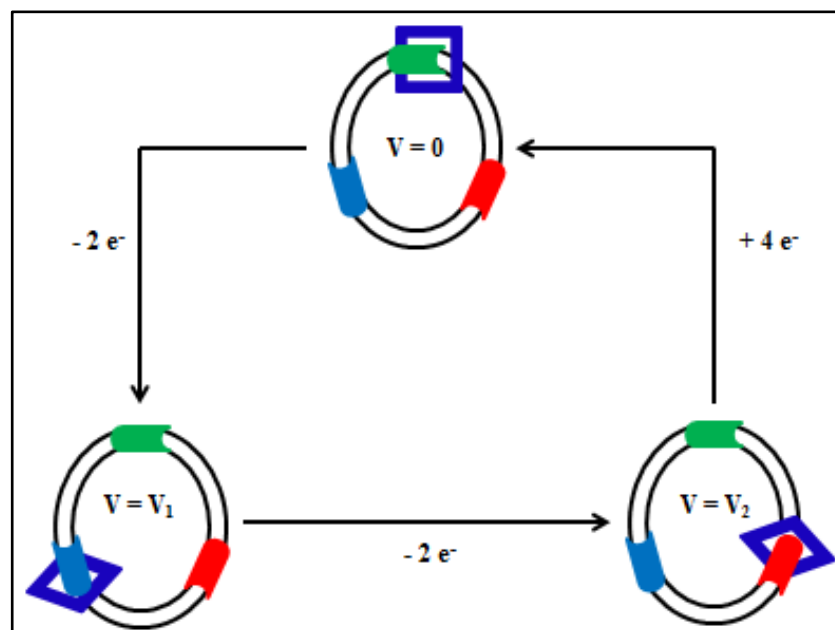


Figure 2.12 A proposed general design of the RGB tri-stable [2]catenane¹⁶³

In this design, three different voltages V_0 , V_1 , and V_2 are used to control the colour, where at V_0 all three donor units are neutral and the CBPQT⁴⁺ ring encircles the TTF unit (green). Under the help of an applied external voltage V_1 , the TTF unit is oxidised and doubly charged, repelling the CBPQT⁴⁺ ring and move to the second donor unit of R-BZD. This geometry of the [2]catenane is associated with the second state, which

affords a blue coloured complex. After the voltage is changed into V_2 , the R-BZD component is oxidised, driving the CBPQT⁴⁺ ring to the DNP unit, leading to a red coloured complex. After the voltage is reset back to V_0 , the CBPQT⁴⁺ ring will move back to the original position of the TTF unit. During the whole process, each of the three colour states is accessed at different voltages, even though the CBPQT⁴⁺ ring may move clockwise or counter-clockwise along the space units (S)¹⁶³. Based on the proposed mechanism, the tri-stable [2]catenane can show three different colour states depending on the applied external voltages. This example provides a simple demonstration of a molecular-scale supramolecular machine.

2.4 The concept of crystal engineering

The original concept of crystal engineering was to control the behaviour of organic molecules in the solid state based on an understanding of intermolecular interactions as developed by Supramolecular Chemistry¹⁶⁴⁻¹⁶⁶. The idea of crystal engineering is to control the way in which the ions or molecules encounter and recognise each other, and then pack together into their optimum orientation based on the effect of intrinsic steric and electronic properties. This ultimately leads to the design of functional organic molecular solids with interesting chemical and physical properties^{164,165}. The subject of crystal engineering can be thought of as research on the synthetic chemistry of crystals, i.e. to understand the way in which ions or molecules crystallise, leading to the design of novel complexes with controlled structures and properties. The process of synthesising crystals is, at present, difficult to control since it depends on both long and short range interactions. With the distance increasing, some interactions fall off rapidly, while other effects such as dipolar interactions and hydrogen bond can exist over longer ranges. The hydrogen bond is one essential instrument for designing molecular structures and aggregates¹⁶⁷.

Therefore, the concept of crystal engineering is concerned about the design and synthesis of a crystalline material associated with a consideration of the effects of steric, electronic and intermolecular interactions between the constituent building blocks¹⁶⁷.

2.4.1 Intermolecular interactions of crystal engineering

Intermolecular interactions can be attractive or repulsive depending on the types of the contacts involved. Intermolecular interactions are weaker than the covalent bonds, which hold molecules together. Table 2.2 shows different types of intermolecular interactions and their relative strengths with examples.

| Interaction | Typical energy (kJ·mol ⁻¹) | Examples |
|-------------------------------|--|-------------------------------------|
| Ion-ion | 100-500 | Na ⁺ Cl ⁻ |
| Ion-dipole | 40-300 | K ⁺ (18C6) |
| Dipole-dipole | 5-80 | H ₂ O, CHCl ₃ |
| Dipole-induced dipole | 2-10 | CO _{2(aq)} |
| Induced dipole-induced dipole | 0.05-40 | Noble gases |

Table 2.2 Different types of intermolecular interactions¹⁶⁸

Ion-ion interactions are the strongest forces, and are largely presented in inorganic compounds. This type of interaction involves small species as opposed to large ones. Although induced dipole-induced dipole interactions are the weakest, and are involved in all substances¹⁶⁸, the dipole-dipole interactions, which are of intermediate strength, exist between organic molecules. For organic molecules, there are electronegative elements presented that introduce a dipole. The electronegative elements involve nitrogen- or oxygen-based substituents. Dipole-dipole interactions are the dominant force to assemble organic molecules. The hydrogen bond is an example of dipole-dipole interactions, and is widely used in chemistry and biology¹⁶⁹⁻¹⁷⁴, such as utilised in DNA and proteins. Hydrogen bonding acts as an important role in determining the three-dimensional structures adopted by nucleic bases and proteins, with further determining the macromolecule's physiological or biochemical role¹⁷⁵⁻¹⁷⁷. In addition, hydrogen bond can determine the structure of polymers, such as porous coordination polymers¹⁷⁸.

2.4.2 Hydrogen bonding in crystal engineering

In this section, the definition of hydrogen bonding will be illustrated with the following examples to prove the significant role of a hydrogen bond for utilisation in crystal engineering.

2.4.2.1 The definition of hydrogen bonding

A hydrogen bond can be formed between an electronegative atom and a hydrogen atom bonded to fluorine, oxygen and nitrogen. The hydrogen bond can be simple (one donor and one acceptor), bifurcated (three-centre), or trifurcated (four-centre)¹⁷². In Figure 2.13, the D elements can be O, N, F, S and C respectively. Meanwhile, the A elements can be O, N, F, S, X⁻, alkene, alkyne and arene respectively.

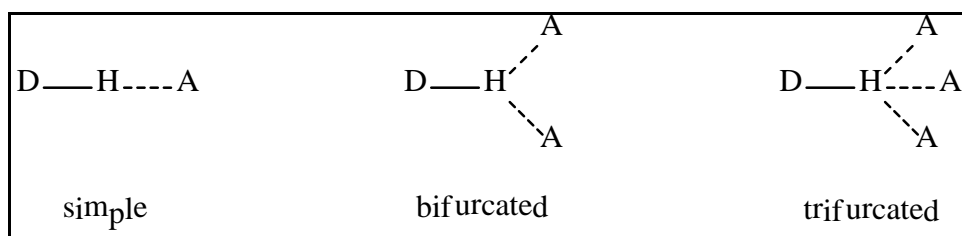


Figure 2.13 Common hydrogen bond arrangements¹⁷²

2.4.2.2 Applications of hydrogen bonding in crystal engineering

Hydrogen bonds are widely used in crystal engineering. For example, the carboxylic acid, which is a functional group, forms various hydrogen bond patterns. Two main hydrogen bond patterns, dimers and catemers, can be formed in crystalline carboxylic acids. Benzoic acid is one of the typical examples of many carboxylic acid crystal structures, with dimerisation occurring via hydrogen bond. From Wilson et al.¹⁷⁹ studies, the positions of the two hydrogen atoms linked the benzoic acid molecules in order to form a dimer through hydrogen bond. Figure 2.14 shows the hydrogen bonds in forming the dimer of benzoic acid.

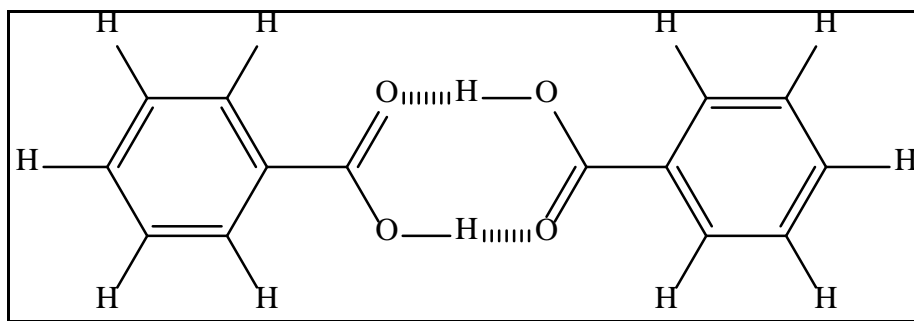
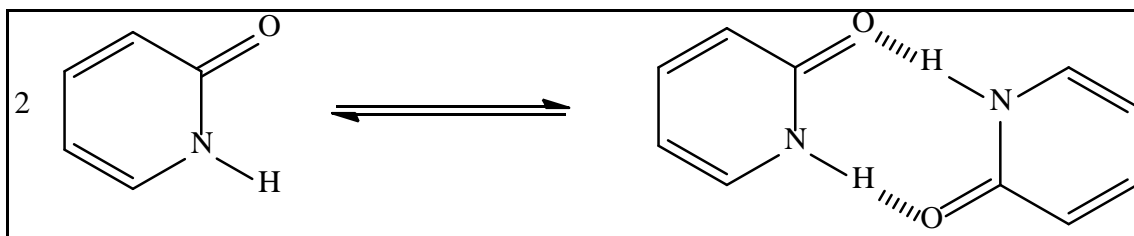


Figure 2.14 Hydrogen bonds in forming the dimer of benzoic acid¹⁷⁹

Motifs, which are similar to the carboxylic acid dimer, can be found in other systems such as 2-Pyridone^{180,181}.

Scheme 2.4 displays the hydrogen bonds formation of a dimer of pyridine.



Scheme 2.4 Hydrogen bonds formation of a dimer of Pyridone^{180,181}

Leiserowitz and Nader^{182,183} studied the motif behaviour of a hydrogen bond in carboxylic acids. The catemer was constructed by an infinite one-dimensional pattern of carboxylic acid groups in crystals, and was assembled via O-H \cdots O hydrogen bonds. Beyer and Price¹⁸⁴ commented that the formation of catemer could only be achieved by molecules with small substituents on the acid group. The steric bulk of an aromatic ring would prevent the formation of catemer. Das and Desiraju^{185,186} suggested that the substituent effects could be separated into steric and electronic in nature. The steric effect referred to the size and shape of substituents and the electronic effect related to the polarity and electronegativity of the group. In addition, a number of conclusions could be drawn by Das and Desiraju^{185,186} from the study of substituted phenylpropionic acids. The authors^{185,186} commented that the catemer was one-dimensional pattern compared with the zero-dimensional dimer formation; For composing catemer, a supportive C-H \cdots O hydrogen bond, from a proximal C-H group located on the phenyl ring and ortho to the ethynyl group, was necessary; catemer formation was uncommon

because most acids could not generate the supportive C-H \cdots O hydrogen bond; The factors for forming different geometries of catemer were based on the intrinsic and steric effects of substituent groups. Both the dimer and catemer formation could not exist in any given carboxylic acid at the same time.

Figure 2.15 shows the catemer hydrogen bond motifs produced by carboxylic acid.

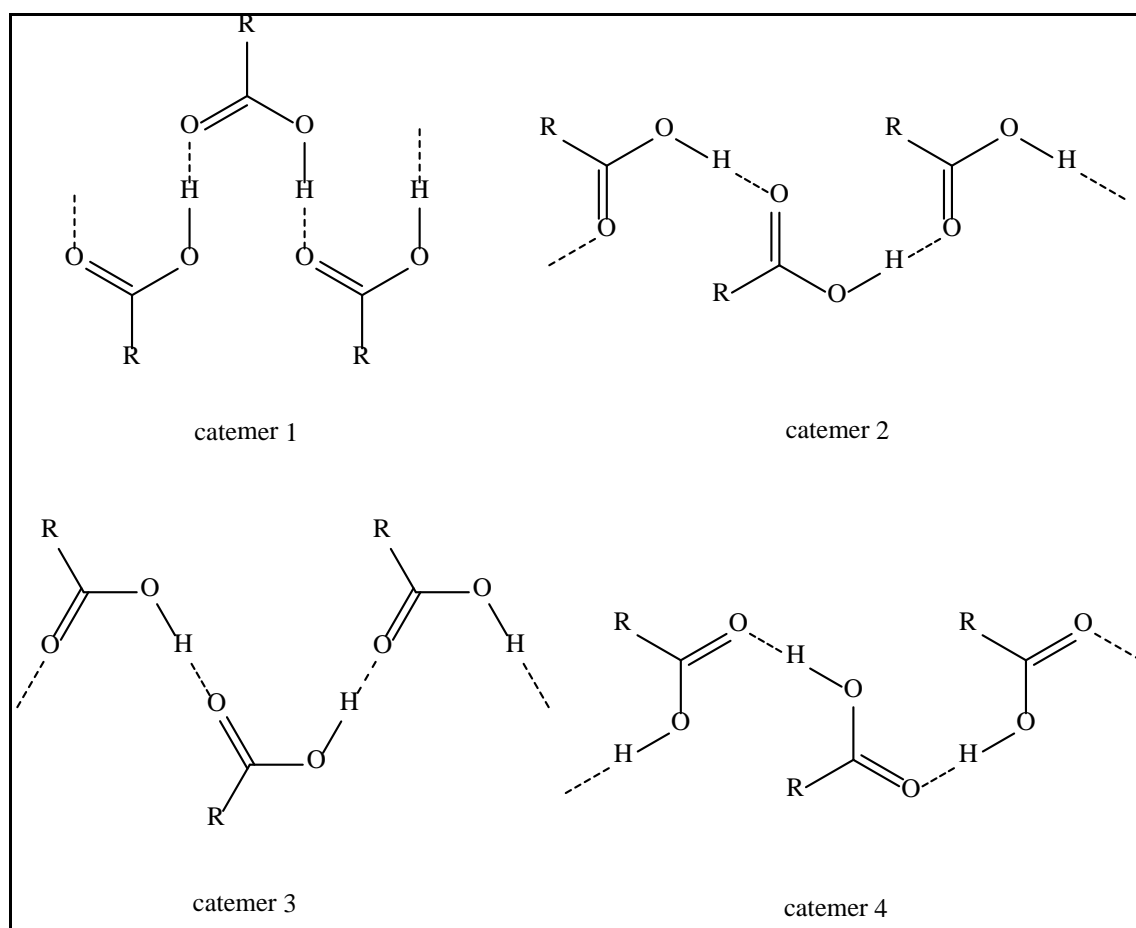


Figure 2.15 Catemer hydrogen bond motifs produced by carboxylic acid¹⁸⁶

Aside from catemer 4, all the other catemers are *syn*-planar formation in catemer 1/2/3. In catemer 4, the complex is obtained by switching H atoms in catemer 2 and is *anti*-planar formation. All of these four catemers are one-dimensional patterns¹⁸⁷. Meanwhile, the less frequent patterns of catemers are sensitive to the steric effects of the substituent group or to O \cdots O lone pair repulsive interactions. However, compared with the *syn*-planar conformation, the *anti*-planar geometry is of much higher energy, which is 6 kcal·mol⁻¹¹⁸⁶.

2.4.3 Multiple hydrogen bond arrays and secondary hydrogen bond interactions

Figure 2.16 displays the hydrogen bond arrays in DNA.

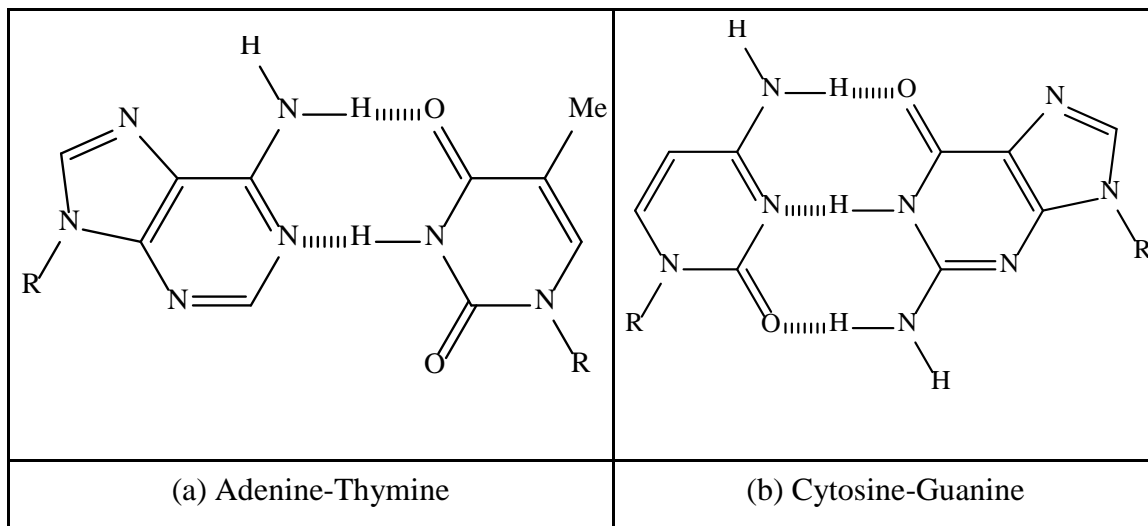


Figure 2.16 Hydrogen bond arrays in DNA¹⁸⁸

The A-T and C-G hydrogen bond bases pairing present in DNA are presented in Figure 2.16. It is shown that more than one hydrogen bond are consists in the formation of the complementary base pairs in both cases. There are three hydrogen bonds presented in the C-G dimer, while the A-T dimer involves only two, which explains why the regions containing C-G dimers are much more stable than A-T ones. In the structure of DNA, the roles of base pairing and π - π stacking in assembling the DNA double helix are significant in determining the function of supramolecular self-assemblies, which enable DNA to replicate and pass its genetic information to RNA¹⁸⁸. Secondary hydrogen bond interactions are also important in determining the stability of multiple hydrogen bond arrays.

Secondary hydrogen bond corresponds to the electrostatic interaction between adjacent hydrogen bond atoms^{189,190}. In this case, the four diagonal electrostatic interactions marked on the array type I are repulsive (+hydrogen with +hydrogen, and –oxygen with –nitrogen). In the array type II, there is no net secondary hydrogen bond effect overall, whereas in the array type III, there are four net attractive secondary hydrogen bond interactions^{189,190}, which lead to the maximum interaction strength. Figure 2.17 shows multiple hydrogen bond arrays.

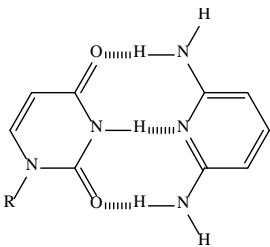
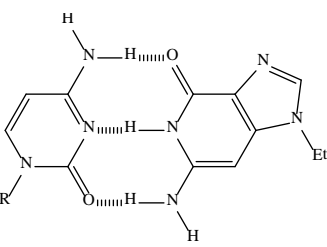
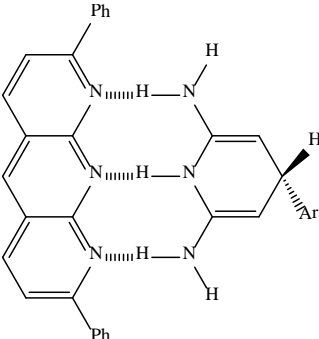
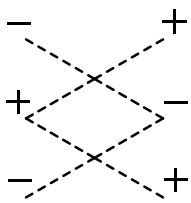
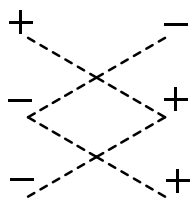
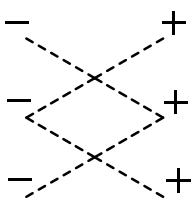
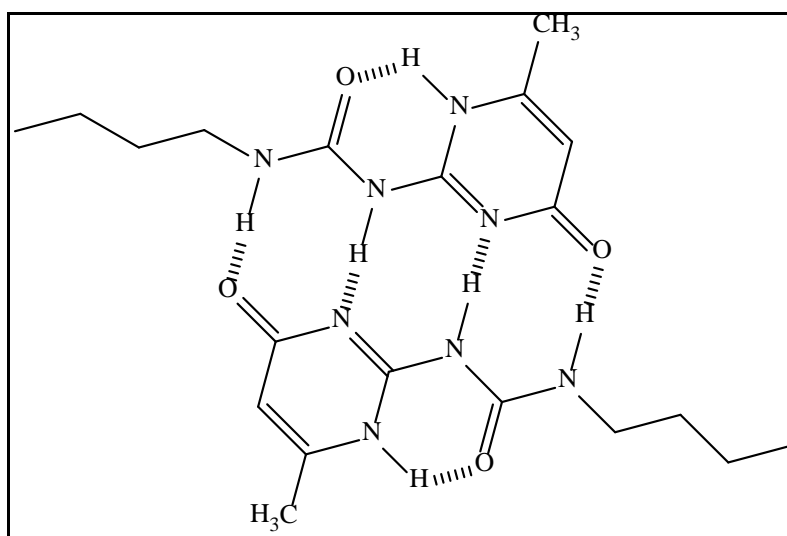
| Array types | I | II | III |
|----------------------|---|---|---|
| Structure |  |  |  |
| Interaction strength | $K_a = 90 \text{ M}^{-1}$ | $K_a = 1 \times 10^4 \text{ M}^{-1}$ | $K_a \geq 1 \times 10^5 \text{ M}^{-1}$ |
| Hydrogen bond arrays |  |  |  |
| D-A interaction | ADA-DAD | DAA-ADD | DDD-AAA |

Figure 2.17 Multiple hydrogen bond arrays^{189,190}

Polymers can be formed through hydrogen bonding. Sijbesma et al.¹⁹¹ had shown a "DDAA" hydrogen bond array. Figure 2.18 shows the hydrogen bonds array of 2-butylureido-6-methylpyrimidone.

Figure 2.18 Hydrogen bonds array of 2-butylureido-6-methylpyrimidone¹⁹¹

Dimer was in chloroform and could essentially be regarded as a reversible alternative to a covalent bond. In solution, each terminal group could form an intermolecular dimer resulting in polymer formation. Association with a monomer led to a block at one end of the polymer chain and this acted as a stopper. After changing the methyl group on each end of the structure into a more complex alkyl groups, a linear supramolecular polymer was obtained by Sherrington and Taskinen¹⁹².

Figure 2.19 shows a linear chain obtained by the dimerization of the ureidopyrimidone units.

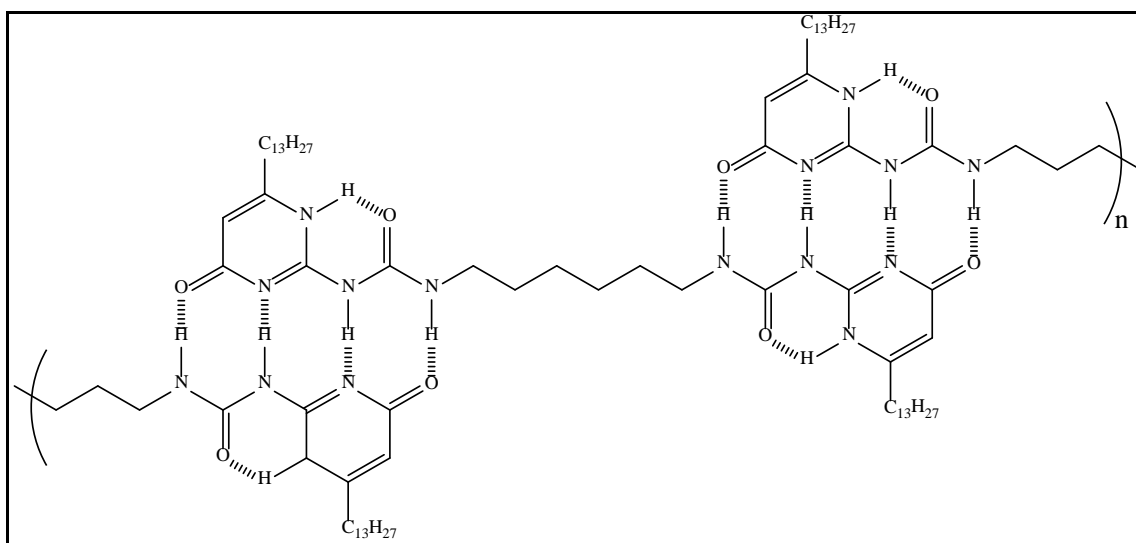


Figure 2.19 A linear chain obtained by the dimerization of the ureidopyrimidone units¹⁹²

2.5 Overview of the solid state structures of MTCNQ salts

Based on the different physical properties and crystal structures, Shirota and Sakai¹⁹³ suggested that MTCNQ salts could be separated into two groups A and B. Group A contains Li, Na-, K- and RbTCNQ(I). LiTCNQ, however, demonstrates somewhat unique properties compared with other salts in Group A. Group B includes RbTCNQ(II) and CsTCNQ. RbTCNQ(III) and NH₄TCNQ(II) are difficult to classify into Group A or B, because they tend to resemble RbTCNQ(I) in some ways, but RbTCNQ(II) in others.

2.5.1 Comparison of Group A and Group B salts in crystal structures

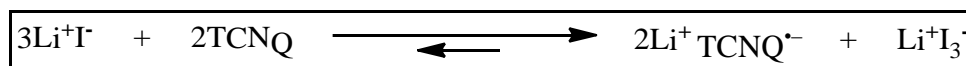
Apart from LiTCNQ, the crystal structures of simple salts of alkali metals in the first group of the Periodic Table have all been obtained¹⁹⁴⁻²⁰¹. These X-ray studies revealed that the TCNQ prefer to form face-to-face π -stacks infinite columns in the solid state. The formation of such columns is associated with the property of enhanced electrical conductivity. Ordinarily, the TCNQ units prefer to form diadic, triadic or even tetradic units, which are associated with low or intermediate conductivity, whereas for high conductivity materials, such as TTF-TCNQ, the TCNQ units stack as a monadic column. In Group A, the column structures of Li-, Na-, K-, and RbTCNQ(I) consist of diadic TCNQ units. However in Rb(II)-, CsTCNQ complexes, a monadic packing motif is adopted, which suggest the conductivity property should be higher than those complexes in Group A at the same temperature¹⁹³.

These materials tend to show phase transitions which are revealed using different measurements, such as electrical conductivity^{202,203}, magnetic susceptibility^{204,205} and other physical properties^{203,205}. Phase transitions in MTCNQ salts, where M represents an alkali metal, have been observed in the temperature region -150 to +300°C¹⁹³. In Group A, the packing of TCNQ⁻ anions in column changed from diadic into monadic motif with increasing temperature. The MTCNQ salts in Group B belong to the high temperature phase, which is monadic, at room temperature¹⁹³.

2.6 An overview of the solid-state behaviour of TCNQ salts

2.6.1 Preparation of TCNQ salts

TCNQ will readily accept one free electron by reaction with relevant alkali metal iodide salts, such as LiI, NaI, and KI in boiling acetonitrile. Scheme 2.5 shows the standard preparation method of LiTCNQ.



Scheme 2.5 Standard preparation method of LiTCNQ

The use of excess alkali metal iodide pushes the equilibrium in this reaction to the right hand side through the formation of I_3^- .

LiTCNQ is a valuable starting compound for the preparation of other TCNQ complexes, especially for transition metal TCNQ complexes, because LiTCNQ is easy to dissolve in common solvents, including deionised water.

In the solid state, the $\text{TCNQ}^{\bullet-}$ anions prefer to form face-to-face π stacks. The 1:1 stoichiometry $\text{TCNQ}^{\bullet-}$ anion salts are semiconductors and usually purple in colour. Crystallisation of these 1:1 salts with a molar equivalent of TCNQ^0 leads to complex salts (cation: TCNQ ratio of 1:2), which exhibits metallic behaviour according to the mixed valence nature of the TCNQ packing motif. The crystal structures and phase transition of each MTCNQ (M = alkali and transition metals) will be discussed in the following paragraphs.

2.6.2 Structural investigations of alkali metal TCNQ salts

There are significant differences between LiTCNQ and the other alkali metal TCNQ salts. For example, only unit cell data has been reported for LiTCNQ¹⁹⁵, whereas full X-ray crystallography information has been published with NaTCNQ (low²⁰⁶- and high²⁰⁷-temperature forms), KTCNQ (low²⁰⁸- and high²⁰⁸-temperature forms), three polymorphs of RbTCNQ (I/II/III)^{195,209,210}, Rb_2TCNQ_3 (113K, 294K)^{211,212}, and Cs_2TCNQ_3 (R.T.)²¹³, respectively.

NaTCNQ crystals were prepared by Konno and Saito²⁰⁶. Below the phase transition temperature (348K), in this structure, the $\text{TCNQ}^{\bullet-}$ anions existed as dimers which were then assembled into a columnar structure with alternating intermolecular distances of 3.21 and 3.49 Å along *a* axis. In addition, six negatively charged nitrogen atoms from $\text{TCNQ}^{\bullet-}$ anions were coordinated to one Na^+ cation in an octahedral coordination environment. In stark contrast, crystals prepared at 353K showed $\text{TCNQ}^{\bullet-}$ anions face-to-face π stacked in columns along *a* axis with the same perpendicular distance between neighbours, as opposed to the alternate spacing seen in the low temperature phase²⁰⁷. Figure 2.20 shows the crystal structure of NaTCNQ at room temperature, in which the $\text{TCNQ}^{\bullet-}$ anions are stacked in alternating columns with six anions surrounding each cation site. The adjacent cation stacks are rotated by $\approx 90^\circ$.

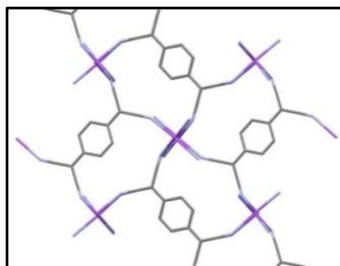


Figure 2.20 Crystal structure of NaTCNQ at room temperature (ref code: NATCNQ)²⁰⁶

The phase transition of KTCNQ occurs at 395K²⁰⁸. Konno et al.²⁰⁸ have characterised the low and high temperature modifications of KTCNQ. Under the phase transition temperature, the packing pattern of TCNQ^{•-} anions is face-to-face π -stacked to form discrete TCNQ^{•-} dimers with further forming columns with alternating intermolecular distances. However, the TCNQ^{•-} anions are packed into evenly spaced columns above the phase transition temperature. Each K⁺ cation lies at the centre of a distorted cube, coordinated to eight negatively charged nitrogen atoms from different TCNQ^{•-} units²⁰⁸. Therefore, this monomer-dimer transition is similar to that already reported for NaTCNQ. Figure 2.21 shows the crystal structure of KTCNQ at room temperature, in which the TCNQ^{•-} anions are stacked in alternating rows with eight anions surrounding each cation site. The adjacent cation stacks are rotated by $\approx 90^\circ$.

In both NaTCNQ and KTCNQ, the negatively charged nitrogen atoms of the cyano groups are coordinated to the metal cation. Simple alkali metal TCNQ salts, such as NaTCNQ and KTCNQ, have lower conductivity behaviour than expected because of Peierls Distortion²¹⁴. It is known that TCNQ^{•-} anion prefers to form face-to-face π stack radical dimer pairs, which allows the unpaired electrons to pair their spin. This leads to greater stability through the splitting of the valence band into two bands, a filled bonding orbital band and an empty anti-bonding orbital band²¹⁴.

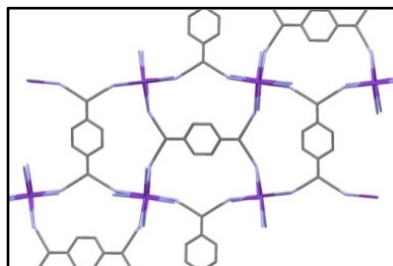


Figure 2.21 Crystal structure of KTCNQ at room temperature (ref code: KTCYQM01)²⁰⁸

The intradimer overlap within NaTCNQ and KTCNQ is frequently referred to as “ring-ring”, which is shortened to R-R, arrangement with a slippage of the molecular centre along the short-axis as seen in Figure 2.22. The other type of overlap is ring-external bond, which is shortened to R-B overlap which means that one quinoid bond lies over the centre of the ring of the adjacent molecule as a result of a shift of the molecular centre along the long axis in Figure 2.23²⁰⁶.

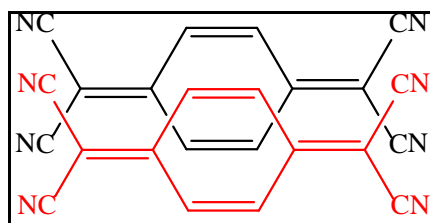


Figure 2.22 Typical ring-ring (R-R) overlap of two TCNQ moieties or “short-axis” slipped

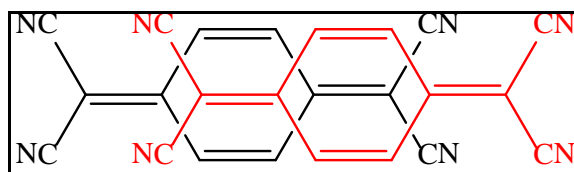


Figure 2.23 Typical ring-external bond (R-B) overlap of two TCNQ moieties or “long-axis” slipped

As the size of the cation is increased, solid state behaviour changes are observed. For example, the salt RbTCNQ can exist in several different stoichiometries. For RbTCNQ itself, two different packing motifs, RbTCNQ(I) and RbTCNQ(II) have been published. Figure 2.24 shows the different packing motifs of RbTCNQ(I) and RbTCNQ(II).

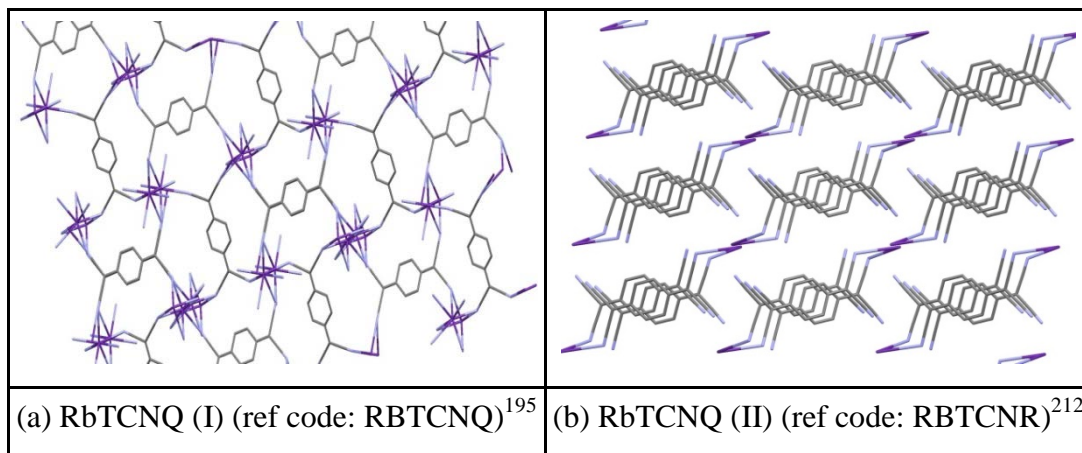


Figure 2.24 The different packing motifs of RbTCNQ(I)¹⁹⁵ and RbTCNQ(II)²¹²

In RbTCNQ(I), the TCNQ^{•−} dimers assembled into infinite columns, with neighbouring columns arranged mutually perpendicular within the crystal structure as previously seen for NaTCNQ and KTCNQ. Each Rb⁺ ion is coordinated by eight nitrogen atoms of adjacent different TCNQ^{•−} anions with the further forming of a distorted cube¹⁹⁵. However, in contrast to NaTCNQ and KTCNQ, the TCNQ^{•−} anion in RbTCNQ(I) adopts a shallow boat conformation as viewed in Figure 2.25, in which the planes through the terminal part of C(CN)₂ groups deviate a few degrees from the plane through the quinoid structure of the molecule^{53,54}.

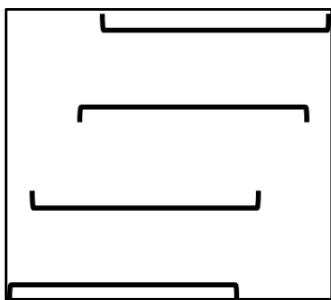


Figure 2.25 A schematic representation of the shallow boat conformation in RbTCNQ(I)

This conformation can be considered to be the result of the presence of the high spin densities on the quinoid methine carbons on neighbouring TCNQ^{•−} anions attracting each other, whereas the nitrile groups tend to repel each other as a result of their high negatively charge density^{53,54}. In RbTCNQ(I), the interplanar distance between the TCNQ^{•−} anions is 3.159 Å alternating with a larger distance of 3.484 Å. Interestingly, the perpendicular distance of 3.159 Å in RbTCNQ(I) is considerably shorter than the corresponding distance of 3.4 Å, which is normally recorded between adjacent aromatic rings¹⁹⁵. Therefore, there is a strong π orbitals interactions within the closely separated TCNQ^{•−} dimer components. On the other hand, in the complex of RbTCNQ(II), the TCNQ^{•−} anion stacks are assembled parallel to each other and form monadic columns. The overlap between neighbouring TCNQ^{•−} anions is the ring-external bond (R-B) type, an arrangement which is characteristic of highly conductive TCNQ complexes^{39,209,215}.

In RbTCNQ(III), the TCNQ^{•−} anions are stacked in a face-to-face behaviour with further assembling into infinite monadic columns²⁰⁹. The ring-external bond (R-B) overlap of two adjacent TCNQ^{•−} units is the same packing motif as viewed in the crystal structure of RbTCNQ(II), whilst the arrangement of the TCNQ^{•−} anions in the stacks is the same in RbTCNQ(I)²⁰⁹. The perpendicular distance between neighbouring TCNQ^{•−}

anions is 3.33 Å, which is slightly shorter than the distance within RbTCNQ(II). The Rb^+ cation is surrounded by eight negatively charged nitrogen atoms from $\text{TCNQ}^{\cdot-}$ anions in a distorted cube geometry²⁰⁹.

Crystal structures of Rb_2TCNQ_3 at 113K and 294K have been published^{211,212}. The crystal structure of Rb_2TCNQ_3 at 294K is isomorphous with Cs_2TCNQ_3 . There are two types of TCNQ environments within the packing patterns, which are centric and noncentric. The definition of centric here refers to molecules lying on the centres of symmetry and those not on these centres are described as noncentric²¹². Because of the formation of TCNQ triads within the crystal structure, the planes (of the quinoid moieties) through adjacent moieties are not exactly parallel. Therefore, the definition of the interplanar distance should be considered^{53,54}. The Rb^+ cation is coordinated by eight nitrogen atoms of different TCNQ molecules, forming a distorted cube. On decreasing the temperature to 113K, the molecule geometries of corresponding TCNQ units in Rb_2TCNQ_3 do not change significantly. The TCNQ groups remain non-planar, with cyano groups bending out of the planes^{211,212}.

Within the crystal structure of Cs_2TCNQ_3 , whilst the aromatic ring and attached methylene carbons lie in a plane, each dicyanomethylene group is nonplanar, being twisted relative to the central aromatic ring²¹³. Fritchie and Arthur²¹³ commented that these major distortions were ascribed to the rigid and close packing patterns within TCNQ columns. For each Cs^+ cation, eight nitrogen atoms from adjacent TCNQ columns are primarily coordinated to the central metal ion forming a cube geometry. For further details about individual TCNQ groups within a column, the TCNQ units and stack, the readers are referred to Van der Wal and Van Bodegom^{211,212}. Figure 2.26 shows the definition of the average bond lengths of TCNQ molecule by assuming D_{2h} symmetry. Table 2.3 lists the structure features of alkali metal TCNQ salts. The average bond lengths (a-f) are defined in Figure 2.26.

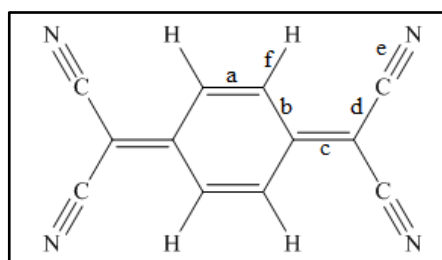


Figure 2.26 Define the bond lengths within TCNQ molecule

Chapter 2

| Compound | T | Colour | Space group | Type of stack | Overlap type | Interplanar distance/Å | Average bond lengths/Å | | | | | |
|--|------|----------------|--------------------|---------------|-------------------------|----------------------------------|------------------------|--------|--------|--------|--------|--------|
| LiTCNQ ¹⁹⁵ | R.T. | Purple | tetragonal | diads | N/A* | N/A* | a | B | c | d | e | f |
| NaTCNQ ²⁰⁶ | R.T. | Purple | C-1 | diads | R-R | 3.223 3.200 3.505 3.480 | N/A* | N/A* | N/A* | N/A* | N/A* | N/A* |
| NaTCNQ ²⁰⁷ | 353K | N/A* | P2 ₁ /n | regular | R-R | 3.385 | 1.355 | 1.427 | 1.419 | 1.420 | 1.141 | 0.979 |
| KTCNQ ²¹⁶ | R.T. | Red | P2 ₁ /c | regular | N/A* | 3.43 3.44 | 1.353 | 1.420 | 1.413 | 1.417 | 1.147 | 0.987 |
| KTCNQ ²⁰⁸ | R.T. | N/A* | P2 ₁ /n | diads | R-R | 3.240 3.234 3.554 3.580 | 1.411 | 1.450 | 1.430 | 1.430 | 1.127 | N/A* |
| KTCNQ ²⁰⁸ | 413K | N/A* | P2 ₁ /c | regular | R-R | 3.479 | 1.366 | 1.417 | 1.420 | 1.416 | 1.144 | 0.997 |
| RbTCNQ(I) ¹⁹⁵ | 113K | reddish-purple | P2 ₁ /c | diads | R-R R-B (slipped) | 3.159 3.484 | 1.348 | 1.416 | 1.399 | 1.420 | 1.133 | 0.936 |
| RbTCNQ(II) ²¹⁰ | R.T. | dark purple | P-1 | regular | R-B | 3.43 | 1.373 | 1.423 | 1.420 | 1.416 | 1.153 | 1.074 |
| RbTCNQ(III) ²⁰⁹ | R.T. | N/A* | P4/n | regular | R-B | 3.33 | 1.343 | 1.406 | 1.355 | 1.401 | 1.151 | N/A* |
| Rb ₂ TCNQ ₃ | R.T. | N/A* | P2 ₁ /c | triads | R-B R-R | 3.26 3.12 | 1.308 | 1.425 | 1.447 | 1.420 | 1.102 | N/A* |
| | | | | | | | 1.368Δ | 1.430Δ | 1.410Δ | 1.426Δ | 1.142Δ | 1.080Δ |
| Rb ₂ TCNQ ₃ ²¹¹ | 113K | dark purple | P2 ₁ /c | triads | R-B R-R | 3.23 3.07 | 1.339¶ | 1.448¶ | 1.376¶ | 1.440¶ | 1.136¶ | 1.081¶ |
| | | | | | | | 1.368Δ | 1.432Δ | 1.419Δ | 1.426Δ | 1.155Δ | 1.077Δ |
| Cs ₂ TCNQ ₃ ²¹³ | R.T. | N/A* | P2 ₁ /c | triads | R-B R-R | 3.22 3.26 | 1.355¶ | 1.448¶ | 1.385¶ | 1.436¶ | 1.153¶ | 1.077¶ |
| | | | | | | | 1.356Δ | 1.427Δ | 1.411Δ | 1.419Δ | 1.153Δ | 0.992Δ |

* N/A: not available

¶: TCNQ⁰

Δ: TCNQ⁻

Table 2.3 Structure features of alkali metal TCNQ salts

2.6.3 Ammonium (NH₄⁺)TCNQ salt

The solid state behaviour of NH₄TCNQ has been studied by Kobayashi²¹⁵. The crystals of NH₄TCNQ exhibit dimorphism with purple NH₄TCNQ(I) crystallising from a

solution of mixed THF and MeOH, whereas bluish-purple $\text{NH}_4\text{TCNQ(II)}$ is grown from a solution of MeCN. It is found that the crystals of $\text{NH}_4\text{TCNQ(I)}$ are twinned and unsuitable for crystal structure analysis^{215,217}. However, a phase transition is recorded at 301K based on the pattern changes on the oscillation photographs²¹⁵.

In the complex of $\text{NH}_4\text{TCNQ(II)}$, $\text{TCNQ}^{\bullet-}$ units form a face-to-face π -stacked monadic column along c axis. The packing motif, which is exhibited in Figure 2.27, is quite similar to that of RbTCNQ(I) . The overlap pattern between the adjacent $\text{TCNQ}^{\bullet-}$ is ring-external bond (R-B) type as seen in RbTCNQ(II) and the intermolecular distance is 3.31 Å. The phase transition from monomer to dimer has been detected at -58°C through resistivity measurements²¹⁵. Figure 2.27 shows the average structure of NH_4TCNQ .

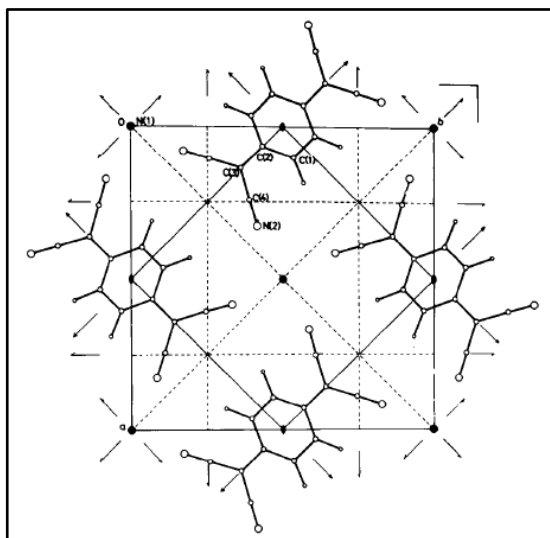


Figure 2.27 The average structure of NH_4TCNQ ²¹⁵

2.6.4 Alkaline earth metal TCNQ salts

Li et al.²¹⁸ have studied three alkaline earth metal TCNQ salts, which were $[[\text{M}_2(\text{TCNQ})_3(\text{H}_2\text{O})_6]^+\text{TCNQ}]_n$ ($\text{M} = \text{Ca}$ (1), Sr (2) and Ba (3)). Each of these were synthesised by reacting of corresponding $\text{MCl}_2 \cdot n\text{H}_2\text{O}$ ($\text{M} = \text{Ca}$ (1), Sr (2) and Ba (3)) with LiTCNQ . X-ray crystallographic analysis revealed that three alkaline earth metal TCNQ salts are isomorphic. The packing pattern of TCNQ units and each alkaline earth metal act as an important role in determining the resulting 3D network structures. For example, in a typical structure of complex $\text{Ca}(\text{TCNQ})_2(\text{H}_2\text{O})_3$, each Ca^{2+} ion is coordinated by four different neighbouring $\text{TCNQ}^{\bullet-}$ anions and four oxygen atoms from neighbouring water molecules, resulting in a distorted square anti-prismatic geometry as

each Ca^{2+} ion is crystallographically equivalent in the 3D network structure. Li et al.²¹⁸ reported that the bond lengths of M-NC and M-O show a continuously decreasing trend, paralleling the decrease from the largest Ba^{2+} to the smallest Ca^{2+} .

FT-IR spectra of three alkaline earth metal TCNQ salts all exhibit sharp stretching bands for the cyano groups, and bands representing for the coordination of the TCNQ to the alkaline earth metal ions and water molecules. Other measurements, such as the cyclic voltammetry and differential pulse voltammetry of alkaline earth metal TCNQ salts, exhibit a reversible one-electron oxidation and reduction process²¹⁸.

2.6.5 Transition metal TCNQ salts

2.6.5.1 Cu(TCNQ) (I/II)

Figure 2.28 shows the different packing motifs of CuTCNQ(I) and CuTCNQ(II).

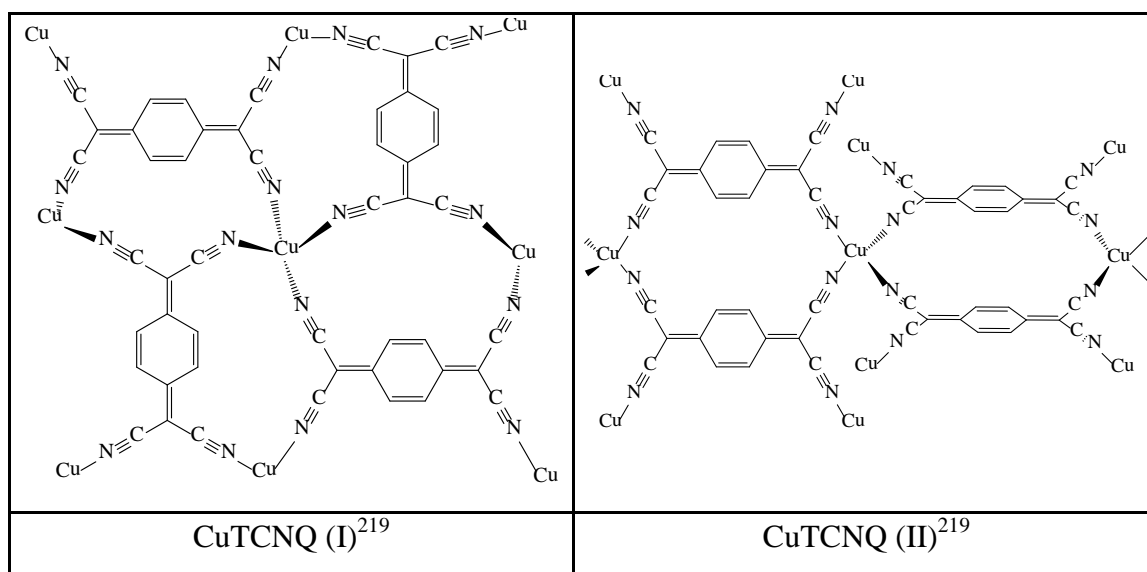


Figure 2.28 The different packing motifs of CuTCNQ(I) and CuTCNQ(II)

The complexes such as charge transfer salts^{220,221}, organometallic compounds^{220,221} and coordination polymers based on the properties of TCNQ^{220,221} have generated considerable attention over the past years, particularly for applications such as electronic storage^{220,221} and light emitting devices^{220,221}. For example, CuTCNQ has received particular attention^{30,219,222}. CuTCNQ forms two polymorphs each based on the repeating pattern of a four-coordination Cu^+ cation and four negatively charged nitrogen atoms from adjacent $\text{TCNQ}^{\bullet-}$ anions. The comparison of these two different phases of CuTCNQ reveals two primary features associated with the different packing motifs of

TCNQ^{•-} anions. First is the different orientation of TCNQ^{•-} anions. In CuTCNQ(I), the TCNQ^{•-} anions are stacked in alternating rows with four negatively charged anions surrounding each metal ion with adjacent TCNQ^{•-} anions rotated in respect to each other by $\approx 90^\circ$. This packing motif is similar to that seen for alkali metal TCNQ salts²¹⁹. In CuTCNQ(II), a new packing motif is presented, in which there is an infinite array of coplanar TCNQ^{•-} units, all of which are orientated in the same direction. The other difference between these two phases concerns the type of interpenetration which occurs. In CuTCNQ(I), the distance between adjacent TCNQ^{•-} anions within a columnar stack is 3.24 Å. Meanwhile, the interpenetration of CuTCNQ(II) does not bring TCNQ^{•-} units close enough to form a face-to-face π stacking pattern, the vertical distance between parallel TCNQ^{•-} anions being 6.8 Å. On the basis of their formulation as compounds containing TCNQ^{•-} anions, IR spectra of the two phases of CuTCNQ are similar²¹⁹. Heintz et al.²¹⁹ suggested that the number of absorption bands representing of cyano groups were different. The kinetic product in phase I was soluble in acetonitrile and could be converted into its corresponding thermodynamic phase, which was phase II, gradually by varying the temperature. Both phases of CuTCNQ were dark purple crystalline salts, which could be distinguished by scanning electron microscopy and powder X-ray diffraction. Different phases of CuTCNQ lead to dramatically different conductivity properties. Both phases of CuTCNQ behave as semiconductors, CuTCNQ(I) has a conductivity of 0.25 S cm^{-1} at room temperature, whereas phase II is nearly insulating with a value of $1.3 \times 10^{-5} \text{ S cm}^{-1}$ at room temperature, respectively. The magnetic properties have been measured for phase I, which is essentially diamagnetic, whereas phase II exhibits Curie-Weiss behaviour when the temperature is low enough²¹⁹.

2.6.5.2 Ag(TCNQ) (II)

Figure 2.29 shows the packing motif of AgTCNQ(II), with forming overlapping orthogonal geometry. Four-fold distorted tetrahedral coordination of the Ag⁺ cations²²³.

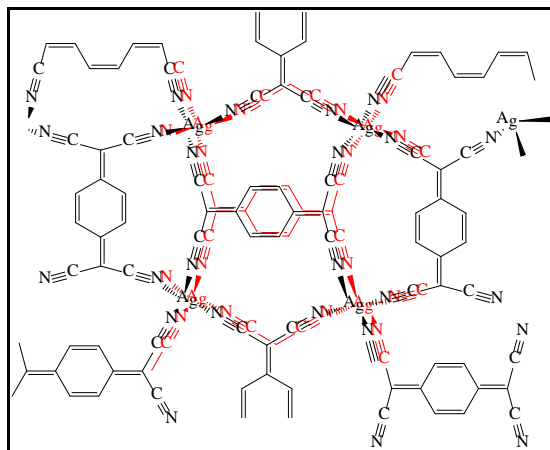


Figure 2.29 The packing motif of AgTCNQ(II)²²³

As viewed in Figure 2.29, the Ag^+ cation and TCNQ^- anion are columnated parallel to the short axis. Distorted tetrahedron geometry is formed, in which one Ag^+ cation is coordinated by four negatively charged nitrogen atoms of cyano groups²²³. The resistivity value of simple AgTCNQ salts is $8 \times 10^5 \Omega \text{cm}$, and the perpendicular distance between the adjacent TCNQ^- planes is 3.50 Å, which is larger than the corresponding value of neighbouring aromatic rings^{195,223}. TCNQ^- units do not display a common shallow “boat” conformation with the nitrogen atoms on each end of cyano groups raised above the mean plane of each TCNQ^- molecule^{223,224}. As O’Kane et al.²²⁵ indicated that both phases of AgTCNQ can be synthesised in bulk using two different synthetic routes. Compared with the case in CuTCNQ(I/II), the kinetic phase AgTCNQ (I) does not easily convert into its corresponding thermodynamic phase II. Both phases of AgTCNQ are similar because of their structural similarities and their basic formation of complexes of TCNQ^- . The corresponding absorption bands represented in cyano groups can be analysed from IR spectra, in which phase I can be distinguished with phase II based on the different wavenumbers²²⁵. From the Raman spectra, researchers can determine the structure of AgTCNQ based on the characteristic principal vibration modes^{224,226}. In addition, in AgTCNQ(II), the strongly dimerised feature of the organic acceptor is such that the thermal activation of the triplet state is difficult to be recorded in the accessible temperature range²²⁵.

2.6.6 Other binary $\text{M}(\text{TCNQ})_2(\text{H}_2\text{O})_2$ family members (M = Mn, Fe, Co, Ni)

A series complexes of binary $\text{M}(\text{TCNQ})_2(\text{H}_2\text{O})_2$ (M = Mn, Fe, Co, Ni) have been studied by Nafady et al.^{29,221,227-229}. All of the complexes are synthesised by the

electrocrystallisation method. Detailed knowledge is elucidated by different measurements, such as cyclic voltammetry, chronoamperometry, electrochemical quartz crystal microbalance and galvanostatic methods together with IR, Raman and other microscopic techniques, clearly establishing the differences in the electrocrystallisation synthesised binary $M(\text{TCNQ})_2(\text{H}_2\text{O})_2$ ($M = \text{Mn, Fe, Co, Ni}$) complexes. Particularly in cyclic voltammetry, the effect of voltammetric scan rate, electrolysis time, electrolyte concentration, temperature, and method of electrode modification on the preferential selection of specific transition metals cations have been explored. For Nafady et al.^{29,221,227-229}, their contribution in this study highlights the significance in using the electrocrystallisation method in synthesising and managing the morphology and stoichiometry of a series of binary $M(\text{TCNQ})_2(\text{H}_2\text{O})_2$ ($M = \text{Mn, Fe, Co, Ni}$) complexes.

2.6.7 Lanthanide TCNQ complexes: Its compounds, derivatives and analogues

Figure 2.30 shows the plots of atomic radii of lanthanides as function of atomic number.

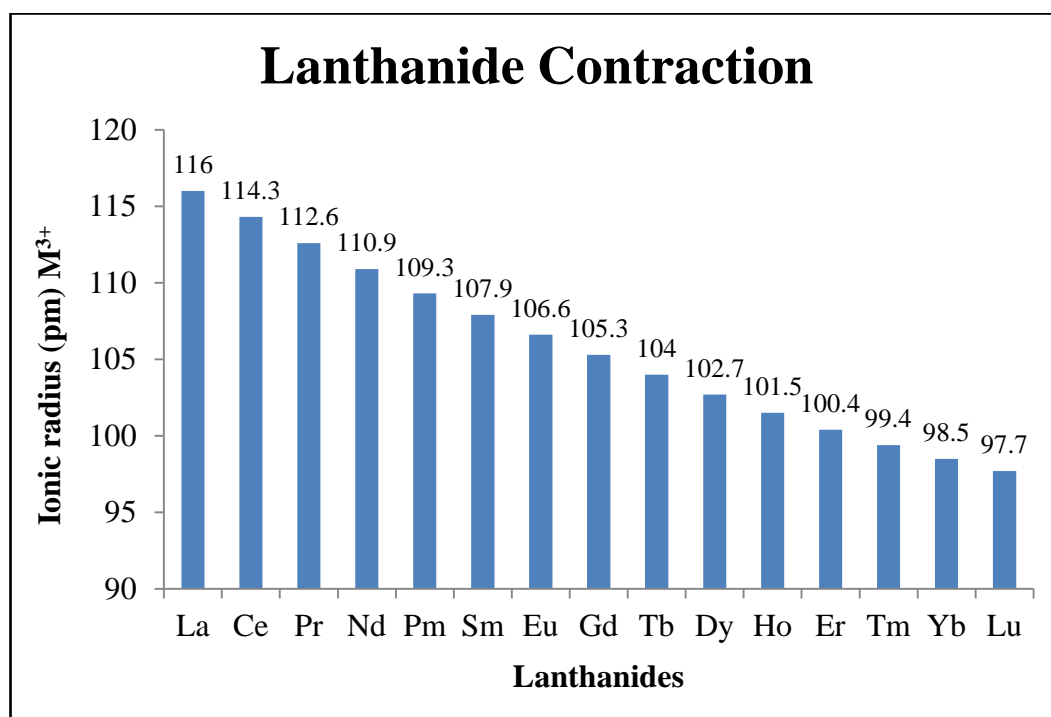


Figure 2.30 Plots of atomic radii of lanthanides as function of atomic number²³⁰

Because of the lanthanide contraction, the size of the lanthanide atoms decreases regularly and steadily with the increasing atomic number. The contraction is because of the f electrons have a poor ability to screen other valence electrons away from the nuclear charge²³⁰. Apart from europium and ytterbium, all of the lanthanide metals are

Chapter 2

considered to consist of Ln^{3+} ions with three electrons per atom dedicated to form metallic bonding. Therefore, europium and ytterbium are best regarded as Ln^{2+} with only two electrons in forming metallic bonding. This accounts for the greater metallic radii of europium and ytterbium in respect to other lanthanides, which have more valence electrons for metallic binding and as a result of small size with the help of stronger force of attraction reducing the inter nuclear distance²³¹.

Lanthanide ions are classed as hard Lewis acids and, with hard bases such as negatively charged groups. They can form non-coordination electrostatic bonds²³². Europium and terbium, which have useful fluorescence properties, are especially interesting. Anion sensing using luminescent lanthanide complexes is a well-established technique. Anion binding leads to changes in the spectra of lanthanide ions, which can provide useful information about the nature of this binding²³³.

The synthesis of ligand lanthanide complexes is of interest in application, such as functional materials²³⁴. In particular, the unique magnetic properties of lanthanide complexes have been of much interest²³⁵. Lanthanide ions show large anisotropic magnetic behaviour²³⁶ and when combined with organic radicals or metal ions, which are paramagnetic, the lanthanide ions can be used to synthesis molecular based magnets²³⁷. Because of their luminescence and paramagnetic properties, the prospect of applications of lanthanide macrocyclic ligand complexes in biology, chemistry and medicine have provided other novel reasons for further research²³⁸⁻²⁴¹. During the past two decades, with the wide variety of macrocycles being made, the number of these complexes is rapidly increasing and includes coronands as well as cryptands¹⁵³, crown ethers^{124,126} and their chemically modified derivatives and calixarenes^{128,242}.

TCNQ lanthanide complexes have become a hot topic for discussion as a result of their potentially interesting optical and ligand moderated magnetic properties²³⁵. According to Zhang et al.²⁴³, reaction between trivalent lanthanide ions $\text{TCNQ}^{\cdot-}$ anions can form different coordination environment of TCNQ lanthanide complexes based on the different reaction solvent, which will affect the packing pattern of crystal structures. The magnetic study of different TCNQ lanthanide complexes reveals an antiferromagnetic coupling interactions, which originate from the π - π interactions between $\text{TCNQ}^{\cdot-}$ anions. Cyclic voltammograms of TCNQ lanthanide complexes exhibit a reversible one electron oxidation and reduction process.

2.6.8 Cyanine dye-TCNQ complexes

The purpose of using cyanine dyes as the counter cations is that the polarisability of these cations and their π -stacking properties can be varied through variation of the heteroatoms present and the crystal structure of the complexes will be influenced by the shape and size of the cation²⁴⁴. Because of their propensity to form face-to-face π stacks and their cationic nature, cyanine dyes have for long been of interest as counter ions for TCNQ^{•-} salts. Klanderman and Hoesterey²⁴⁴ published the preparation of a large number of cyaninium TCNQ salts. Figure 2.31 shows the basic skeleton of cyaninium cations.

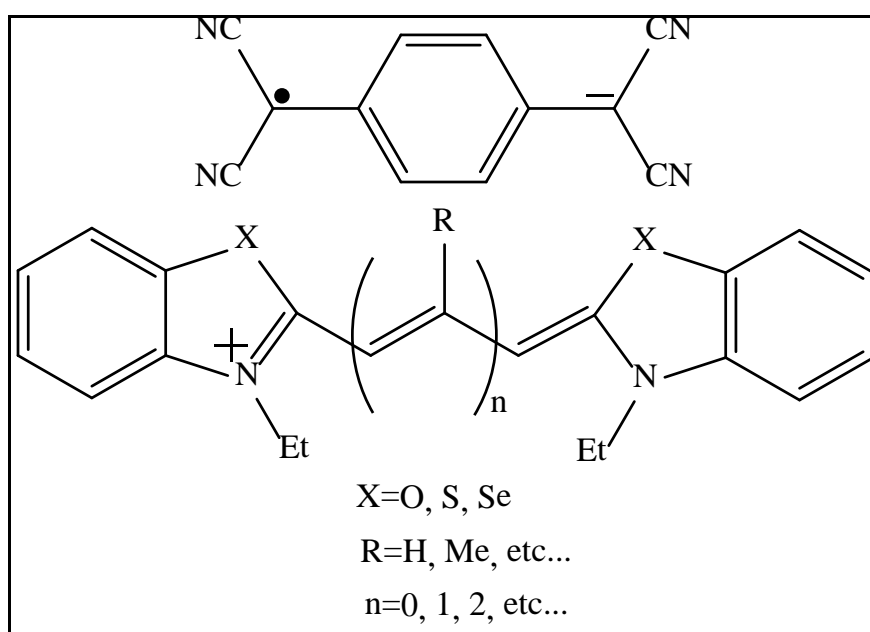


Figure 2.31 Basic skeleton of cyaninium cations used

Although all these four different organic dye complexes have an N-ethyl group, each of them can exhibit distinct properties, by existing as either *cis*- or *trans*- to adjacent units as well as the different substituents on the R position. The counter ions play an important role in determining the solid state architectures. Even slight changes in size or position will lead to huge difference. The halide is a counter ion, which can sit in the cavity between the organic dye columns because its size is small. When the counter ions are bigger or molecules such as TCNQ the packing pattern will be totally different and the infinite mixed or segregated stacks will be formed. Figure 2.32 shows the formation of cyanine dye-TCNQ complexes.

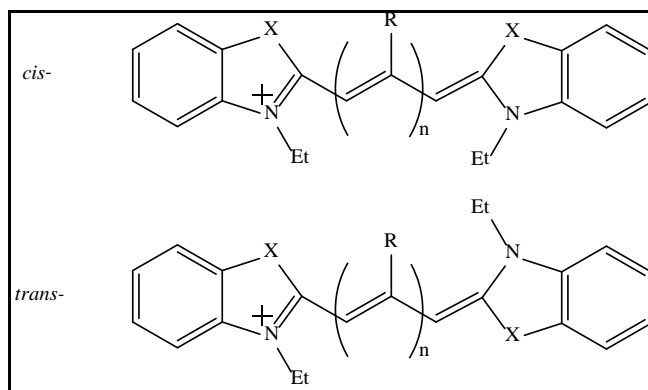


Figure 2.32 The formation of cyanine dye-TCNQ complexes

Figure 2.32 shows the cyanine cation absorption data and corresponding complex TCNQ salt conductivity data²⁴⁴.

| Cation (R^+) | λ_{\max} (nm) | σ_{300} (S/cm) | E_a (eV) | m.p. ($^{\circ}\text{C}$) |
|------------------|-----------------------|-----------------------|------------|-----------------------------|
| <p>1</p> | 375 | 5.0×10^{-3} | 0.27 | 244-247 |
| <p>2</p> | 423 | 6.7×10^{-3} | 0.21 | 276-278 |
| <p>3</p> | 430 | 4.8×10^{-2} | 0.22 | 288-290 |
| <p>4</p> | 519 | 7.0×10^{-1} | 0.058 | 253-255 |
| <p>5</p> | 557 | 1.5×10^{-1} | 0.067 | 267-268 |

Figure 2.33 Cyanine cation absorption data and corresponding complex TCNQ salt²⁴⁴

In Klanderman and Hoesterey²⁴⁴, for the simple cyanine cations **1**, **2** and **3**, the conductivity behaviour of the corresponding TCNQ complexes appears to be associated with the polarisability of the dye-cation. In compounds **4** and **5**, because the carbocyanines have higher polarisability than the simple cyanines, the corresponding TCNQ complexes of these carbocyanines are normally more highly conductive²⁴⁴.

Shibaeva and Atovmyan²⁴⁵ studied the solid state behaviour of a number of conducting TCNQ complexes. In particular, they reported the behaviour of the complexes of 3,3-diethylthiacyanine and the 1:2 complex of 3,3'-diethylcarbocyanine with TCNQ, respectively. In the complex of 3,3-diethylthiacyanine with TCNQ, instead of isolated infinite anion stacks, the crystal packing consists of discrete pairs of anions with a perpendicular distance of 3.23 Å. The stacks of dye molecules lie parallel in respect to each other and the interplanar distance is approximately 3.65-3.68 Å. The conformation of dye molecule is flat and the bending angle is by *ca.* 5° in respect to the conjugated rings²⁴⁵.

In the 1:2 complex of 3,3'-diethylcarbocyanine with TCNQ, the solid-state structure consists of alternating layers. The perpendicular distance within a TCNQ pair is 3.29 Å without any overlap to adjacent pairs. Each TCNQ mean plane is parallel to each other. The conformation of the dye molecules is flat and the bending angle is by *ca.* 6° in respect to the conjugated rings, which is larger than the corresponding angle in the complex of 3,3-diethylthiacyanine with TCNQ²⁴⁵. The conductivity value of 3,3'-diethylcarbocyanine with TCNQ is $1.5 \times 10^5 \text{ S cm}^{-1}$, $E_a = 0.3 \text{ eV}$ ²⁴⁵.

The solid state behaviour of a number of cyanine dye TCNQ complexes has been reported^{245,246}, and two examples of cyaninium TCNQ^{•-} complexes are shown below and illustrate some of the possible structures which can be formed and how the different cations can determine the solid state architecture. Table 2.4 shows two typical cyanine dye-TCNQ complexes.

| Cation name | Abbreviation | X | R | n |
|----------------------------|--------------|---|---|---|
| 3,3'- Diethyloxacyaninium | OC7 | O | H | 0 |
| 3,3'- Diethylthiacyaninium | SC7 | S | H | 0 |

Table 2.4 Two typical cyanine dye-TCNQ complexes

Figure 2.34 shows a stack of OC7-TCNQ complex.

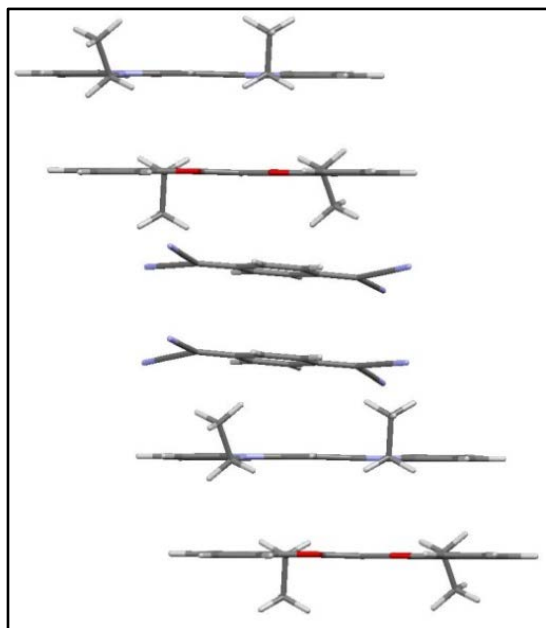


Figure 2.34 A stack of OC7-TCNQ complex (ref code: JEXJEB)³⁶

The complex of OC7-TCNQ forms alternating stacks of cyaninium dimers and TCNQ^{•-} dimers forming $\cdots D^+ D^+ A^- A^- D^+ D^+ \cdots$ columns, which are packed into sheets, forming a herringbone array in relation to neighbouring sheets. The cyanine cation is flat with the ethyl substituents in *cis*- formation. Within the TCNQ dimer, the adjacent TCNQ units are short-axis slipped. The slip angle is 16° and the perpendicular distance is by *ca.* 3.35 Å³⁶. Figure 2.35 shows the packing pattern of SC7-TCNQ complex.

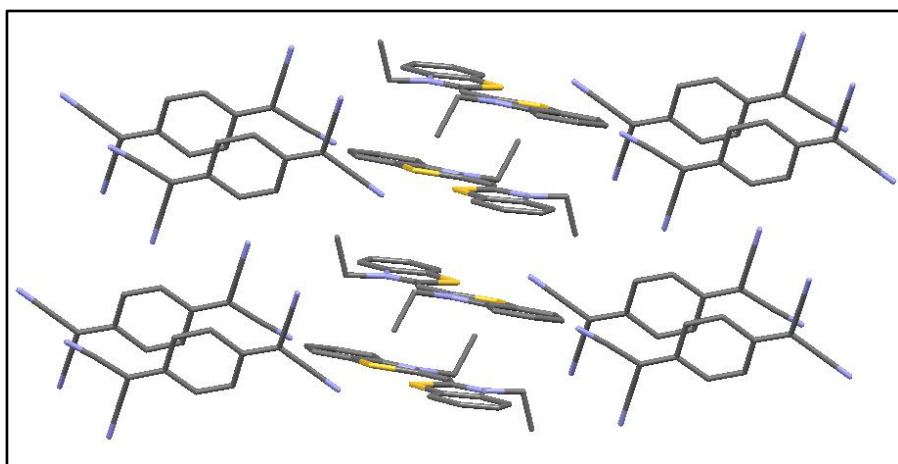


Figure 2.35 Packing pattern of SC7-TCNQ complex (ref code: ECTCN10)²⁴⁷

However, the solid state architecture of the sulphur analogue, SC7-TCNQ is different from the OC7-TCNQ. The TCNQ^{•-} dimers form infinite stacks separated SC7 dye cations. Close contact occurs between the cyano group and sulphur atoms in a manner similar to that seen in TTF-TCNQ and might be the explanation the different solid state architecture²⁴⁷.

A study of the solid state behaviour of the donor-acceptor complexes of organic dye-TCNQ complexes, such as OC7-TCNQ and SC7-TCNQ, can help to lead to a better understanding of the factors, which control the solid state behaviour of TCNQ complexes. Changing the substituents from oxygen to either sulphur or selenium leads to a significantly different crystal architecture, which will affect the physical properties of such molecules. In addition, introduction of different substituents around the cyanine core can also play an important role here.

The counter ion plays an important role in controlling the solid state architecture. Even slightly changes in size, shape or position will lead to huge difference. The halide is used as counter ion for cyanine-dyes and thus can sit in the cavity between organic dye columns because of its size is small. When the counter ions are bigger and non-spherical, such as TCNQ^{•-}, the packing pattern will be totally different and infinite mixed or segregated stacks will be formed. In addition to forming face-to-face π stacks in the solid state, other intramolecular interactions, such as cyano-sulfur contacts, can also play an important role here.

2.6.9 TTF-TCNQ

In TTF-TCNQ, the TTF (electron donor) and TCNQ (electron acceptor) stacks separately, which leads to the formation of segregated columns. The TTF can all too easily lose an electron and form a radical cation, which tends to form π stacked columns in the solid state. When TTF is crystallised with TCNQ, the resulting complex contains alternate stacks, in which the TTF units are partially oxidised and the TCNQ units are partly reduced in turn. At room temperature, the components in each stack are evenly spaced and the material shows metallic behaviour, but when the temperature is decreased below 77K, dimerization occurs within the stacks and a semiconductor is formed. The conductivity of TTF-TCNQ is high at the room temperature, which is $400 \text{ S}\cdot\text{cm}^{-1}$ ²⁴⁸. Figure 2.36 shows the schematic representation of the TTF-TCNQ structure,

the donor and acceptor molecules are arranged in segregated stacks with the molecular plane tilted in respect to the stacking axis of $b[010]$ ²⁴⁸. The complex of TTF-TCNQ is regarded as a two-chain conducting material as the segregated stacks of both TTF and TCNQ contribute to the conductivity behaviour²⁰.

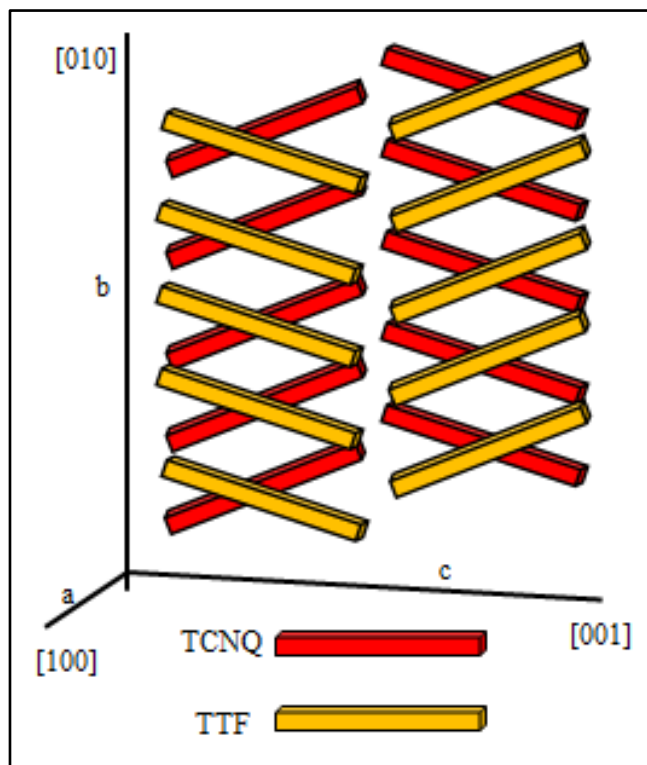


Figure 2.36 Schematic representation of the TTF-TCNQ structure²⁴⁹

2.6.10 Electrical behaviour of alkali metal TCNQ salts

All of the alkali metal TCNQ salts are displayed as semiconductors either above or below the phase transition temperature, with different corresponding activation energies for each phase^{53,54}. As an MTCNQ example of how the temperature dependence with the resistivity ρ exhibited as a reasonable curve was discussed by Afify et al.⁶⁵ Figure 2.37 shows the electrical resistivity against $1000/T$ for the alkali metal TCNQ salts.

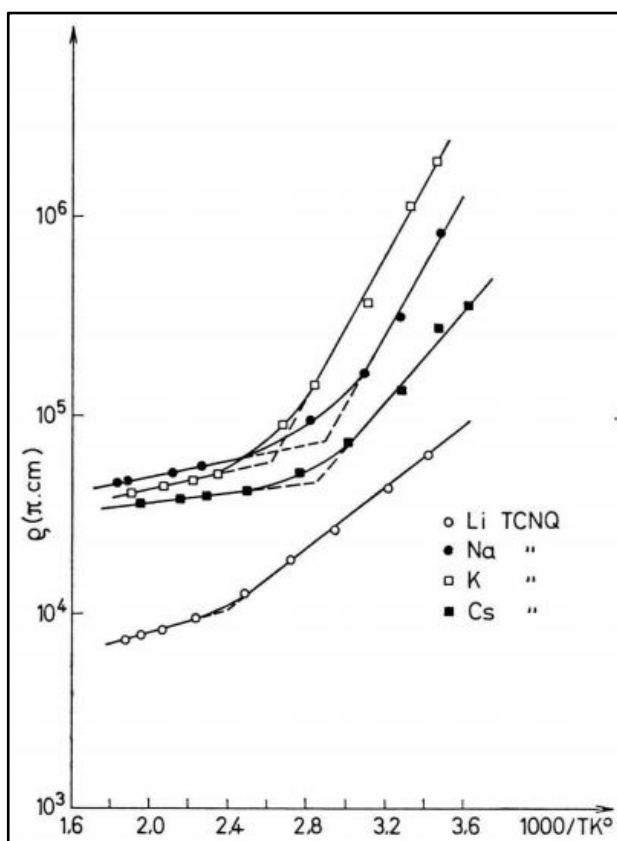


Figure 2.37 Electrical resistivity against $1000/T$ for the alkali metal TCNQ salts⁶⁵

As Afify et al.⁶⁵ said, TCNQ displayed a linear relation between electrical resistivity and temperature, which demonstrated that TCNQ behaved as an intrinsic semiconductor. As viewed in Figure 2.37, each of the curves contained two separated linear sections, connected by an inflection point, which represents the transition temperature. Afify et al.⁶⁵ observed that the resistivity at the transition temperature point was about 13 times lower than that at room temperature. In addition, Afify et al.⁶⁵ summarised the values representing the electrical resistivity of alkali metal TCNQ salts at room temperature ($290 \pm 2\text{K}$), the change of the activation energies during the phase transitions and the high temperatures. Table 2.5 shows the physical properties of TCNQ and its salts at $290 \pm 2\text{K}$.

| Substance | ρ (Ωcm) | E_1^* (e.v) | E_2^{**} (e.v) | E_1^*/E_2^{**} |
|--------------|------------------------------|---------------|------------------|------------------|
| TCNQ | 2.0×10^{10} | 0.56 | N/A*** | N/A*** |
| LiTCNQ | 5.6×10^4 | 0.16 | 0.057 | 2.80 |
| NaTCNQ | 8.8×10^5 | 0.34 | 0.041 | 8.29 |
| KTCNQ | 2.0×10^6 | 0.43 | 0.047 | 9.15 |
| Cs(TCNQ)TCNQ | 2.9×10^5 | 0.25 | 0.023 | 8.69 |

* E_1 : Activation energy for the low temperature range

** E_2 : Activation energy for the high temperature range

***N/A: Not available

Table 2.5 Physical properties of TCNQ and its salts at $290 \pm 2\text{K}$ ⁶⁵

Compared with TCNQ, the resistivity of the alkali metal TCNQ salts are three to six orders of magnitudes lower. This phenomenon can be explained as the quinonoid structure of TCNQ changed into its corresponding benzenoid $\text{TCNQ}^{\cdot-}$ unit. The π - π orbitals interactions will predominate in the process of conduction. In addition, Afify et al.⁶⁵ recorded that the observed resistivity of the alkali metal TCNQ salts followed the order of $\text{Li}^+ < \text{Na}^+ < \text{K}^+$. This trend could be explained as the decreasing cationic radius and, as a result, the interplanar spacing would be decreased correspondingly.

Sakai et al.^{202,203} found that in alkali metal TCNQ salts, the activation energy increased with the higher temperatures. All of the relative data had been summarised in Table 2.6. Especially for CsTCNQ, Sakai et al.^{202,203} observed that the resistivity changed monotonously with the temperature. The rapid increased resistivity value at high temperature was because of the decomposition of the complex. The resistivity for CsTCNQ was $6 \times 10^2 \Omega\text{cm}$ at room temperature. From room temperature to 400K, the activation energy was 0.16eV. Table 2.6 shows the activation energies of alkali metal TCNQ salts.

| Substance | E_1^* (e.v) | E_2^{**} (e.v) |
|-------------------------|---------------|------------------|
| NaTCNQ | 0.23-0.32 | 0.6-1.1 |
| KTCNQ | 0.15-0.45 | 0.4-0.6 |
| RbTCNQ (dark purple) | 0.16-0.22 | 0.22-0.4 |

* E_1 : Activation energy for the low temperature range

** E_2 : Activation energy for the high temperature range

Table 2.6 The activation energies of alkali metal TCNQ salts^{202,203}

The activation energy of NaTCNQ was from 0.23 to 0.32eV below the transition temperature and from 0.16 to 0.22eV above. The activation energy of KTCNQ was from 0.23 to 0.45eV below the transition point and from 0.15 to 0.31eV above. In the case of reddish-purple RbTCNQ, the activation energy was from 0.41 to 0.53eV below the transition point and from 0.28 to 0.37eV above. Table 2.7 shows the conductivity and activation energy measurements at room temperature of a single crystal of alkali metal TCNQ salts.

| MTCNQ Single Crystal | | | | |
|-----------------------------------|-------------------------------------|-----------------------|-------------------|--------------------|
| | Conductivity | Phase Transition Temp | Activation Energy | |
| Material | σ_{rt} (S·cm ⁻¹) | T_t (K) | E_a (low) (e.v) | E_a (high) (e.v) |
| NaTCNQ | 1.0×10^{-3} | 338 | 0.23-0.32 | 0.16-0.22 |
| KTCNQ | 5.0×10^{-3} | 391 | 0.23-0.45 | 0.15-0.31 |
| RbTCNQ(I) | 3.0×10^{-5} | 374 | 0.41-0.53 | 0.28-0.37 |
| RbTCNQ(II) | 1.0×10^{-2} | 231 | 0.16-0.19 | 0.16-0.19 |
| Cs ₂ TCNQ ₃ | 6.0×10^{-2} | 254 | 0.16 | 0.16 |

Table 2.7 Conductivity and activation energy measurements at room temperature^{193,202,203}

As viewed in Table 2.7, the values of conductivity (σ_{rt}) are different among different alkali metal TCNQ salts. This phenomena can be attributed to the various packing motifs in crystal structures. The conductivity properties of TCNQ^{•-} complexes arise

from the motion of the odd electrons along face-to-face π stacks of TCNQ⁻ anions²⁵⁰. In order to display the conductivity properties, the activation energy needs to overcome the Coulomb repulsion effect between adjacent unpaired electrons²⁵⁰.

The phase transitions contribute to a change in the type of packing and volume changes²⁵¹. Various packing motifs will lead to a change in the singlet-triplet separation energy, which can be recorded by ESR technique¹⁰⁷. The phase transition is associated with a change from a dimerised TCNQ⁻ columnar stack within the crystal to a uniform(monodic) column around a phase transition temperature¹⁰⁷.

The simple alkali metal TCNQ salts are all semiconductors with an activation energy, which decreases above the phase transition temperature. This phenomenon can be explained by the effect of temperature on the stacking columns and the intramolecular interactions²⁵¹.

2.6.11 Magnetic properties of TCNQ complexes

In this section, electrons spin/paramagnetic resonance will be stated firstly, with particular focus on the Zeeman Effect. Following this, the magnetic properties of TCNQ complex salts will be illustrated with theory background to support the generation of the triplet excited signal of TCNQ complexes. Finally, examples of TCNQ complexes will be stated with their corresponding ESR results attached.

2.6.11.1 Electron spin/paramagnetic resonance

ESR spectroscopy is a widely used technique for studying materials with unpaired electrons, which is particularly useful for studying metal complexes or organic radicals. Because each electron possesses an intrinsic angular momentum, it is known as 'spin'²⁵². Consequently, because the electron is electrically charged and since there is an external magnetic field, B_0 , associated with any moving charge, the spinning electrons will be correlated with the orientation in respect to an external magnetic field. In other words, by characteristic of its intrinsic angular momentum, an electron can be regarded as a tiny bar magnet²⁵³. By interacting with electromagnetic radiation, each orientation represents a discrete energy level. For example, for a single unpaired electron, there are only two possible orientations in respect to a given axis²⁵². The unpaired electron can either spin clockwise at a particular rate or it can spin anti-clockwise at the same rate. In

terms of the magnetic properties of an electron in an external magnetic field, it can align effectively with the direction of the external magnetic field or against it. It is the phenomenon, which generates the basis of the electron spin resonance method of studying materials with unpaired electrons²⁵³.

2.6.11.2 The Zeeman Effect

The energy levels will degenerate without an external magnetic field (B_0). However, the discrete energy levels studied in ESR spectroscopy are because of the interaction between an unpaired electron and an external magnetic field. This effect is called the Zeeman Effect²⁵⁴. Since energies are quantised, a single unpaired electron can only achieve two separated energy levels, which including a level of lower energy and a higher energy level, respectively. Specifically, a single unpaired electron has a level of lower energy when the momentum of the electron, μ , is parallel with the external magnetic field and a higher energy level with μ is anti-parallel with the external magnetic field. The phenomenon is described as a picture in Figure 2.38.

Along the direction of the external magnetic field, the two different energy levels are mainly affected by the electron spin, m_s . The parallel state is $m_s = -\frac{1}{2}$ and the anti-parallel state is $m_s = +\frac{1}{2}$, respectively. Because of the interaction between the electron spin and the applied external magnetic field, the energies gap between these two different levels can be calculated as:

$$\Delta E = g \mu_B B_0 \Delta m_s = g \mu_B B_0 \quad ^{254}$$

Where g is the g -factor; μ_B is the Bohr magneton, which is the intrinsic electron's magnetic momentum; B_0 is the applied external magnetic field; the change of the spin state $\Delta m_s = \pm 1$.

As discussed in previous paragraphs, without the external magnetic field, the two spin states will have the same energy. Therefore, there is no energy gap to be measured. The energies gap between the two different spin states is linear as a function of the magnetic field increases. Figure 2.38 describes the situation that when the external magnetic field is scanned, the energies of the two spin states of an unpaired electron diverge. With the application of an external magnetic field, the resonance will be generated when there is

an absorption of energy by the spins based on the energy difference between the two electron spin states, in which the gap is equal to $h\nu$ for the spectrometer²⁵⁴.

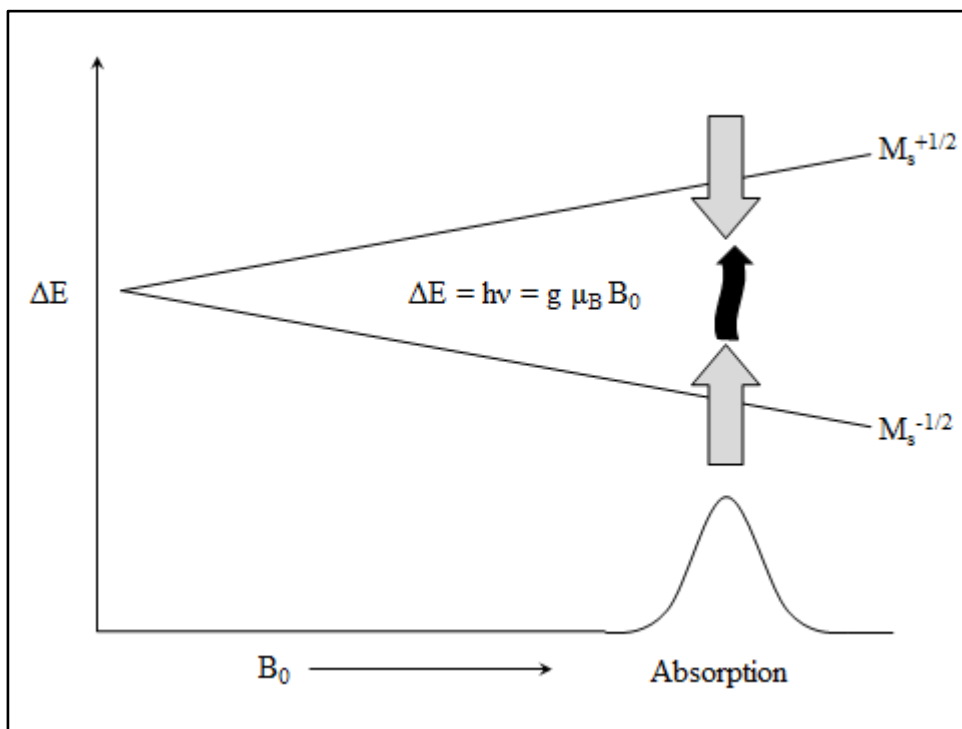


Figure 2.38 Explanation the divergence of the energies of an unpaired electron in a magnetic field²⁵⁴

2.6.11.3 Magnetic properties of TCNQ complexes

The technique of ESR is applied to study the magnetic properties of TCNQ complexes in order to achieve a more comprehensive understanding of the electronic states in these materials, especially crystalline samples which contain $\text{TCNQ}^{\cdot-}$ dimers in the corresponding crystal structures which can generate triplet exciton signals from singlet ground state under specific temperature. Figure 2.39 shows the energy level and ESR transitions as a function of magnetic field for an oriented triplet state molecule.

As seen in Figure 2.39, the energy levels will diverge on application of an external magnetic field. Two resonance absorption lines will be generated corresponding to transitions controlled by the high-field selection rule of $\Delta M = \pm 1$. This anisotropy is a result of the dipolar coupling of the two electrons and these transitions will take place at different fields²⁵².

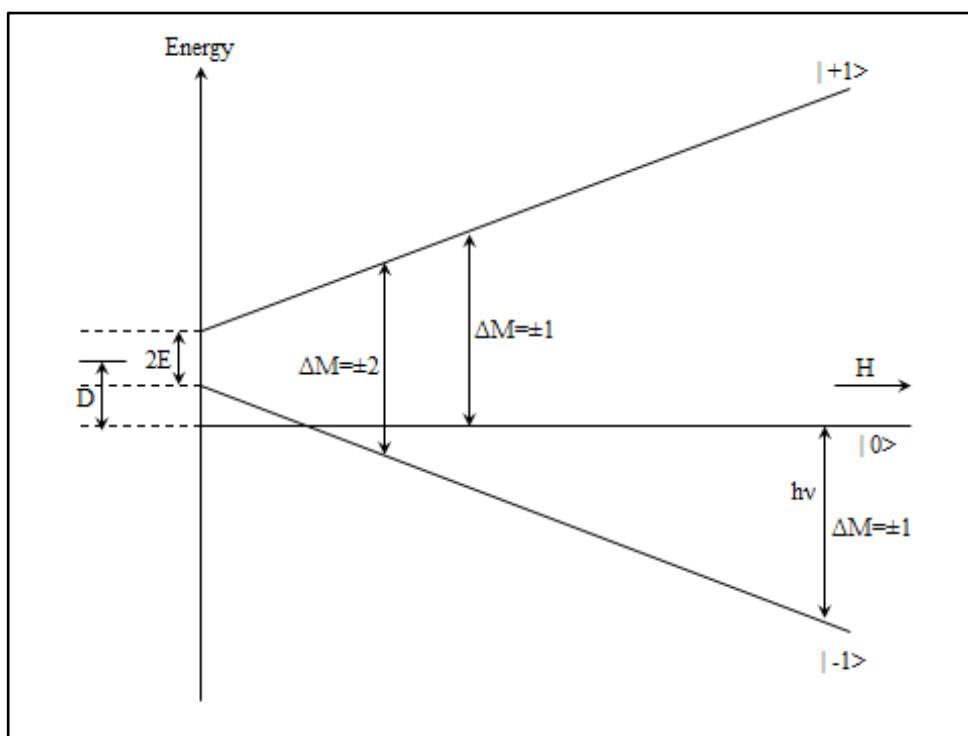


Figure 2.39 Energy level and ESR transitions as a function of magnetic field for an oriented triplet state molecule²⁵³

A detailed ESR studied by Bailey and Chesnut²⁰⁵, Jones and Chesnut²⁵⁵, and Kepler²⁵⁶ had commented on the existence of excited triplet states associated with ground singlet states in TCNQ complexes. If the two electron spins associated with the TCNQ⁻ anions did not interact with each other, which was a doublet electronic state, the line intensities would tend to follow the Curie Law with an easily calculated magnitude in Scheme 2.6, whereas generating a triplet excited state from a singlet ground state, the relative observed properties which should correspond with Scheme 2.7.

$$I = \frac{C}{T}$$

Scheme 2.6 The Curie Law

$$I = \frac{A}{T} \left[\exp\left(\frac{J}{kT}\right) + 3 \right]$$

Scheme 2.7 Relationship between the peak intensities in ESR spectra

2.6.11.4 ESR spectral characteristics associated with triplet excitons in TCNQ complexes

As Kepler²⁵⁶, Chesnut and Arthur Jr.²⁵⁷ mentioned, the complex Cs_2TCNQ_3 had two triplet signals with different orientations per unit cell and a broad central impurity peak resonance. The four outer lines represented the fine structure from two physically equivalent, geometrically non-equivalent triplet signals per unit cell. This situation was related to the two-fold screw axis of the $\text{P2}_1/\text{c}$ space group. The calculation of peak intensity (I) was based on the Scheme 2.7. The value of singlet-triplet separation (J) calculated from the magnitude of the susceptibility at 0, 50, 100, 150 and 200°C were 0.146, 0.136, 0.130, 0.123 and 0.116 eV, respectively. In addition, Kepler²⁵⁶ observed that the recorded value of the diamagnetic susceptibility, 3.28×10^{-4} emu/mol agreed with that calculated from Pascal's constants, which was 3.15×10^{-4} emu/mol. Based on Hibma and Kommandeur²⁵⁸ studies, complexes of KTCNQ, RbTCNQ and $\text{TMB}^+\text{TCNQ}^-$ were measured by the ESR technique. With the observation of dipolar splitting unequivocal, the ESR spectra proved that the signals derived from triplet excitons. From Rembaum et al.²⁵⁹, having a singlet-triplet transition model for simple paramagnetic TCNQ salt, the ESR peak intensity (I) can be calculated by Scheme 2.7. Additionally, Klanderman and Hoesterey²⁴⁴ commented that the ESR measurements on 2,4,6-triphenylpyridinium/-pyrylium/-thiapyrylium TCNQ complexes displayed a single, sharp resonance at $g=2.0038$.

2.6.12 Spectroscopic analysis of TCNQ and its corresponding $\text{TCNQ}^{\bullet-}$ salts

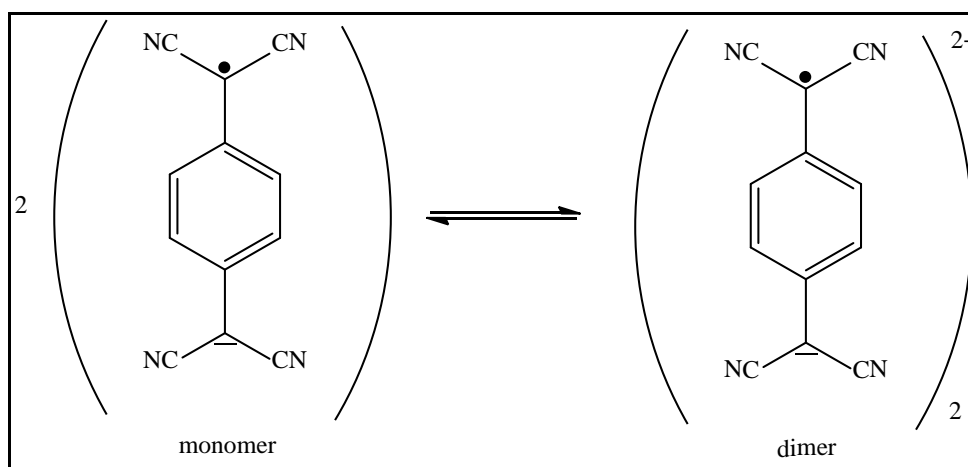
IR, Raman and UV-Vis spectroscopy are useful techniques for analysing TCNQ charge-transfer complexes, especially in distinguishing the presence of TCNQ in respect to its various redox states²⁶⁰, which have been utilised for analysing alkali metal TCNQ salts. Table 2.8 shows a comparison of the IR absorption bands observed of TCNQ and its corresponding $\text{TCNQ}^{\bullet-}$.

| | TCNQ (cm^{-1}) | TCNQ $^{\bullet-}$ (cm^{-1}) |
|--------------------------|---------------------------|---|
| -CN stretch | 2220 | 2190/2180 |
| C-H out of plane bending | 859 | 828 |
| C=C stretch | 1540 | 1581/1512 |

Table 2.8 IR absorption bands observed of TCNQ and its corresponding TCNQ $^{\bullet-}$ ^{261,262}

As TCNQ is reduced, changes are seen in its corresponding IR spectra. Acker and Hertler²⁶¹ reported the IR spectra of TCNQ $^{\bullet-}$ anions, especially in LiTCNQ. As viewed in Table 2.8, it can be seen that several changes occur upon the reduction from TCNQ $^{\circ}$ to its corresponding TCNQ $^{\bullet-}$. Two main variations are the splitting of absorption bands representing cyano groups and the conversion of C=C from conjugated into an aromatic system. Both of the two changes will lower the frequencies of the absorption bands, when the TCNQ is reduced into its corresponding TCNQ $^{\bullet-}$.

For UV-Vis spectroscopy in analyzing MTCNQ salts, the issue of reversible dimerization of TCNQ $^{\bullet-}$ in aqueous solution has been discussed by Boyd and Phillips²⁶³. Upon increasing the concentration of the TCNQ $^{\bullet-}$ solution at 25°C, a new band appears at $\lambda_{\text{max}} = 643 \text{ nm}$ and the corresponding TCNQ $^{\bullet-}$ anion absorption at $\lambda_{\text{max}} = 737 \text{ nm}$ becomes gradually weaker. These changes arise from the presence of a monomer-dimer equilibrium in aqueous solution. Scheme 2.8 shows the monomer-dimer equilibrium of TCNQ $^{\bullet-}$ in aqueous solution.



Scheme 2.8 The monomer-dimer equilibrium of TCNQ $^{\bullet-}$ in aqueous solution

No dimerisation has been observed in solvents other than water near room temperature, monomer being formed in acetonitrile, methanol and methylformamide. The stabilisation of the dimer is attributed to solvation effects, as methylformamide has a higher dielectric constant than water.

2.7 Discussion of 1:1/1:1:1 versus 2:1/2:1:1 TCNQ complexes

In this section, a series of ionophore-complexed MTCNQ complexes will be discussed with supporting information, especially for the ionophore-encapsulated alkali metal TCNQ complexes, which will be discussed in detail with a different packing pattern demonstrated.

2.7.1 Ionophore-complexed MTCNQ salts

Another potentially useful approach for controlling the solid state behaviour of $\text{TCNQ}^{\bullet-}$ salts is through ionophore complexation. In order to investigate this behaviour, Morinaga et al.⁶⁴ decided to study ionophore-complexed TCNQ salts, focusing mainly on metal cations and ammonium TCNQ salts. There were two types of MTCNQ complexes, which were $(\text{crown ether})_m(\text{M}^+\text{TCNQ}^{\bullet-})_n$ and $(\text{crown ether})_m(\text{M}^+\text{TCNQ}^{\bullet-})_n(\text{TCNQ}^0)$ respectively. The interactions between metal cations and $\text{TCNQ}^{\bullet-}$ anions would be weakened because the metal cation was surrounded by crown ether and this situation guided a change in the bulk physical properties of the resulting complex. The characteristics of (crown ether)MTCNQ salts had been listed in Table 2.9 and Table 2.10, respectively.

In addition, most of the complexes are isolated as crystalline materials having different colours. Ionophore complexes MTCNQ salts tend to be synthesised when the cavity of specific crown ether is comparable to the size of the relative metal cation. There are three common complexed situations, which happen between crown ethers and metal cations. If the cavity of crown ethers suits the size of bonding metal cation, the ion will sit in the cavity of crown ether with interactions formed between metal cation and oxygen atoms on the crown ether. Additionally, this situation will lead to synthesis of 1:1 or 1:1:1 (crown ether)MTCNQ salts successfully. However, if the size of the metal cation is larger than the cavity of bonding crown ether, there is a tendency to form a complex, in which the metal cation is sandwiched between the two crown ethers.

Furthermore, if the size of the metal cation is smaller than the cavity of crown ether, the complex will not be formed correspondingly.

Table 2.9 and Table 2.10 show the ammonium/MTCNQ ionophore complexes prepared by Morinaga et al.⁶⁴, with the corresponding values of yield, melting points, stoichiometry and elemental analysis. Morinaga et al.⁶⁴ commented that most of the TCNQ complexes were obtained as crystalline materials. The simple 1:1 salts tended to form when the cavity of the crown ether was comparable to or larger than the corresponding size of the cation, whereas if the crown ether had a cavity smaller than the size of the cation, a 2:1 stoichiometry was seen arising from the cation being sandwiched by crown ethers^{126,264}. Meanwhile, unusual stoichiometry existed in both simple and complex TCNQ salts. Crown ethers, such as 18C6 and DB18C6, formed complexes with different stoichiometries with metal cations, such as Rb^+ and Cs^+ cation. The reasons for explaining this phenomenon could be the existence of polymorphs in Rb/CsTCNQ .

Many of the simple 1:1:1 ionophore complexed MTCNQ salts are insulators with resistivity higher than $10^7 \Omega\text{cm}$. However, the ionophore complexed $\text{M}^+(\text{TCNQ}^{\bullet-})(\text{TCNQ}^0)$ salts are much more conductive than simple MTCNQ salts with resistivity values range from 10^2 to $10^4 \Omega\text{cm}$, which suggest the presence of mixed stacks of TCNQ^0 and $\text{TCNQ}^{\bullet-}$ will display higher conductivity properties. In addition, the resistivity values of simple TCNQ salts are lower than the corresponding MTCNQ salts, which indicates the interactions between metal cations and $\text{TCNQ}^{\bullet-}$ anions are modified when the crown ethers are presented. Additionally, the resistivity of the ‘complex’ $\text{M}^+(\text{TCNQ}^{\bullet-})(\text{TCNQ}^0)$ salts are of nearly the same magnitude as those of the corresponding MTCNQ salts⁶⁴.

The relationship between the colours of the simple ionophore MTCNQ salts and their physical properties had also been studied by Morinaga et al.⁶⁴. The yellow-greenish and yellow TCNQ complexes have higher resistivity with the value $\approx 10^{14} \Omega\text{cm}$. Whereas, the purple, violet and blue coloured salts are much more conductive with the resistivity values $\approx 10^7$ - $10^{11} \Omega\text{cm}$. This is because of the different strength of interactions between adjacent TCNQ units in the crystal structures. In the yellow-greenish, and yellow samples, the $\text{TCNQ}^{\bullet-}$ anions are isolated, which is not good for electrons transfer. In contrast, in the purple, violet and blue salts, π - π stacked dimers are formed⁶⁴.

Chapter 2

| Complex | Yield (%) | M.p. (°C) | Stoichiometry | C | | H | | N | | Remark | Resistivities (Ω cm) |
|---|-----------|-----------|---------------|-------|--------|-------|--------|-------|--------|---------------------|------------------------------|
| | | | | F*(%) | T**(%) | F*(%) | T**(%) | F*(%) | T**(%) | | |
| (12C4)LiTCNQ | <10 | >300 | 1:1 | 61.15 | 62.02 | 5.21 | 5.20 | 14.33 | 14.46 | Black plates | N/A |
| (12C4) ₂ NaTCNQ | 48 | 183-185 | 2:1 | 57.94 | 58.02 | 6.21 | 6.26 | 9.51 | 9.67 | Blue needles | 6.6×10^8 |
| (15C5)NaTCNQ | 19 | 150 | 1:1 | 58.86 | 59.06 | 5.36 | 5.41 | 12.35 | 12.52 | Purple hexahedral | 1.3×10^{10} |
| (18C6)NaTCNQ | <10 | 151-153 | 1:1 | 57.04 | 58.65 | 5.53 | 5.74 | 11.40 | 11.40 | Blue needles | N/A |
| (DB18C6)NaTCNQ | 57 | 214-216 | 1:1 | 65.45 | 65.41 | 4.78 | 4.80 | 9.60 | 9.54 | Yellow green plates | $>10^{14}$ |
| (DC18C6)NaTCNQ | 18 | 173-174 | 1:1 | 64.07 | 64.09 | 6.82 | 6.72 | 9.26 | 9.34 | Purple plates | N/A |
| (C222)NaTCNQ | 60 | 160-161 | 1:1 | 59.69 | 59.69 | 6.63 | 6.68 | 13.90 | 13.92 | Yellow powder | $>10^{14}$ |
| (15C5) ₂ KTCNQ | 46 | 210 | 2:1 | 56.17 | 56.20 | 6.65 | 6.48 | 8.29 | 8.19 | Purple hexahedral | 8.5×10^{11} |
| (18C6)KTCNQ | 58 | 203-205 | 1:1 | 56.50 | 56.79 | 5.57 | 5.56 | 11.30 | 11.04 | Purple needles | 6.7×10^9 |
| (DB18C6)KTCNQ | 65 | 202-204 | 1:1 | 63.71 | 63.67 | 4.65 | 4.68 | 9.19 | 9.28 | Yellow green plates | $>10^{14}$ |
| (DC18C6)KTCNQ | <10 | 189-192 | 1:1 | 62.13 | 62.42 | 6.30 | 6.55 | 9.88 | 9.10 | Violet plates | N/A |
| (C222)KTCNQ | 56 | 137 | 1:1 | 58.21 | 58.14 | 6.50 | 6.51 | 13.58 | 13.56 | Blue hexahedral | 1.3×10^{10} |
| (15C5) ₂ RbTCNQ | 58 | 202-203 | 2:1 | 52.62 | 52.64 | 6.14 | 6.07 | 7.68 | 7.67 | Purple hexahedral | 1.3×10^9 |
| (18C6) ₂ RbTCNQ | 64 | 208-210 | 2:1 | 51.87 | 52.04 | 5.15 | 5.09 | 10.08 | 10.11 | Violet needles | 3.9×10^9 |
| (DB18C6)RbTCNQ | 38 | 173-177 | 1:1 | 61.57 | 61.81 | 5.07 | 5.19 | 5.69 | 5.54 | Green needles | 2.0×10^9 |
| (DC18C6)RbTCNQ | 39 | 190-192 | 1:1 | 58.01 | 58.05 | 6.18 | 6.09 | 8.30 | 8.46 | Purple plates | 2.8×10^{11} |
| (DB24C8)RbTCNQ | 43 | 106-108 | 1:1 | 58.07 | 58.58 | 4.84 | 4.92 | 7.81 | 7.59 | Yellow green plates | N/A |
| (C222)RbTCNQ | 43 | 146-148 | 1:1 | 53.97 | 54.09 | 6.05 | 6.05 | 12.60 | 12.62 | Violet hexahedral | 7.4×10^9 |
| (18C6) ₃ (CsTCNQ) ₂ | 30 | 198-200 | 3:2 | 49.07 | 49.12 | 5.54 | 5.50 | 7.67 | 7.64 | Yellow plates | $>10^{14}$ |

Chapter 2

| Complex | Yield (%) | M.p. (°C) | Stoichiometry | C | | H | | N | | Remark | Resistivities (Ω cm) |
|--|-----------|-----------|---------------|-------|--------|-------|--------|-------|--------|---------------------|------------------------------|
| | | | | F*(%) | T**(%) | F*(%) | T**(%) | F*(%) | T**(%) | | |
| (DB18C6) ₂ CsTCNQ | 42 | 156 | 2:1 | 59.33 | 59.04 | 5.04 | 4.95 | 5.57 | 5.30 | Green needles | 1.1×10^{11} |
| (DB24C8)CsTCNQ | 54 | 137-138 | 1:1 | 55.11 | 55.04 | 4.59 | 4.62 | 7.06 | 7.13 | Yellow green plates | $>10^{14}$ |
| (C222)CsTCNQ | 62 | 151-153 | 1:1 | 50.55 | 50.50 | 5.66 | 5.65 | 11.68 | 11.78 | Violet hexahedral | 2.4×10^{10} |
| (15C5) ₂ NH ₄ TCNQ | 36 | 140-142 | 2:1 | 57.82 | 57.99 | 7.46 | 7.30 | 10.57 | 10.57 | Violet needles | 4.0×10^8 |
| (18C6)NH ₄ TCNQ | 15 | 170-172 | 1:1 | 59.01 | 59.25 | 6.41 | 6.63 | 14.16 | 14.39 | Purple needles | 2.3×10^9 |
| (DB18C6) ₂ NH ₄ TCNQ | 60 | 168-170 | 2:1 | 65.91 | 66.23 | 5.77 | 5.99 | 7.64 | 7.43 | Green needles | 6.6×10^7 |
| (DC18C6)NH ₄ TCNQ | 12 | 156-157 | 1:1 | 64.60 | 64.63 | 7.55 | 7.46 | 11.58 | 11.78 | Blue hexahedral | N/A |
| (15C5) ₂ Ba(TCNQ) ₂ | <10 | 253-255 | 2:1 | 53.43 | 53.48 | 5.09 | 4.91 | 11.42 | 11.36 | Yellow green plates | N/A |
| (18C6)Ba(TCNQ) ₂ | <10 | 249-251 | 1:1 | 52.73 | 52.38 | 4.04 | 3.98 | 13.70 | 13.83 | Purple needles | N/A |

* F: Found in elemental analysis

** T: Theory in elemental analysis

Table 2.9 The characteristics of simple ionophore ammonium/MTCNQ salts⁶⁴

| Complex | Yield (%) | M.p. (°C) | Stoichiometry | C | | H | | N | | Remark | Resistivities (Ω cm) |
|--|-----------|-----------|---------------|-------|--------|-------|--------|-------|--------|------------------|----------------------|
| | | | | F*(%) | T**(%) | F*(%) | T**(%) | F*(%) | T**(%) | | |
| (18C6)NaTCNQTCNQ | 37 | >300 | 1:1:1 | 61.94 | 62.15 | 4.47 | 4.64 | 15.96 | 16.11 | Black needles | 1.9×10^3 |
| (15C5) ₂ KTCNQTCNQ | <10 | >300 | 2:1:1 | 59.49 | 59.51 | 5.42 | 5.45 | 12.41 | 12.62 | Black needles | N/A |
| (DB18C6)KTCNQTCNQ | 36 | 224-225 | 1:1:1 | 65.18 | 65.42 | 3.92 | 3.99 | 13.91 | 13.87 | Black hexahedral | 4.4×10^3 |
| (15C5) ₂ RbTCNQTCNQ | <10 | 260 | 2:1:1 | 56.45 | 56.56 | 5.17 | 5.18 | 12.01 | 11.99 | Black needles | 1.5×10^4 |
| (18C6)RbTCNQTCNQ | 59 | 235 | 1:1:1 | 56.91 | 57.03 | 4.23 | 4.25 | 14.98 | 14.78 | Black plates | 1.2×10^4 |
| (15C5) ₂ CsTCNQTCNQ | <10 | >300 | 2:1:1 | 53.99 | 53.83 | 4.83 | 4.93 | 11.68 | 11.41 | Black hexahedral | N/A |
| (18C6)CsTCNQTCNQ | 58 | >300 | 1:1:1 | 53.56 | 53.67 | 3.93 | 4.00 | 14.00 | 13.91 | Black needles | 2.8×10^3 |
| (DB18C6) ₄ (CsTCNQ) ₂ TCNQ | <10 | 173-174 | 4:2:1 | 59.59 | 60.05 | 4.81 | 4.69 | 7.08 | 7.24 | Black needles | N/A |
| (18C6)NH ₄ TCNQTCNQ | 20 | 160-162 | 1:1:1 | 62.39 | 62.60 | 5.23 | 5.25 | 18.20 | 18.25 | Black hexahedral | 4.6×10^2 |
| (DB18C6) ₂ NH ₄ TCNQTCNQ | <10 | 162-164 | 2:1:1 | 67.98 | 67.17 | 4.63 | 4.61 | 15.93 | 16.02 | Black needles | N/A |
| (DC18C6)NH ₄ TCNQTCNQ | 10 | 167 | 1:1:1 | 66.05 | 66.15 | 6.01 | 6.06 | 15.96 | 15.78 | Black hexahedral | N/A |
| (15C5) ₂ Ba(TCNQ) ₂ TCNQ | <10 | 245-247 | 2:1:1 | 57.71 | 57.99 | 7.53 | 7.30 | 10.60 | 10.57 | Black needles | N/A |
| (18C6)Ba(TCNQ) ₂ TCNQ | <10 | 287-289 | 1:1:1 | 56.47 | 56.84 | 3.62 | 3.77 | 16.53 | 16.57 | Black powder | N/A |

* F: Found in elemental analysis

** T: Theory in elemental analysis

Table 2.10 The characteristics of complex ionophore ammonium/MTCNQ salts⁶⁴

2.7.2 Ionophore-encapsulated alkali metal TCNQ salts

Ionophore complexation of alkali metal TCNQ salts guide a change in intermolecular interactions and modify the physical properties of these materials. Whether the crown ethers can form 1:1 or 2:1 complexes with cations is based on the cavity of the crown ether and the size of the metal cation. Within 1:1 complexes, the cation sits in the middle of the crown ether and anion can still coordinate to the cation. However, in 2:1 complexes, a sandwich will be formed with the cation sitting between the two crown ethers, which will prevent any direct connections with anions.

Two main classes of ionophore MTCNQ salts have been structurally characterised. Firstly, a $\text{TCNQ}^{\bullet-}$ dimer is formed, which involves the 18C6 complex of Ti^+ , K^+ and $\text{Rb}^+\text{TCNQ}^{\bullet-}$ in Figure 2.40^{36,107,131}. From the crystal structures of these complexes, the common feature is that two crown ethers encapsulate metal cations which are coordinated to two nitriles from cyano groups at opposite ends of a $\text{TCNQ}^{\bullet-}$ dimer. This situation demonstrates direct coordination between the metal cations and the $\text{TCNQ}^{\bullet-}$ dimers. Another kind of architecture is adopted with the 15C5 complex of K^+ and $\text{Ti}^+\text{TCNQ}^{\bullet-}$ in Figure 2.41^{107,131}. Here the metal cation is sandwiched between two crown ethers.

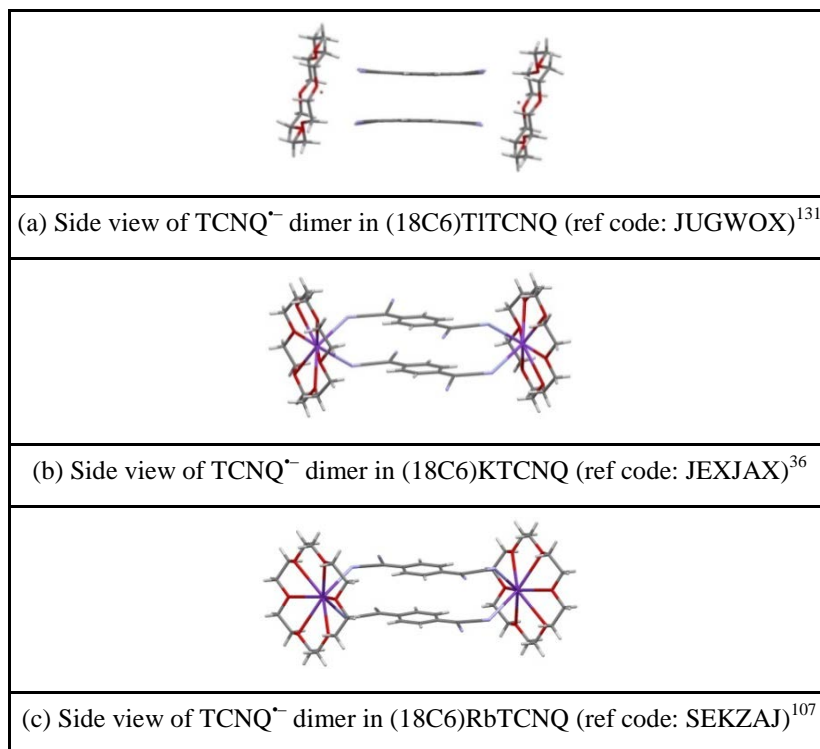


Figure 2.40 The packing arrangement showing the $\text{TCNQ}^{\bullet-}$ dimer^{36,107,131}

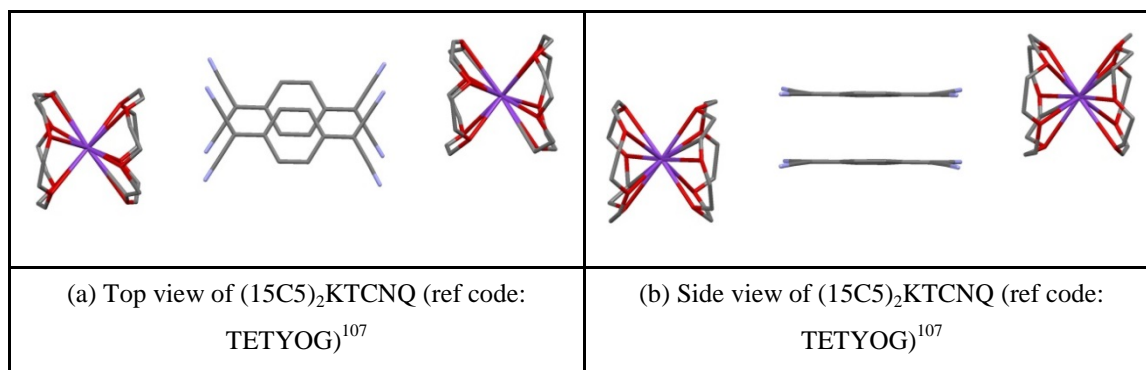


Figure 2.41 Top (a) and side (b) views of a $TCNQ^{\bullet-}$ dimer within $(15C5)_2KTCNQ$

Each of these complexes afford structures containing isolated $TCNQ^{\bullet-}$ dimers. The spectroscopic and electronic behaviour of these $TCNQ^{\bullet-}$ dimer components, which are also found in organic metals and semiconductors, are therefore attractive for detailed studies¹³¹. The dimers found in 1:1:1 crown ether: M^+ : $TCNQ^{\bullet-}$ salts (where $M = K^+$, Rb^+) are packed into a brickwork array, in which the $TCNQ^{\bullet-}$ dimers are isolated from each other. This arrangement is similar to that seen by Dunitz et al.²⁶⁵ in the solid state structures of a series of 18C6 MSCN ($M = Rb^+$ or Cs^+) complexes, whereas a linear chain is formed by the K^+ analogue. In the latter case, both sides of the cation-crown are coordinated by the anions. However, this is not seen for $(18C6)KTCNQ$, since two cyano groups at each end of the $TCNQ^{\bullet-}$ dimer are coordinated to one face of the $K^+(18C6)$ complex¹³¹. In $(15C5)_2KTCNQ$, the $TCNQ^{\bullet-}$ dimers are even more highly screened from each other. In this case, the two crown ethers encapsulate the K^+ cation completely. Grossel and Weston^{55,131} attempted to prepare the C222 complex of KTCNQ. However, they only isolated and characterised $K^+(C222)DCTC$. Figure 2.42 shows the C222 complex of K^+DCTC^- as its acetonitrile solvate and Figure 2.43 displays its corresponding crystal structure.

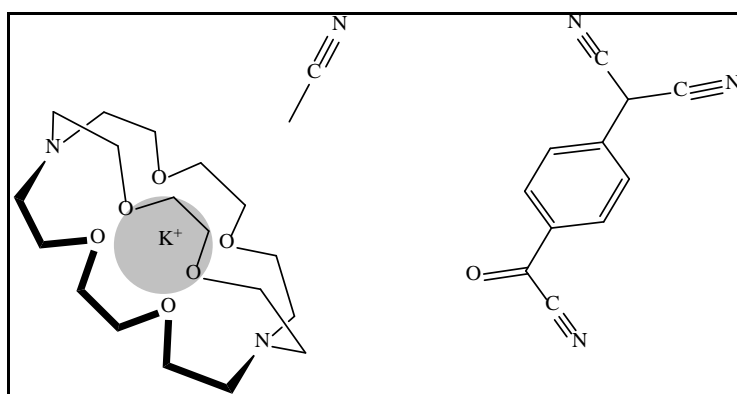


Figure 2.42 The C222 complex of K^+DCTC^- as its acetonitrile solvate

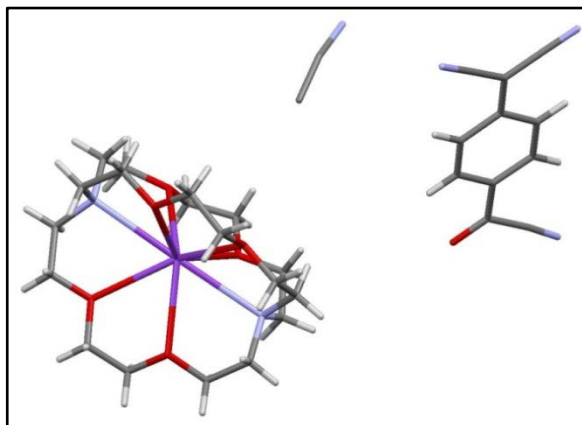


Figure 2.43 Crystal structure of the C222 complex of K^+DCTC^- as its acetonitrile solvate (ref code: QOBYUB)⁵⁵

In parallel with this study, Grossel et al.³⁶ also focused on the solid state behavior of $TCNQ^{\bullet-}$ salts containing organic dye cations. X-ray crystallographic analysis indicated that in general, the $TCNQ^{\bullet-}$ anions formed dimers and that the packing of these complexes depended on the nature of the counter-cation or cation complexes.

The main focus of the present project involves an extended study of the factors which influence the solid state architecture of crown ether encapsulated $TCNQ$ salts and particularly the role of the counter-cation in determining this. This ‘crystal-engineering’ study of a number of simple $TCNQ$ salts and their analogues will involve the preparation of several series of salts involving different alkali metal cations. Crystalline samples of these will be subjected to X-ray structural studies in order to examine the resulting crystal architectures formed and attempt to gain further insight into which parameters control these. The long-term goal is to be able to design particular solid state motifs with a view to controlling the optical and electronic properties of such complexes. The work will then be extended to explore the behaviour of lanthanide crown ether $TCNQ$ complexes.

ESR, optical spectroscopic measurements, conductivity and crystal structures are four significant techniques for characterising $TCNQ$ salts. When the properties of $TCNQ$ and its salts are rationalised and compared, it appears that the conductivity of such complexes is dependent on the uniformity of the electron movement in the $TCNQ$ array^{74,249}. However, if the $TCNQ$ units are not equivalent, the electron movement mechanism will inhibit conductivity through selectively ‘pinning’ the available electrons on some parts of the $TCNQ$ molecules²⁶⁶.

3. Ionophore Encapsulated MTCNQ Salts

The main focus of the present project has involved an extended study of the factors which influence the solid state architecture of crown ether-encapsulated TCNQ salts and particularly the role of the counter-cation in determining this. This ‘crystal-engineering’ study of a number of simple TCNQ salts and their analogues involved the preparation of several series of salts of different alkali metal cations. Crystalline samples of these were subjected to X-ray structural studies in order to examine the resulting crystal architectures formed and to attempt to gain further insight into which parameters control these. The long term goal has been able to design particular solid state motifs with a view to controlling the optical and electronic properties of such complexes.

Electron Paramagnetic Resonance (EPR), optical spectroscopy, conductivity and X-ray crystallography are four significant techniques for characterising TCNQ salts. When the properties of TCNQ and its corresponding salts are rationalised and compared, it appears that the conductivity of such complexes is dependent on the nature of the TCNQ array^{74,249,266}.

3.1 Summarised crystal structures of TCNQ salts

From the Grossel group’s previous studies, the solid state behaviour of the 18-crown-6 complexes of K^+ , Rb^+ and TITCNQ and $(15C5)_2KTCNQ$ have been reported^{36,55,107,131,132,267,268}. A brickwork packing pattern of dimers is observed in the solid state structures of the 18C6 complexes of K^+ and $RbTCNQ$. Such packing architectures reflect the impact of the bulk of the crown ether and tight ion-pair interactions^{107,131,267}. The 18C6 complexes of K^+ , Rb^+ and TITCNQ and $(15C5)_2KTCNQ$ exhibit thermally activated triplet exciton behaviour, which is sensitive to the nature of the counter-ion and the solid state architecture^{36,107,132,267,268}. In $(15C5)_2KTCNQ$, sheets of $TCNQ^{\bullet-}$ dimers are surrounded by $(15C5)_2K^+$ barrels, in contrary to the architecture observed for the 18C6 complexes of K^+ , Rb^+ and TITCNQ^{107,131}. Here the presence of the ionophore inhibits the cation-anion interactions and provides a crystal architecture in which the $TCNQ^{\bullet-}$ dimers can be isolated both from the counter-ion and neighbouring $TCNQ^{\bullet-}$ dimers^{36,55,107,131,132,268}. Therefore, this kind of complex gives a good opportunity to investigate the behaviour of an isolated

TCNQ^{•-} dimer in the solid state^{36,107,268}. Figure 3.1 shows the chemical structures of (a) (18C6)K⁺, Rb⁺ and TITCNQ; and (b) (15C5)₂KTCNQ, respectively. The crystal structures of (a) (18C6)K⁺, Rb⁺ and TITCNQ; and (b) (15C5)₂KTCNQ can be seen in Figure 2.40 and Figure 2.41, respectively.

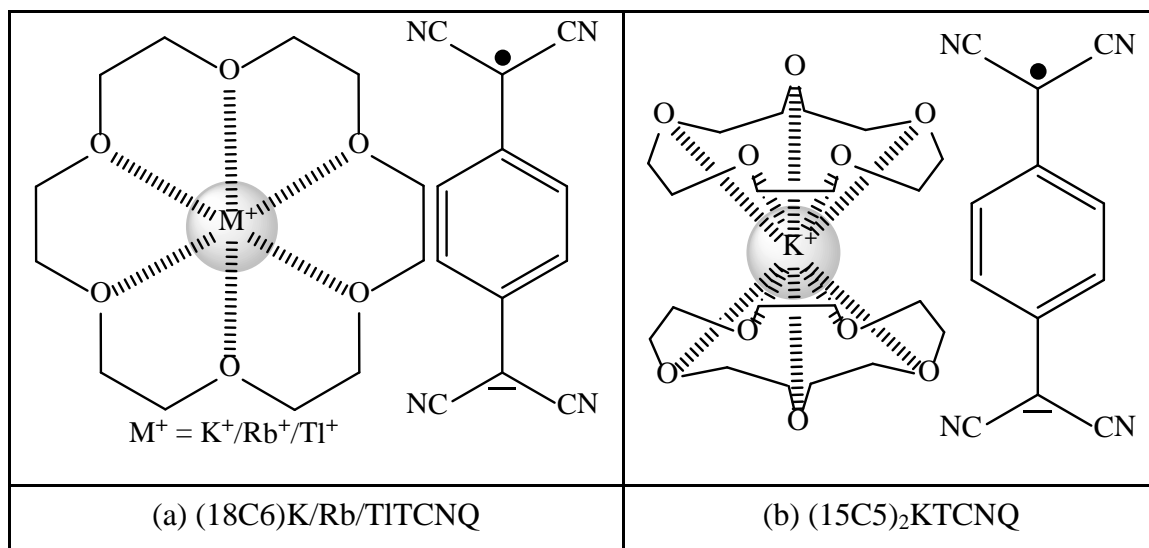


Figure 3.1: The structure of (a) (18C6)K/Rb/TITCNQ; (b) (15C5)₂KTCNQ^{36,107,131,268}

3.2 Crystal growth experiments

For study of the ionophore-encapsulated MTCNQ salts, a key requirement is the preparation of crystalline complexes which are suitable for X-ray structural study. There are several key factors that require attention. Firstly, each component should be completely dissolved in solvent (dry acetonitrile); the ideal situation being to mix all of the reactants without the visible presence of any solids in the solutions. Secondly, the solution must be filtered whilst hot and then left to cool down slowly to room temperature, otherwise, some of the ingredients will remain in the mixture when the temperature is reduced and these will contaminate the product. Thirdly, for achieving good crystals, the solution must be left to evaporate slowly. This step is the most significant factor of the whole experiment since the rate of evaporation will affect the formation of crystals. Normally, the solution needs to be left for several days, or even several weeks. For the preparation of a good quality crystalline complex in this study, the top of the container was covered by parafilm with several holes in it in order to decrease the rate of solvent evaporation, and so generate better solid and even crystals. Finally, when crystals had formed and had been isolated by filtration, dry diethyl ether

was used for washing the resulting solid several times to remove excess crown ether. The use of dry diethyl ether is ideal, since not only does it not seem to dissolve too much of the required products, but it can also remove excess crown ether. Washing the products was continued until the washing solvent did not change colour. This gave product, which was stored under vacuum and then prepared for other measurements.

3.3 Ionophore encapsulated MTCNQ complexes (M = Li, Na, K, Cs)

In this section, each of the ionophore encapsulated MTCNQ (M = Li, Na, K, Cs) complexes obtained in this study will be discussed. Initially TCNQ^o is needed to be purified by recrystallisation from hot dry acetonitrile. Full details of the experiments carried out attempting to prepare various crown ether encapsulated MTCNQ complexes are reported in the Experimental Section. In the TCNQ unit, each centroid and mean plane is defined by the carbon atoms of the benzene ring. Centroid-centroid distance refers to the distance between adjacent TCNQ units. Centroid-mean plane (perpendicular) distance is defined as a centroid of one TCNQ unit pointing to a neighbouring upper TCNQ mean plane. The centroid-centroid and centroid-mean plane distances are taken as the average in each packing pattern of TCNQ repeating units. Table 3.1 shows description of key parameters in TCNQ plane.

| Side view | End view |
|---|------------------------------|
| | |
| r = Perpendicular face-to-face separation | |
| d = Long axis slip distance | s = Short axis slip distance |
| l = Centroid to centroid distance | |
| α = Long axis slip angle | β = Short axis slip angle |

Table 3.1 Description of key parameters in TCNQ plane

3.3.1 Preparation of $(12C4)_2M(TCNQ)_n$ complexes ($M = Li, Na, K$)

In this section, the behaviour of the complexes $(12C4)_2LiTCNQ$, $(12C4)_2NaTCNQ$, $(12C4)_2Li(TCNQ)_2$, $(12C4)_2Na(TCNQ)_2$ and $(12C4)_2K(TCNQ)_2$ will be discussed including a brief summary of the preparative method used and an analysis of each crystal structure obtained.

3.3.1.1 $(12C4)_2MTCNQ$ complexes ($M = Li, Na$)

(a) $(12C4)_2LiTCNQ$

Reaction of 12C4 with LiTCNQ and NaTCNQ in dry acetonitrile (2:1) (using the crown: salt ratio 2:1) afforded in each case a dark blue or a black crystalline solid respectively, which proved suitable for X-ray structural studies. The X-ray structural studies reveal that these two complexes are iso-structural. In each case, the alkali metal cation is sandwiched between two crown ether units and completely screened from the counter anion. The $TCNQ^{\bullet-}$ counterions are face-to-face π -stacked in columns. An unusual feature of these columns is that, within a given column, neighbouring $TCNQ^{\bullet-}$ counterions are twisted (25.94°) relative to each other. Figure 3.2 shows geometries of adjacent $TCNQ^{\bullet-}$ units in $(12C4)_2LiTCNQ$ showing the extent of long-axis slippage [Figure 3.2(a)] and the distortion from planarity [Figure 3.2(b)], respectively.

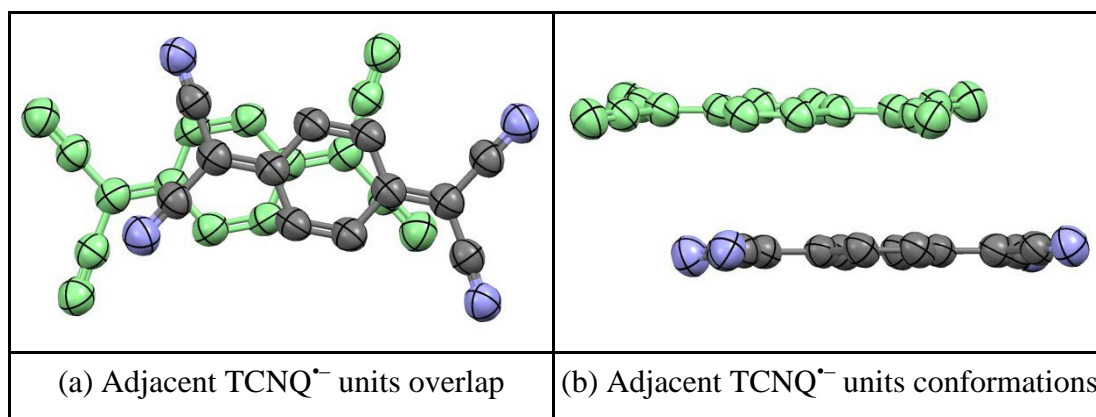


Figure 3.2 Geometries of adjacent $TCNQ^{\bullet-}$ units in $(12C4)_2LiTCNQ$ (one of the $TCNQ^{\bullet-}$ units is highlighted as light green and hydrogen atoms are excluded)

Figure 3.3 shows top (a) and side (b) views of adjacent $TCNQ^{\bullet-}$ units in $(12C4)_2LiTCNQ$, respectively.

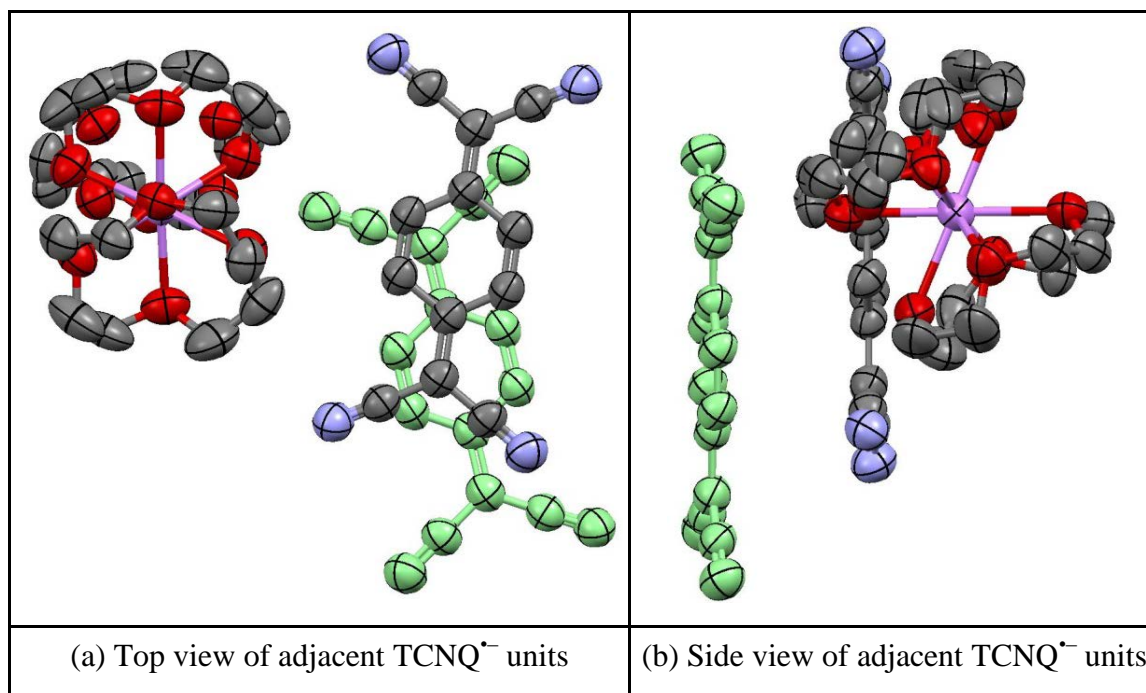


Figure 3.3 Top (a) and side (b) views of adjacent TCNQ^{•-} units in (12C4)₂LiTCNQ (one of the TCNQ^{•-} units is highlighted as light green and hydrogen atoms are excluded)

Within adjacent TCNQ^{•-} units, the vertical π - π distance (r) between neighbouring TCNQ^{•-} units is 3.387 Å. The slip distance (d) and slip angle (α) along the long axis are 2.40 Å and 35.30° respectively. Meanwhile, the slip distance (s) and slip angle (β) along short axis are 0.26 Å and 4.37°. As viewed in Figure 3.3, the pair of adjacent TCNQ^{•-} units is mainly long-axis slipped.

Because of the complete encapsulation of the cation by the two crown ether units in this complex, each TCNQ^{•-} is not coordinated to the metal ion. Unusually, neighbouring TCNQ^{•-} units are twisted in respect to each other. The TCNQ^{•-} units assemble into infinite columns with equal vertical distances between neighbours, which are in close face-to-face π contact with a twist angle of 25.94° and long axis slip of 2.40 Å. Adjacent TCNQ^{•-} units are slightly paddle shaped and twisted in such a way that the cyano groups in neighbouring TCNQ^{•-} units are pushed away from each other. Table 3.2 shows summary of bond distances observed of TCNQ^{•-} in (12C4)₂LiTCNQ, the bonds (a-f) being defined in Figure 2.26 as for Table 3.2.

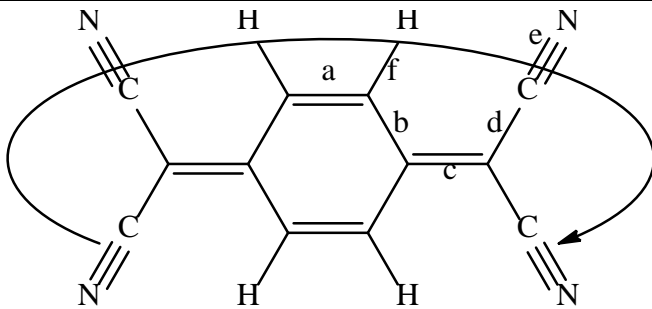
|  | | | | | | |
|--|------------------|-----------|-----------|-----------|-----------|-------|
| (a) Definition of the bond lengths within the TCNQ ^{•-} molecule | | | | | | |
| Structure | Bond lengths (Å) | | | | | |
| | a | b | c | d | e | f |
| (12C4) ₂ LiTCNQ | | 1.426 (4) | | 1.411 (4) | 1.163 (3) | 0.951 |
| | 1.363 (4) | 1.421 (3) | 1.418 (4) | 1.418 (4) | 1.154 (3) | 0.949 |
| | 1.363 (4) | 1.426 (4) | 1.418 (4) | 1.411 (4) | 1.163 (3) | 0.951 |
| | | 1.421 (3) | | 1.418 (4) | 1.154 (3) | 0.949 |

Table 3.2 Summary of bond distances (Å) observed of TCNQ^{•-} in (12C4)₂LiTCNQ

It appears from these observations that TCNQ^{•-} has quinonoidal character because bond 'a' is shorter than bond 'b'. In (12C4)₂LiTCNQ, there are significant differences in the lengths of some of the chemically equivalent sites on the TCNQ^{•-} units, which suggests that it does not possess D_{2h} symmetry anymore. Figure 3.4 shows further views of the solid state behaviour of (12C4)₂LiTCNQ.

As seen in Figure 3.4, some difficulties were encountered during the X-ray crystal structure solution as the crown ethers are found to be disordered. The atomic occupancy is 0.511(4):0.489(4) of disordered crown ether ring. The components of (12C4)₂LiTCNQ form mixed 1:2 alternating sheets as viewed in the packing diagram [Figure 3.4(a)]. Within this arrangement, the 'cation-barrels' insulate the twisted TCNQ^{•-} dimers from each other within the sheet. Perpendicular to these layers, the TCNQ^{•-} dimers form infinite stacks and neighbouring units are mutually twisted by 25.94° relative to each other. The centroid-centroid distance (l) between neighbouring TCNQ^{•-} units is 4.158 Å and the perpendicular π - π distance (r) is 3.387 Å, respectively. Each Li⁺ cation is encapsulated by two molecules of 12C4 and the complex of (12C4)₂Li⁺ lies in the channels between TCNQ^{•-} stacks. There is no direct co-ordination between the TCNQ^{•-} units and the Li⁺ ions. Within the cation complex, the planes of the

two crown ether units (as defined by each set of oxygen atoms) are tilted in respect to each other (by *ca.* 5.39°). Figure 3.5 summarises the various contact distances within the cation complex.

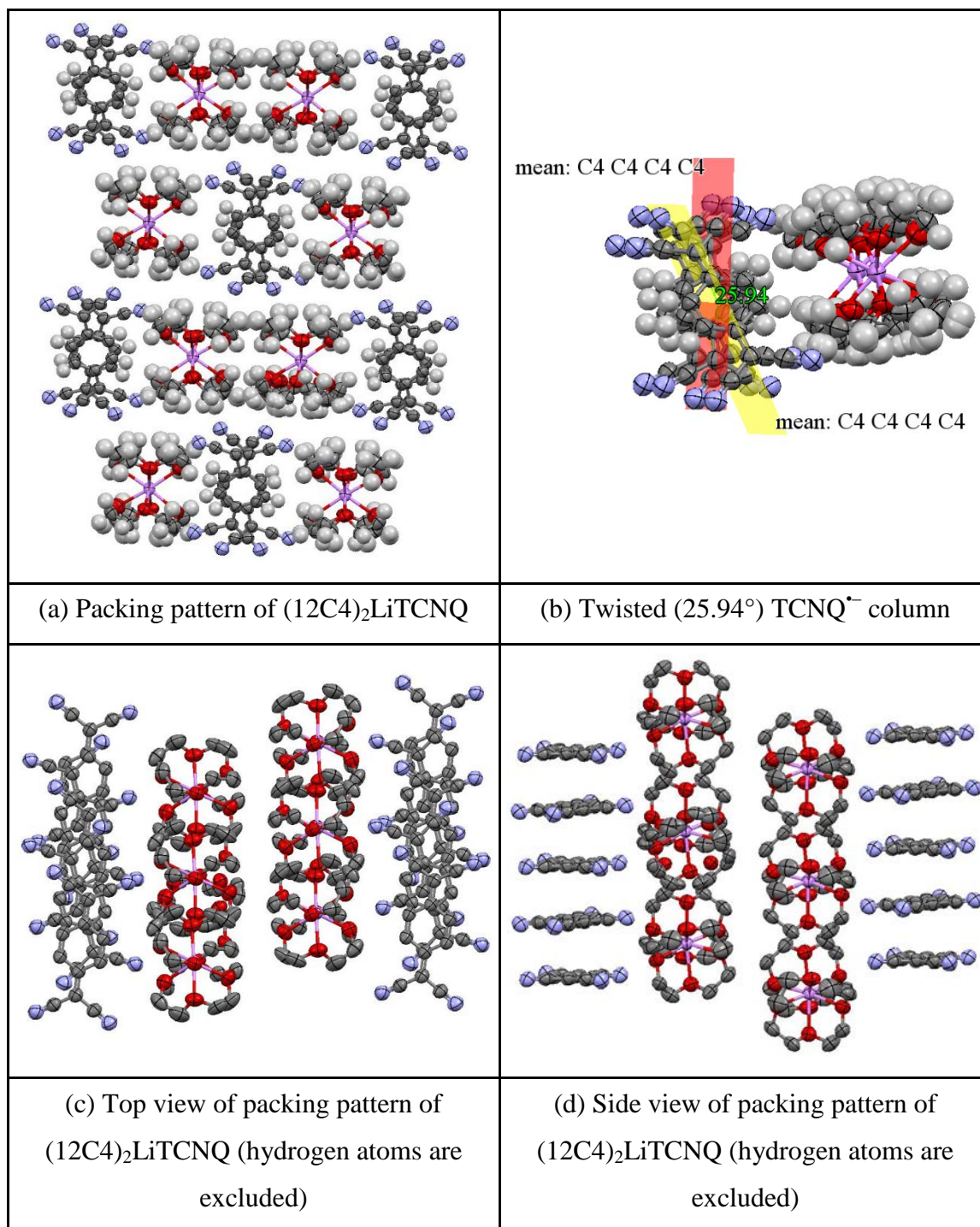


Figure 3.4 Views of the solid state behaviour of (12C4)₂LiTCNQ

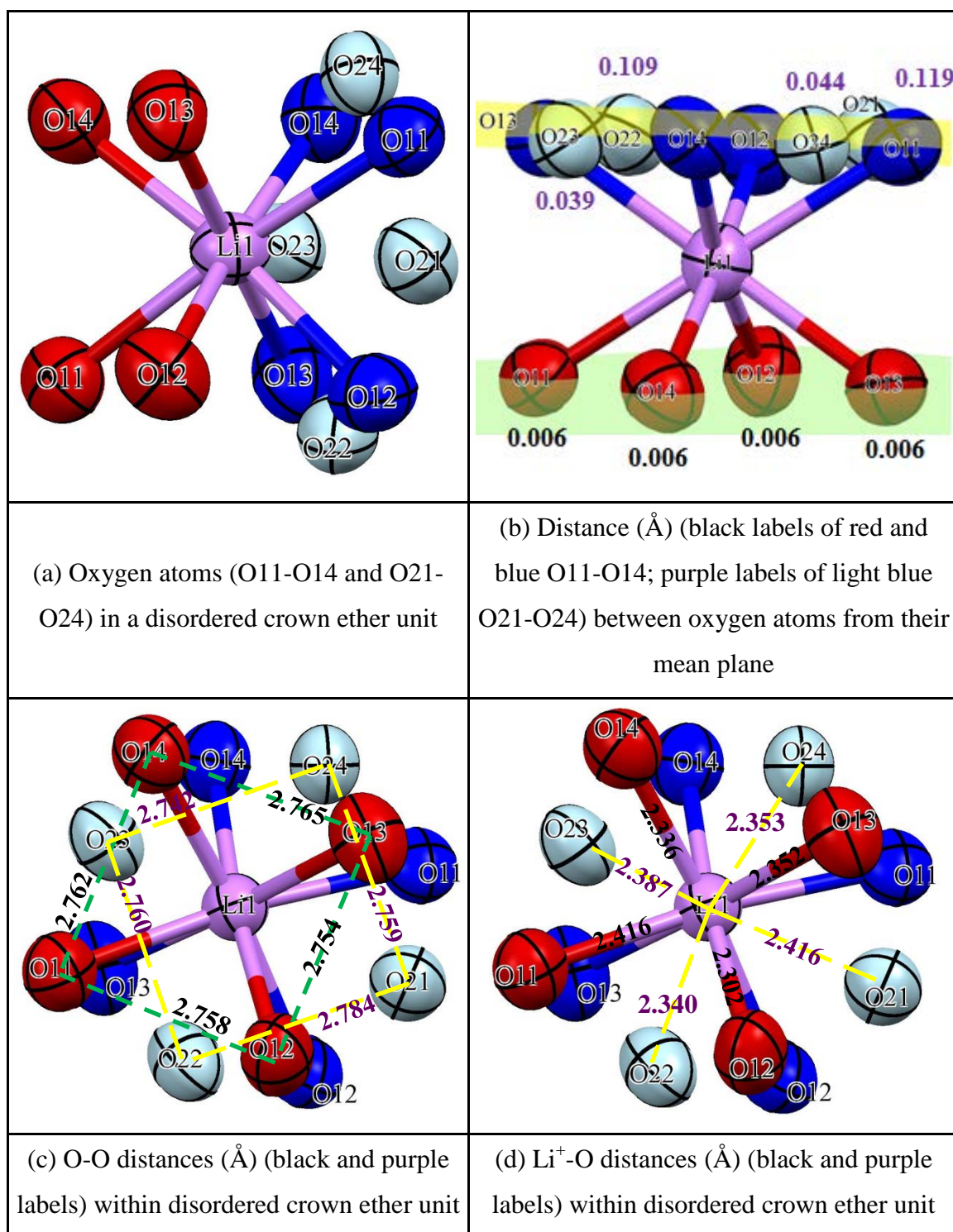


Figure 3.5 Description of the basic unit in (12C4)₂LiTCNQ (carbon and hydrogen atoms are excluded)

As viewed in Figure 3.5, two crown ether rings are identical in respect to each other. In order to improve the visibility, two of the crown ether rings are represented as different colours and one of them is shown as disordered crown ether ring. All of the four oxygen atoms on 12C4 are sited on a plane to form an irregular, nearly planar quadrilateral of

mean side *ca.* 2.760 Å. All of the Li⁺-O distances in (12C4)₂LiTCNQ are not equal and seem to fall into two groups: (i) 2.302, 2.336, 2.352 Å and (ii) 2.416 Å, respectively, which shows that the Li⁺ cation's position is not central within the cavity of 12C4. Key parameters of the crystal structure of (12C4)₂LiTCNQ with full details of the structure solution and refinement are listed in the Experimental Section and the Supporting Information (in the Appendices) respectively.

(b) (12C4)₂NaTCNQ

Figure 3.6 shows a top (a) and side (b) views of the basic unit in (12C4)₂NaTCNQ.

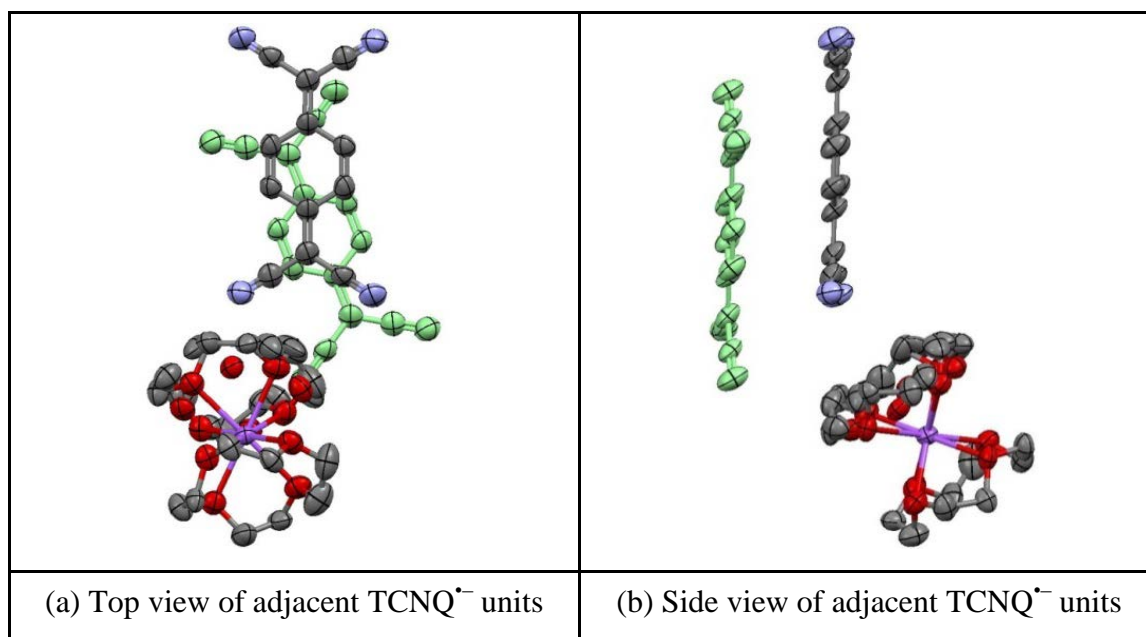


Figure 3.6 Top (a) and side (b) views of adjacent TCNQ^{•-} units in (12C4)₂NaTCNQ (one of TCNQ^{•-} units is highlighted as light green and hydrogen atoms are excluded)

Within adjacent TCNQ^{•-} units, the vertical π - π distance (*r*) between neighbouring TCNQ^{•-} units is 3.426 Å, which is longer than is the case in (12C4)₂LiTCNQ. The slip distance (*d*) and slip angle (α) along the long axis are 2.34 Å and 34.33°, whereas, the slip distance (*s*) and slip angle (β) along short axis are 0.23 Å and 3.80°. As viewed in Figure 3.6, the TCNQ^{•-} dimer pair is mainly long-axis slipped. However, as with its lithium analogue, here neighbouring TCNQ units are rotated relative to each other by 25.96°. Figure 3.7 shows geometries of adjacent TCNQ^{•-} units in (12C4)₂NaTCNQ exhibiting the twisted pattern (overlap view) and the distortion from planarity (conformation), respectively.

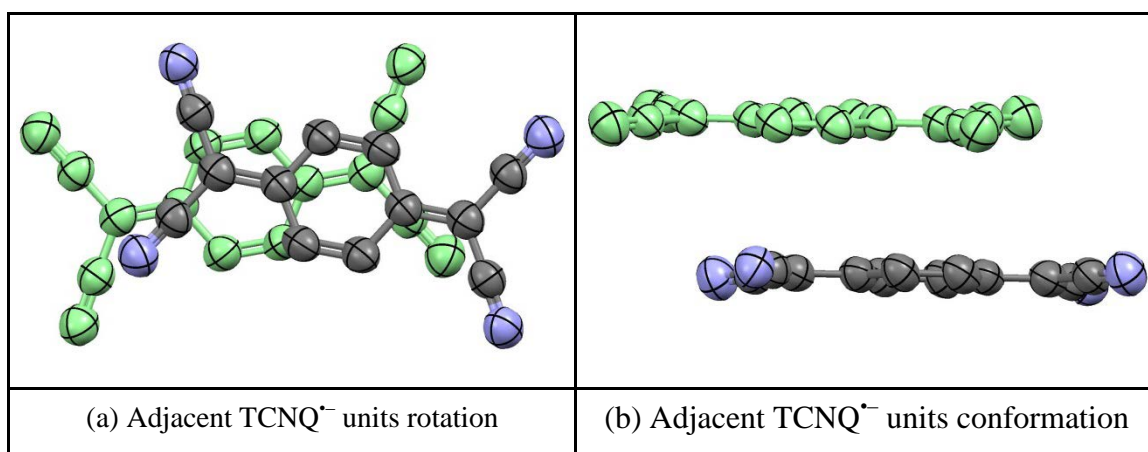


Figure 3.7 Geometries of adjacent TCNQ⁻ units in (12C4)₂NaTCNQ (one of TCNQ⁻ units is highlighted as light green and hydrogen atoms are excluded)

Because of the ‘sandwich’ nature of the crown ether-cation complex, the TCNQ⁻ is not coordinated to metal. Consequently, the TCNQ⁻ forms infinite column with equal vertical distance between adjacent TCNQ⁻ units, which are closely face-to-face π stacked alternately twisted along the stacking axis and long axis slipped. Neighbouring TCNQ⁻ units adopt a shallow paddle conformation twisted in such a way that the cyano groups in neighbouring TCNQ⁻ moieties are pushed away from each other. Table 3.3 shows the summary of bond lengths observed for TCNQ⁻ in (12C4)₂NaTCNQ; the bonds (a-f) being defined in Figure 2.26.

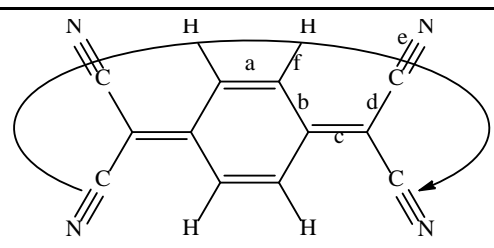
|  | | | | | | |
|--|------------------|-----------|-----------|-----------|-----------|-------|
| (a) Definition of the bond lengths within the TCNQ ⁻ molecule | | | | | | |
| Structure | Bond lengths (Å) | | | | | |
| | a | b | c | d | e | f |
| (12C4) ₂ NaTCNQ | | 1.424 (7) | | 1.421 (7) | 1.138 (6) | 0.950 |
| | 1.351 (7) | 1.425 (7) | 1.424 (7) | 1.422 (7) | 1.151 (6) | 0.949 |
| | 1.351 (7) | 1.424 (7) | 1.424 (7) | 1.421 (7) | 1.138 (6) | 0.950 |
| | | 1.425 (7) | | 1.422 (7) | 1.151 (6) | 0.949 |

Table 3.3 Summary of bond lengths (Å) observed of TCNQ⁻ in (12C4)₂NaTCNQ

These data suggest that the $\text{TCNQ}^{\cdot-}$ unit has quinonoidal character because of bond 'a' is shorter than bond 'b'. In $(12\text{C}_4)_2\text{NaTCNQ}$, there are once again significant differences in the lengths of some of the chemically equivalent $\text{TCNQ}^{\cdot-}$ unit, which suggests that the molecule does not possess D_{2h} symmetry anymore. Figure 3.8 shows further views of the solid state packing behaviour of $(12\text{C}_4)_2\text{NaTCNQ}$.

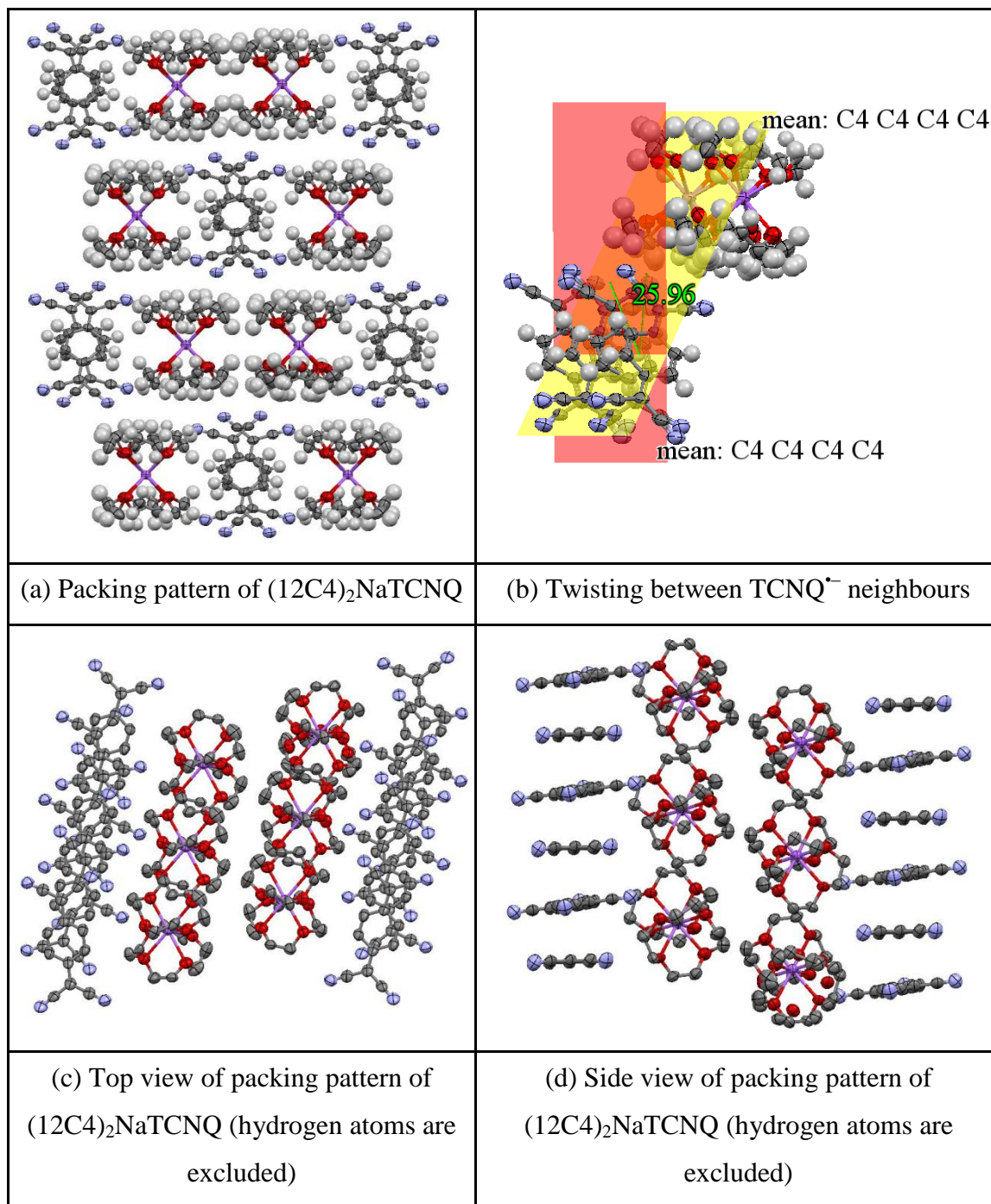


Figure 3.8 Views of the solid state behaviour of $(12\text{C}_4)_2\text{NaTCNQ}$

Figure 3.8 shows different views of the extended crystal structure of $(12C4)_2NaTCNQ$. Once again difficulties were encountered during the X-ray crystal structure solution as the crown ethers were found to be disordered. The atomic occupancy is 0.5:0.5 of disordered crown ether ring. The packing arrangement seen here is the same as that observed for $(12C4)_2LiTCNQ$. The $TCNQ^{\bullet-}$ units lie in infinite stacks with the same centroid and perpendicular distance between adjacent planes and neighbouring units alternately twisted (25.96°) in a manner the similar as that seen for $(12C4)_2LiTCNQ$. In addition, each Na^+ cation is encapsulated by two molecules of 12C4 and the complex of $(12C4)_2Na^+$ lies in the channels between $TCNQ^{\bullet-}$ stacks.

The complexes of $(12C4)_2LiTCNQ$ and $(12C4)_2NaTCNQ$ are iso-structural. The solid state behaviour of both complexes clearly differs from that seen previously for $(15C5)_2KTCNQ$ ^{107,131}. In the latter case, the K^+ cation is sandwiched between two disordered 15C5 ligands and the $TCNQ^{\bullet-}$ counterions form isolated dimers rather than the infinite stacks seen in the present structures. This suggests that the volume of the (crown ether)₂M⁺ complex plays an important role in determining the solid state behaviour of these materials. Figure 3.9 shows the basic unit for $(12C4)_2NaTCNQ$.

As seen in Figure 3.9, two crown ether rings are identical in respect to each other. In order to improve the visibility, two of the crown ether rings are represented as different colours and one of them is shown as disordered crown ether ring. All of the four oxygen atoms on 12C4 are sited on their mean plane to form an irregular quadrilateral of mean side by *ca.* 2.817 Å. The minimum and maximum of Na^+-O distances in $(12C4)_2NaTCNQ$ are 2.469 and 2.486 Å, respectively. The different Na^+-O distances demonstrate that the Na^+ cation lies within a distorted cavity of two 12C4 units, which is similar that seen for $(12C4)_2LiTCNQ$.

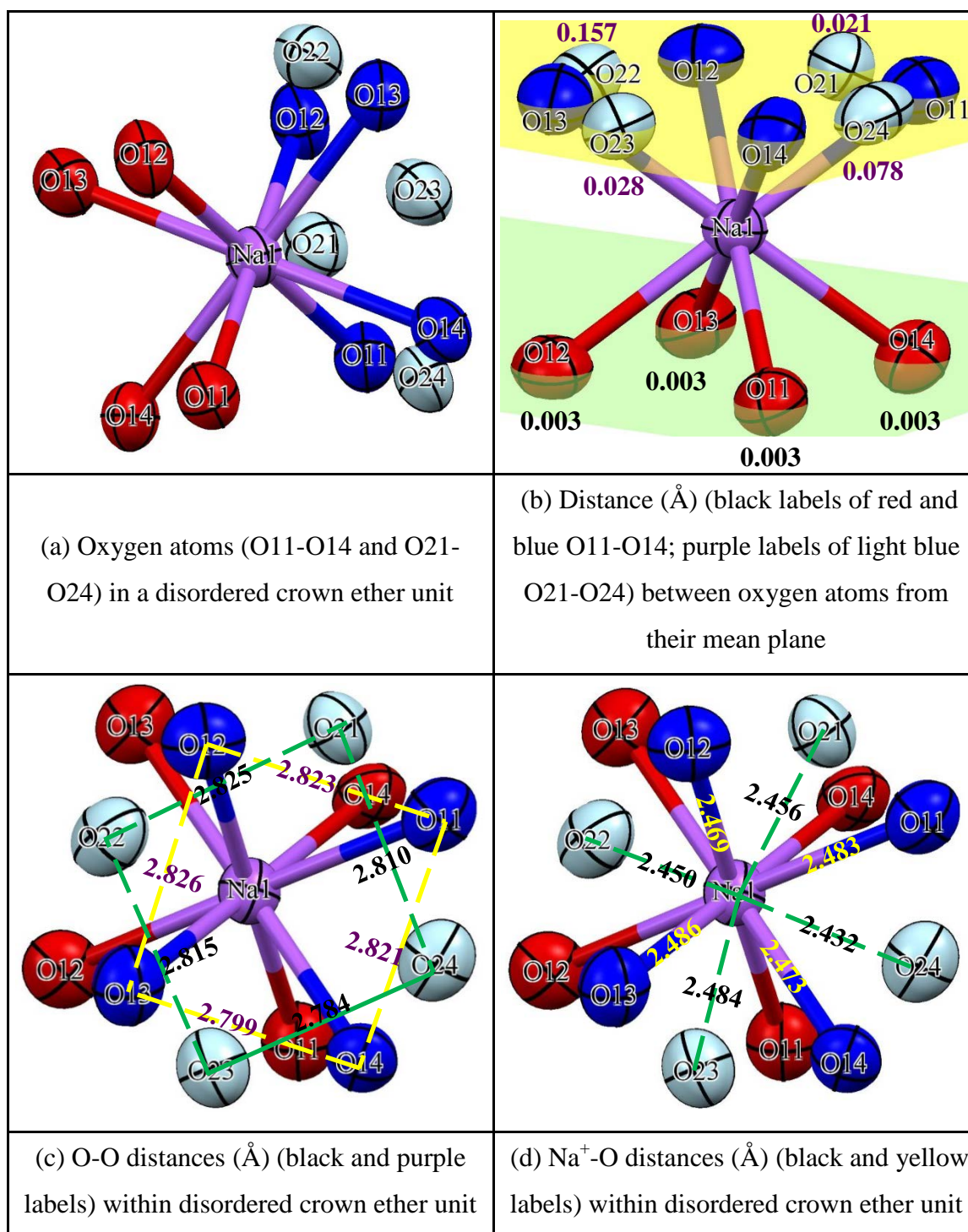


Figure 3.9 Description of the basic unit for (12C4)₂NaTCNQ (carbon and hydrogen atoms are excluded)

3.3.1.2 $(12C4)_2M(TCNQ)_2$ ($M = Li, Na, K$)

(a) $(12C4)_2Li(TCNQ)_2$

Reaction of 12C4 with LiTCNQ and TCNQ⁰ (ratio 2:1:1) in dry acetonitrile afforded a yield (28%) of a dark green crystalline solid which contained single crystals suitable for X-ray structural study. Full details including an account of the structure solution and refinement are reported in the Experimental Section and the Supporting Information (in the Appendices) respectively. The crystals obtained were of $(12C4)_2Li(TCNQ)_2$ and the basic structure is shown in Figure 3.10.

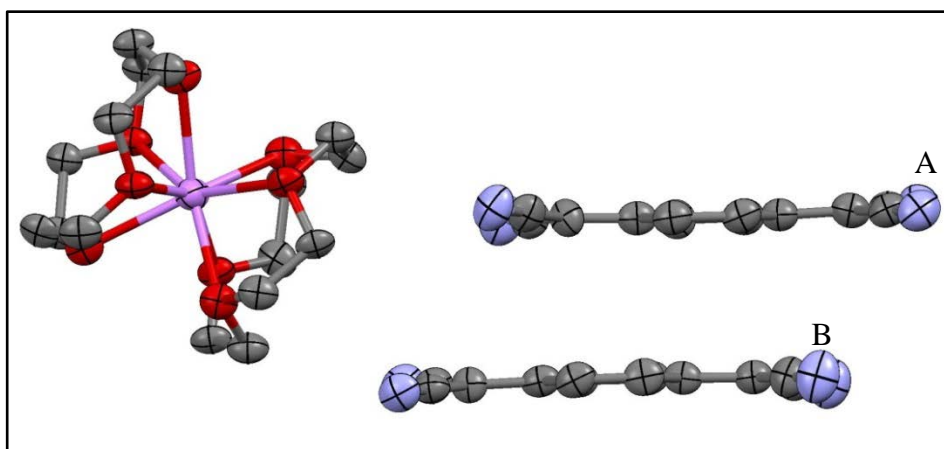


Figure 3.10 Basic structure of $(12C4)_2Li(TCNQ)_2$ (hydrogen atoms are excluded)

Bond lengths within the TCNQ units are summarised in Table 3.4. In this structure, the Li^+ ion is coordinated to and sandwiched between two crown ether units. The TCNQ units form a dimer which is significantly long axis slipped (see Figure 3.11). The similarity of the bond lengths within the two TCNQ units makes it difficult to distinguish between the TCNQ⁻ and TCNQ⁰ components. The data in Table 3.4 suggest that both TCNQ units have some quinonoidal character because bond length “a” is less than “b”. For both components A and B distribution of bond lengths is intermediate between these reported for TCNQ⁰ and TCNQ⁻ respectively²¹³.

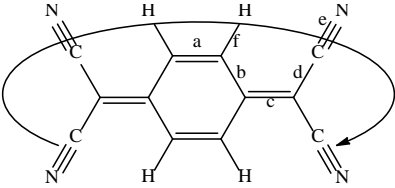
|  | | | | | | |
|---|------------------|-----------|-----------|-----------|-----------|-------|
| (a) Definition of the bond lengths within the TCNQ molecule | | | | | | |
| Structure | Bond lengths (Å) | | | | | |
| | a | b | c | d | e | f |
| TCNQ unit (A) | | 1.435 (5) | | 1.412 (5) | 1.162 (5) | 0.951 |
| | 1.366 (6) | 1.429 (5) | 1.392 (5) | 1.437 (6) | 1.137 (6) | 0.950 |
| | 1.349 (6) | 1.422 (5) | 1.411 (6) | 1.420 (5) | 1.159 (5) | 0.949 |
| | | 1.431 (5) | | 1.422 (6) | 1.153 (5) | 0.950 |
| TCNQ unit (B) | | 1.421 (5) | | 1.414 (5) | 1.160 (5) | 0.950 |
| | 1.357 (6) | 1.428 (5) | 1.419 (5) | 1.422 (5) | 1.141 (5) | 0.950 |
| | 1.363 (6) | 1.430 (5) | 1.413 (5) | 1.413 (5) | 1.160 (5) | 0.950 |
| | | 1.420 (5) | | 1.426 (6) | 1.142 (6) | 0.951 |

Table 3.4 Summary of bond lengths (Å) observed for TCNQ units in
(12C4)₂Li(TCNQ)₂

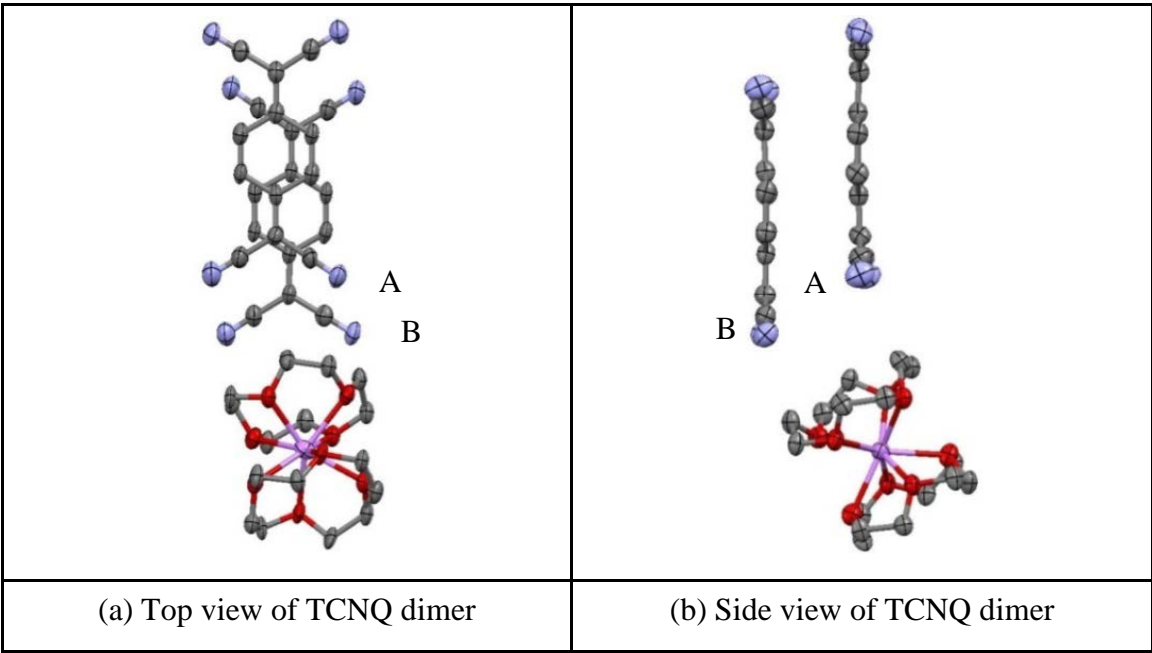


Figure 3.11 Top (a) and side (b) views of TCNQ dimer (AB) in (12C4)₂Li(TCNQ)₂
(hydrogen atoms are excluded)

Within the crystal, the TCNQ dimers assemble into infinite columns in which the individual TCNQ units are assembled in an ABB'A' motif (Figure 3.12) in which neighbouring dimers (AA' and BB') are significantly “diagonally” slipped (Figure 3.13). Distances and angles within the TCNQ stacks are listed in Table 3.5.

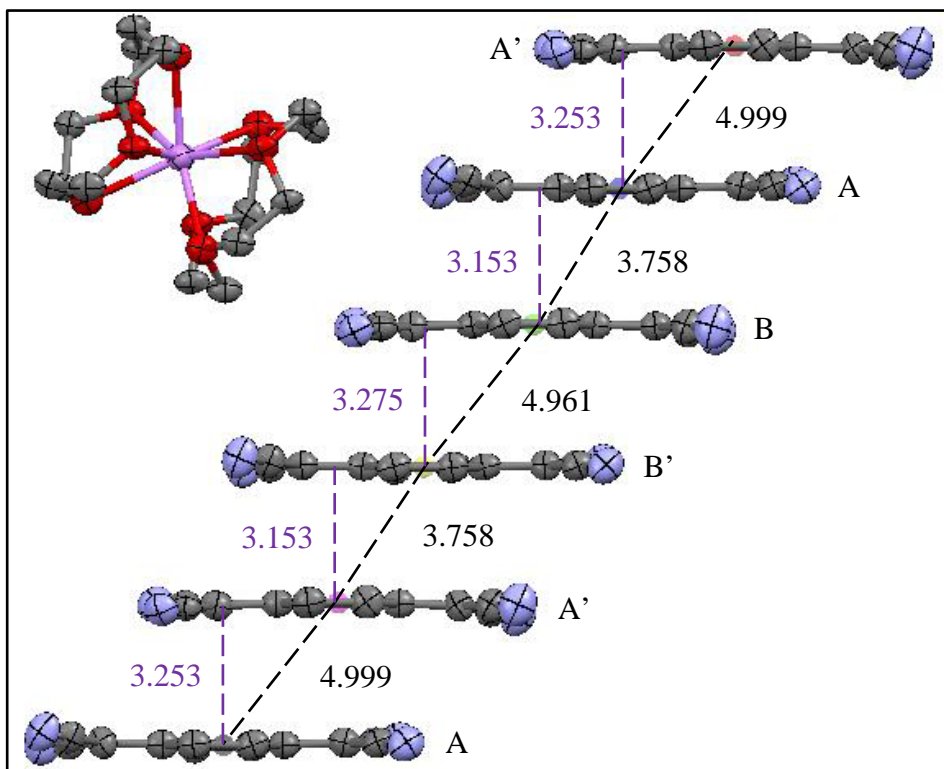


Figure 3.12 The TCNQ column in $(12C4)_2Li(TCNQ)_2$ (hydrogen atoms are excluded)

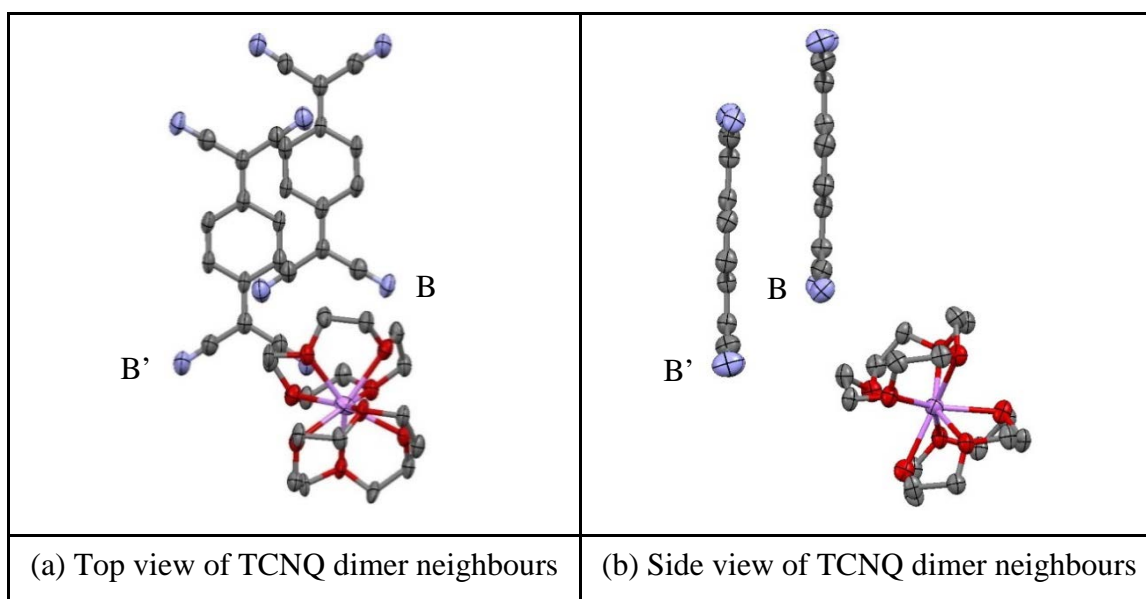


Figure 3.13 Top (a) and side (b) views of TCNQ units (BB'), which is similar as for TCNQ dimer neighbours (AA') in $(12C4)_2Li(TCNQ)_2$ (hydrogen atoms are excluded)

| TCNQ units | | TCNQ dimer | TCNQ dimer neighbours (AA') | TCNQ dimer neighbours (BB') |
|--|--------------|------------|-----------------------------|-----------------------------|
| π - π perpendicular distance (Å) | | 3.15 | 3.25 | 3.28 |
| Short-axis slip | Distance (Å) | 0.48 | 2.72 | 2.70 |
| | Angle (°) | 8.66 | 39.93 | 39.50 |
| Long-axis slip | Distance (Å) | 1.99 | 2.65 | 2.57 |
| | Angle (°) | 32.28 | 39.19 | 38.12 |
| Centroid-centroid distance (Å) | | 3.76 | 5.00 | 4.96 |

Table 3.5 Distances (Å) and angles (°) within the TCNQ stacks of (12C4)₂Li(TCNQ)₂

Within the AB dimer, the individual TCNQ units adopt a shallow boat conformation in which neighbouring $-\text{C}(\text{CN})_2$ units are twisted away from each other. The two TCNQ planes are slightly tilted in respect to each other (by *ca.* 0.19°). Individual TCNQ units adopt a paddle conformation in which one $-\text{C}(\text{CN})_2$ group is tilted in respect to the other side of the same TCNQ unit, by *ca.* 7.98° for TCNQ(A) and by *ca.* 7.00° for TCNQ(B) respectively. From these data, it will be evident that π -facial overlap between neighbouring dimers within a column is not ideal for extended π - π delocalisation within the column.

Each Li^+ cation is sandwiched between two crown ether molecules and resulting complex $[(12\text{C}4)_2\text{Li}^+]$ lies in channels between the TCNQ columns. There is no direct co-ordination between the TCNQ units and the Li^+ ions. Within the cation complex, the planes of the two crown ether units (as defined by each set of oxygen atoms) are slightly tilted in respect to each other (by *ca.* 0.09°). Figure 3.14 summarises the various contact distances within the cation complex.

As viewed in Figure 3.14, the four oxygen atoms of each 12C4 unit are sited on their mean plane to form an irregular quadrilateral of mean side *ca.* 2.764 Å. The minimum and maximum of Li^+ -O distances within the cation complex are 2.332 and 2.396 Å respectively. The different Li^+ -O distances demonstrate that the Li^+ cation is distorted above the cavity of each 12C4 units. Two crown ether units are not disordered and are staggered in respect to each other.

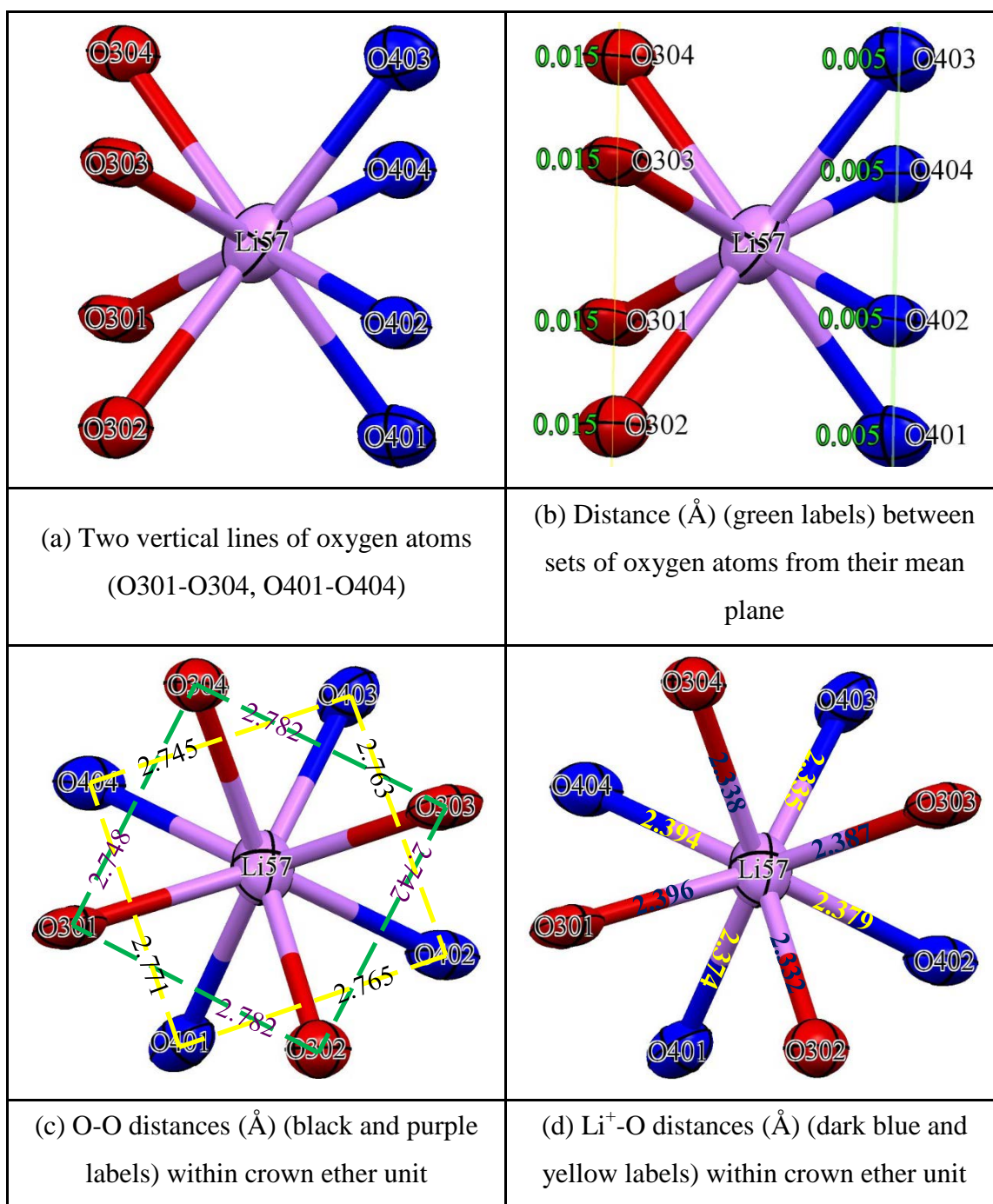


Figure 3.14 The various contact distances (Å) within the cation complex (carbon and hydrogen atoms are excluded)

(b) (12C4)₂Na(TCNQ)₂

Reaction of 12C4 with NaTCNQ and TCNQ⁰ (ratio 2:1:1) in dry acetonitrile afforded a yield (14%) of a dark purple crystalline solid (Combustion Analysis: Calculated: C: 61.30%, H: 5.14%, N: 14.29%. Found: C: 61.17%, H: 4.46%, N: 14.39%.) which contained single crystals suitable for X-ray structural study. Full details including an account of the structure solution and refinement are reported in the Experimental

Section and the Supporting Information (in the Appendices) respectively. The crystals obtained were of $(12C4)_2Na(TCNQ)_2$ and the key components are shown in Figure 3.15.

Bond lengths within the TCNQ units are summarised in Table 3.6. In this structure, the Na^+ ion is coordinated between two crown ether units. The TCNQ units form a dimer which is significantly long axis slipped (see Figure 3.16). The similarity of the bond lengths within the two TCNQ units makes it difficult to distinguish between the $TCNQ^\circ$ and $TCNQ^{\bullet-}$ components.

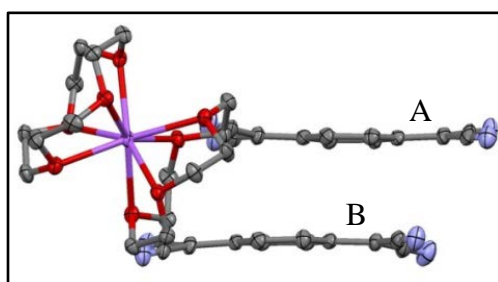


Figure 3.15 Basic unit of $(12C4)_2Na(TCNQ)_2$ (hydrogen atoms are excluded)

| (a) Definition of the bond lengths within the TCNQ molecule | | | | | | |
|---|------------------|-----------|-----------|-----------|-----------|-------|
| Structure | Bond lengths (Å) | | | | | |
| | a | b | c | d | e | f |
| TCNQ unit (A) | | 1.433 (2) | | 1.431 (3) | 1.151 (3) | 0.951 |
| | 1.357 (3) | 1.438 (3) | 1.398 (3) | 1.426 (3) | 1.151 (3) | 0.950 |
| | 1.358 (3) | 1.435 (2) | 1.401 (3) | 1.423 (3) | 1.158 (3) | 0.950 |
| | | 1.438 (3) | | 1.424 (3) | 1.157 (3) | 0.950 |
| TCNQ unit (B) | | 1.438 (2) | | 1.427 (3) | 1.152 (3) | 0.950 |
| | 1.361 (3) | 1.438 (3) | 1.396 (3) | 1.428 (3) | 1.153 (3) | 0.950 |
| | 1.355 (3) | 1.432 (2) | 1.398 (3) | 1.428 (3) | 1.155 (3) | 0.950 |
| | | 1.435 (3) | | 1.426 (3) | 1.153 (3) | 0.949 |

Table 3.6 Summary of bond lengths (Å) observed for TCNQ units in $(12C4)_2Na(TCNQ)_2$

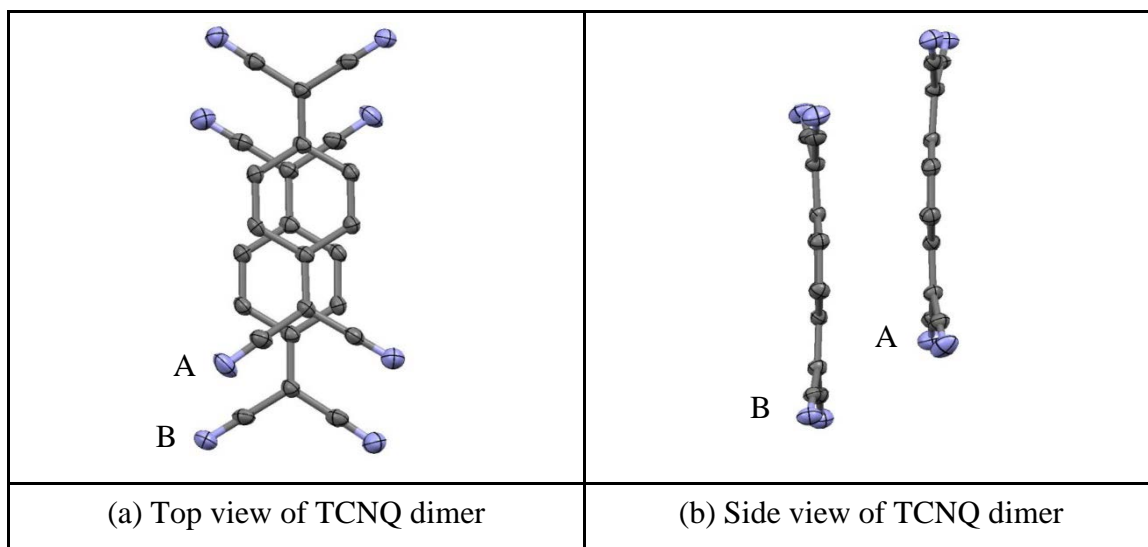


Figure 3.16 Top (a) and side (b) views of TCNQ dimer (AB) in $(12C4)_2Na(TCNQ)_2$ (hydrogen atoms are excluded)

The data in Table 3.6 suggest that both TCNQ units have some quinonoidal character because bond length “a” is less than “b”. For both components A and B, the distribution of bond lengths is intermediate between these reported for $TCNQ^{\circ}$ and $TCNQ^{\bullet-}$ respectively²¹³.

Within the crystal, the TCNQ dimers assemble into infinite columns in which the individual TCNQ units are assembled in an ABB'A' motif (Figure 3.17) and in which neighbouring dimers are significantly “diagonally” slipped [Figure 3.18(a)].

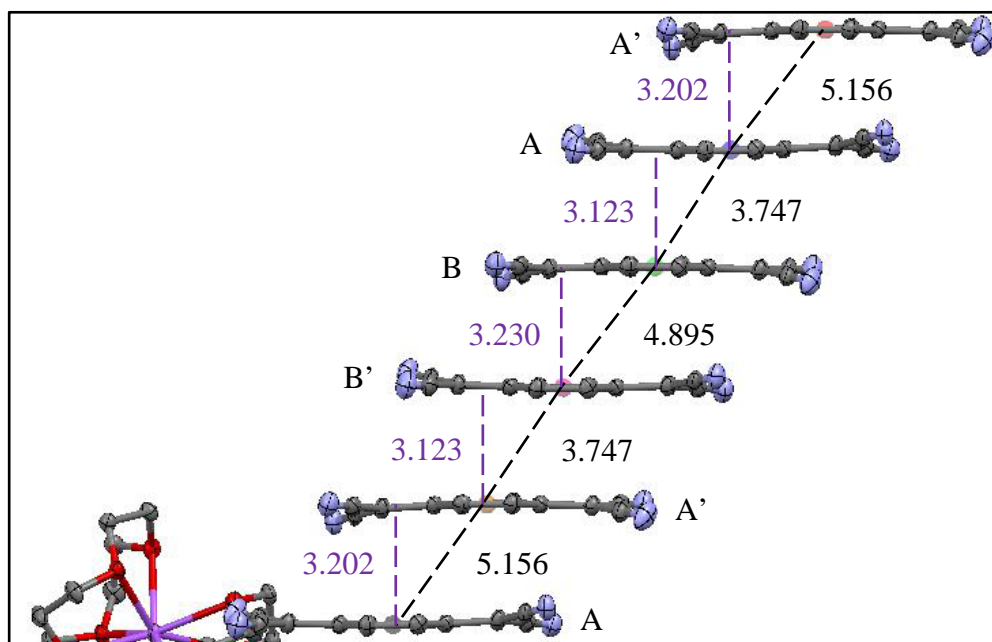


Figure 3.17 The TCNQ column in $(12C4)_2Na(TCNQ)_2$ (hydrogen atoms are excluded)

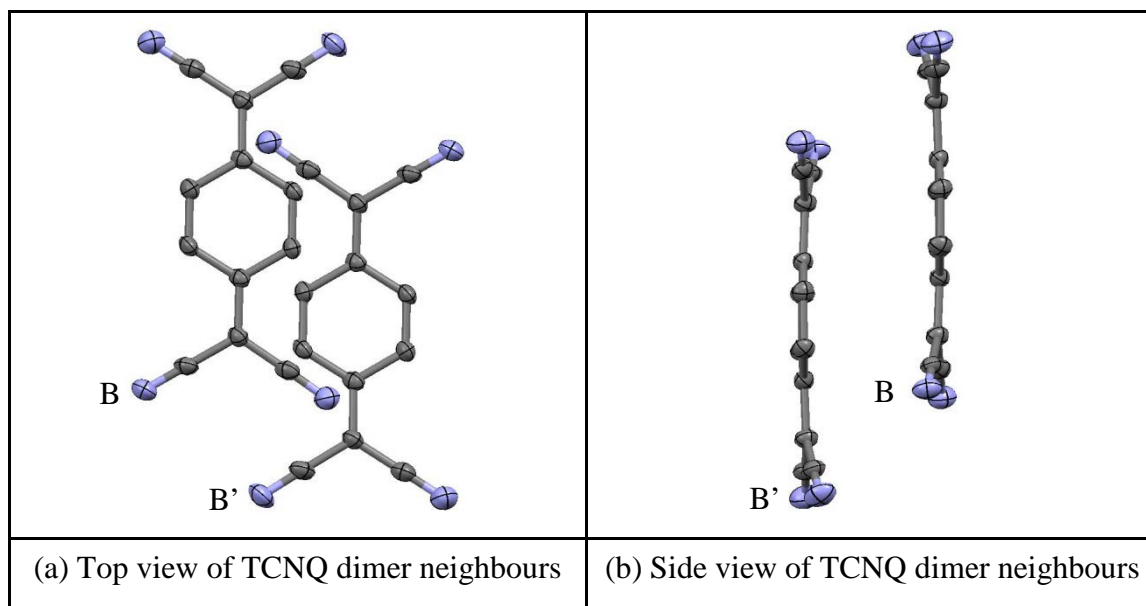


Figure 3.18 Top (a) and side (b) views of TCNQ units (BB'), which is similar as for TCNQ dimer neighbours (AA') in $(12C4)_2Na(TCNQ)_2$ (hydrogen atoms are excluded)

Distances and angles within the TCNQ stacks are summarised in Table 3.7.

| TCNQ units | | TCNQ dimer | TCNQ dimer neighbours (AA') | TCNQ dimer neighbours (BB') |
|--|--------------|------------|-----------------------------|-----------------------------|
| π - π perpendicular distance (Å) | | 3.12 | 3.20 | 3.23 |
| Short-axis slip | Distance (Å) | 0.33 | 3.14 | 2.80 |
| | Angle (°) | 6.04 | 44.44 | 40.92 |
| Long-axis slip | Distance (Å) | 2.04 | 2.55 | 2.39 |
| | Angle (°) | 33.18 | 38.53 | 36.50 |
| Centroid-centroid distance (Å) | | 3.75 | 5.16 | 4.90 |

Table 3.7 Distances (Å) and angles (°) within the TCNQ stacks of $(12C4)_2Na(TCNQ)_2$

Within the AB dimer, the individual TCNQ units adopt a shallow boat conformation in which neighbouring $-C(CN)_2$ units are twisted away from each other. The two TCNQ planes are slightly tilted in respect to each other (by *ca.* 1.06°). Individual TCNQ units adopt paddle conformation in which one $-C(CN)_2$ group is tilted in respect to the other side of the same TCNQ unit by *ca.* 12.97° for TCNQ(A) and by *ca.* 14.07° for TCNQ(B) respectively. From these data, it will be evident that π -facial overlap between

neighbouring dimers within a column is not ideal for extended π - π delocalisation within the column.

Each Na^+ cation is sandwiched between two crown ether molecules and the resulting complex $[(12\text{C}4)_2\text{Na}^+]$ lies in channels between the TCNQ columns. There is no direct coordination between the TCNQ units and the Na^+ ions. Within the cation complex, the planes of the two crown ether units (as defined by each set of oxygen atoms) are slightly tilted in respect to each other (by *ca.* 0.86°). Figure 3.19 summarises the various contact distances within the cation complex.

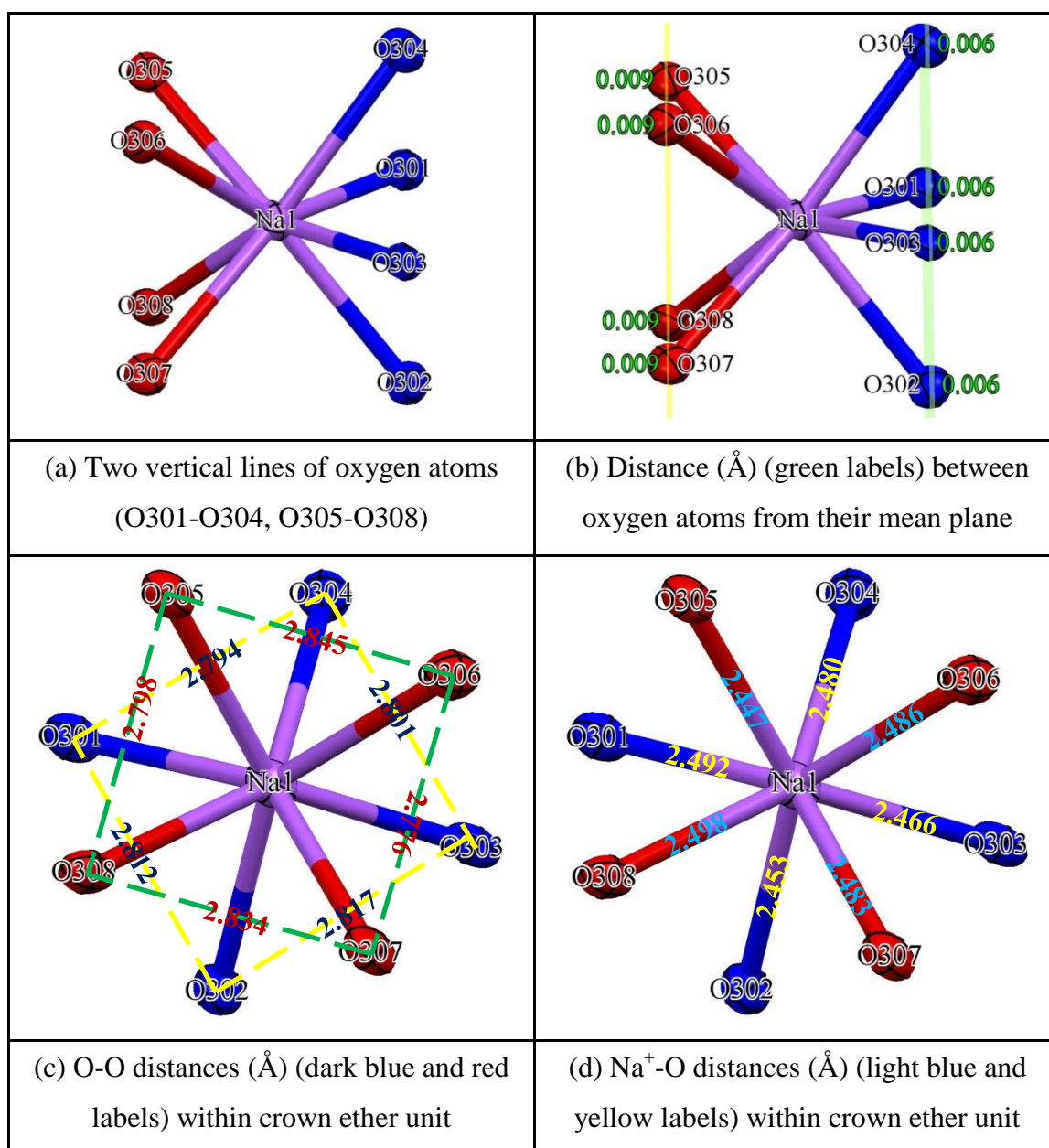


Figure 3.19 The various contact distances (Å) within the cation complex (carbon and hydrogen atoms are excluded)

As can be seen in Figure 3.19 (a and b), each of the four oxygen atoms within a 12C4 unit is accurately located at the same distance from their mean plane. They form an irregular quadrilateral geometry with a mean side of *ca.* 2.813 Å. The four oxygen atoms have different bond lengths to central Na⁺ cation, which demonstrates that the Na⁺ cation is in a distorted position above the cavity of each 12C4 unit. All of the Na⁺-O distances are similar to that of a van der Waals' contact (Na⁺-O = 2.47 Å)^{269,270}. Two crown ether units are not disordered and are staggered in respect to each other.

(c) (12C4)₂K(TCNQ)₂

Reaction of 12C4 with KTCNQ and TCNQ⁰ (ratio 2:1:1) in dry acetonitrile afforded a yield (24%) of a purple crystalline solid (Combustion Analysis: Calculated: C: 60.06%, H: 5.04%, N: 14.00%. Found: C: 59.82%, H: 4.44%, N: 15.74%.) which contained single crystals suitable for X-ray structural study. Full details including an account of the structure solution and refinement are reported in the Experimental Section and the Supporting Information (in the Appendices) respectively. The crystals obtained were of (12C4)₂K(TCNQ)₂ and the core unit is shown in Figure 3.20.

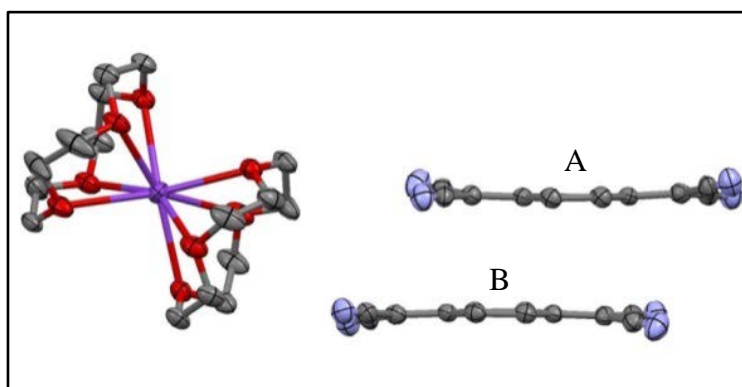


Figure 3.20 Core unit of (12C4)₂K(TCNQ)₂ (hydrogen atoms are excluded)

Bond lengths within each of the TCNQ units are summarised in Table 3.8. In this structure the K⁺ ion is coordinated between two crown ether units. The TCNQ units form a dimer which is significantly long axis slipped (see Figure 3.21). The similarity of the bond lengths within the two TCNQ units makes it difficult to distinguish between the TCNQ⁰ and TCNQ⁻ component.

The data in Table 3.8 suggest that both TCNQ units have some quinonoidal character because bond length “a” is less than “b”. For both components A and B, the distribution

of bond lengths is intermediate between these reported for TCNQ⁰ and TCNQ^{•-} respectively²¹³.

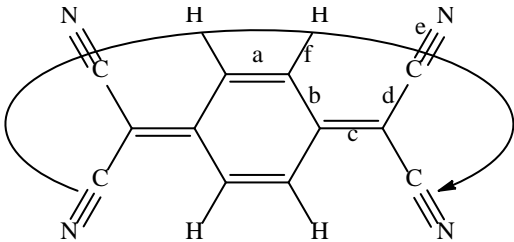
|  | | | | | | |
|--|------------------|-----------|-----------|-----------|-----------|-------|
| (a) Definition of the bond lengths within the TCNQ molecule | | | | | | |
| Structure | Bond lengths (Å) | | | | | |
| | a | b | c | d | e | f |
| TCNQ unit (A) | | 1.434 (2) | | 1.435 (2) | 1.151 (2) | 0.950 |
| | 1.358 (2) | 1.437 (2) | 1.395 (2) | 1.426 (2) | 1.151 (2) | 0.951 |
| | 1.359 (2) | 1.438 (2) | 1.400 (2) | 1.425 (2) | 1.155 (2) | 0.950 |
| | | 1.435 (2) | | 1.426 (2) | 1.154 (2) | 0.950 |
| TCNQ unit (B) | | 1.435 (2) | | 1.428 (2) | 1.154 (2) | 0.949 |
| | 1.359 (2) | 1.442 (2) | 1.398 (2) | 1.427 (2) | 1.153 (2) | 0.949 |
| | 1.354 (2) | 1.435 (2) | 1.391 (2) | 1.437 (2) | 1.148 (2) | 0.950 |
| | | 1.437 (2) | | 1.429 (2) | 1.153 (2) | 0.950 |

Table 3.8 Summary of bond lengths (Å) observed for TCNQ units in (12C4)₂K(TCNQ)₂

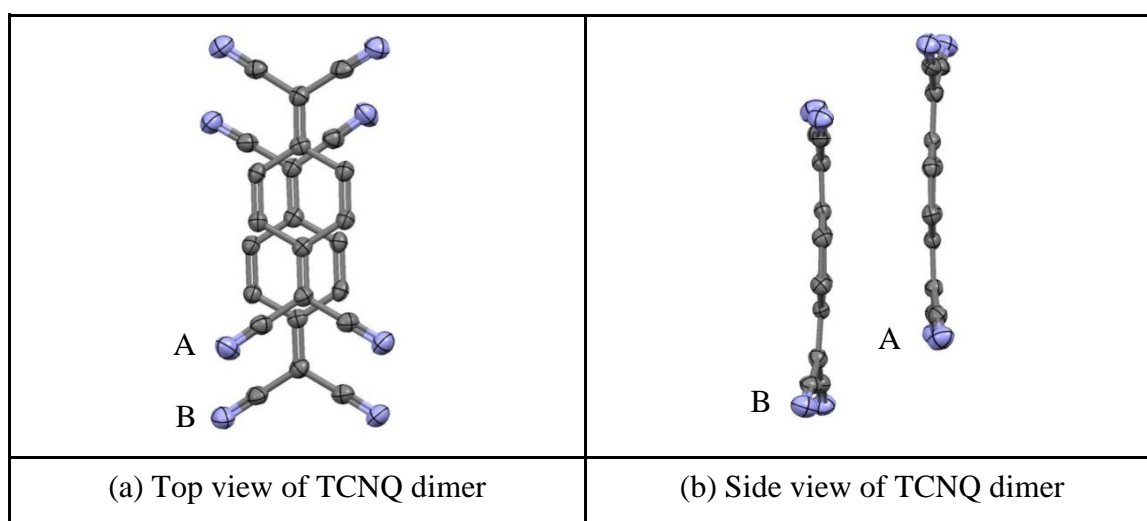


Figure 3.21 Top (a) and side (b) views of TCNQ dimer (AB) in (12C4)₂K(TCNQ)₂ (hydrogen atoms are excluded)

Within the crystal, the TCNQ dimers assemble into infinite columns in which the individual TCNQ units are assembled in an ABB'A' motif (Figure 3.22) in which neighbouring dimers are significantly “diagonally” slipped (Figure 3.23).

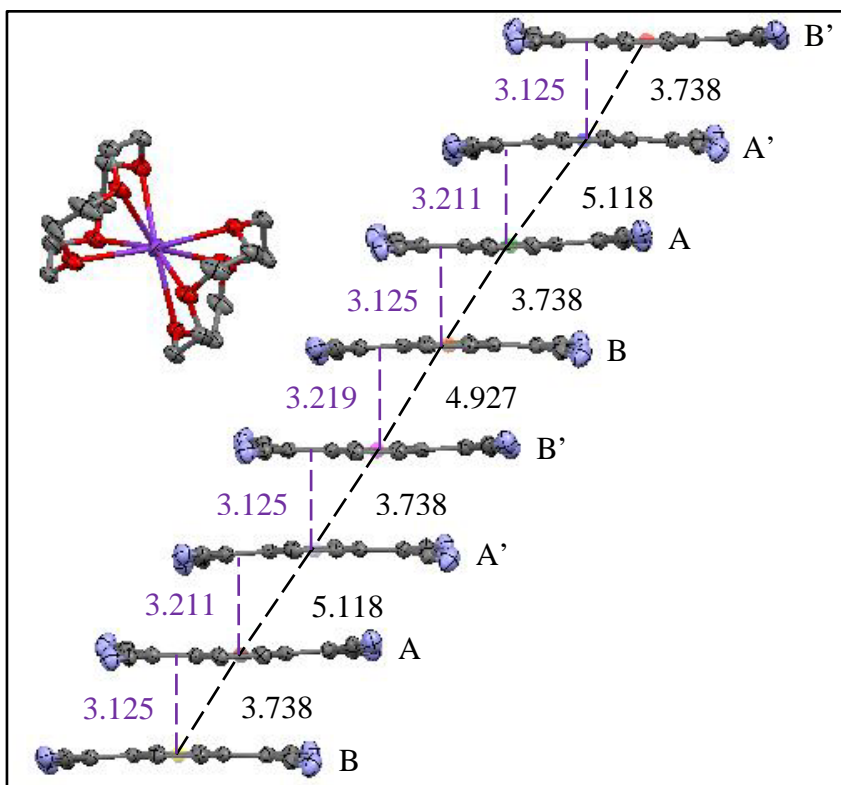


Figure 3.22 The TCNQ column in $(12C4)_2K(TCNQ)_2$ (hydrogen atoms are excluded)

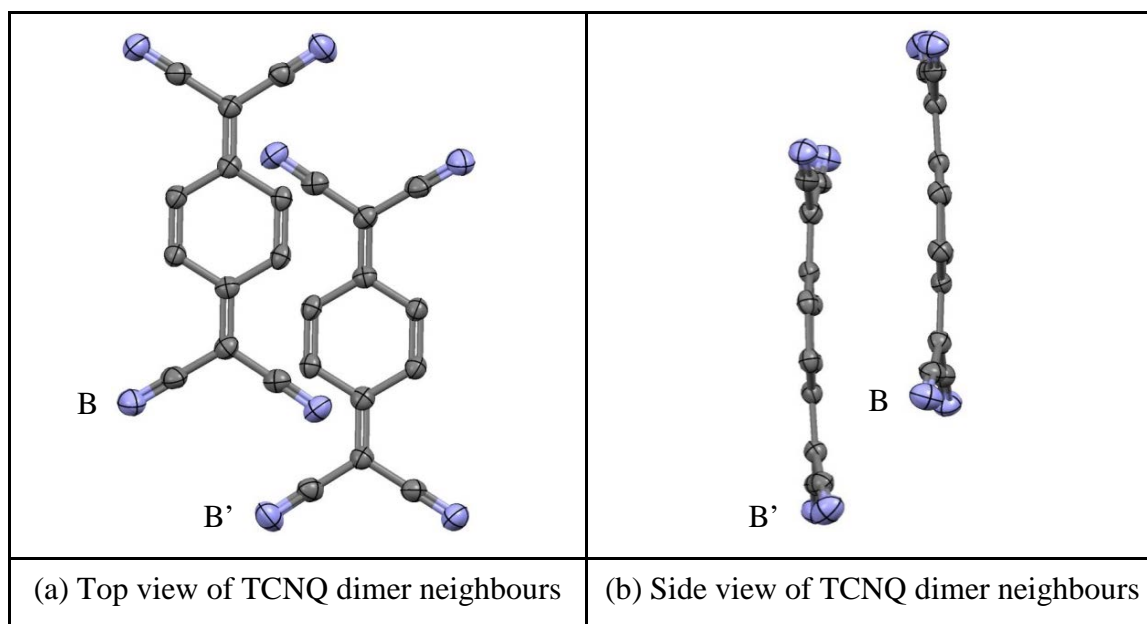


Figure 3.23 Top (a) and side (b) views of TCNQ dimer units (BB'), which is similar to TCNQ dimer neighbours (AA') in $(12C4)_2K(TCNQ)_2$ (hydrogen atoms are excluded)

Distances and angles within the TCNQ stacks are summarised in Table 3.9.

| TCNQ units | | TCNQ dimer | TCNQ dimer neighbours (AA') | TCNQ dimer neighbours (BB') |
|--|--------------|------------|-----------------------------|-----------------------------|
| π - π perpendicular distance (Å) | | 3.13 | 3.21 | 3.22 |
| Short-axis slip | Distance (Å) | 0.30 | 3.13 | 2.92 |
| | Angle (°) | 5.47 | 44.28 | 42.20 |
| Long-axis slip | Distance (Å) | 2.03 | 2.47 | 2.32 |
| | Angle (°) | 32.97 | 37.58 | 35.77 |
| Centroid-centroid distance (Å) | | 3.74 | 5.12 | 4.93 |

Table 3.9 Distances (Å) and angles (°) within the TCNQ stacks of (12C4)₂K(TCNQ)₂

Within the AB dimer the individual TCNQ units adopt a shallow boat conformation in which neighbouring $-C(CN)_2$ units are twisted away from each other. The two TCNQ planes are slightly tilted in respect to each other (by *ca.* 0.92°). Individual TCNQ units adopt paddle conformation in which one $-C(CN)_2$ group is tilted in respect to the other side of the same TCNQ unit, by *ca.* 13.59° for TCNQ(A) and by *ca.* 11.39° for TCNQ(B) respectively. From these data, it will be evident that π -facial overlap between neighbouring dimers within a column is not ideal for extended π - π delocalisation within the column.

Each K⁺ cation is sandwiched between two crown ether molecules and the resulting cation complex [(12C4)₂K⁺] lies in channels between the TCNQ columns. There is no direct coordination between the TCNQ units and the K⁺ ions. Within the cation complex the planes of the two crown ether units (as defined by each set of oxygen atoms) are slightly tilted in respect to each other (by *ca.* 4.18°). Figure 3.24 summarises the various contact distances within the cation complex.

As seen in Figure 3.24, each of the four oxygen atoms of each 12C4 unit is sited at the same distance from their mean plane to form an irregular quadrilateral geometry of mean side *ca.* 2.837 and 2.848 Å respectively. The different K⁺-O distances demonstrate that the K⁺ cation is distorted above the cavity of each 12C4 units. All of the K⁺-O distances are less than that of a van der Waals' contact (K⁺-O = 2.85 Å)^{269,271} and thus it

seems justifiable to regard the metal cations and the oxygen atoms as being in contact. The two crown ether units are not disordered and are staggered in respect to each other.

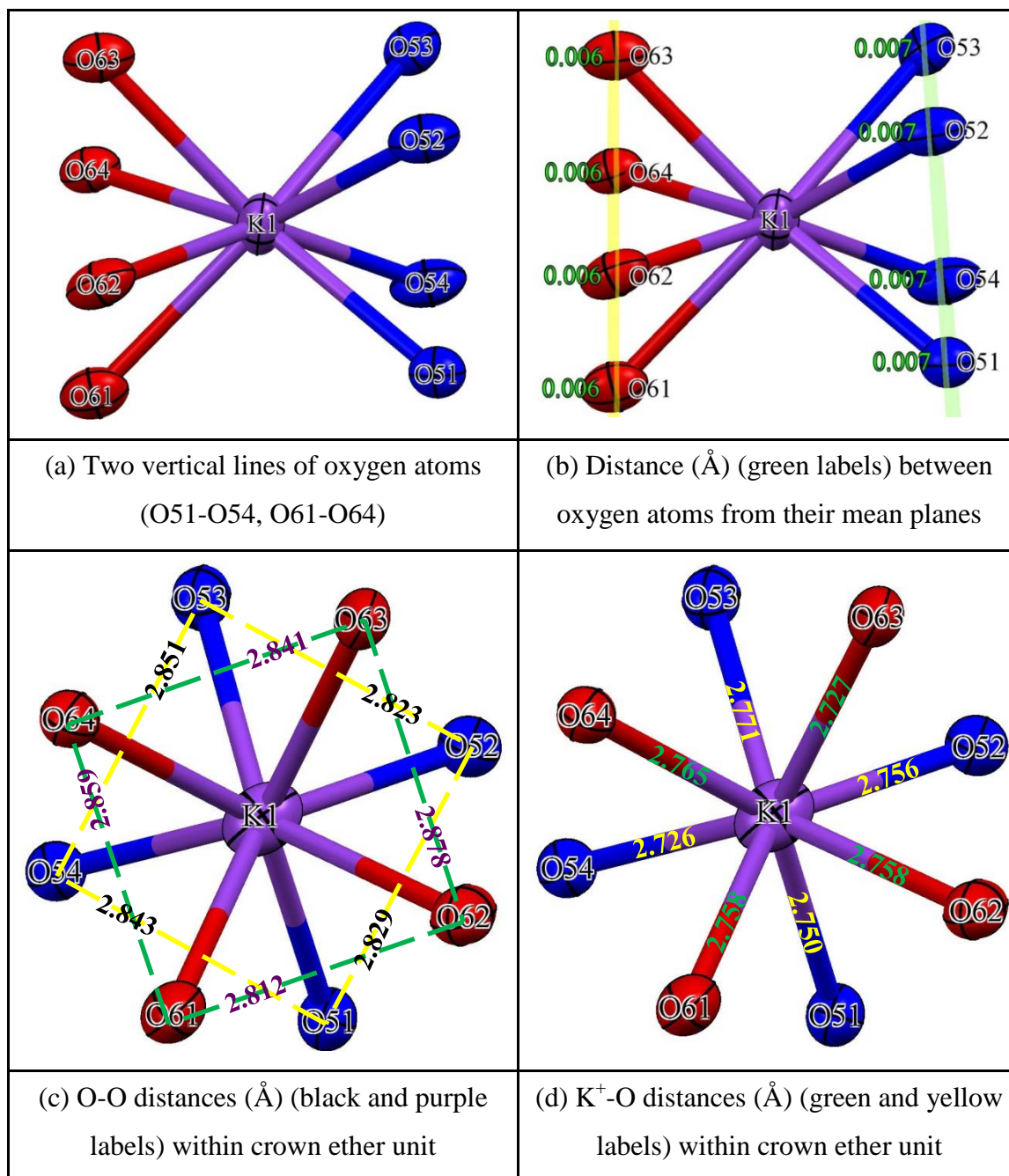


Figure 3.24 Summarises the various contact distances (Å) within the cation complex (carbon and hydrogen atoms are excluded)

3.3.1.3 Comparison of (12C4)₂Li(TCNQ)₂, (12C4)₂Na(TCNQ)₂ and (12C4)₂K(TCNQ)₂ structures

Figure 3.25 shows the spacefilled views of the components of (12C4)₂Li⁺, Na⁺ and

$\text{K}(\text{TCNQ})_2$ respectively. In each of the complexes, two TCNQ units form a dimer. Because each metal cation (Li^+ , Na^+ or K^+) is coordinated in between two crown ether units, there are not any direct metal to TCNQ interactions (M^+-NC) in each of the complexes. The M^+-O bond lengths become longer as the size of the metal cation increases from Li^+ to K^+ . Meanwhile, the cell volume is increased from 1906.4(2) in $(12\text{C}4)_2\text{Li}(\text{TCNQ})_2$ to 1979.3(2) for $(12\text{C}4)_2\text{K}(\text{TCNQ})_2$.

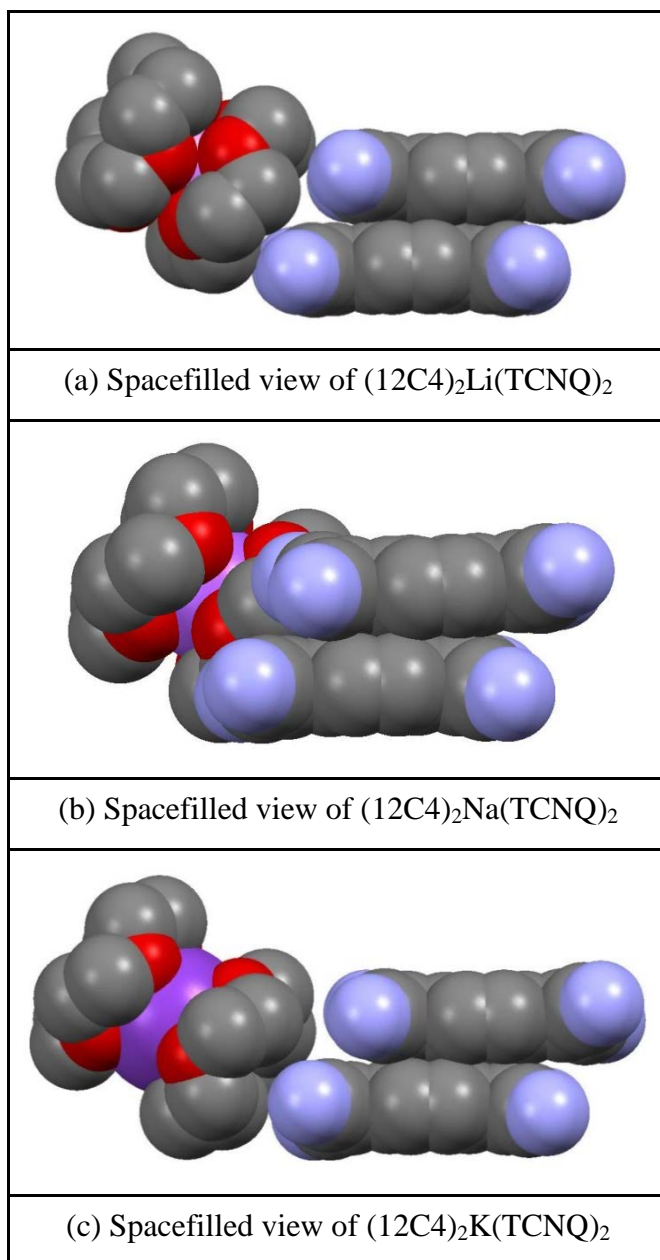


Figure 3.25 Spacefilled view of $(12\text{C}4)_2\text{Li}^+$, Na^+ and $\text{K}(\text{TCNQ})_2$ (hydrogen atoms are excluded)

TCNQ units prefer to form infinite column in these three TCNQ salts with long-axis slipped within TCNQ dimer and TCNQ dimer neighbours as viewed in Figure 3.26. In

each case, the similarity of the bond lengths within the two TCNQ units makes it difficult to distinguish between the TCNQ^0 and $\text{TCNQ}^{\cdot-}$ components, which suggests that electrons are delocalised within in the TCNQ column.

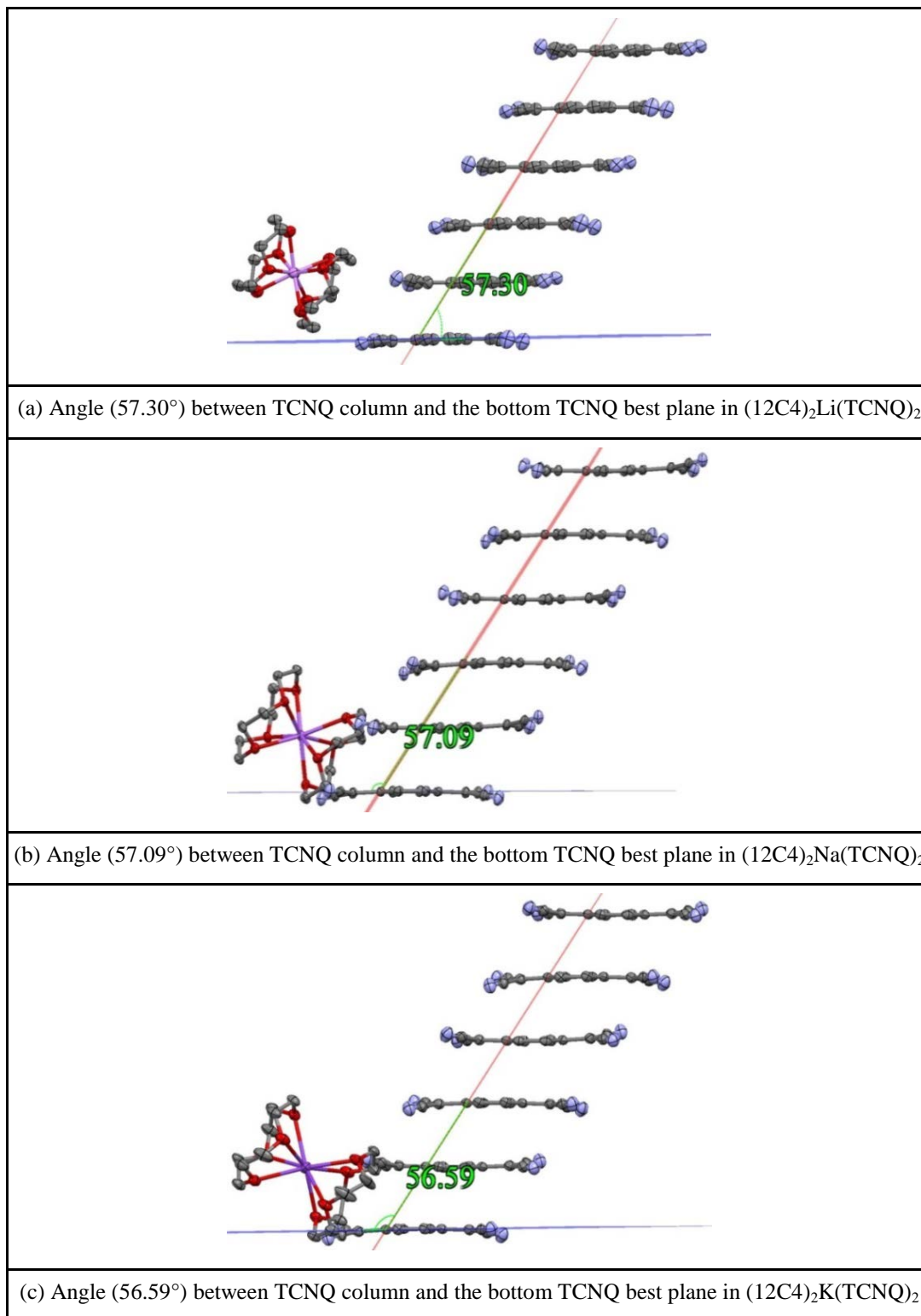


Figure 3.26 Tilt angle between TCNQ column and the bottom TCNQ best plane for $(12\text{C}4)_2\text{Li}^+$, Na^+ and $\text{K}(\text{TCNQ})_2$ (hydrogen atoms are excluded)

| TCNQ units | | (12C4) ₂ Li(TCNQ) ₂ | | (12C4) ₂ Na(TCNQ) ₂ | | (12C4) ₂ K(TCNQ) ₂ | |
|--|--------------|---|-----------------------|---|-----------------------|--|-----------------------|
| | | TCNQ dimer | TCNQ dimer neighbours | TCNQ dimer | TCNQ dimer neighbours | TCNQ dimer | TCNQ dimer neighbours |
| π - π perpendicular distance (Å) | | 3.15 | 3.26 | 3.12 | 3.22 | 3.13 | 3.21 |
| Long-axis slip | Distance (Å) | 1.99 | 2.61 | 2.04 | 2.47 | 2.03 | 2.39 |
| | Angle (°) | 32.28 | 38.68 | 33.18 | 37.49 | 32.97 | 36.67 |
| Centroid-centroid distance (Å) | | 3.76 | 4.98 | 3.75 | 5.03 | 3.74 | 5.02 |

Table 3.10 Comparison of key parameters of TCNQ column geometries in (12C4)₂Li/Na/K(TCNQ)₂

3.3.2 Preparation of (15C5)M(TCNQ)_n complexes (M = Li, Na)

In this section, the solid-state behaviour of the complexes of (15C5)LiTCNQ, (15C5)NaTCNQ, (15C5)Li(TCNQ)₂·H₂O and (15C5)Na(TCNQ)₂·H₂O will be discussed.

3.3.2.1 (15C5)MTCNQ complexes (M = Li, Na)

(a) (15C5)LiTCNQ

Reaction of 15C5 with LiTCNQ (ratio 1:1) in dry acetonitrile afforded a reasonable yield (81%) of a very pure purple crystalline solid (Combustion Analysis: Calculated: C: 61.25%, H: 5.61%, N: 12.98%. Found: C: 61.46%, H: 5.51%, N: 13.29%.) which contained single crystals suitable for X-ray structural study. Full details including an account of the structure solution and refinement are reported in the Experimental Section and the Supporting Information (in the Appendices) respectively. The crystals obtained were of (15C5)LiTCNQ and the basic structural unit is shown in Figure 3.27.

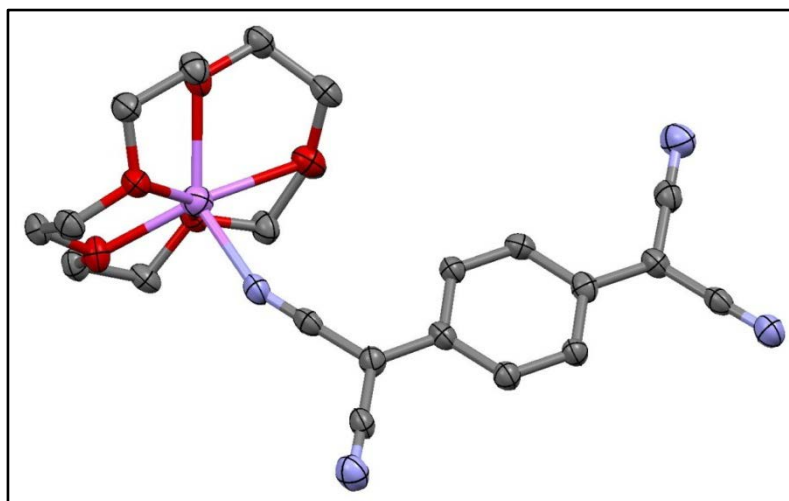


Figure 3.27 Basic structural unit of (15C5)LiTCNQ (hydrogen atoms are excluded)

Bond lengths within the $\text{TCNQ}^{\bullet-}$ anions are summarised in Table 3.11. In this structure, the Li^+ ion is complexed with one crown ether and co-ordinated to one $\text{TCNQ}^{\bullet-}$ anion. The $\text{TCNQ}^{\bullet-}$ anions associate to form a dimer which is significantly short-axis slipped (Figure 3.28). The data in Table 3.11 suggest that the $\text{TCNQ}^{\bullet-}$ has some quinonoidal character because bond length “a” is less than “b”. The distribution of bond lengths is reported for $\text{TCNQ}^{\bullet-}$ ²¹³.

| (a) Definition of the bond lengths within the $\text{TCNQ}^{\bullet-}$ molecule | | | | | | |
|---|------------------|-----------|-----------|-----------|-----------|-----------|
| Structure | Bond lengths (Å) | | | | | |
| | a | b | c | d | e | f |
| $\text{TCNQ}^{\bullet-}$ unit | | 1.420 (3) | | 1.419 (3) | 1.156 (3) | 0.951 (3) |
| | 1.362 (3) | 1.420 (3) | 1.418 (3) | 1.416 (3) | 1.154 (3) | 0.950 (3) |
| | 1.365 (3) | 1.418 (3) | 1.420 (3) | 1.419 (3) | 1.157 (3) | 0.949 (3) |
| | | 1.426 (3) | | 1.413 (3) | 1.158 (3) | 0.949 (3) |

Table 3.11 Summary of bond lengths (Å) observed for $\text{TCNQ}^{\bullet-}$ units in (15C5)LiTCNQ

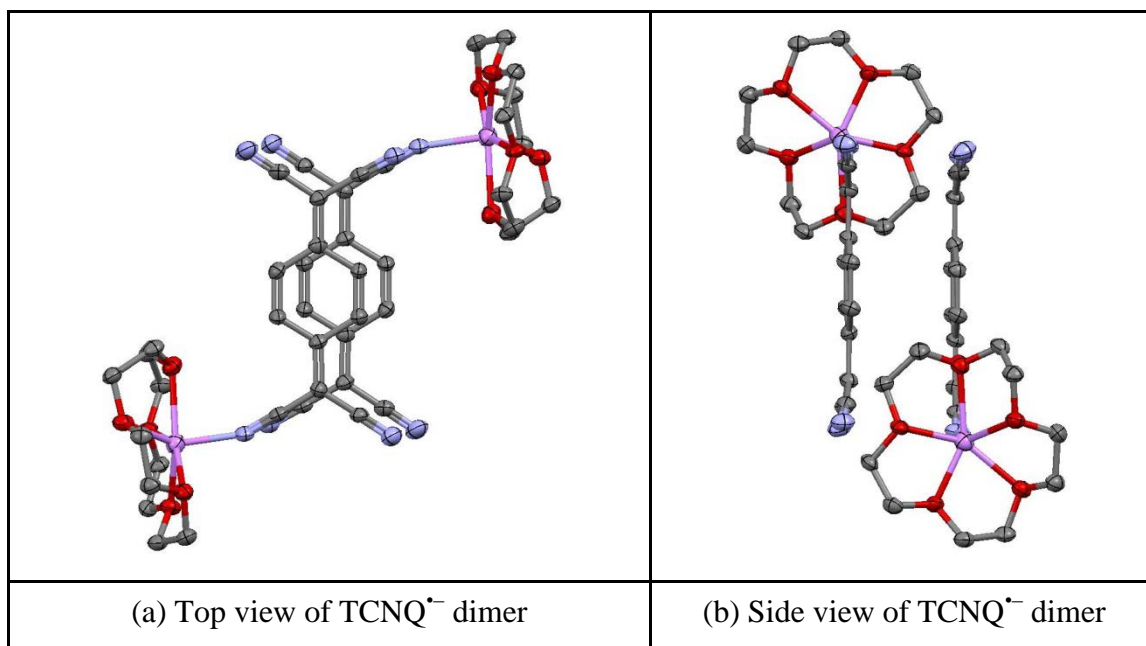


Figure 3.28 Top (a) and side (b) views of TCNQ^{•-} dimer and associated counter ions in (15C5)LiTCNQ (hydrogen atoms are excluded)

Within the crystal, the TCNQ^{•-} units are assembled into separated dimers (Figure 3.29) in which neighbouring dimers are significantly long-axis slipped (Figure 3.30). Distance and angles within the TCNQ^{•-} stacks are listed in Table 3.12.

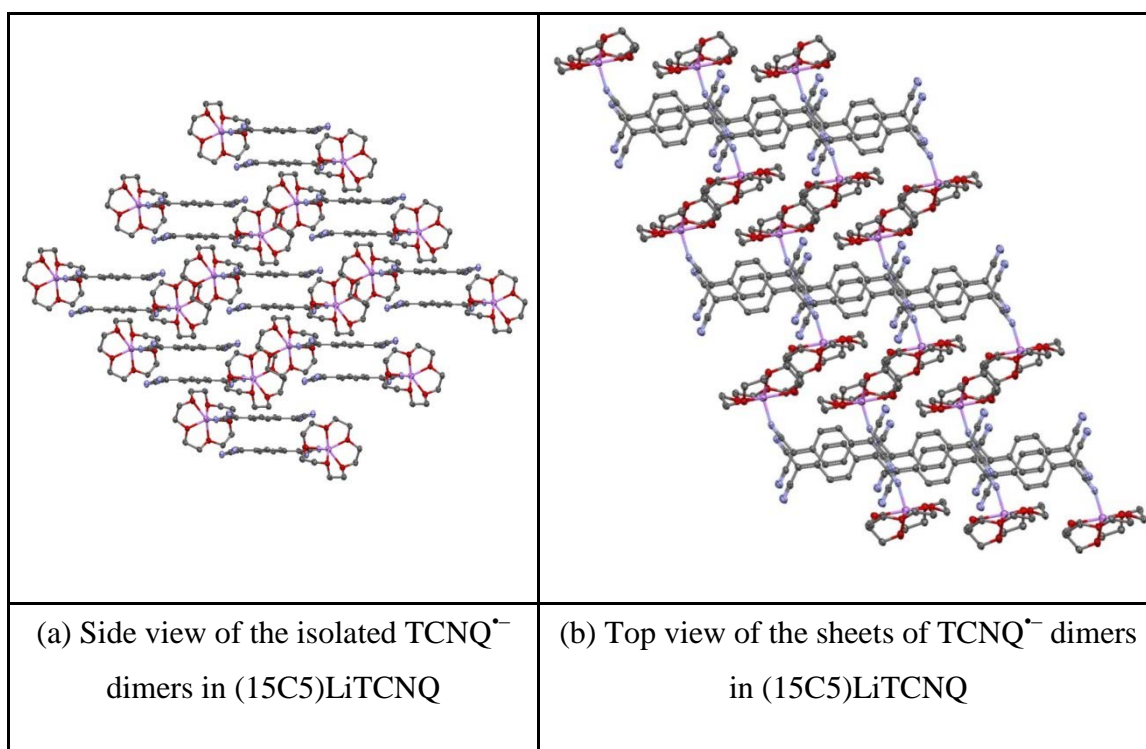


Figure 3.29 Side (a) and Top (b) views of TCNQ^{•-} dimers in (15C5)LiTCNQ (hydrogen atoms are excluded)

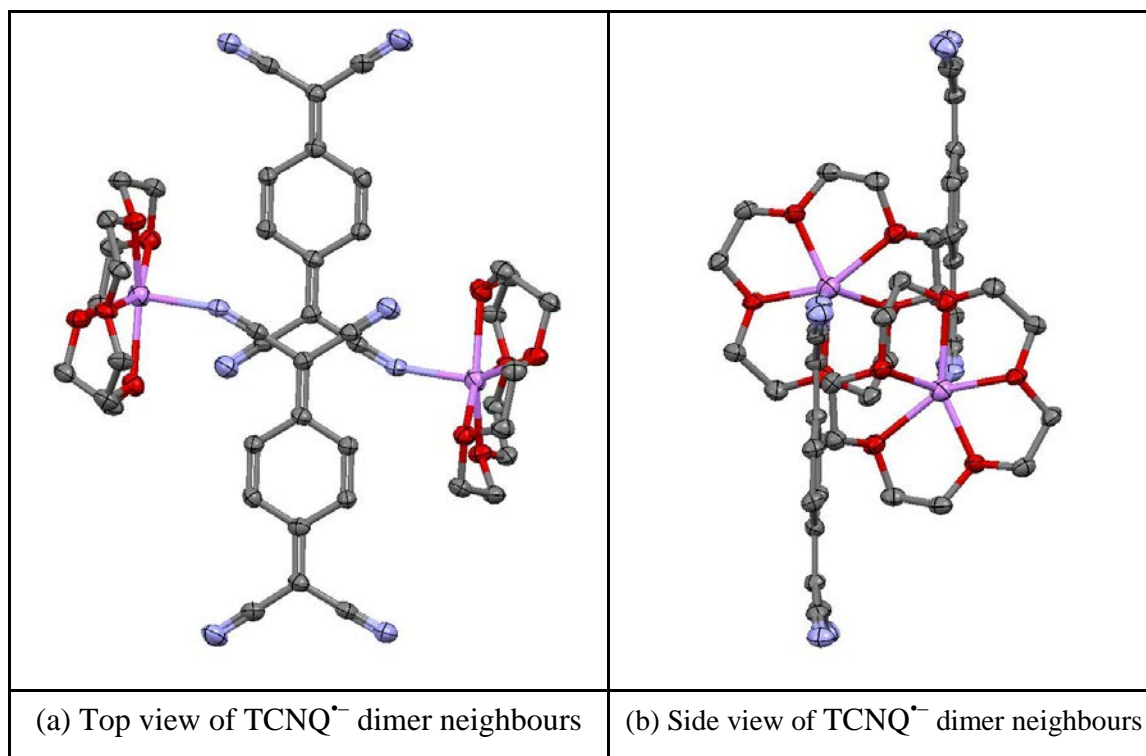


Figure 3.30 Top (a) and side (b) views of TCNQ^{•-} dimer neighbours in (15C5)LiTCNQ (hydrogen atoms are excluded)

| TCNQ units | | TCNQ ^{•-} dimer | TCNQ ^{•-} dimer neighbours |
|--|--------------|--------------------------|-------------------------------------|
| π - π perpendicular distance (Å) | | 3.14 | 3.45 |
| Short-axis slip | Distance (Å) | 0.96 | 0.020 |
| | Angle (°) | 16.99 | 0.33 |
| Long-axis slip | Distance (Å) | 0.25 | 6.93 |
| | Angle (°) | 4.55 | 63.51 |
| Centroid-centroid distance (Å) | | 3.30 | 7.75 |

Table 3.12 Distances (Å) and angles (°) within the TCNQ^{•-} stacks of (15C5)LiTCNQ

In (15C5)LiTCNQ, each TCNQ^{•-} is coordinated to only one metal cation. Consequently, the TCNQ^{•-} forms brickwork packing which is made up of pairs of TCNQ^{•-} dimers. Each pair of TCNQ^{•-} dimer is closely face-to-face π -associated and slightly short axis slipped. However, the TCNQ^{•-} dimer neighbours within the column are significantly long axis slipped. Within individual TCNQ^{•-} dimers, the TCNQ^{•-} units are slightly boat shape with the twisting in such a way that the cyano groups in

neighbouring $\text{TCNQ}^{\bullet-}$ units are pushed away from each other. Figure 3.31 shows $\text{TCNQ}^{\bullet-}$ dimer geometries in $(15\text{C}5)\text{LiTCNQ}$ illustrating the short-axis slip within a dimer (overlap view) and the distortion from planarity (conformation view) respectively, together with the relationship with a next nearest-neighbour dimer.

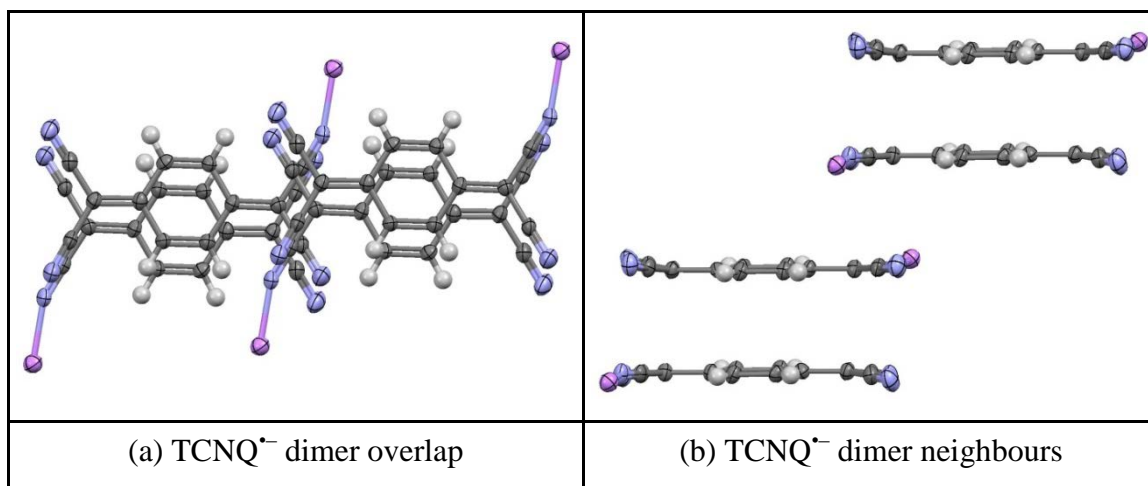


Figure 3.31 $\text{TCNQ}^{\bullet-}$ dimers geometries in $(15\text{C}5)\text{LiTCNQ}$

Figure 3.32 shows torsion angles in the $\text{TCNQ}^{\bullet-}$ units for $(15\text{C}5)\text{LiTCNQ}$.

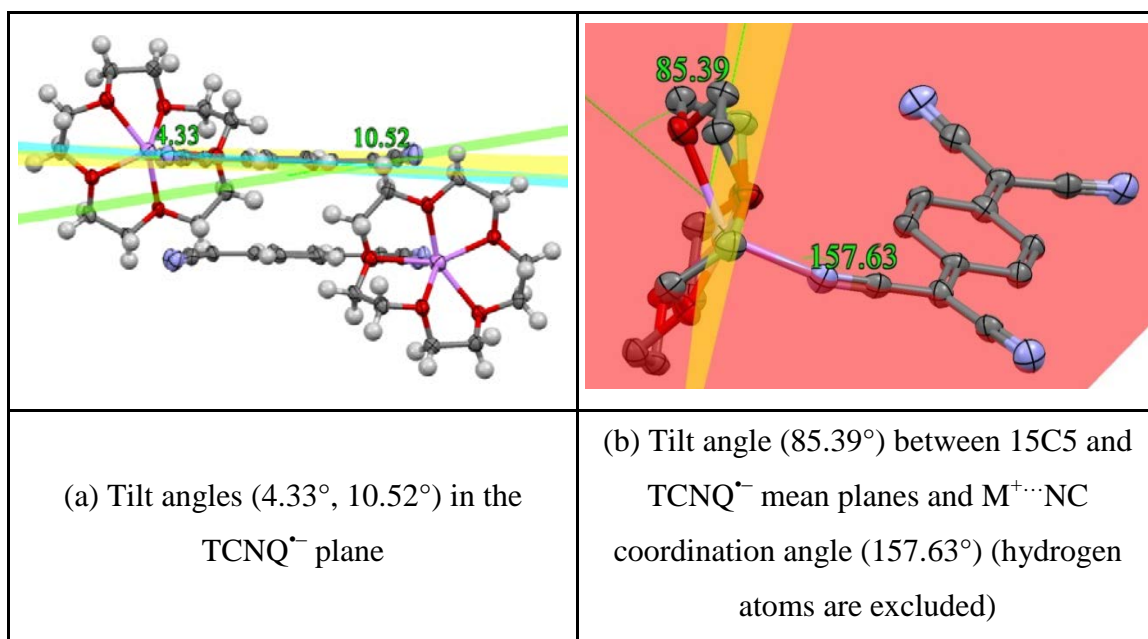


Figure 3.32 Angular relationships in $(15\text{C}5)\text{LiTCNQ}$

Each Li^+ cation is coordinated to one nitrogen atom from cyano group and five oxygen atoms from crown ether unit. Each crown ether complex lies in a channel between the $\text{TCNQ}^{\bullet-}$ stacks. The Li^+ cation sits above the crown ether unit because of the coordination with nitrogen on cyano group from the neighbouring $\text{TCNQ}^{\bullet-}$ unit. The

crown ether plane is tilted at an angle of 85.39° in respect to benzenoid core of the TCNQ $^-$ unit. As viewed in Figure 3.32(b), the coordination angle is not linear between Li $^+$ and NC but subtends a Li $^+ \cdots$ NC angle of 157.63° . The tilt angles (4.33° , 10.52°) in the TCNQ $^-$ plane reflect the fact that only one cyano group from a TCNQ $^-$ unit coordinates to the lithium ion resulting in a twisted geometry. In the packed structure (Figure 3.29), the presence of TCNQ $^-$ dimers is similar to those seen for (18C6)MTCNQ (M = K, Rb) except that in the present case each metal cation only coordinates to one cyano group rather than two in those examples¹³¹. Similarly in the present structure, only TCNQ $^-$ dimer formation occurs there being no extended interactions between TCNQ $^-$ dimers in (15C5)LiTCNQ. Figure 3.33 summarises the various contact distances within the cation complex.

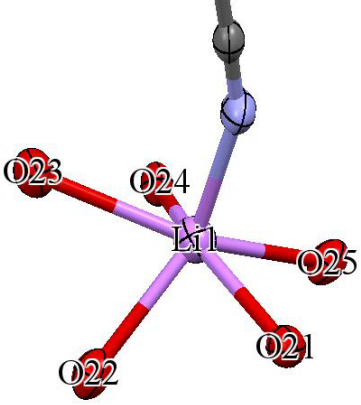
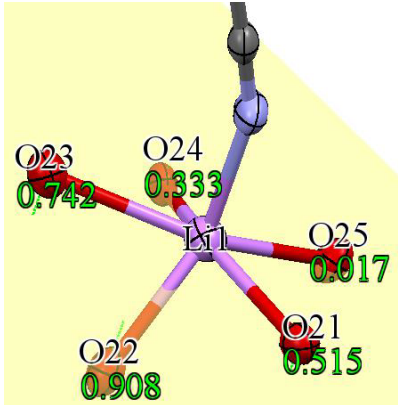
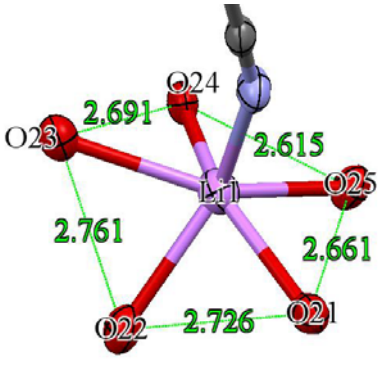
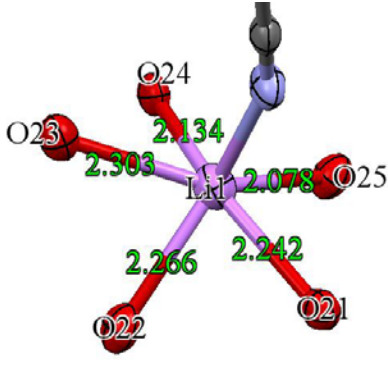
| | |
|---|--|
|  |  |
| (a) Five oxygen atoms (O21-O25) on crown ether unit | (b) Distance (Å) (green labels) between five oxygen atoms from their mean plane |
|  |  |
| (c) O-O distances (Å) (green labels) within 15C5 | (d) Li $^+$ -O distances (Å) (green labels) within 15C5 |

Figure 3.33 The various contact distances (Å) within the cation complex (carbon atoms on crown ether unit and hydrogen atoms are excluded)

As viewed in Figure 3.33, the cation complex of (15C5)Li⁺ form a pentagonal pyramid configuration. Except for O22 which is 0.908 Å away from the oxygen atoms, mean plane, the other four ligating oxygen atoms of the crown ether are located above and below their mean plane. Consequently, all of the five oxygen atoms of the crown ether form irregular pentagonal geometry of mean side by *ca.* 2.691 Å. All of the Li⁺-O distances in (15C5)LiTCNQ lie in the range between 2.078 and 2.303 Å. The Li⁺-N distance (2.078 Å) is slightly less than that of a van der Waals' contact (Li⁺-N = 2.15 Å)²⁶⁹ and thus it seems justifiable to regard the metal cation and the nitrogen atom as being in contact.

(b) (15C5)NaTCNQ

Reaction of 15C5 with NaTCNQ (ratio 1:1) in dry acetonitrile afforded a reasonable yield (48%) of a very pure purple crystalline solid (Combustion Analysis: Calculated: C: 59.06%, H: 5.41%, N: 12.52%. Found: C: 58.76%, H: 5.02%, N: 12.32%.), which contained single crystals suitable for X-ray structural study. Full details including an account of the structure solution and refinement are reported in the Experimental Section and the Supporting Information (in the Appendices) respectively. The crystals obtained were of (15C5)NaTCNQ and the basic building block is shown in Figure 3.34.

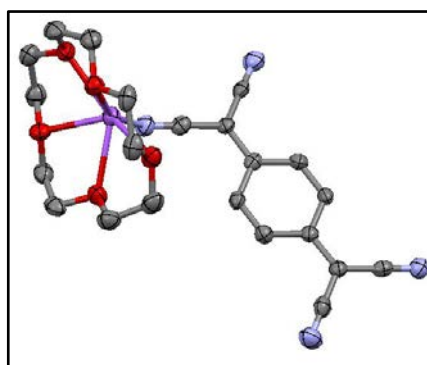


Figure 3.34 Basic unit of (15C5)NaTCNQ (hydrogen atoms are excluded)

Bond lengths within the TCNQ^{•-} units are summarised in Table 3.13. In this structure, each Na⁺ ion is coordinated within one crown ether unit, but also to two TCNQ^{•-} nitrogen atoms of a TCNQ^{•-} dimer in contrast to the behaviour seen for its lithium analogue. The TCNQ^{•-} units form a dimer which is significantly short axis slipped (see Figure 3.35). The data in Table 3.13 suggest that each TCNQ^{•-} unit has some quinonoidal character because bond length “a” is less than “b”. The distribution of bond lengths is reported for TCNQ^{•-}²¹³.

| (a) Definition of the bond lengths within the TCNQ ^{•-} molecule | | | | | | |
|---|------------------|-----------|-----------|-----------|-----------|-------|
| Structure | Bond lengths (Å) | | | | | |
| | a | b | c | d | e | f |
| TCNQ ^{•-} (A) | | 1.421 (4) | | 1.415 (4) | 1.146 (4) | 0.950 |
| | 1.352 (4) | 1.421 (4) | 1.403 (4) | 1.422 (4) | 1.152 (4) | 0.950 |
| | 1.358 (4) | 1.417 (4) | 1.412 (4) | 1.405 (4) | 1.154 (4) | 0.950 |
| | | 1.421 (4) | | 1.423 (4) | 1.148 (4) | 0.950 |

Table 3.13 Summary of bond lengths (Å) observed for TCNQ^{•-} units in (15C5)NaTCNQ

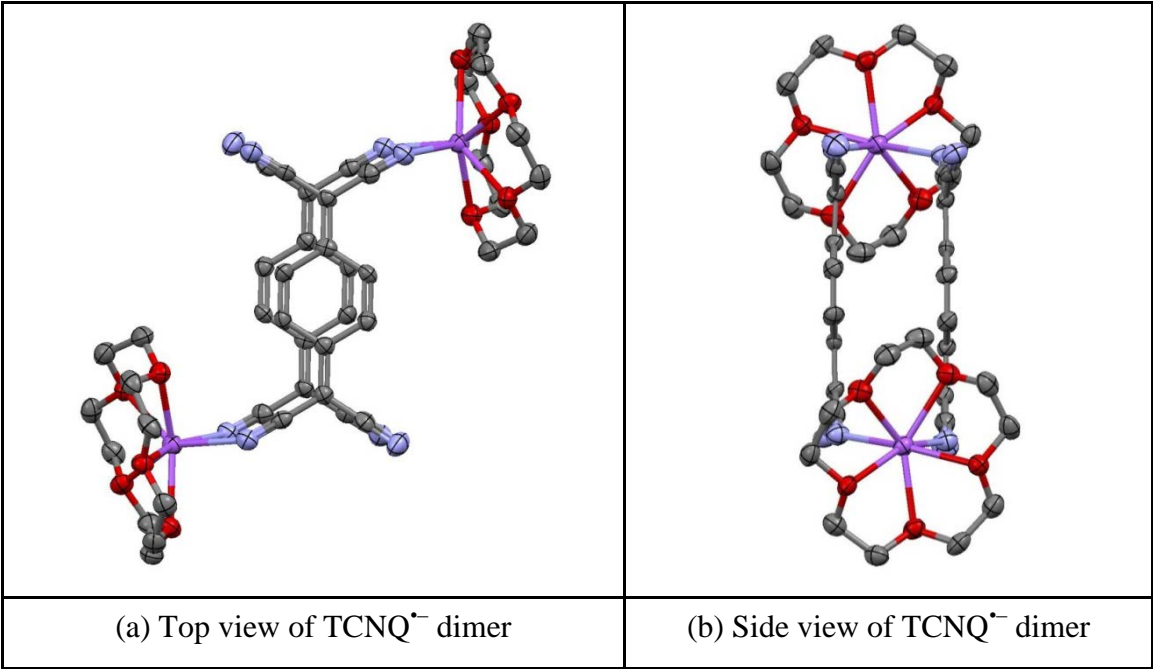


Figure 3.35 Top (a) and side (b) views of TCNQ^{•-} dimer in (15C5)NaTCNQ (hydrogen atoms are excluded)

Within the crystal, the TCNQ^{•-} units are assembled into separated dimers in which TCNQ^{•-} dimer neighbours are significantly long-axis slipped (Figure 3.36 and Figure

3.37) in a manner similar to that seen previously for the 18C6 complexes of K^+ and $RbTCNQ^{131}$. Distance and angles within the $TCNQ^{\bullet-}$ stacks are listed in Table 3.14.

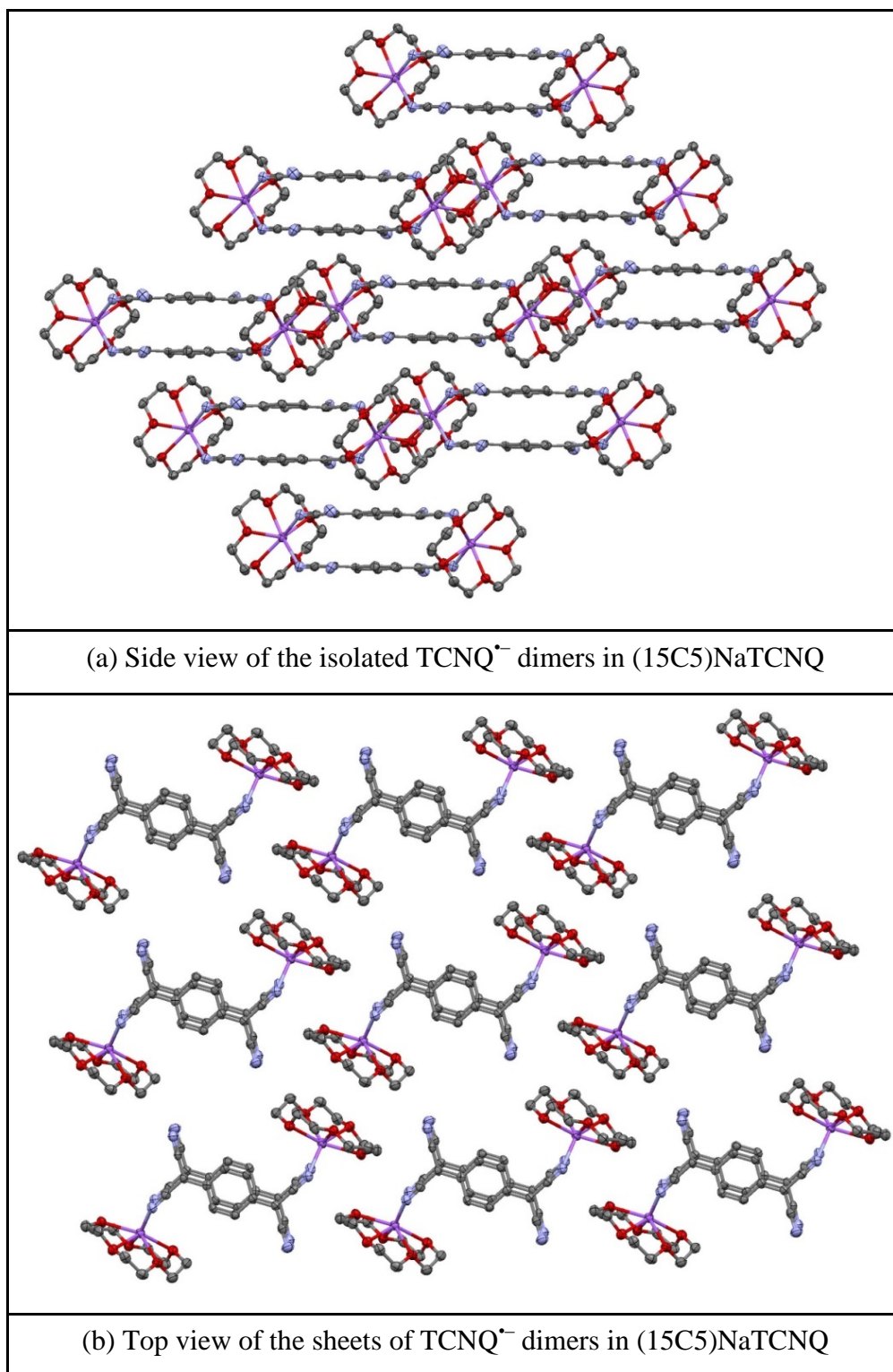


Figure 3.36 Side (a) and top (b) views of $TCNQ^{\bullet-}$ dimers in $(15C5)NaTCNQ$ (hydrogen atoms are excluded)

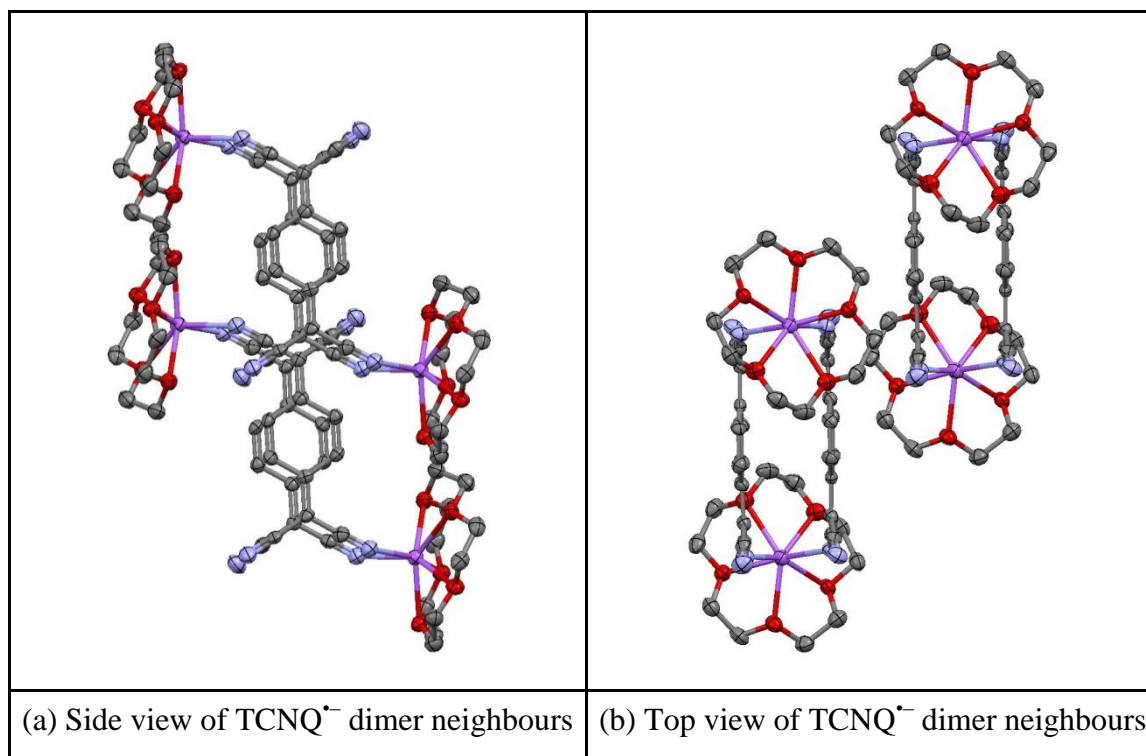


Figure 3.37 Side (a) and top (b) views of TCNQ^{•-} dimer neighbours in (15C5)NaTCNQ (hydrogen atoms are excluded)

| TCNQ units | | TCNQ ^{•-} dimer | TCNQ ^{•-} dimer neighbours |
|--|--------------|--------------------------|-------------------------------------|
| π - π perpendicular distance (Å) | | 3.260 | 3.14 |
| Short-axis slip | Distance (Å) | 0.60 | 0.21 |
| | Angle (°) | 10.43 | 3.83 |
| Long-axis slip | Distance (Å) | 0.18 | 6.46 |
| | Angle (°) | 3.16 | 64.11 |
| Centroid-centroid distance (Å) | | 3.32 | 7.18 |

Table 3.14 Distances (Å) and angles (°) within the TCNQ^{•-} stacks of (15C5)NaTCNQ

In (15C5)NaTCNQ, each TCNQ^{•-} is coordinated to two metal ions. Consequently, the TCNQ^{•-} forms infinite brickwork packing containing pairs of TCNQ^{•-} units, which can be regarded as dimers and are closely face-to-face π -stacked with slight short-axis slipped. Then the nearest neighbour TCNQ^{•-} units within the column are significantly long-axis slipped. Within a TCNQ^{•-} dimer, the TCNQ^{•-} units adopt a slight boat shape and are twisted in such a way that the cyano groups in neighbouring TCNQ^{•-} units are

pushed apart from each other, which is the same as seen in the case of (15C5)LiTCNQ. Figure 3.38 shows geometries of TCNQ^{•-} dimers in (15C5)NaTCNQ.

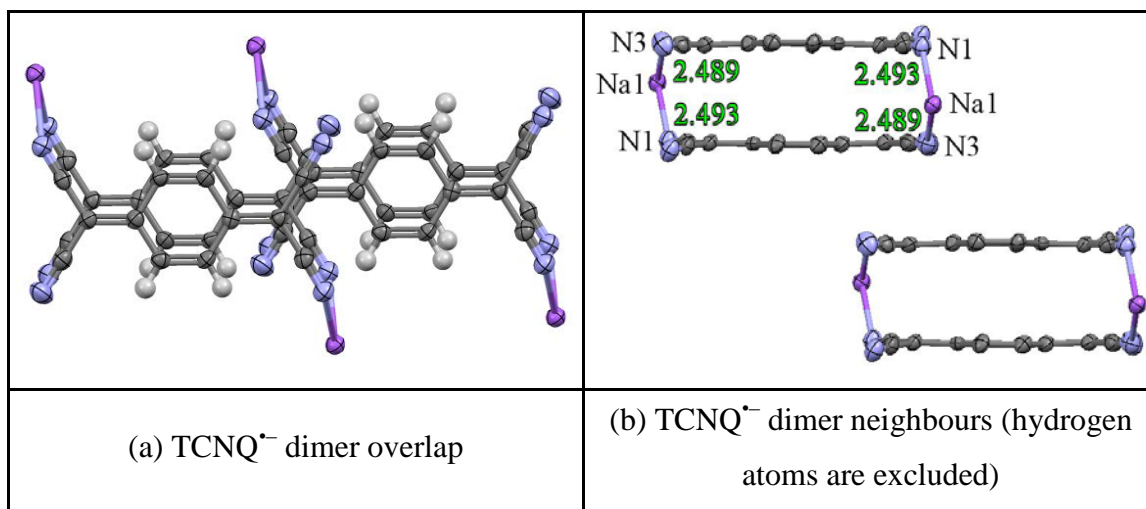


Figure 3.38 TCNQ^{•-} dimers geometries in (15C5)NaTCNQ

Figure 3.39 shows key contact and torsion angles in the TCNQ^{•-} units for (15C5)NaTCNQ.

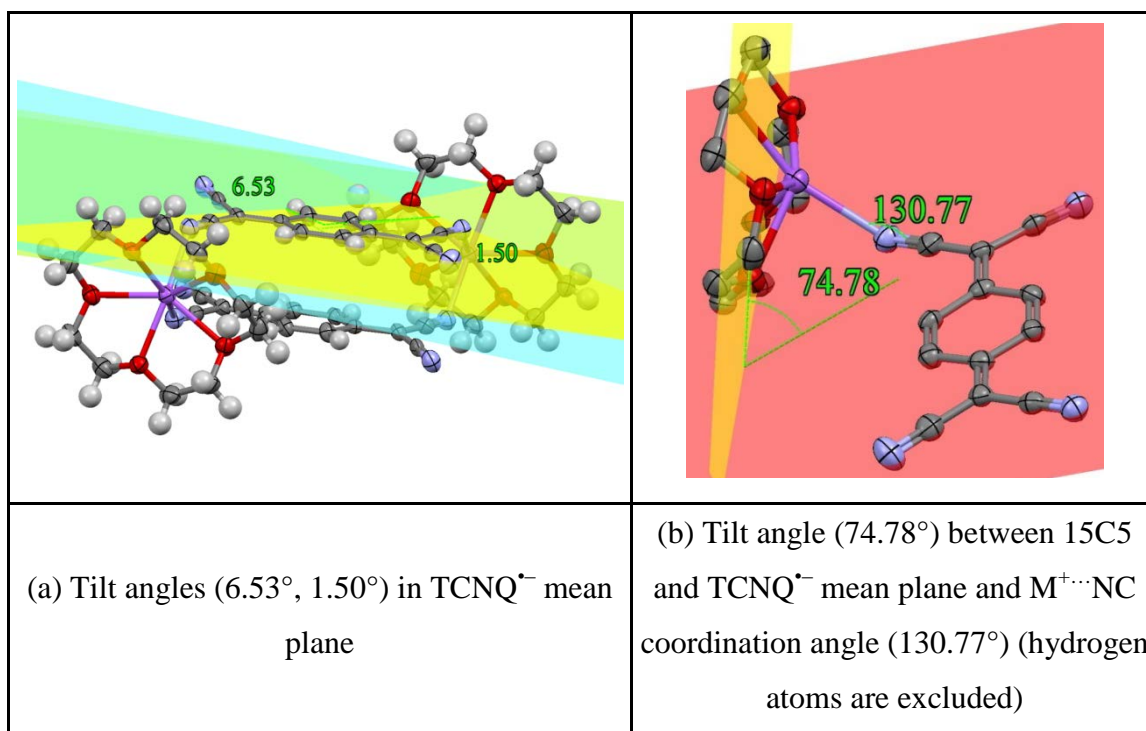


Figure 3.39 Angular relationships within (15C5)NaTCNQ

Each Na⁺ cation is coordinated to two nitrogen atoms from the cyano groups on adjacent TCNQ^{•-} units and five oxygen atoms from the crown ether. The latter lies in the channels between the TCNQ^{•-} stacks. The crown ether plane is twisted at an angle

of 74.78° in respect to the ring of the $\text{TCNQ}^{\cdot-}$ unit. As viewed in Figure 3.39(b), the contact angle between Na^+ and NC is 130.77° . The reason for smaller twist and coordination angles in comparison with those seen in $(15\text{C}5)\text{LiTCNQ}$ is the greater degree of inter-unit co-ordination between the metal cation and cyano groups in the sodium salt. In the present case, the $\text{TCNQ}^{\cdot-}$ coordinates to two metal ions to form a dimer similar to that seen for $(18\text{C}6)\text{MTCNQ}$ ($\text{M} = \text{K}, \text{Rb}$)¹³¹ but in contrast with the behaviour described earlier for $(15\text{C}5)\text{LiTCNQ}$. Because the metal centres lie transoid across the $\text{TCNQ}^{\cdot-}$ dimer, the geometry changes in $(15\text{C}5)\text{NaTCNQ}$ are smaller than in $(15\text{C}5)\text{LiTCNQ}$. Figure 3.40 summarises the various contact distances within the cation complex.

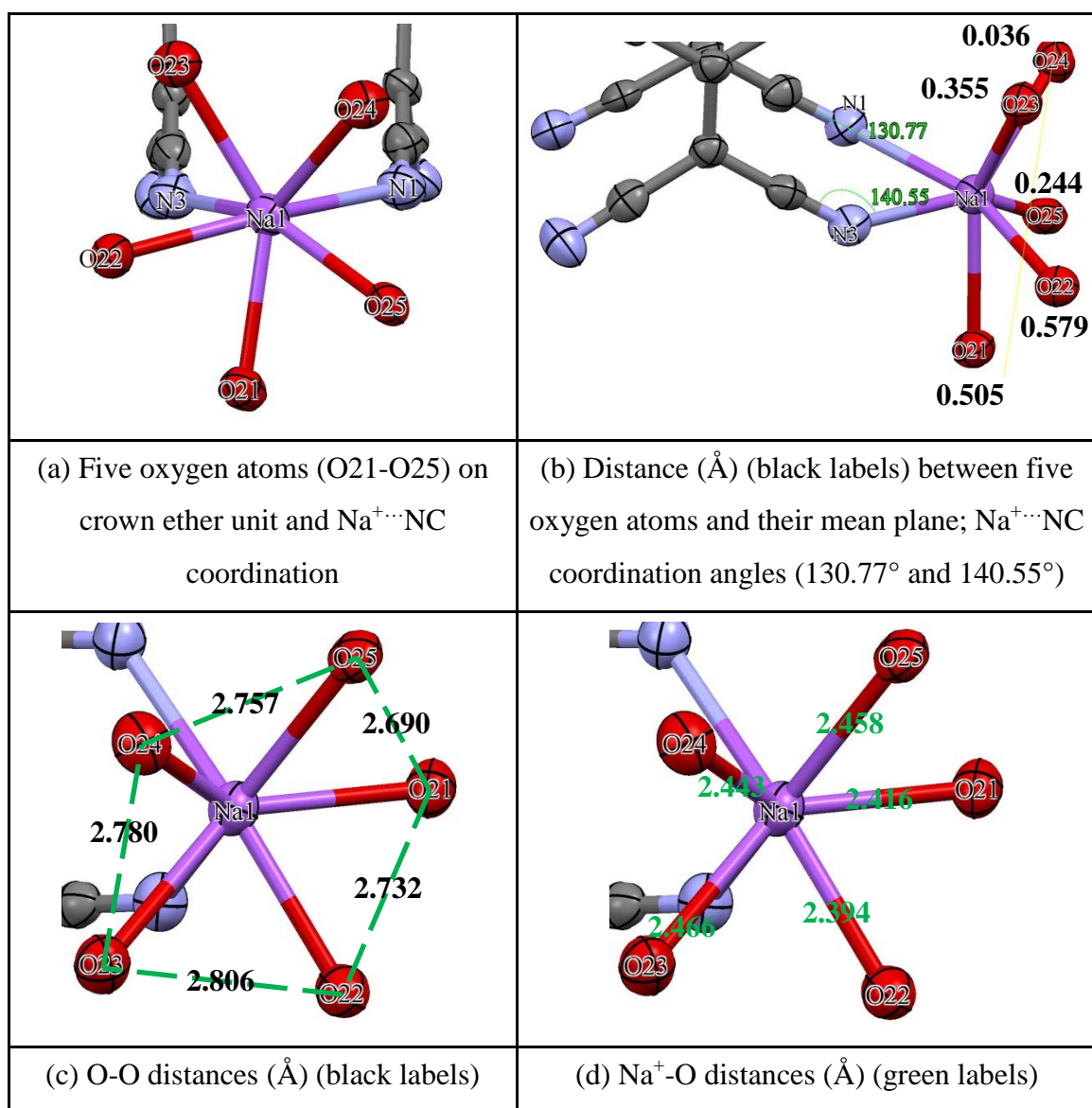


Figure 3.40 The various contact distances (Å) within the cation complex (carbon atoms on crown ether units and hydrogen atoms are excluded)

As viewed in Figure 3.40, except for O22 which is 0.579 Å away from the oxygen atoms mean plane, other four oxygen atoms of the crown ether unit are sited on their mean plane. The ligating oxygen atoms lie above and below their mean plane to form irregular pentagonal geometry of mean side by *ca.* 2.753 Å. Not all of the Na⁺-O distances in (15C5)NaTCNQ are equal but seem to fall into two groups: (i) 2.394 Å and (ii) 2.416, 2.443, 2.458, 2.466 Å respectively, which proves that Na⁺ cation is located above the distorted cavity of 15C5. Consequently, all of the Na⁺-O distances are slightly less than that of a van der Waals' contact (Na⁺-O = 2.47 Å)^{269,270} and thus it seems justifiable to regard the metal cations and the oxygen atoms as being in contact. The distance of Na⁺-N (2.493 Å) is shorter than that of a van der Waals' contact (Na⁺-N = 2.50 Å)^{269,270} and thus it seems justifiable to regard the metal cation and the nitrogen atom as being in contact.

3.3.2.2 Comparison between (15C5)LiTCNQ and (15C5)NaTCNQ

The X-ray structural studies reveal that the two cation complexes show similar but not identical solid-state behaviour. In each case, the alkali metal cation sits above the centre of the crown ether unit. The TCNQ^{•-} anions form face-to-face π -stacked dimers with two metal crown ether complexes oriented approximately perpendicular to the TCNQ^{•-} dimer plane and each located at diagonally opposite ends of the TCNQ^{•-} dimer. In the lithium salt, one of the cyano group nitrogen atoms appears to be coordinated to the lithium cation whereas for the corresponding sodium salt, two cyano groups are associated with the metal cation. The latter arrangement mirrors the behaviour previously seen for (18C6)KTCNQ and its Rb⁺ analogue¹³¹. The difference between the Li and Na salt structures probably reflects the different cation size and maximum coordination potential of these metal cations. The (crown ether)MTCNQ dimer units are assembled into columns, offset relative to their neighbours to achieve efficient packing as seen previously for the corresponding (18C6)MTCNQ salts (M = K, Rb)¹³¹.

Figure 3.41 shows distances to neighbouring dimers in (15C5)Li⁺ and NaTCNQ compared with (18C6)K⁺ and RbTCNQ. All of the dimer neighbours are long axis slipped in these four TCNQ salts. Because of the different TCNQ^{•-} co-ordination behaviour, the geometry changes in (15C5)NaTCNQ are smaller than is the case in (15C5)LiTCNQ as shown in Figure 3.39. The packing pattern of (15C5)NaTCNQ is similar to that seen in (18C6)KTCNQ and (18C6)RbTCNQ, for which the dimer

separation distances are much longer because the increased size of metal ions and the more bulky crown ether units.

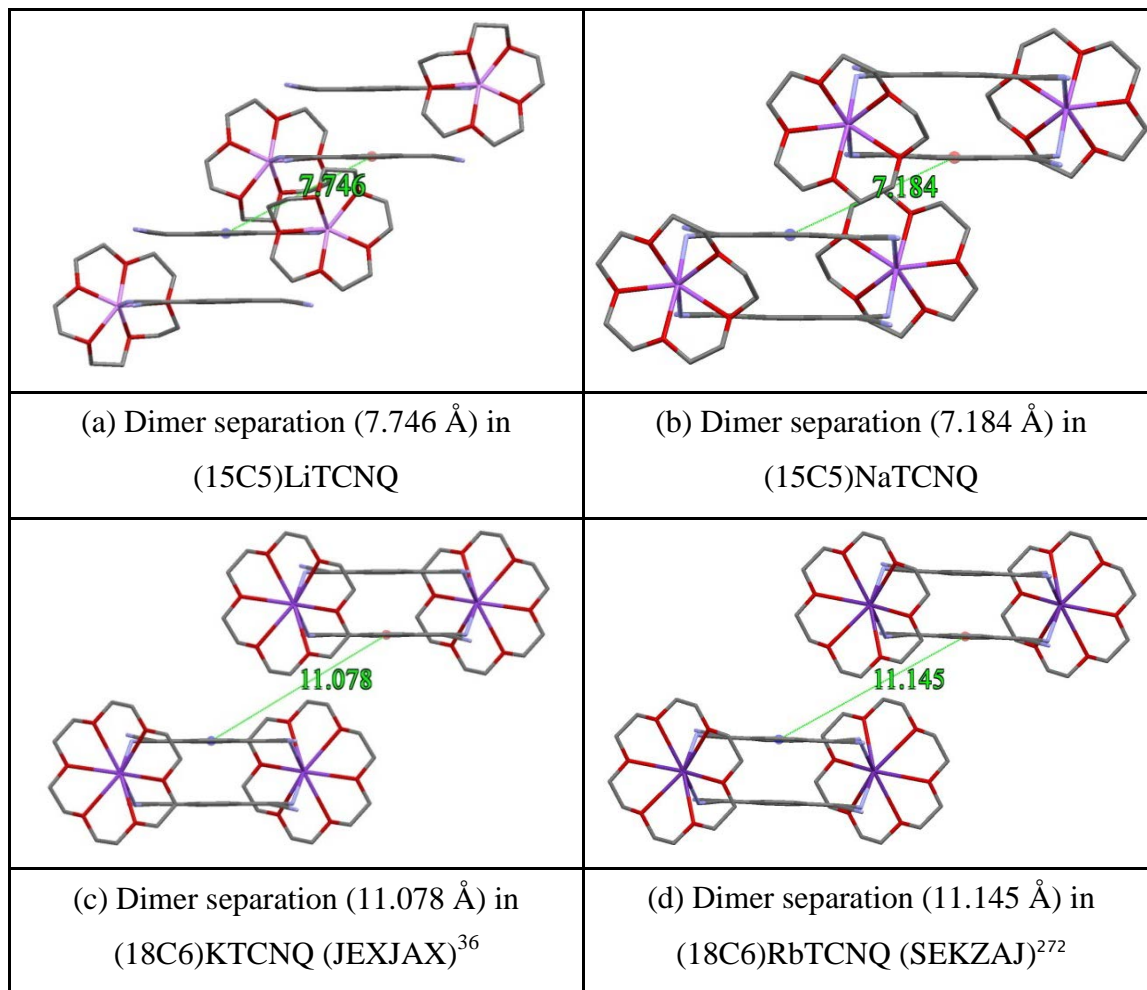


Figure 3.41 Distances to neighbouring dimers in (15C5)Li⁺ and NaTCNQ compared with (18C6)K⁺ and RbTCNQ (hydrogen atoms excluded)

3.3.2.3 (15C5)M(TCNQ)₂·H₂O complexes (M = Li, Na)

(a) (15C5)Li(TCNQ)₂·H₂O

Reaction of 15C5 with LiTCNQ and TCNQ⁰ (ratio 1:1:1) in dry acetonitrile afforded a reasonable yield (56%) of a very pure dark blue crystalline solid (Combustion Analysis: Calculated: C: 62.48%, H: 4.63%, N: 17.14%. Found: C: 62.47%, H: 4.45%, N: 17.38%.), which contained single crystals suitable for X-ray structural study. Full details including an account of the structure solution and refinement are reported in the Experimental Section and the Supporting Information (in the Appendices) respectively. The crystals obtained were of (15C5)Li(TCNQ)₂·H₂O and the components are shown in Figure 3.42.

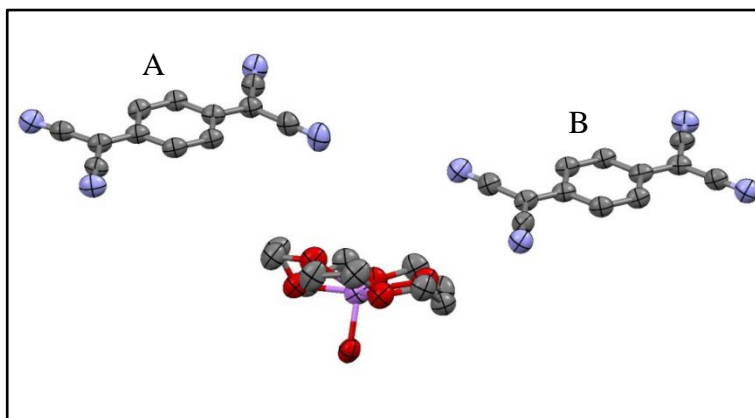


Figure 3.42 Components present in $(15C5)Li(TCNQ)_2 \cdot H_2O$ (hydrogen atoms excluded)

Bond lengths within the TCNQ units are summarised in Table 3.15.

| (a) Definition of the bond lengths within the TCNQ molecule | | | | | | |
|---|------------------|-----------|-----------|-----------|-----------|-------|
| Structure | Bond lengths (Å) | | | | | |
| | a | b | c | d | e | f |
| TCNQ unit (A) | | 1.431 (5) | | 1.434 (5) | 1.157 (4) | 0.950 |
| | 1.356 (5) | 1.444 (5) | 1.396 (5) | 1.426 (6) | 1.156 (5) | 0.951 |
| | 1.359 (5) | 1.436 (5) | 1.395 (5) | 1.427 (5) | 1.168 (5) | 0.950 |
| | | 1.445 (5) | | 1.429 (6) | 1.156 (5) | 0.950 |
| TCNQ unit (B) | | 1.432 (5) | | 1.424 (5) | 1.162 (5) | 0.949 |
| | 1.347 (5) | 1.444 (5) | 1.397 (5) | 1.426 (6) | 1.153 (5) | 0.950 |
| | 1.362 (5) | 1.433 (5) | 1.403 (5) | 1.434 (5) | 1.158 (5) | 0.950 |
| | | 1.444 (5) | | 1.423 (6) | 1.152 (5) | 0.951 |

Table 3.15 Summary of bond distances (Å) observed for TCNQ units

In this structure, the Li^+ ion is coordinated to one crown ether unit and one water molecule. The TCNQ units form a dimer which is significantly long axis slipped (see Figure 3.43).

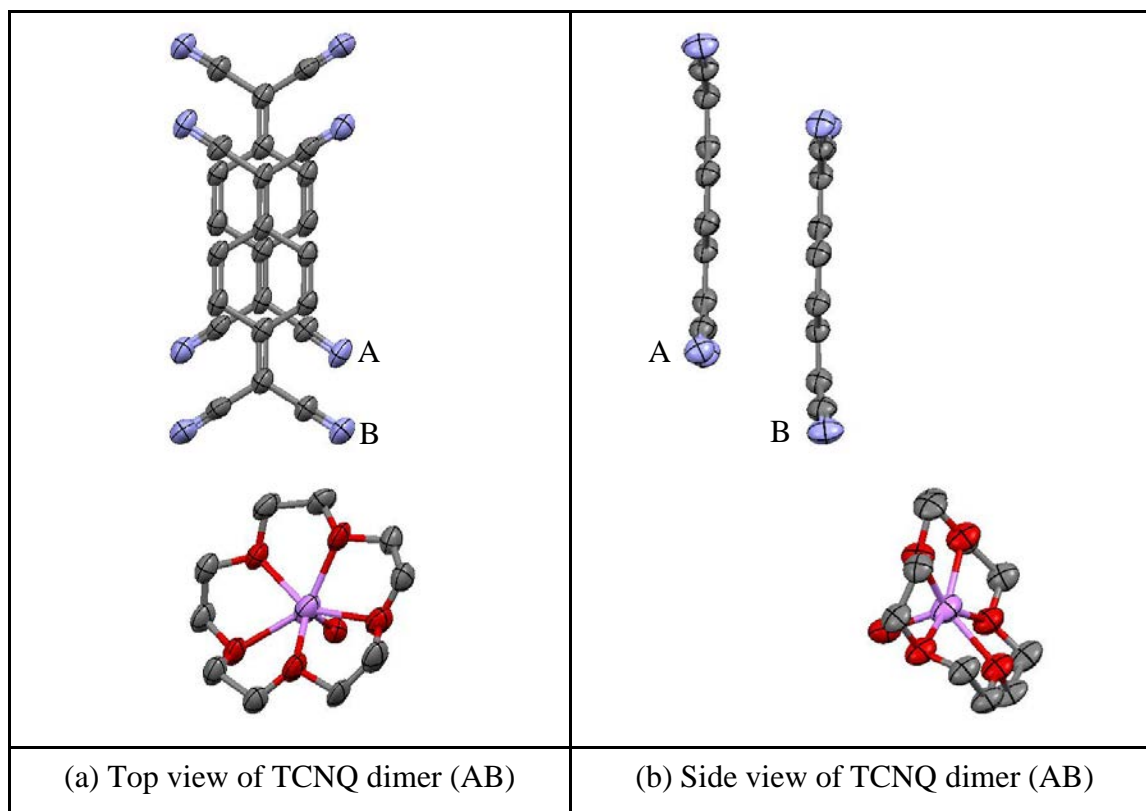


Figure 3.43 Top (a) and side (b) view of TCNQ dimer (AB) in $(15\text{C}5)\text{Li}(\text{TCNQ})_2\cdot\text{H}_2\text{O}$ (hydrogen atoms are excluded)

The similarity of the bond lengths within the two TCNQ units makes it difficult to distinguish between the $\text{TCNQ}^{\bullet-}$ and TCNQ^0 components. The data in Table 3.15 suggest that both TCNQ units have some quinonoidal character because bond length “a” is less than “b”. For both components A and B, the distribution of bond lengths is intermediate between these reported for TCNQ^0 and $\text{TCNQ}^{\bullet-}$ respectively²¹³.

Within the crystal, the TCNQ dimers assemble into infinite columns in which the individual TCNQ units are assembled in an $\text{ABB}'\text{A}'$ motif (see Figure 3.44) in which neighbouring dimers are significant “diagonally slipped” (see Figure 3.45). Distance and angles within the TCNQ stacks are listed in Table 3.16.

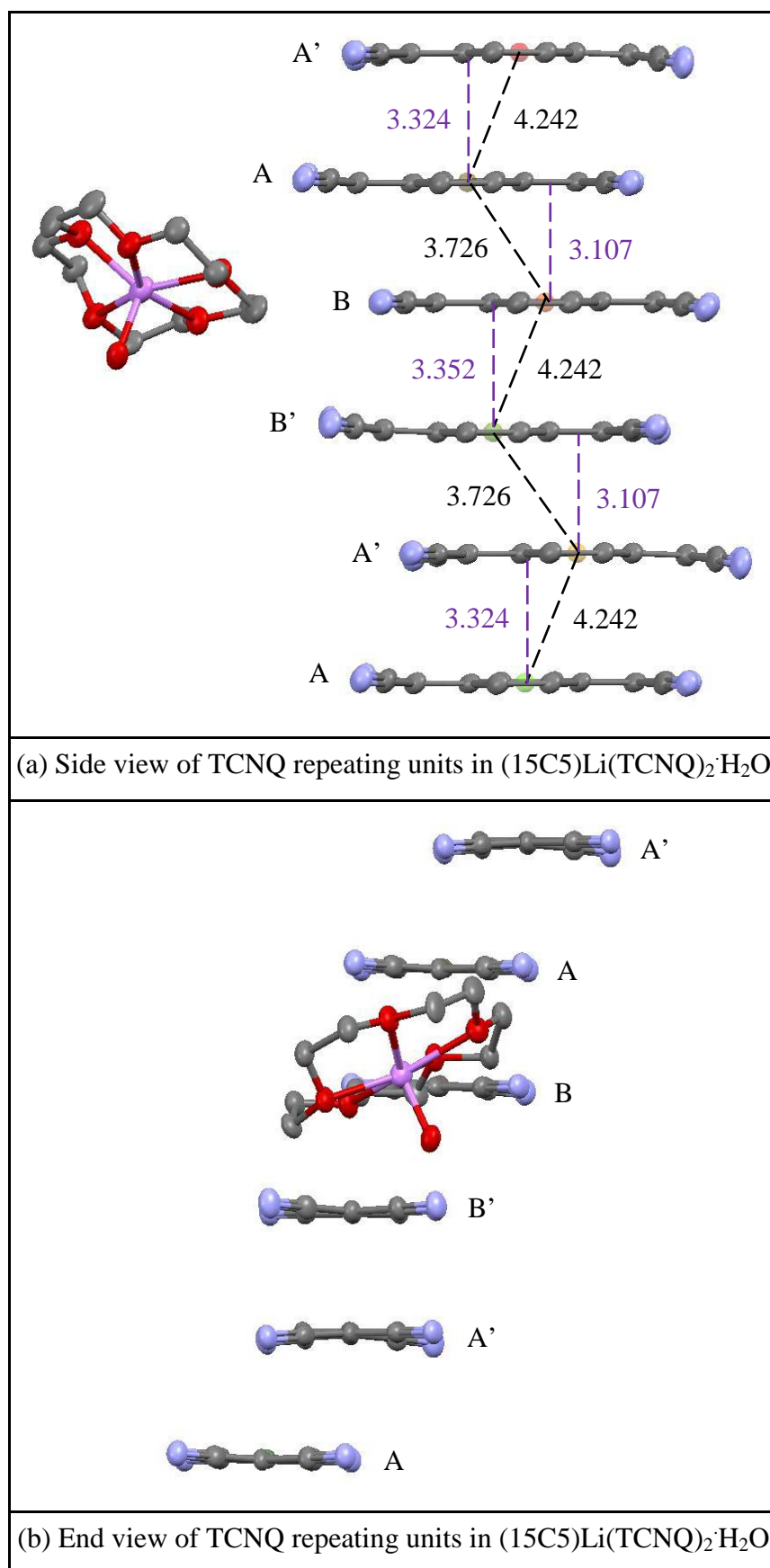


Figure 3.44 Observation of TCNQ repeating units in $(15C5)Li(TCNQ)_2 \cdot H_2O$ (hydrogen atoms are excluded)

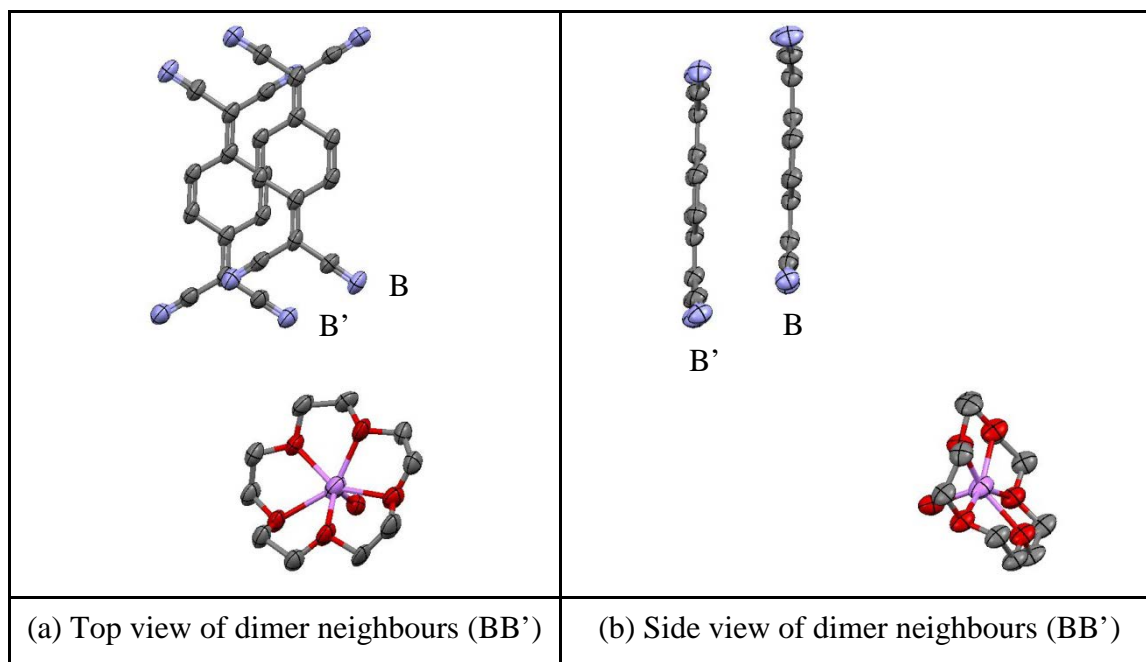


Figure 3.45 Top (a) and side (b) views of dimer neighbours (BB'), which is similar to dimer neighbours (AA') in $(15C5)Li(TCNQ)_2 \cdot H_2O$ (hydrogen atoms are excluded)

| TCNQ units | | TCNQ dimer | TCNQ dimer neighbours (AA') | TCNQ dimer neighbours (BB') |
|--|--------------|------------|-----------------------------|-----------------------------|
| π - π perpendicular distance (Å) | | 3.11 | 3.32 | 3.35 |
| Short-axis slip | Distance (Å) | 0.049 | 2.27 | 2.18 |
| | Angle (°) | 0.90 | 34.36 | 33.05 |
| Long-axis slip | Distance (Å) | 2.04 | 1.33 | 1.42 |
| | Angle (°) | 33.26 | 21.83 | 22.97 |
| Centroid-centroid distance (Å) | | 3.73 | 4.24 | 4.24 |

Table 3.16 Distances (Å) and angles (°) within the TCNQ stacks of $(15C5)Li(TCNQ)_2 \cdot H_2O$

Within the AB dimer, the individual TCNQ units adopt a shallow boat conformation in which neighbouring $-C(CN)_2$ units are tilted away from each other. The two TCNQ planes are also slightly tilted in respect to each other (by *ca.* 1.13°) as viewed in Figure 3.46(b). From these data it will be evident that π -facial overlap between dimer neighbours within a column is not ideal for extended π - π delocalisation within the column.

Unlike the case in (15C5)LiTCNQ, in the present cation complex, a H₂O molecule fills the vacant Li⁺ co-ordination site and neither TCNQ^{•−} nor TCNQ⁰ is coordinated to metal cation. Therefore, compared with the case of (15C5)LiTCNQ, the extra volume of TCNQ⁰ will change the packing motif of crown ether and TCNQ. Consequently, TCNQ units form infinite columns containing pairs of isolated TCNQ dimers, which can be regarded as dimers that are in close face-to-face π contact and significantly long-axis slipped. Figure 3.46 shows torsion angles in the TCNQ units for (15C5)Li(TCNQ)₂·H₂O.

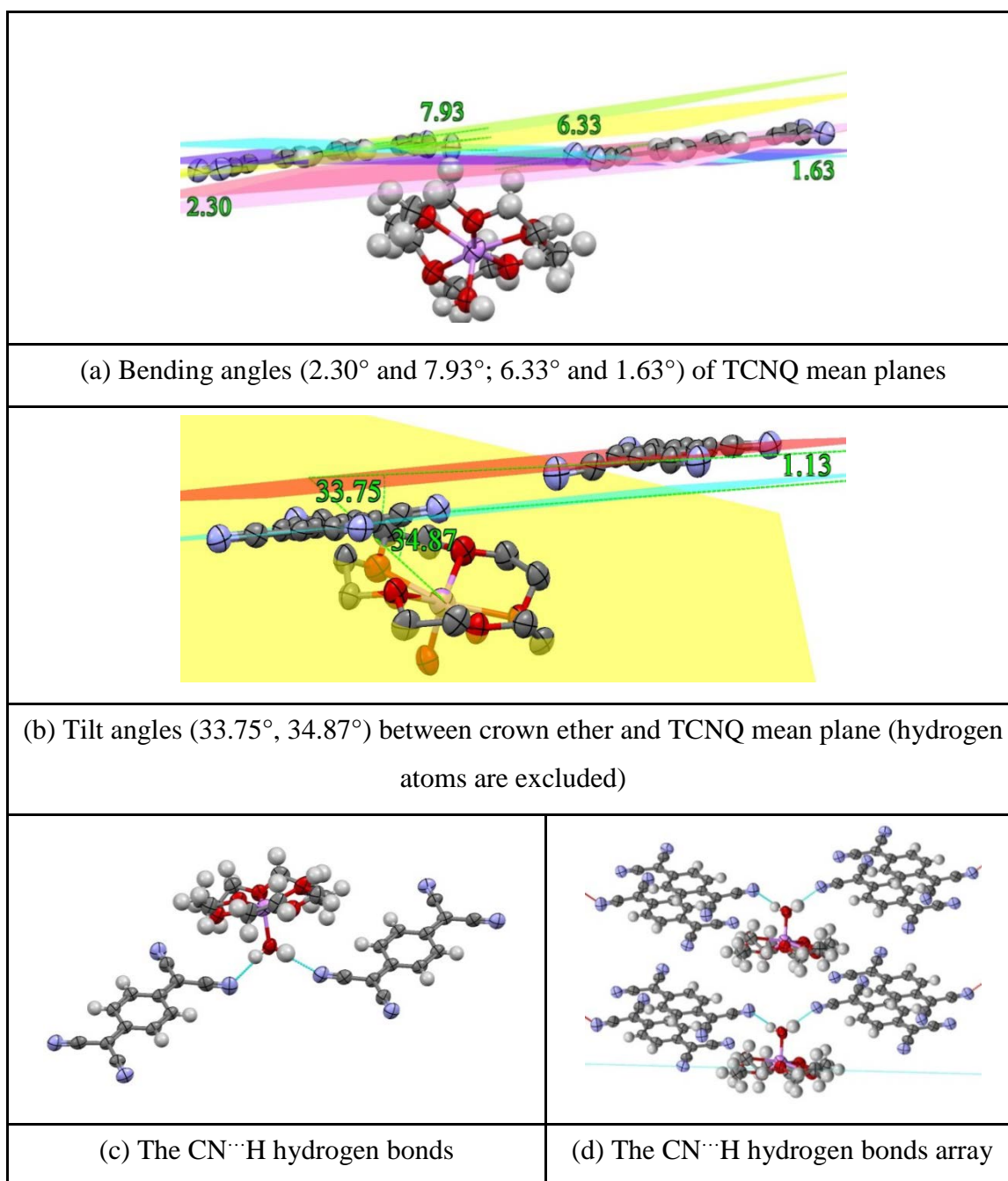


Figure 3.46 Angular relationships in (15C5)Li(TCNQ)₂·H₂O

As viewed in Figure 3.46, each Li^+ cation is coordinated by one oxygen atom from H_2O molecule and five oxygen atoms from crown ether unit respectively. $\text{CN}\cdots\text{H}$ hydrogen bonds are formed between hydrogens from H_2O molecule and nitrogen atoms from the TCNQ units. The cation complex $(15\text{C}5)\text{Li}^+(\text{H}_2\text{O})$ lies in a channel between the TCNQ columns. The crown ether plane is twisted at an angle of 33.75° and 34.87° in respect to benzene rings of the two TCNQ units. Figure 3.47 summarises the various contact distances within the cation complex.

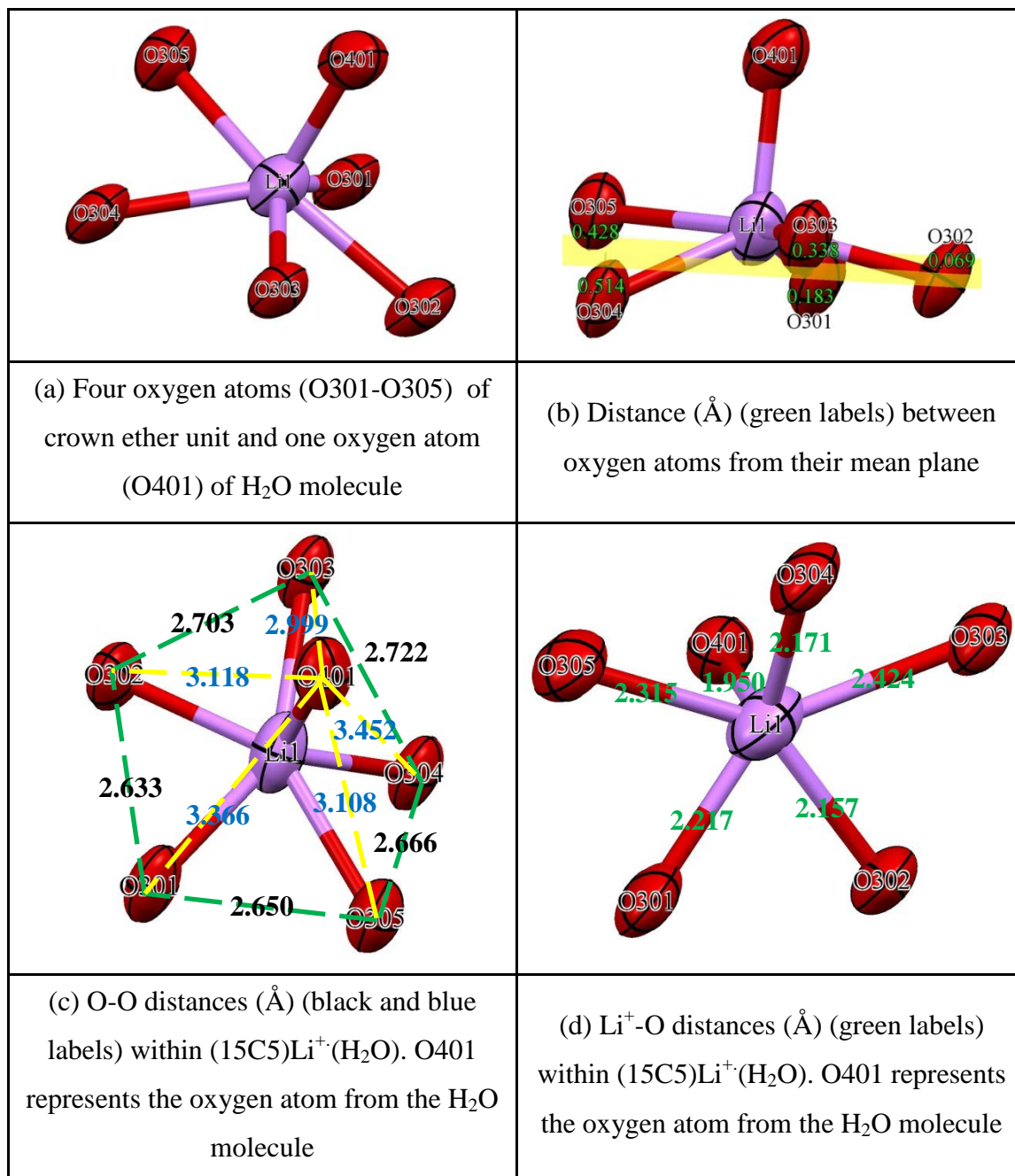


Figure 3.47 The various contact distances (Å) within the cation complex (carbon and hydrogen atoms are excluded)

As viewed in Figure 3.47, except for O304 which is tilted 0.514 \AA away from the oxygen mean plane, other four oxygen atoms of the crown ether unit are sited on the mean plane. The five oxygen atoms on crown ether unit form irregular pentagonal geometry of mean side by *ca.* 2.675 \AA . All of the $\text{Li}^+\text{-O}$ distances in $(15\text{C}5)\text{Li}(\text{TCNQ})_2\cdot\text{H}_2\text{O}$ are in the range between 2.157 \AA and 2.424 \AA respectively, and the Li^+ cation sits above the cavity of the 15C5 unit because of coordination with the H_2O molecule.

(b) $(15\text{C}5)\text{Na}(\text{TCNQ})_2\cdot\text{H}_2\text{O}$

Reaction of 15C5, NaTCNQ and TCNQ^0 (ratio 1:1:1) in dry acetonitrile afforded a reasonable yield (60%) of a very pure dark blue crystalline solid (Combustion Analysis: Calculated: C: 60.98%, H: 4.52%, N: 16.73%. Found: C: 61.28%, H: 4.30%, N: 16.69%.) which contained single crystals suitable for X-ray structural study. Full details including an account of the structure solution and refinement are reported in the Experimental Section and the Supporting Information (in the Appendices) respectively. The crystals obtained were of $(15\text{C}5)\text{Na}(\text{TCNQ})_2\cdot\text{H}_2\text{O}$ and the basic structure is shown in Figure 3.48. Bond lengths within the TCNQ units are summarised in Table 3.17.

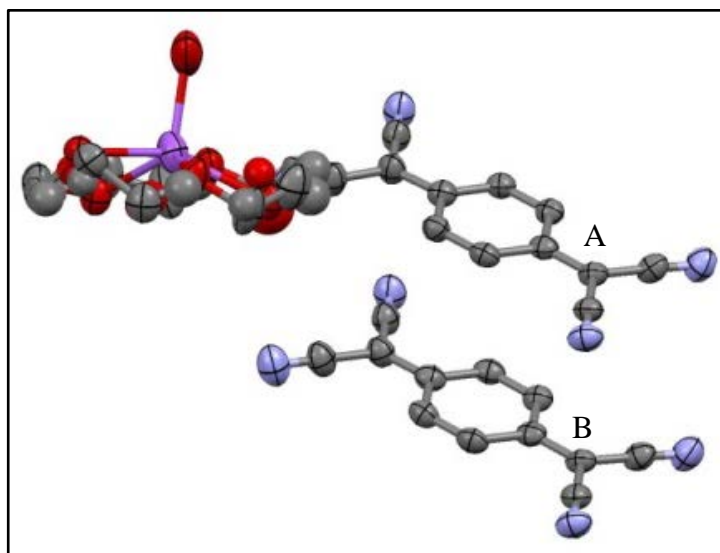


Figure 3.48 Basic structure of $(15\text{C}5)\text{Na}(\text{TCNQ})_2\cdot\text{H}_2\text{O}$ (hydrogen atoms are excluded)

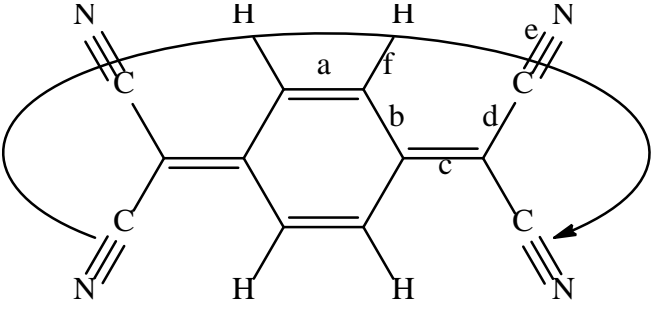
|  | | | | | | |
|--|------------------|-----------|-----------|-----------|-----------|-------|
| (a) Definition of the bond lengths within the TCNQ molecule | | | | | | |
| Structure | Bond lengths (Å) | | | | | |
| | a | b | c | d | e | f |
| TCNQ unit (A) | | 1.437 (5) | | 1.434 (5) | 1.152 (5) | 0.950 |
| | 1.352 (5) | 1.435 (5) | 1.393 (5) | 1.427 (5) | 1.151 (4) | 0.949 |
| | 1.362 (5) | 1.440 (5) | 1.398 (5) | 1.429 (5) | 1.143 (5) | 0.951 |
| | | 1.431 (5) | | 1.427 (5) | 1.147 (5) | 0.950 |
| TCNQ unit (B) | | 1.438 (5) | | 1.428 (5) | 1.154 (5) | 0.950 |
| | 1.360 (5) | 1.437 (5) | 1.393 (5) | 1.420 (5) | 1.153 (5) | 0.950 |
| | 1.358 (5) | 1.426 (5) | 1.400 (5) | 1.422 (5) | 1.155 (5) | 0.950 |
| | | 1.435 (5) | | 1.427 (5) | 1.153 (5) | 0.950 |

Table 3.17 Summary of bond distances (Å) observed for TCNQ units in
(15C5)Na(TCNQ)₂·H₂O

In this structure, the Na⁺ ion is coordinated to one H₂O molecule and one crown ether unit. The TCNQ units form a dimer which is significantly long-axis slip (see Figure 3.49). The similarity of the bond lengths within the two TCNQ units makes it difficult to distinguish between the TCNQ^{•-} and TCNQ⁰ components.

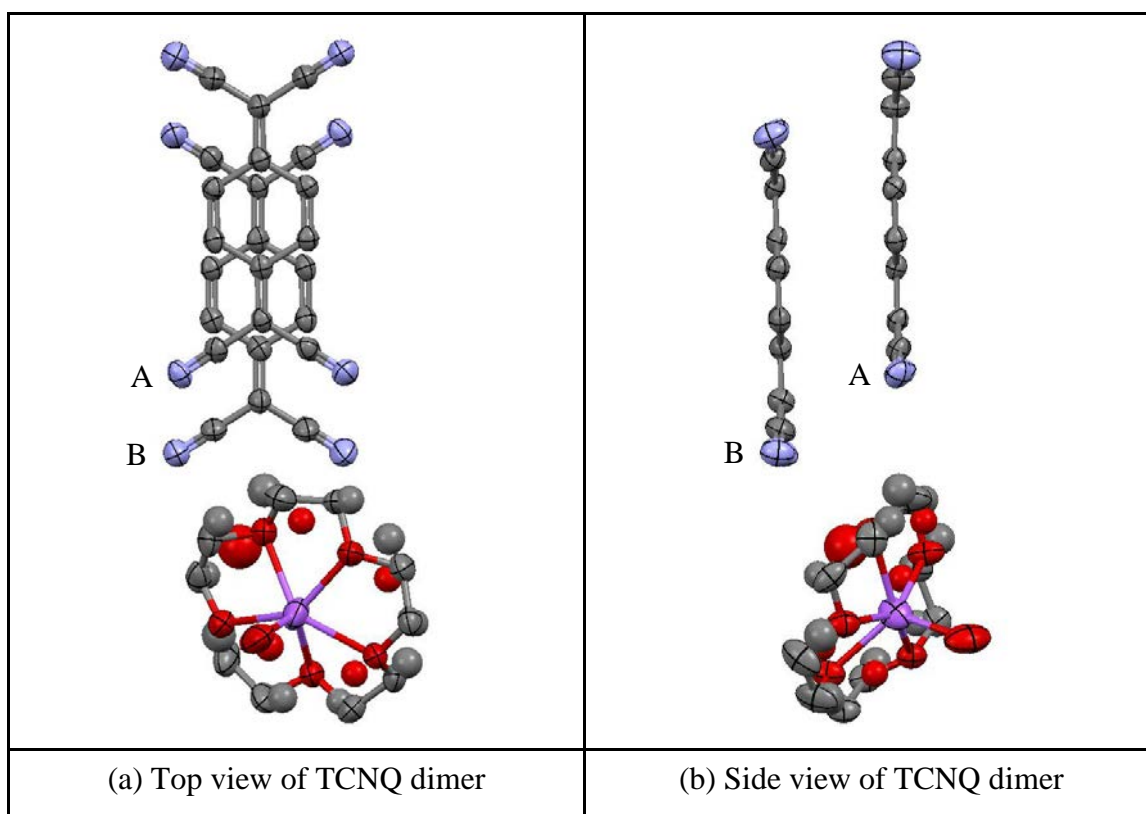


Figure 3.49 Top (a) and side (b) views of TCNQ dimer in $(15C5)Na(TCNQ)_2 \cdot H_2O$ (hydrogen atoms are excluded)

The data in Table 3.17 suggest that both TCNQ units have some quinonoidal character because bond length “a” is less than “b”. For both components of A and B, the distribution of bond lengths is intermediate between these reported for $TCNQ^{\cdot-}$ and $TCNQ^0$ respectively²¹³.

Within the crystal, there is no direct association of the TCNQ units with the Na^+ ion. The TCNQ dimers assemble into infinite columns in which the individual TCNQ units are assembled in an $ABB'A'$ motif (see Figure 3.50) in which dimer neighbours are significantly “diagonally” slipped (see Figure 3.51). Distances and angles within the TCNQ stacks are summarised in Table 3.18.

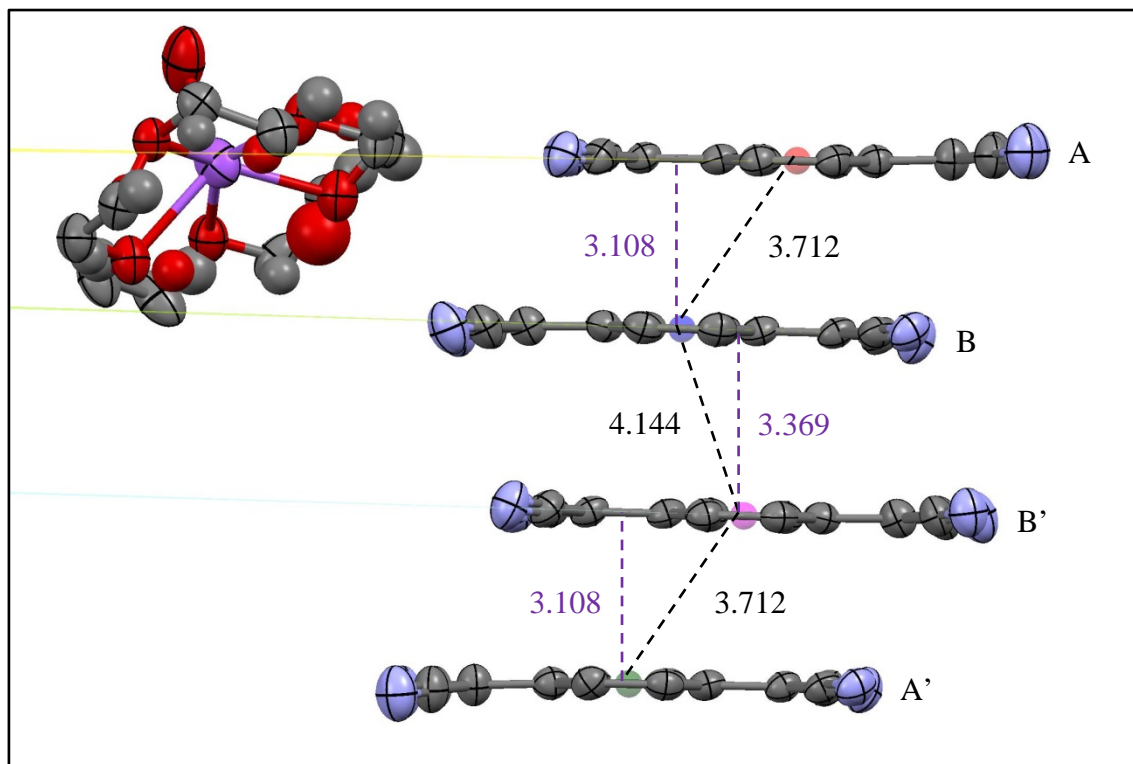


Figure 3.50 Assembly of TCNQ repeating units in $(15C5)Na(TCNQ)_2 \cdot H_2O$ (hydrogen atoms are excluded)

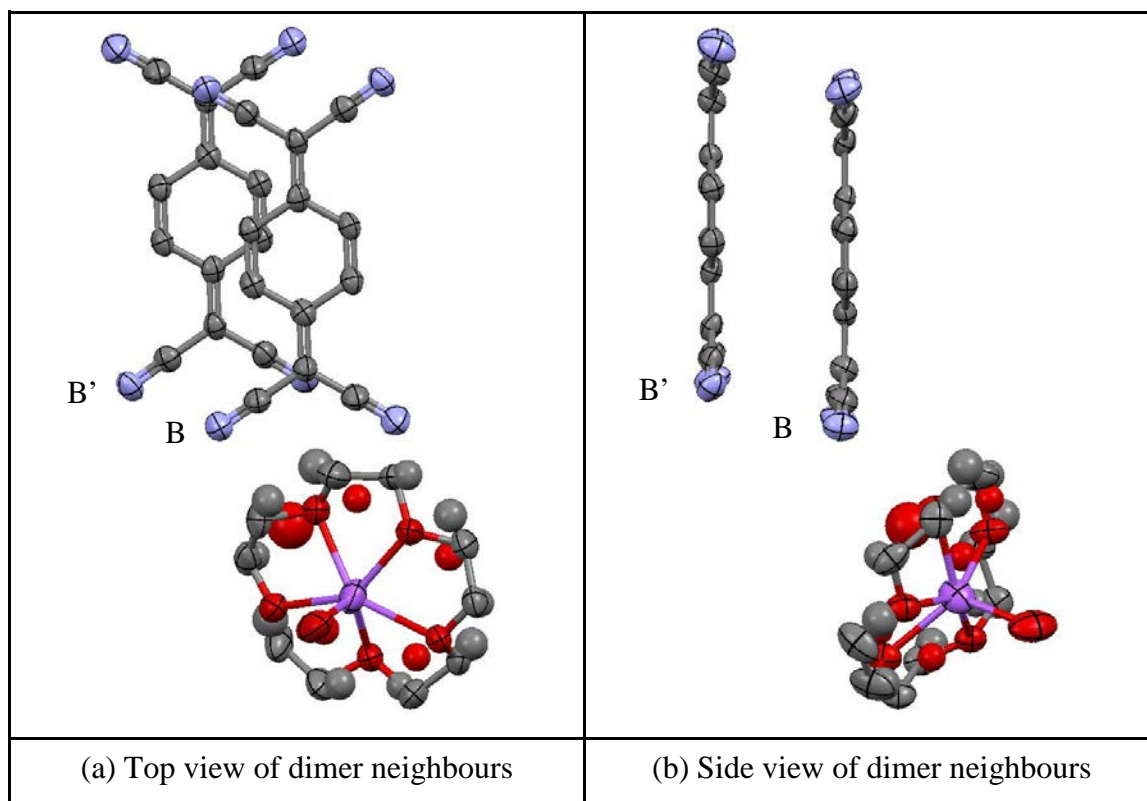


Figure 3.51 Top (a) and side (b) views of TCNQ dimer neighbours in $(15C5)Na(TCNQ)_2 \cdot H_2O$ (hydrogen atoms are excluded)

| TCNQ units | | TCNQ dimer | TCNQ dimer neighbours |
|--|--------------|------------|-----------------------|
| π - π perpendicular distance (Å) | | 3.11 | 3.37 |
| Short-axis slip | Distance (Å) | 0.071 | 2.12 |
| | Angle (°) | 1.31 | 32.12 |
| Long-axis slip | Distance (Å) | 2.03 | 1.16 |
| | Angle (°) | 33.13 | 19.03 |
| Centroid-centroid distance (Å) | | 3.71 | 4.14 |

Table 3.18 Distances (Å) and angles (°) within the TCNQ stacks of (15C5)Na(TCNQ)₂·H₂O

Within the AB dimer, the individual TCNQ units adopt a shallow boat conformation in which neighbouring $-\text{C}(\text{CN})_2$ units are twisted away from each other. The two TCNQ planes are slightly tilted in respect to each other (by *ca.* 0.96°). From these data, it will be evident that π -facial overlap between dimer neighbours within a column is not ideal for extended π - π delocalisation within the column.

Unlike the case of (15C5)NaTCNQ, in this complex, except via H₂O molecule, neither TCNQ^{•-} nor TCNQ⁰ is directly coordinated to the metal cation. In (15C5)Na(TCNQ)₂·H₂O, TCNQ units prefer to form separated tetramer as repeating unit instead of an infinite column. In each tetramer, there are two pairs of isolated TCNQ dimers, which can be regarded as dimers, which are in close face-to-face π contact with a slight long-axis slipped.

As viewed in Figure 3.52, each Na⁺ cation is coordinated by one oxygen atom from a H₂O molecule and five oxygen atoms from crown ether unit respectively. CN^{••}H hydrogen bonds are formed between hydrogen (H₂O molecule) and nitrogen (cyano group). The cation complex of (15C5)Na⁺(H₂O) lies in a channel between the TCNQ stacks. The crown ether mean plane (as defined by each set of oxygen atoms) is tilted at an angle of 37.15° and 36.76° in respect to benzene ring of the two TCNQ units in a dimer. Figure 3.53 summarises the various contact distances within the cation complex.

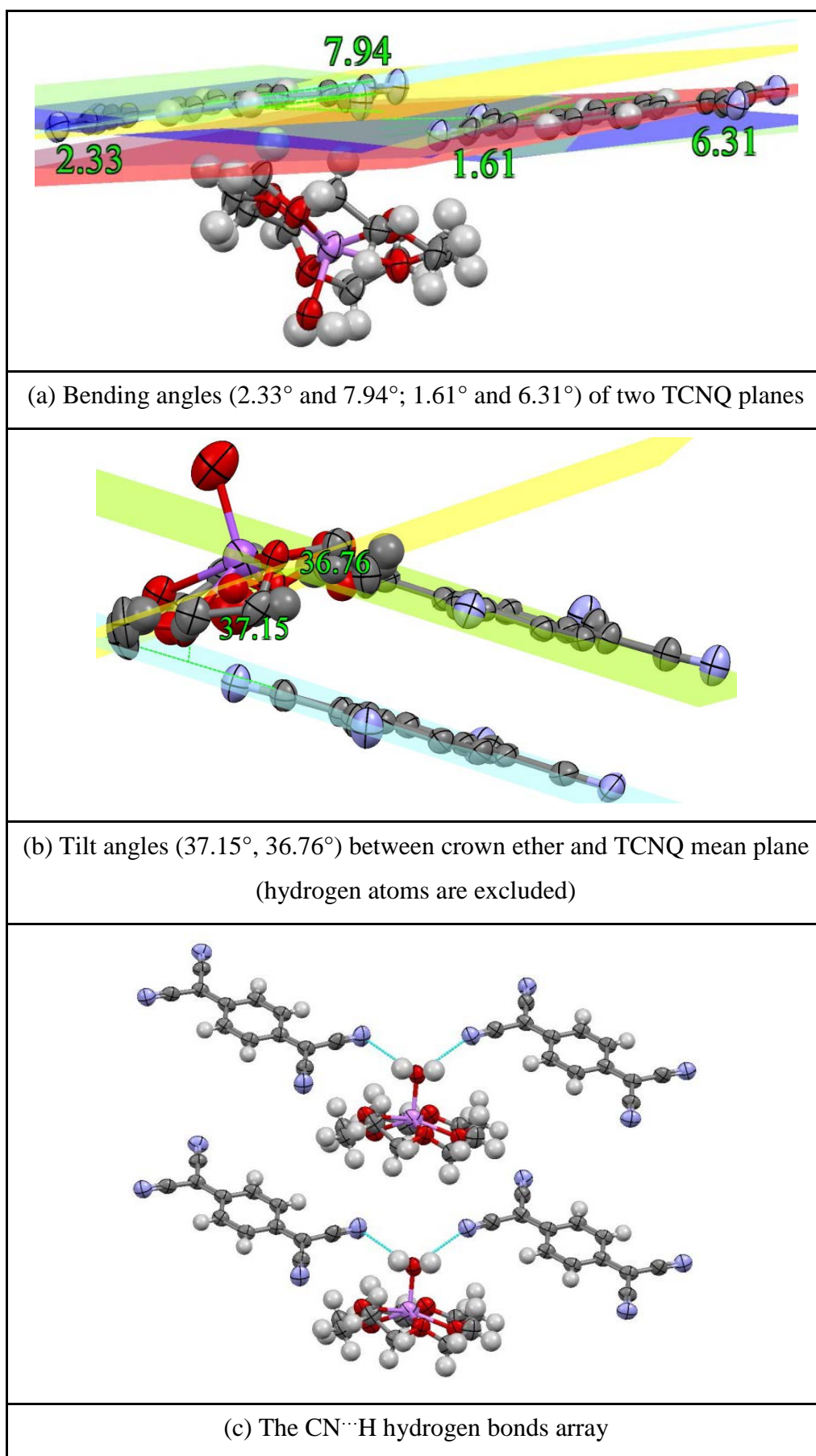


Figure 3.52 Angle descriptions in $(15\text{C}5)\text{Na}(\text{TCNQ})_2\cdot\text{H}_2\text{O}$

Figure 3.53 Various contact distances (Å) within the cation complex (carbon and hydrogen atoms excluded)

As viewed in Figure 3.53, some difficulties were encountered during the X-ray crystal structure solution as the crown ether is found to be disordered. Except for O303 which is 0.515 Å away from the oxygen atom mean plane, the other four oxygen atoms of the crown ether unit are sited on their mean plane. The ligating oxygen atoms sit above and

below their mean plane to form irregular pentagonal geometry of mean side by *ca.* 2.761 Å. All of the Na⁺-O distances in (15C5)Na(TCNQ)₂·H₂O are different, which demonstrates that the Na⁺ cation lies distorted above the cavity of 15C5 because the coordination with H₂O molecule.

3.3.2.4 Comparison between (15C5)Li(TCNQ)₂·H₂O and (15C5)Na(TCNQ)₂·H₂O

Figure 3.54 shows a space-filled view of cation complexes of (15C5)Li⁺ and Na⁺·H₂O respectively. Each metal cation (Li⁺/Na⁺) is coordinated by one H₂O molecule and one crown ether unit. There are not any direct metal-anion interactions (M⁺-NC) in either of these complexes. Both of the metal cations (Li⁺/Na⁺) are situated above the cavity of crown ether unit. Comparing the size of metal cation (Li⁺ < Na⁺), the Na⁺ cation is sited further away (0.573 Å) from the crown ether mean plane (as defined by each set of oxygen atoms) than Li⁺ cation (0.366 Å).

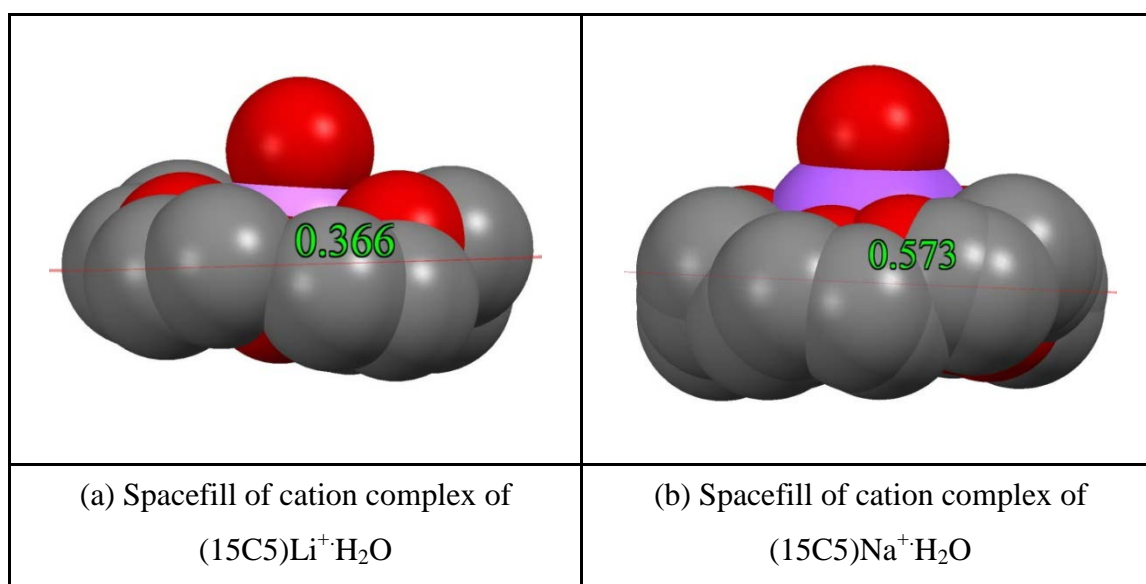


Figure 3.54 Spacefilled view of cation complex of (15C5)Li⁺/Na⁺·H₂O (hydrogen atoms are excluded)

Figure 3.55 shows the tilt angle between TCNQ column and the bottom TCNQ best plane for (15C5)Li⁺(TCNQ)₂·H₂O and (15C5)Na(TCNQ)₂·H₂O respectively. In these two TCNQ salts, TCNQ units prefer to form column. In each case, the similarity of the bond lengths within the two TCNQ units makes it difficult to distinguish between the components of TCNQ⁰ and TCNQ^{•-}, which demonstrates that the electrons are delocalised within the TCNQ column.

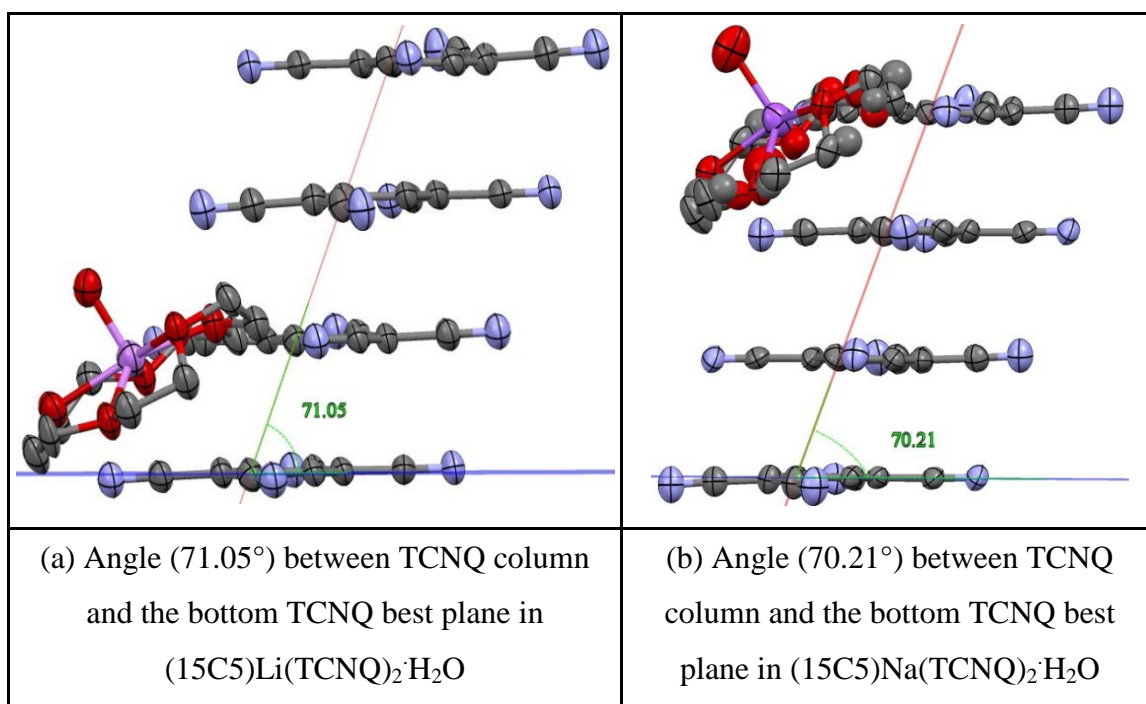


Figure 3.55 Tilt angle between TCNQ column and the bottom TCNQ best plane for $(15C5)Li^+(TCNQ)_2 \cdot H_2O$ and $(15C5)Na(TCNQ)_2 \cdot H_2O$ (hydrogen atoms are excluded)

| TCNQ units | | $(15C5)Li(TCNQ)_2 \cdot H_2O$ | | | $(15C5)Na(TCNQ)_2 \cdot H_2O$ | |
|--|--------------------|-------------------------------|-----------------------------|-----------------------------|-------------------------------|-----------------------------|
| | | TCNQ dimer | TCNQ dimer neighbours (AA') | TCNQ dimer neighbours (BB') | TCNQ dimer | TCNQ dimer neighbours (BB') |
| π - π perpendicular distance (Å) | | 3.11 | 3.32 | 3.35 | 3.11 | 3.37 |
| Long-axis slip | Distance (Å) | 2.04 | 1.33 | 1.42 | 2.03 | 1.16 |
| | Angle ($^\circ$) | 33.26 | 21.83 | 22.97 | 33.13 | 19.03 |
| Centroid-centroid distance (Å) | | 3.73 | 4.24 | 4.24 | 3.71 | 4.14 |

Table 3.19 Comparison of key parameters of TCNQ column geometries in $(15C5)Li^+ \cdot H_2O$ and $(15C5)Na^+ \cdot H_2O$

3.3.3 Preparation of (18C6)M(TCNQ)_n complexes (M = Na, K, Cs)

In this section, cation complexes of (18C6)KTCNQ, (18C6)Na(TCNQ)₂·2H₂O, (18C6)K(TCNQ)_{2.5}, and (18C6)Cs(TCNQ)₂ will be discussed with an analysis of their crystal structures.

(a) (18C6)KTCNQ

The crystal structure of (18C6)KTCNQ (ref code: JEXJAX) has been published by the Grossel group and the X-ray data had been collected at room temperature (283-303K)³⁶. In the course of present study, crystal of (18C6)KTCNQ were obtained which had characterisation data identical with that previously reported. An X-ray structure study of this TCNQ salt was carried out with the data being collected at 100K and the result was essentially identical with those previously found. Table 3.21 compares the key crystallographic data for the two structures solutions.

Reaction of 18C6 with KTCNQ (ratio 1:1) in dry acetonitrile afforded a dark violet crystalline solid (Combustion Analysis: Calculated: C: 56.79%, H: 5.56%, N: 11.03%. Found: C: 57.32%, H: 6.02%, N: 12.86%) which contained single crystals suitable for X-ray structural study. Full details including an account of the structure solution and refinement are reported in the Experimental Section and the Supporting Information (in the Appendices) respectively. The crystals obtained were of (18C6)KTCNQ and the basic structure is shown in Figure 3.56.

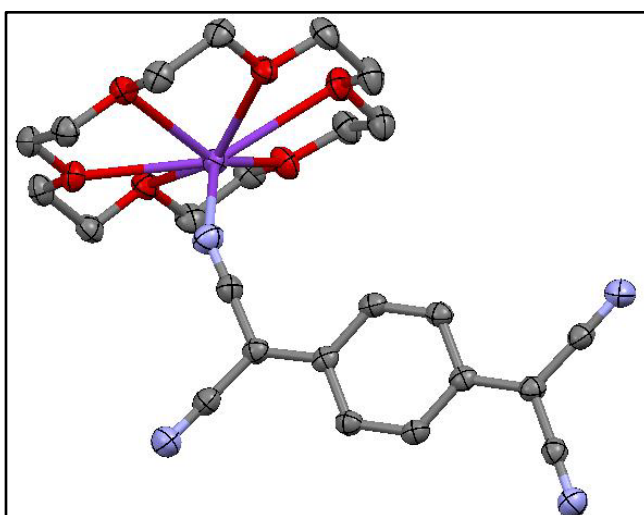


Figure 3.56 Basic structure of (18C6)KTCNQ in this study (hydrogen atoms are excluded)

Bond lengths within the TCNQ^{•-} units are summarised in Table 3.20.

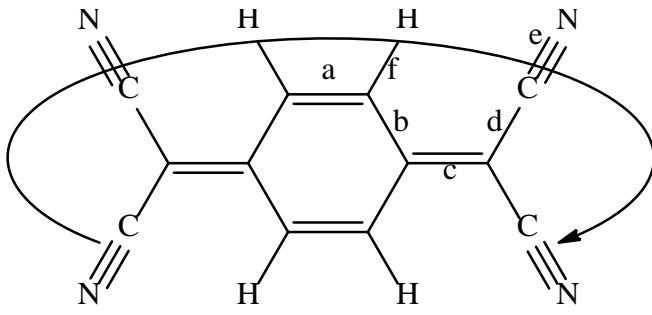
|  | | | | | | |
|--|------------------|-----------|-----------|-----------|-----------|---------|
| (a) Definition of the bond lengths within the TCNQ ^{•-} molecule (ref code: JEXJAX) ³⁶ | | | | | | |
| Structure | Bond lengths (Å) | | | | | |
| | a | b | c | d | e | f |
| TCNQ ^{•-} unit | | 1.425(13) | | 1.417(13) | 1.154(13) | 0.950 |
| | | (1.414) | | (1.419) | (1.146) | (0.970) |
| | 1.364(13) | 1.423(12) | 1.418(13) | 1.423(13) | 1.153(14) | 0.950 |
| | (1.360) | (1.423) | (1.419) | (1.417) | (1.143) | (0.970) |
| | 1.365(13) | 1.421(13) | 1.421(13) | 1.421(12) | 1.155(13) | 0.951 |
| | (1.361) | (1.417) | (1.418) | (1.417) | (1.146) | (0.970) |
| | | 1.427(12) | | 1.419(13) | 1.155(13) | 0.950 |
| | | (1.423) | | (1.409) | (1.155) | (0.970) |

Table 3.20 Summary of bond lengths (Å) observed for TCNQ^{•-} units in (18C6)KTCNQ (literature values³⁶ for comparison are listed in brackets)

A comparison table containing key parameters of crystal structure at the different data collection temperatures is summarised in Table 3.21.

Comparison of the unit cell dimensions of (18C6)KTCNQ at the different temperatures, the representing of unit cell has been rotated because the length along *a* axis under 100K is similar to the corresponding data along *c* axis under room temperature and the statistics along *c* axis under 100K is similar to that found in *a* axis under room temperature respectively. The unit cell dimensions of (18C6)KTCNQ have been extended as the data collection temperature is increased, which leads to a slight increase in the unit-cell volume (from 5126.9 Å³ to 5275.6 Å³).

| (18C6)KTCNQ | | | | |
|--------------------------|---|-------------|---|-----------|
| Key parameters | 100K | | Room temperature (283-303K) ³⁶ | |
| Empirical formula | C ₄₈ H ₅₆ K ₂ N ₈ O ₁₂ | | C ₄₈ H ₅₆ K ₂ N ₈ O ₁₂ | |
| Crystal system | Monoclinic | | Monoclinic | |
| Space group | C2/c | | A2/n | |
| Unit cell dimensions | a/Å | 23.6591(17) | a/Å | 26.670(4) |
| | b/Å | 8.1779(5) | b/Å | 8.223(4) |
| | c/Å | 26.7609(19) | c/Å | 24.341(4) |
| | α /° | 90 | α /° | 90 |
| | β /° | 98.0370(10) | β /° | 81.22(1) |
| | γ /° | 90 | γ /° | 90 |
| Volume (Å ³) | 5126.9 | | 5275.6 | |
| Z | 4 | | 4 | |
| R-Factor (%) | 2.56 | | 4.34 | |

Table 3.21 Comparison of key parameters of (18C6)KTCNQ at different data collection temperatures

In this structure, the K⁺ ion is coordinated by one crown ether unit. The TCNQ^{•-} units form a dimer which is slightly short-axis slip (see Figure 3.57).

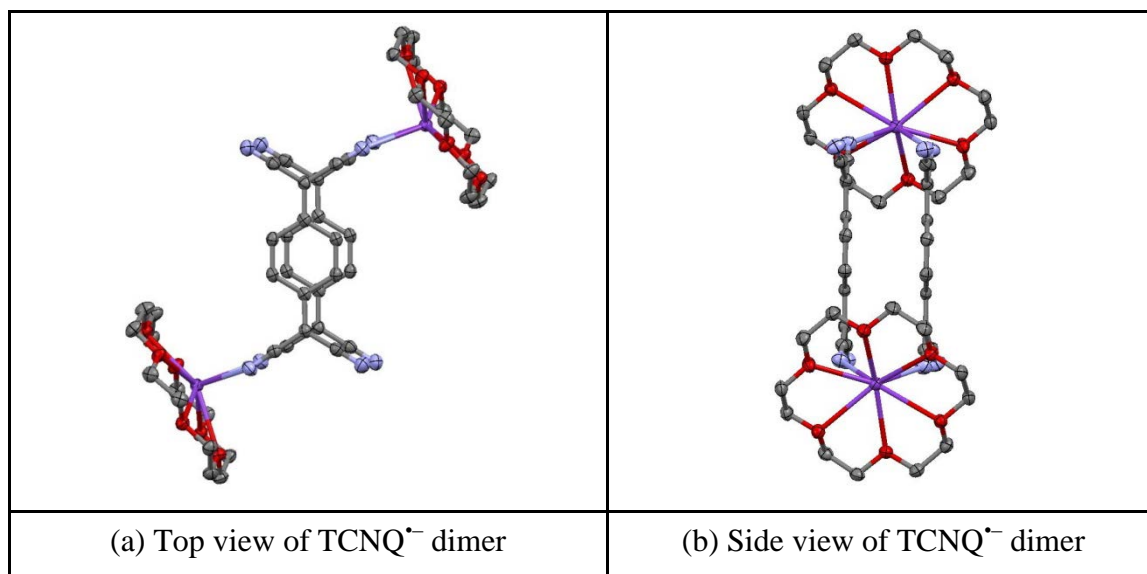


Figure 3.57 Top (a) and side (b) views of TCNQ^{•-} dimer in (18C6)KTCNQ (hydrogen atoms are excluded)

The data in Table 3.20 suggest that $\text{TCNQ}^{\bullet-}$ units have some quinonoidal character because bond length “a” is less than “b”. The distribution of bond lengths is reported for $\text{TCNQ}^{\bullet-}$ ²¹³.

As previously reported^{36,131}, within the crystal, the $\text{TCNQ}^{\bullet-}$ units are assembled into separated dimers in which $\text{TCNQ}^{\bullet-}$ dimer neighbours are significantly long-axis slip (see Figure 3.58). Distances and angles within the $\text{TCNQ}^{\bullet-}$ stacks are summarised in Table 3.22.

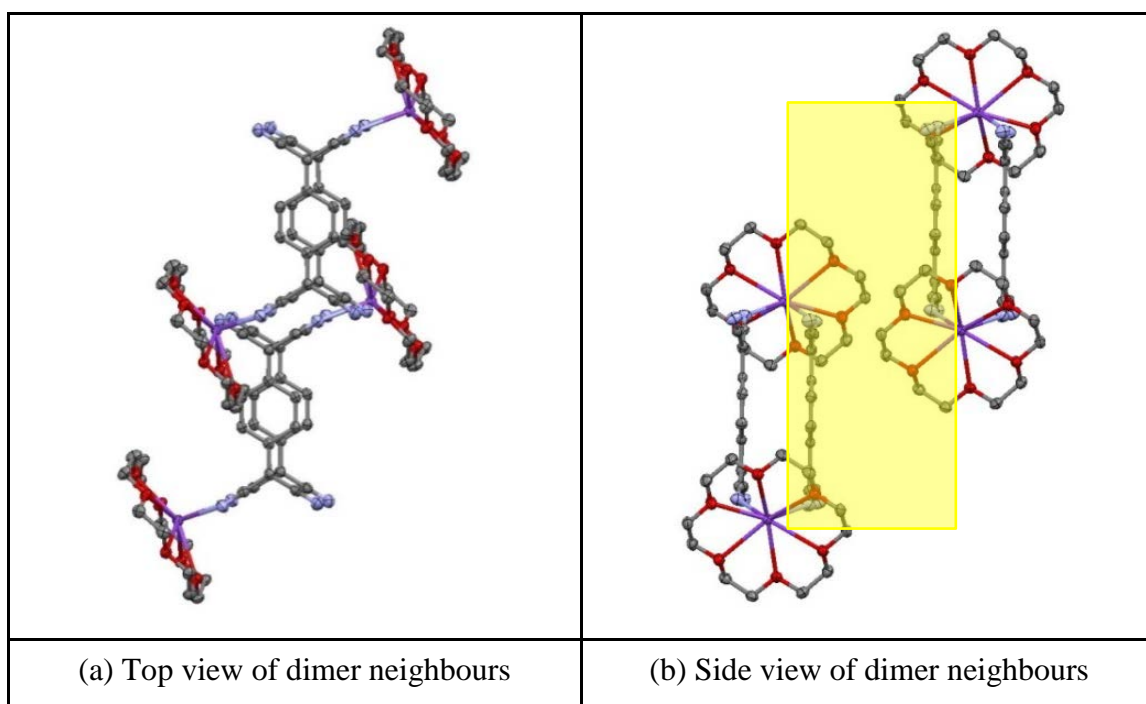


Figure 3.58 Top (a) and side (b) views of dimer neighbours in (18C6)KTCNQ (hydrogen atoms are excluded)

| $\text{TCNQ}^{\bullet-}$ unit [JEXJAX] ³⁶ | | $\text{TCNQ}^{\bullet-}$ dimer | $\text{TCNQ}^{\bullet-}$ dimer neighbours |
|--|--------------|--------------------------------|---|
| π - π perpendicular distance (Å) | | 3.16 [3.23] ¹³¹ | 5.54 |
| Short-axis slip | Distance (Å) | 0.53 [0.33] ¹³¹ | 2.30 |
| | Angle (°) | 9.53 [5.82] ¹³¹ | 22.55 |
| Long-axis slip | Distance (Å) | 0.081 [0.080] ¹³¹ | 8.90 |
| | Angle (°) | 1.47 [1.42] ¹³¹ | 58.11 |
| Centroid-centroid distance (Å) | | 3.20 [3.24] ¹³¹ | 10.74 |

Table 3.22 Distances (Å) and angles (°) within the $\text{TCNQ}^{\bullet-}$ stacks of (18C6)KTCNQ

Each K^+ cation is coordinated to a crown ether unit and two nitriles from adjacent $TCNQ^{\bullet-}$ units within a $TCNQ^{\bullet-}$ dimer. The K^+ cation sits 0.726 \AA above the crown ether mean plane (0.762 \AA in literature)³⁶, as defined by each set of oxygen atoms. As previously reported³⁶, from the side view of the isolated $TCNQ^{\bullet-}$ dimers in (18C6)KTCNQ (see Figure 3.60), the $TCNQ^{\bullet-}$ units adopts a brickwork structure of $TCNQ^{\bullet-}$ dimers bound by the metal-crown ether units. Consequently, each $TCNQ^{\bullet-}$ unit also adopts a non-planar boat geometry analogous with that observed in the simple M-TCNQ salts such as $RbTCNQ(I)$ ¹³¹ twisted in such a way that the cyano groups in neighbouring $TCNQ^{\bullet-}$ units are pushed away from each other. Examining of the top view packing pattern of (18C6)KTCNQ reveals that each $TCNQ^{\bullet-}$ dimer pair is parallel to each other and that the neighbouring columns of $TCNQ^{\bullet-}$ dimers are tilted in respect to each other by *ca.* 7° (compared with 10.84° in the previous literature)³⁶. Figure 3.59 shows $TCNQ^{\bullet-}$ dimer geometries in (18C6)KTCNQ.

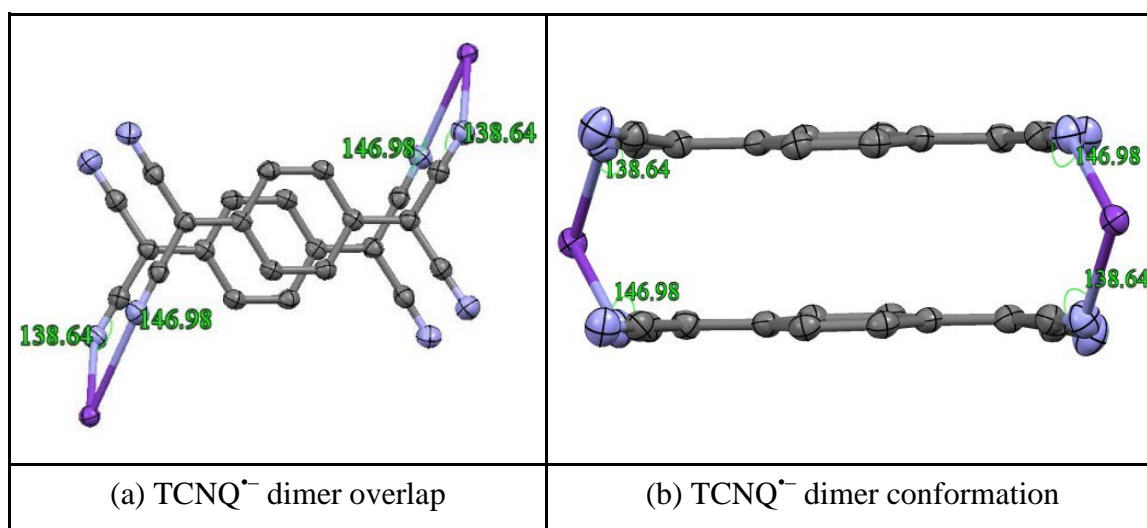


Figure 3.59 $TCNQ^{\bullet-}$ dimer geometries in (18C6)KTCNQ (hydrogen atoms are excluded)

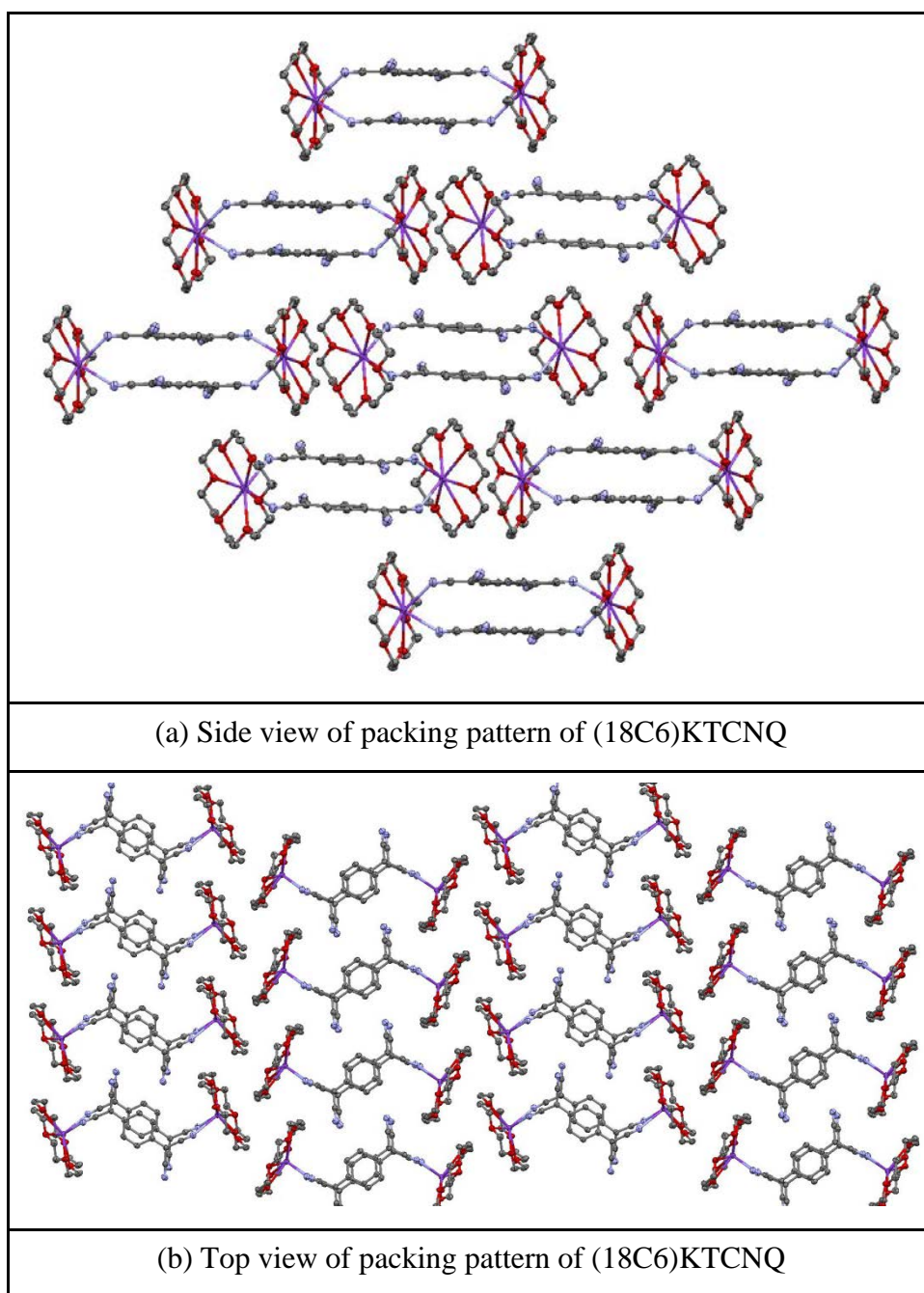


Figure 3.60 Side (a) and top (b) views of packing pattern of (18C6)KTCNQ (hydrogen atoms are excluded)

Figure 3.61 summarises the various contact distances within the cation complex. All of the six oxygen atoms are approximately sited on their mean plane. The ligating oxygen atoms lay above and below their mean plane to form irregular hexagonal geometry of mean side by *ca.* 2.802 Å. All of the K^+ -O distances in (18C6)KTCNQ can be summarised into two main groups, which are (i) 2.805, 2.810, 2.849 Å and (ii) 2.908, 2.919, 2.959 Å respectively. The different K^+ -O distances demonstrate that the K^+ cation is distorted above the cavity of 18C6. The distance of K1-N1, which is 2.819 Å,

is slightly shorter than the sum of the van der Waals' radii ($K^+-N = 2.88 \text{ \AA}$)^{269,271} and thus it seems justifiable to regard the metal cation and the nitrogen atom as being in contact whereas the distance of K1-N3 is a little longer at 2.952 \AA .

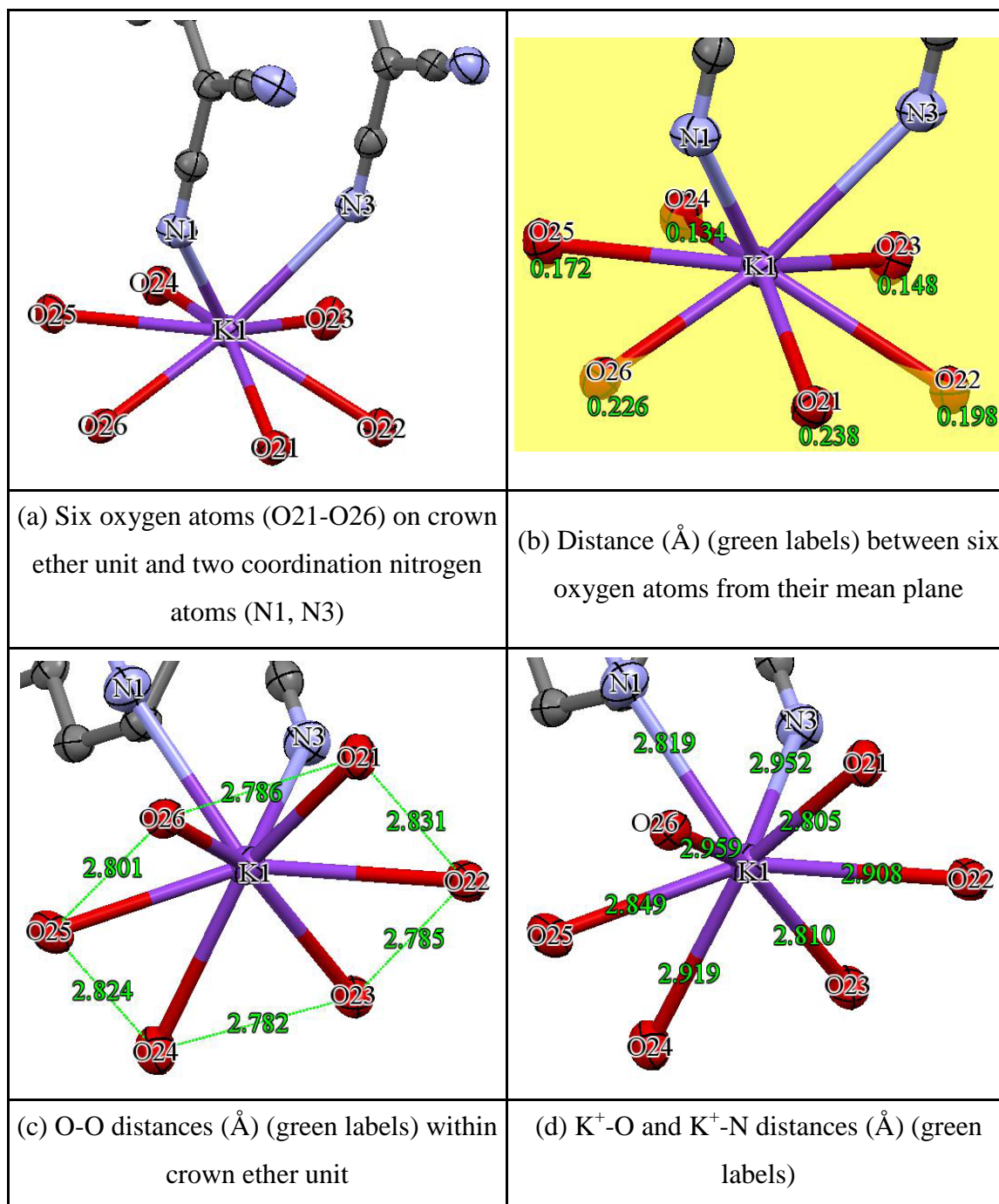


Figure 3.61 The various contact distances (Å) within the cation complex of (18C6)KTCNQ (carbon atoms on crown ether unit and hydrogen atoms are excluded)

(b) (18C6)Na(TCNQ)₂·2H₂O

Reaction of 18C6 with NaTCNQ and TCNQ⁰ (ratio 1:1:1) in dry acetonitrile afforded a yield (5%) of a dark blue crystalline solid which contained single crystals suitable for X-ray structural study (combustion data is awaited). Full details including an account of the structure solution and refinement are reported in the Experimental Section and the Supporting Information (in the Appendices) respectively. The crystals obtained were of (18C6)Na(TCNQ)₂·2H₂O and the basic unit is shown in Figure 3.62. Bond lengths within the TCNQ units are summarised in Table 3.23. In this structure, the Na⁺ ion is disordered and coordinated by one crown ether unit and two H₂O molecules. Figure A.1 shows five closely related structures in which (18C6)Na⁺ is complexed with two H₂O molecules have been found in the Cambridge Database (see Appendix).

The TCNQ units form a dimer which is significantly long-axis slipped (see Figure 3.63). The similarity of the bond lengths within the two TCNQ units makes it difficult to distinguish between the TCNQ^{•-} and TCNQ⁰ components.

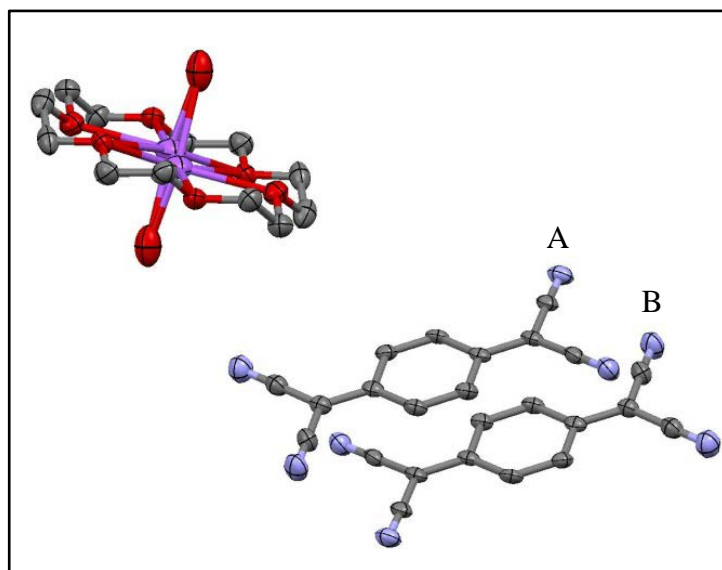


Figure 3.62 Basic unit of (18C6)Na(TCNQ)₂·2H₂O (sodium ion is disordered and hydrogen atoms are excluded)

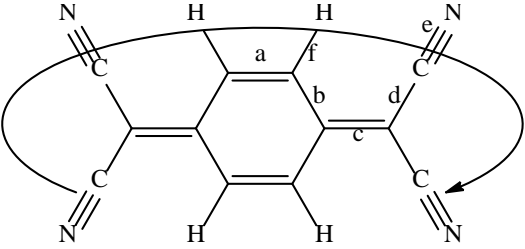
|  | | | | | | |
|---|------------------|-----------|-----------|-----------|-----------|-------|
| (a) Definition of the bond lengths within the TCNQ molecule | | | | | | |
| Structure | Bond lengths (Å) | | | | | |
| | a | b | c | d | e | f |
| TCNQ unit (A) | | 1.440 (2) | | 1.430 (2) | 1.157 (2) | 0.950 |
| | 1.359 (2) | 1.438 (2) | 1.402 (2) | 1.426 (2) | 1.155 (2) | 0.950 |
| | 1.361 (2) | 1.440 (2) | 1.400 (2) | 1.430 (2) | 1.160 (2) | 0.949 |
| | | 1.438 (2) | | 1.427 (2) | 1.157 (2) | 0.950 |
| TCNQ unit (B) | | 1.438 (2) | | 1.427 (2) | 1.157 (2) | 0.950 |
| | 1.361 (2) | 1.440 (2) | 1.400 (2) | 1.430 (2) | 1.160 (2) | 0.949 |
| | 1.359 (2) | 1.438 (2) | 1.402 (2) | 1.426 (2) | 1.155 (2) | 0.950 |
| | | 1.440 (2) | | 1.430 (2) | 1.157 (2) | 0.950 |

Table 3.23 Summary of bond distances (Å) observed for TCNQ units

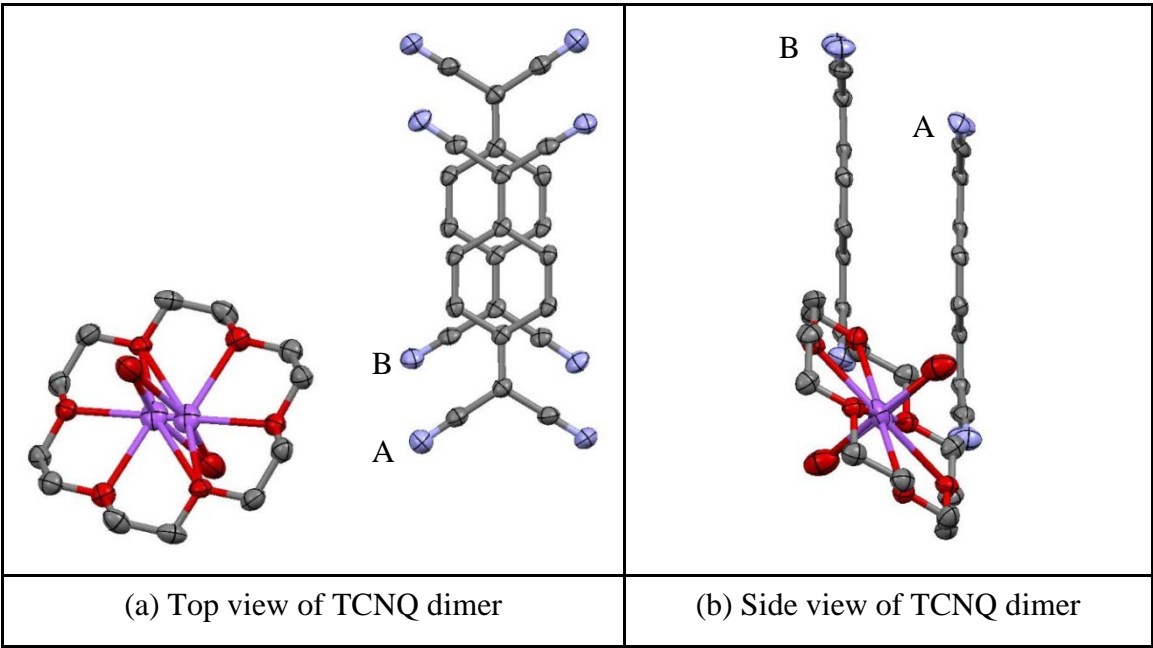


Figure 3.63 Top (a) and side (b) views of TCNQ dimer in $(18C6)Na(TCNQ)_2 \cdot 2H_2O$
(hydrogen atoms are excluded)

The data in Table 3.23 suggest that both TCNQ units have some quinonoidal character because bond length “a” is less than “b”. For both components A and B, the distribution of bond lengths is intermediate between these reported for TCNQ⁰ and TCNQ^{•-213}.

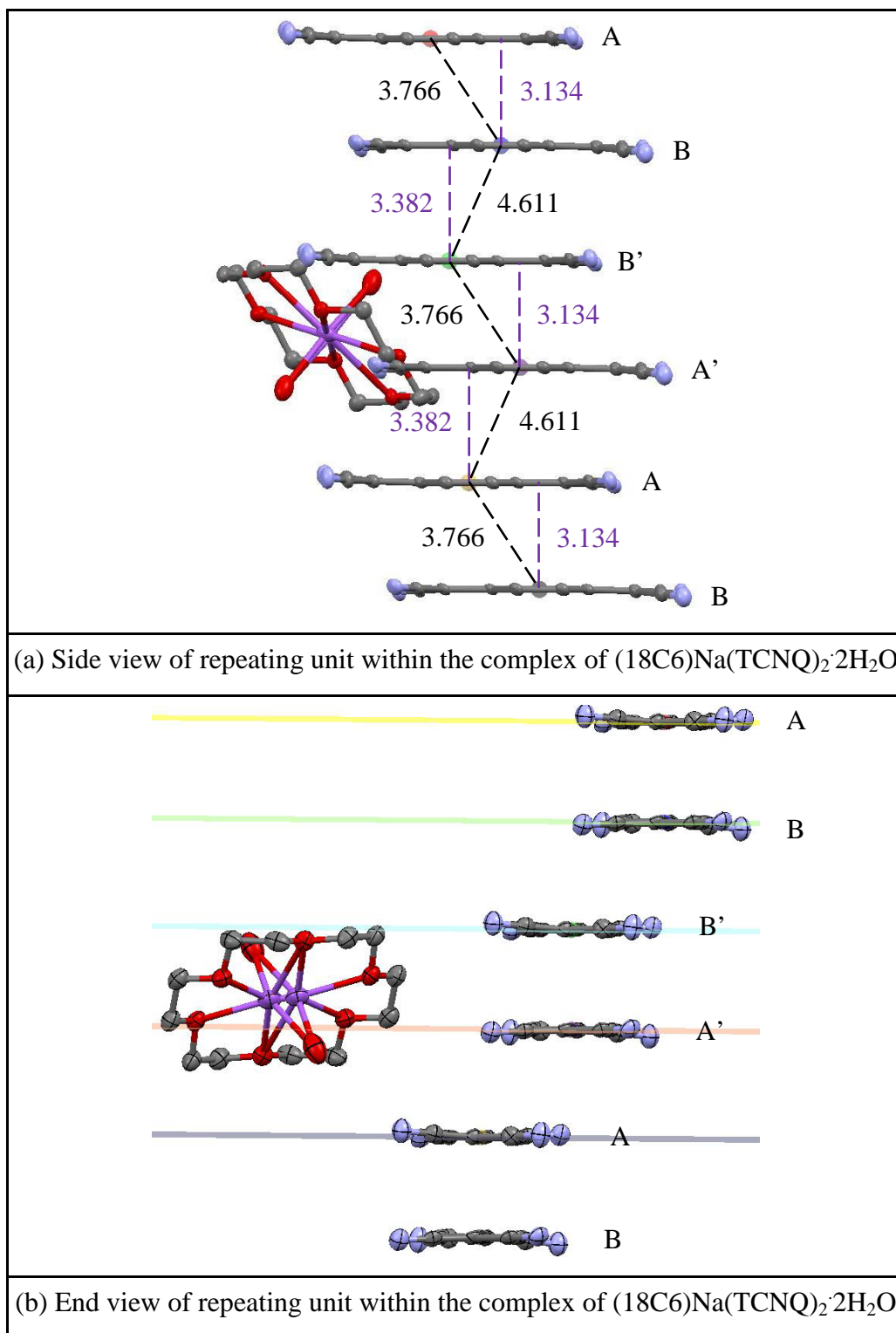


Figure 3.64 Views of repeating unit within the complex of $(18C6)Na(TCNQ)_2 \cdot 2H_2O$ (hydrogen atoms are excluded)

Within the crystal, the TCNQ dimers assembled into infinite columns in which the individual TCNQ units are assembled in an ABB'A' motif (see Figure 3.64) in which dimer neighbours is significantly “diagonally” slipped (see Figure 3.65). Distances and angles within the TCNQ stacks are listed in Table 3.24.

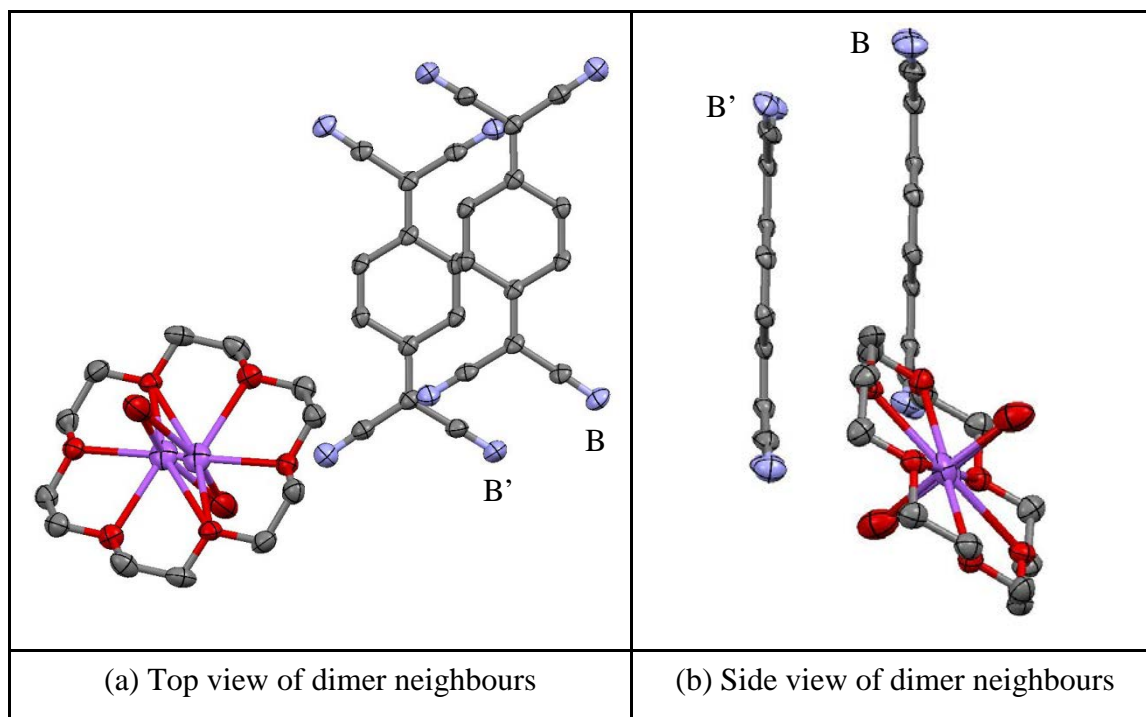


Figure 3.65 Top (a) and side (b) views of dimer neighbours, which is similar to dimer neighbours (AA') in $(18C6)Na(TCNQ)_2 \cdot 2H_2O$ (hydrogen atoms are excluded)

| | | TCNQ dimer | TCNQ dimer neighbours |
|--|--------------|------------|-----------------------|
| π - π perpendicular distance (Å) | | 3.13 | 3.38 |
| Short-axis slip | Distance (Å) | 0.13 | 2.74 |
| | Angle (°) | 2.43 | 39.03 |
| Long-axis slip | Distance (Å) | 2.08 | 1.52 |
| | Angle (°) | 33.62 | 24.24 |
| Centroid-centroid distance (Å) | | 3.77 | 4.61 |

Table 3.24 Distances (Å) and angles (°) within the TCNQ stacks of $(18C6)Na(TCNQ)_2 \cdot 2H_2O$

In the complex of $(18C6)Na(TCNQ)_2 \cdot 2H_2O$, the zigzag formation of TCNQ units affords a column with a wavelike pattern containing pairs of isolated TCNQ dimers. The dimers AB are close face-to-face π stacked with ideal overlap for conforming maximum π -orbital interactions. Moreover, within the dimer, the individual TCNQ units adopt a shallow boat conformation in which neighbouring $-C(CN)_2$ units are twisted away from each other. From the data in Table 3.24, it will be evident that π -facial overlap between dimer neighbours within a column is not ideal for extended π - π delocalisation within the column. Figure 3.66 shows the presence of hydrogen bonding between the TCNQ cyano groups and the two water molecules co-ordinated to each sodium ion.

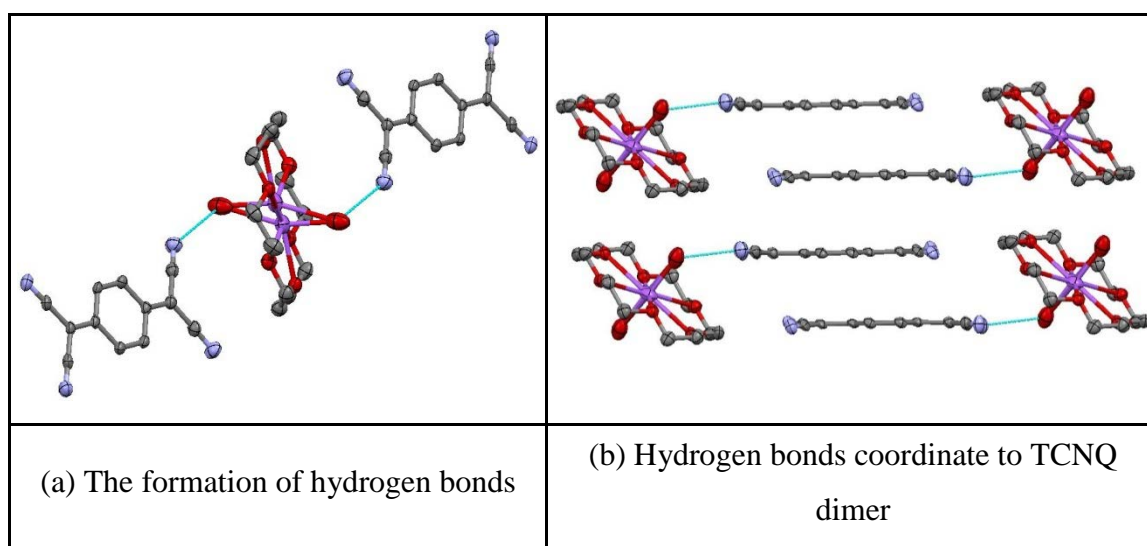


Figure 3.66 The formation of hydrogen bonding in $(18C6)Na(TCNQ)_2 \cdot 2H_2O$ (hydrogen atoms are excluded)

Each Na^+ cation is coordinated by one crown ether unit and two H_2O molecules. The resulting cation complex lies in channels between the TCNQ columns. There is no direct coordination between the TCNQ units and the Na^+ ions. The crown ether mean plane (as defined by each set of oxygen atoms) is twisted at an angle of 32.20° in respect to benzene ring of the TCNQ unit. The position of the Na^+ cation is disordered because the cavity of 18C6 does not exactly matching the size of Na^+ cation. One $-CN \cdots H$ hydrogen bond is formed between each H_2O molecule and adjacent cyano group (see Figure 3.66). Consequently, the H_2O molecules contribute to the coordination sphere around the Na^+ cation. Figure 3.67 summarises the various contact distances within the cation complex of $(18C6)Na(TCNQ)_2 \cdot 2H_2O$, comparing with a similar behaviour as seen for example in $Na(18C6)(H_2O)_2(N_3)$ (ref code: HORZET)²⁷³.

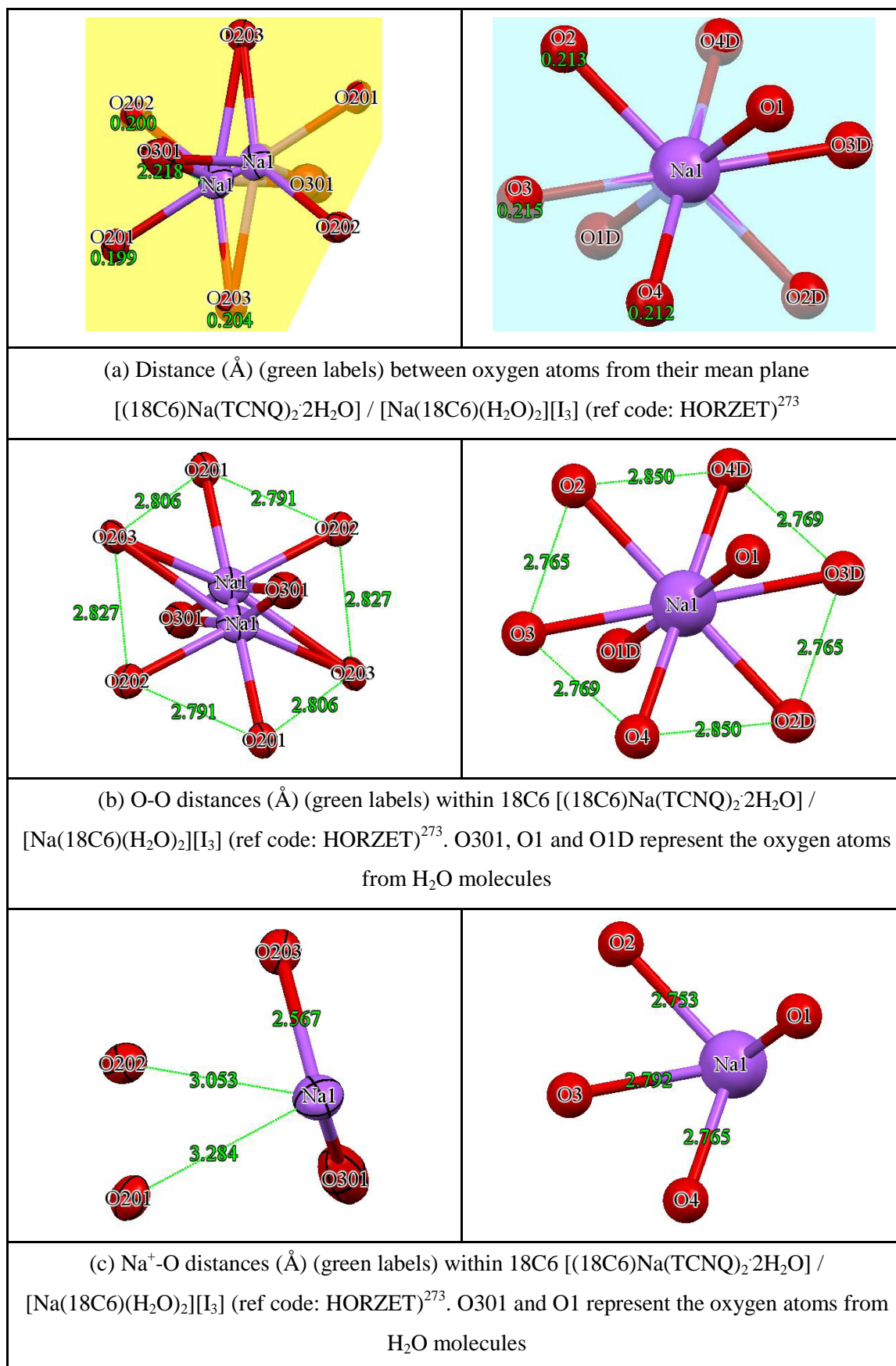


Figure 3.67 The various contact distances (Å) within the cation complex (carbon atoms on crown ether ring and hydrogen atoms are excluded)

As viewed in Figure 3.67, in $(18C6)Na(TCNQ)_2 \cdot 2H_2O$, all of the six oxygen atoms are approximately sited on the mean plane. The ligating six oxygen atoms lie above and below their mean plane to compose irregular hexagon geometry of mean side by *ca.* 2.808 Å. Because the size of Na^+ cation does not match the cavity of 18C6, the metal ion is disordered in the cavity of 18C6.

(c) $(18C6)K(TCNQ)_{2.5}$

Reaction of 18C6 with KTCNQ and $TCNQ^0$ (ratio 1:1:1) in dry acetonitrile afforded a reasonable yield (61%) of a pure bright black crystalline solid (Combustion Analysis: Calculated: C: 61.98%, H: 4.21%, N: 17.21%. Found: C: 61.84%, H: 4.00%, N: 17.08%.) which contained single crystals suitable for an X-ray structural study. Full details including an account of the structure solution and refinement are reported in the Experimental Section and the Supporting Information (in the Appendices) respectively. The crystals obtained were of $(18C6)K(TCNQ)_{2.5}$ and the core unit is shown in Figure 3.68.

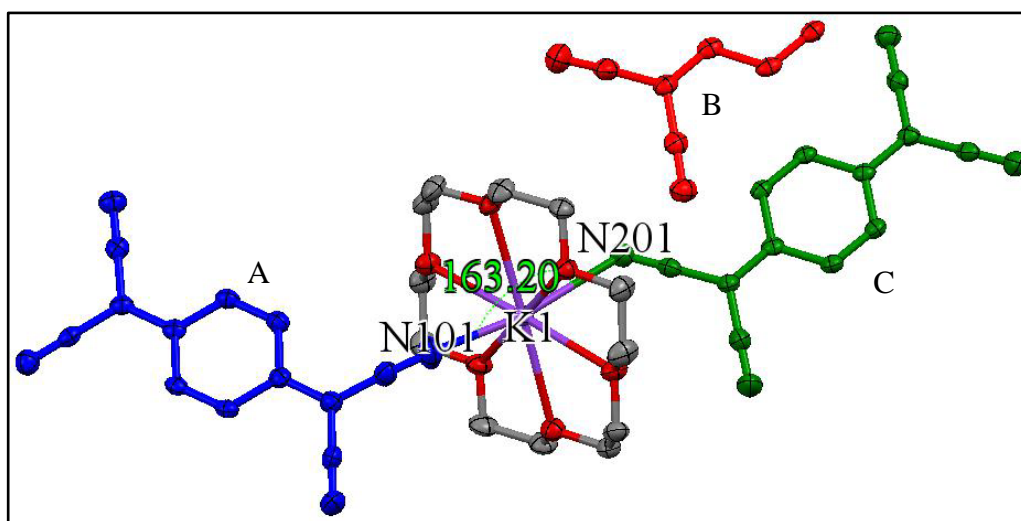


Figure 3.68 Core unit of $(18C6)K(TCNQ)_{2.5}$ (hydrogen atoms are excluded)

Bond lengths within the TCNQ units are summarised in Table 3.25. Figure 3.69 shows the zigzag pseudo-chain formation of cation-crown ether complex in $(18C6)K(TCNQ)_{2.5}$.

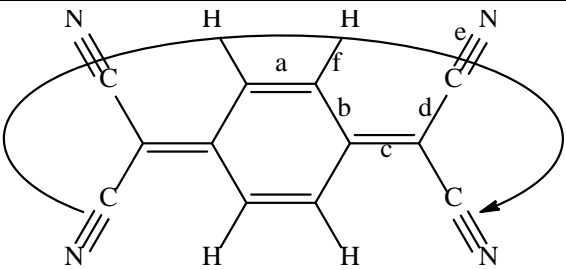
|  | | | | | | |
|--|------------------|------------|-----------|-----------|------------|-------|
| (a) Definition of the bond lengths within the TCNQ molecule | | | | | | |
| Structure | Bond lengths (Å) | | | | | |
| | a | b | c | d | e | f |
| TCNQ unit (A) | | 1.435 (2) | | 1.433 (2) | 1.153 (19) | 0.951 |
| | 1.364 (2) | 1.436 (2) | 1.409 (2) | 1.430 (2) | 1.156 (2) | 0.950 |
| | 1.363 (2) | 1.432 (2) | 1.411 (2) | 1.435 (2) | 1.148 (2) | 0.950 |
| | | 1.438 (2) | | 1.427 (2) | 1.158 (2) | 0.950 |
| TCNQ unit (B) | | 1.449 (2) | | 1.433 (2) | 1.156 (2) | 0.950 |
| | 1.353 (2) | 1.446 (2) | 1.380 (2) | 1.439 (2) | 1.150 (2) | 0.949 |
| | 1.353 (2) | 1.449 (2) | 1.380 (2) | 1.433 (2) | 1.156 (2) | 0.950 |
| | | 1.446 (2) | | 1.439 (2) | 1.150 (2) | 0.949 |
| TCNQ unit (C) | | 1.447 (2) | | 1.438 (2) | 1.153 (2) | 0.950 |
| | 1.359 (2) | 1.443 (2) | 1.395 (2) | 1.436 (2) | 1.153 (19) | 0.949 |
| | 1.356 (2) | 1.443 (19) | 1.396 (2) | 1.434 (2) | 1.160 (2) | 0.950 |
| | | 1.442 (2) | | 1.438 (2) | 1.151 (2) | 0.949 |

Table 3.25 Summary of bond distances (Å) observed for TCNQ units in
(18C6)K(TCNQ)_{2.5}

As viewed in Figure 3.69, in the cation complex of (18C6)K⁺, each K⁺ ion is coordinated by two TCNQ units. The TCNQ units assemble into extended columns in which there is a pentamer repeat pattern in this complex. In these, they are all π -stacked long and short-axis slipped alternately forming a wave-like motif [see Figure 3.72(c)]. A TCNQ unit is co-ordinated to each face of the K⁺-crown ether complex, thereby linking the columns together. The angle between these two TCNQ units, N101-K1-N201, is 163.20°. The chain pattern of TCNQ \cdots K⁺ \cdots TCNQ unit is similar to that seen in

(18C6)KNCS, in which the K^+ ion sits at the centre cavity of crown ether unit, coordinated to two disordered thiocyanate anions²⁶⁵.

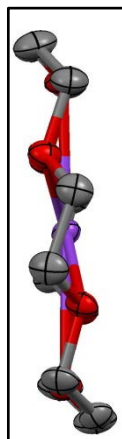


Figure 3.69 Zigzag conformation of cation complex $[(18C6)K^+]$ in $(18C6)K(TCNQ)_{2.5}$ (hydrogen atoms are excluded)

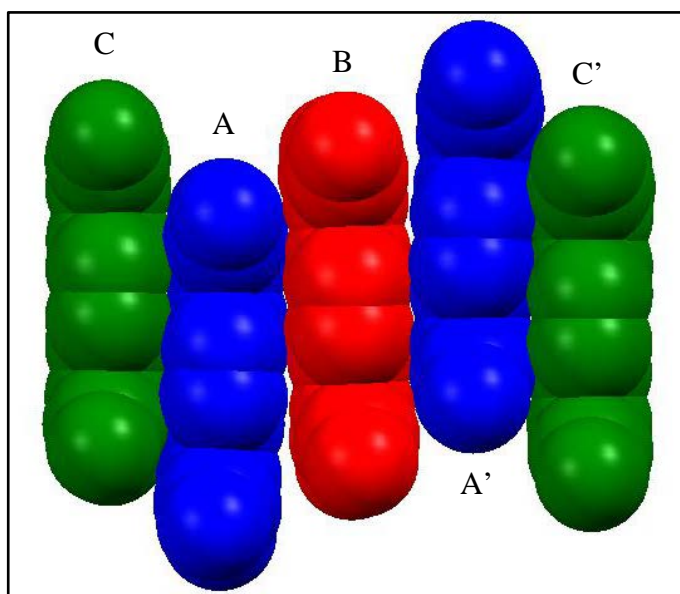


Figure 3.70 Space-fill diagram of TCNQ pentamer stack in $(18C6)K(TCNQ)_{2.5}$ (hydrogen atoms are excluded)

The data in Table 3.25 suggest that all of the TCNQ units have some quinonoidal character because bond length “a” is less than “b”. In the TCNQ pentamer, after measuring the c bond lengths in each TCNQ unit, it seems that both TCNQ unit (B) (red) and TCNQ unit (C) (green) have less electron density, and hence more $TCNQ^0$ character. Consequently, TCNQ unit (A) (blue) has higher electron density, and hence more $TCNQ^{\bullet-}$ character. As suggested, TCNQ units form mixed stacks, approximating a

TCNQ⁰-TCNQ^{•-}-TCNQ⁰-TCNQ^{•-}-TCNQ⁰ pattern similar to that seen previously in (C222)K(TCNQ)_{2.5} (Figure 3.119), which means two electrons are delocalised over the five TCNQ units but more negative charge density appears to reside on the second and fourth TCNQ units (blue ones) based on c bond lengths. Figure 3.71 shows top and side views of pairs of individual TCNQ units within (18C6)K(TCNQ)_{2.5}.

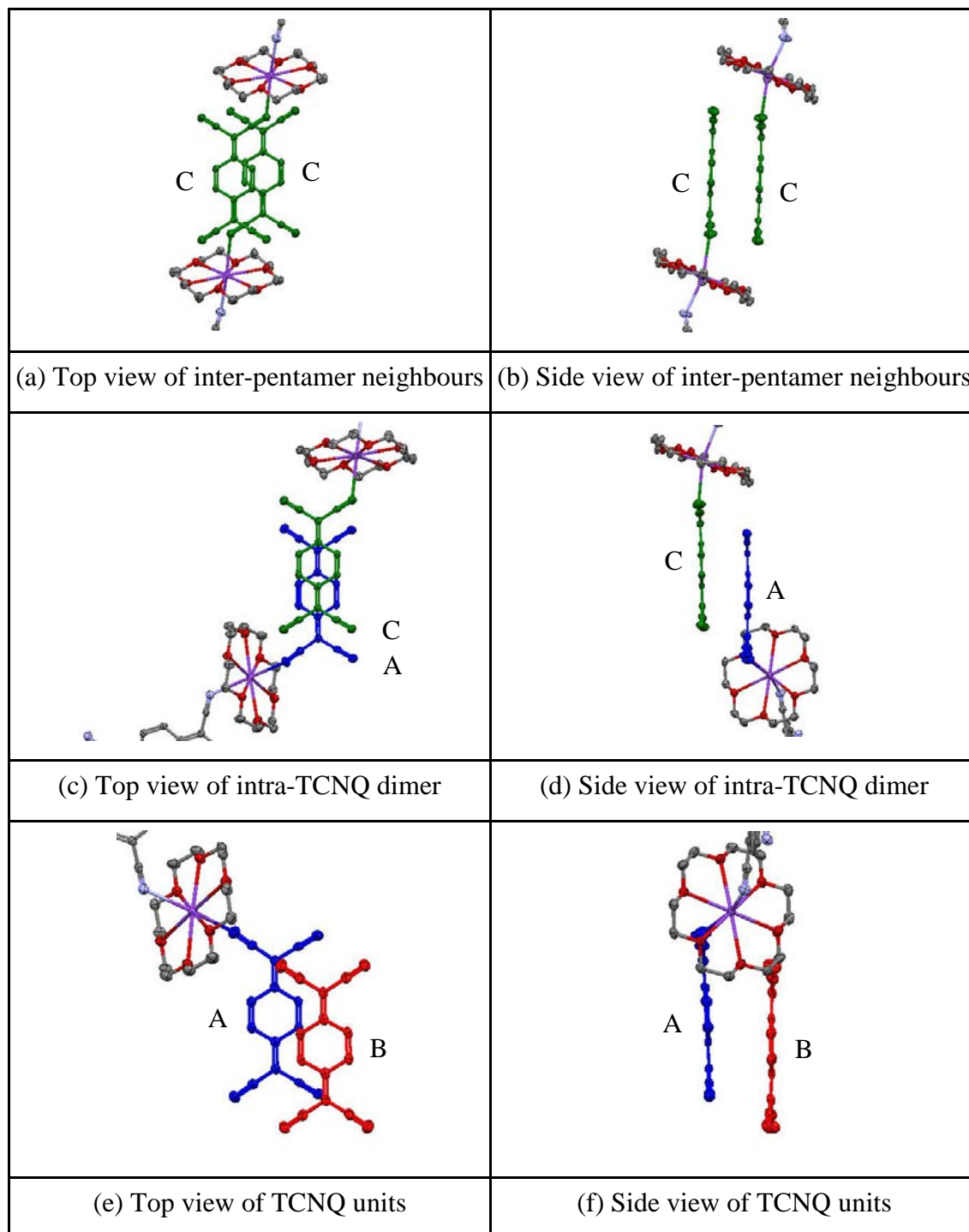


Figure 3.71 Top (a/c/e) and side (b/d/f) views of TCNQ units in (18C6)K(TCNQ)_{2.5}
(hydrogen atoms are excluded)

Within the crystal structure of $(18C6)K(TCNQ)_{2.5}$, the TCNQ pentamer can assemble into an infinite column (see Figure 3.72) with short-axis slippage between neighbouring TCNQ pentamers. The repeating unit (TCNQ pentamer) is composed by two separated dimer pairs separated by a single TCNQ unit (B), which has $TCNQ^0$ character. Neighbouring TCNQ columns form a herringbone packing pattern [see Figure 3.72(b)]. There are more TCNQ units than K^+ and 18C6, which results in the wave-like TCNQ column motif in order to create the cavities to accommodate the required cation complex of $(18C6)K^+$.

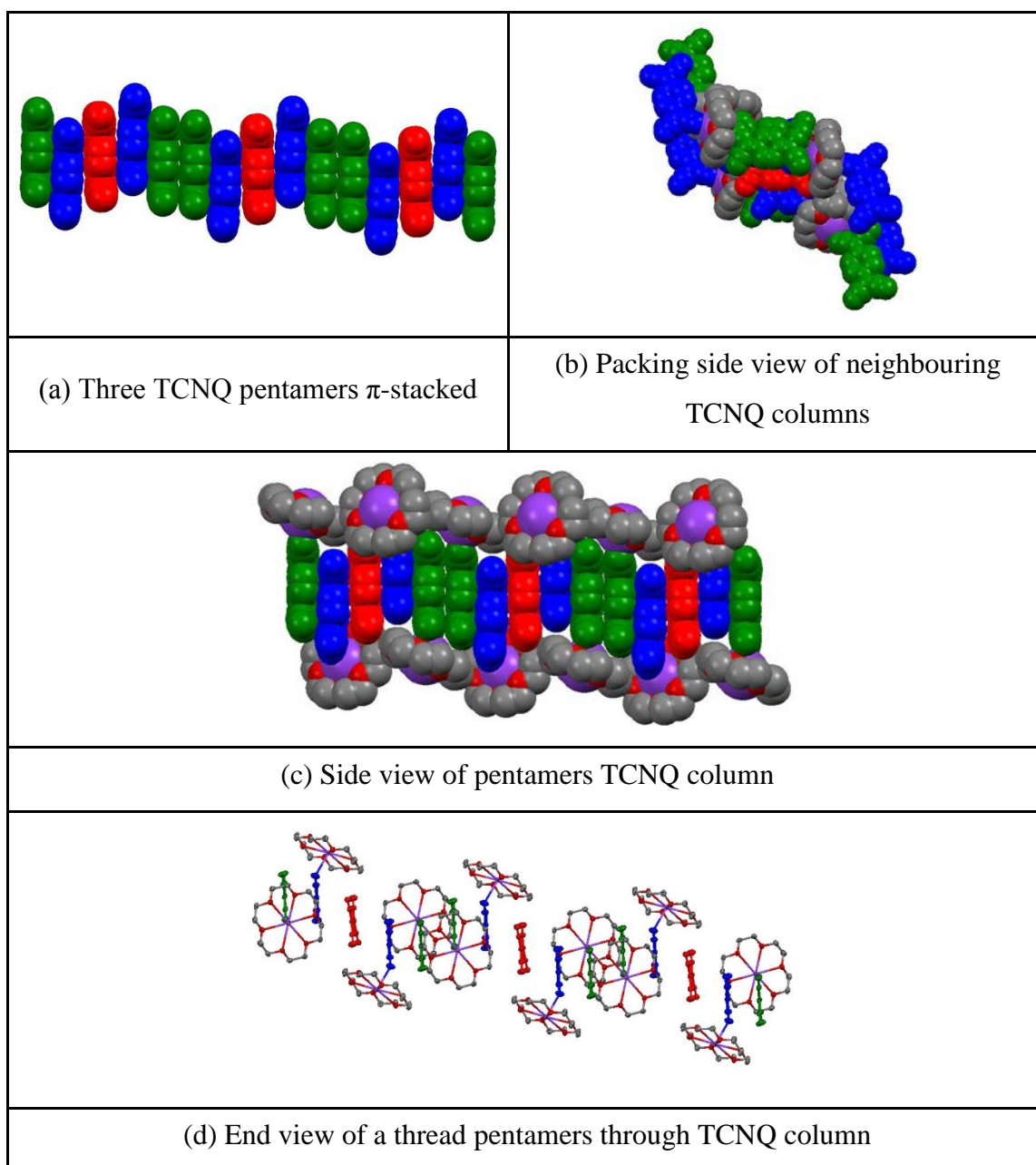


Figure 3.72 Views of pentamers geometry and packing pattern in TCNQ column (hydrogen atoms are excluded)

Distances and angles within the TCNQ stacks are summarised in Table 3.26.

| TCNQ unit | | AC | AB | TCNQ pentamer neighbours |
|--|--------------|-------|-------|--------------------------|
| π - π perpendicular distance (Å) | | 3.13 | 4.55 | 3.37 |
| Short-axis slip | Distance (Å) | 0.32 | 2.39 | 1.89 |
| | Angle (°) | 5.81 | 27.71 | 29.31 |
| Long-axis slip | Distance (Å) | 2.12 | 1.86 | 0.30 |
| | Angle (°) | 34.05 | 22.23 | 5.08 |
| Centroid-centroid distance (Å) | | 3.80 | 3.40 | 3.87 |

Table 3.26 Distances (Å) and angles (°) within the TCNQ stacks and between pentamer neighbours of (18C6)K(TCNQ)_{2.5}

Unlike the situation in (18C6)KTCNQ, the extra volume arising from the presence of TCNQ⁰ will change the packing motif. TCNQ units which can be regarded as dimers are closely face-to-face π contact and slightly long axis slipped. The dimer neighbours of TCNQ units within the column are significantly short-axis slipped but still closely π - π stacked. Consequently, within a TCNQ dimer, the TCNQ units are slightly boat shaped and twisted in such a way that the cyano groups in neighbouring TCNQ units are pushed away from each other. Figure 3.73 summarises the various contact distances within the cation complex.

As viewed in Figure 3.73, the ligating oxygen atoms sit above and below their mean plane (as defined by each set of oxygen atoms) to form an irregular hexagonal geometry of mean side by *ca.* 2.837 Å. The K⁺-O distances in (18C6)K(TCNQ)_{2.5} are not all equal and seem to fall into two groups: (i) 2.778 Å and (ii) 2.807, 2.813, 2.825, 2.828, 2.830 Å respectively. They are slightly shorter than the sum of the van der Waals' radii (K⁺-O = 2.85 Å)²⁷¹ and thus it seems justifiable to regard the metal cations and the oxygen atoms as being in contact. Consequently, the different K⁺-O distances demonstrate that the K⁺ cation does not lie in the centre of the cavity of 18C6. The distances of K⁺-N are 2.822 and 2.892 Å in Figure 3.73(d).

In (18C6)KNCS, the ligating oxygen atoms sit approximately 0.20 Å above and below their mean plane to form a nearly planar hexagon of mean side by *ca.* 2.82 Å, which is

matching with the van der Waals' diameter of oxygen atom and thus it seems justifiable to regard neighbouring oxygen atoms as being in contact²⁶⁵. The distances of K^+ -O are not equal and are slightly longer than the sum of the van der Waals' radii. The N or S, terminal atom in the disordered NCS^- anion, is located 3.19 Å from adjacent K^+ ion and close to the threefold screw axis of the hexagon, thereby satisfying the symmetry of hexagonal bipyramidal coordination²⁶⁵.

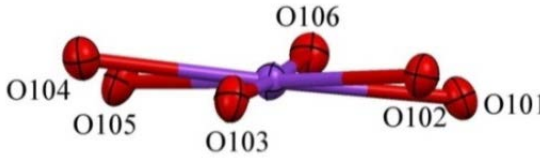
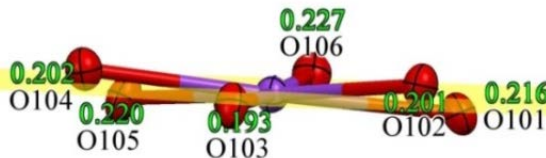
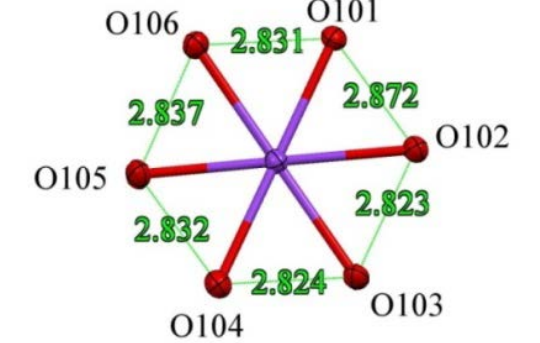
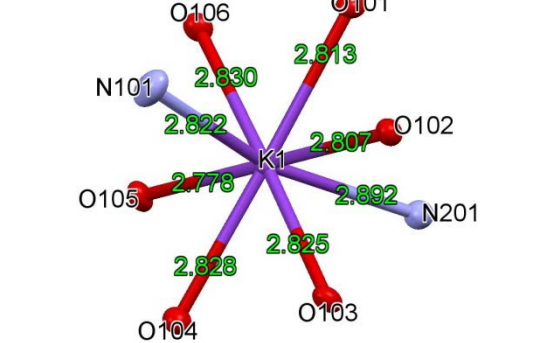
| | |
|--|---|
|  |  |
| (a) Six oxygen atoms (O101-O106) in crown ether unit | (b) Distance (Å) (green labels) between six oxygen atoms from their mean plane |
|  |  |
| (c) O-O distances (Å) (green labels) within 18C6 | (d) K^+ -O and K^+ -N distances (Å) (green labels) within 18C6 |

Figure 3.73 Various contact distances (Å) within the cation complex of $(18C6)K(TCNQ)_{2.5}$ (carbon atoms on crown ether unit and hydrogen atoms are excluded)

(d) $(18C6)Cs(TCNQ)_2$

Reaction of Cs_2TCNQ_3 with $TCNQ^0$ and 18C6 (ratio 1:2:2) in dry acetonitrile afforded a yield (13%) of a dark blue crystalline solid which contained single crystals suitable for X-ray structural study (combustion data is awaited). Full details including an account of the structure solution and refinement are reported in the Experimental Section and the Supporting Information (in the Appendices) respectively. The crystals obtained were of $(18C6)Cs(TCNQ)_2$, in which two $TCNQ$ molecules lie on the symmetry centres, and the basic components are shown in Figure 3.74.

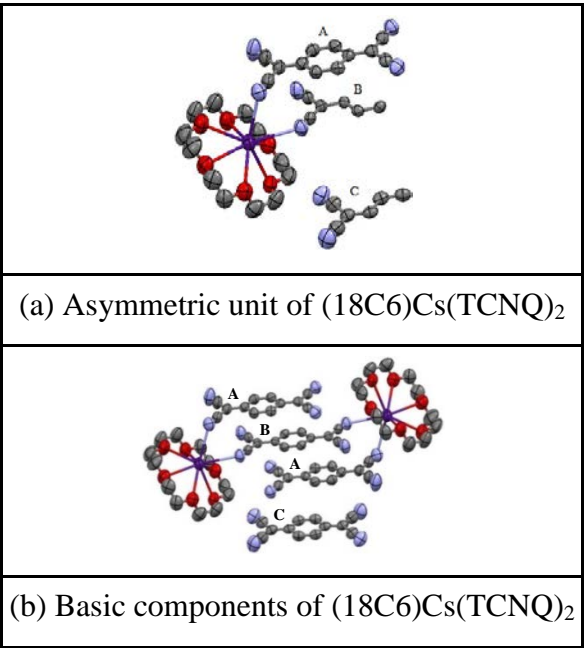


Figure 3.74 Asymmetric unit and basic components of $(18C6)Cs(TCNQ)_2$ (hydrogen atoms are excluded)

Bond lengths within the TCNQ units are summarised in Table 3.27.

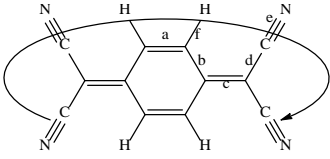
|  | | | | | | |
|---|------------------|-----------|-----------|-----------|-----------|-------|
| (a) Definition of the bond lengths within the TCNQ molecule | | | | | | |
| Structure | Bond lengths (Å) | | | | | |
| | a | b | c | d | e | f |
| TCNQ unit (A) | | 1.430 (6) | | 1.419 (7) | 1.143 (6) | 0.931 |
| | 1.352 (6) | 1.423 (6) | 1.399 (6) | 1.425 (7) | 1.135 (6) | 0.930 |
| | 1.348 (6) | 1.426 (6) | 1.399 (5) | 1.414 (6) | 1.150 (6) | 0.930 |
| | | 1.419 (6) | | 1.430 (6) | 1.145 (5) | 0.930 |
| TCNQ unit (B) | | | | 1.430 (6) | 1.145 (6) | 0.930 |
| | 1.348 (5) | 1.445 (5) | 1.388 (5) | 1.424 (6) | 1.143 (5) | 0.930 |
| TCNQ unit (C) | | | | 1.428 (7) | 1.134 (7) | 0.930 |
| | 1.339 (6) | 1.445 (6) | 1.381 (6) | 1.422 (6) | 1.147 (6) | 0.930 |

Table 3.27 Summary of bond distances (Å) observed for TCNQ units in $(18C6)Cs(TCNQ)_2$

In this structure, the Cs^+ ion is coordinated to one crown ether unit and two nitrile groups on adjacent TCNQ molecules. The TCNQ units form a trimer which is significantly long axis slipped (see Figure 3.75).

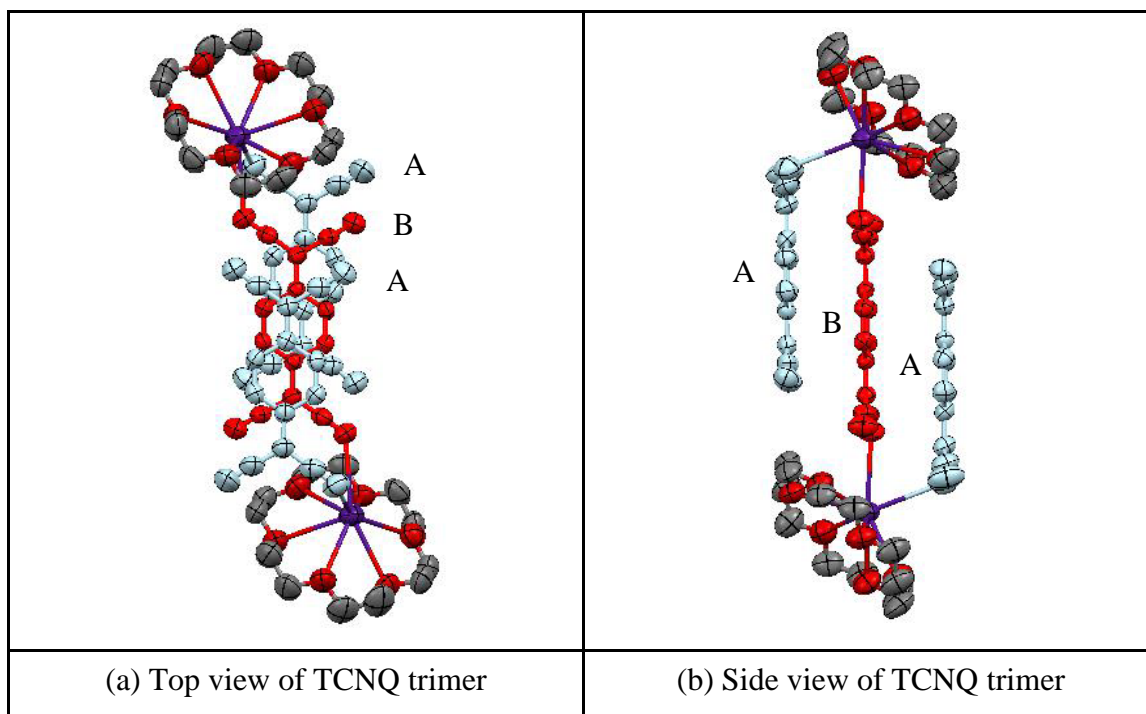


Figure 3.75 Top (a) and side (b) views of TCNQ trimer in $(18\text{C}6)\text{Cs}(\text{TCNQ})_2$ (hydrogen atoms are excluded)

The data in Table 3.27 suggest that all of the TCNQ units have some quinonoidal character because bond length “a” is less than “b”. In the TCNQ trimer, after measuring the c bond lengths in each TCNQ unit, it seems that TCNQ unit (A) has higher electron density, consistent with higher $\text{TCNQ}^{\bullet-}$ character. Consequently, the TCNQ unit (B) and TCNQ unit (C) are less electron rich and therefore have more TCNQ^0 character. Therefore, in each TCNQ trimer, the three TCNQ units form mixed stacks, having a $\text{TCNQ}^{\bullet-} - \text{TCNQ}^0 - \text{TCNQ}^{\bullet-}$ configuration, i.e. with two electrons delocalised over the three TCNQ units but more negative charge density appear to reside on the outer TCNQ units (A). Within the crystal, the TCNQ trimers assemble into infinite columns, separated on either face by an isolated TCNQ^0 (C) unit. The individual TCNQ units being assembled in an ABAC motif (see Figure 3.76) in which neighbouring trimers are significantly “diagonally” slipped (see Figure 3.77).

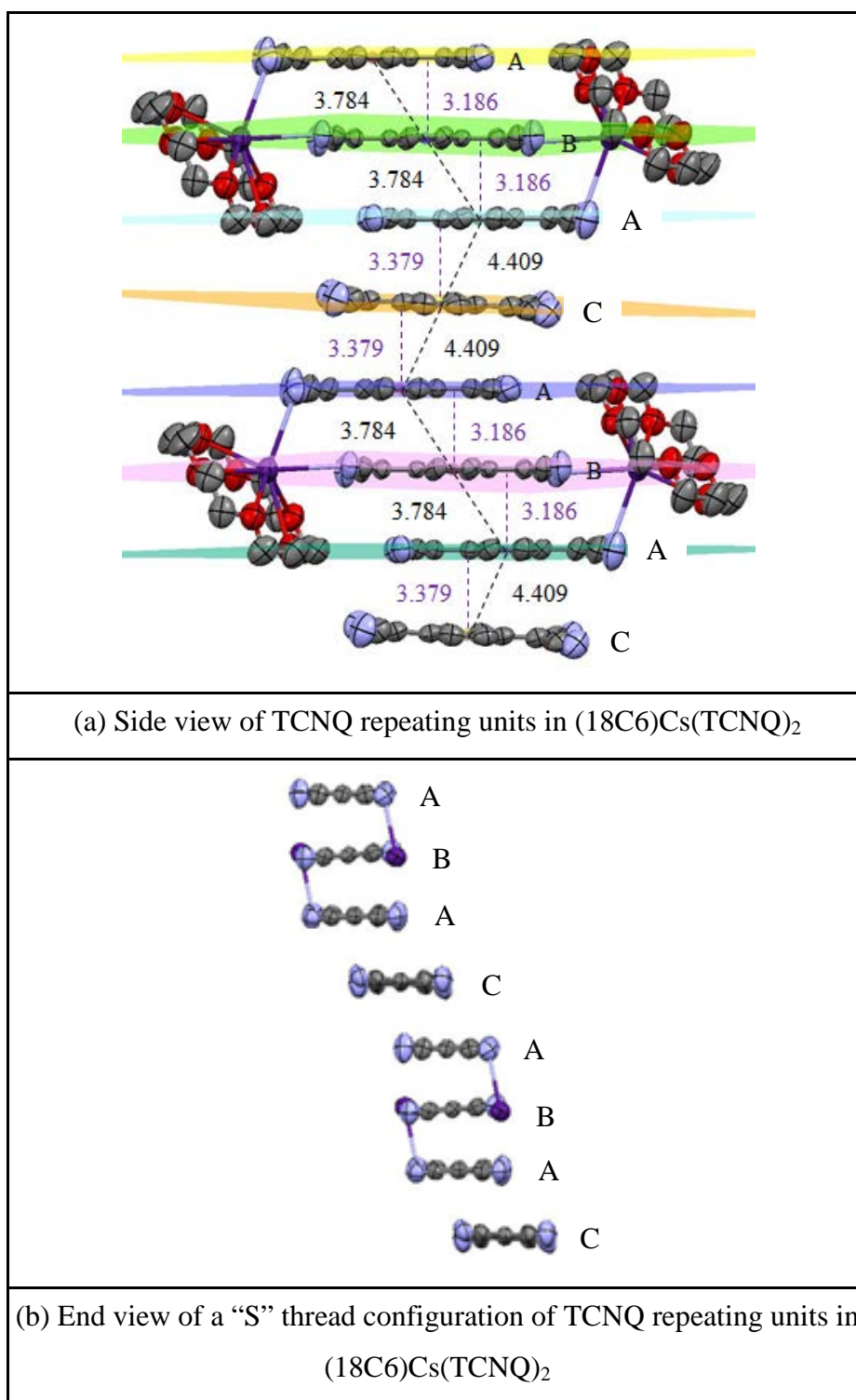


Figure 3.76 Assembly of the TCNQ repeating units in $(18C6)Cs(TCNQ)_2$ (hydrogen atoms are excluded)

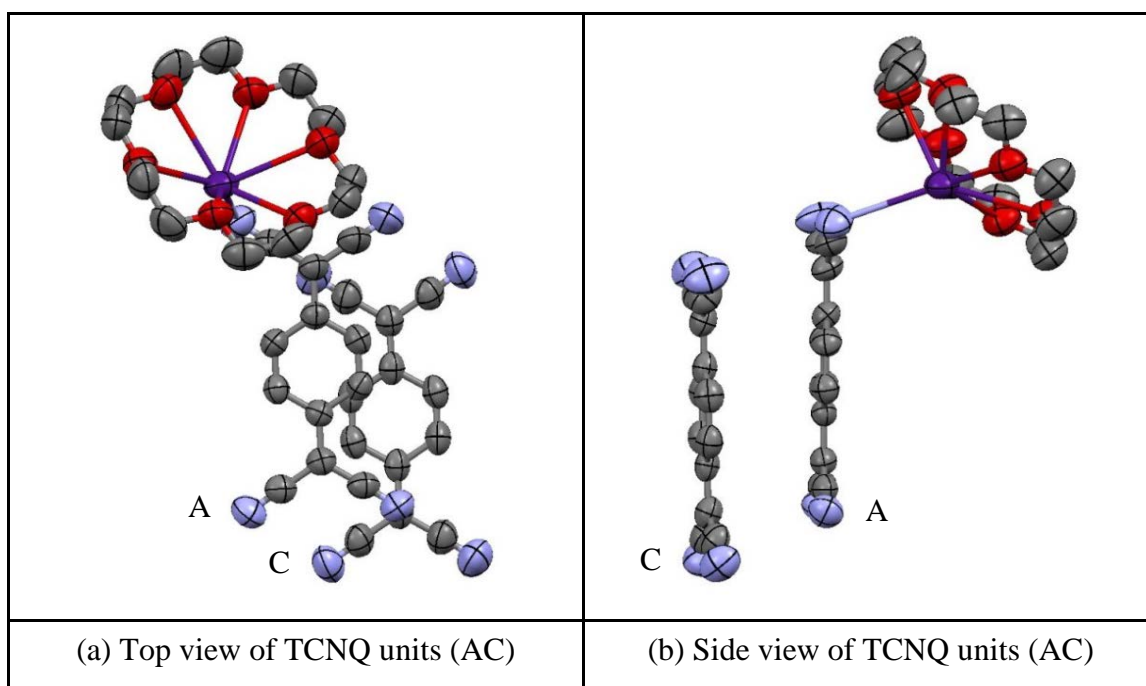


Figure 3.77 Top (a) and side (b) views of TCNQ units (AC) in $(18C6)Cs(TCNQ)_2$ (hydrogen atoms are excluded)

Distances and angles within the TCNQ stacks are listed in Table 3.28.

| TCNQ units | | TCNQ trimer | AC |
|--|--------------|-------------|-------|
| π - π perpendicular distance (Å) | | 3.19 | 3.38 |
| Short-axis slip | Distance (Å) | 0.17 | 2.27 |
| | Angle (°) | 3.05 | 33.89 |
| Long-axis slip | Distance (Å) | 2.03 | 1.70 |
| | Angle (°) | 32.50 | 26.71 |
| Centroid-centroid distance (Å) | | 3.78 | 4.41 |

Table 3.28 Distances (Å) and angles (°) within the TCNQ stacks of $(18C6)Cs(TCNQ)_2$

Within the TCNQ trimer, the individual TCNQ units adopt a shallow boat conformation in which neighbouring $-C(CN)_2$ units are twisted away from each other and the tilt angle between each TCNQ plane is 1.58° . Within the TCNQ trimer neighbours, the tilt angle between adjacent TCNQ planes is 3.89° .

From these data, it will be evident that π -facial overlap between TCNQ units (AC) within a TCNQ column is not ideal for extended π - π delocalisation within the TCNQ column.

Each Cs^+ cation is coordinated by one crown ether unit and two nitrile groups on adjacent TCNQ units and the resulting complex lies in channels between the wave-like TCNQ columns. Figure 3.78 summarises the various contact distances within the cation complex.

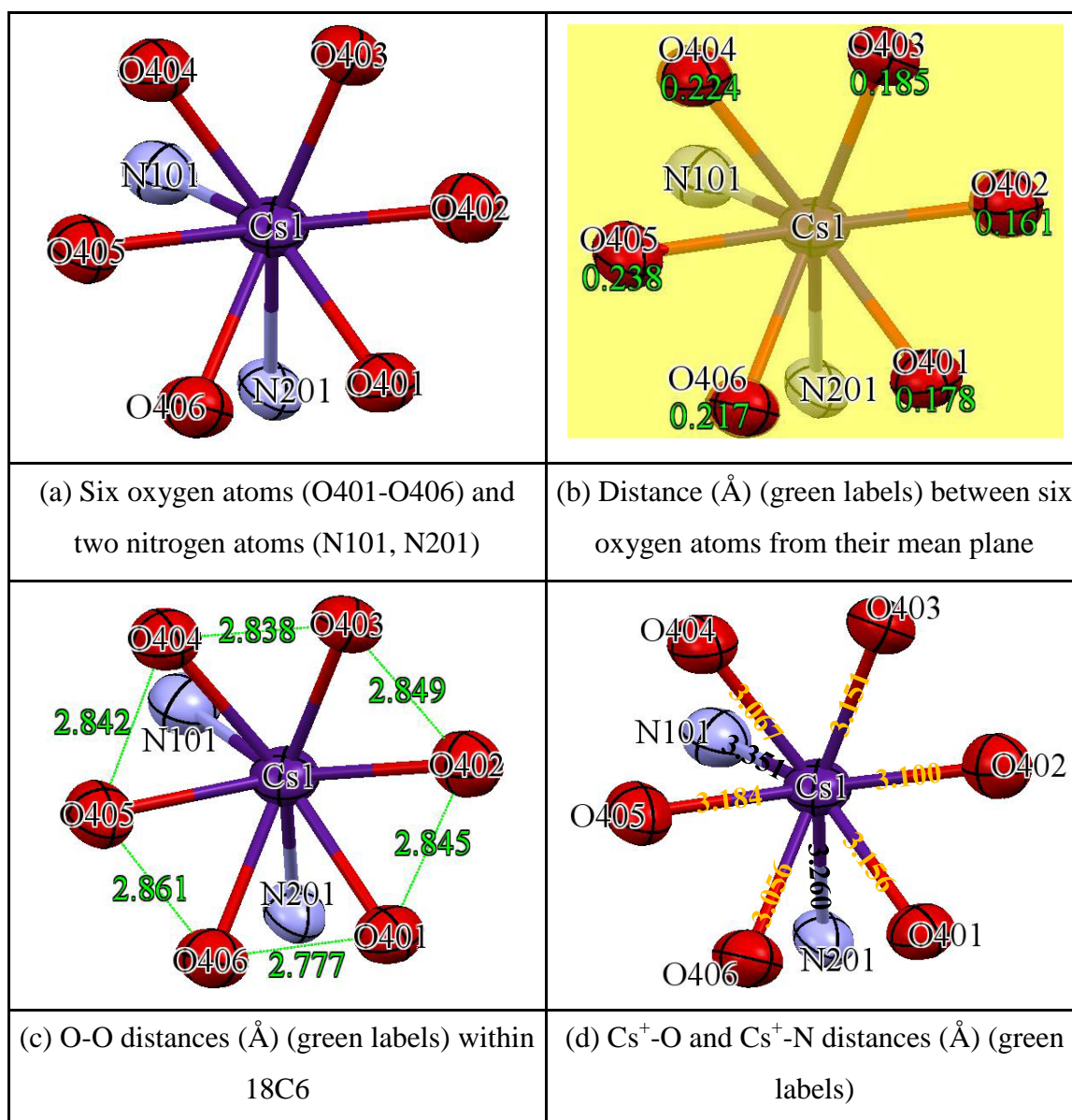


Figure 3.78 The various contact distances (Å) within the cation complex of $(18\text{C}6)\text{Cs}(\text{TCNQ})_2$ (carbon and hydrogen atoms are excluded)

As viewed in Figure 3.78, the ligating oxygen atoms sit above and below their mean plane to form irregular hexagon geometry of mean side by ca. 2.835 Å. The $\text{Cs}^+\text{-O}$ distances in $(18\text{C6})\text{Cs}(\text{TCNQ})_2$ are not all equal but seem to fall into two groups: (i) 3.056, 3.067 Å; (ii) 3.100, 3.151, 3.156 and 3.184 Å respectively. All of the $\text{Cs}^+\text{-O}$ bonds are slightly short than the sum of the van der Waals' radii ($\text{Cs}^+\text{-O} = 3.42 \text{ Å}$)^{270,271} and thus it seems justifiable to regard the metal cation and the oxygen atoms as being in contact. Consequently, the different $\text{Cs}^+\text{-O}$ distances demonstrate that the Cs^+ cation is distorted above the cavity of 18C6. The distances of Cs-N are 3.260 and 3.351 Å, which are slightly shorter than the sum of the van der Waals' radii ($\text{Cs}^+\text{-N} = 3.45 \text{ Å}$)^{270,271} and thus it seems justifiable to regard the metal cation and the nitrogen atom as being in contact.

3.3.4 Preparation of $(\text{B15C5})\text{M}(\text{TCNQ})_n$ ($\text{M} = \text{Li}, \text{Cs}$)

In this section, the solid-state behaviour of the complexes of $(\text{B15C5})\text{LiTCNQ}\cdot\text{H}_2\text{O}$ and $(\text{B15C5})_2\text{Cs}(\text{TCNQ})_3$ will be discussed.

(a) $(\text{B15C5})\text{LiTCNQ}\cdot\text{H}_2\text{O}$

Reaction of B15C5 (Benzo-15-crown-5) with LiTCNQ and TCNQ^0 (ratio 1:1:1) in dry acetonitrile afforded a reasonable yield (30%) of a plate of dark blue crystalline solid which contained single crystals suitable for X-ray structural study (combustion data is awaited). Full details including an account of the structure solution and refinement are reported in the Experimental Section and the Supporting Information (in the Appendices) respectively. The crystals obtained were of $(\text{B15C5})\text{LiTCNQ}\cdot\text{H}_2\text{O}$ and the core unit is shown in Figure 3.79.

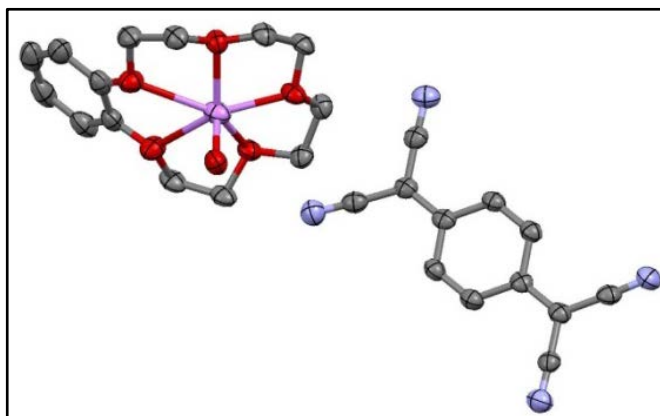


Figure 3.79 Core unit of $(\text{B15C5})\text{LiTCNQ}\cdot\text{H}_2\text{O}$ (hydrogen atoms are excluded)

Bond lengths within the $\text{TCNQ}^{\bullet-}$ unit are summarised in Table 3.29.

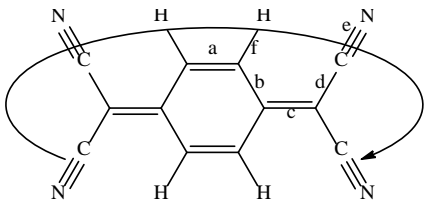
|  | | | | | | |
|---|------------------|-----------|-----------|-----------|-----------|-------|
| (a) Definition of the bond lengths within the $\text{TCNQ}^{\bullet-}$ molecule | | | | | | |
| Structure | Bond lengths (Å) | | | | | |
| | a | b | c | d | e | f |
| $\text{TCNQ}^{\bullet-}$ unit | | 1.426 (2) | | 1.430 (2) | 1.151 (2) | 0.950 |
| | 1.365 (3) | 1.427 (2) | 1.412 (3) | 1.423 (3) | 1.159 (2) | 0.950 |
| | 1.364 (3) | 1.429 (2) | 1.418 (3) | 1.419 (2) | 1.156 (2) | 0.950 |
| | | 1.419 (2) | | 1.432 (2) | 1.150 (2) | 0.950 |

Table 3.29 Summary of bond distances (Å) found for $\text{TCNQ}^{\bullet-}$ in $(\text{B15C5})\text{LiTCNQ}\cdot\text{H}_2\text{O}$

In this structure, the Li^+ ion is coordinated by one crown ether unit and one H_2O molecule. The $\text{TCNQ}^{\bullet-}$ units form a dimer which is significantly short-axis slipped (see Figure 3.80), which is typical of non-coordinated dimers e.g. in $(15\text{C5})_2\text{KTCNQ}^{107}$. In $(15\text{C5})_2\text{KTCNQ}$, the crown ether units inhibit the cation-anion interactions and form a structure in which the $\text{TCNQ}^{\bullet-}$ dimers are separated both from the metal ions and other $\text{TCNQ}^{\bullet-}$ dimers respectively¹⁰⁷.

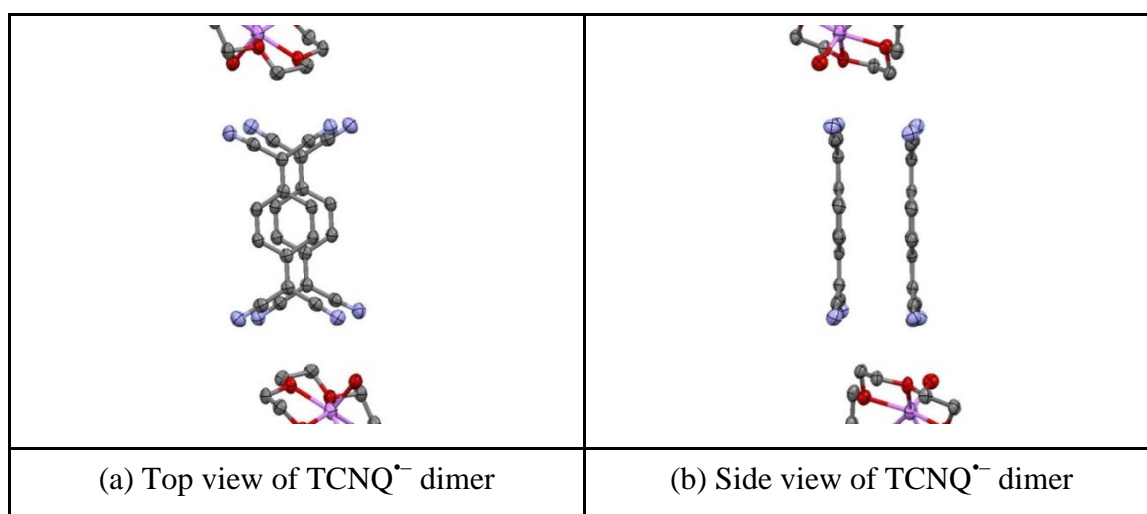


Figure 3.80 Top (a) and side (b) views of $\text{TCNQ}^{\bullet-}$ dimer in $(\text{B15C5})\text{LiTCNQ}\cdot\text{H}_2\text{O}$
(hydrogen atoms are excluded)

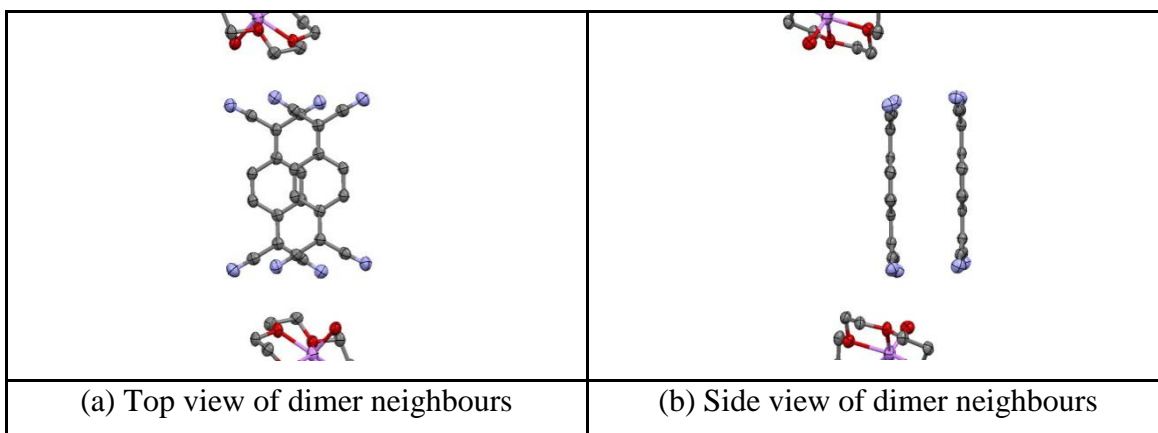


Figure 3.81 Top (a) and side (b) views of dimer neighbours in (B15C5)LiTCNQ·H₂O (hydrogen atoms are excluded)

The data in Table 3.29 suggest that the TCNQ^{•-} unit has some quinonoidal character because bond length “a” is less than “b”. The distribution of bond lengths is typical for these reported for TCNQ^{•-} ²¹³. Within the crystal, the TCNQ^{•-} dimers assemble into infinite columns in which dimer neighbours are significantly short-axis slipped (see Figure 3.81). The centroid-to-centroid distance between adjacent benzene rings of TCNQ units is 3.316 Å and the π - π distance is 3.195 Å respectively.

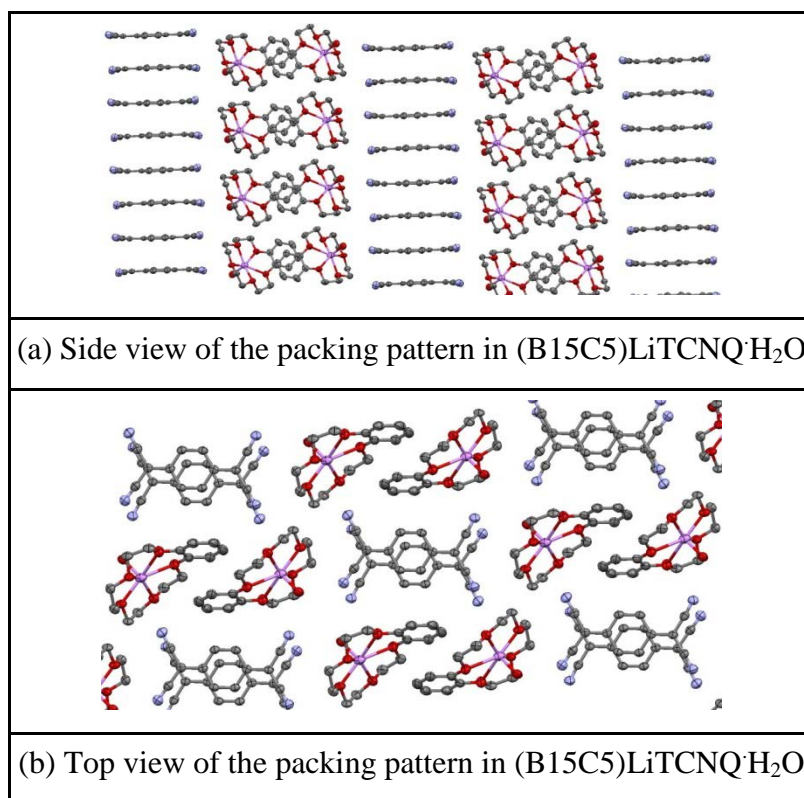


Figure 3.82 Side (a) and top (b) views of the packing pattern in (B15C5)LiTCNQ·H₂O (hydrogen atoms are excluded)

Distance and angles within the TCNQ^{•-} stacks are summarised in Table 3.30.

| TCNQ ^{•-} unit | | TCNQ ^{•-} dimer | Dimer neighbours |
|--|--------------|--------------------------|------------------|
| π - π perpendicular distance (Å) | | 3.20 | 3.61 |
| Short-axis slip | Distance (Å) | 0.88 | 2.05 |
| | Angle (°) | 15.42 | 29.54 |
| Long-axis slip | Distance (Å) | 0.11 | 0.15 |
| | Angle (°) | 1.95 | 2.41 |
| Centroid-centroid distance (Å) | | 3.32 | 4.15 |

Table 3.30 Distances (Å) and angles (°) within the TCNQ^{•-} stacks in (B15C5)LiTCNQ·H₂O

Within TCNQ^{•-} dimer, the individual TCNQ^{•-} unit adopts a shallow boat conformation in which the -C(CN)₂ parts on each end of TCNQ^{•-} unit is tilted in respect to benzene ring. Consequently, in TCNQ^{•-} dimer, the benzene ring on each TCNQ^{•-} unit is parallel in respect to adjacent TCNQ^{•-} unit in which neighbouring -C(CN)₂ units are twisted away from each other with the tilt angle by *ca.* 10.88°. Figure 3.83 shows the TCNQ^{•-} dimer geometries in (B15C5)LiTCNQ·H₂O.

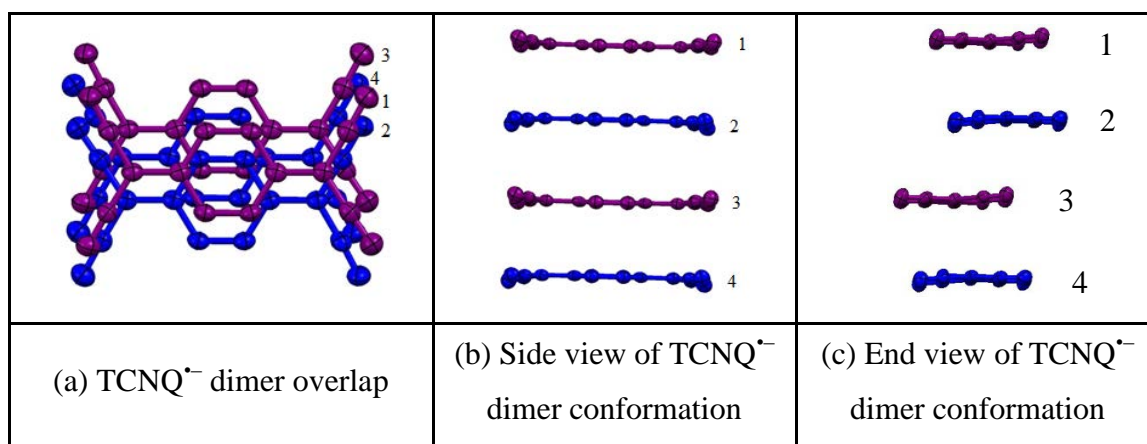


Figure 3.83 TCNQ^{•-} dimers geometries in (B15C5)LiTCNQ·H₂O (hydrogen atoms are excluded)

From these data it will be evident that π -facial overlap between dimer neighbours within a column is not ideal for extended π - π delocalisation within the column. Each Li⁺ cation is coordinated by one crown ether unit and one H₂O molecule and the resulting complex lies in channels between the TCNQ^{•-} columns. There is no direct coordination between

the $\text{TCNQ}^{\cdot-}$ units and the Li^+ ions but a $\text{CN}\cdots\text{H}$ hydrogen bond is formed between H_2O molecule and adjacent nitrile groups on the $\text{TCNQ}^{\cdot-}$ units (see Figure 3.84).

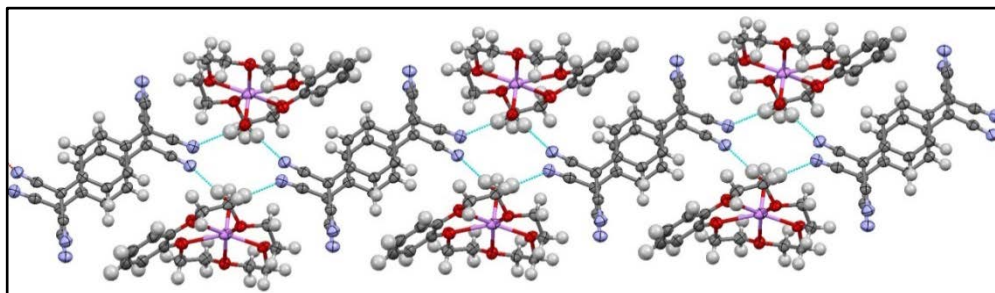


Figure 3.84 Hydrogen bonding coordination pattern to $\text{TCNQ}^{\cdot-}$ dimers

Figure 3.85 summarises the various contact distances within the cation complex.

| | |
|--|---|
| | |
| <p>(a) Five oxygen atoms (O201-O205) in crown ether unit</p> | <p>(b) Distance (Å) (green labels) between five oxygen atoms and their mean plane</p> |
| | |
| <p>(c) O-O distances (Å) (green labels). O301 represent the oxygen atom from H_2O</p> | <p>(d) Li-O distances (Å) (green labels)</p> |

Figure 3.85 The various contact distances (Å) within the cation complex (carbon, except for benzene ring, and hydrogen atoms are excluded)

As viewed in Figure 3.85, the ligating oxygen atoms are sitting above and below their mean plane to form an irregular pentagonal geometry of mean side by *ca.* 2.614 Å. All of the five oxygen atoms on crown ether ring show different distances to the centre of Li^+ cation. The Li^+ cation is placed above the cavity of the crown ether ring and is located above the mean plane of the oxygen atoms by *ca.* 0.427 Å.

(b) $(\text{B15C5})_2\text{Cs}(\text{TCNQ})_3$

Reaction of B15C5 with $\text{Cs}_2(\text{TCNQ})_3$ and TCNQ^0 (ratio 4:1:2) in dry acetonitrile afforded a plate of dark blue crystalline solid which contained single crystals suitable for X-ray structural study (combustion data is awaited). Full details including an account of the structure solution and refinement are reported in the Experimental Section and the Supporting Information (in the Appendices) respectively. The crystals obtained were of $(\text{B15C5})_2\text{Cs}(\text{TCNQ})_3$ and the core unit is shown in Figure 3.86, in which Cs^+ ion and TCNQ (B) are in symmetry elements.

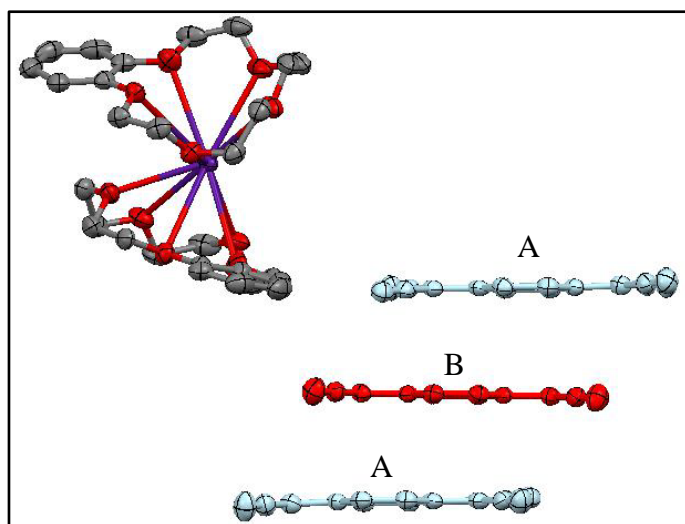


Figure 3.86 Core unit of $(\text{B15C5})_2\text{Cs}(\text{TCNQ})_3$ (hydrogen atoms are excluded)

Bond lengths within the TCNQ units are summarised in Table 3.31. In this structure each Cs^+ ion is coordinated by two crown ether units. The TCNQ units form a trimer which is significantly long axis slipped (see Figure 3.87). In TCNQ trimer, all of the TCNQ units have some quinonoidal character because bond length “a” is less than “b”. After measuring the c bond lengths in each TCNQ unit, it seems reasonable to regard TCNQ unit (A) as having less electron density than B, and suggests that the A units have more TCNQ^0 character and the red TCNQ unit (B) has more TCNQ^- character. Within each repeating units of TCNQ trimer, TCNQ units form mixed stacks, TCNQ^0 -

$\text{TCNQ}^{\bullet-}$ - TCNQ^0 , which means that one electron is delocalised over the three TCNQ units.

Within the crystal, the TCNQ trimers assemble into infinite columns in which the individual TCNQ units are assembled in an ABA motif (see Figure 3.88) in which dimer neighbours are significantly “diagonally” slipped (see Figure 3.89).

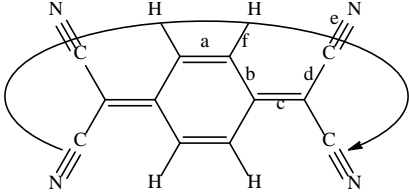
|  | | | | | | |
|--|------------------|-----------|-----------|-----------|-----------|-------|
| (a) Definition of the bond lengths within the TCNQ molecule | | | | | | |
| Structure | Bond lengths (Å) | | | | | |
| | a | b | c | d | e | f |
| TCNQ unit (A) | | 1.442 (4) | | 1.435 (4) | 1.152 (3) | 0.950 |
| | 1.346 (4) | 1.450 (3) | 1.382 (4) | 1.441 (4) | 1.146 (4) | 0.951 |
| | 1.349 (4) | 1.448 (4) | 1.389 (4) | 1.442 (4) | 1.144 (4) | 0.950 |
| | | 1.450 (3) | | 1.432 (4) | 1.146 (4) | 0.950 |
| TCNQ unit (B) | | 1.434 (4) | | 1.431 (3) | 1.151 (3) | 0.949 |
| | 1.361 (4) | 1.436 (3) | 1.402 (4) | 1.432 (4) | 1.147 (4) | 0.950 |
| | 1.361 (4) | 1.434 (4) | 1.402 (4) | 1.431 (3) | 1.151 (3) | 0.949 |
| | | 1.436 (3) | | 1.432 (4) | 1.147 (4) | 0.950 |

Table 3.31 Summary of bond distances (Å) scrutinise for TCNQ units in the cation complex

As viewed in Figure 3.88, it can be seen that $\text{Cs}_2(\text{TCNQ})_3$, TCNQ^0 and B15C5 can form alternating stacks as viewed in packing diagram. The TCNQ units are assembled into infinite π - π stacks. A side view of TCNQ units reveals a wave-like pattern. The cation complex of $(\text{B15C5})_2\text{Cs}^+$ sits in channels between the TCNQ columns. Examining of the packing diagrams in Figure 3.88(b), it reveals that the TCNQ columns pack in a herringbone array. Consequently, neighbouring TCNQ trimers are significantly “diagonally” slipped as viewed in Figure 3.89. Distances and angles within the TCNQ stacks are summarised in Table 3.32.

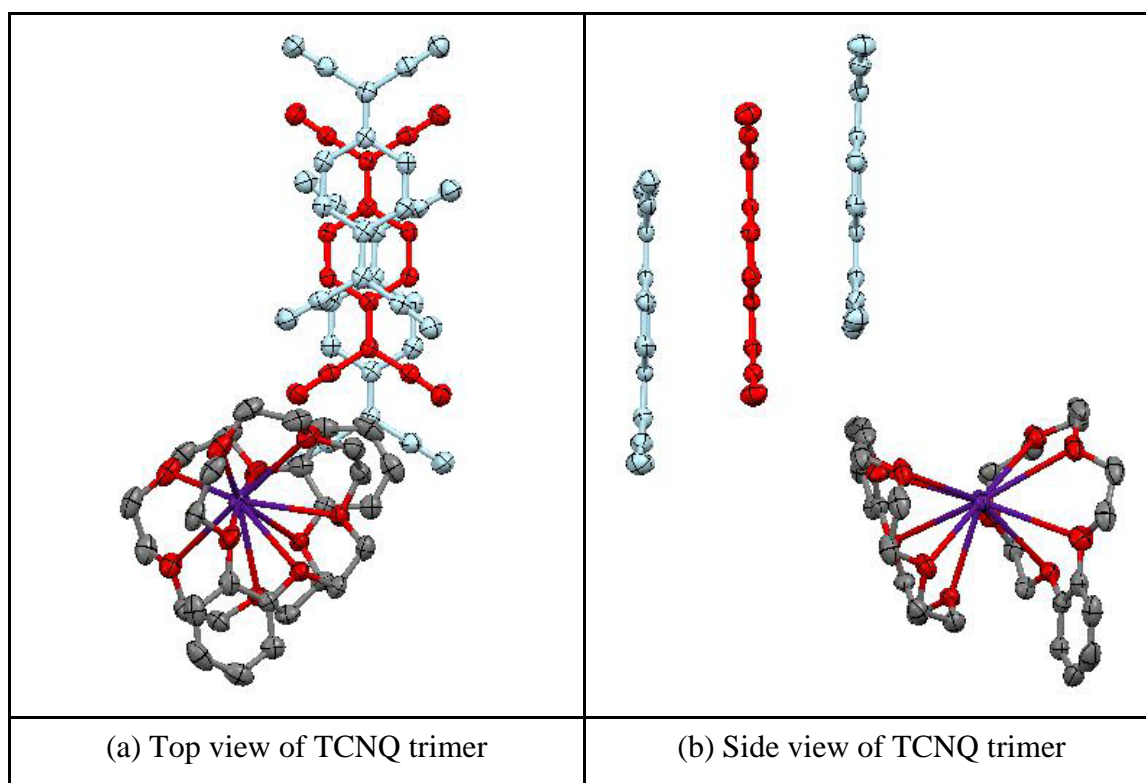


Figure 3.87 Top (a) and side (b) views of TCNQ trimer in $(B15C5)_2Cs(TCNQ)_3$
(hydrogen atoms are excluded)

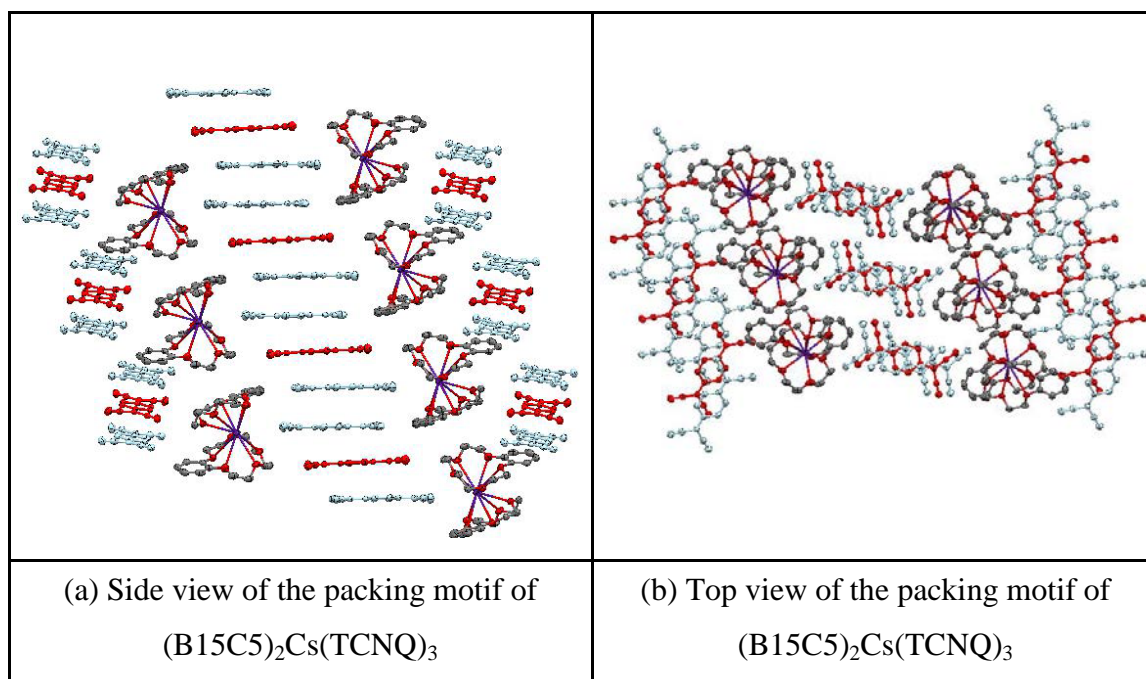


Figure 3.88 Side (a) and top (b) views of the packing motif of $(B15C5)_2Cs(TCNQ)_3$
(hydrogen atoms are excluded)

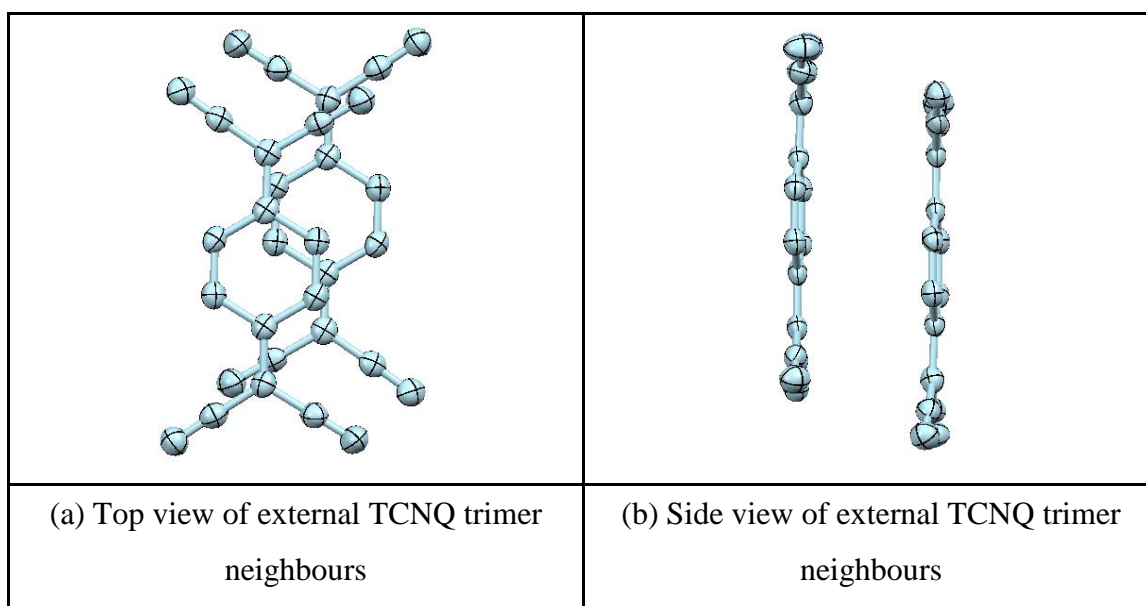


Figure 3.89 Top (a) and side (b) views of external TCNQ trimer neighbours in $(\text{B15C5})_2\text{Cs}(\text{TCNQ})_3$ (hydrogen atoms are excluded)

| TCNQ units | | TCNQ trimer | TCNQ trimer neighbours |
|--|--------------|-------------|------------------------|
| π - π perpendicular distance (Å) | | 3.17 | 3.50 |
| Short-axis slip | Distance (Å) | 0.071 | 1.26 |
| | Angle (°) | 1.28 | 19.82 |
| Long-axis slip | Distance (Å) | 2.14 | 1.29 |
| | Angle (°) | 33.99 | 20.24 |
| Centroid-centroid distance (Å) | | 3.82 | 3.93 |

Table 3.32 Distances (Å) and angles (°) within the TCNQ stacks of $(\text{B15C5})_2\text{Cs}(\text{TCNQ})_3$

Within the TCNQ trimer, adjacent TCNQ units are tilted in respect to each other by *ca.* 1.25° [Figure 3.87(b)]. TCNQ unit (A) adopts a shallow boat conformation in which neighbouring $-\text{C}(\text{CN})_2$ units are twisted away from each other and TCNQ unit (B) is flat configuration. From these data, it will be evident that π -facial overlap between trimer neighbours within a column is not ideal for extended π - π delocalisation within the column.

Each Cs^+ cation is sandwiched between two crown ether molecules and the resulting complex lies in channels between the TCNQ columns. There is no direct co-ordination

between the TCNQ units and the Cs^+ ions. Within the cation complex, the planes of the two crown ether units (as defined by each set of oxygen atoms) are tilted in respect to each other (by *ca.* 30.19°) as viewed in Figure 3.90. Figure 3.91 summarises the various contact distances within the cation complex.

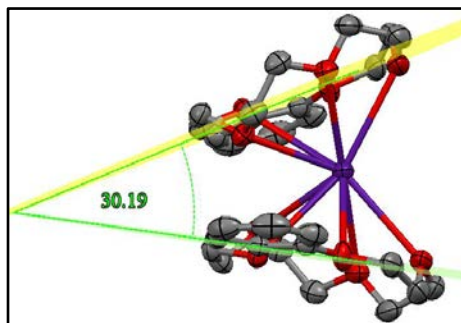


Figure 3.90 Tilt angle between two crown ether mean plane (defined by a set of oxygen atoms) (hydrogen atoms are excluded)

| | |
|---|---|
| | |
| (a) Oxygen atoms (O301-O305) and their mean plane | (b) Distance (Å) (green labels) between oxygen atoms and their mean plane |
| | |
| (c) O-O distances (Å) (green labels) in B15C5 | (d) Cs^+ -O distances (Å) (green labels) in B15C5 |

Figure 3.91 The various contact distances (Å) within the cation complex (carbon, except for benzene ring, and hydrogen atoms are excluded)

As the Cs^+ ion sits at the screw axis, two crown ether rings are exactly symmetric in respect to each other. As viewed in Figure 3.91, except for O303, other four oxygen atoms of each B15C5 unit are sited on their mean plane. The ligating oxygen atoms are sitting above and below their mean plane to form an irregular pentagonal geometry with mean side by *ca.* 2.766 Å. The different Cs^+ -O distances demonstrate that the Cs^+ cation is distorted above the cavity of crown ether unit.

3.3.5 Preparation of $(\text{B18C6})\text{K}(\text{TCNQ})_2$

Reaction of B18C6 (Benzo-18-crown-6) with KTCNQ and TCNQ^0 (ratio 1:1:1) in dry acetonitrile afforded a reasonable yield (57%) of a needle of dark blue crystalline solid (Combustion Analysis: Calculated: C: 63.40%, H: 3.99%, N: 14.78%. Found: C: 62.88%, H: 3.70%, N: 15.02%.) which contained single crystals suitable for X-ray structural study. Full details including an account of the structure solution and refinement are reported in the Experimental Section and the Supporting Information (in the Appendices) respectively. The crystals obtained were of $(\text{B18C6})\text{K}(\text{TCNQ})_2$ and the basic unit is shown in Figure 3.92.

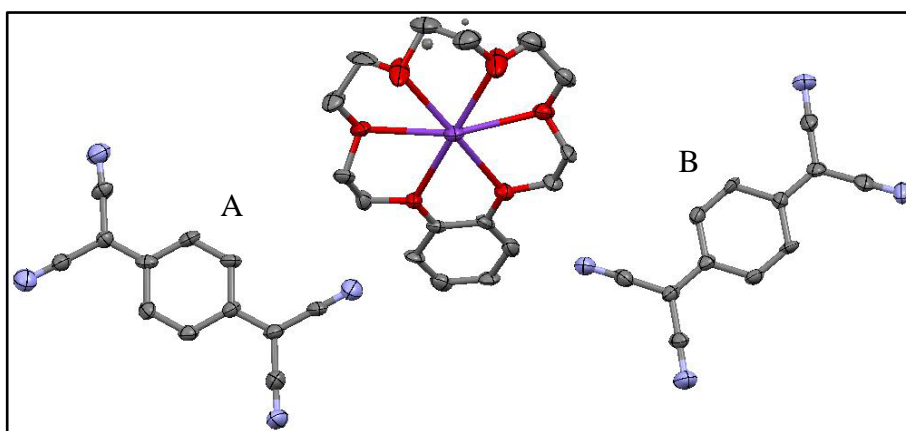


Figure 3.92 Basic unit of $(\text{B18C6})\text{K}(\text{TCNQ})_2$ (hydrogen atoms are excluded)

Bond lengths within the TCNQ units are summarised in Table 3.33. In this structure, the K^+ ion is coordinated by one crown ether unit. The TCNQ units form a dimer which is significantly long-axis slipped (see Figure 3.93). The similarity of the bond lengths within the two TCNQ units makes it difficult to distinguish between the $\text{TCNQ}^{\cdot-}$ and TCNQ^0 components.

The data in Table 3.33 suggest that both TCNQ units have some quinonoidal character because bond length “a” is less than “b”. For both TCNQ components A and B, the distribution of bond lengths is intermediate between these reported for TCNQ⁰ and TCNQ^{•-} respectively²¹³.

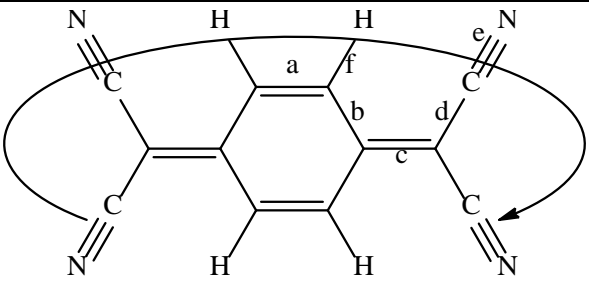
|  | | | | | | |
|--|------------------|-----------|-----------|-----------|-----------|-------|
| (a) Definition of the bond lengths within the TCNQ molecule | | | | | | |
| Structure | Bond lengths (Å) | | | | | |
| | a | b | c | d | e | f |
| TCNQ unit (A) | | 1.443 (9) | | 1.427 (9) | 1.166 (9) | 0.949 |
| | 1.381 (9) | 1.408 (9) | 1.385 (8) | 1.440 (8) | 1.130 (9) | 0.950 |
| | 1.381 (8) | 1.435 (8) | 1.417 (9) | 1.410 (9) | 1.138 (9) | 0.949 |
| | | 1.421 (9) | | 1.437 (9) | 1.137 (9) | 0.950 |
| TCNQ unit (B) | | 1.447 (8) | | 1.413 (9) | 1.175 (9) | 0.950 |
| | 1.340 (9) | 1.433 (9) | 1.394 (9) | 1.436 (9) | 1.162 (9) | 0.951 |
| | 1.340 (9) | 1.462 (7) | 1.411 (8) | 1.417 (9) | 1.183 (9) | 0.950 |
| | | 1.429 (8) | | 1.430 (9) | 1.136 (9) | 0.949 |

Table 3.33 Summary of bond distances (Å) observed for TCNQ units in (B18C6)K(TCNQ)₂

In (B18C6)K(TCNQ)₂, pairs of TCNQ dimers assemble into infinite columns in which the individual TCNQ units are assembled in an ABB'A' motif (see Figure 3.94). As viewed in Figure 3.95, it can be seen that the K(TCNQ)₂ and B18C6 can form alternating stacks as viewed in packing diagram. The solvent molecule of MeCN has been removed after this cation complex is recrystallized from hot dry DCM. TCNQ units are assembled into infinite face-to-face π -stacks, for forming further columns. From the top view of the packing pattern of (B18C6)K(TCNQ)₂, adjacent TCNQ columns form into a herringbone packing pattern.

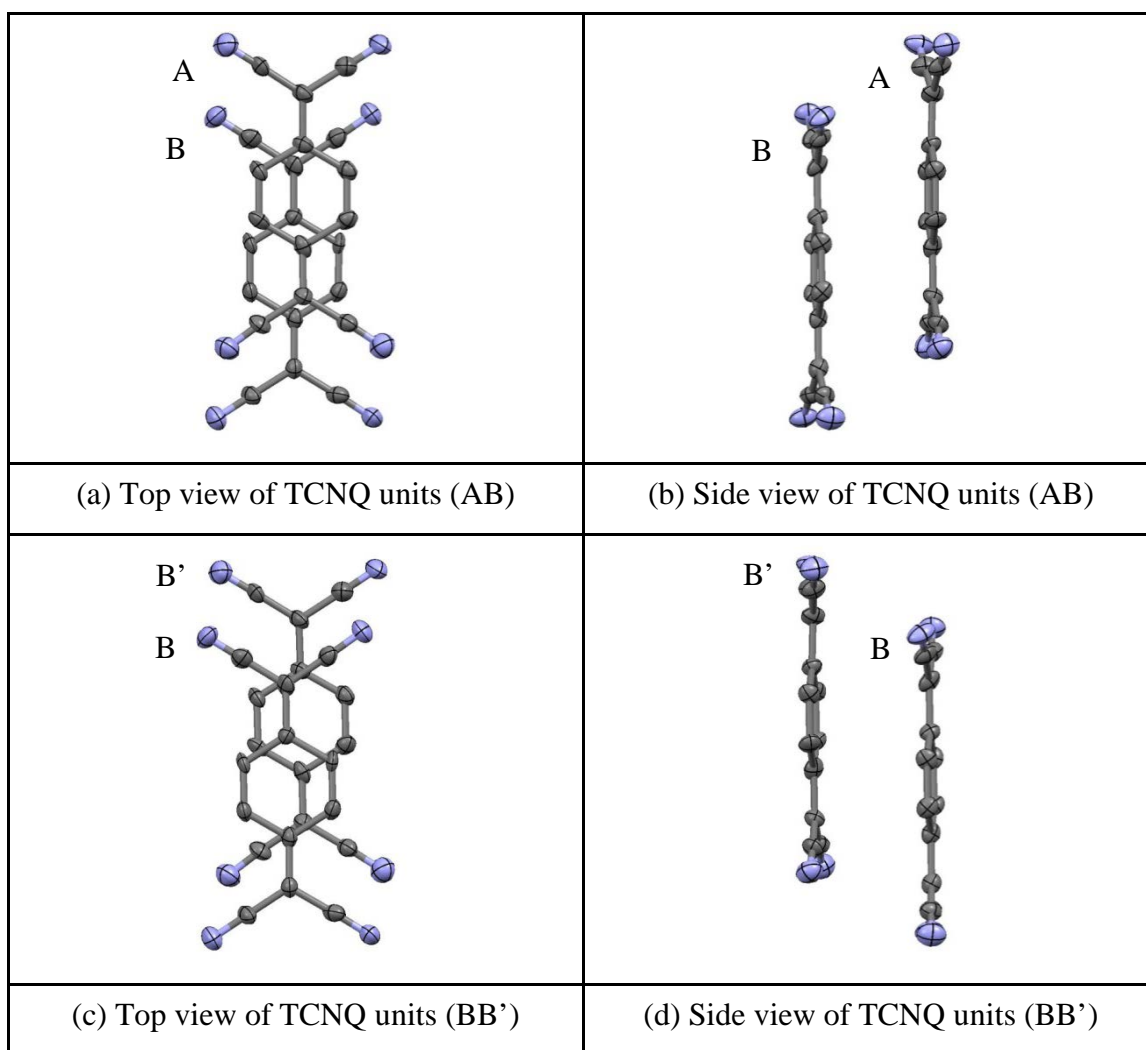


Figure 3.93 Top (a/c) and side (b/d) views of TCNQ units in $(\text{B18C6})\text{K}(\text{TCNQ})_2$ (hydrogen atoms are excluded)

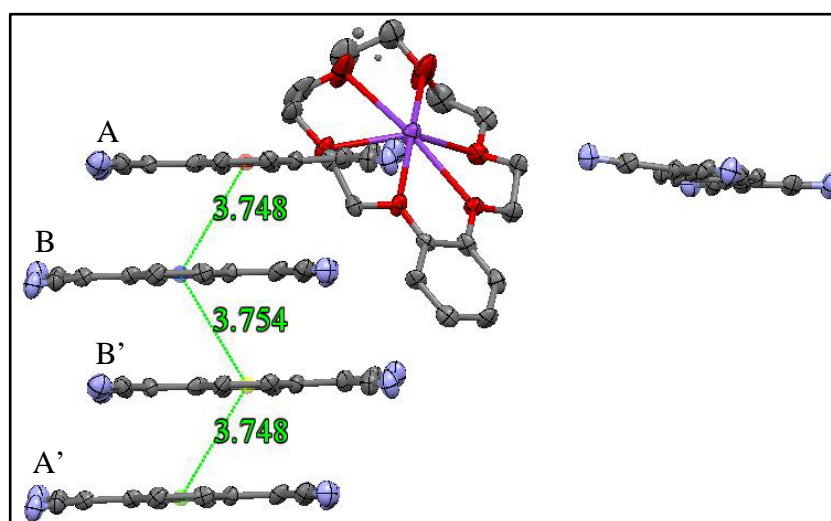


Figure 3.94 Observation of TCNQ repeating units in $(\text{B18C6})\text{K}(\text{TCNQ})_2$ (hydrogen atoms are excluded)

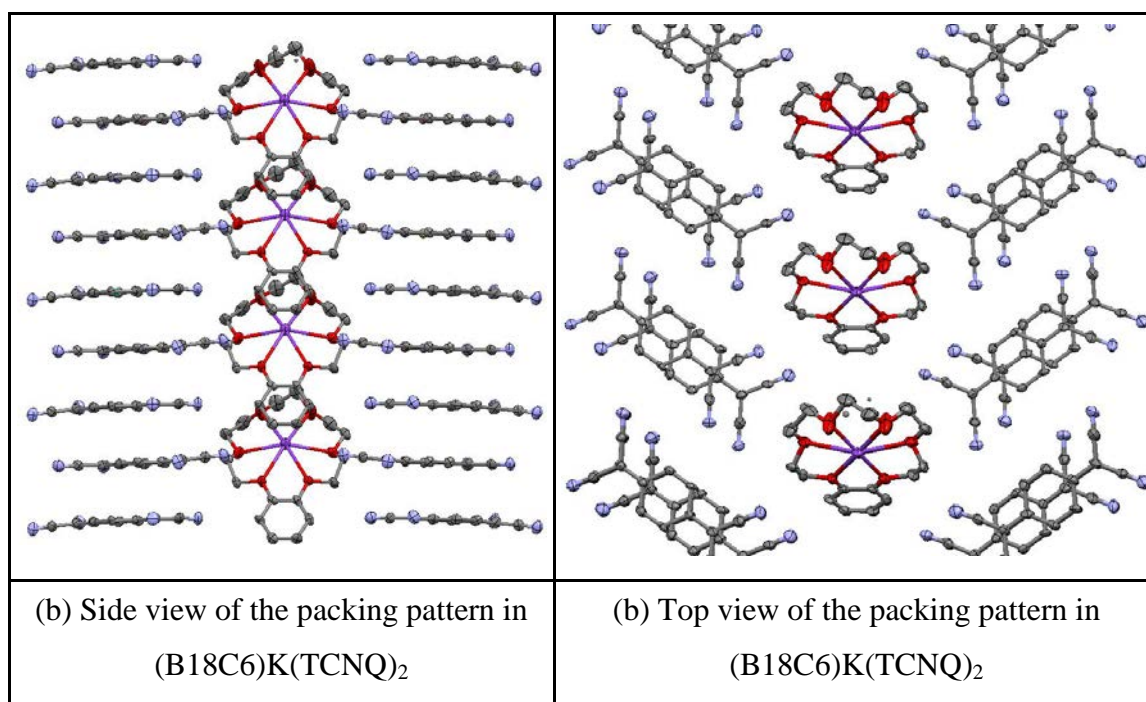


Figure 3.95 Side (a) and top (b) views of the packing pattern in $(\text{B18C6})\text{K}(\text{TCNQ})_2$, yellow area represents the repeating TCNQ dimer (hydrogen atoms are excluded)

Figure 3.96 shows the packing pattern of $(\text{B18C6})\text{K}^+$ cation complex, which forms one-dimensional infinite chain structure through $\text{K}^+-\pi$ interactions with adjacent units. The cation complex of $(\text{B18C6})\text{K}^+$ is off-set π -stacked geometry oriented in order to minimise the π - π repulsion between nearby benzene rings and maximises the π - σ attraction between the σ framework of the inner edge of the cavity of one B18C6 with the π electrons of the neighbouring benzene ring. Consequently, the K^+ ion sits above the π electron cloud of adjacent benzene ring. The cation complex of $(\text{B18C6})\text{K}^+$ is sited in the cavity between the TCNQ columns (Figure 3.95), and part of the crown ether ring is disordered, in which the atomic occupancy is 66% in respect to 34%. Each $(\text{B18C6})\text{K}^+$ cation complex is long-axis slipped by *ca.* 5.106 Å in respect to adjacent cation complex and the corresponding slip angle is 37.61°. Distances and angles within the TCNQ stacks are summarised in Table 3.34. In $(\text{B18C6})\text{K}(\text{TCNQ})_2$, the average distance of K^+ ion to carbon atoms on the phenyl ring of the B18C6 is 3.013 Å, which is significantly shorter than the corresponding distance of the two core complexes in Zhu et.al. study²⁷⁴ and indicates that there are stronger $\text{K}^+-\pi$ interactions in $(\text{B18C6})\text{K}(\text{TCNQ})_2$.

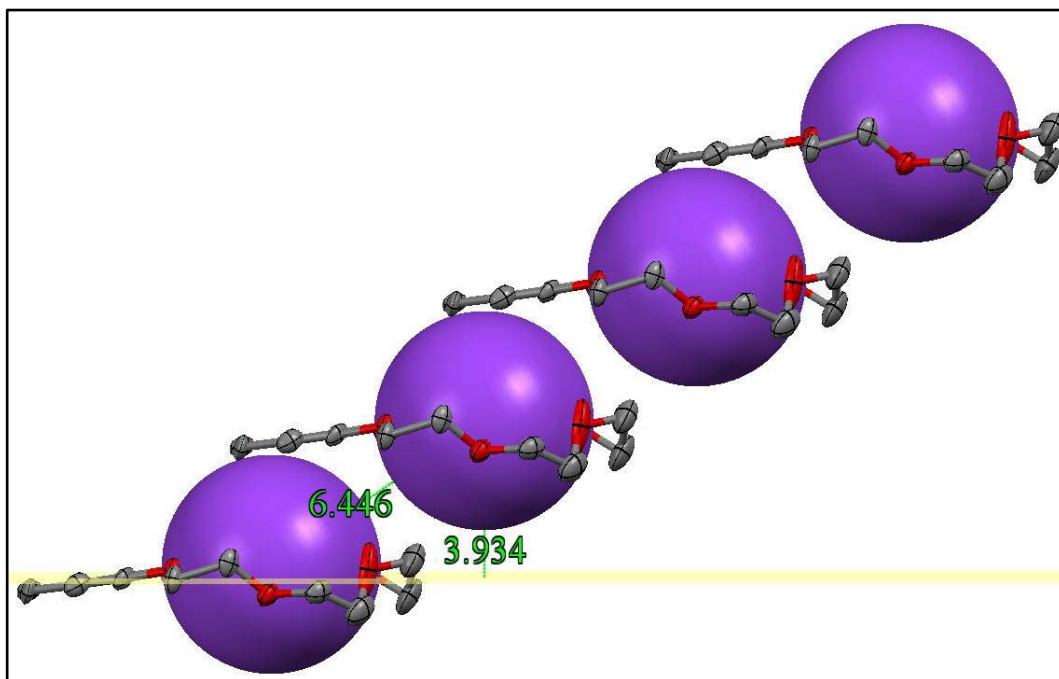


Figure 3.96 Packing pattern of (B18C6)K⁺ (hydrogen atoms are excluded)

| TCNQ units | | AB | BB' |
|--|--------------|-------|-------|
| π - π perpendicular distance (Å) | | 3.18 | 3.26 |
| Short-axis slip | Distance (Å) | 0.028 | 0.18 |
| | Angle (°) | 0.50 | 3.17 |
| Long-axis slip | Distance (Å) | 1.98 | 1.85 |
| | Angle (°) | 31.81 | 29.58 |
| Centroid-centroid distance (Å) | | 3.75 | 3.75 |

Table 3.34 Distances (Å) and angles (°) within the TCNQ stacks of (B18C6)K(TCNQ)₂

Within the TCNQ dimer, the individual TCNQ units adopt a shallow boat conformation in which neighbouring –C(CN)₂ units are twisted away from each other. In TCNQ dimer, the neighbouring TCNQ units are tilted in respect to each other by *ca.* 0.17°. Figure 3.97 summarises the various contact distances within the cation complex.

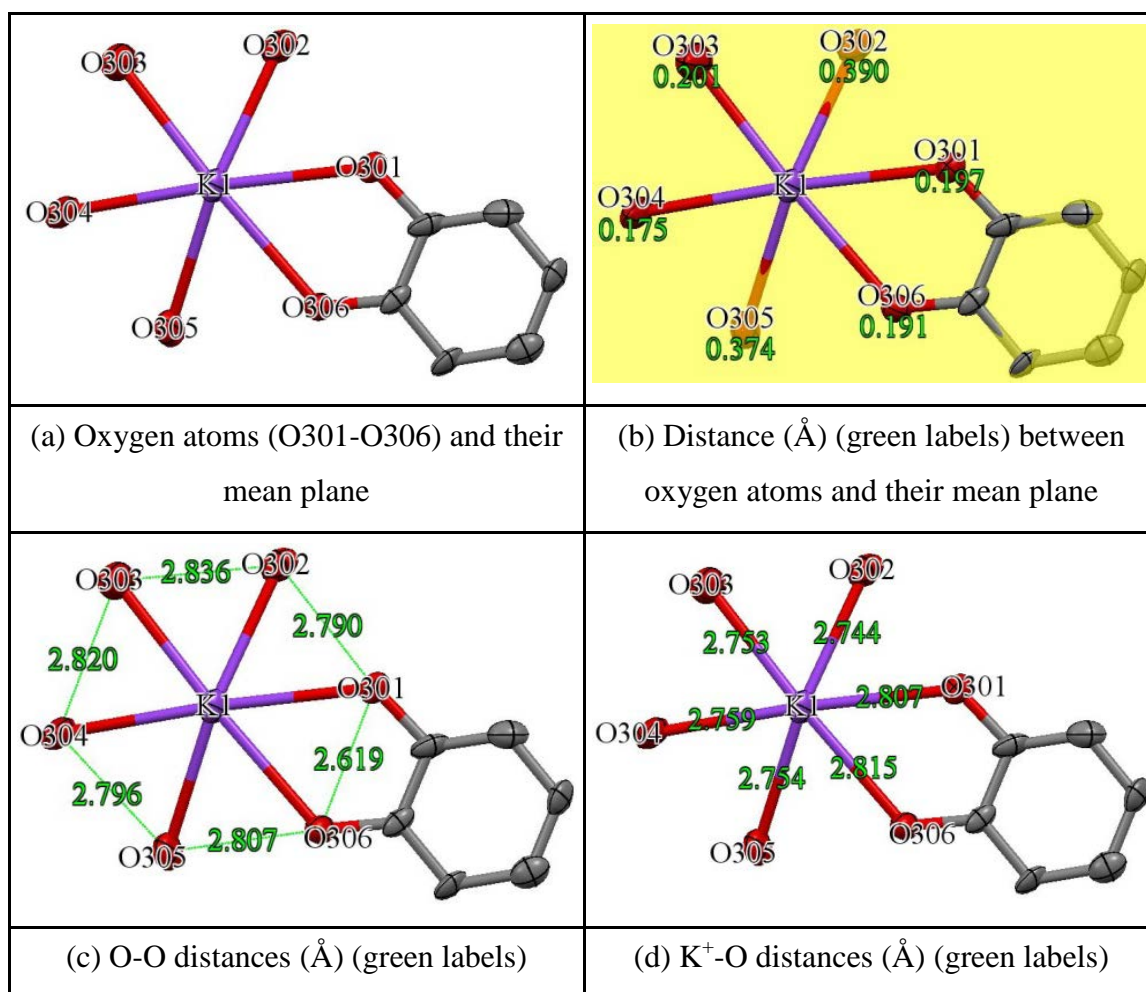


Figure 3.97 Various contact distances (Å) in (B18C6)K(TCNQ)₂ (carbon, except for benzene ring, and hydrogen atoms are excluded)

As viewed in Figure 3.97, the ligating oxygen atoms are sitting above and below their mean plane to form irregular hexagon with mean side by *ca.* 2.778 Å, which is less than those of van der Waals contact (K⁺-O = 2.85 Å)²⁷¹ and thus it seems justifiable to regard the metal cation and the oxygen atoms as being in contact. The different K⁺-O distances demonstrate that the K⁺ cation is distorted in the cavity of crown ether unit.

3.3.6 Preparation of (DB18C6)K(TCNQ)₂

Reaction of DB18C6 (Dibenzo-18-crown-6) with KTCNQ and TCNQ⁰ (ratio (1:1:1) in dry acetonitrile afforded a reasonable yield (70%) of a block of black crystalline solid (Combustion Analysis: Calculated: C: 65.42%, H: 3.99%, N: 13.86%. Found: C: 65.95%, H: 2.85%, N: 16.06%) which contained single crystals suitable for X-ray structural study (combustion data is awaited). Full details including an account of the

structure solution and refinement are reported in the Experimental Section and the Supporting Information (in the Appendices) respectively. The crystals obtained were of (DB18C6)K(TCNQ)₂ and the basic unit is shown in Figure 3.98.

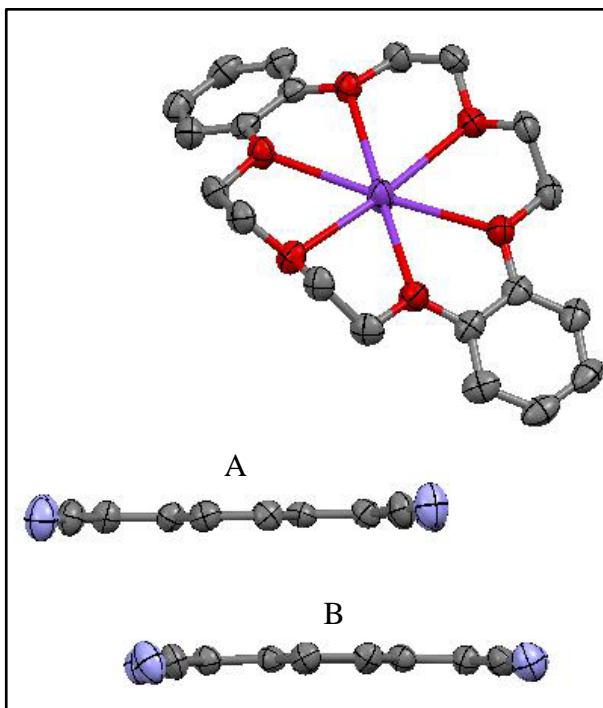


Figure 3.98 Basic unit of (DB18C6)K(TCNQ)₂ (hydrogen atoms are excluded)

Bond lengths within the TCNQ units are summarised in Table 3.35. In this structure, the K⁺ ion is coordinated by one crown ether unit. The TCNQ units form a dimer which is significantly long axis slipped (see Figure 3.99). The data in Table 3.35 suggest that both TCNQ units have some quinonoidal character because bond length “a” is less than “b”. After measuring the c bond lengths in each TCNQ unit, it seems that TCNQ unit (B) was less electron density, which suggests TCNQ⁰ character. Consequently, the TCNQ unit (A) has greater electron negative density, consistent with TCNQ^{•-} character. Within each repeating unit of the TCNQ dimer, TCNQ units form mixed stacks of TCNQ⁰-TCNQ^{•-} components (see Figure 3.100), which means one extra electron is delocalised over the two TCNQ units but more negative charge density appears to reside on the TCNQ unit (A) based on the corresponding c bond lengths as viewed in Table 3.35.

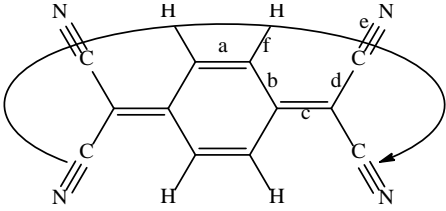
|  | | | | | | |
|---|------------------|-----------|-----------|-----------|-----------|-------|
| (a) Definition of the bond lengths within the TCNQ molecule | | | | | | |
| Structure | Bond lengths (Å) | | | | | |
| | a | b | c | d | e | f |
| TCNQ unit (A) | | 1.434 (4) | | 1.423 (5) | 1.160 (4) | 0.950 |
| | 1.354 (4) | 1.439 (4) | 1.403 (4) | 1.425 (4) | 1.154 (4) | 0.950 |
| | 1.350 (4) | 1.432 (4) | 1.396 (4) | 1.431 (5) | 1.144 (4) | 0.950 |
| | | 1.437 (4) | | 1.431 (4) | 1.149 (4) | 0.951 |
| TCNQ unit (B) | | 1.440 (4) | | 1.427 (5) | 1.151 (4) | 0.950 |
| | 1.357 (4) | 1.439 (4) | 1.389 (4) | 1.434 (4) | 1.151 (4) | 0.951 |
| | 1.350 (4) | 1.434 (4) | 1.390 (4) | 1.422 (5) | 1.154 (4) | 0.950 |
| | | 1.440 (4) | | 1.435 (4) | 1.146 (4) | 0.950 |

Table 3.35 Summary of bond distances (Å) observed for TCNQ units in (DB18C6)K(TCNQ)₂

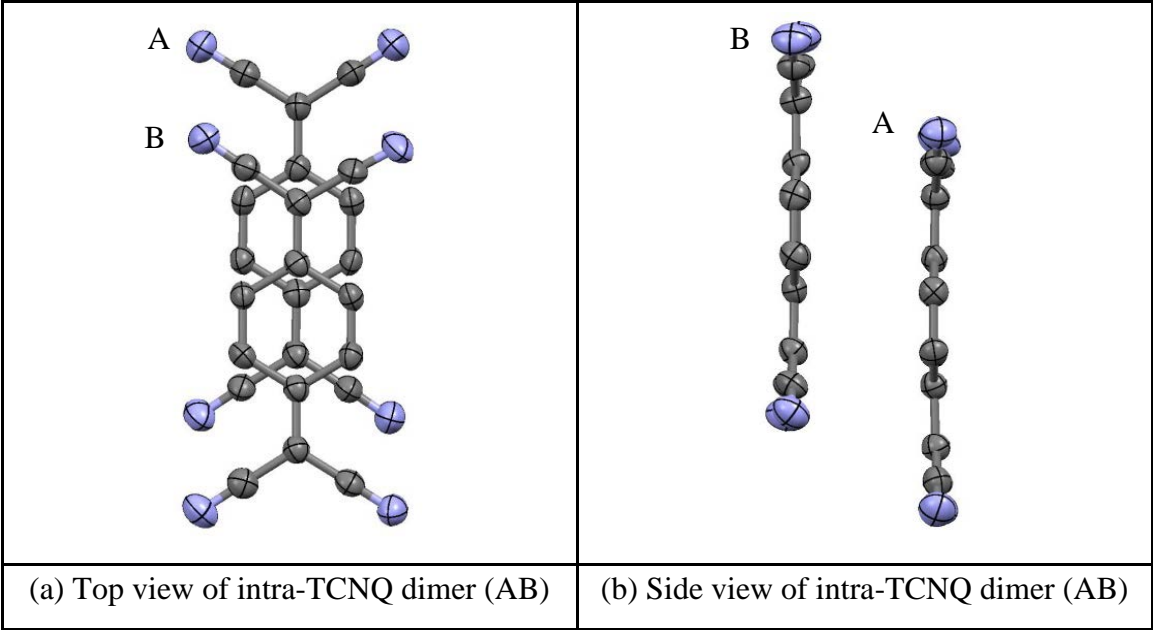


Figure 3.99 Top (a) and side (b) views of TCNQ dimer (AB) in (DB18C6)K(TCNQ)₂ (hydrogen atoms are excluded)

Within the crystal, the TCNQ dimers assemble into infinite columns in which the individual TCNQ units are assembled in an $ABB'A'$ motif (see Figure 3.100) in which dimer neighbours is significantly “diagonally” slipped (see Figure 3.101).

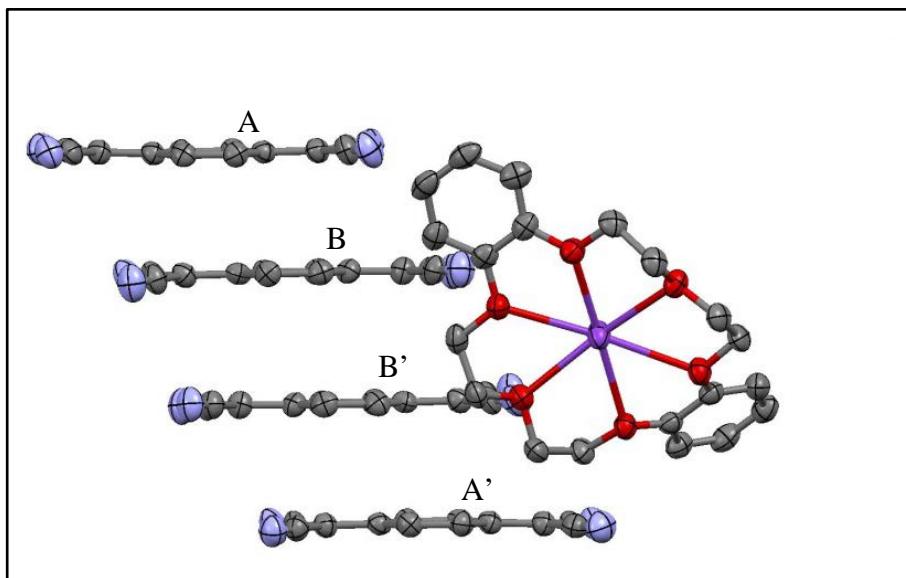


Figure 3.100 Observation of TCNQ repeating unit in $(\text{DB18C6})\text{K}(\text{TCNQ})_2$ (hydrogen atoms are excluded)

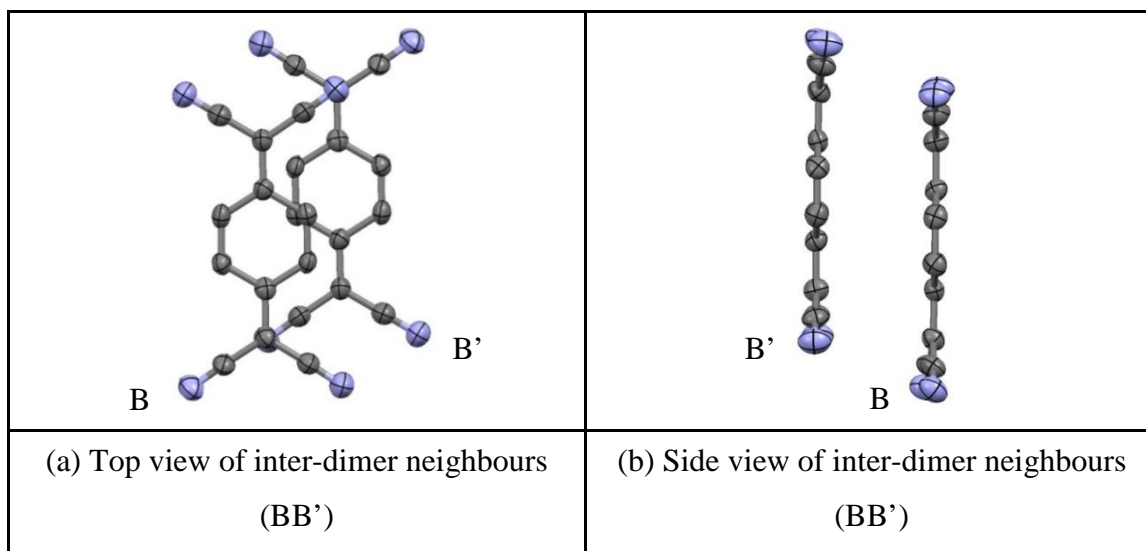


Figure 3.101 Top (a) and side (b) views of dimer neighbours (BB') of $(\text{DB18C6})\text{K}(\text{TCNQ})_2$ (hydrogen atoms are excluded)

Figure 3.102 shows the packing pattern of $(\text{DB18C6})\text{K}(\text{TCNQ})_2$. TCNQ units are assembled into infinite face-to-face π -stacks. The cation complex of $(\text{DB18C6})\text{K}^+$ form dimeric structure through K^+ - π interactions (see Figure 3.103), which is an off-set π -stacked geometry oriented in order to minimise the π - π repulsion between nearby

benzene rings and maximises the π - σ attraction between the σ framework of the inner edge of the cavity of one DB18C6 with the π electrons of the neighbouring benzene ring. The ligand of DB18C6 adopts a “butterfly” configuration, which is not symmetrical. The angle between mean planes of two benzene rings is 127.01° , and these mean planes form angles of 14.90° and 38.16° with mean plane of six oxygen atoms of DB18C6.

The dimeric structure of cation complex in $(\text{DB18C6})\text{K}(\text{TCNQ})_2$ is similar to that seen in Zhu et. al. studies²⁷⁴ in which two molecules of $[\text{K}(\text{DB18C6})]_2[\text{Hg}(\text{SCN})_4]$ form dimeric structure through K^+ - π interactions²⁷⁴. In $[\text{K}(\text{DB18C6})]_2[\text{Pt}(\text{SCN})_6] \cdot 2\text{H}_2\text{O} \cdot \text{C}_2\text{H}_4\text{Cl}_2$, DB18C6 adopts a symmetric boat conformation, further forming dimeric structure in respect to adjacent cation complex through K^+ - π interactions²⁷⁵. $[\text{K}(\text{DB18C6})_2\text{Cu}_2\text{Cl}_6]$ uses K^+ - π interactions to form polymeric endless chains²⁷⁶.

The distance between K^+ ion and carbon atoms on the mean plane of the phenyl ring of DB18C6 is 3.076 \AA , which are significantly shorter than the corresponding distance of the comparative complex in Zhu et.al. study²⁷⁴ and indicates that there are stronger K^+ - π interactions in $(\text{DB18C6})\text{K}(\text{TCNQ})_2$. Consequently, the cation complex of $(\text{DB18C6})\text{K}^+$ is situated in the cavity between the TCNQ columns. As seen in Figure 3.102(b), TCNQ units form separated dimers, which are sited between the crown ether columns. Distance and angles within the TCNQ stacks are listed in Table 3.36.

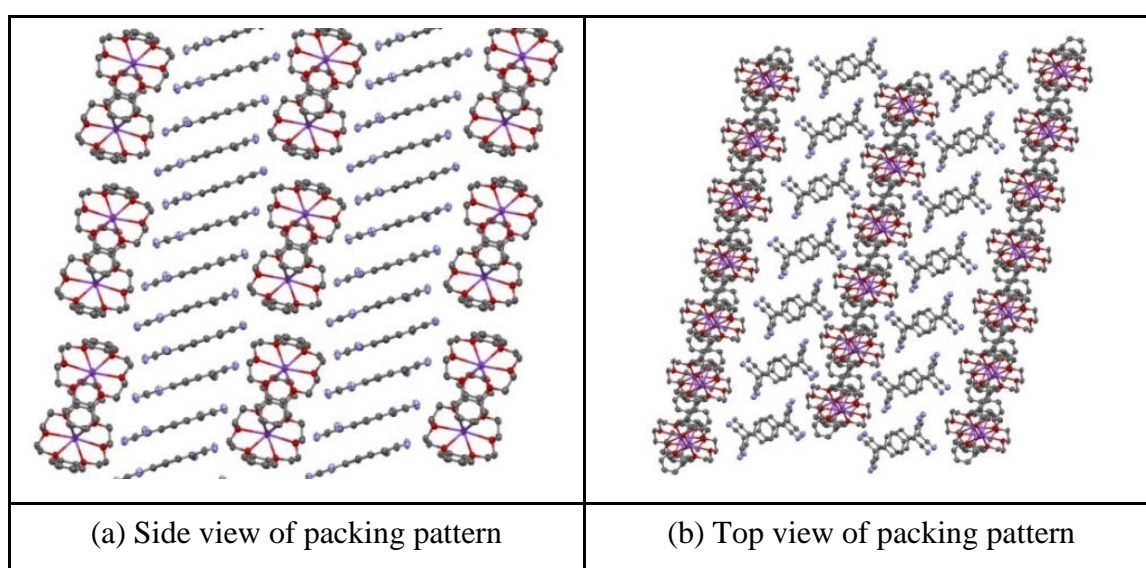


Figure 3.102 Side (a) and top (b) views of packing pattern within $(\text{DB18C6})\text{K}(\text{TCNQ})_2$ (hydrogen atoms are excluded)

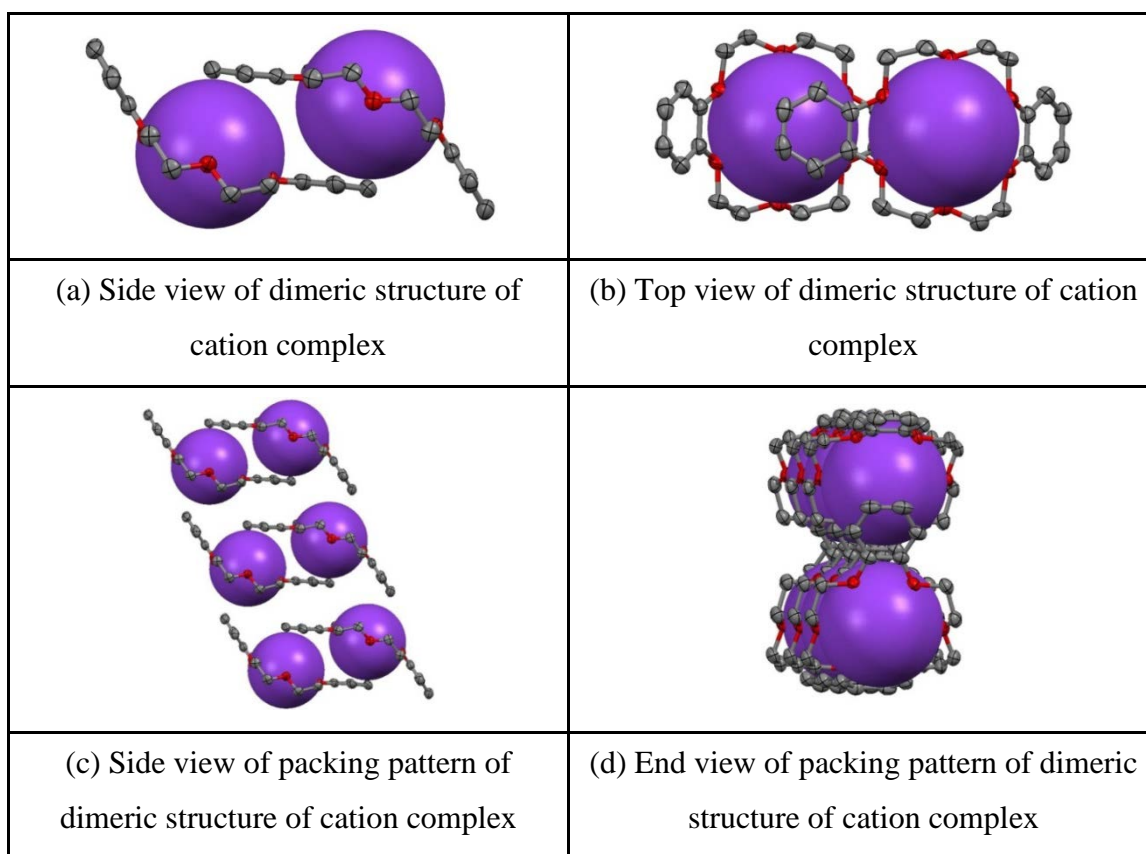


Figure 3.103 Dimeric structure of cation complex through K^+ - π interactions in $(DB18C6)K(TCNQ)_2$ (hydrogen atoms are excluded)

| TCNQ units | | AB | BB' |
|--|--------------|-------|-------|
| π - π perpendicular distance (Å) | | 3.10 | 3.37 |
| Short-axis slip | Distance (Å) | 0.012 | 2.16 |
| | Angle (°) | 0.22 | 32.66 |
| Long-axis slip | Distance (Å) | 2.15 | 1.31 |
| | Angle (°) | 34.74 | 34.74 |
| Centroid-centroid distance (Å) | | 3.78 | 4.21 |

Table 3.36 Distances (Å) and angles (°) within the TCNQ stacks of $(DB18C6)K(TCNQ)_2$

Within the TCNQ dimer, the individual TCNQ units adopt a shallow boat conformation in which neighbour $-C(CN)_2$ units are twisted away from each other. The two TCNQ planes are slightly tilted in respect to each other by *ca.* 1.32° . From these data, it will be evident that π -facial overlap between dimer neighbours within a column is not ideal for

extended π - π delocalisation within the TCNQ column. Figure 3.104 summarises the various contact distances within the cation complex.

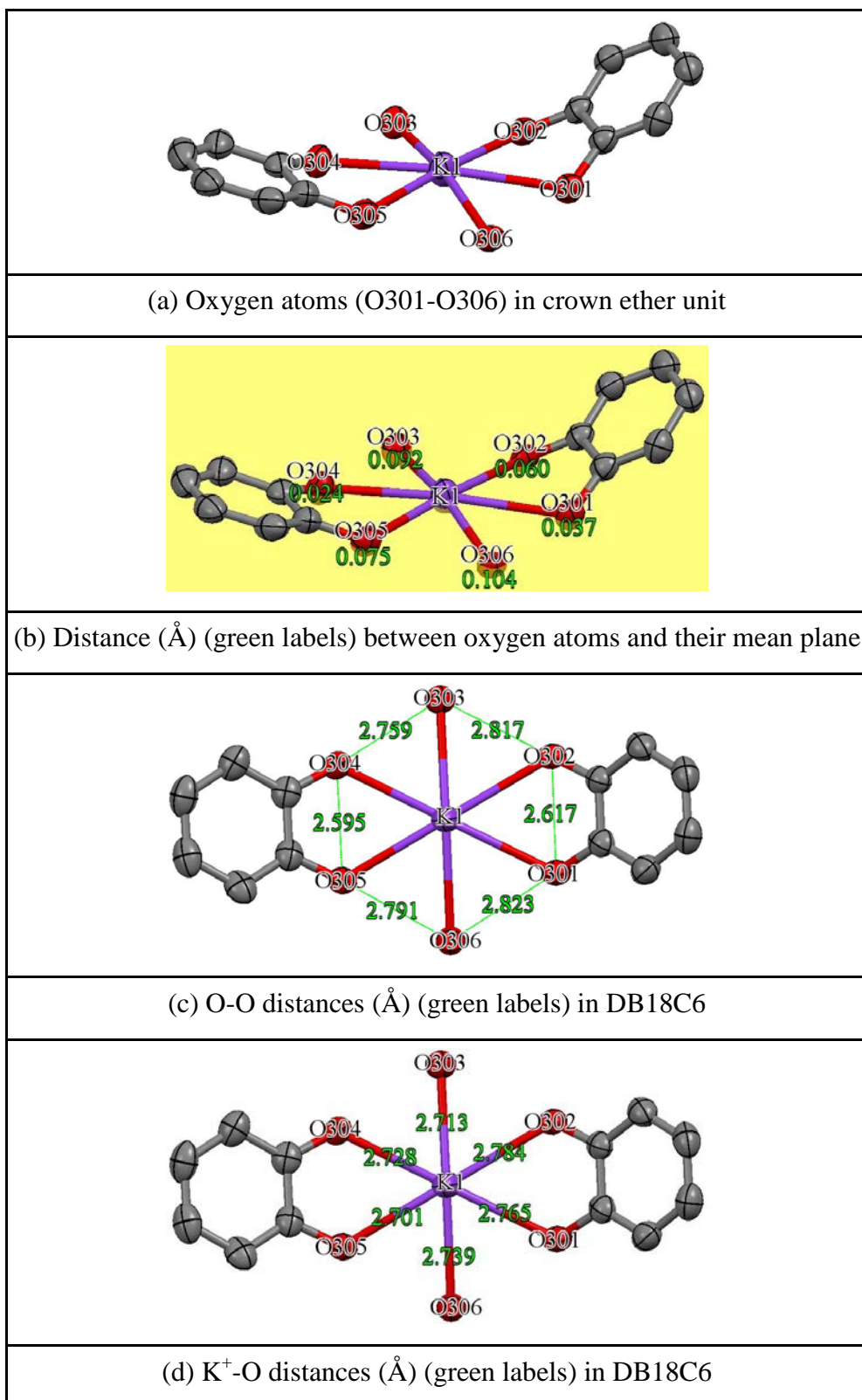


Figure 3.104 Various contact distances (Å) within the cation complex (carbon atoms on crown ether ring and hydrogen atoms are excluded)

As viewed in Figure 3.104, the cation complex of (DB18C6) K^+ unit adopts a shallow boat conformation in which the oxygen atoms of O303 and O306 are bent away from their mean plane (as defined by each set of oxygen atoms). Different O-O distances of DB18C6 form irregular hexagon geometry as mean side by *ca.* 2.734 Å. The minimum and maximum of K^+ -O distances within the cation complex are 2.701 and 2.784 Å which are less than those of van der Waals contact (K^+ -O = 2.85 Å)²⁷¹ and thus it seems justifiable to regard the metal cation and the oxygen atoms as being in contact. The different K^+ -O distances demonstrate that the position of K^+ cation is distorted inside the cavity of each DB18C6 unit.

3.3.7 Preparation of (Dicyc18C6)M(TCNQ)_n (M = K, Cs) (n = 2, 3)

3.3.7.1 (Dicyc18C6)K(TCNQ)₃

Reaction of Dicyc18C6 (Dicyclohexano-18-crown-6) with KTCNQ and TCNQ⁰ (ratio 1:1:1) in dry acetonitrile afforded a reasonable yield (70%) of a pure block of black crystalline solid which contained single crystals suitable for X-ray structural study (Combustion Analysis: Calculated: C: 65.67%, H: 4.72%, N: 16.41%. Found: C: 65.85%, H: 4.79%, N: 16.66%). Full details including an account of the structure solution and refinement are reported in the Experimental Section and the Supporting Information (in the Appendices) respectively. The crystals obtained were of (Dicyc18C6)K(TCNQ)₃ and the basic unit is shown in Figure 3.105. Bond lengths within the TCNQ units are summarised in Table 3.37.

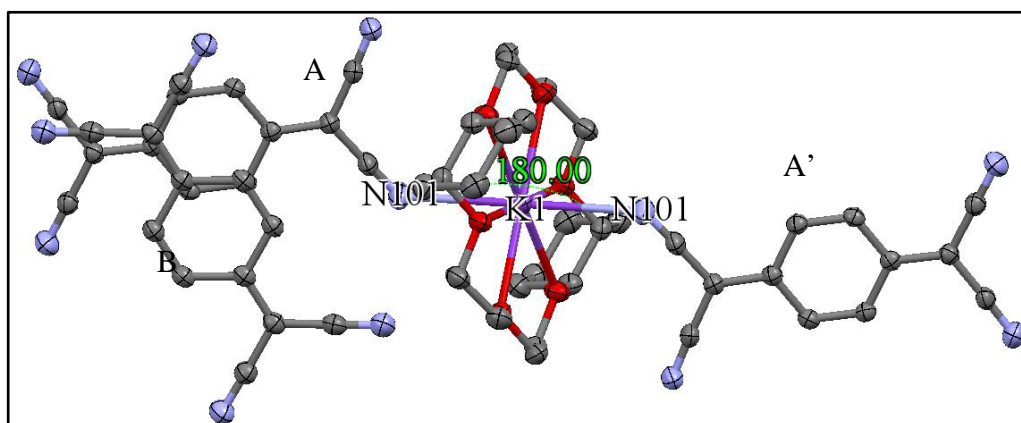


Figure 3.105 Basic unit of (Dicyc18C6)K(TCNQ)₃ (hydrogen atoms are excluded)

As viewed in Figure 3.106, the cation complex of (Dicyc18C6)K⁺ adopts a chair conformation (see Figure 3.106) and each K⁺ ion is coordinated by one crown ether unit and two nitrile groups on adjacent TCNQ units, which form a dimer with significantly long axis slippage (see Figure 3.107). The angle of N101-K1-N101 is 180° because the K⁺ ion sits on the inversion centre and bonded directly to the N atoms on adjacent TCNQ units. The centroid-centroid distance between neighbouring K⁺ ion is 7.961 Å and the perpendicular distance of K⁺ ion to an adjacent cation complex mean plane (defined by a set of oxygen atoms) is 4.255 Å. Therefore, the slip distance in respect to an adjacent cation complex is *ca.* 6.728 Å. Consequently, the angle between cyclohexane best plane and the mean plane of crown ether ring is 62.37°. The chain configuration of TCNQ⋯K⁺⋯TCNQ unit is similar to that seen in (18C6)K(TCNQ)_{2.5} and KO₈C₃₂H₄₇²⁷⁷, respectively. In the latter case, the K⁺ ion is sited at the centre of symmetry and in the centre cavity of crown ether unit, coordinated by six oxygen atoms. A chain conformation, linked by the hydrogen atoms, of phenol / phenoxide – potassium - phenol / phenoxide (K⁺⋯O⋯H⋯O⋯K⁺) is formed in the potassium phenoxide complex²⁷⁷.

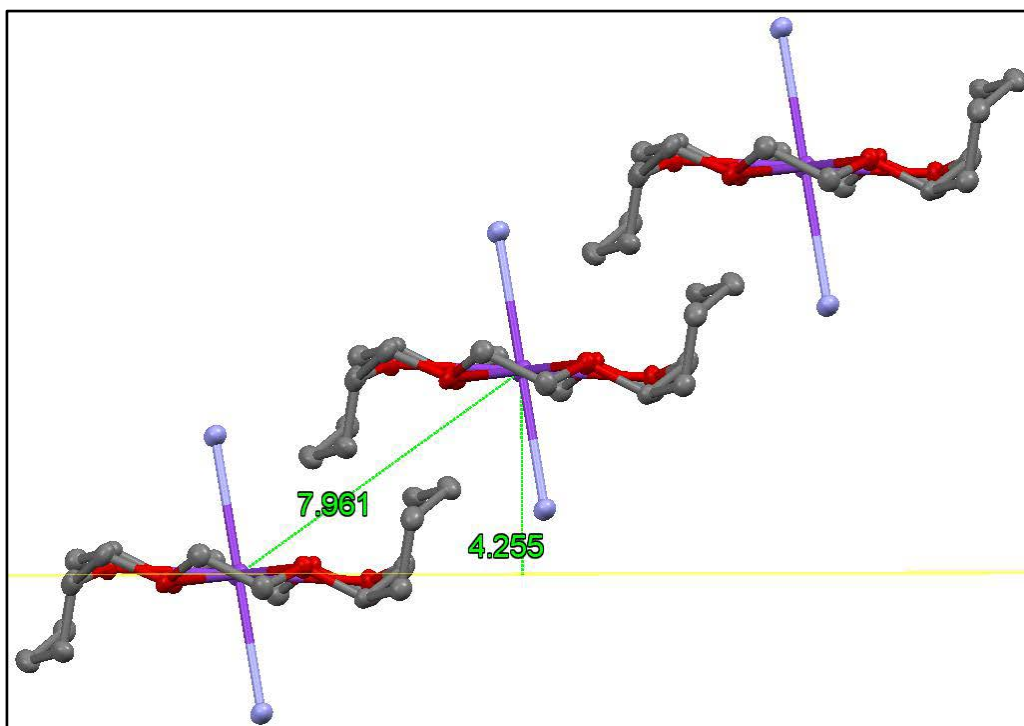


Figure 3.106 An “S” formation of cation complex in (Dicyc18C6)K(TCNQ)₃ (hydrogen atoms are excluded)

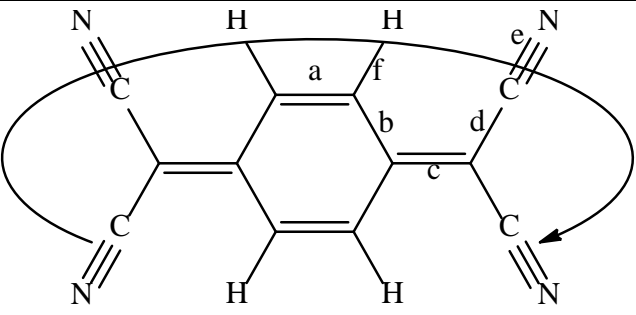
|  | | | | | | |
|--|------------------|------------|------------|------------|------------|-------|
| (a) Definition of the bond lengths within the TCNQ molecule | | | | | | |
| Structure | Bond lengths (Å) | | | | | |
| | a | b | c | d | e | f |
| TCNQ unit (A) | | 1.438 (15) | | 1.431 (16) | 1.150 (16) | 0.950 |
| | 1.359 (15) | 1.437 (15) | 1.398 (15) | 1.430 (15) | 1.151 (16) | 0.950 |
| | 1.360 (15) | 1.438 (15) | 1.402 (15) | 1.427 (16) | 1.150 (16) | 0.950 |
| | | 1.436 (15) | | 1.430 (15) | 1.151 (16) | 0.950 |
| TCNQ unit (B) | | 1.444 (15) | | 1.437 (16) | 1.147 (16) | 0.950 |
| | 1.350 (16) | 1.448 (16) | 1.381 (16) | 1.435 (16) | 1.146 (16) | 0.950 |
| | 1.350 (16) | 1.444 (15) | 1.381 (16) | 1.437 (16) | 1.147 (16) | 0.950 |
| | | 1.448 (16) | | 1.435 (16) | 1.146 (16) | 0.950 |

Table 3.37 Summary of bond distances (Å) observed for TCNQ units in
(Dicyc18C6)K(TCNQ)₃

In this structure, the K^+ ion is coordinated by one crown ether unit and two nitrile groups on adjacent TCNQ units (see Figure 3.105). The TCNQ units form a dimer which is significantly long axis slipped (see Figure 3.107). The similarity of the bond lengths within the two TCNQ units makes it difficult to distinguish between the $TCNQ^{\cdot-}$ and $TCNQ^0$ components.

The data in Table 3.37 suggest that both TCNQ units have some quinonoidal character because bond length “a” is less than “b”. After measuring the c bond lengths in each TCNQ unit, it seems likely that TCNQ unit (A) has more electron density, which suggests $TCNQ^{\cdot-}$ character. Consequently, the TCNQ unit (B) is less electron negative density, which suggests $TCNQ^0$ character.

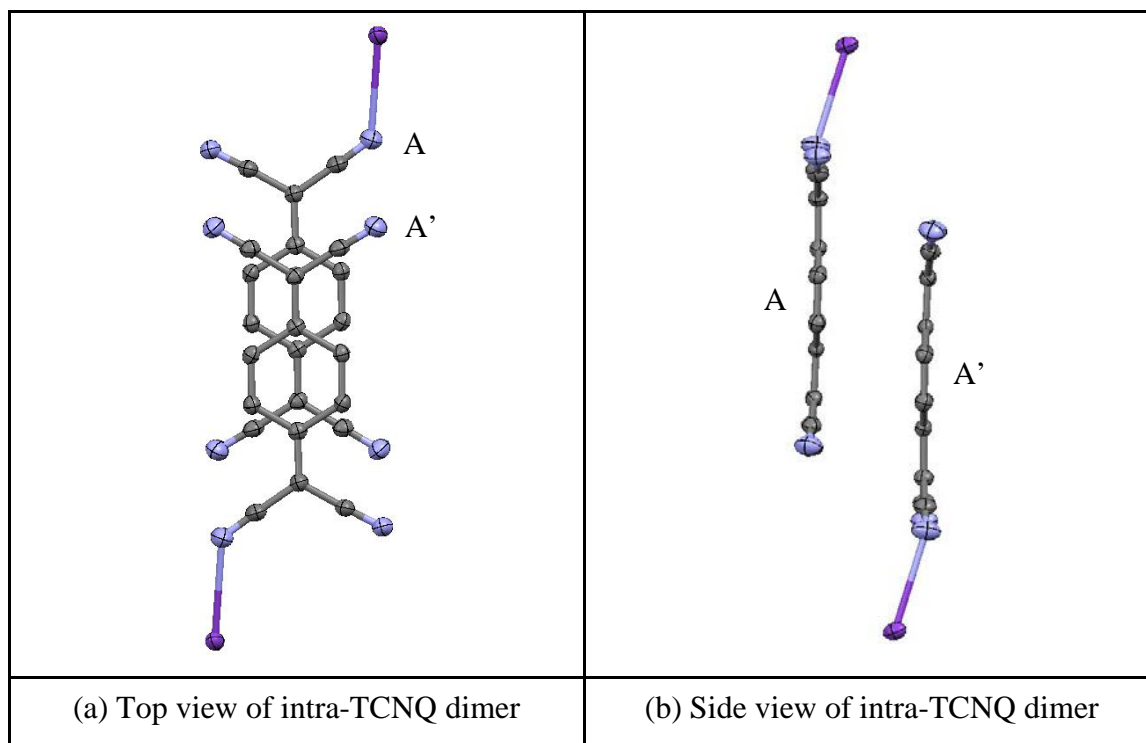


Figure 3.107 Top (a) and side (b) views of TCNQ dimer in (Dicyc18C6)K(TCNQ)₃ (hydrogen atoms are excluded)

Within the TCNQ dimer, the individual TCNQ units adopt a shallow boat conformation in which neighbouring $-\text{C}(\text{CN})_2$ units are twisted away from each other. The two TCNQ planes are parallel in respect to each other.

Within the crystal, the TCNQ dimers assemble into zig-zag infinite columns in which the individual TCNQ units are assembled in an AA'BAA' motif (Figure 3.108) in which extended dimer neighbours is significantly twisted by *ca.* 65.75° in respect to each other (Figure 3.109).

Figure 3.108 shows the packing pattern of (Dicyc18C6)K(TCNQ)₃. TCNQ units are assembled into infinite face-to-face π -stacks, forming infinite columns. Each TCNQ dimer is separated by one single molecule of TCNQ⁰ unit. The cation complex of (Dicyc18C6)K⁺ is located in the cavity between TCNQ columns.

Distance and angles within the TCNQ dimer are listed in Table 3.38.

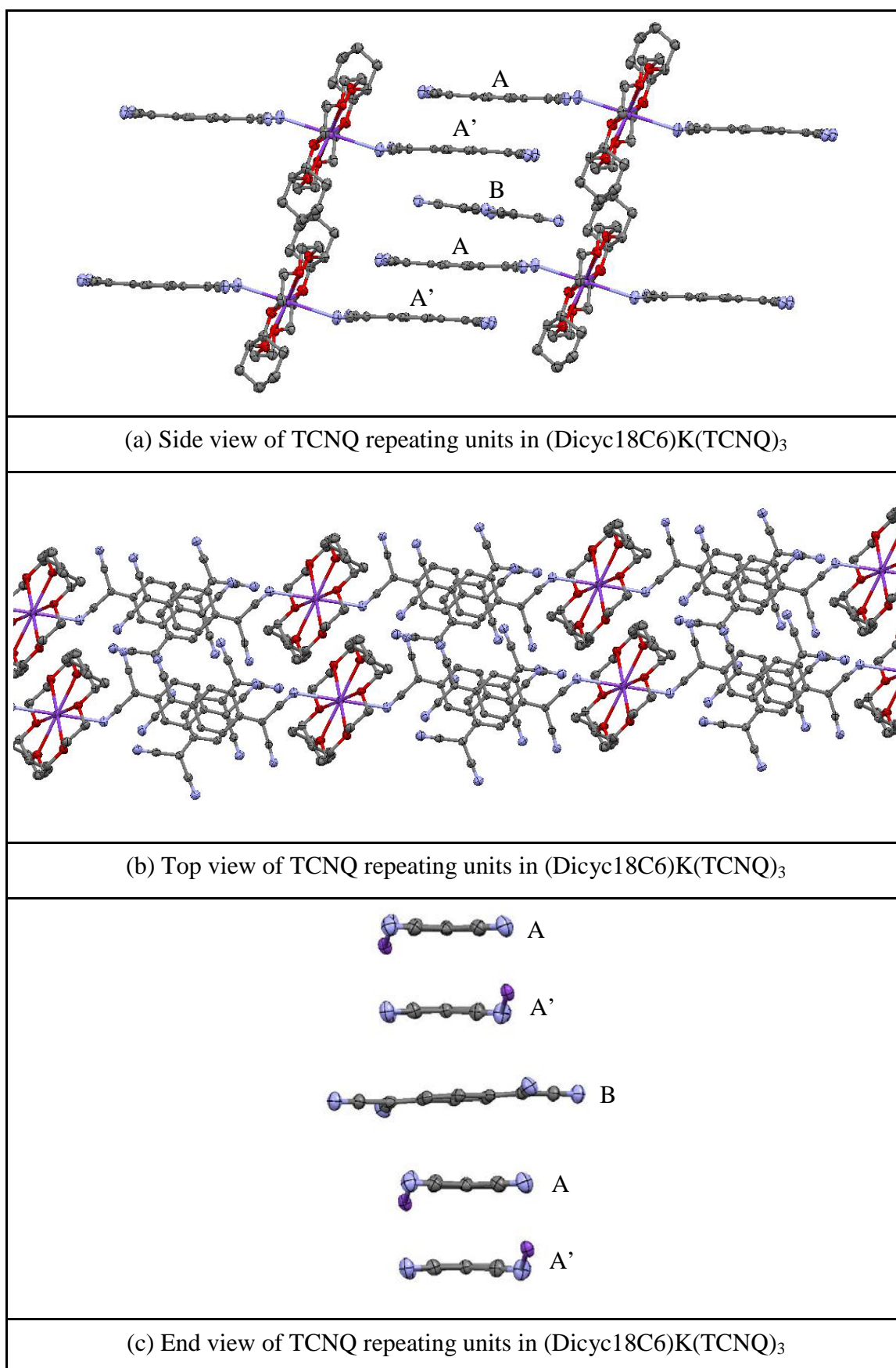


Figure 3.108 Observation of TCNQ repeating units in $(\text{Dicyc18C6})\text{K}(\text{TCNQ})_3$
(hydrogen atoms are excluded)

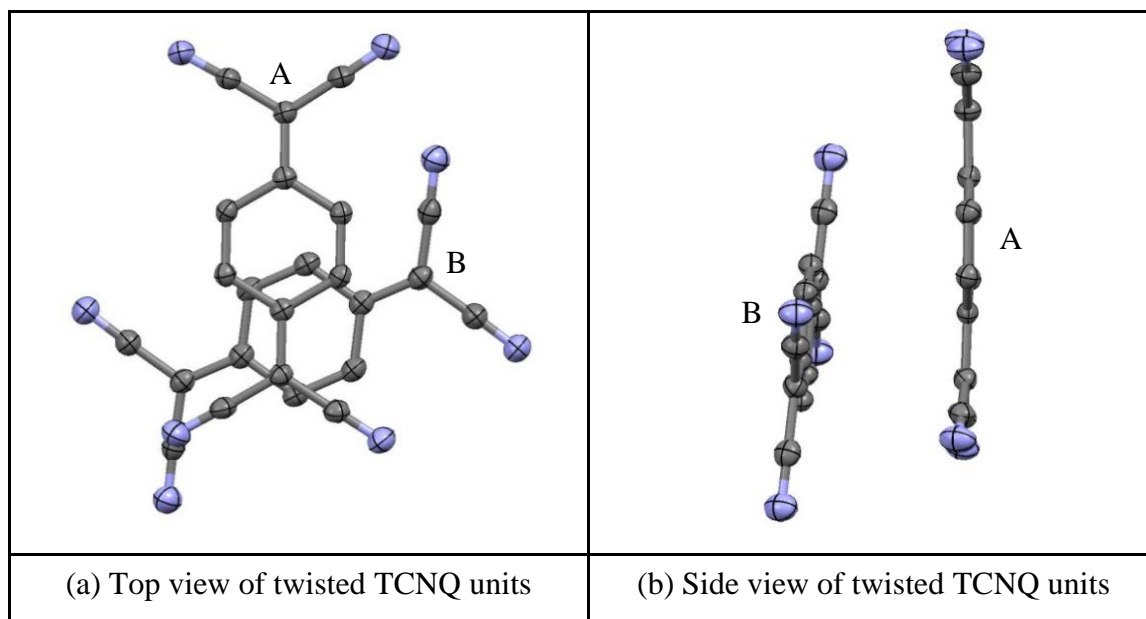


Figure 3.109 Top (a) and side (b) views of external dimer neighbours in $(\text{Dicyc18C6})\text{K}(\text{TCNQ})_3$ (hydrogen atoms are excluded)

| TCNQ units | | TCNQ dimer |
|--|--------------|------------|
| π - π perpendicular distance (Å) | | 3.05 |
| Short-axis slip | Distance (Å) | 0.015 |
| | Angle (°) | 0.28 |
| Long-axis slip | Distance (Å) | 2.17 |
| | Angle (°) | 35.43 |
| Centroid-centroid distance (Å) | | 3.74 |

Table 3.38 Distances (Å) and angles (°) within the TCNQ dimer of $(\text{Dicyc18C6})\text{K}(\text{TCNQ})_3$

From these data, it will be evident that π -facial overlap between dimer neighbouring within a column is not ideal for extended π - π delocalisation within the column. The two TCNQ planes are tilted in respect to each other by *ca.* 4.02° . Figure 3.110 summarises the various contact distances within the cation complex.

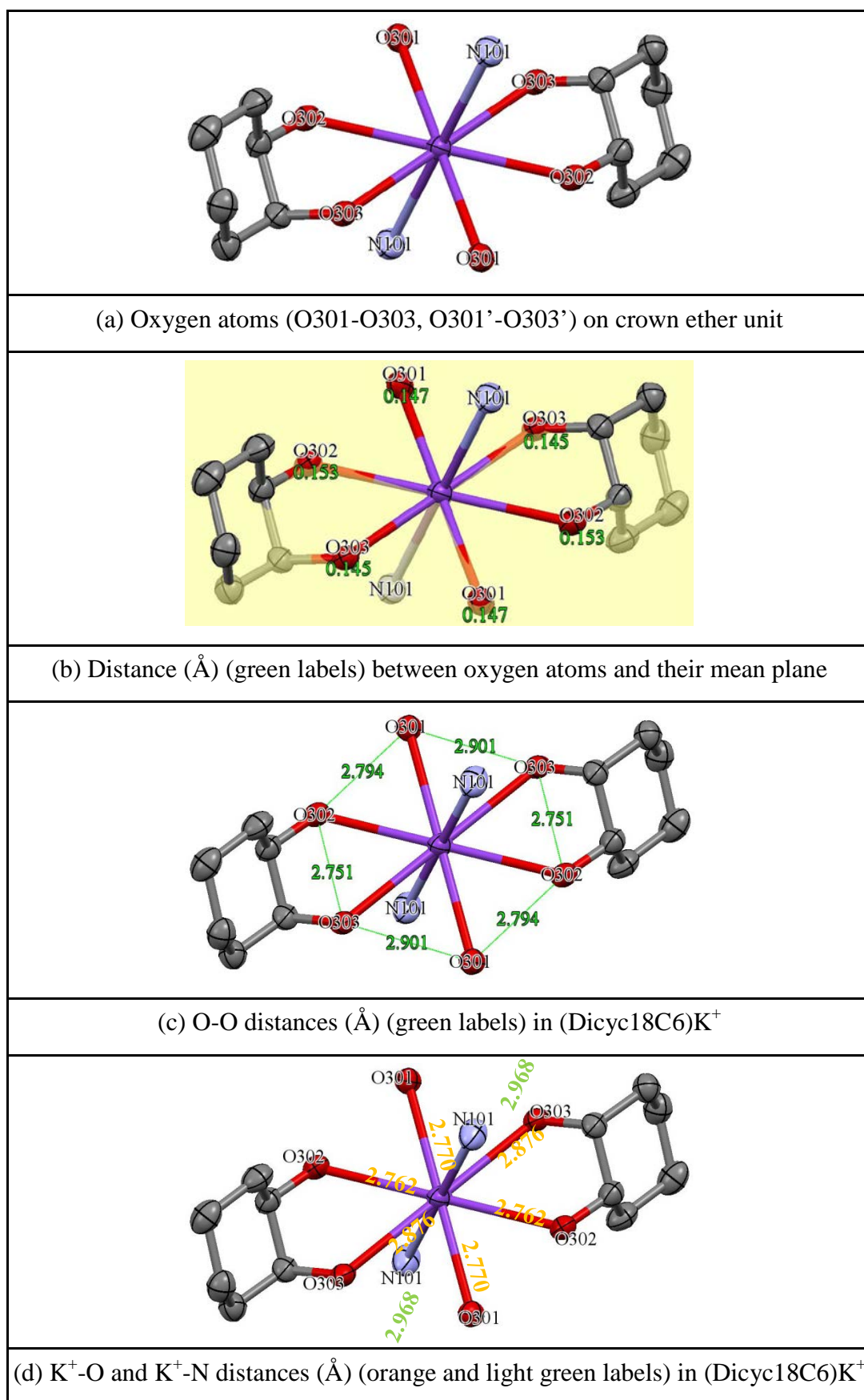


Figure 3.110 Various contact distances (Å) within the cation complex (carbon atoms on crown ether ring and hydrogen atoms are excluded)

As viewed in Figure 3.110, the ligating oxygen atoms are sitting above and below their mean plane (as defined by each set of oxygen atoms) forming irregular hexagon geometry with mean side by *ca.* 2.815 Å. The average K^+ -O distance by *ca.* 2.803 Å, which is less than those of van der Waals contact (K^+ -O = 2.85 Å)²⁷¹ and thus it seems justifiable to regard the metal cations and the oxygen atoms as being in contact. The different K^+ -O distances in Dicyc18C6 demonstrate that the K^+ cation is distorted inside the cavity of crown ether unit. The distance of K1-N101 is 2.968 Å, which is slightly longer than the sum of the van der Waals' radii (K^+ -N = 2.88 Å)^{269,271}.

3.3.7.2 (Dicyc18C6)Cs(TCNQ)₂

Reaction of Dicyc18C6 with $Cs_2(TCNQ)_3$ and $TCNQ^0$ (ratio 2:1:2) in dry acetonitrile afforded a reasonable yield (57%) of a plate of dark blue crystalline solid which contained single crystals suitable for X-ray structural study (combustion data is awaited). Full details including an account of the structure solution and refinement are reported in the Experimental Section and the Supporting Information (in the Appendices) respectively. The crystals obtained were of (Dicyc18C6)Cs(TCNQ)₂ and the basic unit is shown in Figure 3.111. Bond lengths within the TCNQ units are summarised in Table 3.39.

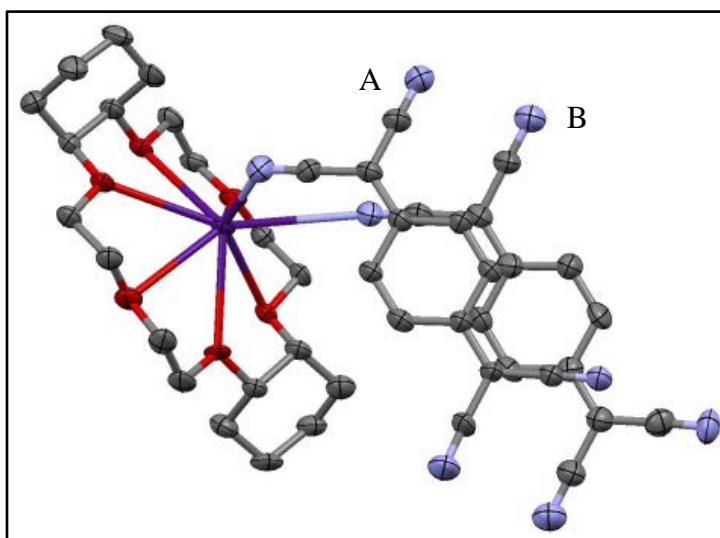


Figure 3.111 Basic unit of (Dicyc18C6)Cs(TCNQ)₂ (hydrogen atoms are excluded)

As seen in Figure 3.112, the cation complex of (Dicyc18C6)Cs⁺ adopts a chair conformation and each Cs⁺ ion is coordinated by one crown ether unit and two nitrile groups on adjacent TCNQ units, which form a dimer with significantly long axis

slippage (see Figure 3.113). Consequently, because of the $\text{Cs}^+\text{-N}$ coordination, each Cs^+ ion is located 1.333 Å above the cavity of crown ether unit. The centroid-centroid distance between Cs^+ ions is 8.270 Å and the perpendicular distance of Cs^+ ion to adjacent cation complex mean plane (defined by a set of oxygen atoms) is 5.829 Å. Therefore, the slip distance in respect to neighbouring cation complex is by *ca.* 6.941 Å. Two cyclohexane rings are not parallel in respect to each other, with the angles between cyclohexane plane and the crown ether mean plane (defined by a set of oxygen atoms) are 61.27° and 65.08°, respectively. The tilt angle between two cyclohexane planes on each end of ligand is 5.31° (see Figure 3.112).

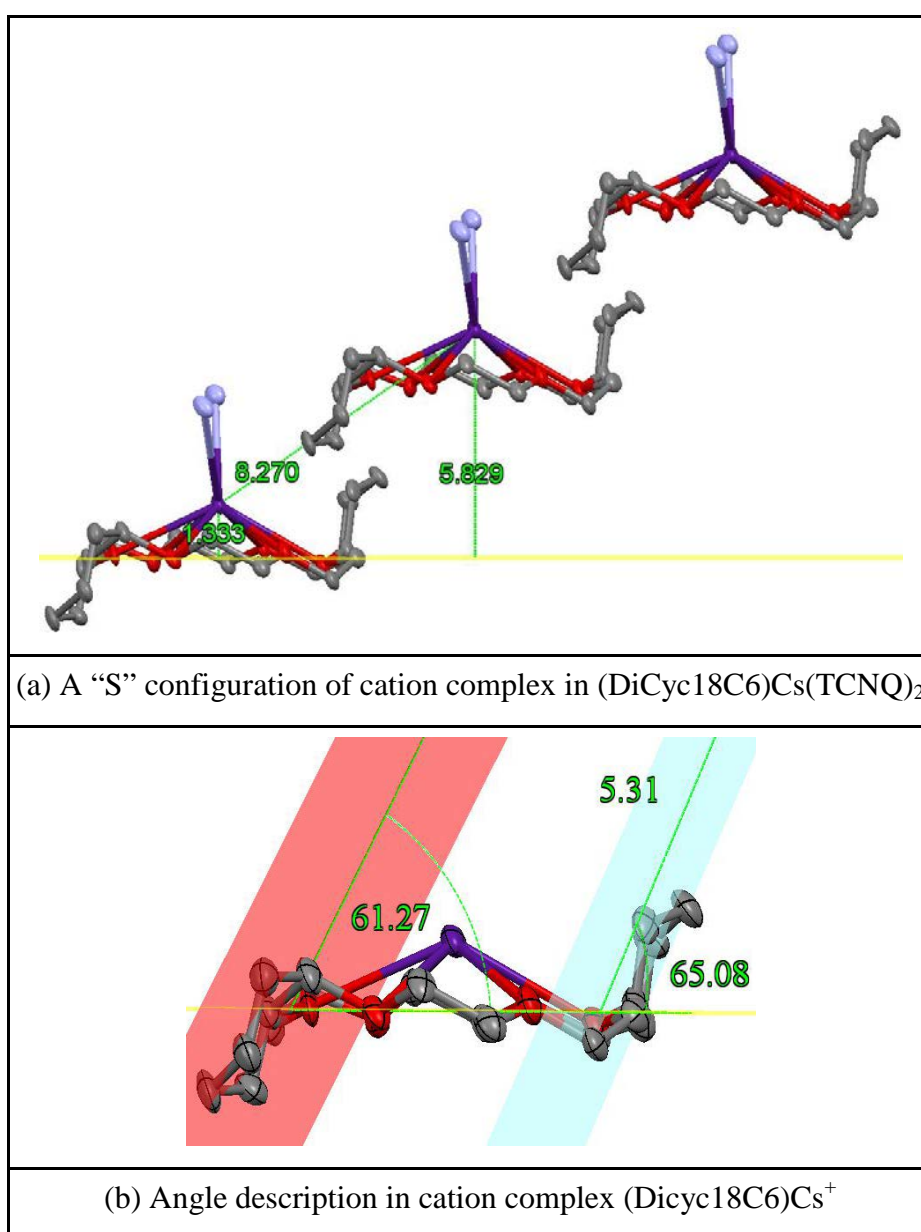


Figure 3.112 Geometry of cation complex in $(\text{DiCyc18C6})\text{Cs}(\text{TCNQ})_2$ (hydrogen atoms are excluded)

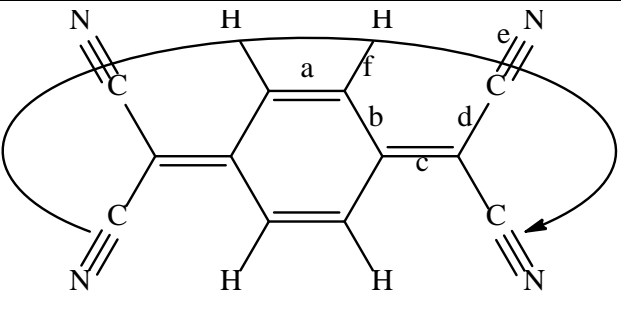
|  | | | | | | |
|--|------------------|------------|------------|------------|------------|-------|
| (a) Definition of the bond lengths within the TCNQ molecule | | | | | | |
| Structure | Bond lengths (Å) | | | | | |
| | a | b | c | d | e | f |
| TCNQ unit (A) | | 1.456 (12) | | 1.436 (13) | 1.145 (13) | 0.952 |
| | 1.355 (13) | 1.435 (12) | 1.393 (13) | 1.446 (13) | 1.169 (14) | 0.951 |
| | 1.365 (14) | 1.441 (13) | 1.406 (13) | 1.422 (13) | 1.141 (13) | 0.948 |
| | | 1.429 (13) | | 1.445 (12) | 1.169 (14) | 0.950 |
| TCNQ unit (B) | | 1.454 (13) | | 1.448 (13) | 1.150 (13) | 0.948 |
| | 1.369 (14) | 1.427 (13) | 1.387 (13) | 1.431 (13) | 1.168 (14) | 0.951 |
| | 1.361 (15) | 1.448 (13) | 1.398 (14) | 1.425 (14) | 1.160 (14) | 0.948 |
| | | 1.436 (14) | | 1.452 (14) | 1.159 (15) | 0.950 |

Table 3.39 Summary of bond distances (Å) observed for TCNQ units in
(Dicyc18C6)Cs(TCNQ)₂

In this structure, the Cs⁺ ion is coordinated by one crown ether unit and two nitrile groups on adjacent TCNQ units, which can be regarded as inter-dimer neighbours. The TCNQ units form a dimer which is diagonally slipped with both significant long and short axis slip (see Figure 3.113). The similarity of the bond lengths within the two TCNQ units makes it difficult to distinguish between the TCNQ^{•-} and TCNQ⁰ components.

The data in Table 3.39 suggest that both TCNQ units have some quinonoidal character because bond length “a” is less than “b”. For both components A and B, the distribution of bond lengths is intermediate between these reported for TCNQ⁰ and TCNQ^{•-} respectively²¹³.

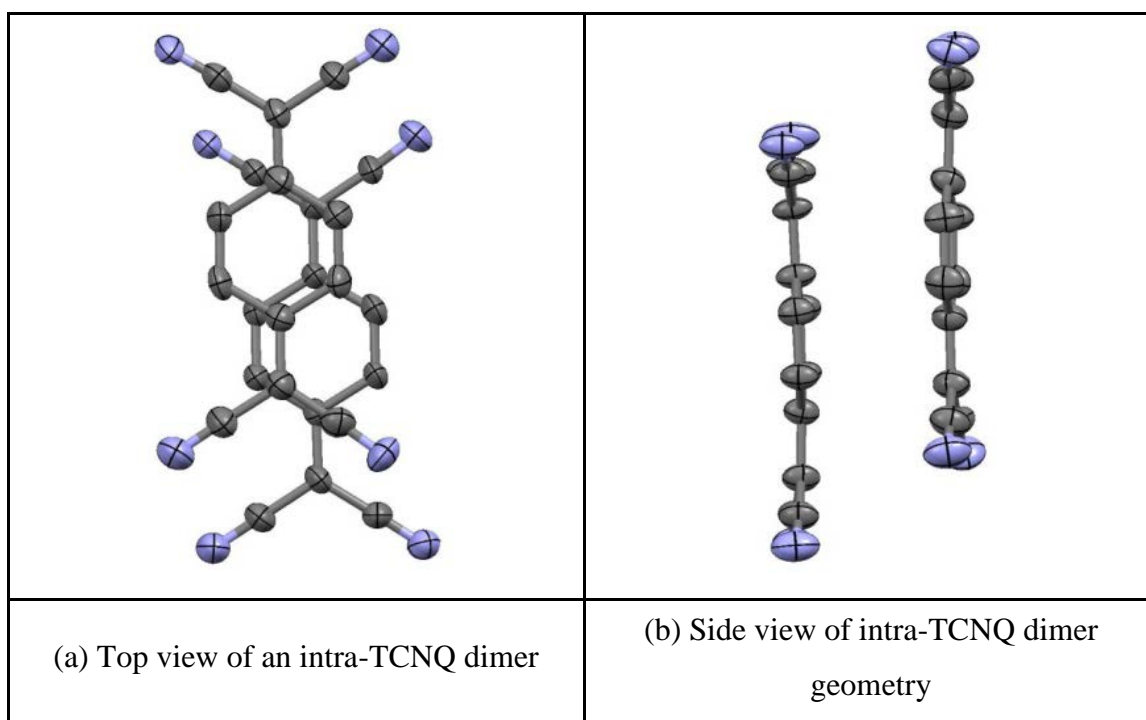


Figure 3.113 Top (a) and side (b) views of TCNQ dimer in (Dicyc18C6)Cs(TCNQ)₂ (hydrogen atoms are excluded)

Within the TCNQ dimer (see Figure 3.113), the individual TCNQ units adopt a shallow boat conformation in which neighbouring $-\text{C}(\text{CN})_2$ units are twisted away from each other. The two TCNQ planes are slightly tilted in respect to each other by *ca.* 3.26° . Within the crystal, the TCNQ dimers assemble into infinite columns in which the individual TCNQ units are assembled in an ABB'A' motif (Figure 3.115) and in which dimer neighbours are significantly “diagonally” slipped (Figure 3.116) and tilted in respect to each other by *ca.* 11.97° .

In (Dicyc18C6)Cs(TCNQ)₂, both intra-TCNQ dimer and inter-TCNQ dimer neighbours are diagonally slipped (Figure 3.113 and Figure 3.116). Each pair of TCNQ dimer neighbours, which has a significantly tilt angle in respect to each other, is coordinated to Cs^+ ion (see Figure 3.111). Consequently, dimer pairs of TCNQ units form infinite zigzag columns as viewed in Figure 3.114. Neighbouring TCNQ columns are twisted 70.15° in respect to each other. Consequently, the reason for forming a wave-like infinite TCNQ column is because there is no extra space to fit in the terminal part of cyclohexane group, which will “push” TCNQ units up and down. Distances and angles within the TCNQ stacks are summarised in Table 3.40.

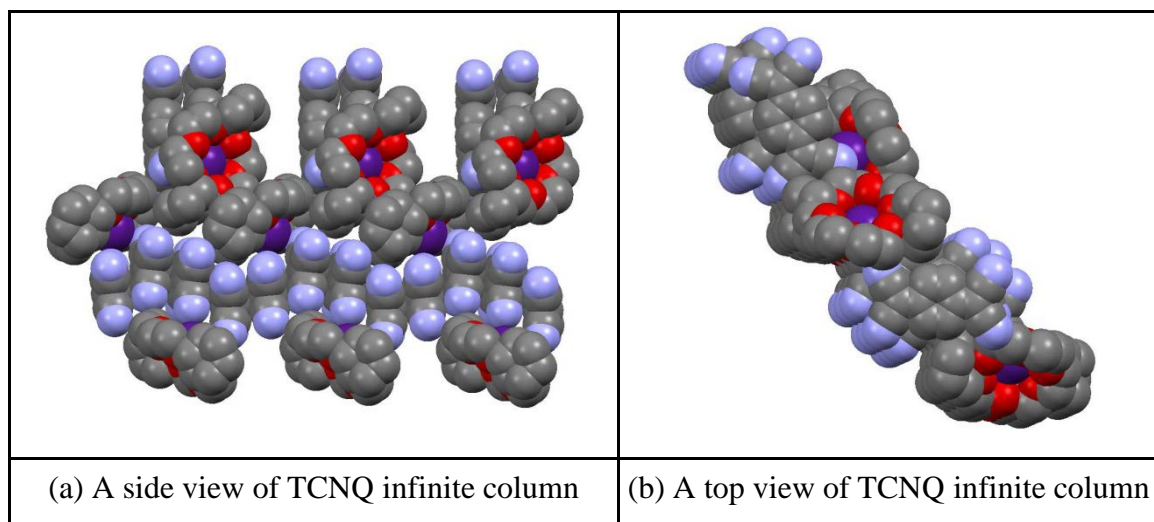


Figure 3.114 A wave-like configuration of TCNQ infinite column in $(\text{Dicyc18C6})\text{Cs}(\text{TCNQ})_2$ (hydrogen atoms are excluded)

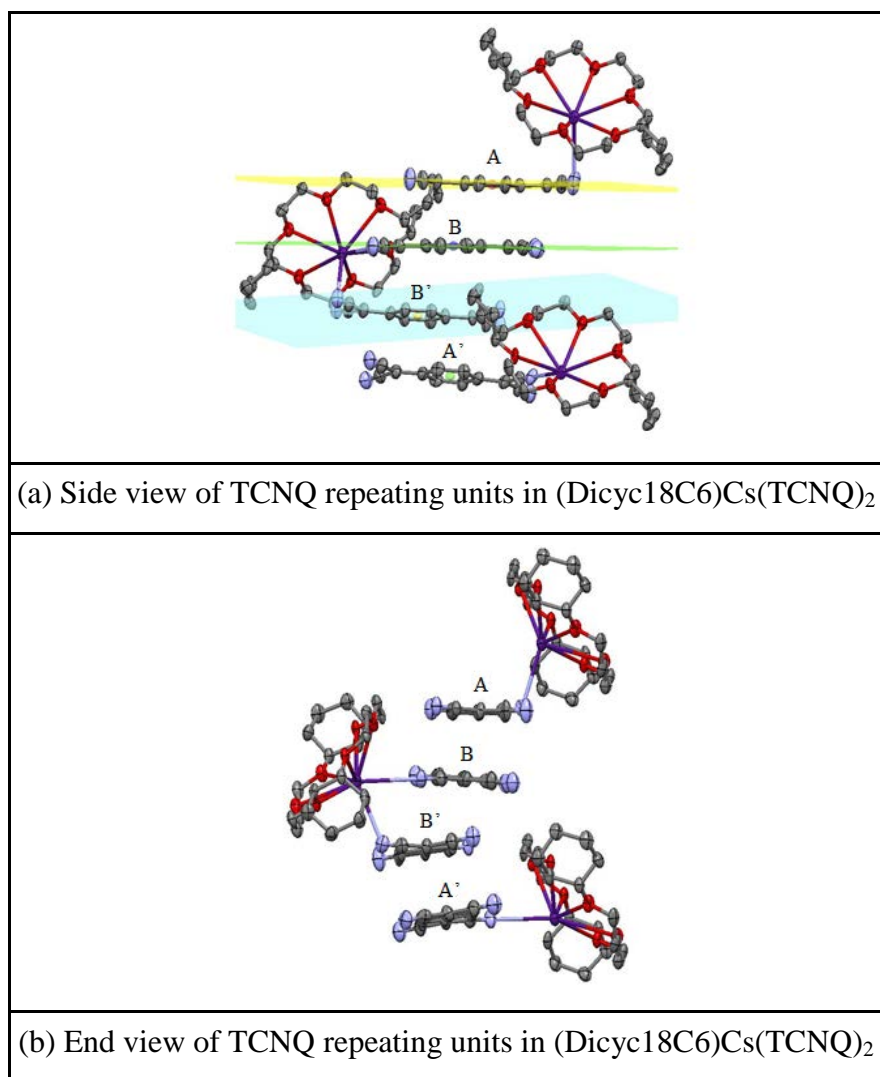


Figure 3.115 Observation of TCNQ repeating units in $(\text{Dicyc18C6})\text{Cs}(\text{TCNQ})_2$ (hydrogen atoms are excluded)

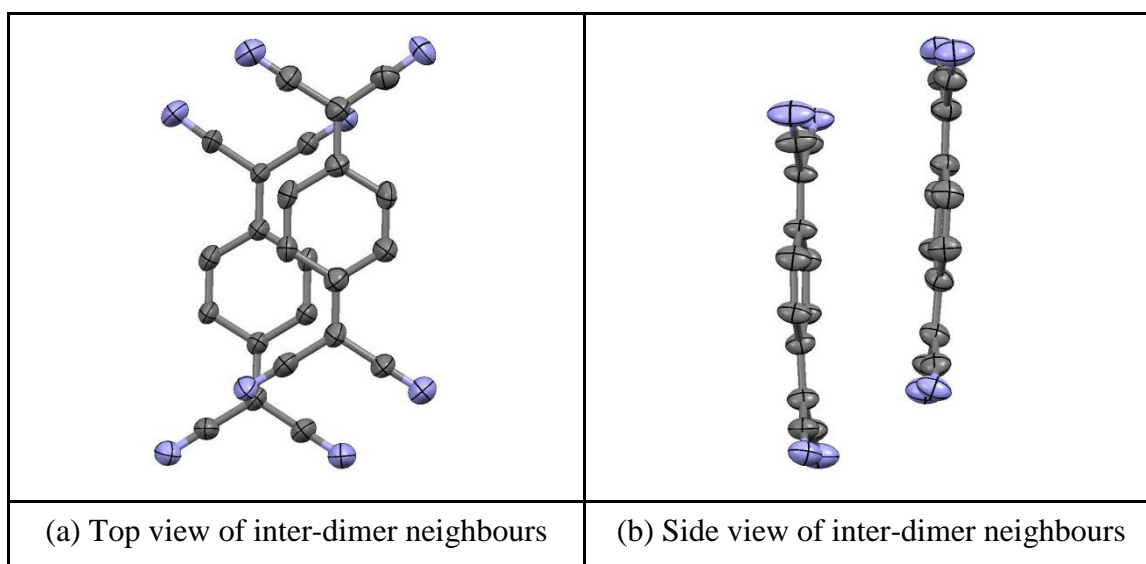


Figure 3.116 Top (a) and side (b) views of dimer neighbours in (Dicyc18C6)Cs(TCNQ)₂ (hydrogen atoms are excluded)

| TCNQ units | | TCNQ dimer | TCNQ dimer neighbours |
|--|--------------|------------|-----------------------|
| π - π perpendicular distance (Å) | | 3.20 | 3.61 |
| Short-axis slip | Distance (Å) | 0.51 | 1.66 |
| | Angle (°) | 9.06 | 24.69 |
| Long-axis slip | Distance (Å) | 1.96 | 1.79 |
| | Angle (°) | 31.49 | 26.37 |
| Centroid-centroid distance (Å) | | 3.78 | 4.36 |

Table 3.40 Distances (Å) and angles (°) within the TCNQ stacks of (Dicyc18C6)Cs(TCNQ)₂

In (DC18C6)Cs(TCNQ)₂, each TCNQ unit is coordinated to one metal ion. Consequently, each TCNQ unit assembles into infinite columns containing pairs of TCNQ dimers, which can be regarded as dimers since they are closely face-to-face π -stack. Each Cs⁺ cation is coordinated to two nitrogen atoms from cyano groups on adjacent TCNQ units and one crown ether unit. The cation complex of (Dicyc18C6)Cs⁺ lies in the channels between the TCNQ stacks (see Figure 3.114). Each TCNQ unit coordinates to one metal to form a dimer similar to that seen for (15C5)LiTCNQ but, in contrast with the behaviour described above for (15C5)LiTCNQ, in (Dicyc18C6)Cs(TCNQ)₂ each metal cation is coordinated by two TCNQ units and both

of the intra-TCNQ dimer and inter-TCNQ dimer neighbours are diagonally slipped. Figure 3.117 summarises the various contact distances within the cation complex of (Dicyc18C6)Cs(TCNQ)₂.

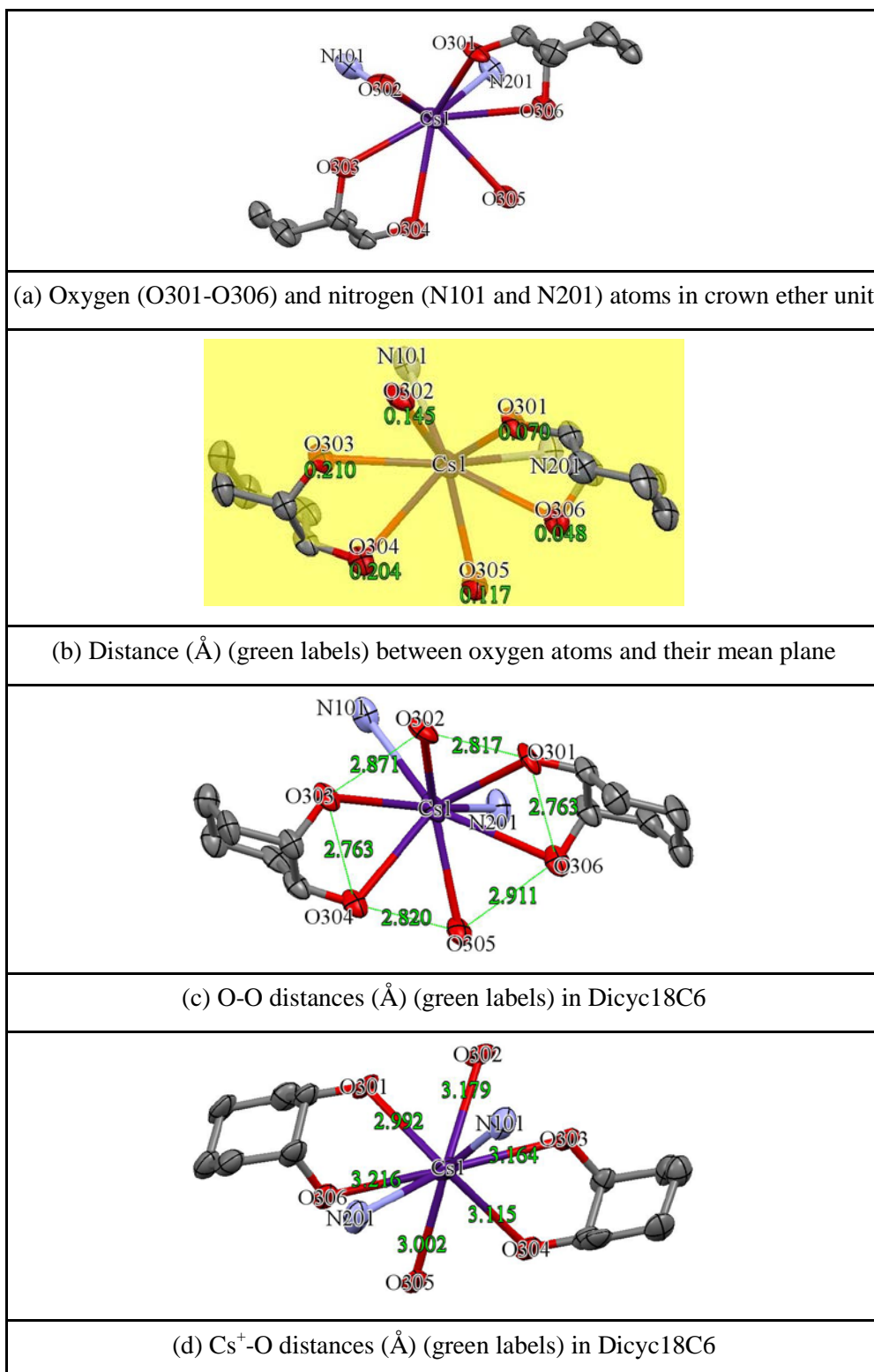


Figure 3.117 Various contact distances (Å) within the cation complex (carbon, except for the TCNQ and cyclohexane, and hydrogen atoms are excluded)

As viewed in Figure 3.117, the ligating oxygen atoms form irregular hexagon geometry of mean side by *ca.* 2.824 Å. The minimum and maximum of Cs⁺-O distances are 2.992 and 3.216 Å respectively. The different Cs⁺-O distances demonstrate that the Cs⁺ cation is in a distorted environment above the cavity of the crown ether unit. All of the distances of Cs⁺-O are less than that for van der Waals' contact (Cs⁺-O = 3.42 Å)^{269,270} and thus it seems justifiable to regard the metal cations and the oxygen atoms as being in contact in respect to each other.

3.3.8 Preparation of (C222)K(TCNQ)_{2.5}

In previous attempts to prepare this complex only crystals of (2.2.2)KDCTC were obtained⁵⁵. However, in the present study, reaction of C222 (2.2.2-Cryptand) and KTCNQ with TCNQ⁰ in dry acetonitrile (1:1:1) (using the crown ether: salt ratio 1:2) gave a fair yield (49%) of a very pure black crystalline solid (Combustion Analysis: Calculated: C: 62.25%, H: 5.01%, N: 18.15%. Found: C: 62.18%, H: 5.02%, N: 18.06%). These crystals proved to be single and of a quality suitable for an X-ray structural study. Full details including an account of the structure solution and refinement are reported in the Experimental Section and the Supporting Information (in the Appendices) respectively. The crystals obtained were of (C222)K(TCNQ)_{2.5} and the basic unit is shown in Figure 3.118.

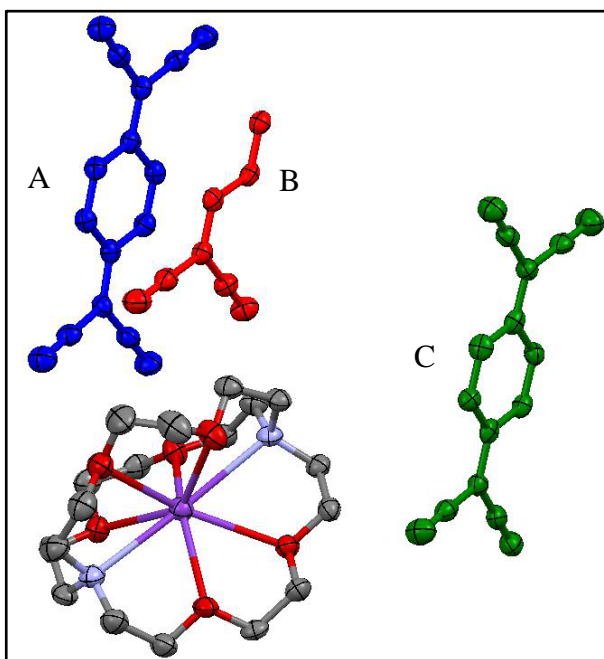


Figure 3.118 Basic unit of (C222)K(TCNQ)_{2.5} (hydrogen atoms are excluded)

Bond lengths within the TCNQ units are summarised in Table 3.41.

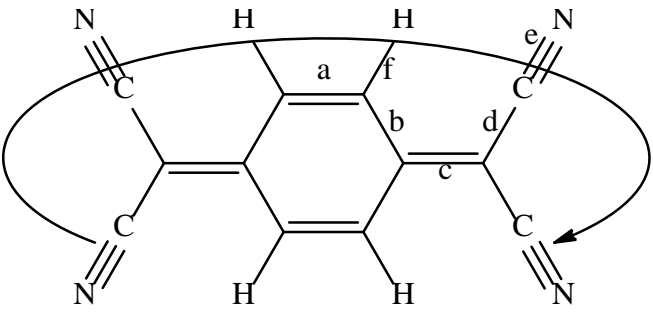
|  | | | | | | |
|--|------------------|-----------|-----------|-----------|-----------|-------|
| (a) Definition of the bond lengths within the TCNQ molecule | | | | | | |
| Structure | Bond lengths (Å) | | | | | |
| | a | b | c | d | e | f |
| TCNQ unit (A) | | 1.433 (5) | | 1.440 (5) | 1.157 (5) | 0.949 |
| | 1.361 (5) | 1.447 (5) | 1.413 (5) | 1.432 (5) | 1.160 (5) | 0.951 |
| | 1.359 (5) | 1.441 (5) | 1.405 (5) | 1.432 (6) | 1.169 (5) | 0.950 |
| | | 1.439 (5) | | 1.436 (5) | 1.162 (5) | 0.951 |
| TCNQ unit (B) | | 1.449 (5) | | 1.444 (5) | 1.149 (5) | 0.950 |
| | 1.357 (5) | 1.446 (5) | 1.385 (5) | 1.452 (5) | 1.156 (5) | 0.951 |
| | 1.357 (5) | 1.449 (5) | 1.385 (5) | 1.444 (5) | 1.149 (5) | 0.950 |
| | | 1.446 (5) | | 1.452 (5) | 1.156 (5) | 0.951 |
| TCNQ unit (C) | | 1.446 (5) | | 1.441 (6) | 1.155 (5) | 0.950 |
| | 1.362 (5) | 1.440 (5) | 1.392 (5) | 1.444 (5) | 1.157 (5) | 0.951 |
| | 1.358 (5) | 1.449 (5) | 1.383 (5) | 1.441 (6) | 1.160 (5) | 0.950 |
| | | 1.449 (5) | | 1.446 (5) | 1.159 (5) | 0.951 |

Table 3.41 Summary of bond lengths (Å) observed for TCNQ units in
(C222)K(TCNQ)_{2.5}

In this structure, the K^+ ion is bound within the cryptand cavity preventing direct contact with the TCNQ units. The TCNQ units form a pentamer, in which they are all π -stacked long-axis slipped alternately up and down thereby forming a wave-like motif (see Figure 3.119).

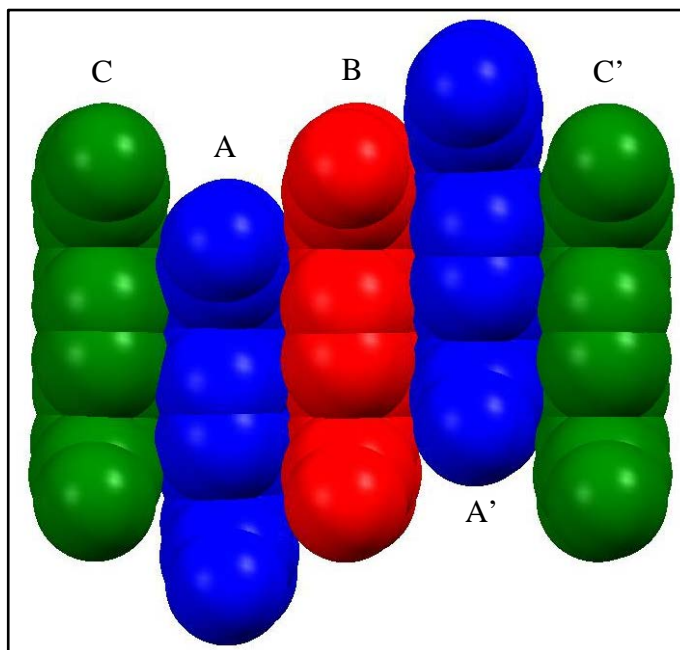


Figure 3.119 Space-fill of TCNQ pentamer stack in $(C222)K(TCNQ)_{2.5}$ (hydrogen atoms are excluded)

The data in Table 3.41 suggest that all of the TCNQ units have some quinonoidal character because bond length “a” is less than “b”. In TCNQ pentamer, after measuring the c bond lengths in each TCNQ unit, it seems reasonable to regard both red and green TCNQ units as having lower electron density, which suggests the assignment of $TCNQ^0$ character. Consequently, the blue TCNQ units are more electron rich suggesting $TCNQ^{\cdot-}$ character. Therefore, TCNQ units form mixed stacks, which is $TCNQ^0$ - $TCNQ^{\cdot-}$ - $TCNQ^0$ - $TCNQ^{\cdot-}$ - $TCNQ^0$ configuration as viewed in the TCNQ pentamer stack, in which two electrons are delocalised over the five TCNQ units but more negative charge density appears to reside on second and fourth TCNQ units (blue ones) based on c bond lengths. Figure 3.120 shows top and side views of individual TCNQ units within and outside the TCNQ pentamer.

Within the crystal structure of $(C222)K(TCNQ)_{2.5}$, the TCNQ pentamer can assemble into infinite columns (see Figure 3.121). There are more TCNQ units than K^+ and C222, which results in a wave-like pattern in the TCNQ column in order to create the cavity in which to fit the cation complex $(C222)K^+$. The packing pattern is probably purely steric because there is no direct association between K^+ ion and nitrogen atoms from adjacent TCNQ units.

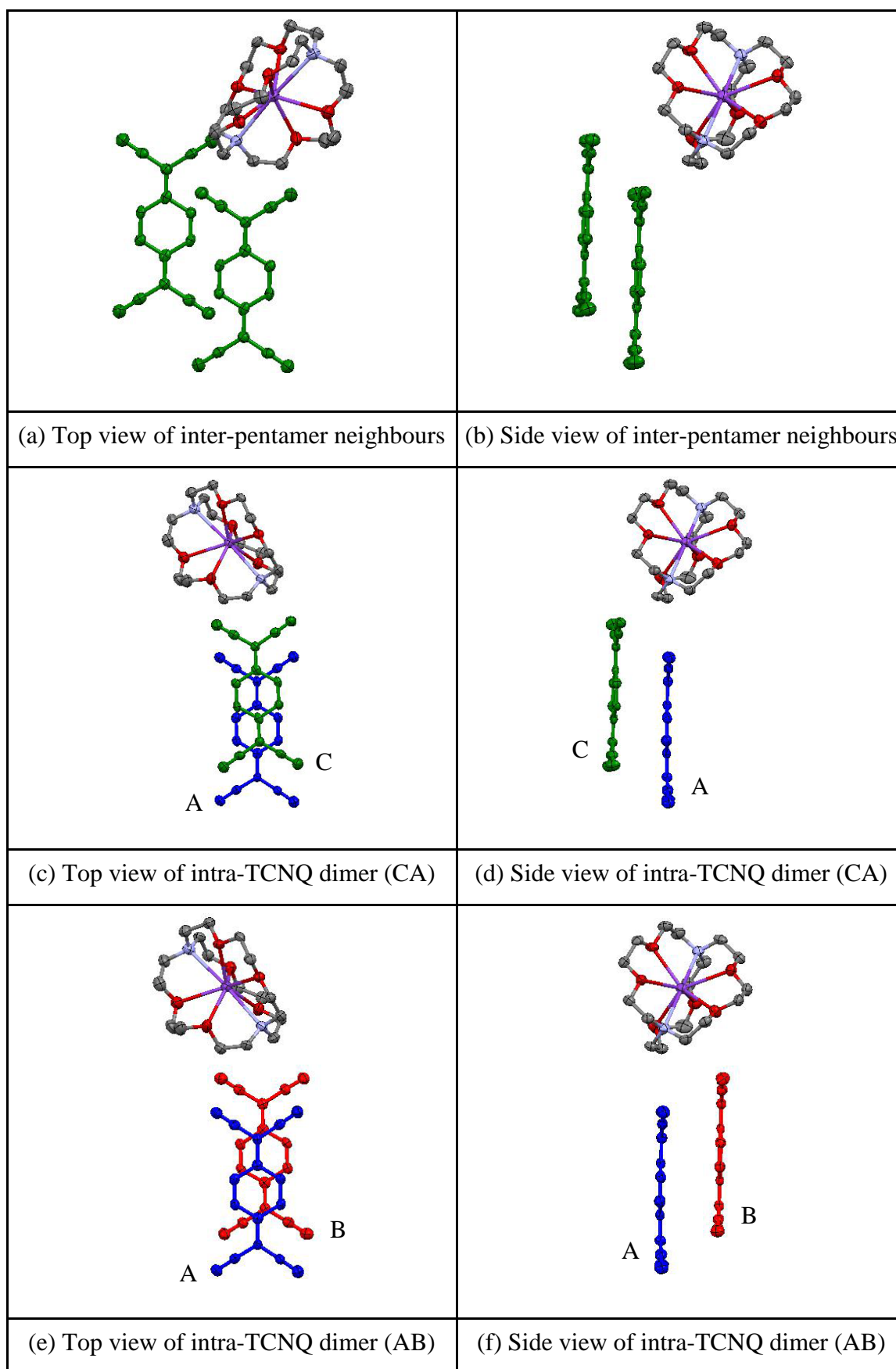


Figure 3.120 Top (a/c/e) and side (b/d/f) views of TCNQ units in $(C_{222})K(TCNQ)_{2.5}$
(hydrogen atoms are excluded)

Within the CA and AB dimer, the individual TCNQ units adopt a shallow boat conformation in which neighbouring $-\text{C}(\text{CN})_2$ units are twisted away from each other. The two TCNQ planes are slightly tilted in respect to each other by *ca.* 4.40° in CA dimer and 1.93° in AB dimer respectively.

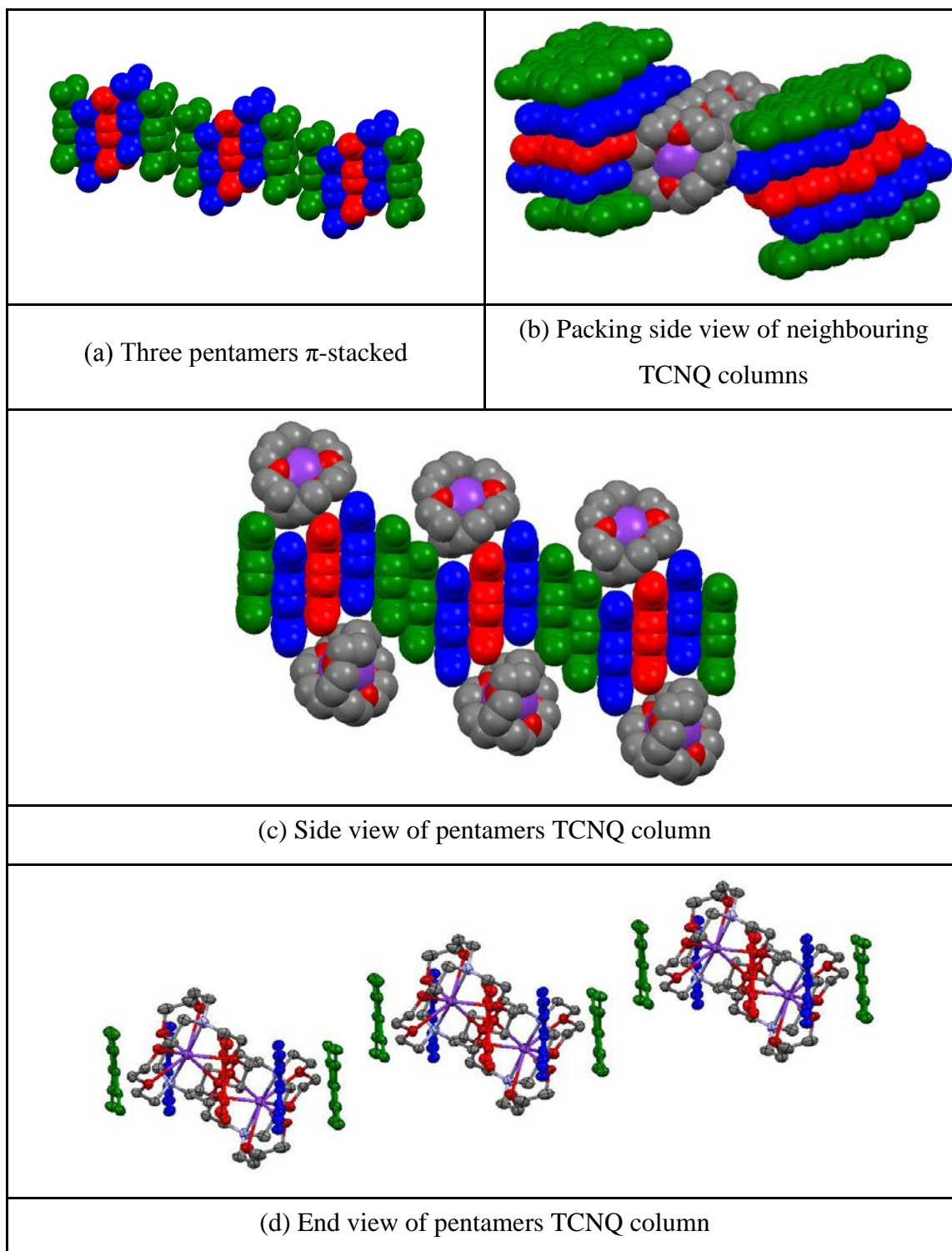


Figure 3.121 Views of pentamers geometry and packing pattern in TCNQ column
(hydrogen atoms are excluded)

As viewed in Figure 3.121, the X-ray structural studies reveal that this is a 2:5 (C222)K(TCNQ)_{2.5} complex. It consists of two cation complexes K⁺(C222) together with three TCNQ⁰ and two TCNQ^{•-} units. The K(TCNQ)_{2.5} and C222 can form alternating stacks as viewed in packing diagram. The TCNQ units are assembled into infinite π - π stacks, which are lying between two layers of (C222)K⁺ cation complexes. A side view of the TCNQ units reveals a wave-like pattern of infinite stack with long-axis slippage between adjacent TCNQ units. The cation complexes of (C222)K⁺ sit in the cavities formed between the TCNQ columns. Distance and angles within the TCNQ stacks are summarised in Table 3.42.

| TCNQ units | | CA | AB | Inter-pentamer neighbours |
|--|--------------|-------|-------|---------------------------|
| π - π perpendicular distance (Å) | | 3.12 | 3.27 | 3.00 |
| Short-axis slip | Distance (Å) | 0.15 | 0.38 | 3.68 |
| | Angle (°) | 2.71 | 6.64 | 50.78 |
| Long-axis slip | Distance (Å) | 1.95 | 1.96 | 2.45 |
| | Angle (°) | 31.80 | 30.96 | 39.19 |
| Centroid-centroid distance (Å) | | 3.70 | 3.83 | 5.34 |

Table 3.42 Distances (Å) and angles (°) within the TCNQ stacks of (C222)K(TCNQ)_{2.5}.

From these data, it will be evident that π -facial overlap between inter-pentamer neighbours within a column is not ideal for extended π - π delocalisation within the column. Figure 3.122 shows K⁺-N and K⁺-O distances in (C222)K(TCNQ)_{2.5}.

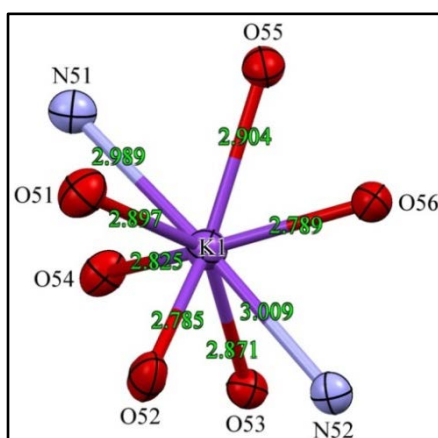


Figure 3.122 K⁺-N and K⁺-O distances (Å) (green labels) in (C222)K(TCNQ)_{2.5} (carbon and hydrogen atoms are excluded)

Each K^+ cation is coordinated with six oxygen atoms and two nitrogen atoms on one crown ether unit as viewed in Figure 3.122. Not all of the K^+ -O distances in $(C222)K(TCNQ)_{2.5}$ are equal, which indicates that the K^+ cation is distorted inside the cavity of cryptand. Two K^+ -N distances, which are 2.989 and 3.009 Å respectively, are slightly longer than the sum of the van der Waals' radii (K^+ -N = 2.88 Å)^{269,271} and thus it seems justifiable to regard the metal cation and the nitrogen atoms as not being directly co-ordinated.

3.3.9 Conclusion

It seems that simple ionophore-MTCNQ salts will form if the cavity of crown ether is comparable to the size of the metal ion. Consequently, a sandwich configuration, in which each metal ion will be coordinated by two molecules of crown ether, will be formed if the size of the metal ion is larger than the cavity of crown ether.

Using LiTCNQ, complexes of $(12C4)_2LiTCNQ$, $(12C4)_2Li(TCNQ)_2$, $(15C5)LiTCNQ$, $(15C5)Li(TCNQ)_2 \cdot H_2O$ and $(B15C5)LiTCNQ \cdot H_2O$ have been synthesised. In $(12C4)_2LiTCNQ$, neighbouring $TCNQ^{\bullet-}$ units are twisted (25.94°) in respect to each other in $TCNQ^{\bullet-}$ column. After adding in another molar equivalent of $TCNQ^0$, neighbouring $TCNQ$ units are no longer twisted, but because of the similarity of the c bond length within each $TCNQ$ units, it is hard to distinguish between $TCNQ^0$ and $TCNQ^{\bullet-}$, which suggests that the electrons are delocalised between the $TCNQ$ units. In $(15C5)LiTCNQ$, the Li^+ ion can fit into the cavity of crown ether and is coordinated by one adjacent $TCNQ^{\bullet-}$ unit. Consequently, the $TCNQ^{\bullet-}$ units form infinite columns made up of pairs of $TCNQ^{\bullet-}$ dimers. Meanwhile, in $(15C5)Li(TCNQ)_2 \cdot H_2O$, the Li^+ ion is coordinated by one H_2O molecule instead of either $TCNQ^0$ or $TCNQ^{\bullet-}$. The similarity of c bond lengths make it difficult to distinguish between $TCNQ^0$ and $TCNQ^{\bullet-}$, which indicates the electrons are delocalised between the $TCNQ$ units. In $(B15C5)LiTCNQ \cdot H_2O$, the Li^+ ion is coordinated to one H_2O molecule and there is no direct coordination between the $TCNQ^{\bullet-}$ units. However, a $CN \cdots H$ hydrogen bond is formed between H_2O molecule and adjacent nitrile group on the $TCNQ^{\bullet-}$ unit. Each $TCNQ^{\bullet-}$ column is made up of pairs of $TCNQ^{\bullet-}$ dimers with cation complex of $(B15C5)Li^+ \cdot H_2O$ sitting in the cavity between the $TCNQ^{\bullet-}$ columns.

Using NaTCNQ, in this study, complexes of $(12C4)_2NaTCNQ$, $(12C4)_2Na(TCNQ)_2$, $(15C5)NaTCNQ$, $(15C5)Na(TCNQ)_2 \cdot H_2O$ and $(18C6)Na(TCNQ)_2 \cdot 2H_2O$ have been isolated and characterised. The size of Na^+ matches that of the cavity in 15C5 very well but is larger than that of 12C4, which results in formation of a sandwich complex, and is smaller than the cavity of 18C6, in which the Na^+ ion is found to be disordered.

$(12C4)_2NaTCNQ$ is iso-structural with $(12C4)_2LiTCNQ$, in which adjacent $TCNQ^{\bullet-}$ units are twisted (25.96°) in respect to each other in $TCNQ^{\bullet-}$ column. After mixing with $TCNQ^0$, dimer pairs of TCNQ units form columns with cation complex of $(12C4)_2Na^+$ sitting in the channels between the TCNQ columns; neighbouring TCNQ units are not twisted in respect to each other. The electrons appear to be delocalised within TCNQ columns because it is difficult to distinguish between the components $TCNQ^0$ and $TCNQ^{\bullet-}$ based on the corresponding c bond lengths. $(15C5)NaTCNQ$ is iso-structural with $(15C5)LiTCNQ$. However, two cyano groups are associated with the Na^+ ion instead of one for the corresponding lithium salt. In $(15C5)Na(TCNQ)_2 \cdot H_2O$, each Na^+ ion is directly coordinated to one H_2O molecule instead of $TCNQ^0$ or $TCNQ^{\bullet-}$.

Consequently, TCNQ units form separated tetramer, which is made up of two pairs of isolated TCNQ dimers as the repeating units instead of an infinite column. A $CN \cdots H$ hydrogen bond is formed between a hydrogen atom from H_2O molecule and a nitrogen atom from adjacent TCNQ unit. Similarly, in $(15C5)Li(TCNQ)_2 \cdot H_2O$, the electrons are delocalised within TCNQ dimer because it is hard to distinguish the components of $TCNQ^0$ and $TCNQ^{\bullet-}$ based on c bond lengths. In $(18C6)Na(TCNQ)_2 \cdot 2H_2O$ each Na^+ ion is disordered inside the cavity of 18C6, the H_2O molecules contribute to the coordination sphere around the Na^+ ion. Each TCNQ column is made up of a TCNQ dimer with cation complex $(18C6)Na^+ \cdot 2H_2O$ fitting in the channels between the TCNQ columns. Consequently, a $CN \cdots H$ hydrogen bond is formed between each H_2O molecule and adjacent cyano group.

For K^+ ion salts in this study, complexes of $(12C4)_2K(TCNQ)_2$, $(18C6)KTCNQ$, $(18C6)K(TCNQ)_{2.5}$, $(B18C6)K(TCNQ)_2$, $(DB18C6)K(TCNQ)_2$, $(Dicyc18C6)K(TCNQ)_3$ and $(C222)K(TCNQ)_{2.5}$ have been synthesised. The K^+ ion can fit into the cavity of 18C6, B18C6, DB18C6, Dicyc18C6 and C222 but is larger than the cavity of 12C4 and 15C5, and forms a sandwich complex in $(12C4)_2K(TCNQ)_2$ and $(15C5)_2KTCNQ^{107,131}$, respectively. In $(12C4)_2K(TCNQ)_2$, dimer pairs of TCNQ units form infinite columns with cation complex $(12C4)_2K^+$ sitting in the cavity between

TCNQ columns. The electrons are delocalised between TCNQ units because it is difficult to distinguish the components TCNQ^0 and $\text{TCNQ}^{\bullet-}$ from the corresponding bond lengths. In $(18\text{C}6)\text{KTCNQ}^{131}$, each K^+ ion is coordinated to two neighbouring $\text{TCNQ}^{\bullet-}$ units, and assembles into a brickwork structure of $\text{TCNQ}^{\bullet-}$ dimers associated with the metal-crown ether units. In both $(18\text{C}6)\text{K}(\text{TCNQ})_{2.5}$ and $(\text{C}222)\text{K}(\text{TCNQ})_{2.5}$, TCNQ units form pentamer as the repeating unit, which assembles into infinite columns with the corresponding cation complex $(18\text{C}6)\text{K}^+$ or $(\text{C}222)\text{K}^+$ sitting in the cavity between TCNQ columns. Within the TCNQ pentamer, TCNQ units prefer to form mixed stacks, in which the average negative charge on the five TCNQ units is -0.4 electrons. The difference between these two TCNQ salts is that the packing pattern of neighbouring pentamer units in $(18\text{C}6)\text{K}(\text{TCNQ})_{2.5}$ have dimer character with significant short-axis slip in respect to each other. In both $(\text{B}18\text{C}6)\text{K}(\text{TCNQ})_2$ and $(\text{DB}18\text{C}6)\text{K}(\text{TCNQ})_2$, neighbouring cation complexes forms a $\text{K}^+-\pi$ associated dimer structure of $[(\text{B}18\text{C}6)\text{K}^+]_2$ and $[(\text{DB}18\text{C}6)\text{K}^+]_2$, respectively. The associated TCNQ units form dimers, which are assembled into infinite columns with the corresponding cation complexes sitting in the cavity between TCNQ columns. The electrons are delocalised within TCNQ units because it is difficult to distinguish TCNQ^0 and $\text{TCNQ}^{\bullet-}$ from the corresponding bond lengths. In $(\text{Dicyc}18\text{C}6)\text{K}(\text{TCNQ})_3$, each K^+ ion is coordinated by one crown ether and two nitrile groups on adjacent TCNQ units. In the TCNQ repeating motif, each pair of TCNQ dimers is separated by an isolated TCNQ unit thereby forming infinite TCNQ columns. The cation complex of $(\text{Dicyc}18\text{C}6)\text{K}^+$ is sitting in the cavity between TCNQ columns.

For the Cs^+ salts prepared in this study, complexes of $(18\text{C}6)\text{Cs}(\text{TCNQ})_2$ and $(\text{B}15\text{C}5)_2\text{Cs}(\text{TCNQ})_3$ have been synthesised. In both of these, TCNQ units form a trimer as the repeating unit, which can be assembled into an infinite column with the corresponding cation complexes sitting in the cavity between TCNQ columns. In the TCNQ trimer, TCNQ units prefer to form mixed stacks as indicated by the corresponding c bond lengths.

3.4 Ionophore Encapsulated MTCNQ Salts (M = Rb)

In a parallel study, it had been decided to prepare a significant number of RbTCNQ complexes to provide a useful data set for one particular metal ion. Complexes of $(12C4)Rb(TCNQ)_{1.5}$, $(15C5)_2RbTCNQ$, $(18C6)Rb(TCNQ)_2$, $(DB18C6)RbTCNQ$, $(DC18C6)Rb(TCNQ)_3$ and $(C222)Rb(TCNQ)_{2.5}$ will be described together with the preparative method used and an analysis of the crystal structures obtained.

3.4.1 Preparation of $(12C4)Rb(TCNQ)_{1.5}$

Reaction of 12C4 with $Rb_2(TCNQ)_3$ (ratio 4:1) in dry acetonitrile afforded a yield (23%) of a plate of blue crystalline solid which contained single crystals suitable for X-ray structural study (combustion data is awaited). Full details including an account of the structure solution and refinement are reported in the Experimental Section and the Supporting Information (in the Appendices) respectively. The crystals obtained were of $(12C4)Rb(TCNQ)_{1.5}$ and the core unit being shown in Figure 3.123.

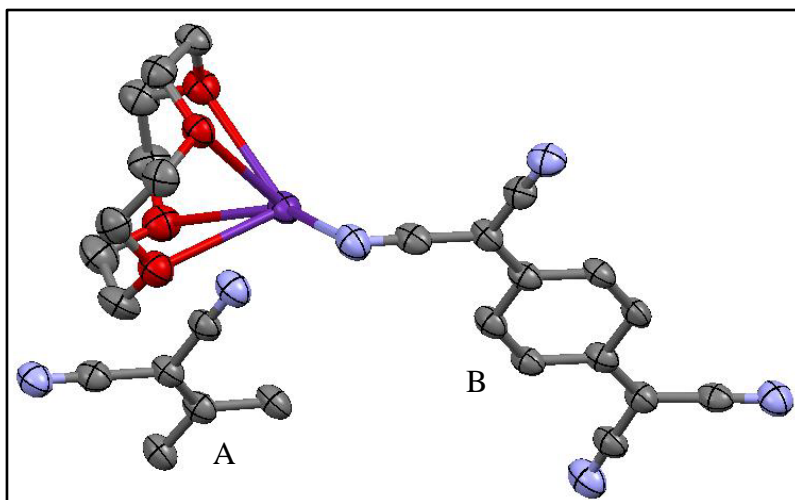


Figure 3.123 Core unit of $(12C4)Rb(TCNQ)_{1.5}$ (hydrogen atoms are excluded)

Bond lengths within the TCNQ units are summarised in Table 3.43. In this structure, the Rb^+ ion is coordinated by four oxygen atoms from 12C4 and four nitrogen atoms from adjacent TCNQ units. The TCNQ units form a dimer which is significantly short-axis slipped (see Figure 3.124). Figure 3.125 shows the TCNQ dimer geometries in $(12C4)Rb(TCNQ)_{1.5}$ exhibiting short-axis slip and distortion from planarity.

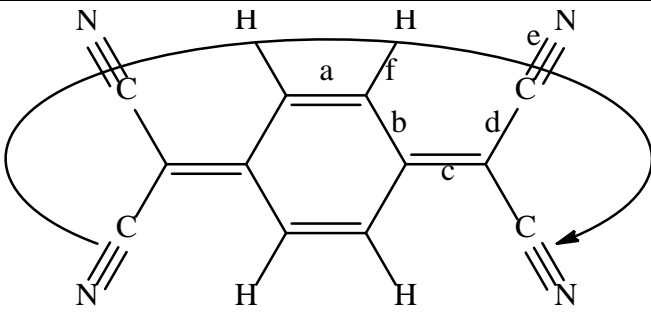
|  | | | | | | |
|--|------------------|-----------|-----------|-----------|-----------|-------|
| (a) Definition of the bond lengths within the TCNQ molecule | | | | | | |
| Structure | Bond lengths (Å) | | | | | |
| | a | b | c | d | e | f |
| TCNQ unit (A) | | 1.442 (5) | | 1.445 (5) | 1.146 (5) | 0.949 |
| | 1.354 (5) | 1.446 (5) | 1.377 (5) | 1.443 (4) | 1.140 (4) | 0.950 |
| | 1.354 (5) | 1.442 (5) | 1.377 (5) | 1.445 (5) | 1.146 (5) | 0.949 |
| | | 1.446 (5) | | 1.443 (4) | 1.140 (4) | 0.950 |
| TCNQ unit (B) | | 1.435 (4) | | 1.421 (5) | 1.157 (5) | 0.950 |
| | 1.374 (5) | 1.425 (5) | 1.417 (5) | 1.425 (5) | 1.156 (5) | 0.950 |
| | 1.363 (5) | 1.423 (5) | 1.425 (5) | 1.420 (5) | 1.154 (5) | 0.951 |
| | | 1.422 (4) | | 1.417 (5) | 1.154 (5) | 0.950 |

Table 3.43 Summary of bond lengths (Å) observed for TCNQ units in $(12C_4)Rb(TCNQ)_{1.5}$

The data in Table 3.43 suggest that both TCNQ units (A and B) have some quinonoidal character because bond length “a” is less than “b”. After measuring the c bond lengths in each TCNQ unit, it seems that TCNQ unit (A) has less electron density, which suggests the assignment of $TCNQ^0$ character. Consequently, TCNQ unit (B) is more electron rich, which supports the assignment of $TCNQ^{\cdot-}$ character. Neighbouring TCNQ dimers are separated by an isolated TCNQ unit, and form a ladder array with significant long-axis slippage as viewed in Figure 3.126.

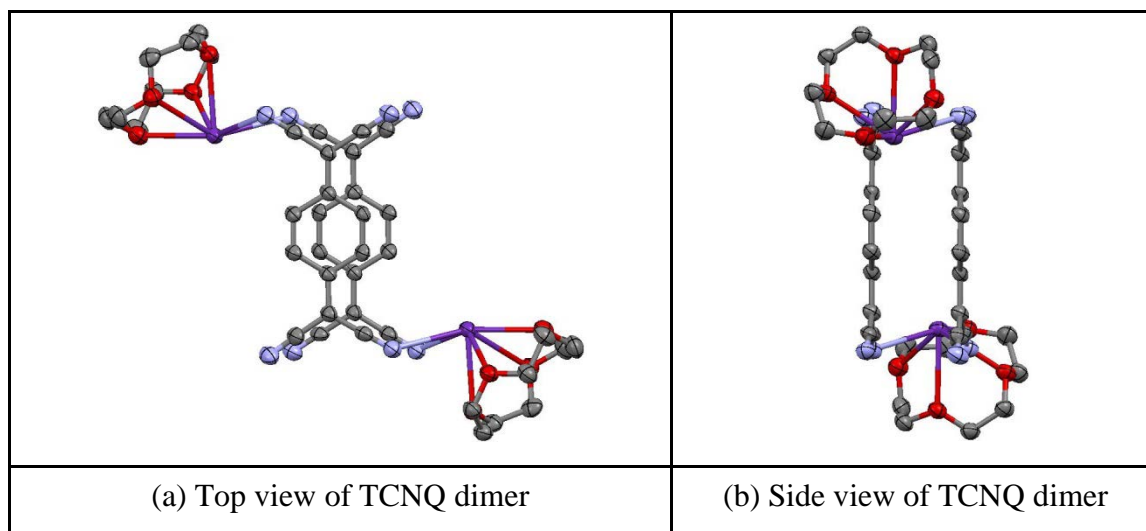


Figure 3.124 Top (a) and side (b) views of TCNQ dimer in $(12C4)Rb(TCNQ)_{1.5}$
(hydrogen atoms are excluded)

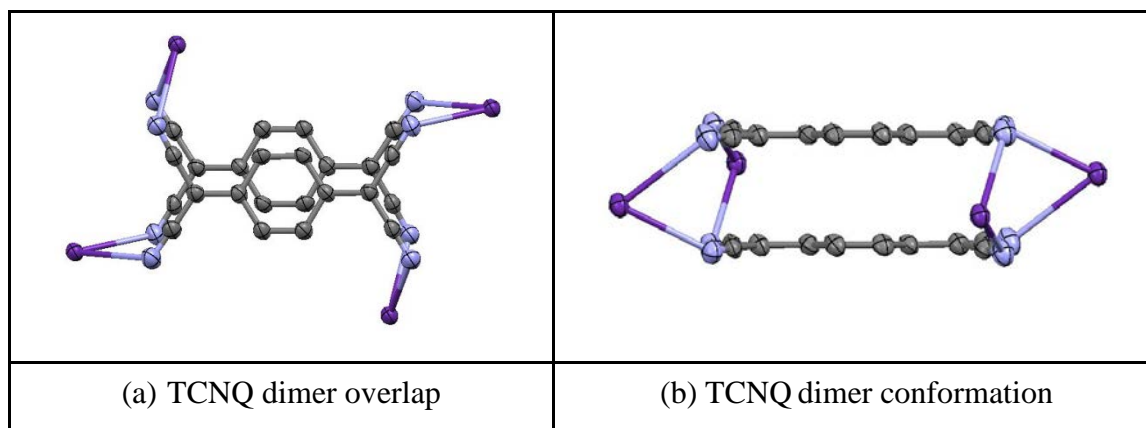


Figure 3.125 TCNQ dimers geometries in $(12C4)Rb(TCNQ)_{1.5}$ (hydrogen atoms are excluded)

Figure 3.126 shows the packing pattern of the TCNQ dimers in $(12C4)Rb(TCNQ)_{1.5}$. As viewed in Figure 3.126, the packing pattern of $(12C4)Rb(TCNQ)_{1.5}$ can be regarded as forming a polymeric chain, in which each Rb^+ ion is coordinated to one crown ether unit and four adjacent TCNQ units. The resulting cation complex of $(12C4)Rb^+$ is located at both ends of TCNQ dimer sheet. Because the size of the Rb^+ ion is much larger than the cavity of 12C4, four surrounding nitrogen atoms compensate in the coordination sphere of the Rb^+ ion. Within each TCNQ dimer, the individual TCNQ mean planes (as defined by benzene ring) are parallel and have equal π - π perpendicular distances in respect to adjacent TCNQ units. The TCNQ dimer here refers to two TCNQ units which are closely face-to-face π -stacked and short-axis slipped, further forming an infinite sheet as viewed in the overall packing pattern of $(12C4)Rb(TCNQ)_{1.5}$. Each TCNQ unit adopts a

planar paddle geometry, in which both ends of $-\text{C}(\text{CN})_2$ groups are tilted by *ca.* 5.16° and 6.16° in respect to the central benzene ring. Consequently, each pair of TCNQ dimer is separated by an isolated TCNQ unit with significant long-axis slip. The extra volume of the additional TCNQ molecule changes the packing motif in $(12\text{C}4)\text{Rb}(\text{TCNQ})_{1.5}$ compared to the brickwork packing pattern seen in $(18\text{C}6)\text{RbTCNQ}$ (ref code: SEKZAJ)²⁷². In the latter, each Rb^+ ion is coordinated to two adjacent $\text{TCNQ}^{\bullet-}$ units and results in a brickwork motif of $\text{TCNQ}^{\bullet-}$ dimers bounded by the cation complexes, neighbouring $\text{TCNQ}^{\bullet-}$ columns forming a herringbone packing pattern²⁷².

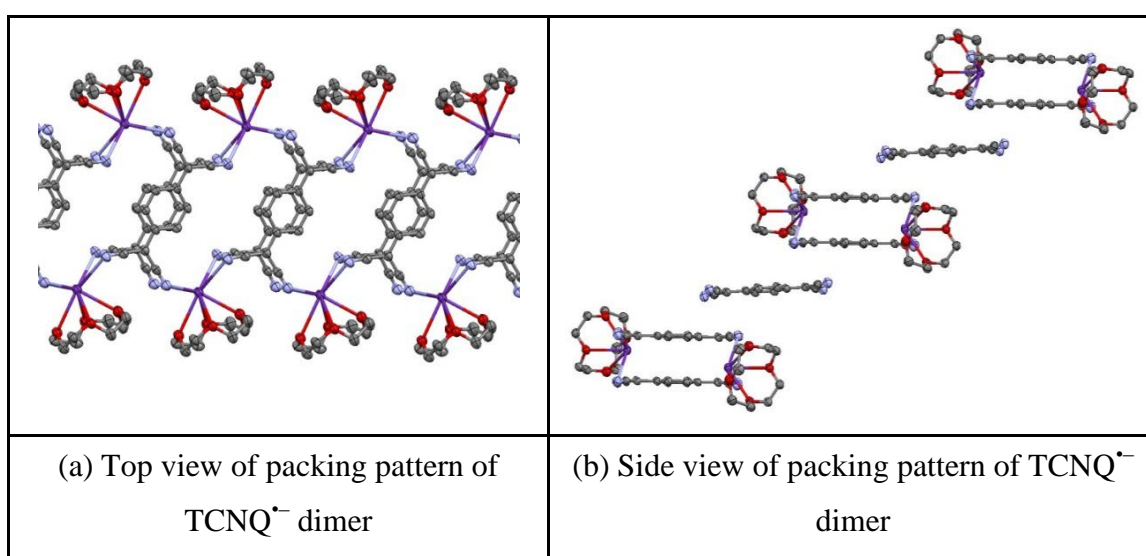


Figure 3.126 Top (a) and side (b) views of packing pattern of $\text{TCNQ}^{\bullet-}$ dimer in $(12\text{C}4)\text{Rb}(\text{TCNQ})_{1.5}$ (hydrogen atoms are excluded)

Distances and angles within the TCNQ stacks are summarised in Table 3.44.

| TCNQ units | | TCNQ dimer |
|--|--------------------|------------|
| π - π perpendicular distance (Å) | | 3.15 |
| Short-axis slip | Distance (Å) | 0.89 |
| | Angle ($^\circ$) | 15.77 |
| Long-axis slip | Distance (Å) | 0.039 |
| | Angle ($^\circ$) | 0.71 |
| Centroid-centroid distance (Å) | | 3.28 |

Table 3.44 Distances (Å) and angles ($^\circ$) within the TCNQ stacks of $(12\text{C}4)\text{Rb}(\text{TCNQ})_{1.5}$

Figure 3.127 summarises the various contact distances within the cation complex of $(12C4)Rb(TCNQ)_{1.5}$.

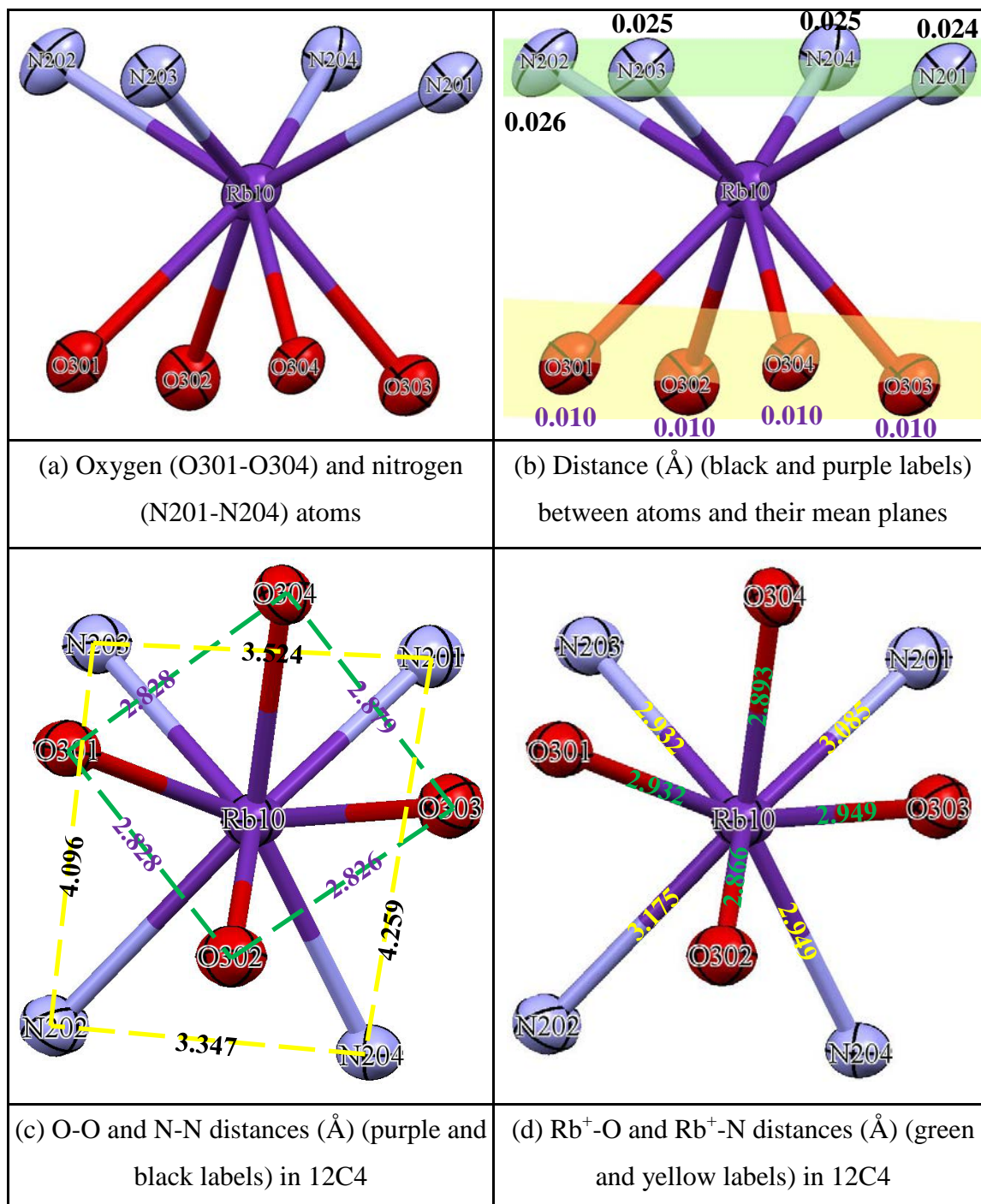


Figure 3.127 Various contact distances (Å) within the cation complex of $(12C4)Rb(TCNQ)_{1.5}$ (carbon and hydrogen atoms are excluded)

As viewed in Figure 3.127, all of the four oxygen atoms are sitting exactly on their mean plane (as defined by each set of oxygen atoms). Each set of four oxygen atoms forms an irregular quadrilateral geometry of mean side by *ca.* 2.840 Å. Not all of the

$\text{Rb}^+\text{-O}$ distances are equal, and the Rb^+ cation is distorted above the cavity of the crown ether unit. Consequently, each set of four nitrogen atoms forms an irregular rectangular geometry of mean side *ca.* 3.807 Å. The average distance of $\text{Rb}^+\text{-N}$ is by *ca.* 3.035 Å, which is slightly shorter than the corresponding bond length in $(18\text{C}6)\text{RbTCNQ}$ (3.037 Å)²⁷².

3.4.2 Preparation of $(15\text{C}5)_2\text{RbTCNQ}$

Reaction of 15C5 with $\text{Rb}_2(\text{TCNQ})_3$ and TCNQ^0 (ratio 4:1:2) in dry acetonitrile afforded a yield (14%) of a dark blue crystalline solid which contained single crystals suitable for X-ray structural study (combustion data is awaited). The product after reaction is a mixture of dark blue and bright yellow crystalline solids. The former is the single crystal sample of $(15\text{C}5)_2\text{RbTCNQ}$ but the latter is TCNQ^0 . Full details including an account of the structure solution and refinement are reported in the Experimental Section and the Supporting Information (in the Appendices) respectively. The crystals obtained were of $(15\text{C}5)_2\text{RbTCNQ}$ and the core unit is shown in Figure 3.128. Bond lengths within the TCNQ units are summarised in Table 3.45.

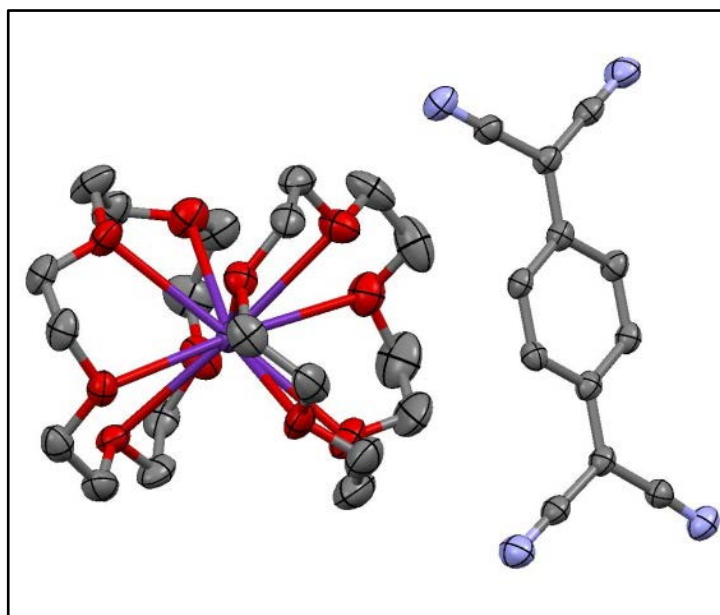


Figure 3.128 Core unit of $(15\text{C}5)_2\text{RbTCNQ}$ (hydrogen atoms are excluded)

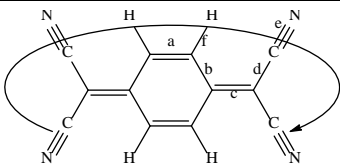
|  | | | | | | |
|---|------------------|-----------|-----------|-----------|-----------|-------|
| (a) Definition of the bond lengths within the TCNQ ^{•-} molecule | | | | | | |
| Structure | Bond lengths (Å) | | | | | |
| | a | b | c | d | e | f |
| TCNQ ^{•-} unit | | 1.417 (3) | | 1.429 (3) | 1.149 (3) | 0.950 |
| | 1.370 (3) | 1.433 (3) | 1.426 (3) | 1.420 (4) | 1.155 (3) | 0.950 |
| | 1.372 (3) | 1.425 (3) | 1.418 (3) | 1.430 (3) | 1.149 (3) | 0.950 |
| | | 1.423 (3) | | 1.418 (4) | 1.156 (3) | 0.950 |

Table 3.45 Summary of bond lengths (Å) observed for TCNQ^{•-} units in (15C5)₂RbTCNQ

In this structure, the Rb⁺ ion is sandwiched between two crown ether units. The TCNQ^{•-} units form a dimer which is significantly short axis slipped and not directly co-ordinated to the Rb⁺ ion (see Figure 3.129).

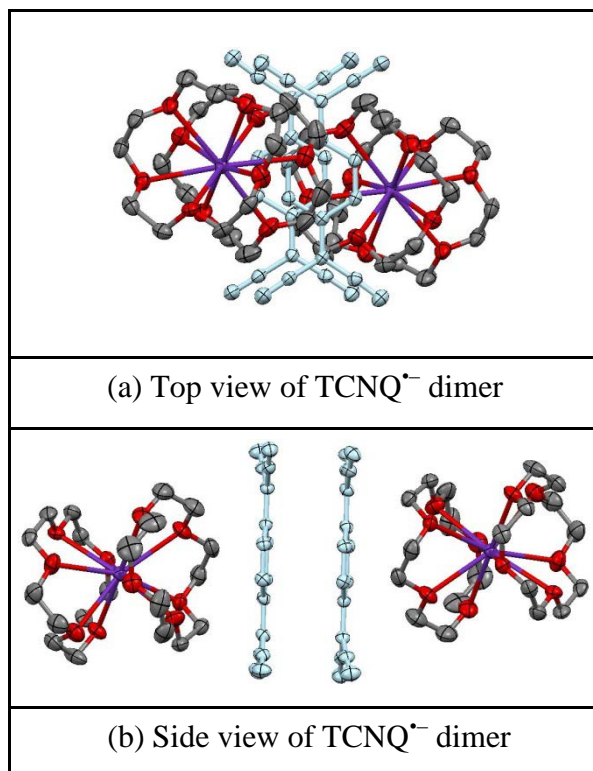


Figure 3.129 Top (a) and side (b) views of TCNQ^{•-} dimer in (15C5)₂RbTCNQ (hydrogen atoms are excluded)

As viewed in Figure 3.129, the packing pattern of $(15C5)_2RbTCNQ$ is similar to that seen in $(15C5)_2KTCNQ$ (ref code: TETYOG)¹⁰⁷. In the latter, each K^+ ion is encapsulated by two molecules of crown ether units. The presence of the ionophore of 15C5 inhibits direct cation-anion interactions and gives an architecture, in which each pair of $TCNQ^{\bullet-}$ dimer is isolated from other $TCNQ^{\bullet-}$ dimers. Consequently, each pair of $TCNQ^{\bullet-}$ dimers is horizontal face-to-face π -stacked between two cation complexes of $(15C5)_2K^+$. In contrast, in $(15C5)_2RbTCNQ$, there are sheets of TCNQ dimer units separated by sheets of cation complexes (see Figure 3.129)¹⁰⁷.

The data in Table 3.45 suggest that $TCNQ^{\bullet-}$ units have some quinonoidal character because bond length “a” is less than “b”. The distribution of bond lengths is the same as those reported for $TCNQ^{\bullet-}$ ²¹³. In $(15C5)_2KTCNQ$, the TCNQ units are of course $TCNQ^{\bullet-}$ and in that case the c bond lengths values which compare well with those in the present structure¹⁰⁷.

Figure 3.130 shows top and side views of the packing pattern of $(15C5)_2RbTCNQ$. $TCNQ^{\bullet-}$ and $(15C5)_2Rb^+$ form 1:1 alternating stacks. The ‘sandwich’ nature of the cation complex prevents the $TCNQ^{\bullet-}$ unit directly coordinating to the metal cation. Surprisingly, the extra $TCNQ^0$ [present in the reaction mixture because of the use of $Rb_2(TCNQ)_3$] does not participate in the reaction as shown by the crystal structure studies of this complex. Individual $TCNQ^{\bullet-}$ units lie parallel in respect to each other within each $TCNQ^{\bullet-}$ dimer. Consequently, the $TCNQ^{\bullet-}$ forms separated dimers with equal π - π perpendicular distance between adjacent $TCNQ^{\bullet-}$ units, which are closely face-to-face π contact and short-axis slipped. The $TCNQ^{\bullet-}$ dimers assemble into infinite parallel sheets as viewed in Figure 3.130(a). Therefore, there is no direct interaction between adjacent pairs of $TCNQ^{\bullet-}$ dimers. Within a $TCNQ^{\bullet-}$ dimer, each $TCNQ^{\bullet-}$ unit adopts a shallow paddle conformation, in which the cyano groups on adjacent $TCNQ^{\bullet-}$ units are pushed away from each other. Figure 3.131 shows the $TCNQ^{\bullet-}$ dimer geometry and the extent of the short-axis slip.

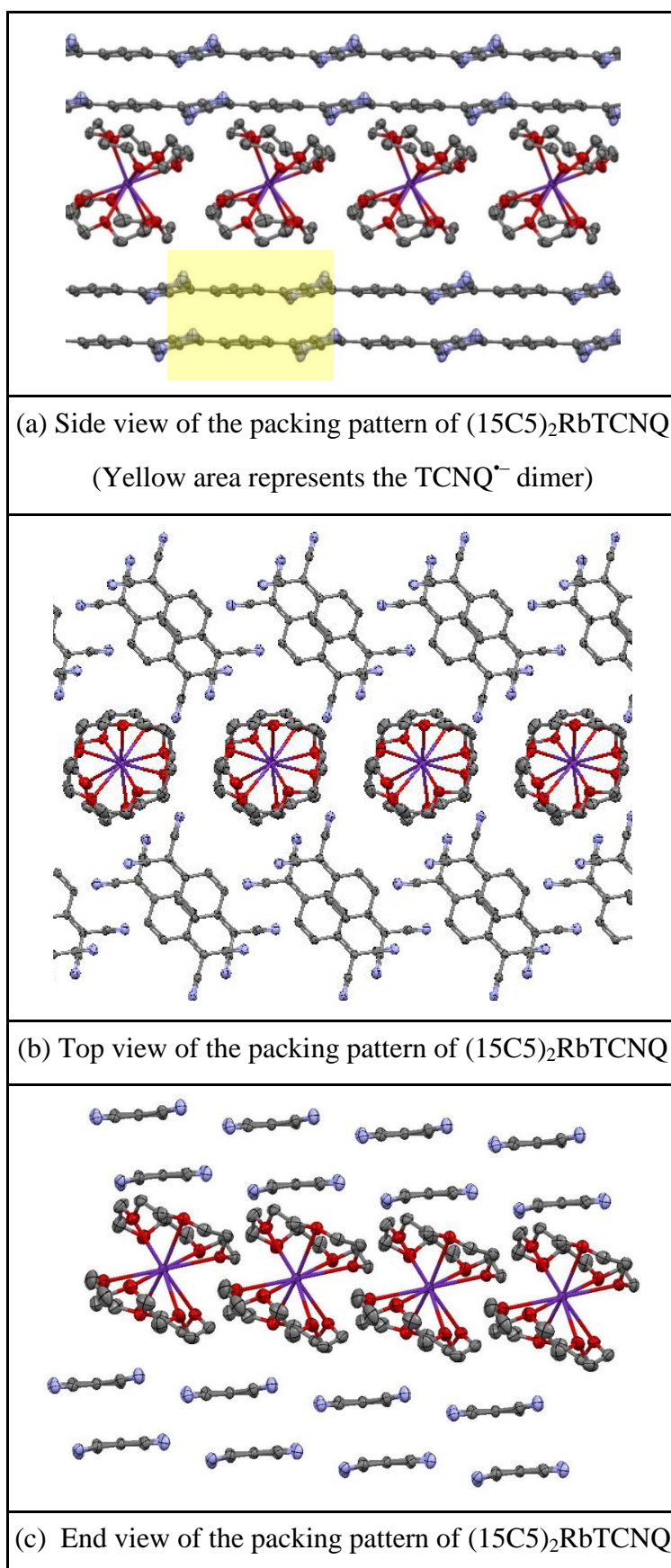


Figure 3.130 Side (a), top (b) and end (c) views of the infinite layers of $(15C5)_2RbTCNQ$ (hydrogen atoms are excluded)

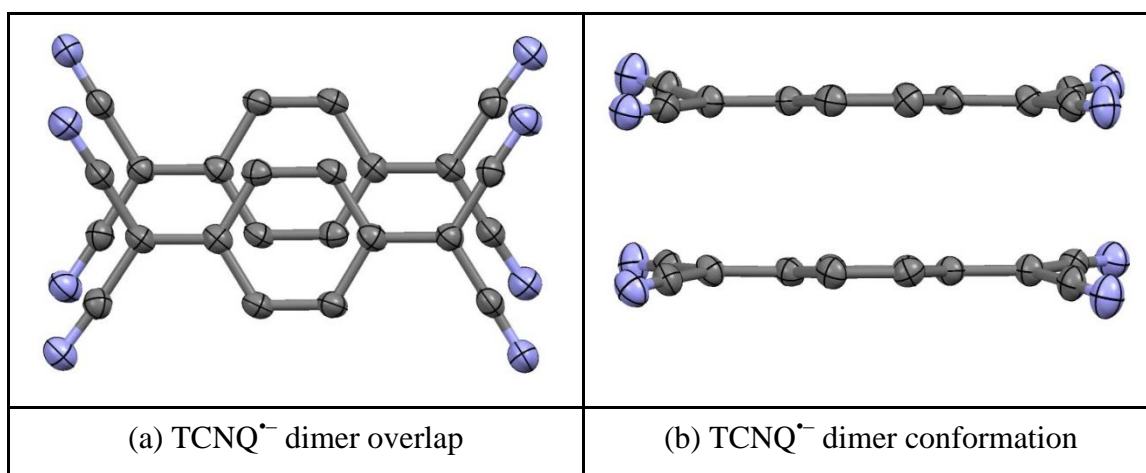


Figure 3.131 TCNQ^{•-} dimers geometries in (15C5)₂RbTCNQ (hydrogen atoms are excluded)

Distance and angles within the TCNQ stacks are summarised in Table 3.46.

| TCNQ ^{•-} units | | TCNQ ^{•-} dimer |
|--|--------------|--------------------------|
| π - π perpendicular distance (Å) | | 3.07 |
| Short-axis slip | Distance (Å) | 1.25 |
| | Angle (°) | 22.11 |
| Long-axis slip | Distance (Å) | 0.0095 |
| | Angle (°) | 0.18 |
| Centroid-centroid distance (Å) | | 3.31 |

Table 3.46 Distances (Å) and angles (°) within the TCNQ^{•-} stacks of (15C5)₂RbTCNQ

Figure 3.132 summarises the various contact distances within the cation complex. The ligating oxygen atoms lay above and below their mean plane (as defined by each set of oxygen atoms) to form irregular pentagon geometry of mean side by *ca.* 2.865 (red) and 2.866 Å (blue), respectively. Not all of the Rb⁺-O distances in the complex of (15C5)₂RbTCNQ are equal but range between 2.938 and 3.119 Å respectively, which demonstrates that the Rb⁺ cation is distorted above the cavity of crown ether unit. Consequently, two crown ether mean planes (defined by a set of oxygen atoms) are tilted in respect to each other by *ca.* 8.66° as viewed in Figure 3.132(b). Compared with the case in (15C5)₂KTCNQ¹⁰⁷, where each set of five oxygen atoms form irregular pentagon geometry of mean side by *ca.* 2.903 and 2.937 Å, which is longer than the

corresponding data in $(15C5)_2RbTCNQ$. Not all of the K^+ -O distances in $(15C5)_2KTCNQ$ are equal but range between 2.815 and 3.204 Å. Consequently, two crown ether mean planes (as defined by a set of oxygen atoms) are tilted in respect to each other by *ca.* 3.77°, which is smaller than the case in $(15C5)_2RbTCNQ$.

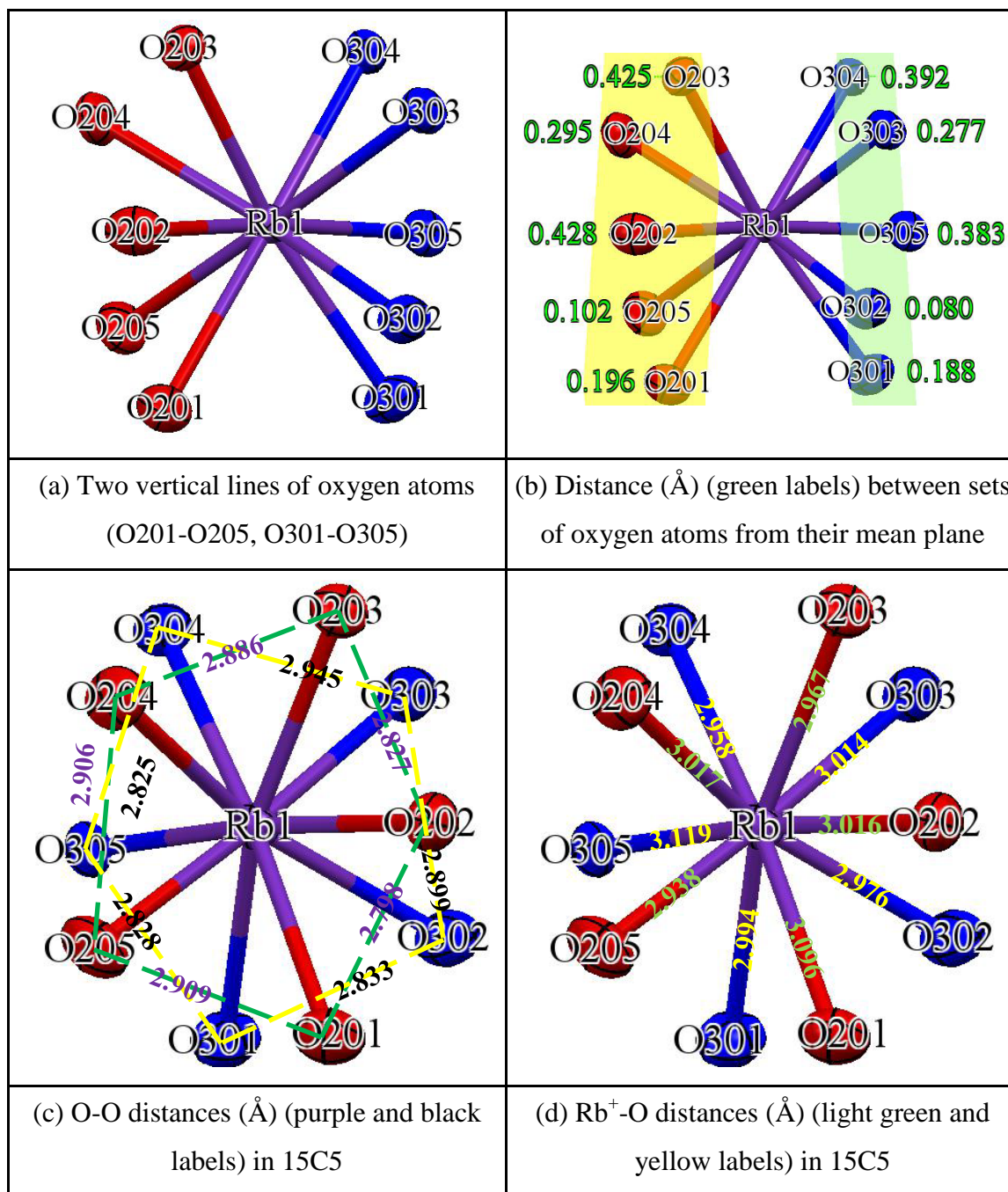


Figure 3.132 Various contact distances (Å) within the cation complex of $(15C5)_2RbTCNQ$ (carbon and hydrogen atoms are excluded)

3.4.3 Preparation of $(18C6)Rb(TCNQ)_2$

Reaction of 18C6 and $Rb_2(TCNQ)_3$ with $TCNQ^0$ (ratio 2:1:2) in dry acetonitrile afforded a reasonable yield (61%) of a plate of dark blue crystalline solid which contained single crystals suitable for X-ray structural study (combustion data is awaited). Full details including an account of the structure solution and refinement are reported in the Experimental Section and the Supporting Information (in the Appendices) respectively. The crystals obtained were of $(18C6)Rb(TCNQ)_2$, in which TCNQ (B) lies on symmetry element, and the core unit is shown in Figure 3.133.

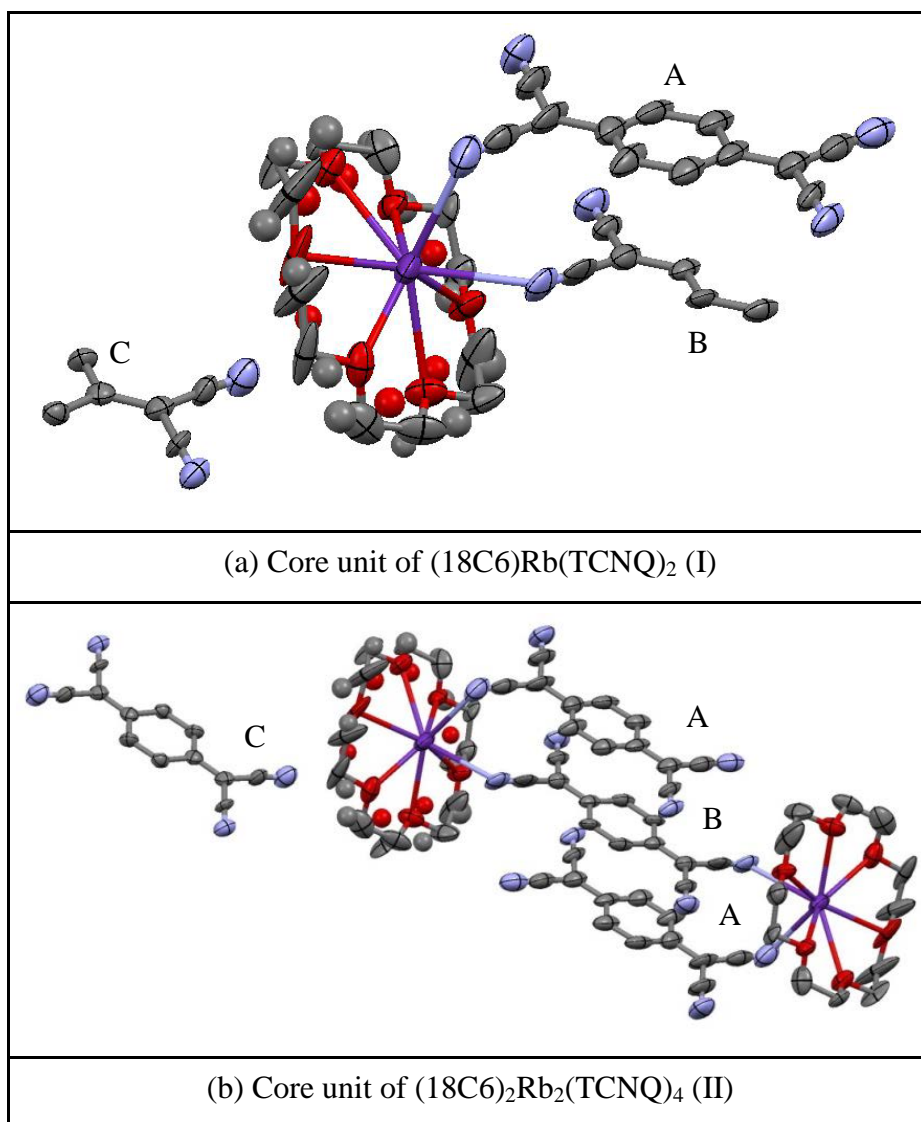


Figure 3.133 Core unit of $(18C6)Rb(TCNQ)_2$ (hydrogen atoms are excluded)

Bond lengths within the TCNQ units are summarised in Table 3.47.

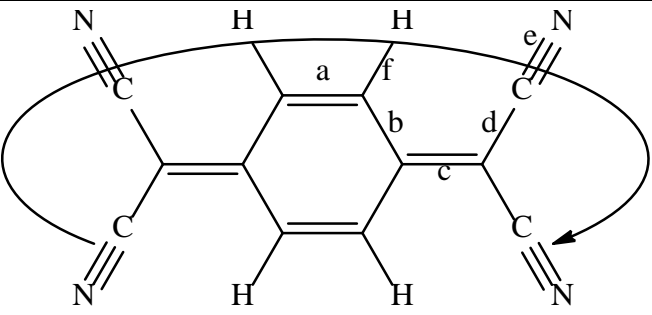
|  | | | | | | |
|--|------------------|------------|------------|------------|------------|-------|
| (a) Definition of the bond lengths within the TCNQ molecule | | | | | | |
| Structure | Bond lengths (Å) | | | | | |
| | a | b | c | d | e | f |
| TCNQ unit (A) | | 1.391 (16) | | 1.492 (19) | 1.124 (15) | 0.950 |
| | 1.400 (14) | 1.397 (17) | 1.437 (14) | 1.418 (18) | 1.130 (16) | 0.950 |
| | 1.364 (14) | 1.431 (15) | 1.412 (13) | 1.387 (17) | 1.176 (15) | 0.950 |
| | | 1.422 (16) | | 1.451 (15) | 1.144 (12) | 0.950 |
| TCNQ unit (B) | | 1.437 (13) | | 1.431 (16) | 1.165 (13) | 0.950 |
| | 1.370 (12) | 1.433 (13) | 1.403 (12) | 1.429 (14) | 1.137 (12) | 0.950 |
| | 1.370 (12) | 1.437 (13) | 1.403 (12) | 1.431 (16) | 1.165 (13) | 0.950 |
| | | 1.433 (13) | | 1.429 (14) | 1.137 (12) | 0.950 |
| TCNQ unit (C) | | 1.431 (15) | | 1.387 (17) | 1.176 (15) | 0.950 |
| | 1.364 (14) | 1.422 (16) | 1.412 (13) | 1.451 (15) | 1.144 (12) | 0.950 |
| | 1.400 (14) | 1.391 (16) | 1.437 (14) | 1.492 (19) | 1.124 (15) | 0.950 |
| | | 1.397 (17) | | 1.418 (18) | 1.130 (16) | 0.950 |

Table 3.47 Summary of bond lengths (Å) observed for TCNQ units in
(18C6)Rb(TCNQ)₂

In this structure, the Rb⁺ ion is coordinated to one crown ether unit and two nitrile groups on adjacent TCNQ units. The TCNQ units form a trimer which is significantly long axis slipped (see Figure 3.134).

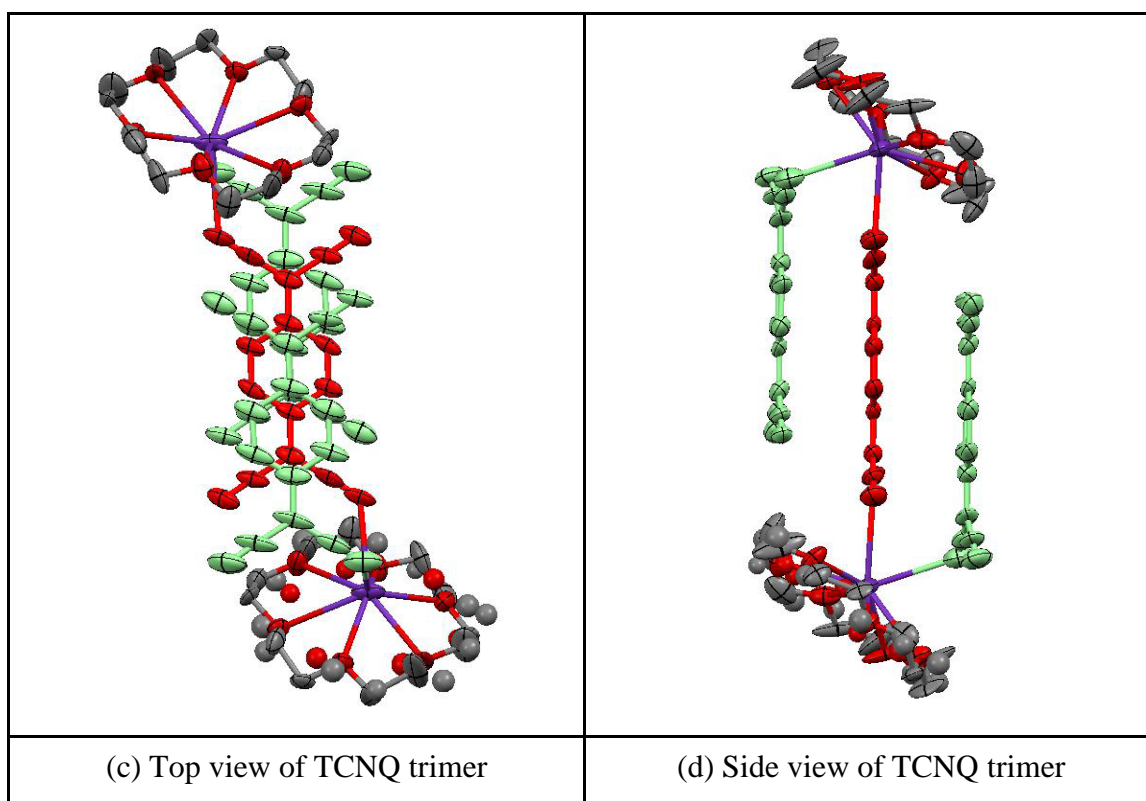


Figure 3.134 Top (a/c) and side (b/d) views of TCNQ trimer in $(18C6)Rb(TCNQ)_2$ (hydrogen atoms are excluded)

The data in Table 3.47 suggest that all of the TCNQ units have some quinonoidal character because bond length “a” is less than “b”. In the TCNQ trimer, after measuring the c bond lengths in each TCNQ unit, it seems that TCNQ unit (A) has more electron density, which suggests $TCNQ^{\cdot-}$ character. Consequently, the TCNQ unit (B) and TCNQ unit (C) have $TCNQ^0$ character. Therefore, in each TCNQ trimer, TCNQ units form mixed stacks, which is $TCNQ^{\cdot-} - TCNQ^0 - TCNQ^{\cdot-}$ configuration as viewed in TCNQ trimer stack in $(18C6)Rb(TCNQ)_2$, which means two electrons delocalised over the three TCNQ units but more negative charge density appears to reside on TCNQ unit (A). Within the crystal, the TCNQ trimers assemble into infinite columns, separated by an isolated TCNQ unit, i.e. the individual TCNQ units are assembled in an ABAC motif (see Figure 3.135), in which trimer neighbours are significantly “diagonally” slipped (see Figure 3.136).

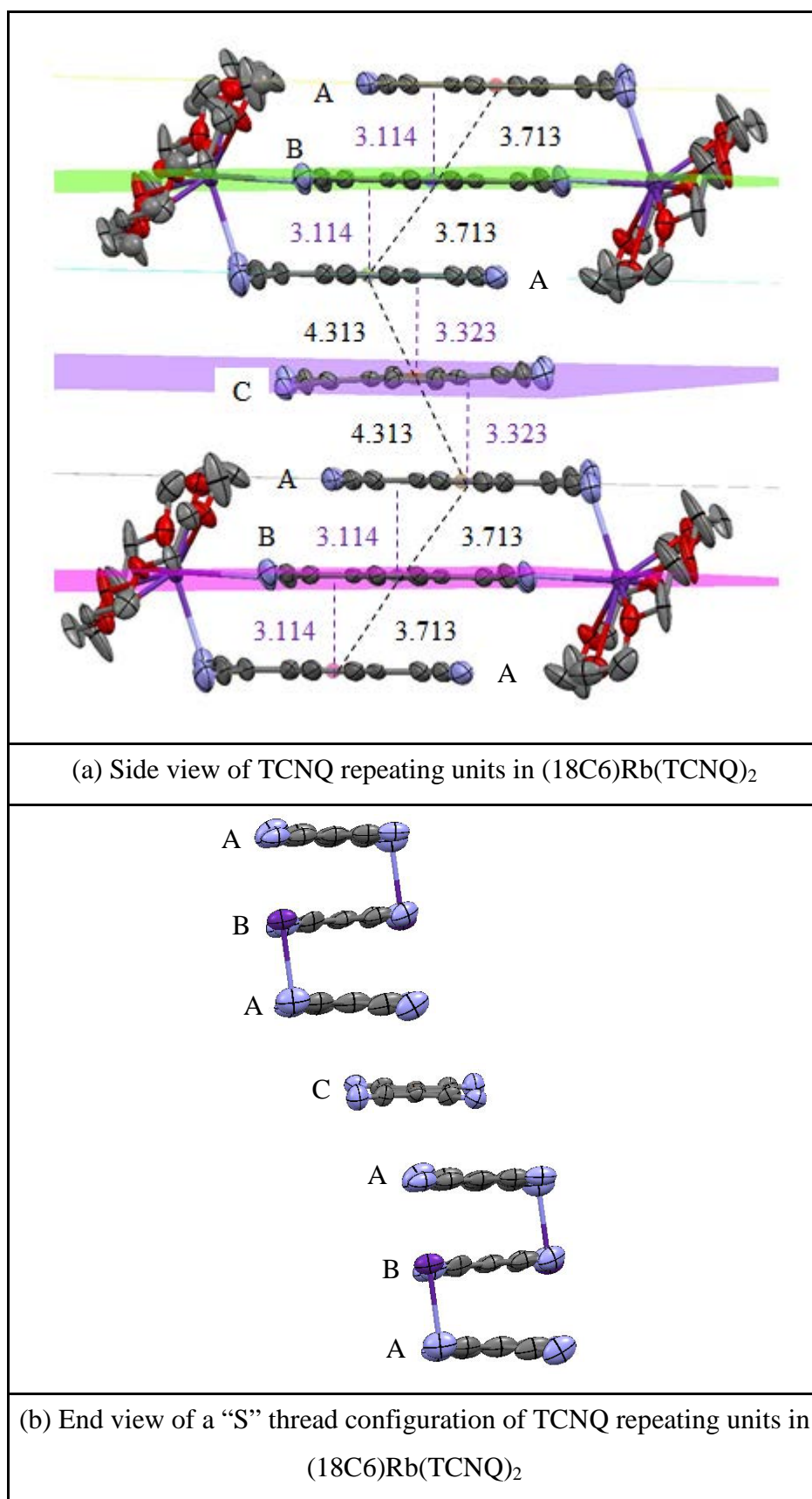


Figure 3.135 Observation of TCNQ repeating units in $(18C6)Rb(TCNQ)_2$ (hydrogen atoms are excluded)

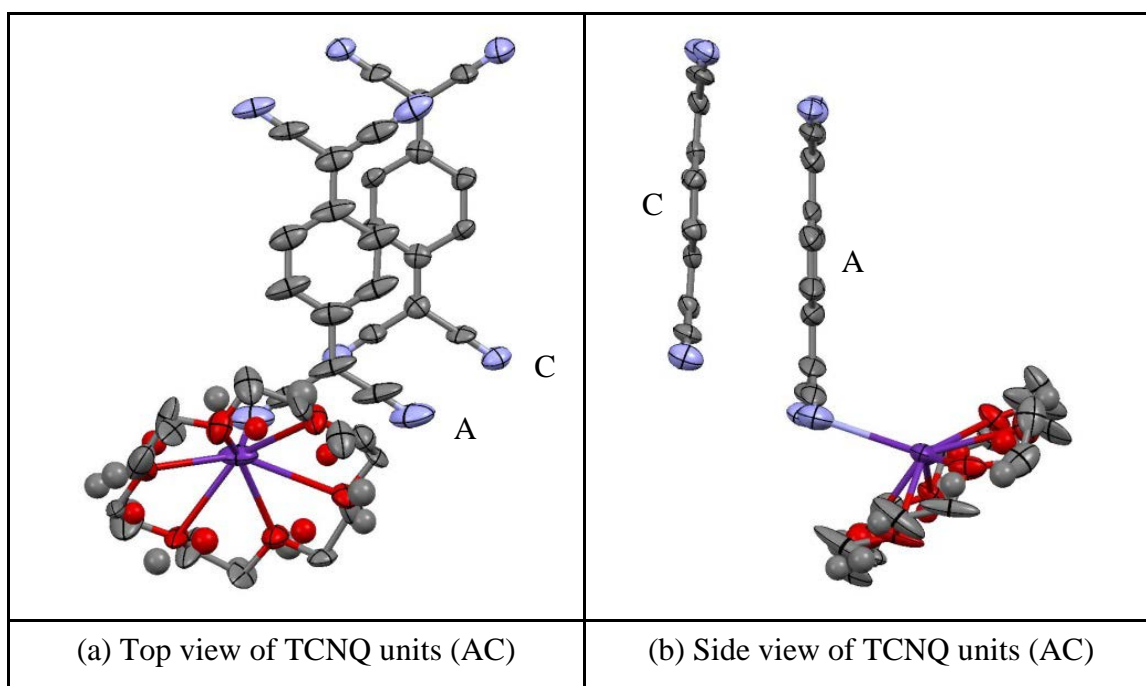


Figure 3.136 Top (a) and side (b) views of TCNQ units (AC) in $(18C6)Rb(TCNQ)_2$ (hydrogen atoms are excluded)

Distances and angles within the TCNQ stacks are summarised in Table 3.48.

| TCNQ units | | TCNQ trimer | AC |
|--|--------------|-------------|-------|
| π - π perpendicular distance (Å) | | 3.11 | 3.32 |
| Short-axis slip | Distance (Å) | 0.15 | 2.20 |
| | Angle (°) | 2.76 | 33.51 |
| Long-axis slip | Distance (Å) | 2.02 | 1.65 |
| | Angle (°) | 32.97 | 26.41 |
| Centroid-centroid distance (Å) | | 3.71 | 4.31 |

Table 3.48 Distances (Å) and angles (°) within the TCNQ stacks of $(18C6)Rb(TCNQ)_2$

From these data, it will be evident that π -facial overlap between TCNQ units (AC) within a column is not ideal for extended π - π delocalisation within the column. As viewed in Figure 3.135, adjacent TCNQ trimers are separated by a $TCNQ^0$ molecule and a side view of the TCNQ units reveals a wave-like pattern of infinite stack with long-axis slippage between adjacent TCNQ units. Each Rb^+ cation is coordinated by one crown ether unit and two adjacent TCNQ units and the resulting complex lies in

channels between the TCNQ columns. The packing pattern in $(18C6)Rb(TCNQ)_2$ is similar as seen for $(18C6)Cs(TCNQ)_2$. In the TCNQ trimer, the individual TCNQ units are tilted in respect to each other by *ca.* 1.54° and having equal π - π perpendicular distance. Consequently, each cation complex of $(18C6)Rb^+$ is coordinated to two cyano groups of the TCNQ trimer. Figure 3.137 shows TCNQ trimer geometries in $(18C6)Rb(TCNQ)_2$.

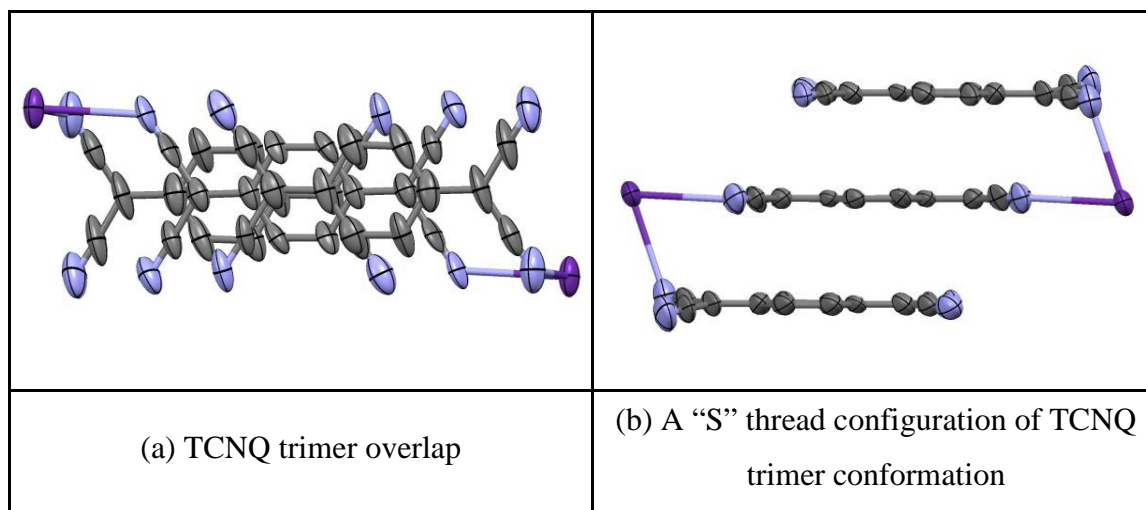


Figure 3.137 TCNQ trimer geometries in $(18C6)Rb(TCNQ)_2$ (hydrogen atoms are excluded)

Figure 3.138 summarises the various contact distances within the cation complex. The crown ether unit is disordered and the atomic occupancy for crown ether ring is 68.2% (ellipsoids atoms) in respect to 31.8% (circle atoms). The ligating ellipsoid oxygen atoms (red) are sitting above and below of their mean plane (as defined by each set of oxygen atoms) to form irregular pentagon geometry of mean side by *ca.* 2.821 \AA and for the circle oxygen atoms (blue), the pentagon geometry of mean side by *ca.* 2.840 \AA . Because of coordination with two adjacent TCNQ units, the Rb^+ cation is "pulled" out of the cavity of crown ether mean plane by *ca.* 0.879 \AA . Not all of the Rb^+-O distances are equal, the Rb^+ ion lying above the cavity of crown ether unit. Two of the Rb^+-N distances are slightly longer than that of a van der Waals' contact ($Rb^+-N = 3.03 \text{ \AA}$)^{269,271}.

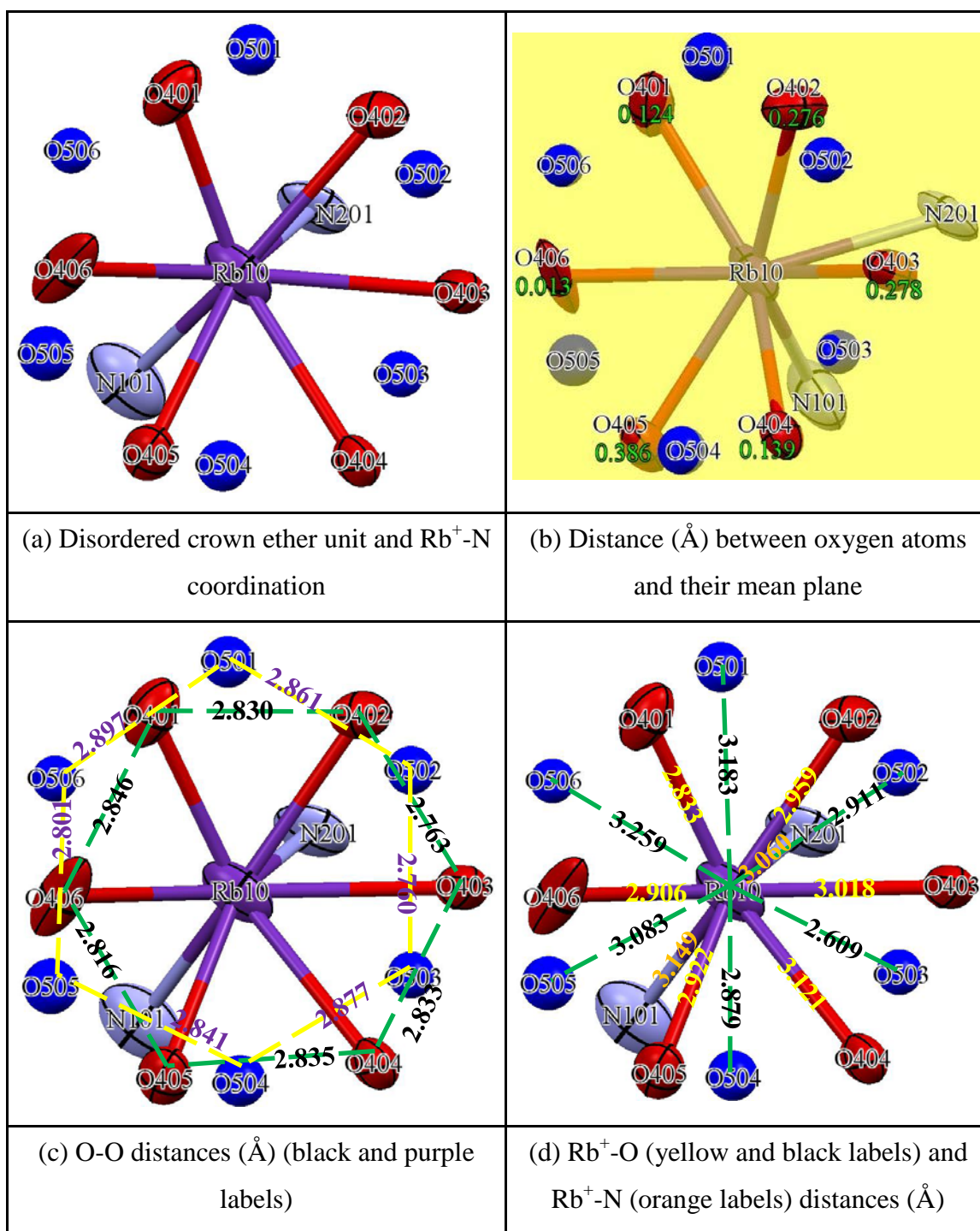


Figure 3.138 Various contact distances (\AA) within the cation complex of $(18\text{C}6)\text{Rb}(\text{TCNQ})_2$ (carbon and hydrogen atoms are excluded)

3.4.4 Preparation of $(\text{DB}18\text{C}6)\text{RbTCNQ}$

Reaction of DB18C6 (Dibenzo-18-crown-6) with $\text{Rb}_2(\text{TCNQ})_3$ and TCNQ^0 (ratio 2:1:2) in dry acetonitrile afforded a yield (25%) of a plate of dark violet crystalline solid (Combustion Analysis: Calculated: C: 59.13%, H: 4.34%, N: 8.61%. Found: C: 59.95%,

H: 4.91%, N: 11.94%) which contained single crystals suitable for X-ray structural study. Full details including an account of the structure solution and refinement are reported in the Experimental Section and the Supporting Information (in the Appendices) respectively. The crystals obtained were of (DB18C6)RbTCNQ and the core unit is shown in Figure 3.139. Bond lengths within the TCNQ units are summarised in Table 3.49.

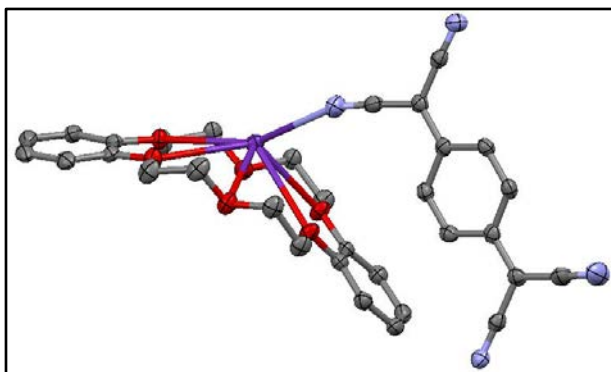
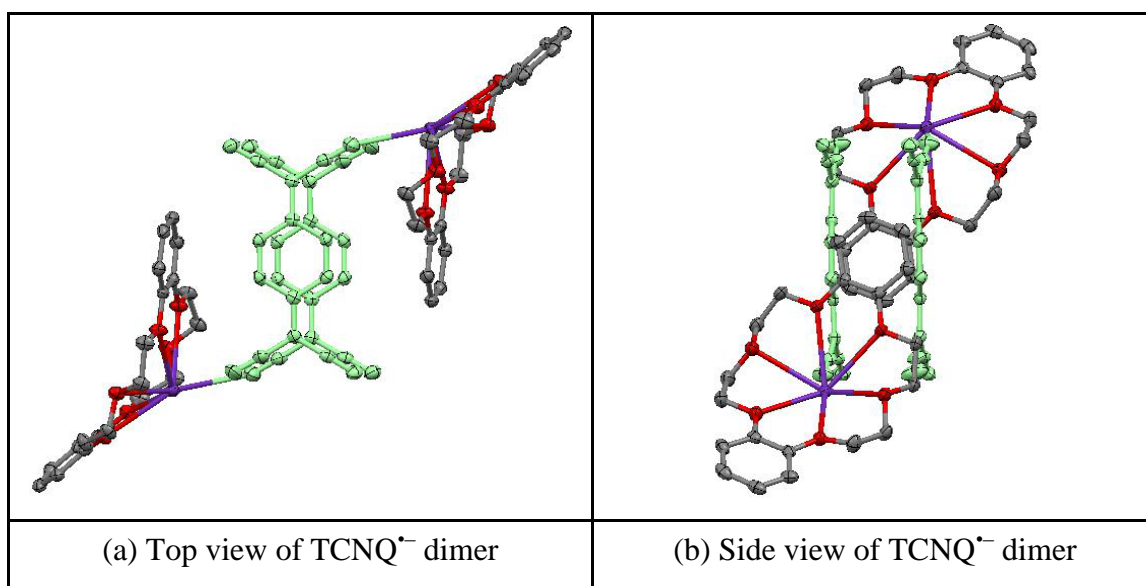


Figure 3.139 Core unit of (DB18C6)RbTCNQ (hydrogen atoms are excluded)

| (a) Definition of the bond lengths within the TCNQ ^{•-} molecule | | | | | | |
|---|------------------|-----------|-----------|-----------|-----------|-------|
| Structure | Bond lengths (Å) | | | | | |
| | a | b | c | d | e | f |
| TCNQ ^{•-} unit | | 1.424 (3) | | 1.421 (3) | 1.152 (3) | 0.950 |
| | 1.363 (3) | 1.424 (3) | 1.421 (3) | 1.419 (3) | 1.148 (3) | 0.950 |
| | 1.367 (3) | 1.427 (3) | 1.421 (3) | 1.423 (3) | 1.150 (3) | 0.950 |
| | | 1.419 (3) | | 1.421 (3) | 1.153 (3) | 0.950 |

Table 3.49 Summary of bond lengths (Å) observed for TCNQ^{•-} units in (DB18C6)RbTCNQ

In this structure, the Rb⁺ ion is coordinated by one crown ether unit and three nitrogen atoms on cyano groups from adjacent TCNQ^{•-} units. The TCNQ^{•-} units form a dimer which is significantly short-axis slipped (see Figure 3.140).

Figure 3.140 Top (a) and side (b) views of TCNQ^{•-} dimer

The data in Table 3.49 suggest that the TCNQ^{•-} has some quinonoidal character because bond length “a” is less than “b”. The distribution of bond lengths is reported for TCNQ^{•-} ²¹³.

Figure 3.142 shows various views of the packing pattern within (DB18C6)RbTCNQ. The TCNQ^{•-} dimers and (DB18C6)Rb⁺ cation complexes form dimers which co-ordinate with lateral neighbours to form extended linear tapes through the structure. Surprisingly, the TCNQ⁰ from Rb₂(TCNQ)₃ does not participate in the crystal structure formed. Indeed the product obtained is a mixture containing a dark violet and a bright yellow crystalline complex. After separation under a microscope and studies by X-ray crystallography, the former is the single crystal sample of (DB18C6)RbTCNQ and the latter is TCNQ⁰. In TCNQ^{•-} dimer, the individual TCNQ^{•-} units are parallel in respect to adjacent TCNQ^{•-} units. Consequently, in the TCNQ^{•-} dimer, the TCNQ^{•-} anions are closely face-to-face π -stack and short-axis slipped (see Figure 3.141). Figure 3.141 shows TCNQ^{•-} dimer geometries in (DB18C6)RbTCNQ, exhibiting the short-axis slip (overlap view) and the distortion from planarity (conformation view). Within the TCNQ^{•-} dimer, the TCNQ^{•-} units are approximately planar with slight twisting at each end of TCNQ^{•-} unit, which allows the cyano groups in adjacent TCNQ^{•-} anions pushed away in respect to each other. Therefore, the packing in (DB18C6)RbTCNQ is dominated by the need to accommodate the volume of the two benzene rings on each crown ether unit and the greater rigidity of DB18C6 when compared with 18C6 itself. Compared with the case in (18C6)RbTCNQ (ref code: SEKZAJ)²⁷², both of the Rb⁺

ions are sitting above the crown ether mean plane (defined by a set of oxygen atoms). For Rb^+ ion in $(\text{DB18C6})\text{RbTCNQ}$, the metal cation has a high coordination environment, six coordinating by oxygen atoms from the crown ether ring and three coordinating by adjacent cyano groups from $\text{TCNQ}^{\bullet-}$ units, which will “pull” the metal ion further away from the crown ether mean plane and will affect the packing pattern of $\text{TCNQ}^{\bullet-}$ dimers. Consequently, the benzene rings on the crown results in the formation of extended polymer chains. In contrast, with the case in $(\text{DB18C6})\text{K}(\text{TCNQ})_2$ in this study, there are no cation- π interactions between adjacent cation complexes.

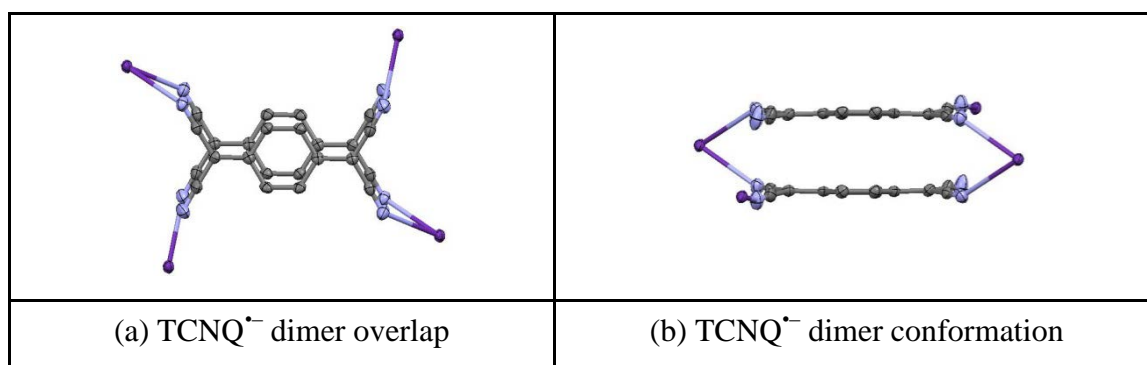


Figure 3.141 $\text{TCNQ}^{\bullet-}$ dimer geometries in $(\text{DB18C6})\text{RbTCNQ}$ (hydrogen atoms are excluded)

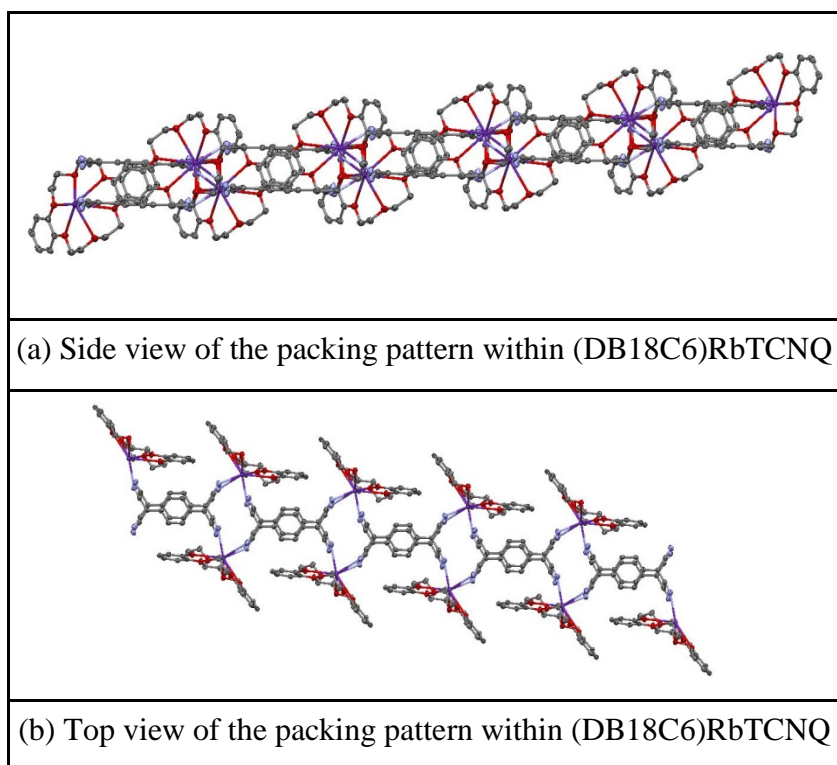


Figure 3.142 Side (a) and top (b) views of the packing pattern within $(\text{DB18C6})\text{RbTCNQ}$ (hydrogen atoms are excluded)

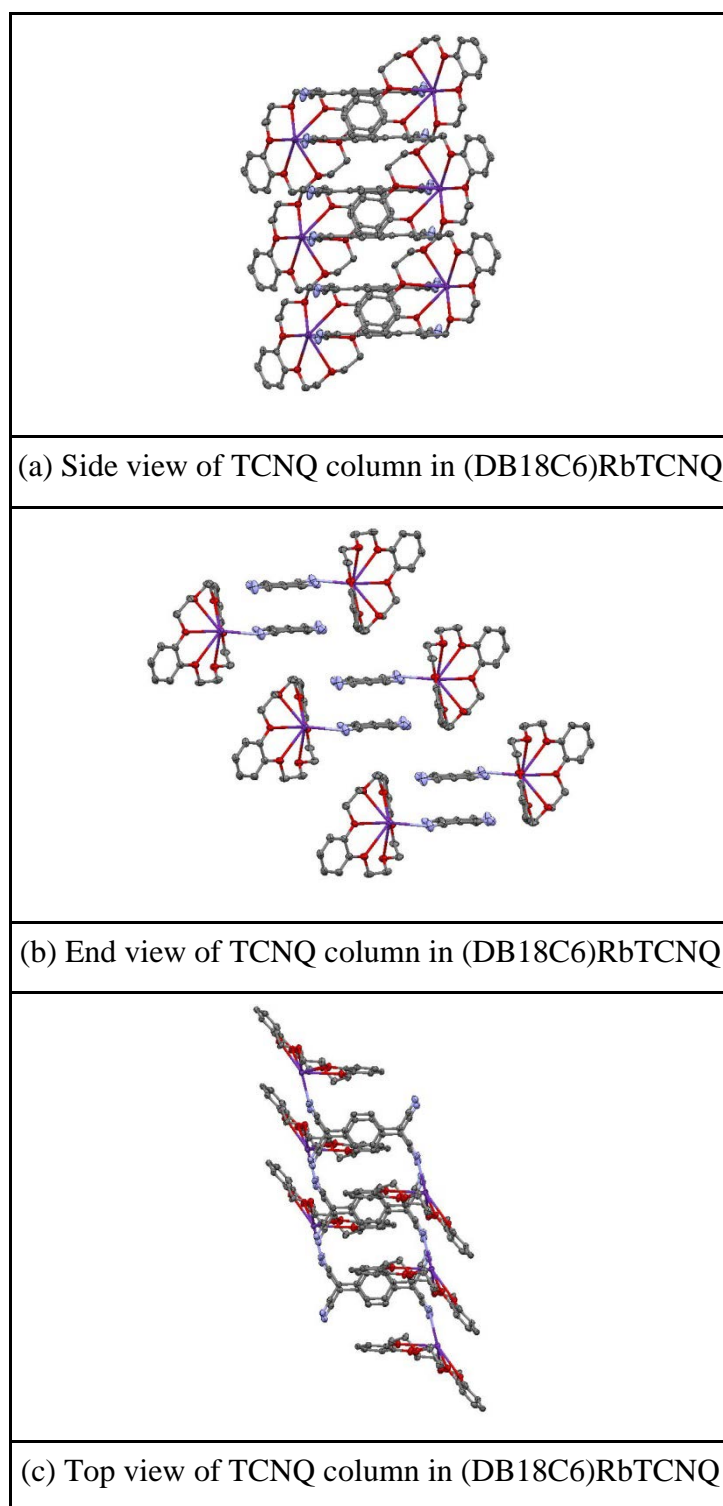


Figure 3.143 Various views of TCNQ column in (DB18C6)RbTCNQ (hydrogen atoms are excluded)

Figure 3.143 shows various views of TCNQ column formation. Each TCNQ infinite column is formed by separated TCNQ^{•-} dimers, in which TCNQ^{•-} dimer neighbours are significantly long-axis slipped [Figure 3.143(b)]. Distances and angles within the TCNQ^{•-} stacks are summarised in Table 3.50.

| TCNQ ⁻ units | | TCNQ ⁻ dimers | TCNQ ⁻ dimer neighbours |
|--|--------------|--------------------------|------------------------------------|
| π - π perpendicular distance (Å) | | 3.18 | 3.29 |
| Short-axis slip | Distance (Å) | 0.62 | 5.80 |
| | Angle (°) | 11.03 | 60.44 |
| Long-axis slip | Distance (Å) | 0.0023 | 0.090 |
| | Angle (°) | 0.041 | 1.57 |
| Centroid-centroid distance (Å) | | 3.24 | 6.67 |

Table 3.50 Distances (Å) and angles (°) within the TCNQ⁻ stacks of (DB18C6)RbTCNQ

Figure 3.144 shows an angular analysis of the (DB18C6)RbTCNQ structure. The cation complex lies in a channel between the sheets of TCNQ⁻ dimers. Because of the coordination between metal cation and cyano groups, the Rb⁺ cation is “pulled” and sits above the crown ether mean plane (as defined by each set of oxygen atoms) by *ca.* 1.337 Å. The bending angle of the DB18C6 mean plane is 48.57°, which is twisted at an angle of 83.10° relative to benzene ring of the TCNQ⁻ unit. The coordination angle between Rb⁺ and NC is 158.14° and so is not linear. As seen in the packing pattern of (DB18C6)RbTCNQ, the presence of a TCNQ⁻ dimer is similar to that seen for (15C5)MTCNQ (M = Li, Na) and (18C6)MTCNQ (M = K, Rb)¹³¹ except that in this case each metal ion coordinates to three different cyano groups, which has not been seen before.

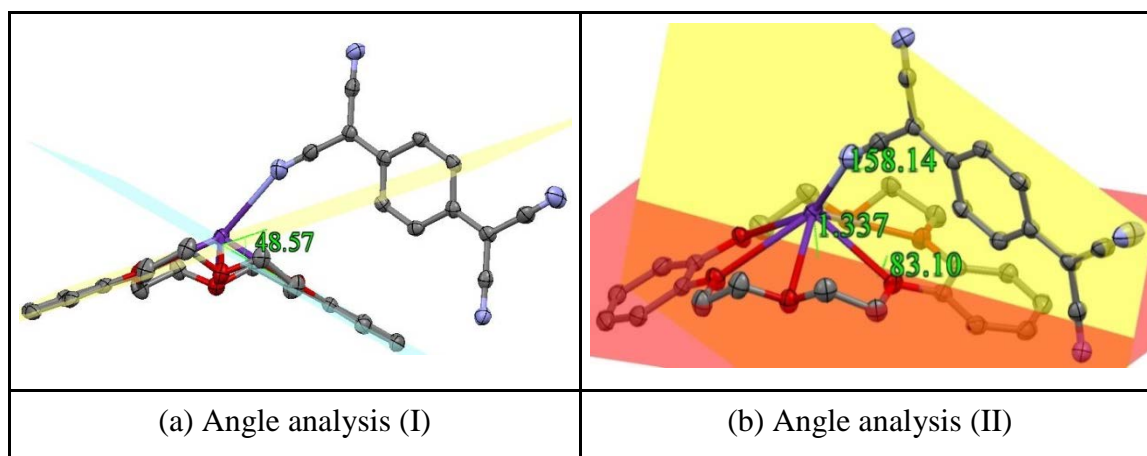


Figure 3.144 Angle analysis of (DB18C6)RbTCNQ (hydrogen atoms are excluded)

Figure 3.145 summarises the various contact distances within the cation complex.

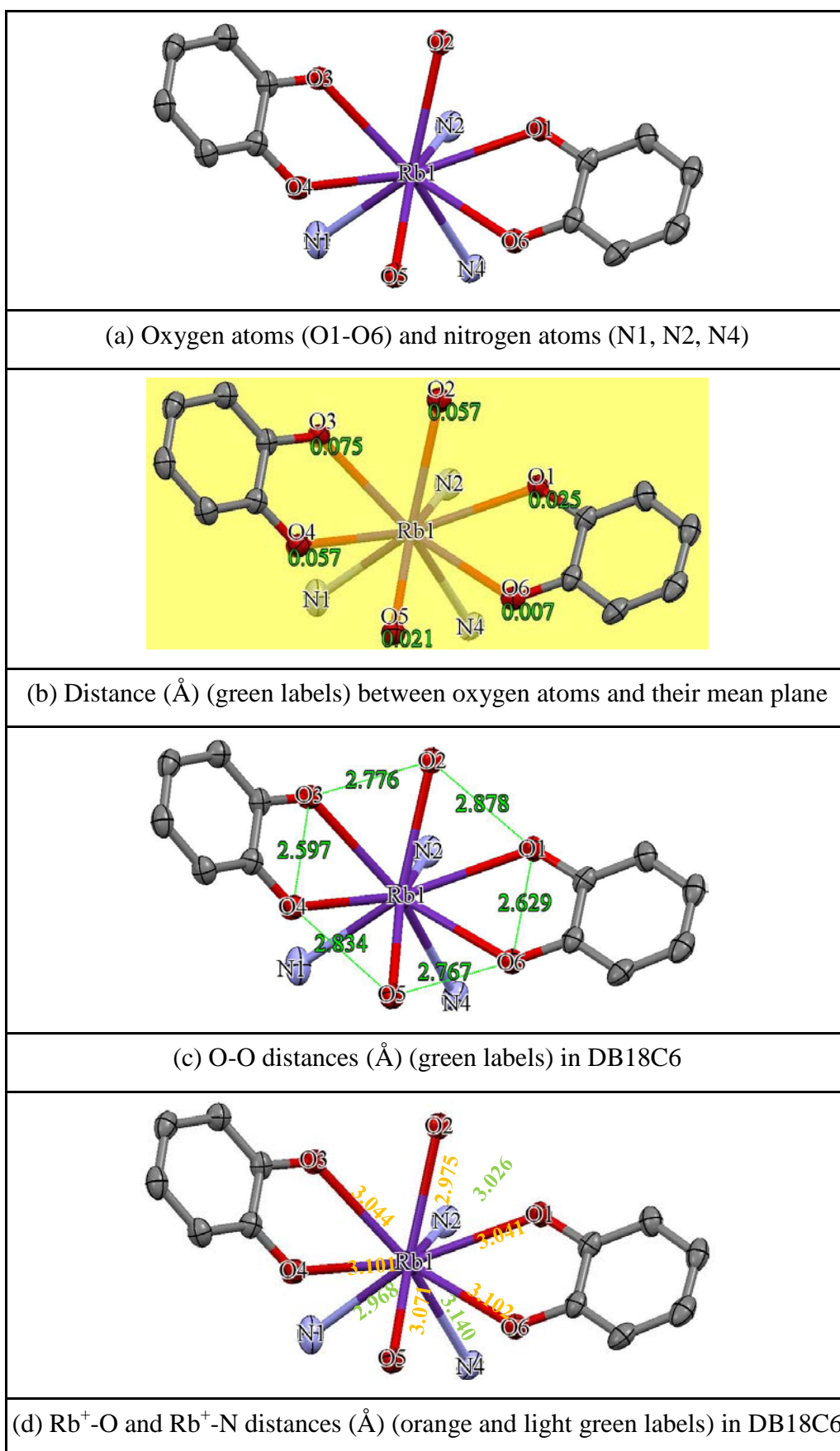


Figure 3.145 Various contact distances (Å) within the cation complex of (DB18C6)RbTCNQ (hydrogen atoms are excluded)

As viewed in Figure 3.145, the ligating oxygen atoms lay above and below their mean plane to form irregular hexagon geometry of mean side by *ca.* 2.747 Å. The minimum and maximum of Rb⁺-O distances are 2.975 and 3.102 Å respectively. The different distances of Rb⁺-O demonstrate that the Rb⁺ cation is distorted above the cavity of crown ether unit. Consequently, all of the Rb⁺-O and Rb⁺-N distances are similar to those of a van der Waals' contact (Rb⁺-O = 3.00 Å, Rb⁺-N = 3.03 Å)^{269,270}.

3.4.5 Preparation of (Dicyc18C6)Rb(TCNQ)₃

Reaction of Dicyc18C6 (Dicyclohexano-18-crown-6) with Rb₂(TCNQ)₃ and TCNQ⁰ (ratio 2:1:2) in dry acetonitrile afforded a plate of dark blue crystalline solid which contained single crystals suitable for X-ray structural study (combustion data is awaited). Full details including an account of the structure solution and refinement are reported in the Experimental Section and the Supporting Information (in the Appendices) respectively. The crystals obtained were of (Dicyc18C6)Rb(TCNQ)₃ and the basic unit is shown in Figure 3.146.

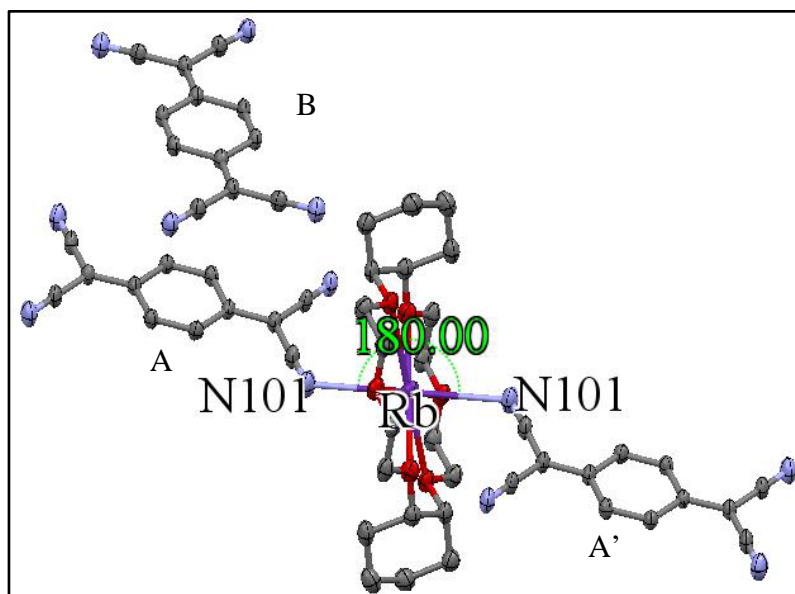


Figure 3.146 Basic unit of (Dicyc18C6)Rb(TCNQ)₃ (hydrogen atoms are excluded)

Bond lengths within the TCNQ units are summarised in Table 3.51. In this structure the Rb⁺ ion is coordinated by one crown ether unit and two adjacent TCNQ units on both sides of metal cation. The TCNQ units form a dimer which is significantly long axis slipped (see Figure 3.148). The similarity of the bond lengths within the two TCNQ units makes it difficult to distinguish between the TCNQ^{•-} and TCNQ⁰ component.

The data in Table 3.51 suggest that both TCNQ units have some quinonoidal character because bond length “a” is less than “b”. For both components A and B, the distribution of bond lengths is intermediate between these reported for TCNQ⁰ and TCNQ^{•-} respectively²¹³.

As viewed in Figure 3.147, the cation complex of (Dicyc18C6)Rb⁺ is in an “S”-shaped conformation and each Rb⁺ ion is coordinated by one crown ether unit and two nitrile groups on adjacent TCNQ units, which form a dimer with significant long axis slippage (see Figure 3.148). The angle of N101-Rb⁺-N101 is 180° because the Rb⁺ ion is located at the centre of symmetry and bond directly to the nitrogen atoms on adjacent TCNQ units. The centroid-centroid distance between Rb⁺ ions is 7.970 Å and the perpendicular distance of Rb⁺ ion to adjacent cation complex mean plane (defined by a set of oxygen atoms) is 4.244 Å. Therefore, the slip distance in respect to an adjacent cation complex is *ca.* 6.746 Å. Consequently, the angle between the cyclohexane plane and the mean plane is 62.31°. The chain configuration of TCNQ^{•-}·Rb⁺·TCNQ unit is similar to that seen in (Dicyc18C6)K(TCNQ)₃ in this study.

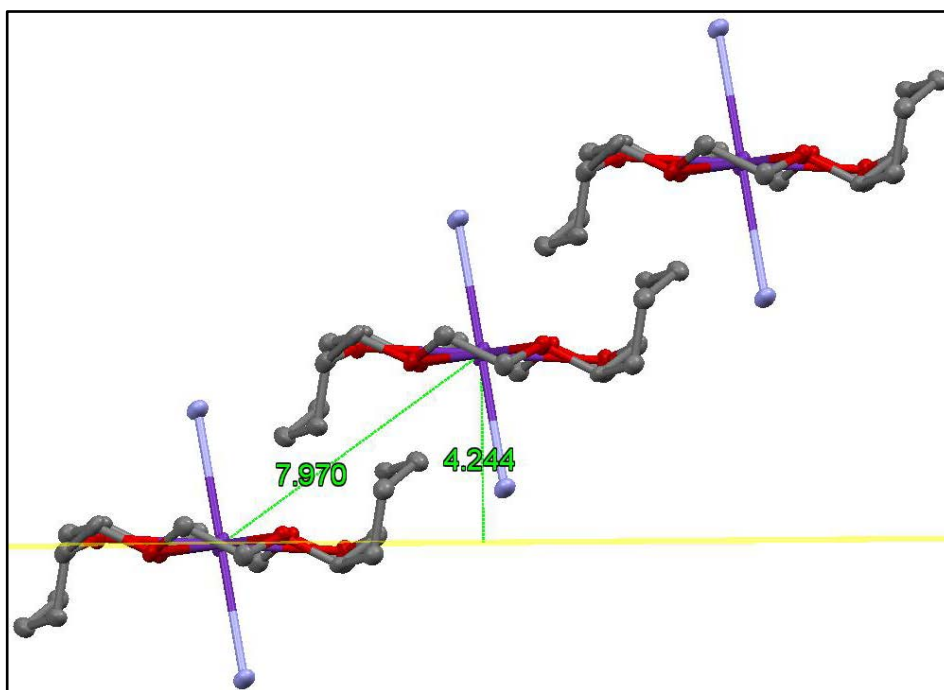


Figure 3.147 A “S”-shaped formation of cation complex in (Dicyc18C6)Rb(TCNQ)₃
(hydrogen atoms are excluded)

The bond distances observed for TCNQ units in (Dicyclo18C6)Rb(TCNQ)₃ are summarised in Table 3.51.

| (a) Definition of the bond lengths within the TCNQ molecule | | | | | | |
|---|------------------|-----------|-----------|-----------|-----------|-------|
| Structure | Bond lengths (Å) | | | | | |
| | a | b | c | d | e | f |
| TCNQ unit (A) | | 1.439 (3) | | 1.432 (3) | 1.152 (3) | 0.951 |
| | 1.359 (2) | 1.441 (2) | 1.399 (2) | 1.434 (3) | 1.148 (3) | 0.949 |
| | 1.364 (2) | 1.444 (3) | 1.403 (2) | 1.431 (3) | 1.148 (3) | 0.950 |
| | | 1.439 (2) | | 1.435 (3) | 1.146 (3) | 0.949 |
| TCNQ unit (B) | | 1.447 (2) | | 1.437 (2) | 1.152 (3) | 0.950 |
| | 1.352 (3) | 1.456 (2) | 1.377 (3) | 1.435 (3) | 1.148 (3) | 0.950 |
| | 1.352 (3) | 1.447 (2) | 1.377 (3) | 1.437 (2) | 1.152 (3) | 0.950 |
| | | 1.456 (2) | | 1.435 (3) | 1.148 (3) | 0.950 |

Table 3.51 Summary of bond lengths (Å) observed for TCNQ units in
(Dicyc18C6)Rb(TCNQ)₃

Each Rb^+ ion is coordinated by one crown ether unit and two adjacent TCNQ units, in which the resulting cation complex lies in channels between the wave-like TCNQ columns. After measuring the c bond lengths in each TCNQ unit, it seems that TCNQ unit (A) has more electron density, which suggests $\text{TCNQ}^{\cdot-}$ character. Consequently, the TCNQ unit (B) is less electron density, which suggests TCNQ^0 character. Within the crystal, the TCNQ dimers assemble into infinite column (see Figure 3.150). Each pair of TCNQ dimers is separated by an isolated TCNQ unit, which is twisted by *ca.* 65.63° in respect to adjacent TCNQ units (see Figure 3.149).

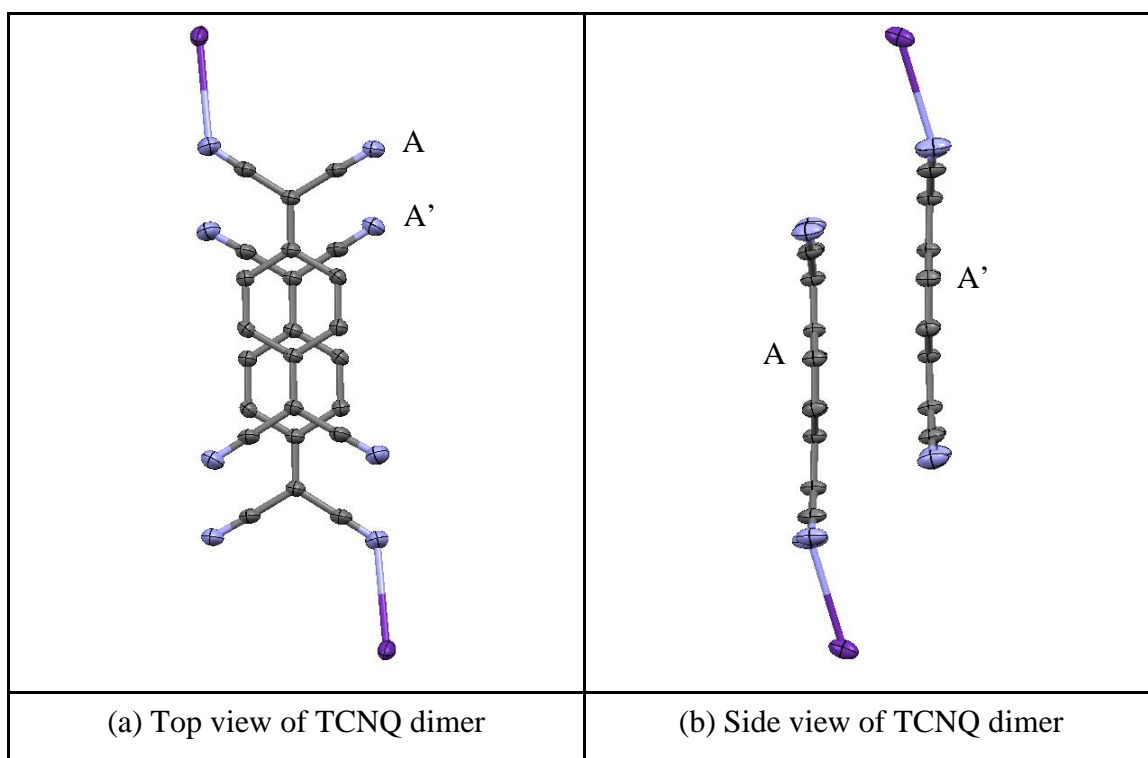


Figure 3.148 Top (a) and side (b) views of TCNQ dimer in $(\text{Dicyc18C6})\text{Rb}(\text{TCNQ})_3$ (hydrogen atoms are excluded)

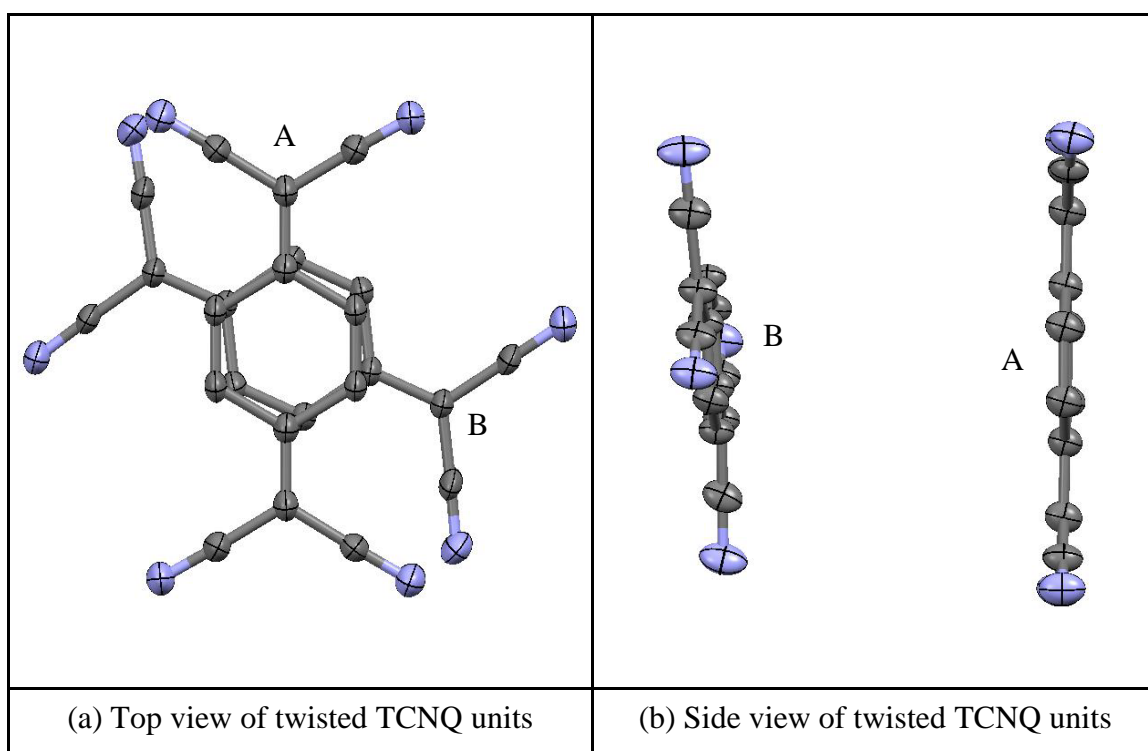


Figure 3.149 Top (a) and side (b) views of twisted TCNQ units in $(\text{Dicyc18C6})\text{Rb}(\text{TCNQ})_3$ (hydrogen atoms are excluded)

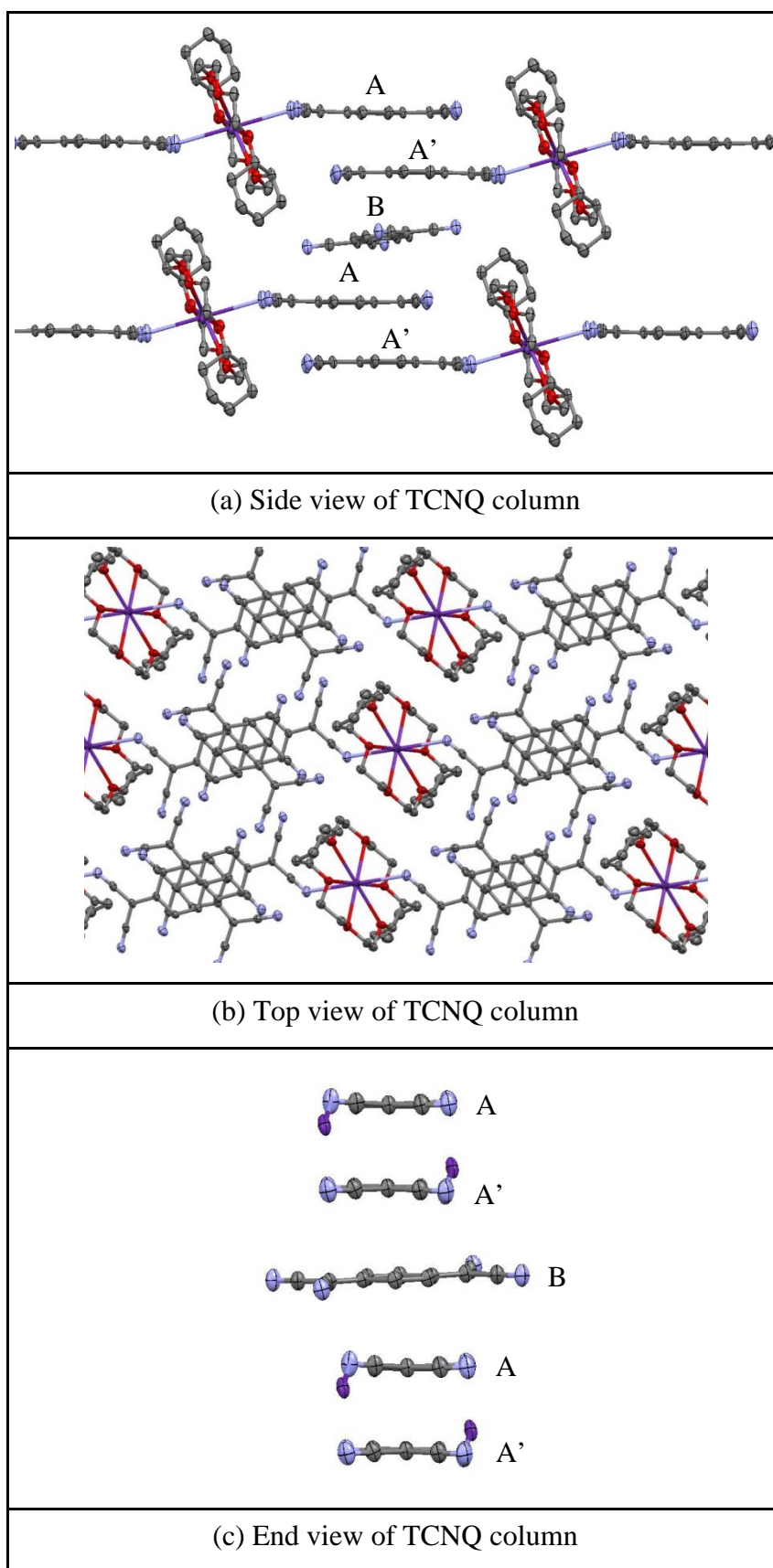


Figure 3.150 Various views of TCNQ column in $(\text{Dicyc18C6})\text{Rb}(\text{TCNQ})_3$ (hydrogen atoms are excluded)

Distances and angles within the TCNQ stacks of (Dicyc18C6)Rb(TCNQ)₃ are summarised in Table 3.52.

| TCNQ units | | TCNQ dimer |
|--|--------------|------------|
| π - π perpendicular distance (Å) | | 3.05 |
| Short-axis slip | Distance (Å) | 0.014 |
| | Angle (°) | 0.26 |
| Long-axis slip | Distance (Å) | 2.16 |
| | Angle (°) | 35.29 |
| Centroid-centroid distance (Å) | | 3.74 |

Table 3.52 Distances (Å) and angles (°) within the TCNQ stacks of (Dicyc18C6)Rb(TCNQ)₃

Within the TCNQ dimer, the individual TCNQ units adopt a shallow boat conformation in which neighbouring –C(CN)₂ units are twisted away from each other. The two TCNQ planes are parallel in respect to each other. From these data, it will be evident that π -facial overlap between dimer neighbours within a column is not ideal for extended π - π delocalisation within the TCNQ column. Figure 3.151 summarises the various contact distances within the cation complex.

As viewed in Figure 3.151, the ligating oxygen atoms are sitting above and below their mean plane (as defined by each set of oxygen atoms) to form irregular hexagon geometry as mean side by *ca.* 2.860 Å. All of the Rb⁺-O distances are different and are less than those of van der Waals contact (Rb⁺-O = 3.00 Å)^{269,271}, thus it seems justifiable to regard the metal cation and the oxygen atoms as being in contact. The different Rb⁺-O distances demonstrate that the Rb⁺ cation is distorted inside the cavity of each crown ether unit. The distance of Rb⁺-N (3.104 Å) is similar to those of van der Waals' contact (Rb⁺-N = 3.03 Å)^{269,271}.

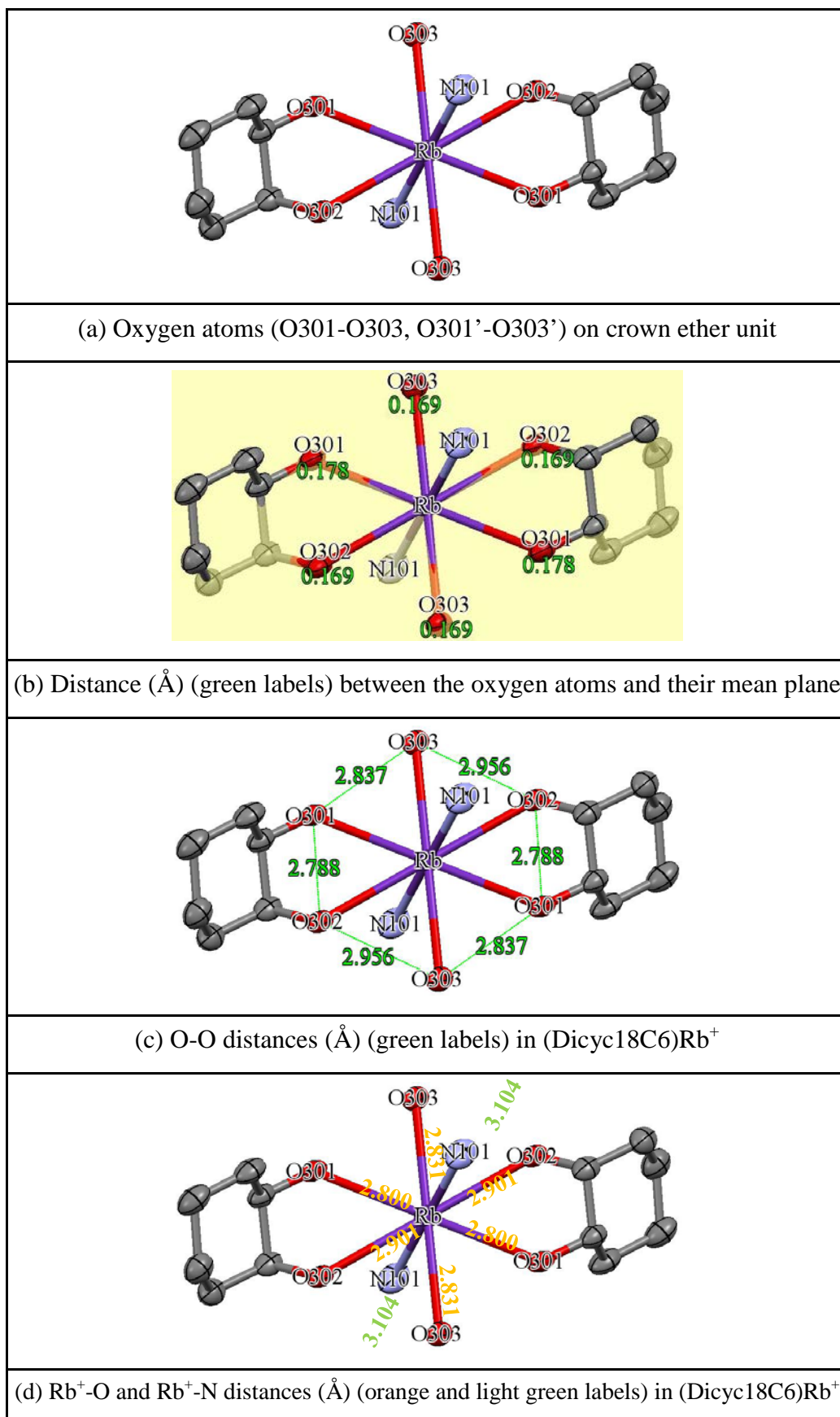


Figure 3.151 Various contact distances (Å) within the cation complex of (Dicyc18C6)Rb(TCNQ)₃ (hydrogen atoms are excluded)

3.4.6 Preparation of (C222)Rb(TCNQ)_{2.5}

Reaction of C222 (2.2.2-Cryptand) with Rb(TCNQ)_{1.5} and TCNQ⁰ (ratio 2:1:2) in dry acetonitrile afforded a reasonable yield (59%) of a plate of dark blue crystalline solid which contained single crystals suitable for X-ray structural study (combustion data is awaited). Full details including an account of the structure solution and refinement are reported in the Experimental Section and the Supporting Information (in the Appendices) respectively. The crystal obtained were of (C222)Rb(TCNQ)_{2.5} and the core unit is shown in Figure 3.152.

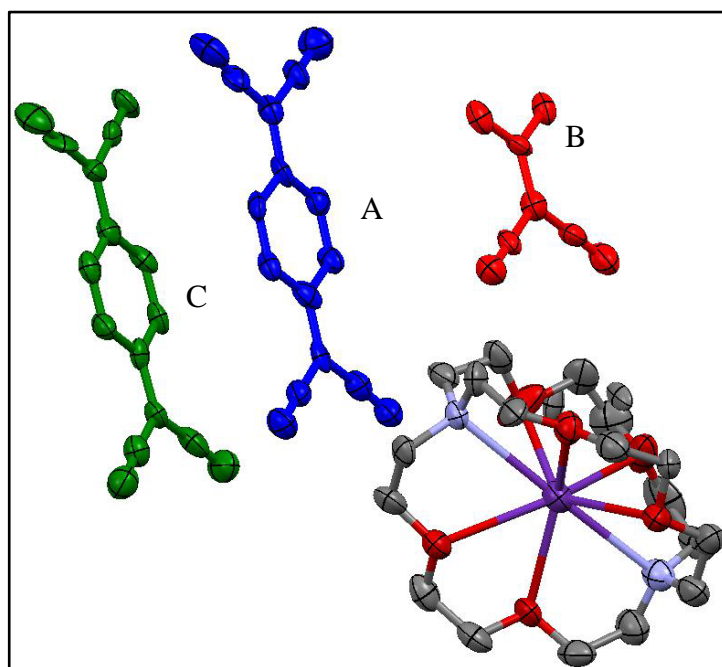


Figure 3.152 Core unit of (C222)Rb(TCNQ)_{2.5} (hydrogen atoms are excluded)

In this structure, the Rb⁺ ion is encapsulated by the cryptand, which prevents direct contact with the TCNQ units. The TCNQ units form a pentamer, in which they are all π -stacked long-axis slipped with alternate up and down with further forming a wave-like configuration (see Figure 3.153).

Bond lengths within the TCNQ units are summarised in Table 3.53. The data in Table 3.53 suggest that all of the TCNQ units have some quinonoidal character because bond length “a” is less than “b”. Within the TCNQ pentamer, after measuring the c bond lengths in each TCNQ unit, it seems that both red and green TCNQ units have lower electron density, and therefore have TCNQ⁰ character. Consequently, the blue TCNQ units are more electron rich, and have TCNQ⁻ character. Therefore, in TCNQ

pentamer, TCNQ units form mixed stacks, with a $\text{TCNQ}^0 - \text{TCNQ}^{\cdot-} - \text{TCNQ}^0 - \text{TCNQ}^{\cdot-} - \text{TCNQ}^0$ motif (see Figure 3.153), which means that two electrons are delocalised over the five TCNQ units but more negative charge density appears to reside on second and fourth TCNQ units (blue ones) based on the c bond lengths. Figure 3.154 shows top and side views of individual TCNQ units within and without TCNQ pentamer of $(\text{C222})\text{Rb}(\text{TCNQ})_{2.5}$.

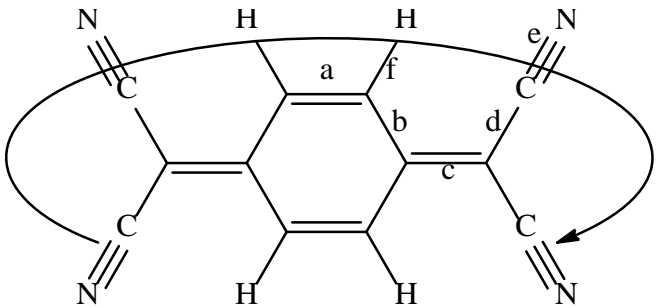
|  | | | | | | |
|--|------------------|------------|------------|------------|------------|-------|
| (a) Definition of the bond lengths within the TCNQ molecule | | | | | | |
| Structure | Bond lengths (Å) | | | | | |
| | a | b | c | d | e | f |
| TCNQ unit (A) | | 1.430 (11) | | 1.410 (13) | 1.155 (11) | 0.948 |
| | 1.344 (12) | 1.418 (12) | 1.411 (12) | 1.422 (12) | 1.158 (11) | 0.950 |
| | 1.362 (12) | 1.430 (11) | 1.414 (12) | 1.405 (12) | 1.156 (11) | 0.949 |
| | | 1.431 (12) | | 1.444 (12) | 1.149 (10) | 0.950 |
| TCNQ unit (B) | | 1.434 (12) | | 1.434 (13) | 1.145 (11) | 0.951 |
| | 1.350 (12) | 1.442 (12) | 1.391 (12) | 1.454 (12) | 1.137 (10) | 0.951 |
| | 1.350 (12) | 1.434 (12) | 1.391 (12) | 1.434 (13) | 1.145 (11) | 0.951 |
| | | 1.442 (12) | | 1.454 (12) | 1.137 (10) | 0.951 |
| TCNQ unit (C) | | 1.437 (12) | | 1.442(13) | 1.131 (13) | 0.951 |
| | 1.357 (12) | 1.430 (12) | 1.399 (12) | 1.437(12) | 1.139 (12) | 0.950 |
| | 1.356 (12) | 1.431 (11) | 1.400 (12) | 1.427(13) | 1.154 (13) | 0.950 |
| | | 1.428 (12) | | 1.426(12) | 1.160 (12) | 0.950 |

Table 3.53 Summary of bond lengths (Å) observed for TCNQ units in $(\text{C222})\text{Rb}(\text{TCNQ})_{2.5}$

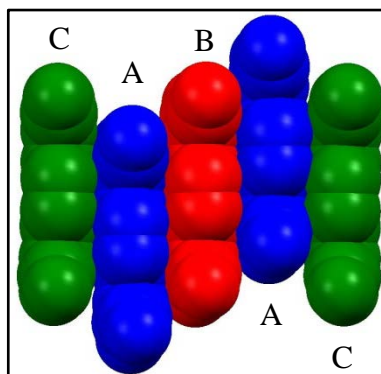


Figure 3.153 Space-fill of TCNQ pentamer stack in $(C222)Rb(TCNQ)_{2.5}$ (hydrogen atoms are excluded)

| | |
|---|--|
| | |
| (a) Top view of inter-TCNQ pentamer neighbours (CC) | (b) Side view of inter-TCNQ pentamer neighbours (CC) |
| | |
| (a) Top view of intra-TCNQ dimer (AC) | (b) Side view of intra-TCNQ dimer (AC) |
| | |
| (c) Top view of intra-TCNQ dimer (AB) | (d) Side view of intra-TCNQ dimer (AB) |

Figure 3.154 Top (a/c/e) and side (b/d/f) views of TCNQ units in $(C222)Rb(TCNQ)_{2.5}$ (hydrogen atoms are excluded)

Within the crystal, the TCNQ pentamers can assemble into infinite columns (see Figure 3.155).

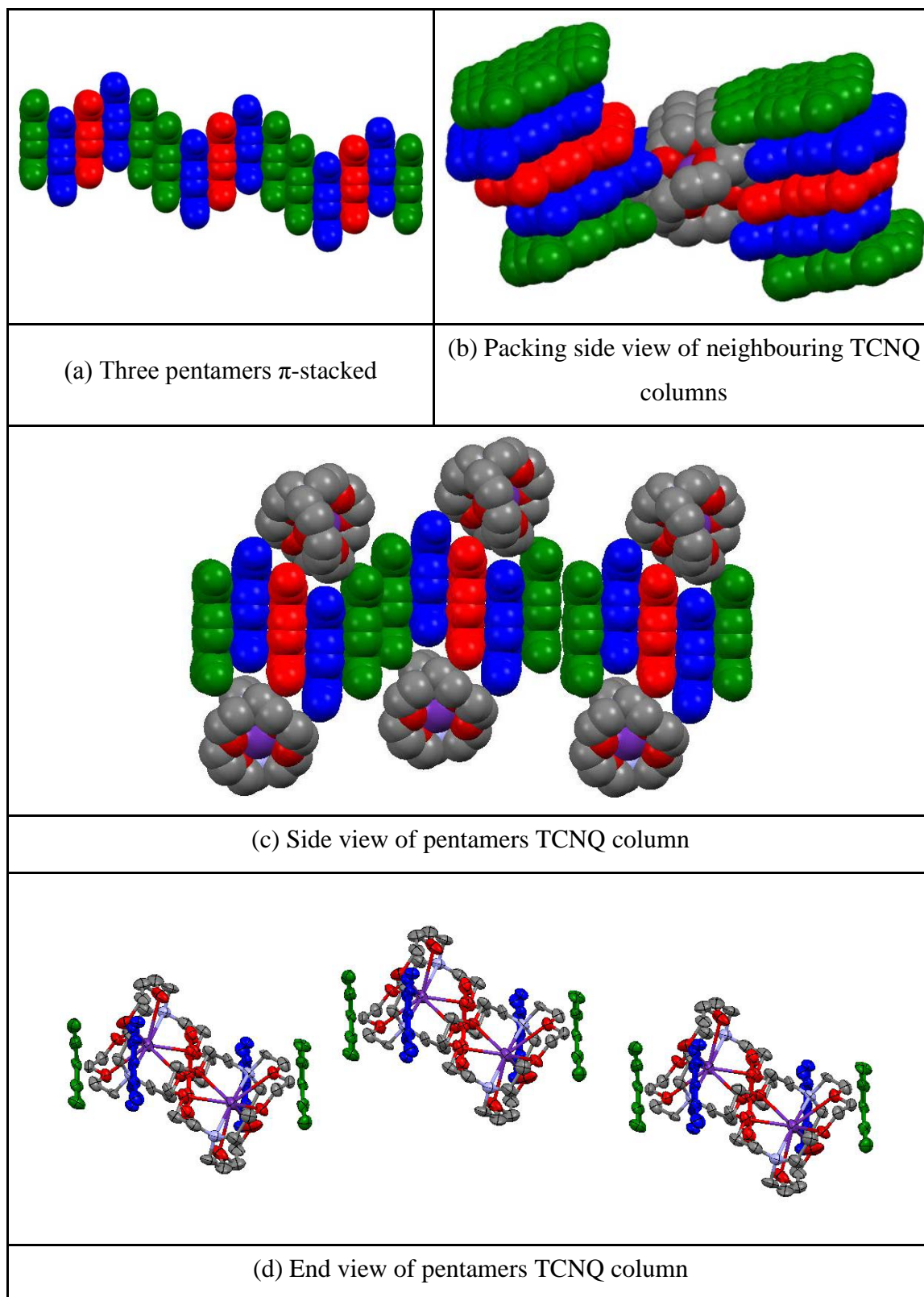


Figure 3.155 Views of pentamers geometry and packing pattern in TCNQ column
(hydrogen atoms are excluded)

There are more TCNQ units than Rb^+ and C222, which making the wave-like TCNQ column to create the cavity to fit the cation complex of $(\text{C222})\text{Rb}^+$. The packing pattern is probably purely steric because there is no direct association between Rb^+ ion and nitrogen atoms from neighbouring TCNQ units.

The X-ray structural studies reveal that this is a 2:5 $(\text{C222})\text{Rb}(\text{TCNQ})_{2.5}$ complex, which is exactly the same as $(\text{C222})\text{K}(\text{TCNQ})_{2.5}$ also prepared in this study. It consists of two cation complexes of $(\text{C222})\text{Rb}^+$ together with three TCNQ^0 and two $\text{TCNQ}^{\bullet-}$ units. Because of the similarity of bond lengths, the electrons are delocalised between TCNQ stacks. The TCNQ units are assembled into infinite π - π stacks, which are sitting between two layers of $(\text{C222})\text{Rb}^+$ cation complexes. A side view of the TCNQ units reveals a wave-like pattern of infinite stack with long-axis slippage between adjacent TCNQ units. The cryptates sit in the cavities between the TCNQ columns. Because Rb^+ cation is fully coordinated by crown ether unit, there is no direct coordination between metal cation and TCNQ units.

Distances and angles within the TCNQ stacks are summarised in Table 3.54.

| TCNQ units | | AC | AB | Inter-pentamer neighbours |
|--|--------------|-------|-------|---------------------------|
| π - π perpendicular distance (Å) | | 3.12 | 3.26 | 2.99 |
| Short-axis slip | Distance (Å) | 0.17 | 0.34 | 3.67 |
| | Angle (°) | 3.12 | 2.95 | 50.83 |
| Long-axis slip | Distance (Å) | 1.95 | 1.95 | 2.44 |
| | Angle (°) | 32.00 | 30.89 | 39.22 |
| Centroid-centroid distance (Å) | | 3.68 | 3.81 | 5.32 |

Table 3.54 Distances (Å) and angles (°) within the TCNQ stacks of $(\text{C222})\text{Rb}(\text{TCNQ})_{2.5}$

Within the TCNQ dimer (AC and AB), the individual TCNQ units adopt a shallow boat conformation in which neighbouring $-\text{C}(\text{CN})_2$ units are twisted away from each other. The two TCNQ planes are slightly tilted in respect to each other by *ca.* 4.44° in AC and 2.12° in AB respectively. From these data, it will be evident that π -facial overlap between dimer neighbours within a TCNQ column is not ideal for extended π - π

delocalisation within the TCNQ column. Descriptions of $\text{Rb}^+\text{-O}$ and $\text{Rb}^+\text{-N}$ distances of cation complex have been summarised in Figure 3.156.

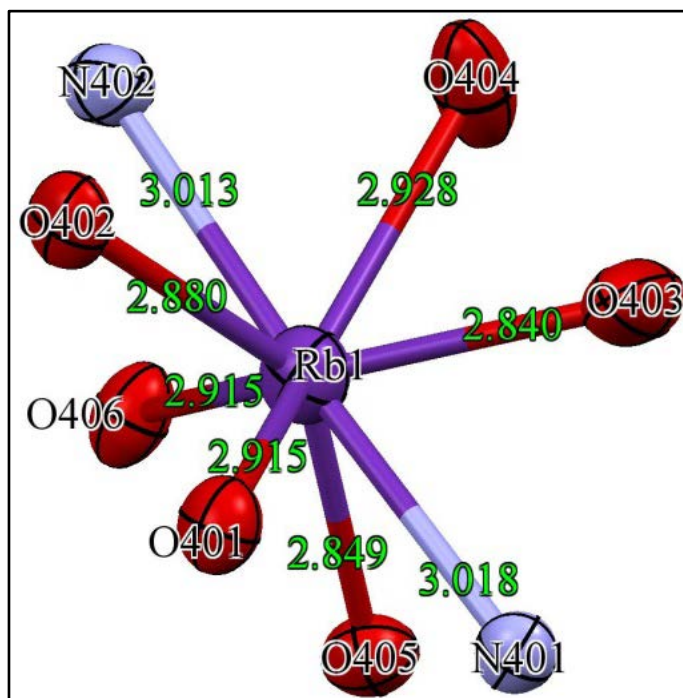


Figure 3.156 $\text{Rb}^+\text{-O}$ and $\text{Rb}^+\text{-N}$ distances in cation complex of $(\text{C222})\text{Rb}(\text{TCNQ})_{2.5}$ (carbon and hydrogen atoms are excluded)

Each Rb^+ cation is coordinated with six oxygen atoms and two nitrogen atoms on one crown ether unit as viewed in Figure 3.156. Not all of the $\text{Rb}^+\text{-O}$ distances in $(\text{C222})\text{Rb}(\text{TCNQ})_{2.5}$ are equal, which shows the Rb^+ cation is distorted inside the cavity of crown ether unit. Consequently, all of the $\text{Rb}^+\text{-O}$ distances are less than that of a van der Waals' contact ($\text{Rb}^+\text{-O} = 3.00 \text{ \AA}$)^{269,271} and thus it seems justifiable to regard the metal cation and the oxygen atoms as being in contact. Two $\text{Rb}^+\text{-N}$ distances, which are 3.013 and 3.018 \AA respectively, are slightly shorter than those of van der Waals contact ($\text{Rb}^+\text{-N} = 3.03 \text{ \AA}$)^{269,271} and thus it seems justifiable to regard the metal cation and the nitrogen atoms as being in contact, respectively.

3.4.7 Conclusion

Concerning the Ionophore-RbTCNQ complexes prepared in this study, complexes of $(12\text{C4})\text{Rb}(\text{TCNQ})_{1.5}$, $(15\text{C5})_2\text{RbTCNQ}$, $(18\text{C6})\text{Rb}(\text{TCNQ})_2$, $(\text{DB18C6})\text{RbTCNQ}$, $(\text{Dicyc18C6})\text{Rb}(\text{TCNQ})_3$ and $(\text{C222})\text{Rb}(\text{TCNQ})_{2.5}$ have been synthesised and characterised.

In $(12C4)Rb(TCNQ)_{1.5}$, a polymeric chain is formed, in which each Rb^+ ion is coordinated to one crown ether unit and four adjacent TCNQ units. The four nitrogen atoms are involved in the coordination sphere of the Rb^+ ion, forming “sandwich” configuration because the size of Rb^+ ion is much larger than the cavity of 12C4. In $(15C5)_2RbTCNQ$, $(15C5)_2Rb^+$ and $TCNQ^{\bullet-}$ can form 1:1 alternating stacks. Each Rb^+ ion is coordinated by two crown ether units, which prevents any direct interactions with $TCNQ^{\bullet-}$ anions. $TCNQ^{\bullet-}$ anions form dimers as the repeating unit, which can be assembled into parallel sheets with cation complex of $(15C5)_2Rb^+$ sitting between them. In $(18C6)Rb(TCNQ)_2$, TCNQ units prefer to form a trimer as repeating unit, which can be assembled into infinite column with the corresponding cation complex of $(18C6)Rb^+$ sitting in the cavity between TCNQ columns. Consequently, each TCNQ trimer is separated by an isolated TCNQ unit and the TCNQ units prefer to form mixed stacks. In $(DB18C6)RbTCNQ$, the $TCNQ^{\bullet-}$ dimers and $(DB18C6)Rb^+$ cation complexes form dimers which co-ordinate with lateral neighbours to form extended linear tapes through the crystal structure. The Rb^+ ion achieves a high coordination environment, in which six oxygen atoms from a crown ether unit and three adjacent cyano groups from neighbouring $TCNQ^{\bullet-}$ units are involved. Consequently, the presence of benzene rings on the crown results in the formation of extended polymer chains but there are no cation- π interactions between adjacent cation complexes. In $(Dicyc18C6)Rb(TCNQ)_3$, each Rb^+ ion is coordinated by one crown ether unit and two nitrile groups on adjacent TCNQ units. In the TCNQ repeating unit, each pair of TCNQ dimer is separated by an isolated TCNQ unit further forming infinite TCNQ columns. The cation complex of $(Dicyc18C6)Rb^+$ is sitting in the cavity between TCNQ columns. In $(C222)Rb(TCNQ)_{2.5}$, TCNQ units form pentamer as the repeating unit, which can be assembled into infinite column with the corresponding cation complex of $(C222)Rb^+$ sitting in the cavity between TCNQ columns. In TCNQ pentamer, TCNQ units prefer to form mixed stacks, in which two electrons are delocalised over five TCNQ units and the average negative charge is -0.4 electrons.

3.5 Optical Behaviour of Ionophore-M-TCNQ Salts

The Infrared (IR) spectra of all the above Ionophore-M-TCNQ salts were recorded as KBr discs and the main features are compared in Table 3.56. The Raman spectra of these complexes have also been recorded and the main characteristics are compared in Table 3.58. Only the key bands of interest are given below, full details of each Ionophore-M-TCNQ salt being reported in the Experimental Section.

3.5.1 IR spectra of Ionophore Encapsulated M-TCNQ Salts

IR provides a valuable insight into the electronic nature of a TCNQ species since the cyanide group resonances are particularly sensitive to the redox state of the TCNQ molecule and whether it is coordinated to a metal cation. Table 3.55 shows the literature values of MTCNQ and Ionophore-Metal TCNQ salts.

| NO. | Complex | IR Spectra region (cm ⁻¹) | |
|-----|--|---------------------------------------|------------------------|
| | | saturated CH stretch | CN stretch |
| 1. | LiTCNQ ²⁶² | - | 2211, 2196, 2182, 2145 |
| 2. | NaTCNQ ²⁷⁸ | - | 2206, 2195, 2175 |
| 3. | KTCNQ ²⁷⁹ | - | 2200, 2185, 2170 |
| 4. | RbTCNQ ^{280,281} | - | 2219, 2187, 2160 |
| 5. | Cs ₂ TCNQ ₃ ²⁸² | - | 2225, 2212, 2180, 2157 |
| 6. | (15C5) ₂ KTCNQ ²⁸³ | 2922 | 2202, 2183, 2154 |
| 7. | (18C6)KTCNQ ²⁸³ | 2901 | 2201, 2187, 2177, 2158 |
| 8. | (18C6)RbTCNQ ²⁸³ | 2900 | 2202, 2187, 2177, 2158 |
| 9. | (18C6)TITCNQ ²⁸³ | 2889 | 2181, 2154 |

Table 3.55 Literature values of MTCNQ and Ionophore-Metal TCNQ salts

Table 3.56 shows the IR spectra of all the Ionophore Encapsulated M-TCNQ Salts in this study.

| NO. | Complex | IR Spectra region (cm ⁻¹) | |
|-----|--|---------------------------------------|------------------------|
| | | saturated CH stretch | CN stretch |
| 1. | (12C4) ₂ LiTCNQ | 2968, 2915, 2875 | 2173, 2151 |
| 2. | (12C4) ₂ NaTCNQ | 2962, 2916, 2875 | 2172, 2150 |
| 3. | (12C4) ₂ Li(TCNQ) ₂ | 2970, 2928, 2882 | 2222, 2198, 2165 |
| 4. | (12C4) ₂ Na(TCNQ) ₂ | 2969, 2935, 2881 | 2223, 2201, 2177 |
| 5. | (12C4) ₂ K(TCNQ) ₂ | 2965, 2926, 2877 | 2195, 2179, 2167 |
| 6. | (12C4)Rb(TCNQ) _{1.5} | 2978, 2955 | 2224, 2212, 2184, 2152 |
| 7. | (15C5)LiTCNQ | 2930, 2878 | 2195, 2174, 2153 |
| 8. | (15C5)NaTCNQ | 2908, 2875 | 2179, 2152 |
| 9. | (15C5)Li(TCNQ) ₂ ·H ₂ O | 2878 | 2197, 2170 |
| 10. | (15C5)Na(TCNQ) ₂ ·H ₂ O | 2872 | 2196, 2167 |
| 11. | (15C5) ₂ RbTCNQ | 2900, 2864 | 2182, 2161 |
| 12. | (18C6)KTCNQ | 2889 | 2174, 2156 |
| 13. | (18C6)Na(TCNQ) ₂ ·2H ₂ O | 2971 | 2223, 2196, 2179 |
| 14. | (18C6)K(TCNQ) _{2.5} | 2899 | 2209, 2196, 2176 |
| 15. | (18C6)Rb(TCNQ) ₂ | 2851 | 2209, 2196, 2171 |
| 16. | (18C6)Cs(TCNQ) ₂ | 2900 | 2209, 2196, 2170 |
| 17. | (B15C5)LiTCNQ·H ₂ O | 2942, 2888 | 2196, 2168 |
| 18. | (B15C5) ₂ Cs(TCNQ) ₃ | 3050, 2971 | 2225, 2195, 2169 |
| 19. | (B18C6)K(TCNQ) ₂ | 3052, 2937 | 2226, 2195, 2166 |
| 20. | (DB18C6)K(TCNQ) ₂ | 2968, 2935, 2887 | 2214, 2189 |
| 21. | (DB18C6)RbTCNQ | 2925, 2885, 2805 | 2189, 2181, 2168, 2157 |
| 22. | (DC18C6)K(TCNQ) ₃ | 2932, 2883 | 2222, 2201, 2174 |
| 23. | (DC18C6)Rb(TCNQ) ₃ | 2972, 2923, 2874 | 2223, 2202, 2174, 2152 |
| 24. | (DC18C6)Cs(TCNQ) ₂ | 3050, 2937 | 2222, 2201, 2179, 2157 |
| 25. | (C222)K(TCNQ) _{2.5} | 2961, 2885, 2810 | 2200, 2178, 2152 |
| 26. | (C222)Rb(TCNQ) _{2.5} | 3054, 2978, 2873 | 2232, 2203, 2173 |

Table 3.56 IR spectra of Ionophore Encapsulated M-TCNQ Salts in this study

In $(12C4)_2MTCNQ$ ($M = Li, Na$), two complexes which are iso-structural, there are observed absorptions corresponding to the aliphatic (sp^3) CH in the region expected for crown ether unit (three bands at ≈ 2970 - 2875 cm^{-1} which are identical with the free 12C4 ligand)^{284,285}, and CN stretches (two bands at $\approx 2150\text{ cm}^{-1}$) for $TCNQ^{\bullet-}$, which conforming closely with the behaviour of the MTCNQ salts. These are shifted relative to those seen for the sample salts no matter what alkali metal is involved.

In $(12C4)_2M(TCNQ)_2$ ($M = Li, Na, K$), there are observed absorptions corresponding to the aliphatic (sp^3) CH in the region expected for the crown ether ring (bands at ≈ 2970 - 2875 cm^{-1})^{284,285}. With the presence of $TCNQ^0$, there is a band (at $\approx 2200\text{ cm}^{-1}$) characteristic of this unit. CN stretch bands (2230 - 2160 cm^{-1}) represent TCNQ units, which conform closely to the behaviour of the MTCNQ salts. These are shifted related to those seen for the sample MTCNQ salts. In $(12C4)Rb(TCNQ)_{1.5}$, there are observed absorptions corresponding to the aliphatic (sp^3) CH in the region expected for the crown ether ring (bands at $2978, 2955\text{ cm}^{-1}$). There are four CN stretch bands represent TCNQ units.

For $(15C5)Li/NaTCNQ$, the results of IR are as expected as listed in Table 3.56. The peaks, representing for the functional groups of aliphatic (sp^3) CH (two bands at ≈ 2930 - 2870 cm^{-1} which is identical with the free 15C5 ligand)²⁸⁶ and CN (bands at ≈ 2180 - 2150 cm^{-1}) can be distinguished and the cyano group resonances appear at positions similar to those observed for the corresponding $(12C4)_2MTCNQ$ ($M = Li, Na$) complexes. It is interesting to note that despite of the markedly different solid-state structures of these materials and the $(12C4)_2MTCNQ$ ($M = Li, Na$) complexes, there is little change in the position of the cyano group resonances. However, in $(15C5)_2RbTCNQ$, the aliphatic (sp^3) CH stretches (bands at $2900, 2864\text{ cm}^{-1}$) are slightly shifted. Consequently, the CN stretch (two bands at $2182, 2161\text{ cm}^{-1}$) represent for $TCNQ^{\bullet-}$, which conforming closely to the behaviour of the MTCNQ salts.

In $(15C5)M(TCNQ)_2 \cdot H_2O$ ($M = Li, Na$), there is observed absorption corresponding to the aliphatic (sp^3) CH in the region expected for crown ether unit (band at $\approx 2875\text{ cm}^{-1}$ which is identical with the free 15C5 ligand)²⁸⁶. CN stretch bands in the region (2200 - 2165 cm^{-1}) represent TCNQ units, which conform closely to the behaviour of the MTCNQ salt. Consequently, there is a broad band (at $\approx 3500\text{ cm}^{-1}$), which is shifted to a

lower wavenumber²⁸⁷, represent the hydrogen bonding in $(15C5)M(TCNQ)_2 \cdot H_2O$ ($M = Li, Na$).

In $(18C6)KTCNQ$, there is absorption corresponding to the aliphatic (sp^3) CH in the region expected for crown ether unit (band at 2889 cm^{-1} which is identical with the free $18C6$ ligand)²⁸⁸. Two CN stretch bands representing $TCNQ^{\bullet -}$ unit can be distinguished and the cyano group resonances appear at positions similar to those observed for the corresponding $(12C4)_2MTCNQ$ ($M = Li, Na$) and $(15C5)MTCNQ$ ($M = Li, Na$) complexes respectively. Consequently, the CN stretch bands conform closely to the behaviour of the MTCNQ salt.

In $(18C6)Na(TCNQ)_2 \cdot 2H_2O$, $(18C6)K(TCNQ)_{2.5}$, $(18C6)Rb(TCNQ)_2$ and $(18C6)Cs(TCNQ)_2$, there are observed absorptions corresponding to the aliphatic (sp^3) CH in the region expected for crown ether ring (bands at $\approx 3060\text{-}2880\text{ cm}^{-1}$ which is identical with the free $18C6$ ligand)²⁸⁸. With the presence of $TCNQ^0$, there is another band (at $\approx 2200\text{ cm}^{-1}$) representing for this unit. The rest CN stretching bands conform closely to the behaviour of the MTCNQ salt. Except for $(18C6)Na(TCNQ)_2 \cdot 2H_2O$, the metal cation of the rest three complexes are coordinated to adjacent $TCNQ$ units. However, the values of CN stretching bands (three bands at $\approx 2211\text{-}2156\text{ cm}^{-1}$) are similar within these four complexes. Consequently, there is a broad band (at $\approx 3400\text{ cm}^{-1}$) representing the hydrogen bonding in $(18C6)Na(TCNQ)_2 \cdot 2H_2O$.

In $(B15C5)LiTCNQ \cdot H_2O$ and $(B15C5)_2Cs(TCNQ)_3$, there are observed absorptions corresponding to the aliphatic (sp^3) CH in the region expected for crown ether unit (bands at $\approx 3050\text{-}2888\text{ cm}^{-1}$). There is a band associated with the presence of $TCNQ^0$ (at $\approx 2200\text{ cm}^{-1}$). Other CN stretch bands (at $\approx 2196\text{-}2168\text{ cm}^{-1}$) conform closely to the behaviour of the MTCNQ salt. Consequently, in $(B15C5)LiTCNQ \cdot H_2O$, there is a broad band (at $\approx 3500\text{ cm}^{-1}$), which is shifted to a lower wavenumber²⁸⁷, represent the hydrogen bonding in this complex.

In $(B18C6)K(TCNQ)_2$, there are observed absorptions corresponding to the aliphatic (sp^3) CH in the region expected for crown ether unit (two bands at $\approx 3052, 2937\text{ cm}^{-1}$). The CN stretches (three bands at $2226\text{-}2166\text{ cm}^{-1}$) represent for $TCNQ$ unit conform closely to the behaviour of the MTCNQ salts.

For (DB18C6)K(TCNQ)₂ and (DB18C6)RbTCNQ, there are observed absorptions corresponding to the aliphatic (*sp*³) CH in the region expected for crown ether unit (three bands at ≈ 2968 - 2805 cm^{-1}). In (DB18C6)K(TCNQ)₂, there is a band indicating the presence of TCNQ⁰ (at $\approx 2214\text{ cm}^{-1}$). Other CN stretching bands (at ≈ 2189 - 2157 cm^{-1}) represent TCNQ units conform closely to the behaviour of the MTCNQ salt.

In (DC18C6)M(TCNQ)₃ (M = K, Rb) and (DC18C6)Cs(TCNQ)₂, there are observed absorptions corresponding to the aliphatic (*sp*³) CH in the region expected for crown ether unit (bands at ≈ 3050 - 2874 cm^{-1}). There is a band associated with the presence of TCNQ⁰ (at $\approx 2200\text{ cm}^{-1}$) and there are three CN stretching bands (at ≈ 2222 , 2201 , 2174 cm^{-1}) in (DC18C6)K(TCNQ)₃, which indicate the weak TCNQ-TCNQ interactions as the slip distance longer than the case in (DC18C6)Rb(TCNQ)₃. Additionally, the CN stretch bands (at ≈ 2223 - 2152 cm^{-1}) represent TCNQ units in these three TCNQ complexes conform closely to the behaviour of the MTCNQ salt.

In (C222)M(TCNQ)_{2.5} (M = K, Rb), there are observed absorption corresponding to the aliphatic (*sp*³) CH in the region expected for the cryptand unit (bands at ≈ 3054 - 2810 cm^{-1}). There is a band (at $\approx 2200\text{ cm}^{-1}$) indicating the presence of TCNQ⁰. The rest of the CN stretching bands conform closely to the behaviour of the MTCNQ salt.

Consequently, the low wavenumbers of CN stretch bands in (C222)K(TCNQ)_{2.5}, which indicate the weak TCNQ-TCNQ interactions as the data of π - π perpendicular distance and slip distance along long or short-axis are slightly longer than the case of (C222)Rb(TCNQ)_{2.5}. Table 3.57 shows the description of cyanide (CN) groups in TCNQ and its five complexes.

| Complex | CN stretch / cm^{-1} |
|----------------------------------|-------------------------------|
| TCNQ ⁰ ²⁸⁹ | 2225 |
| KTCNQ ²⁷⁹ | 2200, 2185, 2170 |
| (12C4) ₂ LiTCNQ | 2173, 2151 |
| (12C4) ₂ NaTCNQ | 2172, 2150 |
| (C222)KTCNQ ⁵⁵ | 2180, 2153 |
| (C222)K(TCNQ) _{2.5} | 2200, 2178, 2152 |

Table 3.57 Description of cyanide (CN) groups in TCNQ and its five complexes

Additionally, the bands representing for cyanide (CN) group of $(12C4)_2LiTCNQ$, $(12C4)_2NaTCNQ$, $(C222)KTCNQ$ and $(C222)K(TCNQ)_{2.5}$ have been shifted to lower energy region compared with $TCNQ^0$ or $KTCNQ$ respectively. This important shift to lower frequency indicates that the CN groups are more weakly bonded consistent with charge delocalisation²⁹⁰. There is an IR spectra sample of $(12C4)_2LiTCNQ$ which has been shown in Figure 3.157. The rest of IR spectra of Ionophore Encapsulated MTCNQ salts have been listed in Appendices.

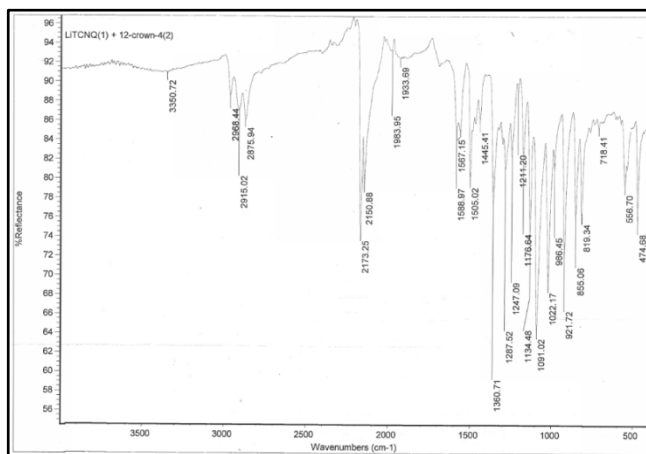


Figure 3.157 IR spectra of $(12C4)_2LiTCNQ$ in this study

3.5.2 Raman spectra of Ionophore Encapsulated M-TCNQ Salts

Vibrational spectroscopy of Raman is applied to identify the vibrational modes that can distinguish the chemical nature of TCNQ species²⁹¹. Raman spectroscopy is a very useful technique which can prove the charge transfer in TCNQ salts²⁹². Faulques et al.²⁹² have shown that the C-CN stretching band (see Figure 3.158) is sensitive to reduction from $TCNQ^0$ to $TCNQ^{\bullet-}$. Faulques et al.²⁹² also found that in one-electron reduction of $LiTCNQ$, the position of the C-CN stretching band is around 1394 cm^{-1} , whereas no band appears at 1453 cm^{-1} , which is represented as $TCNQ^0$ state.

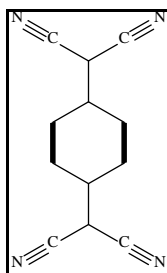


Figure 3.158 Key vibrational motion (black highlighted lines) in the TCNQ molecule

As viewed in Table 3.58, because the π electrons are strongly polarisable, the C=C and CN stretching bands of TCNQ units will generate strong Raman bands²⁹². The peaks sitting in a range between 2221 and 2190 cm^{-1} are ascribed to stretching bands represented cyano groups in TCNQ molecule²⁹². The peak at around 1600 cm^{-1} represents a mixture of C-C and C=C stretching bands, which is because the charge transfer (CT) leading to the redistribution of the electron density on TCNQ molecule²⁹². The peak at 1454 cm^{-1} which is C-CN stretching band, is typical of TCNQ⁰. The lower peak at $\approx 1390\text{-}1380\text{ cm}^{-1}$ proves the electron transfer from TCNQ⁰ to TCNQ⁻, which is a significant peak distinguishing the TCNQ phases^{292,293}. The peak at around 1206 cm^{-1} is ascribed to the C=C-H bending band. The wavenumber below 1200 cm^{-1} is probably because the carbon-carbon bonds of the C(CN)₂ units on TCNQ molecule²⁹². Two stretching bands at around 1454 cm^{-1} of TCNQ⁰ character and with that at around 1390-1380 cm^{-1} of TCNQ⁻ state appear in those of complex TCNQ salts, (crown ether)_mM(TCNQ)_n, especially in Cs⁺ analogues, (DC18C6)_mM(TCNQ)_n and (C222)K(TCNQ)_{2.5}. It seems justifiable to regard these complex TCNQ salts exhibit both TCNQ⁰ and TCNQ⁻ assignments in this study.

Faulques et al.²⁹² indicate that the stretching frequencies of nitrile group in Raman spectra are sensitive to charge transfer in TCNQ salts. The corresponding frequencies of nitrile group of TCNQ⁰ and TCNQ⁻ are found to be around $2227\pm 5\text{ cm}^{-1}$ and $2180\pm 5\text{ cm}^{-1}$, respectively²⁹². There seems to be a resonance structure of the nitrile group is possible between the forms of C[•]-CN or C-C⁺=N⁻, in which this resonance structure of nitrile group is in respect to the electron transfer and the effect of electron delocalisation²⁹².

Compared with the peaks representing for the aliphatic (*sp*³) CH in the region expected for crown ether unit, the corresponding peaks won't show in each Raman spectrum. The reason probably because the coordination of the ligating atoms of the crown ether ring to the metal ions will significantly influences the vibrational modes of the ligands, in which the symmetry of ligands will be broken after coordinating with metal ion through electrostatic interactions²⁹⁴.

| NO. | Complex | Raman Spectra region (cm ⁻¹) | | | |
|-----|---|--|------------------|--------------|---------------|
| | | CN stretch | C=C ring stretch | C-CN stretch | C=C-H bending |
| 1. | TCNQ° in this study | 2230 | 1603 | 1454 | 1206 |
| 2. | (12C4) ₂ LiTCNQ | 2214 | 1604 | 1384 | 1208 |
| 3. | (12C4) ₂ NaTCNQ | 2206 | 1609 | 1389 | 1206 |
| 4. | (12C4) ₂ Li(TCNQ) ₂ | 2216 | 1606 | 1385 | 1207 |
| 5. | (12C4) ₂ Na(TCNQ) ₂ | 2212 | 1602 | 1382 | 1206 |
| 6. | (12C4) ₂ K(TCNQ) ₂ | 2217 | 1608 | 1390 | 1204 |
| 7. | (12C4)Rb(TCNQ) _{1.5} | 2203 | 1604 | 1389 | 1203 |
| 8. | (15C5)LiTCNQ | 2216 | 1605 | 1379 | 1208 |
| 9. | (15C5)NaTCNQ | 2207 | 1602 | 1380 | 1205 |
| 10. | (15C5)Li(TCNQ) ₂ ·H ₂ O | 2216 | 1606 | 1384 | 1206 |
| 11. | (15C5)Na(TCNQ) ₂ ·H ₂ O | 2206 | 1603 | 1384 | 1206 |
| 12. | (15C5) ₂ RbTCNQ | 2203 | 1604 | 1389 | 1203 |
| 13. | (18C6)K(TCNQ) _{2.5} | 2203 | 1603 | 1386 | 1204 |
| 14. | (18C6)Rb(TCNQ) ₂ | 2205 | 1604 | 1390 | 1203 |
| 15. | (18C6)Cs(TCNQ) ₂ | 2197 | 1606 | 1390, 1435 | 1198 |
| 16. | (B15C5)LiTCNQ·H ₂ O | 2188 | 1608 | 1388 | 1197 |
| 17. | (B15C5) ₂ Cs(TCNQ) ₃ | 2201 | 1605 | 1391, 1433 | 1200 |
| 18. | (B18C6)K(TCNQ) ₂ | 2207 | 1606 | 1390 | 1205 |
| 19. | (DB18C6)K(TCNQ) ₂ | 2204 | 1605 | 1388 | 1205 |
| 20. | (DB18C6)RbTCNQ | 2203 | 1603 | 1385 | 1196 |
| 21. | (DC18C6)K(TCNQ) ₃ | 2203 | 1605 | 1389 | 1195, 1204 |
| 22. | (DC18C6)Rb(TCNQ) ₃ | 2226 | 1601 | 1388, 1451 | 1194, 1205 |
| 23. | (DC18C6)Cs(TCNQ) ₂ | 2201 | 1605 | 1390, 1430 | 1197 |
| 24. | (C222)K(TCNQ) _{2.5} | 2189 | 1600, 1614 | 1389, 1434 | 1195 |

Table 3.58 Raman spectra of Ionophore Encapsulated M-TCNQ Salts in this study

A summary of Raman peaks within each of the Ionophore-Encapsulated MTCNQ salts (M = alkali metals) has been posted in Figure 3.159.

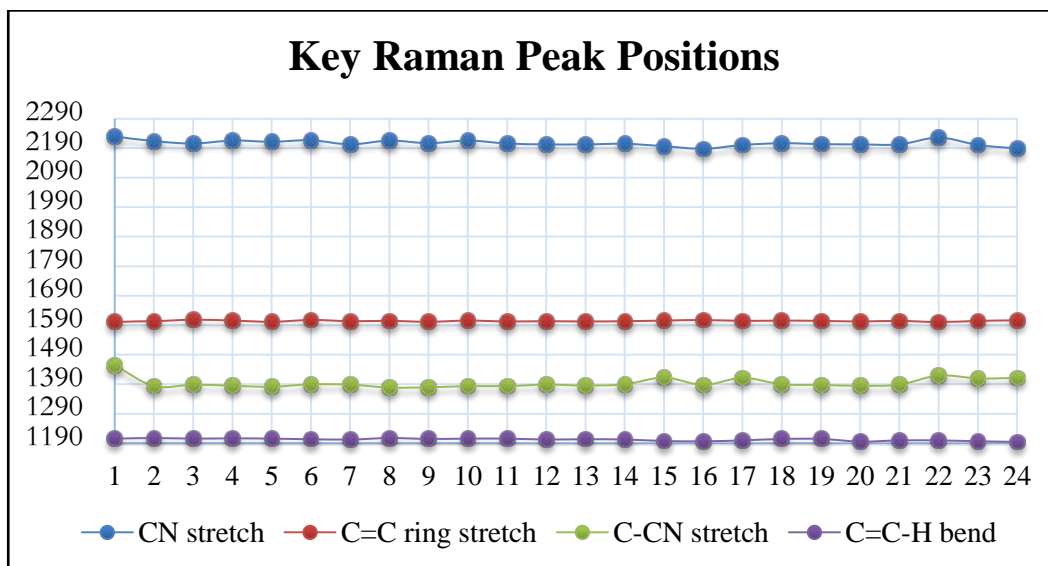


Figure 3.159 A summary of Raman peaks of Ionophore Encapsulated MTCNQ salts

As viewed in Figure 3.159, the aromatic ring in TCNQ unit is not affected, since the peaks representing of the C=C ring stretch (red) and C=C-H bend (purple) show no significant change no matter whether TCNQ⁰ (sample 1) or ionophore encapsulated MTCNQ salts (M = alkali metals) (2-24) are involved. However, the CN stretch bands (2-24) are affected and move to a lower wavenumber compared with TCNQ⁰ (1), which is corroborated by changes in the C-CN stretch band. This suggests that the cation probably perturbs the –CN vibration consistent with the crystal structures. A typical Raman spectrum, (DB18C6)K(TCNQ)₂, is shown in Figure 3.160. The Raman spectra of the other ionophore encapsulated MTCNQ salts are detailed in Appendices.

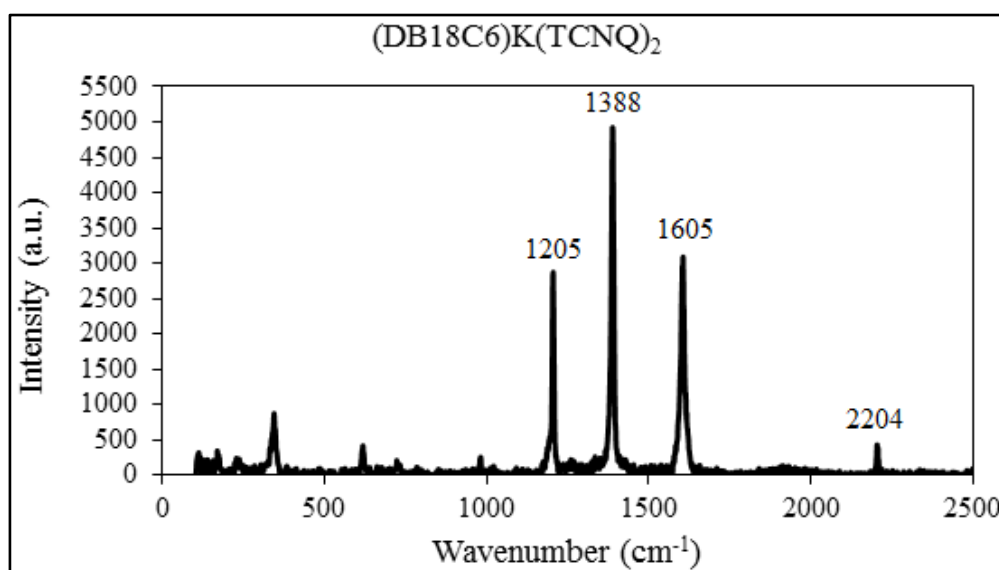


Figure 3.160 Raman spectra sample of (DB18C6)K(TCNQ)₂ in this study

3.6 Conductivity of Ionophore Encapsulated M-TCNQ Salts

| No. | Complex | Resistance (M Ω) at R.T. | Conductivity (S \cdot cm ⁻¹) at R.T. |
|-----|---|----------------------------------|--|
| 1. | (12C4) ₂ LiTCNQ | > 200 | < 2.5 \times 10 ⁻⁸ |
| 2. | (12C4) ₂ NaTCNQ | > 200 | < 2.5 \times 10 ⁻⁸ |
| 3. | (12C4) ₂ Li(TCNQ) ₂ | 1.2 | 4.2 \times 10 ⁻⁶ |
| 4. | (12C4) ₂ Na(TCNQ) ₂ | > 200 | < 2.5 \times 10 ⁻⁸ |
| 5. | (12C4)Rb(TCNQ) _{1.5} | > 200 | < 2.5 \times 10 ⁻⁸ |
| 6. | (15C5)LiTCNQ | > 200 | < 5 \times 10 ⁻⁸ |
| 7. | (15C5)NaTCNQ | > 200 | < 2.9 \times 10 ⁻⁹ |
| 8. | (15C5)Li(TCNQ) ₂ ·H ₂ O | 1.6 | 3.1 \times 10 ⁻⁶ |
| 9. | (15C5)Na(TCNQ) ₂ ·H ₂ O | 29.4 | 3.4 \times 10 ⁻⁷ |
| 10. | (15C5) ₂ RbTCNQ | 30.0 | 3.3 \times 10 ⁻⁷ |
| 11. | (18C6)K(TCNQ) _{2.5} | 87.1 | 3.8 \times 10 ⁻⁸ |
| 12. | (18C6)Rb(TCNQ) ₂ | 28.4 | 1.2 \times 10 ⁻⁷ |
| 13. | (B15C5)LiTCNQ·H ₂ O | 1.9 | 1.8 \times 10 ⁻⁶ |
| 14. | (B18C6)K(TCNQ) ₂ | 1.2 | 2.1 \times 10 ⁻⁶ |
| 15. | (DB18C6)K(TCNQ) ₂ | 4.7 | 1.1 \times 10 ⁻⁶ |
| 16. | (DC18C6)K(TCNQ) ₃ | > 200 | < 5 \times 10 ⁻⁸ |
| 17. | (DC18C6)Rb(TCNQ) ₃ | 153.4 | 3.3 \times 10 ⁻⁸ |
| 18. | (DC18C6)Cs(TCNQ) ₂ | 2.7 | 1.9 \times 10 ⁻⁶ |
| 19. | (C222)K(TCNQ) _{2.5} | 1.1 | 4.0 \times 10 ⁻⁸ |

Table 3.59 Conductivity of Ionophore Encapsulated M-TCNQ Salts in this study

Electrical conductivity measurements have been carried out on compressed circle disc of TCNQ salt. The resistivity (ρ) was calculated from the equation in Scheme 3.1, in which (R) represent for the electrical resistance, (l) equals to the length of the piece of material and the (A) stands for the cross-sectional area of the specimen. Consequently,

the value of conductivity (σ) can be calculated in Scheme 3.2. Because of the limited amount of specific TCNQ salts and mixture achieved product, not every TCNQ sample has been measured of conductivity. The results of the Ionophore Encapsulated M-TCNQ Salts have been listed in Table 3.59.

$$\rho = R \frac{A}{l}$$

Scheme 3.1 Calculation of resistivity (ρ)

$$\sigma \times \rho = 1$$

Scheme 3.2 The relationship between conductivity (σ) and resistivity (ρ)

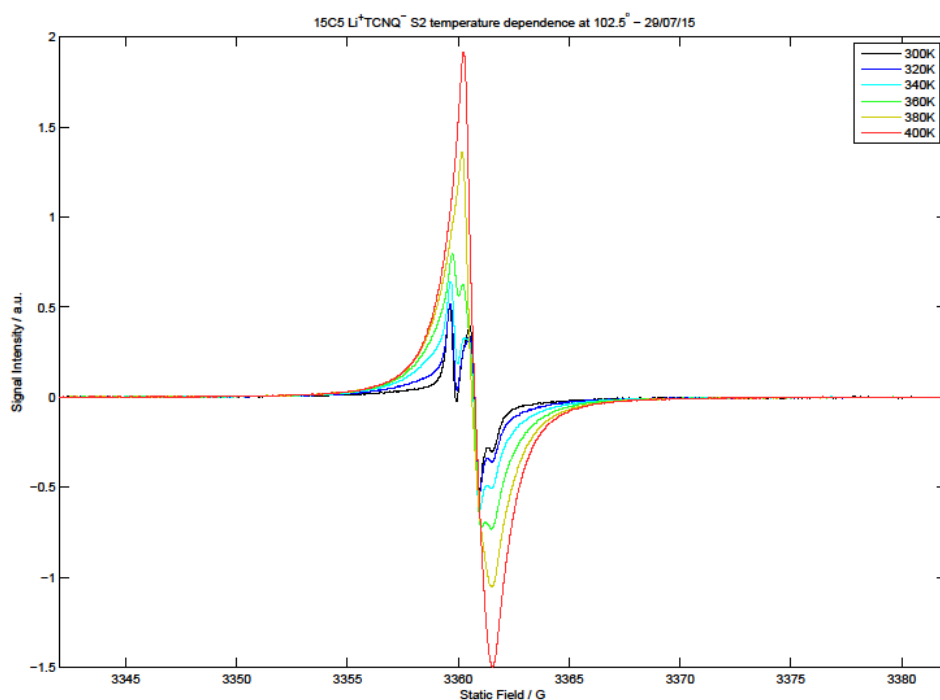
As viewed in Table 3.59, the electrical resistivities at R.T. of the simple TCNQ salts in this study are larger than 200M Ω and the corresponding conductivities at R.T. are less than $2.5 \times 10^{-8} \text{ S cm}^{-1}$, respectively. Consequently, the complex TCNQ salts in this study are much more conductive than the simple TCNQ salts, which is identical with what Morinaga et al. found⁶⁴. The reasons are probably because the π - π orbital interactions between neighbouring TCNQ unit in an infinite column offer a good channel for electrons to transfer and the Coulomb repulsion between the mobile electrons is much more reduced in the complex TCNQ salts, which leading to a higher conductivity effect, than the corresponding simple TCNQ salts⁶⁴. The resistivities of simple and complex TCNQ salts are higher than their corresponding original TCNQ salts (see Table 2.5), such as (12C4)₂LiTCNQ, (12C4)₂Li(TCNQ)₂; (15C5)LiTCNQ, (15C5)Li(TCNQ)₂·H₂O compared with LiTCNQ and (12C4)₂NaTCNQ, (12C4)₂Na(TCNQ)₂; (15C5)NaTCNQ, (15C5)Na(TCNQ)₂·H₂O compared with NaTCNQ. Consequently, the conductivity of simple and complex TCNQ salts are less than their corresponding original TCNQ salts (see Table 2.7), respectively.

3.7 Preliminary Electron Paramagnetic Resonance of Ionophore Encapsulated M-TCNQ Salts

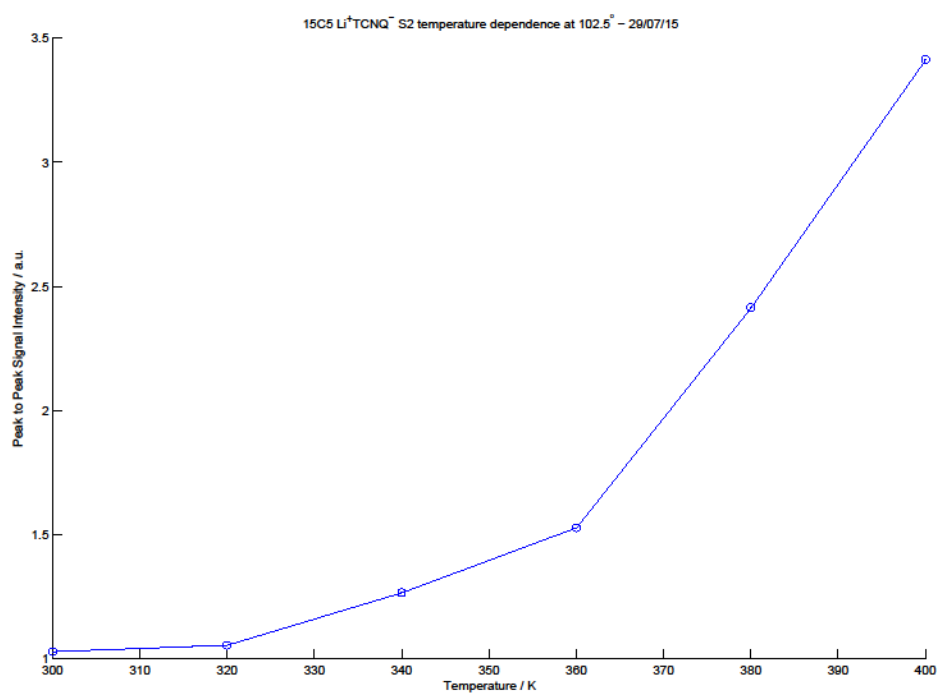
In this section, EPR spectra results of (15C5)LiTCNQ, (15C5)NaTCNQ, (15C5)Li(TCNQ)₂·H₂O, (15C5)Na(TCNQ)₂·H₂O, (18C6)KTCNQ²⁶⁸ and (18C6)K(TCNQ)_{2.5} will be illustrated.

After completing the X-ray structural studies, a number of the compounds have been studied by single crystal EPR Spectroscopy. In each case, a good diffracting single crystal was sealed in a capillary, the diameter of which is 0.5mm. The data of crystal's main face and rotation axis were recorded and the position of the crystal's main face was marked on the capillary. When measuring the electronic behaviour (EPR) of each sample, the starting position was identical to the position where the tube had been marked.

The electronic behaviour of a single crystal of (15C5)LiTCNQ has been measured using variable-temperature EPR spectral experiments. The angular dependence of EPR spectra of a single crystal of (15C5)LiTCNQ was recorded through a 360° rotation (0°-360°, at 5° increments) over a temperature range of 300 to 400K. Figure 3.162 shows the roadmap as a function of angular displacement of an (15C5)LiTCNQ crystal at 300K in this study. As viewed in Figure 3.161, there is a significant increase in EPR signal intensity as a function of increasing temperature. This trend implies a thermally generated material, but it is difficult to determine for certain that this is a triplet (a central sharp resonance increasing in intensity with increasing temperature is usually indicative of a thermally activated migrating triplet exciton). Looking at the rotation roadmap (see Figure 3.162), it seems justifiable to regard that there are spectral components crossing over as would be expected for a triplet excited signal, but nothing is well resolved and if that is a triplet, the zero-field splitting is rather small.



(a) EPR signal intensity as a function of temperature in (15C5)LiTCNQ



(b) The relationship between temperature and peak to peak signal intensity in (15C5)LiTCNQ

Figure 3.161 The EPR signal intensity as a function of temperature in (15C5)LiTCNQ

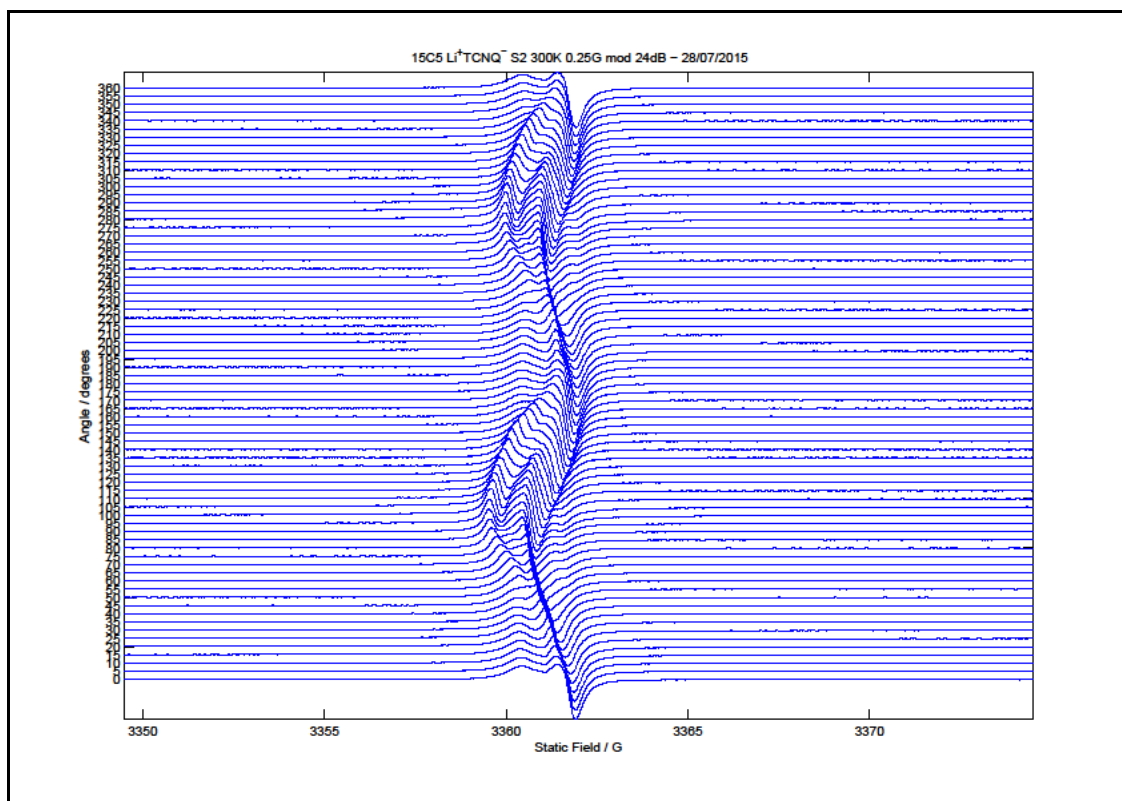


Figure 3.162 Roadmap as a function of angular displacement of an (15C5)LiTCNQ crystal at 300K

The electronic behaviour of single crystal of (15C5)NaTCNQ has been measured by variable-temperature EPR spectra experiments. The angular dependence of EPR spectra of a single crystal of (15C5)NaTCNQ are recorded for a 180° rotation (-130°-60°, at 10° increments) and over a temperature range (298-315K). Figure 3.163 shows the roadmap as a function of angular displacement of an (15C5)NaTCNQ crystal at 315K in this study. In (15C5)NaTCNQ, significant site-splitting is observed, which shows the characteristic of a localised thermally activated triplet state within the isolated TCNQ⁻ dimer¹⁰⁷. The position of the central peak is not orientation dependent. As the temperature is increased to 315K, weak satellites signals will be appeared gradually whose position change rapidly with orientation, in which the weak satellites signals exhibit characteristic of a localised thermally activated triplet state within the isolated TCNQ⁻ dimer^{36,107,132}, which is identical with the property of the dipolar fine structure (zero-field splitting) of an excited triplet exciton state²⁶⁸.

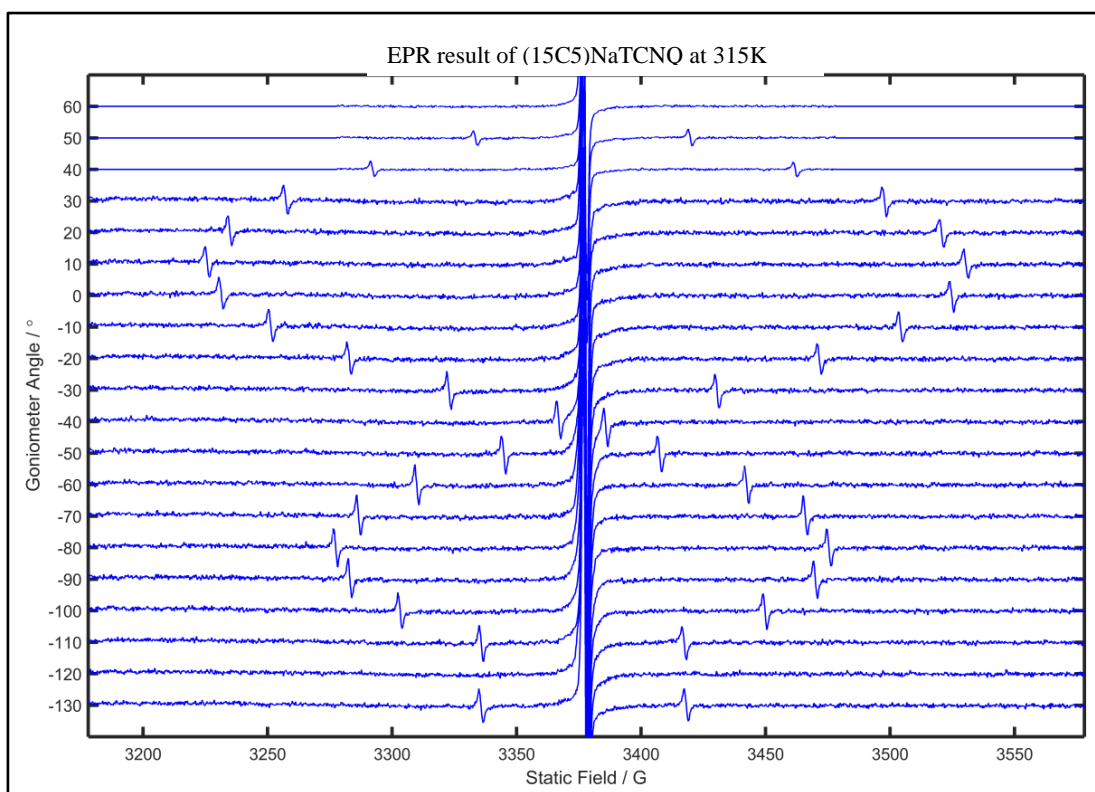
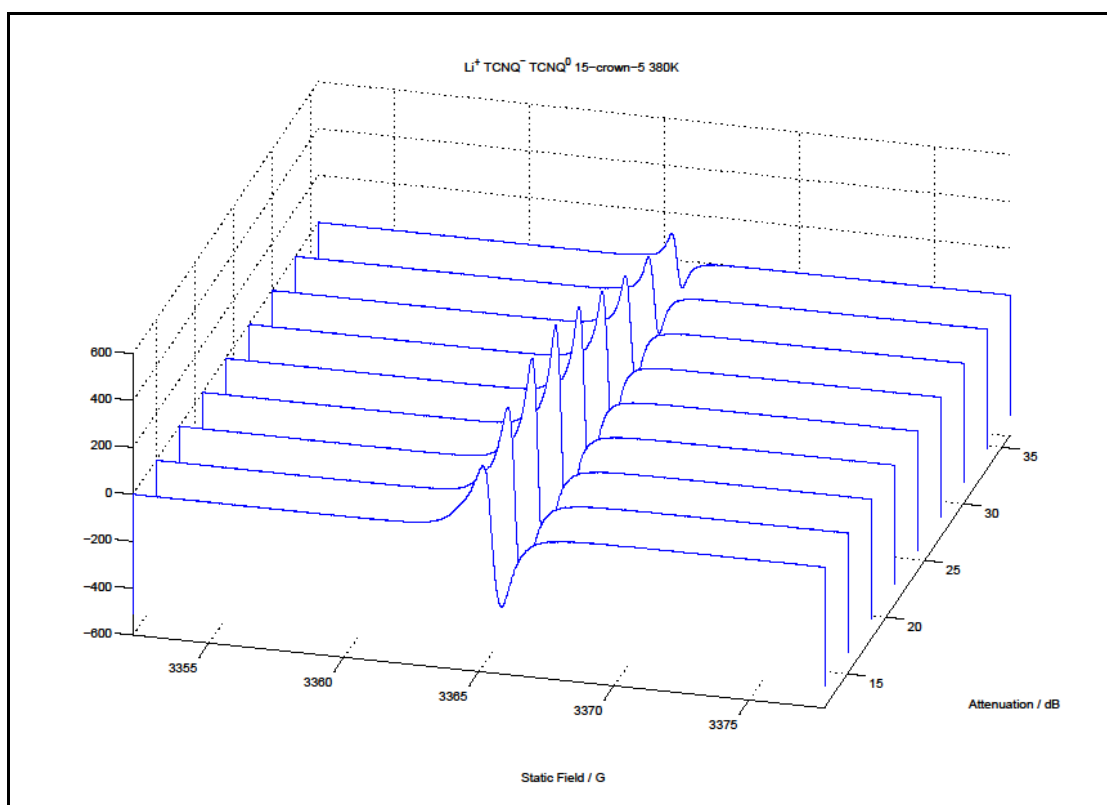
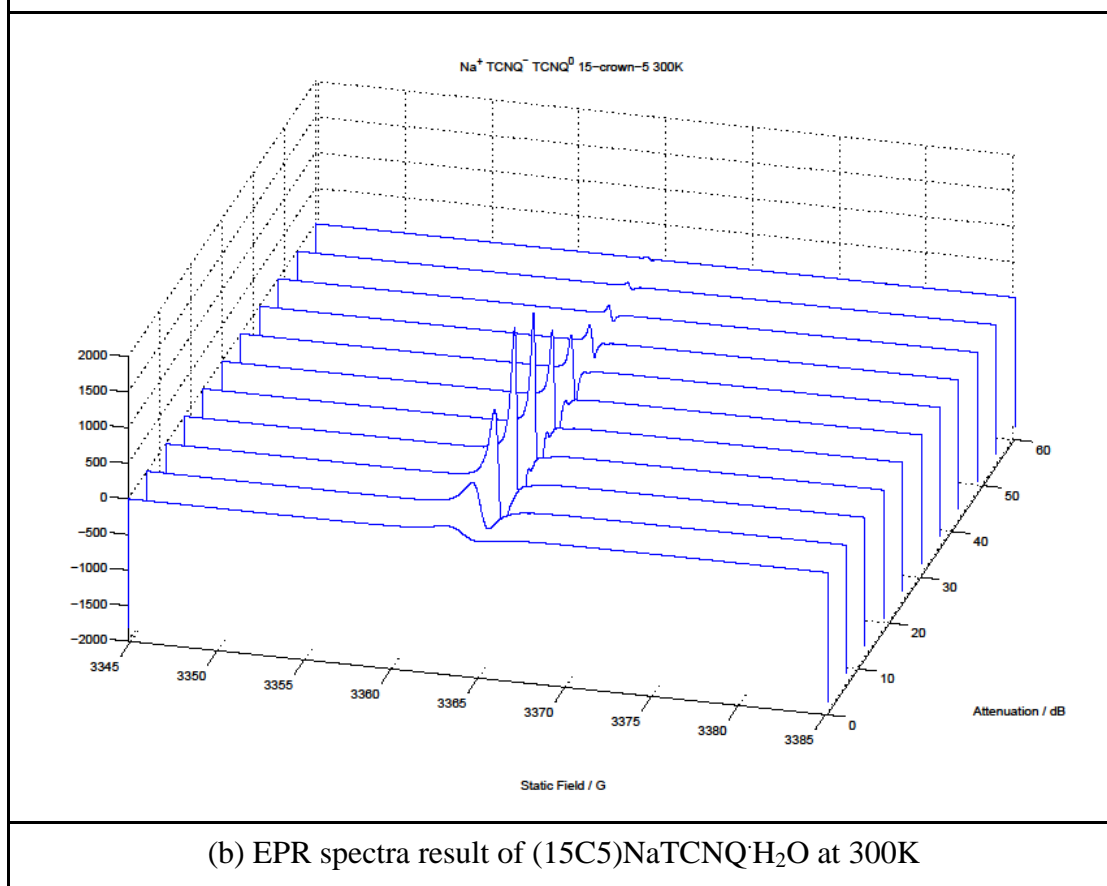


Figure 3.163 Roadmap as a function of angular displacement of an (15C5)NaTCNQ crystal at 315K

The electronic behaviour of single crystals of (15C5)Li/N_a(TCNQ)₂·H₂O have been measured by variable-temperature EPR spectra experiments. As viewed in Figure 3.164, only the central peak can be observed in the EPR spectra, which is not orientation dependent. As the temperature is increasing, there is no evidence for such localised triplet excited states in both of the TCNQ salts. The reason is probably because the electron is delocalised in both of the TCNQ salts, which may affect the spin-spin interaction between electrons, which will further affect the zero-field splitting of an excited migrating triplet exciton state.

(a) EPR spectra result of (15C5)LiTCNQ·H₂O at 380K(b) EPR spectra result of (15C5)NaTCNQ·H₂O at 300KFigure 3.164 EPR spectra results of (15C5)Li/NaTCNQ·H₂O at different temperatures

The electronic behaviour of single crystal of (18C6)KTCNQ has been measured by variable-temperature EPR spectra experiments. The angular dependence of EPR spectra of a single crystal of (18C6)KTCNQ are recorded at a 140° rotation (40° - 180° , 10° increments) and over a temperature range (298K-380K). Figure 3.165 shows the roadmap as a function of angular displacement of an (18C6)KTCNQ crystal at 380K in this study, in which it is identical with what Grossel et al., have found²⁶⁸. In (18C6)KTCNQ, significant site-splitting is observed, which shows the characteristic of a localised thermally activated triplet state within the isolated TCNQ $^{\cdot-}$ dimer. The position of central peak is not orientated dependent. As the temperature is increased to 380K, weak satellites appear whose position change rapidly with orientation, in which the weak satellites signals exhibit the characteristic of a localised thermally activated triplet state within the isolated TCNQ $^{\cdot-}$ dimer^{36,107,132}, which is identical with the property of the dipolar fine structure (zero-field splitting) of an excited triplet exciton state²⁶⁸.

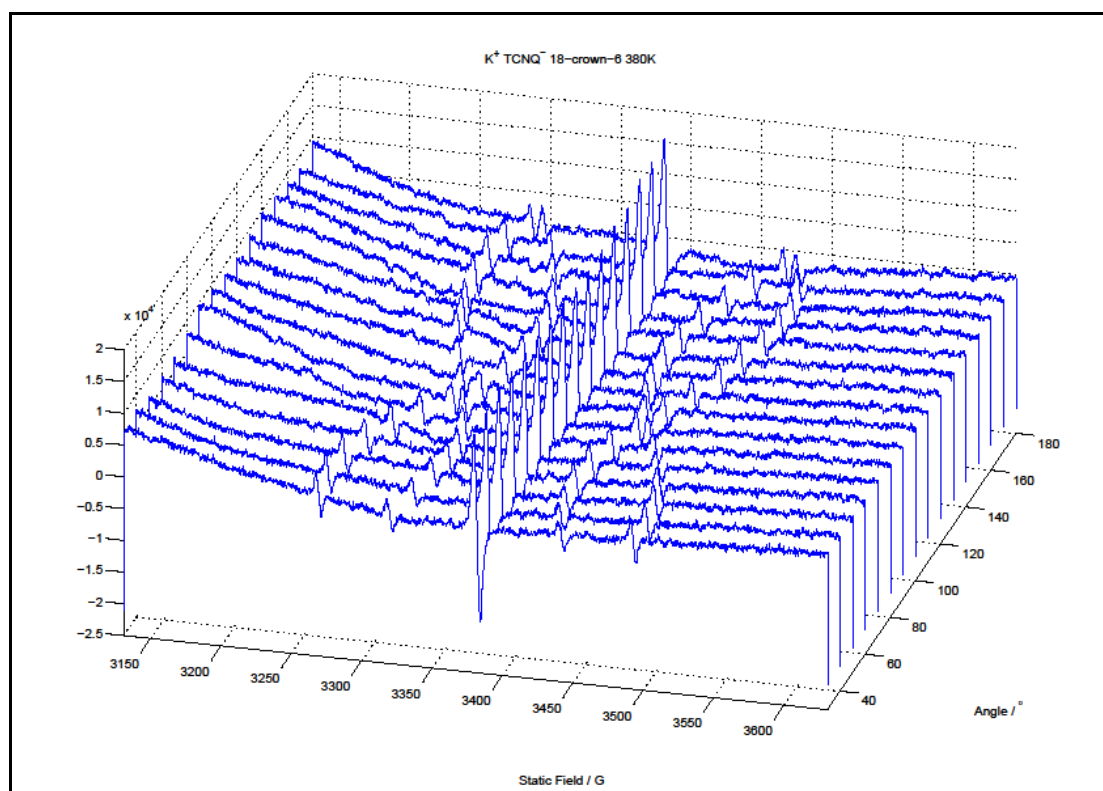


Figure 3.165 Roadmap as a function of angular displacement of a (18C6)KTCNQ at 380K

The electronic behaviour of single crystal of $(18C6)K(TCNQ)_{2.5}$ has been measure by variable-temperature EPR spectra experiments. Compared with the case in $(18C6)KTCNQ$, when the temperature is raised to 380K, only the central peak, which is not orientation dependent, can be detected in the EPR spectra without any satellites signals. There is no evidence for such localised triplet excited states in $(18C6)K(TCNQ)_{2.5}$.

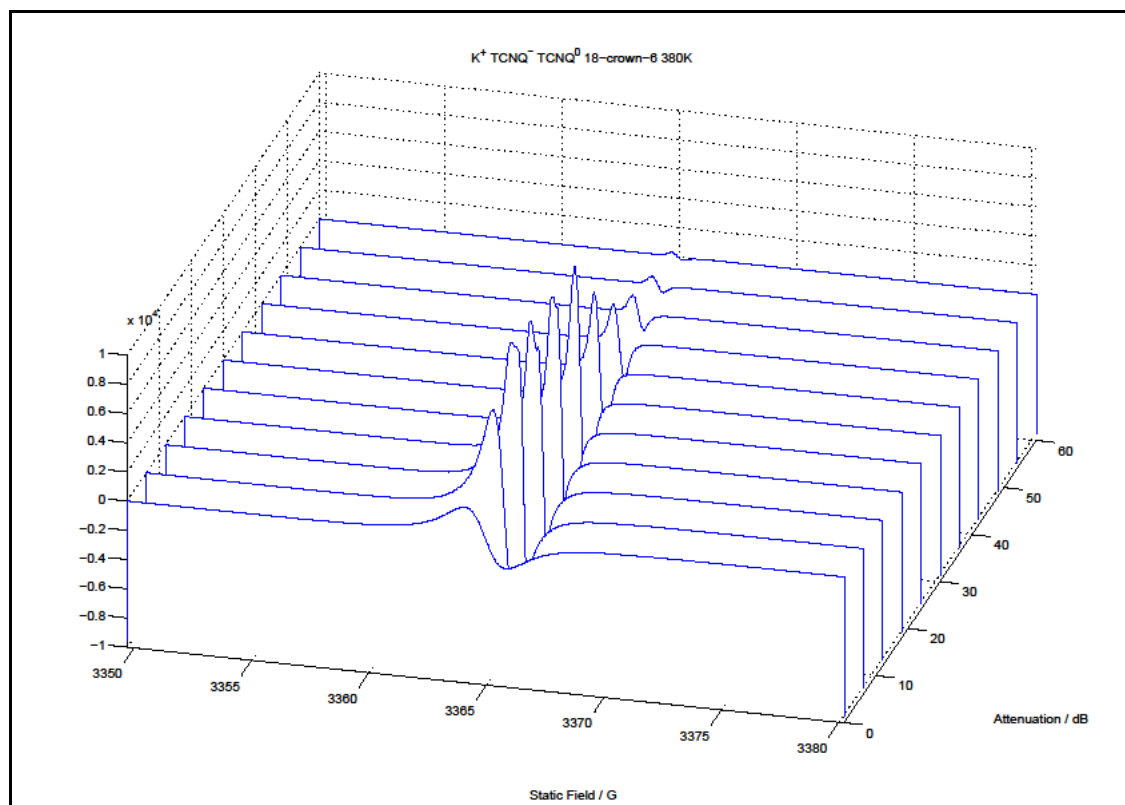


Figure 3.166 EPR spectra result of $(18C6)K(TCNQ)_{2.5}$ at 380K

Therefore, for simple complexes of MTCNQ with crown ether, such as $(15C5)Li/NaTCNQ$ in this study, the spin-spin interaction of the excited triplet observed and measured by EPR spectra of a single crystal has principal values and directions appropriate for the location of the intrinsic pair within the crystal structure. Consequently, for MTCNQ with crown ether and $TCNQ^0$, such as $(15C5)Li/Na(TCNQ)_2 \cdot H_2O$, $(18C6)K(TCNQ)_{2.5}$ in this study, only the central peak can be observed from EPR spectra and there is no evidence for such localised triplet excited states observed.

4. TCNQ Salts of Some Lanthanide Cations

In the current study, two novel lanthanide TCNQ complexes have been synthesised in deionised water and that two of these gave crystals suitable for X-ray structural study. Reaction of lanthanide ions (Tb^{3+} and Yb^{3+}) with LiTCNQ in deionised water (1:3) (the ratio of Ln: salt is 1:3) afforded in each case, crystals of two novel complexes of $\text{Tb}(\text{TCNQ})_3(\text{H}_2\text{O})_6 \cdot 3\text{H}_2\text{O}$ and $\text{Yb}(\text{TCNQ})_3(\text{H}_2\text{O})_6 \cdot 3\text{H}_2\text{O}$ and the solid-state behaviour of these has been investigated.

Hong and co-workers²⁹⁵ have recently reported the solid-state behaviour and properties of a number of lanthanide TCNQ salts including $[\text{Yb}(\text{TCNQ})_2(\text{H}_2\text{O})_6][\text{TCNQ}] \cdot \text{H}_2\text{O} \cdot 2\text{MeOH}$. This latter contains both water and methanol ligands. In this structure, each Yb^{3+} ion is coordinated to two nitrogen atoms from neighbouring $\text{TCNQ}^{\bullet-}$ anions and six oxygen atoms from six water molecules, which conform a square antiprismatic coordination geometry²⁹⁵. Two of the methanol molecules are not coordinated to Yb^{3+} ion. The relevant structural parameters of this complex have been listed in Table 4.5.

4.1 Crystal structure description of $\text{Tb}(\text{TCNQ})_3(\text{H}_2\text{O})_6 \cdot 3\text{H}_2\text{O}$

Reaction of TbCl_3 with LiTCNQ (ratio 1:3) in deionised water afforded a bright blue powder (41%) which contained single crystals suitable for X-ray structural study (combustion data is awaited). Full details including an account of the structure solution and refinement are reported in the Experimental Section and the Supporting Information (in the Appendices) respectively. The crystals obtained were of $\text{Tb}(\text{TCNQ})_3(\text{H}_2\text{O})_6 \cdot 3\text{H}_2\text{O}$ and the basic unit being shown in Figure 4.1.

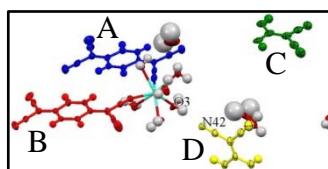


Figure 4.1 Basic unit of $\text{Tb}(\text{TCNQ})_3(\text{H}_2\text{O})_6 \cdot 3\text{H}_2\text{O}$ [showing two halves of TCNQ units (C and D)]

As viewed in Figure 4.1, each Tb^{3+} ion is coordinated by two nitrogen atoms from two adjacent TCNQ units (A and B) and six oxygen atoms from six water molecules. There

are in addition two uncoordinated TCNQ units (C and D), which lie on crystallographic centres of symmetry, in the basic structure of $\text{Tb}(\text{TCNQ})_3(\text{H}_2\text{O})_6 \cdot 3\text{H}_2\text{O}$. The mean plane of TCNQ unit (A) (defined by the central aromatic ring) is tilted 2.84° in respect to TCNQ unit (B). The TCNQ unit (D) can sit between TCNQ unit (A) and TCNQ unit (B) and its molecular plane is tilted 87.97° in respect to that of the TCNQ unit (A) and 88.87° in respect to that of the TCNQ unit (B). A cyano group to water $\text{CN}(\text{N}42) \cdots \text{H}(\text{O}3)$ hydrogen bond is formed, with a distance of 2.038 \AA in the basic unit. Bond lengths within the TCNQ units are summarised in Table 4.1.

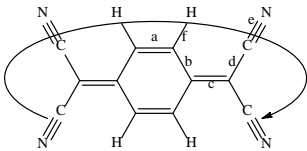
|  | | | | | | |
|---|-------------------------------|-----------|-----------|-----------|-----------|-------|
| (a) Definition of the bond lengths within the TCNQ molecule | | | | | | |
| Structure | Bond lengths (\AA) | | | | | |
| | a | b | c | d | e | f |
| TCNQ unit (A) | | 1.429 (6) | | 1.424 (7) | 1.149 (7) | 0.950 |
| | 1.373 (6) | 1.425 (6) | 1.407 (6) | 1.420 (7) | 1.145 (7) | 0.949 |
| | 1.357 (6) | 1.425 (6) | 1.428 (6) | 1.413 (6) | 1.147 (6) | 0.949 |
| | | 1.418 (6) | | 1.406 (6) | 1.150 (6) | 0.950 |
| TCNQ unit (B) | | 1.420 (6) | | 1.425 (7) | 1.146 (6) | 0.950 |
| | 1.365 (6) | 1.430 (6) | 1.416 (6) | 1.432 (7) | 1.160 (7) | 0.950 |
| | 1.369 (6) | 1.411 (6) | 1.425 (6) | 1.425 (6) | 1.156 (6) | 0.950 |
| | | 1.433 (6) | | 1.406 (6) | 1.149 (6) | 0.949 |
| TCNQ unit (C) | | 1.432 (7) | | 1.424 (7) | 1.156 (7) | 0.949 |
| | 1.359 (8) | 1.437 (7) | 1.396 (8) | 1.419 (7) | 1.155 (7) | 0.949 |
| | 1.359 (8) | 1.432 (7) | 1.396 (8) | 1.424 (7) | 1.156 (7) | 0.949 |
| | | 1.437 (7) | | 1.419 (7) | 1.155 (7) | 0.949 |
| TCNQ unit (D) | | 1.427 (7) | | 1.421 (7) | 1.148 (6) | 0.950 |
| | 1.372 (8) | 1.418 (7) | 1.415 (8) | 1.423 (8) | 1.158 (7) | 0.950 |
| | 1.372 (8) | 1.427 (7) | 1.415 (8) | 1.421 (7) | 1.148 (6) | 0.950 |
| | | 1.418 (7) | | 1.423 (8) | 1.158 (7) | 0.950 |

Table 4.1 Summary of bond lengths (\AA) observed for TCNQ units in $\text{Tb}(\text{TCNQ})_3(\text{H}_2\text{O})_6 \cdot 3\text{H}_2\text{O}$

The data in Table 4.1 suggest that all of the TCNQ units have some quinonoidal character because bond length “a” is less than “b”. In this structure, the TCNQ units (A, B and C) form a pentamer, in which they are all π -stacked long-axis slipped alternately up and down, thereby forming a wave-like motif which is shown in Figure 4.2. Within the TCNQ pentamer, after measuring the c bond lengths in each TCNQ unit, it seems that green TCNQ unit (C) has lower electron density, and therefore have TCNQ^0 character. Consequently, the blue and red TCNQ units (A and B) are more electron rich and have $\text{TCNQ}^{\cdot-}$ character. TCNQ units (B, A and C) form an angle of 123.37° and TCNQ units (A, C and A') for an angle of 164.36° as viewed in Figure 4.2.

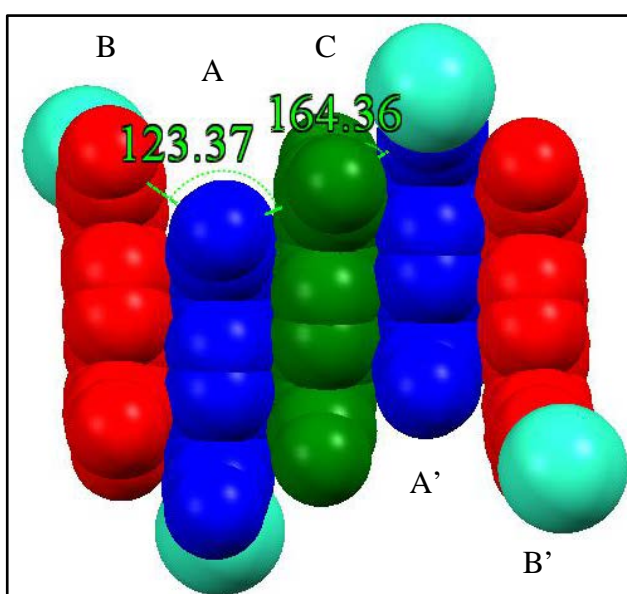


Figure 4.2 Space-fill of TCNQ pentamer stack in $\text{Tb}(\text{TCNQ})_3(\text{H}_2\text{O})_6 \cdot 3\text{H}_2\text{O}$ with Tb^{3+} ions shown in cyan (hydrogen atoms and interstitial solvents are excluded)

The π - π stacking interactions between neighbouring TCNQ units generate infinite one-dimensional columns. These run throughout the entire crystal structure of $\text{Tb}(\text{TCNQ})_3(\text{H}_2\text{O})_6 \cdot 3\text{H}_2\text{O}$. Therefore, intermolecular hydrogen bonds, π -stacking interactions and electrostatic interactions coexist in the crystal structure of $\text{Tb}(\text{TCNQ})_3(\text{H}_2\text{O})_6 \cdot 3\text{H}_2\text{O}$.

Except for TCNQ unit (B) which is flat, TCNQ unit (A) and TCNQ unit (C) adopt a shallow boat conformation in which neighbouring $-\text{C}(\text{CN})_2$ units are twisted away from each other. The two TCNQ planes are slightly tilted in respect to each other by 2.84° in BA dimer and 1.24° in AC dimer, respectively. Consequently, TCNQ unit (A) and TCNQ unit (C) are rotated 14.34° and 6.97° in respect to TCNQ unit (B), respectively.

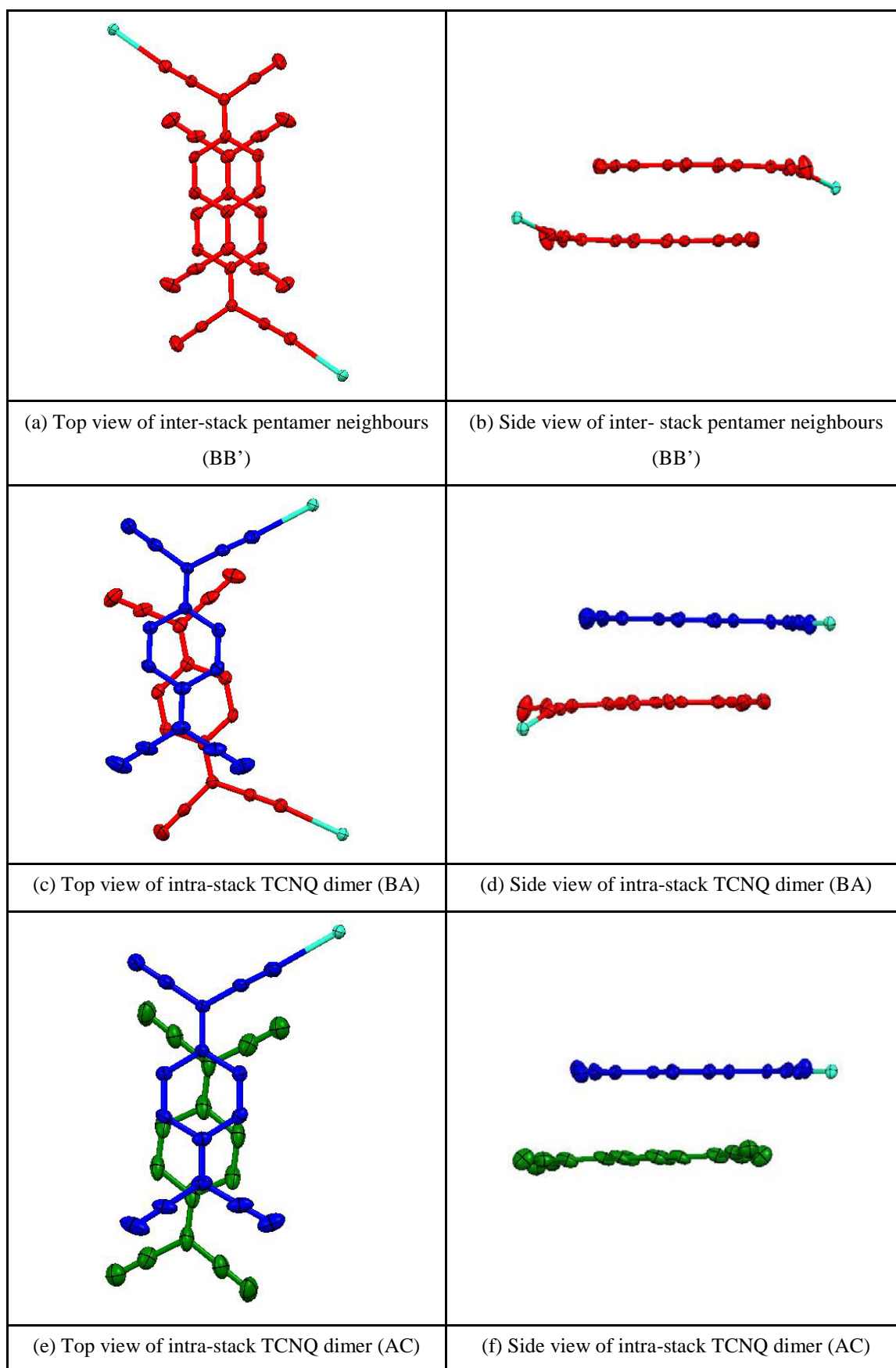


Figure 4.3 Top (a/c/e) and side (b/d/f) views of TCNQ units in $\text{Tb}(\text{TCNQ})_3(\text{H}_2\text{O})_6 \cdot 3\text{H}_2\text{O}$
(hydrogen atoms are excluded)

The packing diagram of $\text{Tb}(\text{TCNQ})_3(\text{H}_2\text{O})_6 \cdot 3\text{H}_2\text{O}$ is shown in Figure 4.4. The TCNQ units lie in infinite stacks with slight rotational twisting between adjacent anion units. These infinite stacks adopt wave-like motif with slight long-axis slippage between adjacent anions (see Figure 4.5). An uncoordinated TCNQ unit (D) is sited in the cavity between neighbouring TCNQ columns. One sheet of uncoordinated TCNQ units (D) is rotated with respect to adjacent sheets by 18.84° as viewed in Figure 4.4(b). Distances and angles within the TCNQ stacks are summarised in Table 4.2.

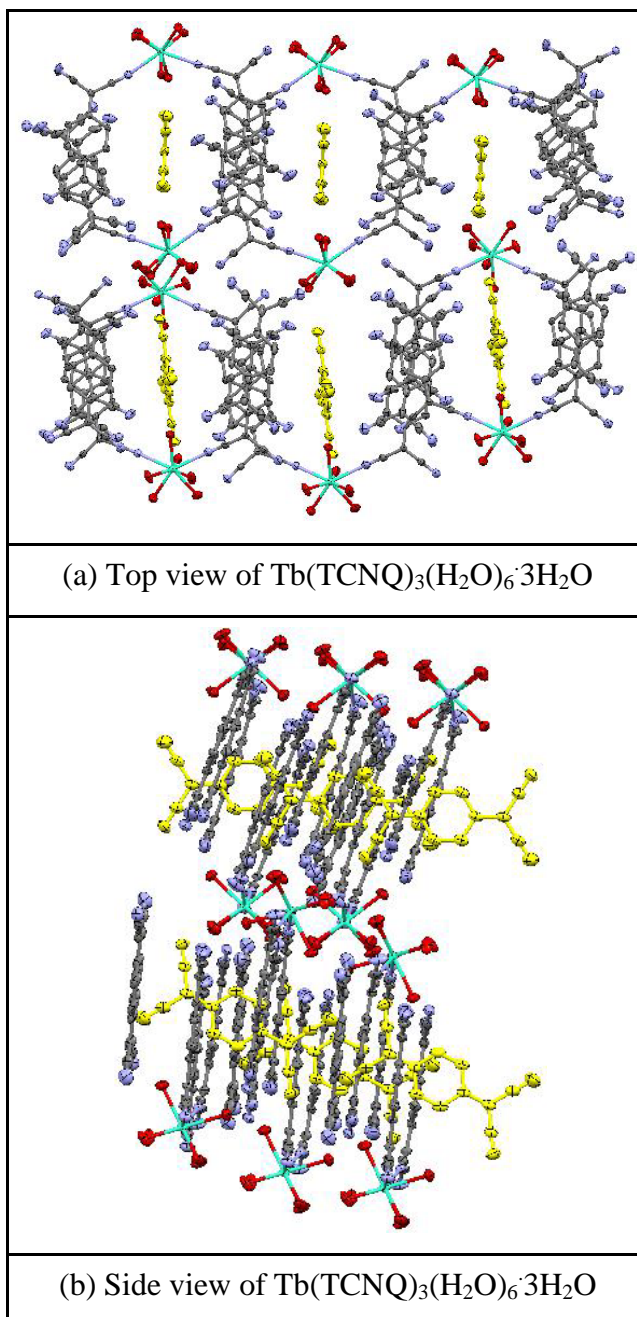


Figure 4.4 Packing diagram of $\text{Tb}(\text{TCNQ})_3(\text{H}_2\text{O})_6 \cdot 3\text{H}_2\text{O}$ viewed along vertical axis (hydrogen atoms and interstitial solvents are excluded)

| TCNQ units | | BA | AC | Inter-stack pentamer neighbours (BB') |
|--|--------------|-------|-------|---------------------------------------|
| π - π perpendicular distance (Å) | | 3.19 | 3.19 | 3.14 |
| Short-axis slip | Distance (Å) | 0.50 | 0.11 | 0.051 |
| | Angle (°) | 8.91 | 1.97 | 0.93 |
| Long-axis slip | Distance (Å) | 1.88 | 1.84 | 2.14 |
| | Angle (°) | 30.51 | 29.98 | 34.28 |
| Centroid-centroid distance (Å) | | 3.73 | 3.69 | 3.80 |

Table 4.2 Distances (Å) and angles (°) within the TCNQ stacks of
 $\text{Tb}(\text{TCNQ})_3(\text{H}_2\text{O})_6 \cdot 3\text{H}_2\text{O}$

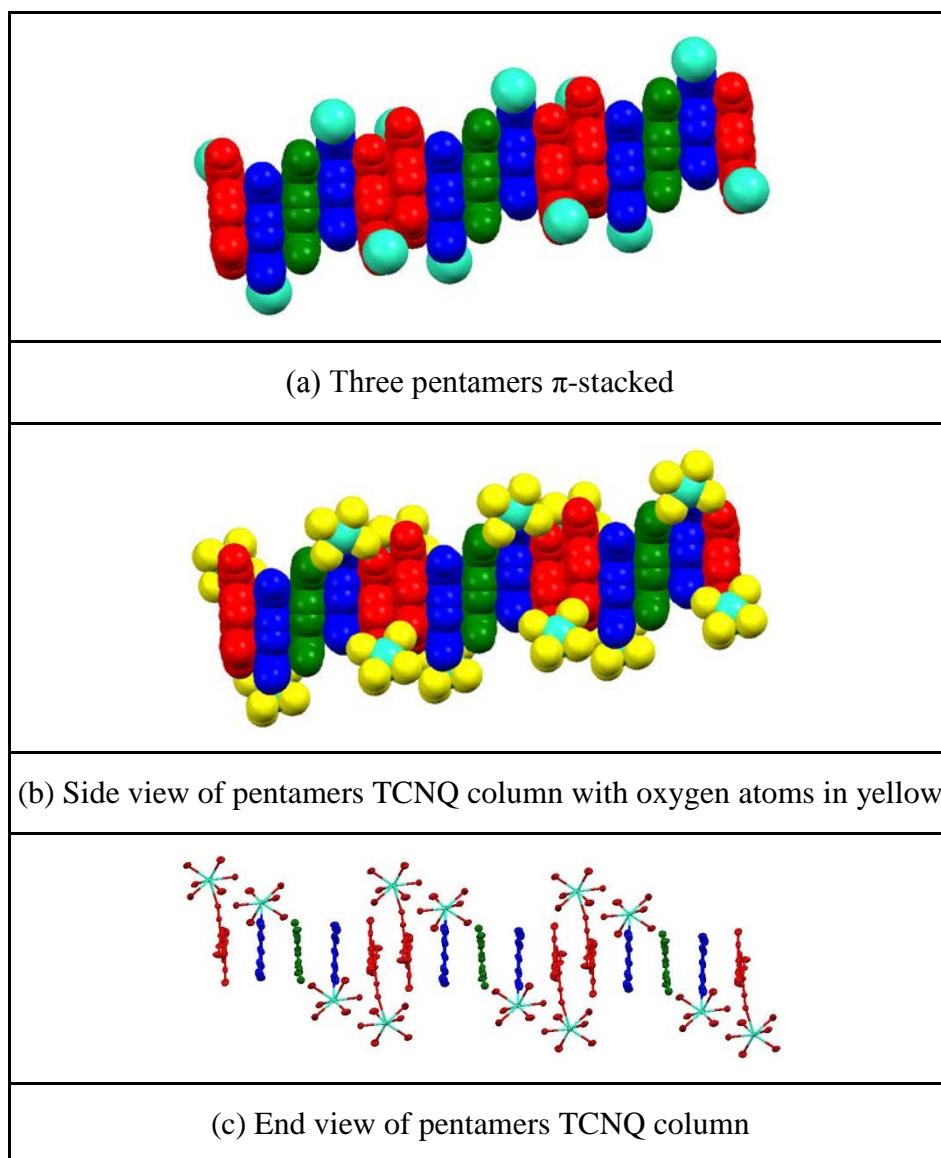


Figure 4.5 Views of pentamers' geometry and packing pattern in the TCNQ stack with
 Tb^{3+} cations in cyan (hydrogen atoms are excluded)

The eight coordinating atoms at Tb^{3+} ion afford a bicapped trigonal prism coordination geometry²³⁶, which is shown in Figure 4.6.

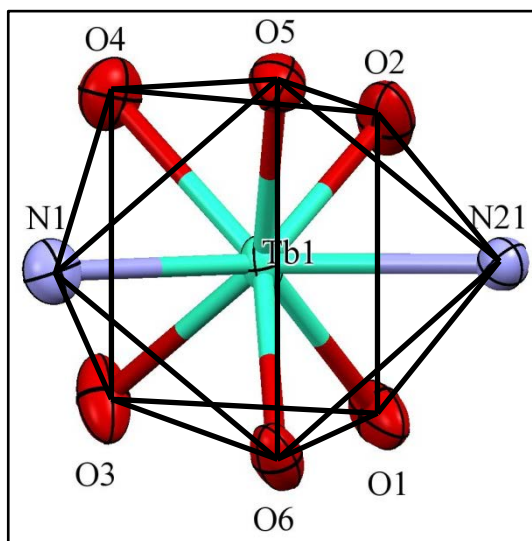


Figure 4.6 Perspective view of coordination geometry in $\text{Tb}(\text{TCNQ})_3(\text{H}_2\text{O})_6 \cdot 3\text{H}_2\text{O}$

One of the two triangular faces is defined by three oxygen atoms (O2, O4 and O5) from three water molecules and the other one is defined by three oxygen atoms (O1, O3 and O6) from the other three water molecules. The tilt angle between the two triangular faces is by 14.59° . The two distances of Tb^{3+} -N are 2.446 and 2.515 Å, and the six distances of Tb^{3+} -O are in the range of 2.330-2.392 Å. The angle of N1-Tb1-N21 is 126.13° . The tilt angle between the two TCNQ mean planes (as defined by each set of aromatic ring) is 2.84° .

4.2 Crystal structure description of $\text{Yb}(\text{TCNQ})_3(\text{H}_2\text{O})_6 \cdot 3\text{H}_2\text{O}$

Reaction of YbCl_3 with LiTCNQ (ratio 1:3) in deionised water afforded a bright blue powder (40%) which contained single crystals suitable for X-ray structural study (combustion data is awaited). Full details including an account of the structure solution and refinement are reported in the Experimental Section and the Supporting Information (in the Appendices) respectively. The crystals obtained were of $\text{Yb}(\text{TCNQ})_3(\text{H}_2\text{O})_6 \cdot 3\text{H}_2\text{O}$ and the basic unit being shown in Figure 4.7.

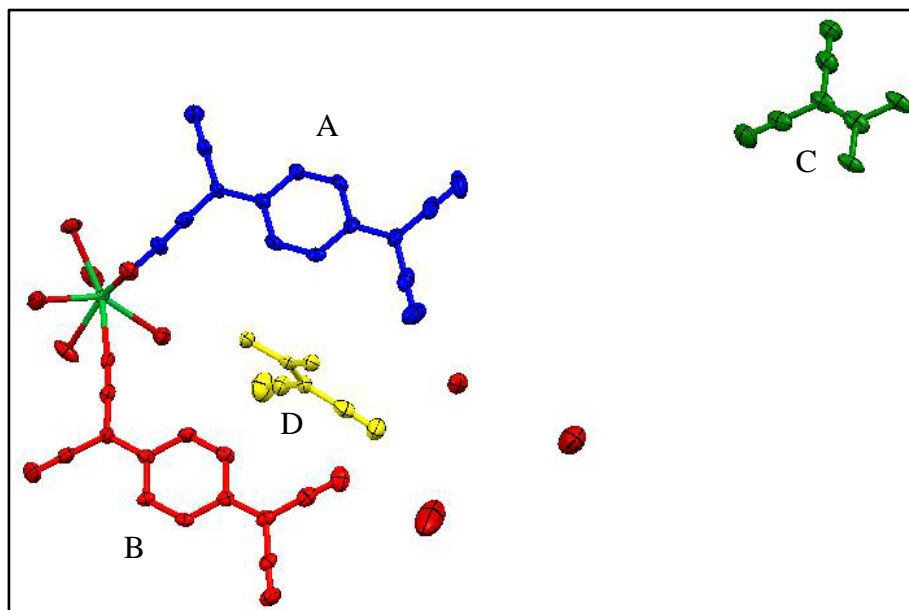


Figure 4.7 Cationic structure of $\text{Yb}(\text{TCNQ})_3(\text{H}_2\text{O})_6 \cdot 3\text{H}_2\text{O}$ [showing two halves of TCNQ units (C and D), hydrogen atoms are excluded]

As viewed in Figure 4.7, each Yb^{3+} ion is coordinated by two nitrogen atoms from adjacent TCNQ units (A and B) and six oxygen atoms from six water molecules. There are two uncoordinated TCNQ units (C and D), which lie on crystallographic centres of symmetry, in the basic structure of $\text{Yb}(\text{TCNQ})_3(\text{H}_2\text{O})_6 \cdot 3\text{H}_2\text{O}$. The mean plane of TCNQ unit (A) (defined by the central aromatic ring) is tilted 2.75° in respect to TCNQ unit (B). The TCNQ unit (D) can sit between TCNQ unit (A) and TCNQ unit (B) and is tilted 88.19° in respect to the TCNQ unit (A) and 87.81° in respect to the TCNQ unit (B). Bond lengths within the $\text{TCNQ}^{\cdot-}$ units are summarised in Table 4.3.

The data in Table 4.3 suggest that all of the TCNQ units have some quinonoidal character because bond length “a” is less than “b”. In this structure, the TCNQ units form a pentamer as repeating unit, in which they are all π -stacked long-axis slipped alternately up and down thereby forming a wave-like motif which is shown in Figure 4.8. Within the TCNQ pentamer, after measuring the c bond lengths in each TCNQ unit, it seems that green TCNQ unit (C) has lower electron density, and therefore has TCNQ^0 character. Consequently, the blue and red TCNQ units (A and B) are more electron rich, and have $\text{TCNQ}^{\cdot-}$ character. TCNQ units (B, A and C) form an angle of 123.06° and TCNQ units (A, C and A') for an angle of 165.02° as viewed in Figure 4.8.

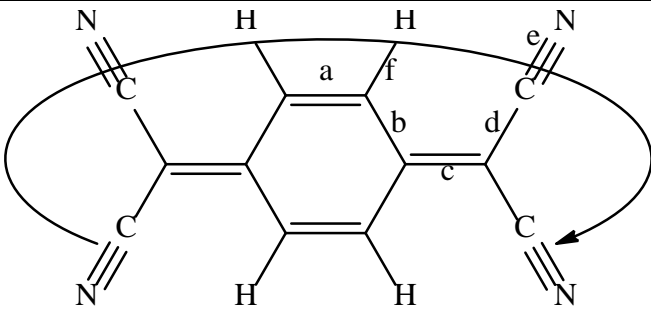
|  | | | | | | |
|--|------------------|-----------|-----------|-----------|-----------|-------|
| (a) Definition of the bond lengths within the TCNQ molecule | | | | | | |
| Structure | Bond lengths (Å) | | | | | |
| | a | b | c | d | e | f |
| TCNQ unit (A) | | 1.418 (7) | | 1.404 (7) | 1.145 (6) | 0.950 |
| | 1.372 (7) | 1.419 (7) | 1.432 (7) | 1.413 (7) | 1.150 (7) | 0.950 |
| | 1.359 (7) | 1.433 (7) | 1.409 (7) | 1.418 (8) | 1.156 (8) | 0.950 |
| | | 1.432 (7) | | 1.426 (8) | 1.145 (8) | 0.949 |
| TCNQ unit (B) | | 1.417 (7) | | 1.406 (7) | 1.157 (7) | 0.951 |
| | 1.359 (7) | 1.426 (7) | 1.434 (7) | 1.404 (7) | 1.154 (7) | 0.950 |
| | 1.382 (7) | 1.431 (7) | 1.411(7) | 1.419 (6) | 1.159 (8) | 0.950 |
| | | 1.424 (7) | | 1.427 (6) | 1.149 (7) | 0.949 |
| TCNQ unit (C) | | 1.431 (8) | | 1.433 (8) | 1.140 (8) | 0.950 |
| | 1.353 (9) | 1.443 (8) | 1.397 (9) | 1.426 (8) | 1.147 (7) | 0.950 |
| | 1.353 (9) | 1.431 (8) | 1.397 (9) | 1.433 (8) | 1.140 (8) | 0.950 |
| | | 1.443 (8) | | 1.426 (8) | 1.147 (7) | 0.950 |
| TCNQ unit (D) | | 1.434 (7) | | 1.435 (8) | 1.146 (8) | 0.950 |
| | 1.368 (8) | 1.420 (8) | 1.411 (8) | 1.433 (8) | 1.151 (8) | 0.949 |
| | 1.368 (8) | 1.434 (7) | 1.411 (8) | 1.435 (8) | 1.146 (8) | 0.950 |
| | | 1.420 (8) | | 1.433 (8) | 1.151 (8) | 0.949 |

Table 4.3 Summary of bond lengths (Å) observed for TCNQ units in
 $\text{Yb}(\text{TCNQ})_3(\text{H}_2\text{O})_6 \cdot 3\text{H}_2\text{O}$

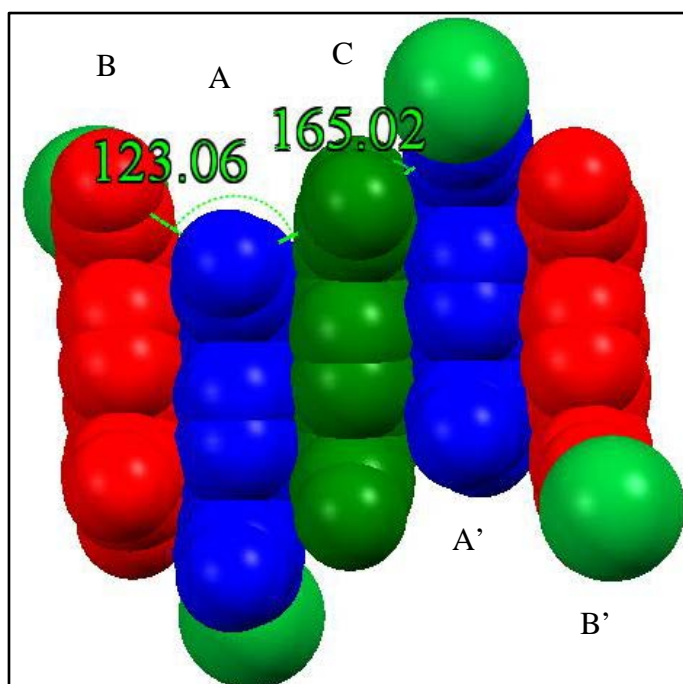


Figure 4.8 Space-fill of TCNQ pentamer stack in $\text{Yb}(\text{TCNQ})_3(\text{H}_2\text{O})_6 \cdot 3\text{H}_2\text{O}$ (Yb^{3+} ions in light green, hydrogen atoms and interstitial solvents are excluded)

The π - π stacking interactions between neighbouring TCNQ units generate one-dimensional columns. These form one-dimensional channels that run throughout the entire crystal structure of $\text{Yb}(\text{TCNQ})_3(\text{H}_2\text{O})_6 \cdot 3\text{H}_2\text{O}$. Therefore, intermolecular hydrogen bonds, π -stacking interactions and electrostatic interactions coexist in the crystal structure of $\text{Yb}(\text{TCNQ})_3(\text{H}_2\text{O})_6 \cdot 3\text{H}_2\text{O}$.

Except for TCNQ unit (B), which is flat, TCNQ unit (A and C) adopt a shallow boat conformation in which neighbouring $-\text{C}(\text{CN})_2$ units are twisted away from each other. The two TCNQ planes are slightly tilted in respect to each other by 2.75° in BA dimer and 0.62° in AC dimer, respectively. Consequently, TCNQ unit (A) and TCNQ unit (C) are rotated 14.73° and 21.23° in respect to TCNQ unit (B), respectively.

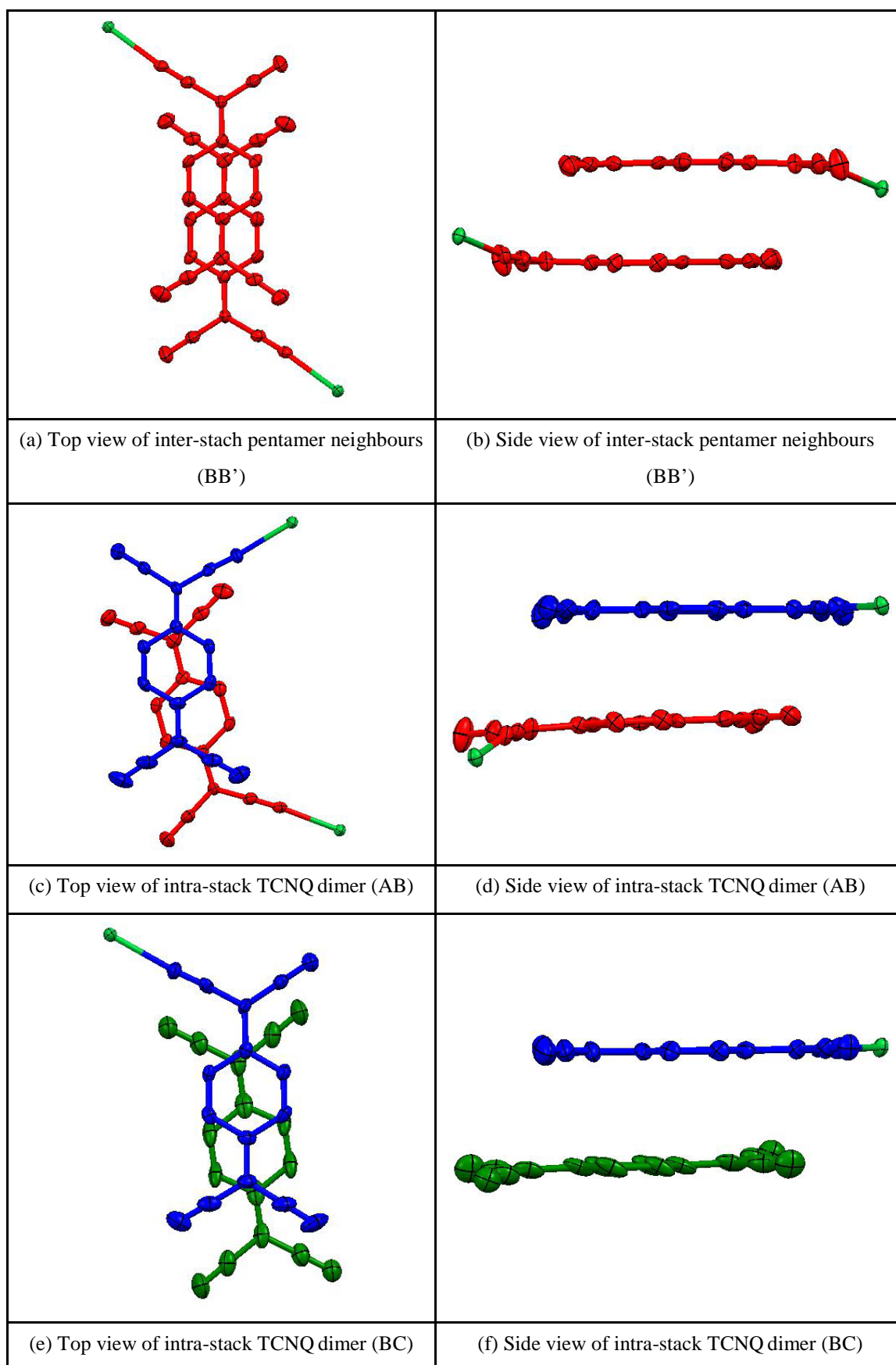


Figure 4.9 Top (a/c/e) and side (b/d/f) views of TCNQ units in $\text{Yb}(\text{TCNQ})_3(\text{H}_2\text{O})_6 \cdot 3\text{H}_2\text{O}$ (hydrogen atoms are excluded)

Figure 4.10 shows the packing diagram of $\text{Yb}(\text{TCNQ})_3(\text{H}_2\text{O})_6 \cdot 3\text{H}_2\text{O}$ viewed along vertical axis. The TCNQ unit lie in an infinite stack with slight rotational twisting between adjacent TCNQ units. The TCNQ units assemble as wave-like infinite stacks with slight long-axis slippage between adjacent TCNQ units. An uncoordinated TCNQ unit is situated vertically between infinite TCNQ columns. One sheet of uncoordinated TCNQ units (D) is rotated with respect to adjacent sheets by 26.20° as viewed in Figure 4.10(b). Distances and angles within the TCNQ stacks are summarised in Table 4.4

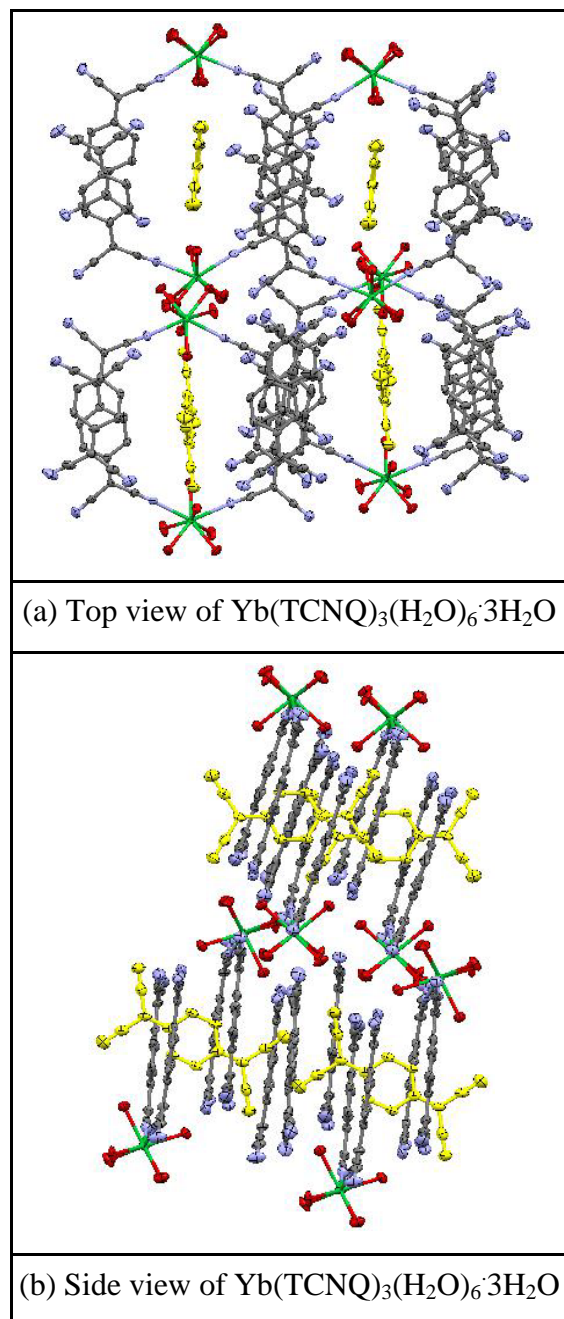


Figure 4.10 Packing diagram of $\text{Yb}(\text{TCNQ})_3(\text{H}_2\text{O})_6 \cdot 3\text{H}_2\text{O}$ viewed along vertical axis
(hydrogen atoms and interstitial solvents are excluded)

| TCNQ units | | BA | AC | Inter-pentamer neighbours |
|--|--------------|-------|-------|---------------------------|
| π - π perpendicular distance (Å) | | 3.19 | 3.17 | 3.13 |
| Short-axis slip | Distance (Å) | 0.48 | 0.10 | 0.058 |
| | Angle (°) | 8.56 | 1.81 | 1.06 |
| Long-axis slip | Distance (Å) | 1.86 | 1.83 | 2.13 |
| | Angle (°) | 30.25 | 30.00 | 34.24 |
| Centroid-centroid distance (Å) | | 3.72 | 3.67 | 3.79 |

Table 4.4 Distances (Å) and angles (°) within the TCNQ stacks of $\text{Yb}(\text{TCNQ})_3(\text{H}_2\text{O})_6 \cdot 3\text{H}_2\text{O}$

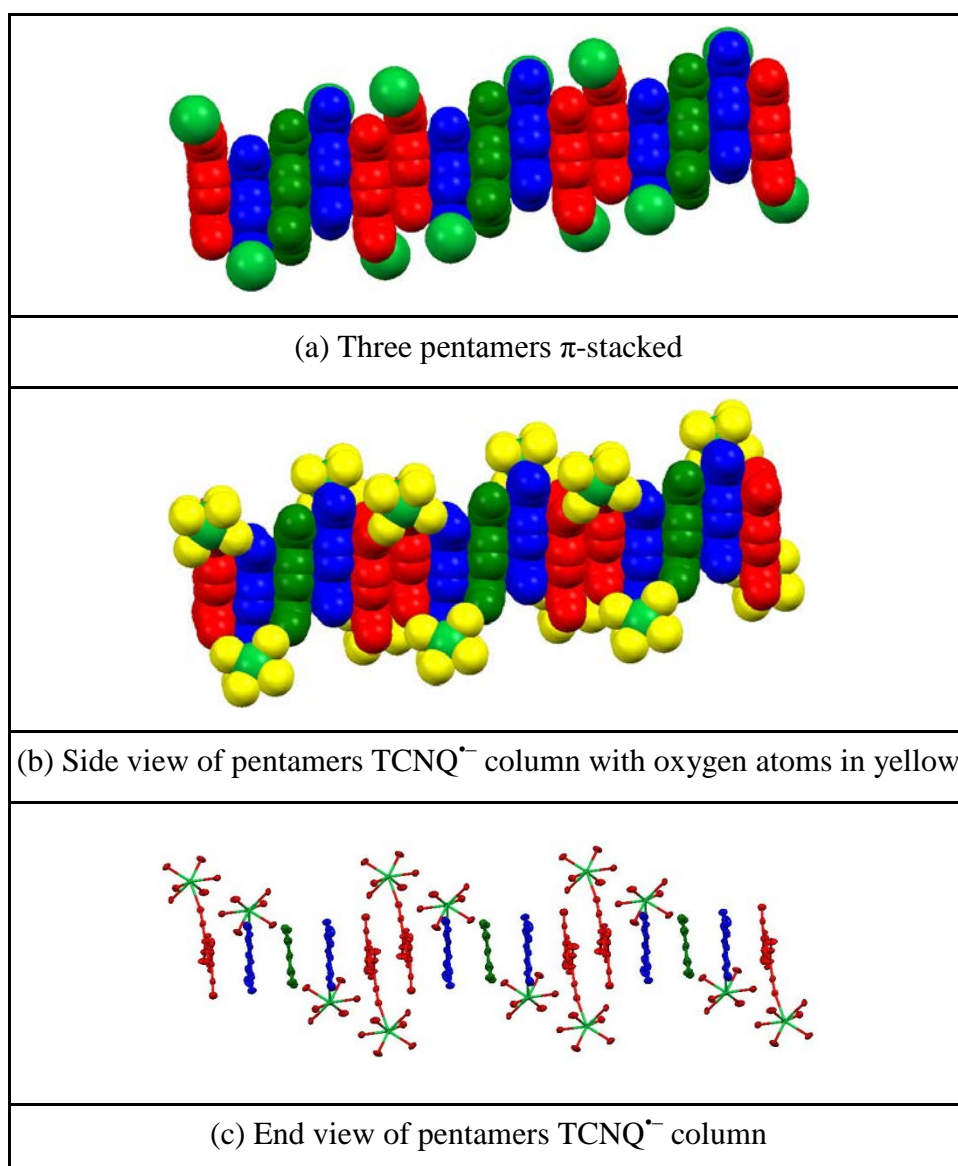


Figure 4.11 Views of pentamers' geometry and packing pattern in the TCNQ stack (hydrogen atoms are excluded)

The eight coordinating atoms around Yb^{3+} adopt a bicapped trigonal prism coordination geometry²³⁶ as viewed in Figure 4.12.

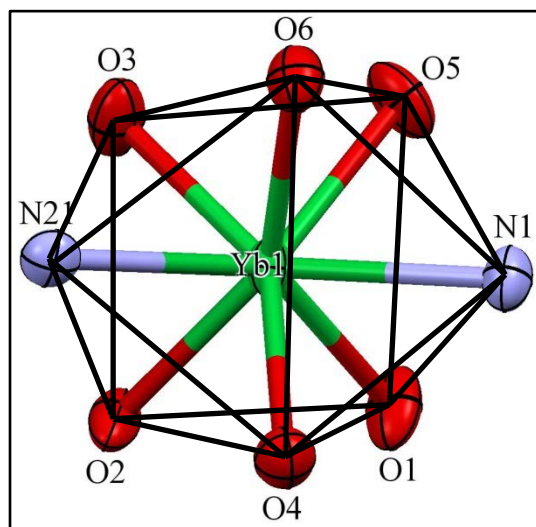


Figure 4.12 Perspective view of coordination geometry in $\text{Yb}(\text{TCNQ})_3(\text{H}_2\text{O})_6 \cdot 3\text{H}_2\text{O}$

One of the two triangular faces is defined by three oxygen atoms (O3, O5 and O6) from three water molecules and the other one is defined by three oxygen atoms (O1, O2 and O4) from the other three water molecules. The tilt angle between the two triangular planes is by 14.44° . The two distances of $\text{Yb}^{3+}\text{-N}$ are 2.390 and 2.466 \AA , and the six distances of $\text{Yb}^{3+}\text{-O}$ are in the range between 2.278 and 2.351 \AA . The angle of N1-Yb1-N21 is 126.30° . The tilt angle between the two $\text{TCNQ}^{\bullet-}$ mean planes (as defined by each set of aromatic ring) is 2.75° .

4.3 Comparison between $\text{Tb}(\text{TCNQ})_3(\text{H}_2\text{O})_6 \cdot 3\text{H}_2\text{O}$ and $\text{Yb}(\text{TCNQ})_3(\text{H}_2\text{O})_6 \cdot 3\text{H}_2\text{O}$ complexes

The important bond distances, coordination number, ligands and coordination geometry of $\text{Tb}(\text{TCNQ})_3(\text{H}_2\text{O})_6 \cdot 3\text{H}_2\text{O}$ (**1**), $\text{Yb}(\text{TCNQ})_3(\text{H}_2\text{O})_6 \cdot 3\text{H}_2\text{O}$ (**2**) and $[\text{Yb}(\text{TCNQ})_2(\text{H}_2\text{O})_6][\text{TCNQ}]\text{H}_2\text{O} \cdot 2\text{MeOH}$ (**3**) are summarised in Table 4.5.

| No. | lanthanide | $\text{Ln}^{3+}\text{-N}$ (Å) | $\text{Ln}^{3+}\text{-O}$ (Å) | $\text{Ln}\cdots\text{Ln}$ (Å) | Coordination number | Coordination geometry |
|-------------------|------------|-------------------------------|-------------------------------|--------------------------------|---------------------|-------------------------|
| 1. | Tb | 2.45, 2.52 | 2.33-2.39 | 8.005 | 8 | bicapped trigonal prism |
| 2. | Yb | 2.39, 2.47 | 2.28-2.35 | 10.62 | 8 | bicapped trigonal prism |
| 3. ²⁹⁵ | Yb | 2.43, 2.51 | 2.28-2.34 | 11.02 | 8 | square antiprismatic |

Table 4.5 Significant structural parameters for **1-3**

In these two complexes (**1** and **2**), except for the $\text{Ln}\cdots\text{Ln}$ distance, the distances of $\text{Ln}^{3+}\text{-N}$ and $\text{Ln}^{3+}\text{-O}$ show a slight decrease along with the size of the lanthanide ions from the larger Tb^{3+} ion to the smaller Yb^{3+} ion²³⁶. The longer $\text{Ln}\cdots\text{Ln}$ distance in $\text{Yb}(\text{TCNQ})_3(\text{H}_2\text{O})_6\cdot 3\text{H}_2\text{O}$ compared with the case in $\text{Tb}(\text{TCNQ})_3(\text{H}_2\text{O})_6\cdot 3\text{H}_2\text{O}$ is because one extra $\text{TCNQ}^{\bullet-}$ unit is inserted vertically in respect to the plane of two coordinated $\text{TCNQ}^{\bullet-}$ units. The trend in structural parameters of **1** and **2** verifies the law of lanthanide contraction²³⁶.

A notable feature of both structures reported here is the formation of TCNQ pentamer stacks similar to those seen in two structures reported earlier in this study namely $(\text{C}222)\text{K}(\text{TCNQ})_{2.5}$ and $(\text{C}222)\text{Rb}(\text{TCNQ})_{2.5}$, respectively. In both of the previous examples, the TCNQ column consisted of mixed valence TCNQ stacks, *i.e.* stacks containing a mixture of TCNQ^0 and $\text{TCNQ}^{\bullet-}$, adopting a wave-like motif. Such a situation may also occur in the two structures under discussion here since; (i) there is significant variation in bond lengths in the three different TCNQ components A, B and C suggesting mixed redox states; and (ii) it is not clear whether the crystals only contain H_2O molecules or whether some of these are actually hydroxide ions. If the latter were true it would compensate (in charge terms) for the presence of a neutral TCNQ component. Furthermore, over a period of two years the crystals of $\text{Tb}(\text{TCNQ})_3(\text{H}_2\text{O})_6\cdot 3\text{H}_2\text{O}$ and $\text{Yb}(\text{TCNQ})_3(\text{H}_2\text{O})_6\cdot 3\text{H}_2\text{O}$ have changed from dark blue to green in colour consistent with, for example, oxidation of $\text{TCNQ}^{\bullet-}$ to TCNQ^0 which could occur if water molecules were being converted into hydroxide ions. In order to test this, an X-ray structural study of the degraded green crystals is to be attempted in an attempt to gain insight into this degradation process. In addition it is hoped that samples of the original complexes might be able to be analysed by neutron diffraction techniques in the hope of detecting the locations of the hydrogen atoms in the sample.

5. Conclusions and Further Work

In the course of this project, a number of novel simple and complex TCNQ salts have been synthesised and the solid-state behaviour of these new compounds has been studied with a view to gaining further insight into the potential for crystal engineering of the properties of such materials.

The simple 1:1 TCNQ salts tended to form when the cavity of the crown ether was comparable to or larger than the corresponding size of the cation, whereas when the crown ether had a cavity smaller than the size of the cation, a 2:1 stoichiometry was seen arising from the cation being sandwiched between two crown ether units^{126,264}. For much larger cations, such as in (12C4)Rb(TCNQ)_{1.5}, four nitrogen atoms from adjacent TCNQ units compensate for the failure of the crown ether to satisfy the coordination of the metal cation. In simple TCNQ salts, the TCNQ^{•-} units prefer to form dimers which are then further packed into infinite columns.

From the table of Infrared frequencies, there are certain characteristics which highlight the reduction of TCNQ⁰ into TCNQ^{•-}. These contain: (a) the splitting of the nitrile frequencies; and (b) conversion of a quinonoid structure into an aromatic system. Intense EPR spectra observed in M⁺(15-crown-5)TCNQ^{•-} (M = Li, Na) at ambient temperature and above, in single crystal samples, are typical of thermally excited triplet state species (S = 1).

Some of the materials show more complex or unusual behaviour. For example, in (15C5)₂RbTCNQ, TCNQ^{•-} dimers assemble into infinite parallel sheets. In (DB18C6)RbTCNQ, the TCNQ^{•-} dimers and cation complex of (DB18C6)Rb⁺ form assemblies which coordinate with lateral neighbours to form infinite linear tapes through the crystal structure. Within the series of complex TCNQ salts studied, in (18C6)Rb(TCNQ)₂, (18C6)Cs(TCNQ)₂ and (B15C5)₂Cs(TCNQ)₃, the TCNQ units prefer to form trimers which further assemble into infinite columns. In (15C5)Na(TCNQ)₂·H₂O, TCNQ units form a tetramer as repeating unit. In (18C6)K(TCNQ)_{2.5}, (C222)K(TCNQ)_{2.5} and (C222)Rb(TCNQ)_{2.5}, the TCNQ units prefer to form pentamer as the repeating unit which further assembles into wave-like infinite TCNQ column. In (12C4)Rb(TCNQ)_{1.5}, (Dicyc18C6)K(TCNQ)₃ and (Dicyc18C6)Rb(TCNQ)₃, each TCNQ dimer is separated by an isolated TCNQ unit. In

complex TCNQ salts, the electrons are delocalised within the TCNQ repeating unit and these materials have a higher electrical conductivity than the corresponding simple TCNQ salts.

This study has led to the discovery of a number of novel packing motifs of ionophore-complexed alkali metal TCNQ salts. Future work would involve the synthesis of 1:1 ratio of RbTCNQ, CsTCNQ and reacting of these with different sizes of crown ethers in order to investigate the packing pattern of such TCNQ “simple” complexes.

Initial studies of the conductivity and EPR behaviour of these materials needs to be extended to see how different packing patterns influence their behaviour. For simple ionophore-complexed alkali metal TCNQ salts prepared in this study, the spin-spin interaction of the excited triplet has been studied by EPR spectroscopy of a single crystal and has principal values and directions appropriate for the location of the intrinsic pair within the crystal structure. For complex TCNQ salts prepared in this study, there is no evidence for such localised triplet excited states. In future work, conductivity measurements over a range of different temperatures will also be needed in order to measure the activation energies for charge migration in each of the TCNQ salts.

Two lanthanide TCNQ complexes have also been prepared: $\text{Tb}(\text{TCNQ})_3(\text{H}_2\text{O})_6 \cdot 3\text{H}_2\text{O}$ and $\text{Yb}(\text{TCNQ})_3(\text{H}_2\text{O})_6 \cdot 3\text{H}_2\text{O}$. Both of the lanthanide TCNQ salts were synthesised in 2012 and since that time the colour of both complexes has changed from dark blue to green. This is probably because the $\text{TCNQ}^{\cdot -}$ anion has been oxidised into TCNQ^0 .

Consequently, the packing motif of TCNQ unit may have changed. This needs further X-ray crystallographic study to identify any changes. Within the two lanthanide TCNQ salts in this study, the wave-motif of the repeating unit of TCNQ pentamer implies that there is probably TCNQ^0 present within the pentamer and if so coordinated H_2O molecules might have been converted to OH^- in order to maintain charge balance. In future work, these two complexes need to be studied by UV-Vis to identify the oxidation state of the lanthanide cations.

6. Experimental Details

6.1 General Details and Instrumentation

6.1.1 Melting Points

Melting points were measured on an Electrothermal melting point apparatus and are uncorrected.

6.1.2 Elemental Analysis

Elemental combustion analyses were performed by Medac Ltd, Chobham Business Centre, Chertsey Road, Chobham, Surrey, GU24 8JB.

6.1.3 Nuclear Magnetic Resonance Spectra

6.1.3.1 Bruker AVII400 FT-NMR Spectrometer (400/1)²⁹⁶

The 400/1 is equipped with a 5mm BBFO probe for routine observation of proton, carbon, fluorine and phosphorous with deuterium lock fitted with z-gradient coils and an automatic sample changer.

The 400/1 is intended for rapid acquisition of routine NMR experiments (1D ^1H , ^{13}C , ^{19}F , ^{31}P spectra, HH COSY, HH TOCSY, HMQC, HMBC, FF COSY). Samples can be entered into an automated queue using the 60 position sample changer.

Data are available for remote processing once acquisition has been completed.

6.1.3.2 Bruker AVIIIHD400 FT-NMR Spectrometer (400/3)²⁹⁷

The 400/3 is equipped with a 5mm SMART probe for routine observation of proton, carbon, fluorine and phosphorous with deuterium lock fitted with z-gradient coils and an automatic sample changer.

The 400/3 is intended for rapid acquisition of routine NMR experiments (1D ^1H , ^{13}C , ^{19}F , ^{31}P spectra, HH COSY, HH TOCSY, HMQC, HMBC, FF COSY). Samples can be entered into an automated queue using the 60 position sample changer.

Data are available for remote processing once acquisition has been completed.

6.1.4 Infra-Red Spectroscopy

IR (KBr discs) spectra were obtained using a Golden Gate sampling attachment on a Mattson Satellite 3000 FTIR at the University of Southampton.

6.1.5 UV / Vis Spectroscopy

UV/Vis spectra were recorded on a Shimadzu 1601 UV-Visible spectrophotometer. Samples were prepared as a solution in a quartz cell.

6.1.6 Raman Spectroscopy

Raman Spectra were collected using a Renishaw In-Via system with a high powered near Infrared (HPNIR) 785nm laser and microscope using a 50× objective at the University of Southampton.

6.1.7 Mass Spectroscopy²⁹⁸

6.1.7.1 MaXis ELECTROSPRAY IONISATION

Samples were analysed using a MaXis (Bruker Daltonics, Bremen, Germany) mass spectrometer equipped with a Time of Flight (TOF) analyser. Samples were introduced to the mass spectrometer *via* a Dionex Ultimate 3000 autosampler and uHPLC pump. Ultra performance liquid chromatography was undertaken *via* a Waters UPLC BEH C18 (50 mm x 2.1mm 1.7µm) column. Gradient 20% acetonitrile (0.2% formic acid) to 100% acetonitrile (0.2% formic acid) in five minutes at a flow rate of 0.6 mL/min. High resolution mass spectra were recorded using positive/negative ion electrospray ionisation.

6.1.7.2 solariX ELECTROSPRAY IONISATION/APPI IONISATION

Samples were analysed using a solariX (Bruker Daltonics, Bremen, Germany) mass spectrometer equipped with a 4.7T magnet and FT-ICR cell. Samples were introduced to the mass spectrometer *via* infusion at a flow rate of 5µL/min into an electrospray ionisation source. High resolution mass spectra were recorded using positive/negative ion electrospray ionisation or Atmospheric pressure photoionization.

6.1.8 Single Crystal X-ray Diffraction²⁹⁹

Crystal structures of the charge transfer TCNQ complexes were measured using Rigaku FR-E+ Ultra High Flux Diffractometer AKA Ros, Rigaku FR-E+ Ultra High Flux Diffractometer AKA Kat and Rigaku 007-HF Diffractometer AKA Dot at the University of Southampton. The structures were solved by direct methods (SHELXS)³⁰⁰ and refined by full-matrix least squares techniques based on F^2 (SHELXL)³⁰⁰ within Olex2³⁰¹. The non-H atoms were refined with anisotropic displacement parameters, except for the disordered crown ether TCNQ complexes, in which the less percentage of the component is kept as isotropic. Molecular illustrations were made with Mercury³⁰². Each of the crystal structure's data were processed by CrystalClear³⁰³⁻³⁰⁵.

6.1.8.1 Rigaku FR-E+ Ultra High Flux Diffractometer AKA Ros

Named after Rosalind Franklin, Ros is the left-hand port on new FR-E+ SuperBright Molybdenum X-Ray generator. This side has a highly focused beam (70 μ m) achieved with the new VariMax VHF (Very High Flux) optics. The setup is completed with an AFC12 goniometer and an enhanced sensitivity Saturn 724+ 18bit CCD detector. Ros is possibly THE most powerful laboratory-based diffractometer in the world! Data is routinely collected at 100K with the aid of an Oxford Cryosystems Cobra.

6.1.8.2 Rigaku FR-E+ Very High Flux Diffractometer AKA Kat

Named in honour of Kathleen Lonsdale, Kat is the right-hand port on new FR-E+ SuperBright Molybdenum X-Ray generator. This side is equipped with VariMax HF (High Flux) optics and the beam is slightly de-focused (100 μ m). As for Ros, the diffractometer also features the AFC12 goniometer and an enhanced sensitivity Saturn 724 + 18bit CCD detector. Kat and Ros together offer the most powerful diffraction equipment that can be found in a departmental laboratory for Chemical Crystallography. Data is routinely collected at 100K with the aid of an Oxford Cryosystems Cobra.

6.1.8.3 Rigaku 007-HF Diffractometer AKA Dot

In honour of Dorothy Hodgkin, the new Rigaku 007 HF (High Flux) diffractometer was named Dot. This Copper rotating anode, equipped with a Saturn 944+ enhanced sensitivity detector, is a very popular solution for macromolecular crystallography, but also provides numerous advantages over the traditional Mo-based systems for chemical

Chapter 6

crystallography. Data is routinely collected at 100K through the use of an Oxford Cryosystems 700 Series CryoStream.

6.1.9 Electron Paramagnetic Resonance

Bruker EMX X/Q-band EPR spectrometer. All of the measurements were performed at X-band which means microwave frequency ~ 10 GHz and magnetic field ~ 3500 G. The exact field and frequency depends on the sample for each individual experiment.

A Bruker High Sensitivity resonator (part number ER 4119HS) or a Super High Q (ER 4122 SHQE) were used for the earlier measurements. The programmable goniometer was Bruker ER 218PG1. Temperature control was achieved using nitrogen gas flow from a B-VT 2000 temperature controller with a quartz dewar insert. The dewar insert holder is Bruker part number ER 169DIS. The data were collected and the results were solved by Dr. Christopher Wedge (University of Warwick – Department of Physics).

6.1.10 Resistance

Resistance data were recorded by MASTECH MY64 Digital Multimeter AC/DC Voltage Current Resistance Tester Detector with Diode.

6.2 Preparation & Purification of Starting Materials, Solvent & Reagents

- (i). Acetonitrile was dried over calcium hydride and distilled before use.
- (ii). Diethyl ether was dried over sodium wire and was freshly decanted before use.
- (iii). Methanol was dried over calcium sulphate and distilled before use.
- (iv). Ethanol was dried over calcium sulphate and distilled before use.
- (v). DCM was dried over calcium hydride and distilled before use.

6.3 Preparation of TCNQ complexes

6.3.1 Purification of TCNQ²⁸³

Pure TCNQ (2.15g, 10.5mmol) is a yellow crystalline solid which was purified by recrystallization from dry acetonitrile (50ml). This procedure was repeated until crystals were yellow-gold, without hint of green. IR $\nu_{\max}/\text{cm}^{-1}$ 2220 (CN stretch). Raman $\nu_{\max}/\text{cm}^{-1}$ 2229 (CN stretch), 1602 (C=C ring stretch), 1454 (C-CN stretch), 1206 (C=C-H bending). Raman $\nu_{\max}/\text{cm}^{-1}$ 2230 (CN stretch), 1603 (C=C ring stretch), 1454 (C-CN stretch), 1206 (C=C-H bending). M.p.>250°C. (lit²⁸³. 287-289°C (dec.))

6.3.2 Preparation of NaTCNQ²⁸³

To a boiling solution of TCNQ (1.02g, 5mmol) in dry acetonitrile (CH_3CN , 50ml) was added a boiling solution of sodium iodide (1.12g, 7.5mmol) in dry acetonitrile (CH_3CN , 50ml). The mixture was stirred for several minutes, then left to cool down, and the precipitate was filtered off. The solid was washed with acetonitrile until washings changed from purple to bright green. The solid was then further washed with diethyl ether (50ml). The residue was dried in vacuum to give a bright purple powder of NaTCNQ (0.97g, 86%). IR $\nu_{\max}/\text{cm}^{-1}$ 2187, 2147 (CN stretch), 1568 (C=C(CN)₂ stretch), 1501 (C=C ring stretch), 1360 (CH bend), 1319 (C-C ring stretch), 1164 (C-CN and C-C ring stretch), 983 (C-C ring stretch), 817, 716 (CH out of plane bend). (lit²⁸³. 2181(plus two more in the same envelope)). M.p.>250°C. (lit²⁸³. >300°C).

6.3.3 Preparation of LiTCNQ²⁸³

To a boiling solution of TCNQ (0.80g, 4mmol) in dry acetonitrile (50ml) was added a boiling solution of lithium iodide (0.95g, 7mmol) in dry acetonitrile (50ml). The mixture was stirred for several minutes, left to cool down. The precipitate was filtered off. The solid was then washed with acetonitrile until washings changed from purple to bright green, and then further washed with diethyl ether (50ml). The solid was dried in vacuum to give a dark purple powder of LiTCNQ (0.70g, 85%). IR $\nu_{\max}/\text{cm}^{-1}$ 2201, 2171 (CN stretch) (lit²⁸³. 2204, 2193), 1580 (C=C(CN)₂ stretch), 1501 (C=C ring stretch), 1360 (CH bend), 1325 (C-C ring stretch), 1165 (C-CN and C-C ring stretch), 985 (C-C ring stretch), 821, 718 (CH out of plane bend). M.p.>250°C. (lit²⁸³. >300°C).

6.3.4 Preparation of KTCNQ⁸⁰

To a boiling solution of TCNQ (1.02g, 5mmol) in dry acetonitrile (50ml) was added a boiling solution of potassium iodide (1.25g, 7.5mmol) in dry acetonitrile (50ml). The mixture was stirred for several minutes (longer than used for making LiTCNQ and NaTCNQ, because the potassium iodide does not dissolve in acetonitrile very well at lower temperatures), and then left to cool down. The precipitate was filtered off. The solid was then washed with acetonitrile until washings changed from purple to bright green, and the further washed with diethyl ether (50ml). The solid was dried in vacuum to give a bright purple powder of KTCNQ (0.94g, 83%). IR $\nu_{\text{max}}/\text{cm}^{-1}$ 2215, 2152 (CN stretch), 1578 ($\text{C}=\text{C}(\text{CN})_2$ stretch), 1505 ($\text{C}=\text{C}$ ring stretch), 1366 (CH bend), 1332 ($\text{C}-\text{C}$ ring stretch), 1175 ($\text{C}-\text{CN}$ and $\text{C}-\text{C}$ ring stretch), 988 ($\text{C}-\text{C}$ ring stretch), 825, 720 (CH out of plane bend). M.p. >250°C. (lit⁸⁰. >300°C).

6.3.5 Preparation of Rb₂(TCNQ)₃

RbI (0.1908g, 0.9mmol) was placed in 250ml round bottom flask and TCNQ⁰ (0.1224g, 0.6mmol) was added. The mixture was dissolved in dry acetonitrile and the resulting solution was left to reflux and stir overnight. The product was filtered while still warm and was washed with dry acetonitrile (100ml) with the washings were bright green. Further washing was completed using dry diethyl ether (100ml) and the product was dried in vacuum over CaCl₂ to give a bright purple crystalline solid (0.12693g, 81%). IR $\nu_{\text{max}}/\text{cm}^{-1}$ 2229, 2214, 2181, 2162 (CN stretch), 15779 ($\text{C}=\text{C}(\text{CN})_2$ stretch), 1503 ($\text{C}=\text{C}$ ring stretch), 1367 (CH bend), 1352 ($\text{C}-\text{C}$ ring stretch), 1183 ($\text{C}-\text{CN}$ and $\text{C}-\text{C}$ ring stretch), 984 ($\text{C}-\text{C}$ ring stretch), 825, 717 (CH out of plane bend). M.p. >250°C.

6.3.6 Preparation of Cs₂(TCNQ)₃

CsI (0.234g, 0.9mmol) was placed in 250ml round bottom flask and TCNQ⁰ (0.1224g, 0.6mmol) was added. The mixture was dissolved in dry acetonitrile and the resulting solution was left to reflux and stir overnight. The product was filtered while still warm and was washed with dry acetonitrile (100ml) until the washings were bright green. Further washing was completed using dry diethyl ether (100ml) and the product was dried in vacuum over CaCl₂ to give a bright purple crystalline solid (0.14498g, 83%). IR $\nu_{\text{max}}/\text{cm}^{-1}$ 2225, 2210, 2180, 2160 (CN stretch), 1579 ($\text{C}=\text{C}(\text{CN})_2$ stretch), 1503 ($\text{C}=\text{C}$

ring stretch), 1368 (CH bend), 1326 (C-C ring stretch), 1182 (C-CN and C-C ring stretch), 963 (C-C ring stretch), 823, 716 (CH out of plane bend). M.p.>250°C.

6.3.7 Preparation of (12C4)₂LiTCNQ

A solution of LiTCNQ (0.424g, 2mmol) and 12-crown-4 (0.700g, 4mmol) in dry acetonitrile (50ml) was boiled for five minutes, and filtered whilst hot and the mixture was then left to cool. The solvent was allowed to evaporate slowly over a period of several days during which a solid was formed which was separated by filtration. The solid was washed with diethyl ether (50ml) and dried in vacuum to give small black chunks (0.437g, 78%). MS (solution) (MeCN) (ESI⁻) m/z: 204.1 (TCNQ⁻). (ESI⁺) m/z: 375.2 (2 × Crown + Na⁺), 199.2 (Crown + Na⁺). IR $\nu_{\max}/\text{cm}^{-1}$ 2968, 2915, 2875 (saturated CH stretch), 2173, 2151 (CN stretch), 1589 (C=C(CN)₂ stretch), 1505 (C=C ring stretch), 1361 (CH bend), 1177 (C-CN and C-C ring stretch), 986 (C-C ring stretch), 819, 718 (CH out of plane bend). Raman $\nu_{\max}/\text{cm}^{-1}$ 2214 (CN stretch), 1604 (C=C ring stretch), 1384 (C-CN stretch), 1208 (C=C-H bending). M.p. 234°C (dec.). Combustion Analysis: Calculated: C: 59.68%, H: 6.44%, N: 9.94%. Found: C: 59.80%, H: 6.15%, N: 10.36%.

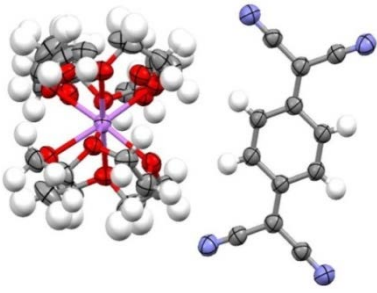
| | | |
|--|---|-----------------------------------|
|  | | |
| $\text{C}_{28}\text{H}_{36}\text{LiN}_4\text{O}_8$ | $a = 16.854(4) \text{ \AA}$ | $\alpha = 90^\circ$ |
| $M_r = 563.55$ | $b = 20.568(5) \text{ \AA}$ | $\beta = 90.539(16)^\circ$ |
| Monoclinic, C2/c | $c = 8.316(3) \text{ \AA}$ | $\gamma = 90^\circ$ |
| $T = 100(2) \text{ K}$ | $V = 2882.8(14) \text{ \AA}^3$ | $Z = 4$ |
| $\lambda = 1.54187 \text{ \AA}$, Dot | $0.36 \times 0.32 \times 0.05 \text{ mm}^3$ | Chunks; Black |
| $D_c = 1.298 \text{ Mg / m}^3$ | $\mu = 0.787 \text{ mm}^{-1}$ | Completeness = 99.6% |
| Independent reflections = 2657 [$R_{\text{int}} = 0.1317$] | $R_1 [I \geq 2\sigma(I)] = 0.0922$ | $wR_2 [\text{all data}] = 0.2795$ |

Table 6.1 Crystal structure information of (12C4)₂LiTCNQ in this study

6.3.8 Preparation of (12C4)₂NaTCNQ²⁸³

A solution of NaTCNQ (0.454g, 2mmol) and 12-crown-4 (0.700g, 4mmol) in dry acetonitrile (50ml) was boiled for five minutes, and filtered whilst hot. The mixture was then left to cool. The solvent was allowed to evaporate slowly over a period of several days during which a solid was formed separately filtration. The solid was washed with diethyl ether (50ml) and dried in vacuum to give small bright black needles (0.269g, 47%). MS (solution) (MeCN) (ESI⁻) m/z: 204.1 (TCNQ⁻). (ESI⁺) m/z: 375.2 (2 × Crown + Na⁺), 199.2 (Crown + Na⁺). IR $\nu_{\max}/\text{cm}^{-1}$ 2962, 2916, 2875 (saturated CH stretch), 2172, 2150 (CN stretch) (lit²⁸³. 2177, 2156), 1567 (C=C(CN)₂ stretch), 1505 (C=C ring stretch), 1361 (CH bend), 1177 (C-CN and C-C ring stretch), 986 (C-C ring stretch), 820, 718 (CH out of plane bend). Raman $\nu_{\max}/\text{cm}^{-1}$ 2257 (CN stretch), 1609 (C=C ring stretch), 1389 (C-CN stretch), 1206 (C=C-H bending). M.p. 226°C (dec.) (lit²⁸³. 185-187°C). Combustion Analysis: Calculated: C: 58.03%, H: 6.22%, N: 9.67%. Found: C: 57.64%, H: 6.16%, N: 9.48%.

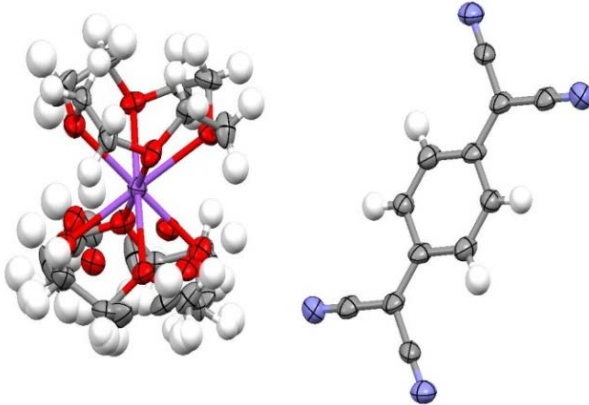
| | | |
|--|---|-----------------------------------|
|  | | |
| $\text{C}_{28}\text{H}_{36}\text{N}_4\text{NaO}_8$ | $a = 17.191(2) \text{ \AA}$ | $\alpha = 90^\circ$ |
| $M_r = 579.60$ | $b = 20.518(2) \text{ \AA}$ | $\beta = 90.131(6)^\circ$ |
| Monoclinic, C2/c | $c = 8.3079(9) \text{ \AA}$ | $\gamma = 90^\circ$ |
| $T = 120(2) \text{ K}$ | $V = 2930.4(5) \text{ \AA}^3$ | $Z = 4$ |
| $\lambda = 0.71075 \text{ \AA}$, Ros | $0.56 \times 0.06 \times 0.02 \text{ mm}^3$ | Needles; Black |
| $D_c = 1.314 \text{ Mg / m}^3$ | $\mu = 0.109 \text{ mm}^{-1}$ | Completeness = 99.9% |
| Independent reflections = 3352 [$R_{\text{int}} = 0.1059$] | $R_1 [I \geq 2\sigma(I)] = 0.0852$ | $wR_2 [\text{all data}] = 0.3046$ |

Table 6.2 Crystal structure information of (12C4)₂NaTCNQ in this study

6.3.9 Preparation of (12C4)₂Li(TCNQ)₂

A solution of LiTCNQ (0.0211g, 0.1mmol), TCNQ⁰ (0.0204g, 0.1mmol) and 12-crown-4 (0.0352g, 0.2mmol) in dry acetonitrile (50ml) was heated under reflux for three hours, filtered whilst hot and then left to cool. The solvent was left to evaporate slowly over a period of several days and the solid which formed was then separated by filtration. The solid was washed with diethyl ether (50ml) and dried in vacuum to form a plate of a dark green crystalline solid (0.02122g, 28%). MS (solution) (MeCN) (ESI⁺) m/z: 204.7 (TCNQ⁻). (ESI⁺) m/z: 375.6 (2 × Crown + Na⁺), 199.4 (Crown + Na⁺). IR $\nu_{\text{max}}/\text{cm}^{-1}$ 2970, 2940 (saturated CH stretch), 2215, 2188 (CN stretch), 1558 (C=C(CN)₂ stretch), 1507 (C=C ring stretch), 1327 (CH bend), 1134 (C-CN and C-C ring stretch), 953 (C-C ring stretch), 861, 694 (CH out of plane bend). Raman $\nu_{\text{max}}/\text{cm}^{-1}$ 2216 (CN stretch), 1606 (C=C ring stretch), 1385 (C-CN stretch), 1207 (C=C-H bending). M.p. 312°C (dec.).

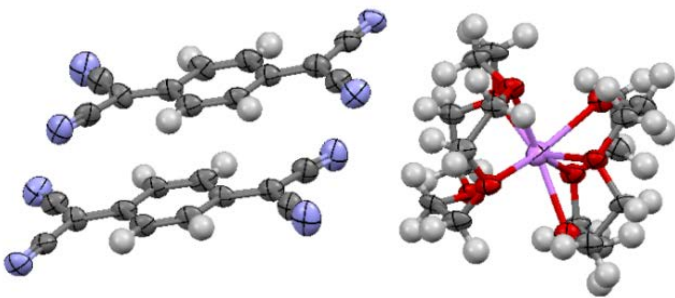
| | | |
|--|---|-----------------------------------|
|  | | |
| $\text{C}_{40}\text{H}_{40}\text{N}_8\text{LiO}_8$ | $a = 8.2048(5) \text{ \AA}$ | $\alpha = 72.456(6)^\circ$ |
| $M_r = 767.74$ | $b = 13.7261(10) \text{ \AA}$ | $\beta = 83.046(7)^\circ$ |
| Triclinic, P-1 | $c = 17.8891(13) \text{ \AA}$ | $\gamma = 86.624(7)^\circ$ |
| $T = 100(2) \text{ K}$ | $V = 1906.3(2) \text{ \AA}^3$ | $Z = 2$ |
| $\lambda = 0.71075 \text{ \AA}$, Ros | $0.05 \times 0.04 \times 0.02 \text{ mm}^3$ | Plate; Dark Green |
| $D_c = 1.338 \text{ Mg / m}^3$ | $\mu = 0.095 \text{ mm}^{-1}$ | Completeness = 98.1% |
| Independent reflections = 8615 [$R_{\text{int}} = 0.4704$] | $R_1 [I \geq 2\sigma(I)] = 0.1055$ | $wR_2 [\text{all data}] = 0.3544$ |

Table 6.3 Crystal structure information of (12C4)₂Li(TCNQ)₂ in this study

6.3.10 Preparation of (12C4)₂Na(TCNQ)₂

A solution of NaTCNQ (0.0227g, 0.1mmol), TCNQ⁰ (0.0204g, 0.1mmol) and 12-crown-4 (0.0352g, 0.2mmol) in dry acetonitrile (50ml) was heated under reflux for three hours, filtered whilst hot and then left to cool. The solvent was left to evaporate slowly over a period of several days and the solid which formed was then separated by filtration. The solid was washed with diethyl ether (50ml) and dried in vacuum to afford plates of metallic black crystalline solid (0.01085g, 14%). MS (solution) (MeCN) (ESI) m/z: 204.5 (TCNQ⁻). (ESI⁺) m/z: 375.7 (2 × Crown + Na⁺), 199.5 (Crown + Na⁺). IR $\nu_{\text{max}}/\text{cm}^{-1}$ 2969, 2935, 2881 (saturated CH stretch), 2223, 2201, 2177 (CN stretch), 1560 (C=C(CN)₂ stretch), 1506 (C=C ring stretch), 1302 (CH bend), 1136 (C-CN and C-C ring stretch), 951 (C-C ring stretch), 848, 689 (CH out of plane bend). Raman $\nu_{\text{max}}/\text{cm}^{-1}$ 2212 (CN stretch), 1602 (C=C ring stretch), 1382 (C-CN stretch), 1206 (C=C-H bending). M.p. 310°C (dec.). Combustion Analysis: Calculated: C: 61.30%, H: 5.14%, N: 14.29%. Found: C: 61.17%, H: 4.46%, N: 14.39%.

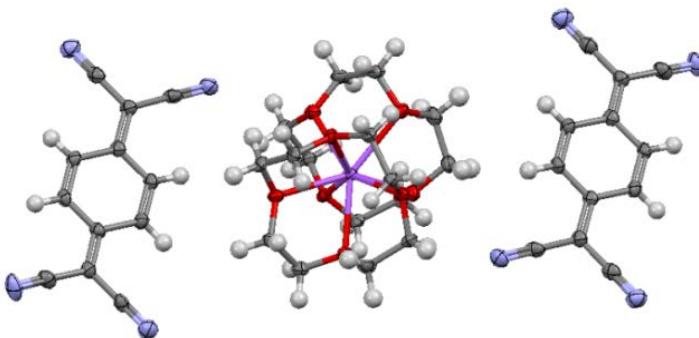
| | | |
|--|-------------------------------------|-------------------------------------|
|  | | |
| C ₄₀ H ₄₀ N ₈ NaO ₈ | a = 8.1038(5) Å | α = 78.713(5)° |
| M _r = 783.79 | b = 13.6922(10) Å | β = 86.236(5)° |
| Triclinic, P-1 | c = 17.7103(11) Å | γ = 85.684(5)° |
| T = 100(2) K | V = 1919.0(2) Å ³ | Z = 2 |
| λ = 0.71075 Å, Ros | 0.10 × 0.09 × 0.02 mm ³ | Block; Black |
| D _c = 1.356 Mg / m ³ | μ = 0.106 mm ⁻¹ | Completeness = 98.4% |
| Independent reflections = 8692 [R _{int} = 0.1518] | R ₁ [I ≥ 2σ(I)] = 0.0625 | wR ₂ [all data] = 0.1703 |

Table 6.4 Crystal structure information of (12C4)₂Na(TCNQ)₂ in this study

6.3.11 Preparation of (12C4)₂K(TCNQ)₂

A solution of KTCNQ (0.0972g, 0.4mmol), TCNQ⁰ (0.0816g, 0.4mmol) and 12-crown-4 (0.1408g, 0.8mmol) in dry acetonitrile (50ml) was heated under reflux for three hours, filtered whilst hot and then left to cool. The solvent was left to evaporate slowly over a period of several days and the solid which formed was then separated by filtration. The solid was washed with diethyl ether (50ml) and dried in vacuum to form a block of metallic black crystalline solid (0.01942g, 24%). MS (solution) (MeCN) (ESI⁻) m/z: 204.4 (TCNQ⁻). (ESI⁺) m/z: 375.6 (2 × Crown + Na⁺), 199.4 (Crown + Na⁺). IR $\nu_{\max}/\text{cm}^{-1}$ 2965, 2926, 2877 (saturated CH stretch), 2195, 2179, 2167 (CN stretch), 1560 (C=C(CN)₂ stretch), 1508 (C=C ring stretch), 1363 (CH bend), 1181 (C-CN and C-C ring stretch), 956 (C-C ring stretch), 828, 700 (CH out of plane bend). Raman $\nu_{\max}/\text{cm}^{-1}$ 2217 (CN stretch), 1608 (C=C ring stretch), 1390 (C-CN stretch), 1204 (C=C-H bending). M.p.>300°C (dec.). Combustion Analysis: Calculated: C: 60.06%, H: 5.04%, N: 14.00%. Found: C: 59.82%, H: 4.44%, N: 15.74%.

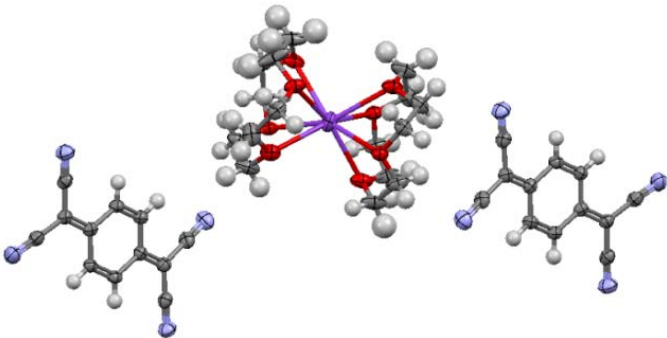
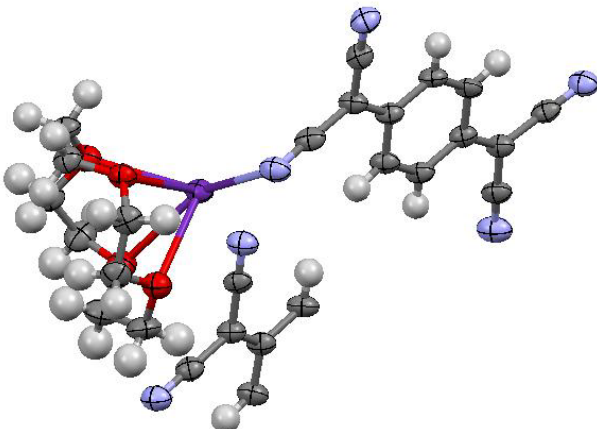
| | | |
|--|-------------------------------------|-------------------------------------|
|  | | |
| C ₄₀ H ₄₀ KN ₈ O ₈ | a = 8.0286(5) Å | α = 80.496(3)° |
| M _r = 799.90 | b = 13.6593(10) Å | β = 85.502(3)° |
| Triclinic, P-1 | c = 18.3991(13) Å | γ = 85.407(3)° |
| T = 100(2) K | V = 1979.3(2) Å ³ | Z = 2 |
| λ = 0.71075 Å, Kat | 0.11 × 0.06 × 0.02 mm ³ | Block; Black |
| D _c = 1.342 Mg / m ³ | μ = 0.197 mm ⁻¹ | Completeness = 99.3% |
| Independent reflections = 9058 [R _{int} = 0.1413] | R ₁ [I ≥ 2σ(I)] = 0.0514 | wR ₂ [all data] = 0.1537 |

Table 6.5 Crystal structure information of (12C4)₂K(TCNQ)₂ in this study

6.3.12 Preparation of (12C4)Rb(TCNQ)_{1.5}

A solution of Rb₂(TCNQ)₃ (0.0784g, 0.1mmol) and 12-crown-4 (0.0704g, 0.4mmol) in dry acetonitrile (50ml) was heated under reflux for three hours, filtered whilst hot and then left to cool. The solvent was left to evaporate slowly over a period of several days and the solid which formed was then separated by filtration. The solid was washed with dry diethyl ether (50ml) and dried in vacuum to form a bright purple plate of crystalline solid (0.01302g, 23%). MS (solution) (MeCN) (ESI⁻) m/z: 204.4 (TCNQ⁻). (ESI⁺) m/z: 375.6 (2 × Crown + Na⁺), 199.4 (Crown + Na⁺). IR $\nu_{\text{max}}/\text{cm}^{-1}$ 2978, 2955 (saturated CH stretch), 2224, 2212, 2184, 2152 (CN stretch), 1569 (C=C(CN)₂ stretch), 1507 (C=C ring stretch), 1361 (CH bend), 1129 (C-CN and C-C ring stretch), 941 (C-C ring stretch), 823 (CH out of plane bend). Raman $\nu_{\text{max}}/\text{cm}^{-1}$ 2203 (CN stretch), 1604 (C=C ring stretch), 1389 (C-CN stretch), 1203 (C=C-H bending). M.p. 235°C (dec.).

Combustion data is awaited.



| | | |
|--|-------------------------------------|-------------------------------------|
| C ₂₆ H ₂₂ N ₆ O ₄ Rb | a = 7.6697(5) Å | α = 90° |
| M _r = 567.96 | b = 13.8448(10) Å | β = 95.695(2)° |
| Monoclinic, P2 ₁ /n | c = 23.7805(17) Å | γ = 90° |
| T = 100(2) K | V = 2512.7(3) Å ³ | Z = 4 |
| λ = 0.71075 Å, Kat | 0.09 × 0.08 × 0.02 mm ³ | Plate; Purple |
| D _c = 1.501 Mg / m ³ | μ = 2.015 mm ⁻¹ | Completeness = 99.4% |
| Independent reflections = 5727 [R _{int} = 0.3024] | R ₁ [I ≥ 2σ(I)] = 0.0703 | wR ₂ [all data] = 0.1892 |

Table 6.6 Crystal structure information of (12C4)Rb(TCNQ)_{1.5} in this study

6.3.13 Preparation of (15C5)LiTCNQ

A solution of LiTCNQ (0.280g, 1.321mmol) and 15-crown-5 (0.291g, 1.321mmol) in dry acetonitrile (50ml) was boiled for five minutes, and filtered whilst hot and then left to cool. The solvent was left to evaporate slowly over a period of several days during which a solid formed which was separated by filtration. The solid was washed with diethyl ether (50ml) and dried in vacuum to give small crystals of a purple solid (0.459g, 81%). MS (solution) (MeCN) (ESI⁻) m/z: 204.1 (TCNQ⁻). (ESI⁺) m/z: 243.2 (Crown + Na⁺). IR $\nu_{\max}/\text{cm}^{-1}$ 2930, 2878 (saturated CH stretch), 2195, 2174, 2153 (CN stretch), 1579 (C=C(CN)₂ stretch), 1503 (C=C ring stretch), 1347 (CH bend), 1179 (C-CN and C-C ring stretch), 985 (C-C ring stretch), 829, 717 (CH out of plane bend). Raman $\nu_{\max}/\text{cm}^{-1}$ 2216 (CN stretch), 1605 (C=C ring stretch), 1379 (C-CN stretch), 1208 (C=C-H bending). M.p. 202°C (dec.). Combustion Analysis: Calculated: C: 61.25%, H: 5.61%, N: 12.98%. Found: C: 61.46%, H: 5.51%, N: 13.29%.

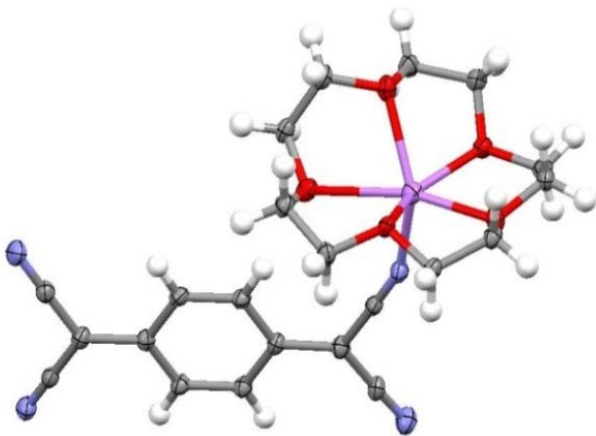
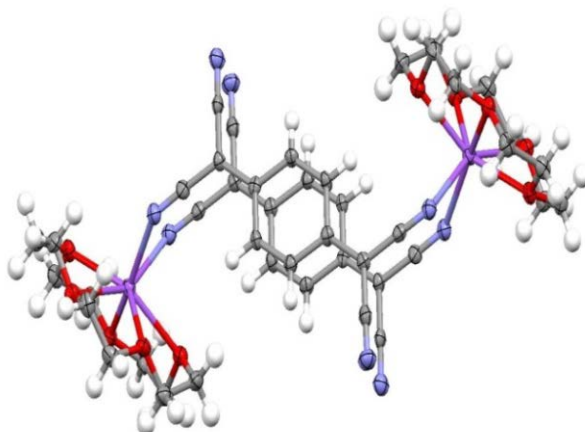
| | | |
|---|---|-----------------------------------|
|  | | |
| $\text{C}_{22}\text{H}_{24}\text{LiN}_4\text{O}_5$ | $a = 9.7939(7) \text{ \AA}$ | $\alpha = 90^\circ$ |
| $M_r = 431.39$ | $b = 15.2363(12) \text{ \AA}$ | $\beta = 102.087(7)^\circ$ |
| Monoclinic, $P2_1/c$ | $c = 14.7146(12) \text{ \AA}$ | $\gamma = 90^\circ$ |
| $T = 100(2) \text{ K}$ | $V = 2147.1(3) \text{ \AA}^3$ | $Z = 4$ |
| $\lambda = 0.71075 \text{ \AA}$, Ros | $0.05 \times 0.04 \times 0.01 \text{ mm}^3$ | Plate; Purple |
| $D_c = 1.335 \text{ Mg / m}^3$ | $\mu = 0.095 \text{ mm}^{-1}$ | Completeness = 99.7% |
| Independent reflections = 4910 [$R_{\text{int}} = 0.1117$] | $R_1 [I \geq 2\sigma(I)] = 0.0575$ | $wR_2 [\text{all data}] = 0.1454$ |

Table 6.7 Crystal structure information of (15C5)LiTCNQ in this study

6.3.14 Preparation of (15C5)NaTCNQ

A solution of NaTCNQ (0.450g, 2mmol) and 15-crown-5 (0.440g, 2mmol) in dry acetonitrile (50ml) was boiled for five minutes, and filtered whilst hot and then left to cool. The solvent was left to evaporate slowly over a period of several days during which a solid formed which was separated by filtration. The solid was washed with diethyl ether (50ml) and dried in vacuum to give small crystals of a purple solid (0.426g, 48%). MS (solution) (MeCN) (ESI⁻) m/z: 204.1 (TCNQ⁻). (ESI⁺) m/z: 243.2 (Crown + Na⁺). IR $\nu_{\max}/\text{cm}^{-1}$ 2908, 2875 (saturated CH stretch), 2179, 2152 (CN stretch), 1576 (C=C(CN)₂ stretch), 1504 (C=C ring stretch), 1343 (CH bend), 1177 (C-CN and C-C ring stretch), 986 (C-C ring stretch), 820, 717 (CH out of plane bend). Raman $\nu_{\max}/\text{cm}^{-1}$ 2207 (CN stretch), 1602 (C=C ring stretch), 1380 (C-CN stretch), 1205 (C=C-H bending). M.p. 160°C (lit⁶⁴. 150°C). Combustion Analysis: Calculated: C: 59.06%, H: 5.41%, N: 12.52%. Found: C: 58.76%, H: 5.02%, N: 12.32%.



| | | |
|--|---|-----------------------------------|
| $\text{C}_{44}\text{H}_{48}\text{N}_8\text{Na}_2\text{O}_{10}$ | $a = 9.2479(14) \text{ \AA}$ | $\alpha = 83.755(7)^\circ$ |
| $M_r = 894.88$ | $b = 11.0432(17) \text{ \AA}$ | $\beta = 89.933(6)^\circ$ |
| Triclinic, P-1 | $c = 11.8476(17) \text{ \AA}$ | $\gamma = 68.656(8)^\circ$ |
| $T = 100(2) \text{ K}$ | $V = 1119.3(3) \text{ \AA}^3$ | $Z = 1$ |
| $\lambda = 0.71075 \text{ \AA, Kat}$ | $0.08 \times 0.06 \times 0.01 \text{ mm}^3$ | Plate; Purple |
| $D_c = 1.328 \text{ Mg / m}^3$ | $\mu = 0.112 \text{ mm}^{-1}$ | Completeness = 98.8% |
| Independent reflections = 5059 [$R_{\text{int}} = 0.0748$] | $R_1 [I \geq 2\sigma(I)] = 0.0698$ | $wR_2 [\text{all data}] = 0.1581$ |

Table 6.8 Crystal structure information of (15C5)NaTCNQ in this study

6.3.15 Preparation of (15C5)Li(TCNQ)₂·H₂O

A solution of LiTCNQ (0.0211g, 0.1mmol), TCNQ⁰ (0.0204g, 0.1mmol) and 15-crown-5 (0.044g, 0.2mmol) in dry acetonitrile (50ml) was heated under reflux for three hours, filtered whilst hot and then left to cool. The solvent was left to evaporate slowly over a period of several days and the solid which formed was then separated by filtration. The solid was washed with diethyl ether (50ml) and dried in vacuum to form plates of a bright black crystalline solid (0.03565g, 56%). MS (solution) (MeCN) (ESI⁻) m/z: 204.1 (TCNQ⁻). (ESI⁺) m/z: 243.2 (Crown + Na⁺). IR $\nu_{\max}/\text{cm}^{-1}$ ~3500 (OH stretch), 2878 (saturated CH stretch), 2201, 2173 (CN stretch), 1560 (C=C(CN)₂ stretch), 1507 (C=C ring stretch), 1340 (CH bend), 1100 (C-CN and C-C ring stretch), 954 (C-C ring stretch), 836, 700 (CH out of plane bend). Raman $\nu_{\max}/\text{cm}^{-1}$ 2216 (CN stretch), 1606 (C=C ring stretch), 1384 (C-CN stretch), 1206 (C=C-H bending). M.p. 270°C (dec.). Combustion Analysis: Calculated: C: 62.48%, H: 4.63%, N: 17.14%. Found: C: 62.47%, H: 4.45%, N: 17.38%.

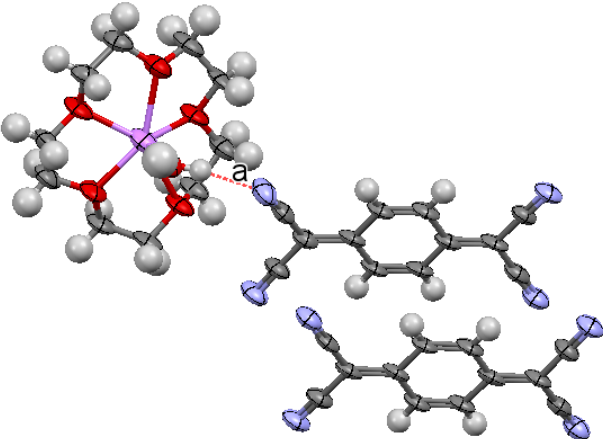
| | | |
|--|-------------------------------------|-------------------------------------|
|  | | |
| C ₃₄ H ₃₀ LiN ₈ O ₆ | a = 8.3276(5) Å | α = 97.533(8)° |
| M _r = 653.60 | b = 12.4763(9) Å | β = 100.335(9)° |
| Triclinic, P-1 | c = 16.6170(11) Å | γ = 99.982(9)° |
| T = 100(2) K | V = 1648.6(2) Å ³ | Z = 2 |
| λ = 0.71075 Å, Ros | 0.08 × 0.05 × 0.02 mm ³ | Plate; Black |
| D _c = 1.316 Mg / m ³ | μ = 0.093 mm ⁻¹ | Completeness = 95.6% |
| Independent reflections = 7259 [R _{int} = 0.1159] | R ₁ [I ≥ 2σ(I)] = 0.0949 | wR ₂ [all data] = 0.2865 |

Table 6.9 Crystal structure information of (15C5)Li(TCNQ)₂·H₂O in this study

6.3.16 Preparation of (15C5)Na(TCNQ)₂·H₂O

A solution of NaTCNQ (0.0277g, 0.1mmol), TCNQ⁰ (0.0204g, 0.1mmol) and 15-crown-5 (0.044g, 0.2mmol) in dry acetonitrile (50ml) was heated under reflux for three hours, filtered whilst hot and then left to cool. The solvent was left to evaporate slowly over a period of several days and the solid which formed was then separated by filtration. The solid was washed with diethyl ether (50ml) and dried in vacuum to form plates of a bright black crystalline solid (0.03906g, 60%). MS (solution) (MeCN) (ESI⁺) m/z: 204.1 (TCNQ⁻). (ESI⁺) m/z: 243.2 (Crown + Na⁺). IR $\nu_{\max}/\text{cm}^{-1}$ ~3500 (OH stretch), 2872 (saturated CH stretch), 2277, 2195, 2165 (CN stretch), 1560 (C=C(CN)₂ stretch), 1508 (C=C ring stretch), 1343 (CH bend), 1112 (C-CN and C-C ring stretch), 948 (C-C ring stretch), 836, 697 (CH out of plane bend). Raman $\nu_{\max}/\text{cm}^{-1}$ 2206 (CN stretch), 1603 (C=C ring stretch), 1384 (C-CN stretch), 1206 (C=C-H bending). M.p. 252°C (dec.). Combustion Analysis: Calculated: C: 60.98%, H: 4.52%, N: 16.73%. Found: C: 61.28%, H: 4.30%, N: 16.69%.

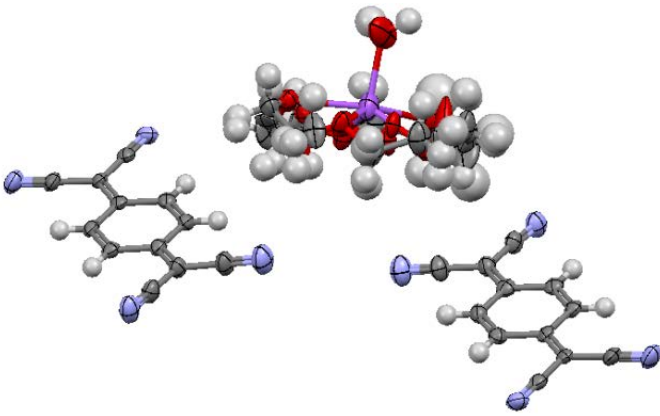
| | | |
|--|---|-----------------------------------|
|  | | |
| $\text{C}_{34}\text{H}_{30}\text{N}_8\text{NaO}_6$ | $a = 8.3578(5) \text{ \AA}$ | $\alpha = 102.623(7)^\circ$ |
| $M_r = 669.65$ | $b = 12.4677(9) \text{ \AA}$ | $\beta = 92.032(6)^\circ$ |
| Triclinic, P-1 | $c = 16.7424(11) \text{ \AA}$ | $\gamma = 99.911(7)^\circ$ |
| $T = 100(2) \text{ K}$ | $V = 1672.2(2) \text{ \AA}^3$ | $Z = 2$ |
| $\lambda = 0.71075 \text{ \AA}$, Ros | $0.16 \times 0.08 \times 0.02 \text{ mm}^3$ | Plate; Black |
| $D_c = 1.330 \text{ Mg / m}^3$ | $\mu = 0.105 \text{ mm}^{-1}$ | Completeness = 98.0% |
| Independent reflections = 7499 [$R_{\text{int}} = 0.0449$] | $R_1 [I \geq 2\sigma(I)] = 0.0835$ | $wR_2 [\text{all data}] = 0.2748$ |

Table 6.10 Crystal structure information of (15C5)Na(TCNQ)₂·H₂O in this study

6.3.17 Preparation of (15C5)₂RbTCNQ

A solution of Rb₂(TCNQ)₃ (0.0782g, 0.1mmol), TCNQ⁰ (0.0408g, 0.2mmol) and 15-crown-5 (0.088g, 0.4mmol) in dry acetonitrile (50ml) was heated under reflux for three hours, filtered whilst hot and then left to cool. The solvent was left to evaporate slowly over a period of several days and the solid which formed was then separated by filtration. The solid was washed with diethyl ether (50ml) and dried in vacuum to form a mixture of a plate of metallic dark blue and a bright yellow-green crystalline solid (0.01046g, 14%). The product of bright yellow-green was proved to be TCNQ⁰ after analysis by an X-ray crystallographic study. The dark blue solid had: MS (solution) (MeCN) (ESI⁻) m/z: 204.5 (TCNQ⁻). (ESI⁺) m/z: 243.5 (Crown + Na⁺). IR $\nu_{\max}/\text{cm}^{-1}$ 2900, 2864 (saturated CH stretch), 2182, 2161 (CN stretch), 1561 (C=C(CN)₂ stretch), 1507 (C=C ring stretch), 1349 (CH bend), 1182 (C-CN and C-C ring stretch), 983 (C-C ring stretch), 829, 714 (CH out of plane bend). Raman $\nu_{\max}/\text{cm}^{-1}$ 2203 (CN stretch), 1604 (C=C ring stretch), 1389 (C-CN stretch), 1203 (C=C-H bending). M.p. 210°C (lit⁶⁴. 202-203°C). Combustion data is awaited.

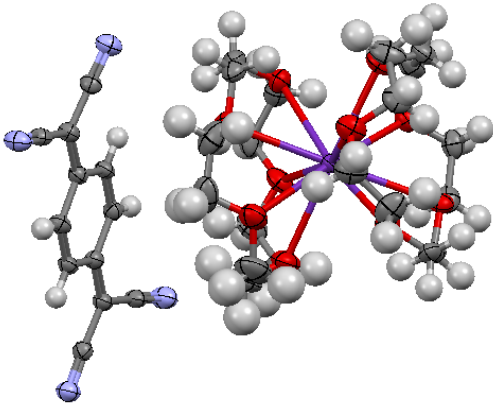
| | | |
|--|-------------------------------------|-------------------------------------|
|  | | |
| C ₃₂ H ₄₄ N ₄ O ₁₀ Rb | a = 8.9191(5) Å | α = 66.628(4)° |
| M _r = 730.18 | b = 14.1097(10) Å | β = 83.769(5)° |
| Triclinic, P-1 | c = 15.2376(11) Å | γ = 77.738(5)° |
| T = 100(2) K | V = 1719.5(2) Å ³ | Z = 2 |
| λ = 0.71075 Å, Ros | 0.11 × 0.05 × 0.02 mm ³ | Plate; Dark Blue |
| D _c = 1.410 Mg / m ³ | μ = 1.500 mm ⁻¹ | Completeness = 99.7% |
| Independent reflections = 7874 [R _{int} = 0.0425] | R ₁ [I ≥ 2σ(I)] = 0.0440 | wR ₂ [all data] = 0.1143 |

Table 6.11 Crystal structure information of (15C5)₂RbTCNQ in this study

6.3.18 Preparation of (B15C5)LiTCNQ·H₂O

A solution of LiTCNQ (0.0211g, 0.1mmol), TCNQ⁰ (0.0204g, 0.1mmol) and Benzo-15-crown-5 (0.0268g, 0.2mmol) in dry acetonitrile (50ml) was heated under reflux for three hours, filtered whilst hot and then left to cool. The solvent was let to evaporate slowly over a period of several days and the solid which formed was then separated by filtration. The solid was washed with diethyl ether (50ml) and dried in vacuum to form a mixture of a block of bright yellow-green and a plate of metallic dark blue crystalline solid (0.01491g, 30%). The bright yellow-green solid was shown to be TCNQ⁰ by an X-ray crystallographic study. The dark blue solid had: MS (solution) (MeCN) (ESI⁺) m/z: 204.5 (TCNQ⁻). (ESI⁺) m/z: 291.6 (Crown + Na⁺). IR $\nu_{\max}/\text{cm}^{-1}$ ~3500 (OH stretch), 2942, 2888 (saturated CH stretch), 2196, 2168 (CN stretch), 1560 (C=C(CN)₂ stretch), 1508 (C=C ring stretch), 1342 (CH bend), 1128 (C-CN and C-C ring stretch), 958 (C-C ring stretch), 838, 754 (CH out of plane bend). Raman $\nu_{\max}/\text{cm}^{-1}$ 2188 (CN stretch), 1608 (C=C ring stretch), 1388 (C-CN stretch), 1197 (C=C-H bending). M.p 220°C (dec.). Combustion data is awaited.

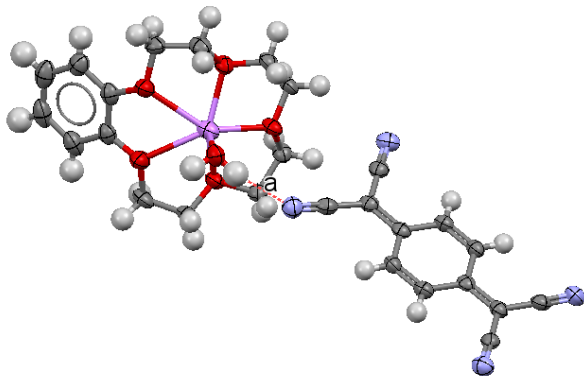
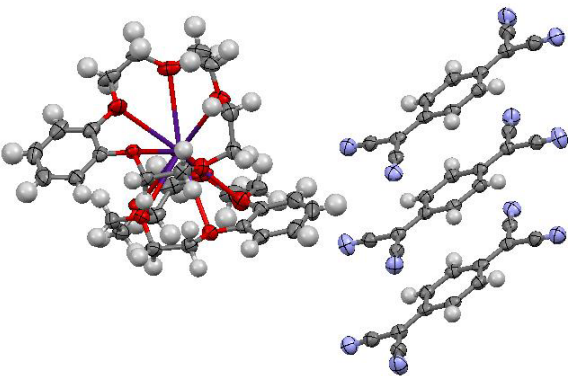
| | | |
|--|---|-----------------------------------|
|  | | |
| $\text{C}_{26}\text{H}_{26}\text{LiN}_4\text{O}_6$ | $a = 6.9047(5) \text{ \AA}$ | $\alpha = 64.605(5)^\circ$ |
| $M_r = 497.45$ | $b = 14.1536(10) \text{ \AA}$ | $\beta = 80.543(6)^\circ$ |
| Triclinic, P-1 | $c = 14.1883(10) \text{ \AA}$ | $\gamma = 80.656(6)^\circ$ |
| $T = 100(2) \text{ K}$ | $V = 1228.98(16) \text{ \AA}^3$ | $Z = 2$ |
| $\lambda = 0.71075 \text{ \AA}$, Ros | $0.09 \times 0.05 \times 0.02 \text{ mm}^3$ | Plate; Dark Blue |
| $D_c = 1.344 \text{ Mg / m}^3$ | $\mu = 0.096 \text{ mm}^{-1}$ | Completeness = 99.6% |
| Independent reflections = 5598 [$R_{\text{int}} = 0.1442$] | $R_1 [I \geq 2\sigma(I)] = 0.0503$ | $wR_2 [\text{all data}] = 0.1338$ |

Table 6.12 Crystal structure information of (B15C5)LiTCNQ·H₂O in this study

6.3.19 Preparation of (B15C5)₂Cs(TCNQ)₃

A solution of Cs₂(TCNQ)₃ (0.0878g, 0.1mmol), TCNQ⁰ (0.0408g, 0.2mmol) and Benzo-15-crown-5 (0.1072g, 0.4mmol) in dry acetonitrile (50ml) was heated under reflux for three hours, filtered whilst hot and then left to cool. The solvent was left to evaporate slowly over a period of several days and the solid which formed was then separated by filtration. The solid was washed with diethyl ether (50ml) and dried in vacuum to form a mixture of a bright yellow-green block and a plate of metallic dark blue crystalline solid (0.00683g, 5%). The bright yellow-green product was shown to be TCNQ⁰ after an X-ray crystallographic study. The dark blue solid had: MS (solution) (MeCN) (ESI⁻) m/z: 204.1 (TCNQ⁻). (ESI⁺) m/z: (Crown + Na⁺). IR $\nu_{\max}/\text{cm}^{-1}$ 3050, 2970 (saturated CH stretch), 2225, 2195, 2169 (CN stretch), 1569 (C=C(CN)₂ stretch), 1506 (C=C ring stretch), 1353 (CH bend), 1126 (C-CN and C-C ring stretch), 938 (C-C ring stretch), 862, 746 (CH out of plane bend). Raman $\nu_{\max}/\text{cm}^{-1}$ 2201 (CN stretch), 1605 (C=C ring stretch), 1391, 1433 (C-CN stretch), 1200 (C=C-H bending). M.p. 280°C (dec.). Combustion data is awaited.



| | | |
|--|---|-----------------------------------|
| $\text{C}_{64}\text{H}_{52}\text{CsN}_{12}\text{O}_{10}$ | $a = 18.7775(13) \text{ \AA}$ | $\alpha = 90^\circ$ |
| $M_r = 1282.09$ | $b = 8.8172(5) \text{ \AA}$ | $\beta = 99.453(1)^\circ$ |
| Monoclinic, C2/c | $c = 35.982(3) \text{ \AA}$ | $\gamma = 90^\circ$ |
| $T = 100(2) \text{ K}$ | $V = 5876.5(7) \text{ \AA}^3$ | $Z = 4$ |
| $\lambda = 0.71075 \text{ \AA, Kat}$ | $0.10 \times 0.10 \times 0.02 \text{ mm}^3$ | Plate; Dark Blue |
| $D_c = 1.449 \text{ Mg / m}^3$ | $\mu = 0.702 \text{ mm}^{-1}$ | Completeness = 99.7% |
| Independent reflections = 6746 [$R_{\text{int}} = 0.0828$] | $R_1 [I \geq 2\sigma(I)] = 0.0411$ | $wR_2 [\text{all data}] = 0.1011$ |

Table 6.13 Crystal structure information of (B15C5)₂Cs(TCNQ)₃ in this study

6.3.20 Preparation of (18C6)KTCNQ²⁸³

A solution of KTCNQ (0.0243g, 0.1mmol) and 18-crown-6 (0.0264g, 0.1mmol) in dry acetonitrile (50ml) was boiled for five minutes, and filtered whilst hot and then left to cool. The solvent was left to evaporate slowly over a period of several days during which a solid formed which was separated by filtration. The solid was washed with diethyl ether (50ml) and dried in vacuum to give small crystals of a metallic dark violet solid (0.02839g, 56%). MS (solution) (MeCN) (ESI⁻) m/z: 204.1 (TCNQ⁻). (ESI⁺) m/z: 287.6 (Crown + Na⁺). IR $\nu_{\text{max}}/\text{cm}^{-1}$ 2889 (saturated CH stretch), 2174, 2156 (CN stretch) (lit²⁸³. 2177, 2156), 1581 (C=C(CN)₂ stretch), 1504 (C=C ring stretch), 1346 (CH bend), 1178 (C-CN and C-C ring stretch), 961 (C-C ring stretch), 830, 721 (CH out of plane bend). M.p. 202°C (lit³⁶. 185°C)

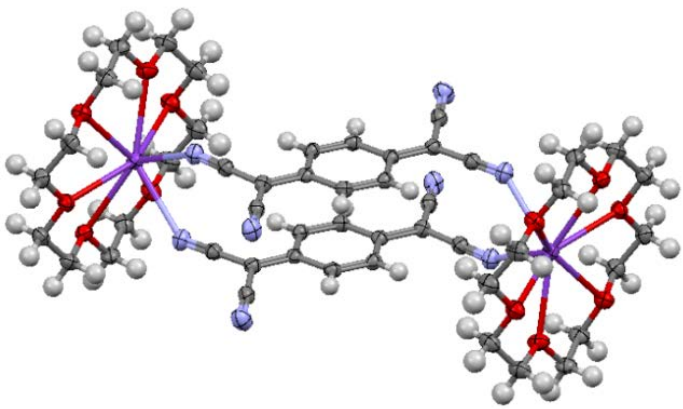
| | | |
|---|---|-----------------------------------|
|  | | |
| $\text{C}_{48}\text{H}_{56}\text{K}_2\text{N}_8\text{O}_{12}$ | $a = 23.6591(17) \text{ \AA}$ | $\alpha = 90^\circ$ |
| $M_r = 1015.22$ | $b = 8.1779(5) \text{ \AA}$ | $\beta = 98.037(1)^\circ$ |
| Monoclinic, C2/c | $c = 26.7609(19) \text{ \AA}$ | $\gamma = 90^\circ$ |
| $T = 100(2) \text{ K}$ | $V = 5126.9(6) \text{ \AA}^3$ | $Z = 4$ |
| $\lambda = 0.71075 \text{ \AA, Kat}$ | $0.26 \times 0.25 \times 0.04 \text{ mm}^3$ | Plate; Dark Violet |
| $D_c = 1.315 \text{ Mg / m}^3$ | $\mu = 0.252 \text{ mm}^{-1}$ | Completeness = 99.7% |
| Independent reflections = 5883 [$R_{\text{int}} = 0.0291$] | $R_1 [I \geq 2\sigma(I)] = 0.0256$ | $wR_2 [\text{all data}] = 0.0712$ |

Table 6.14 Crystal structure information of (18C6)KTCNQ in this study

6.3.21 Preparation of (18C6)Na(TCNQ)₂·2H₂O

A solution of NaTCNQ (0.0227g, 0.1mmol), TCNQ⁰ (0.0204g, 0.1mmol) and 18-crown-6 (0.0264g, 0.1mmol) in dry acetonitrile (50ml) was heated under reflux for three hours, filtered whilst hot and then left to cool. The solvent was let to evaporate slowly over a period of several days and the solid which formed was then separated by filtration. The solid was washed with diethyl ether (50ml) and dried in vacuum to form a plate of metallic dark blue crystalline solid (0.00343g, 5%). MS (solution) (MeCN) (ESI⁻) m/z: 204.3 (TCNQ⁻). (ESI⁺) m/z: 287.6 (Crown + Na⁺). IR $\nu_{\text{max}}/\text{cm}^{-1}$ ~3400 (OH stretch), 2970 (saturated CH stretch), 2223, 2196, 2179 (CN stretch), 1569 (C=C(CN)₂ stretch), 1507 (C=C ring stretch), 1353 (CH bend), 1125 (C-CN and C-C ring stretch), 961 (C-C ring stretch), 862, 750 (CH out of plane bend). M.p. 275°C (dec.). Combustion data is awaited.

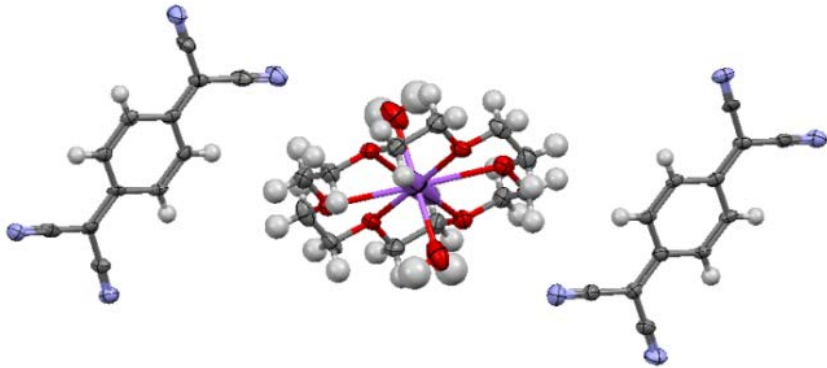
| | | |
|---|-------------------------------------|-------------------------------------|
|  | | |
| C ₃₆ H ₃₆ N ₈ NaO ₈ | a = 7.1430(5) Å | α = 88.618(6)° |
| M _r = 731.72 | b = 8.2470(5) Å | β = 78.909(7)° |
| Triclinic, P-1 | c = 17.5533(13) Å | γ = 64.488(5)° |
| T = 100(2) K | V = 913.77(12) Å ³ | Z = 1 |
| λ = 0.71075 Å, Ros | 0.13 × 0.08 × 0.02 mm ³ | Plate; Dark Blue |
| D _c = 1.330 Mg / m ³ | μ = 0.106 mm ⁻¹ | Completeness = 99.4% |
| Independent reflections = 4163 [R _{int} = 0.1636] | R ₁ [I ≥ 2σ(I)] = 0.0606 | wR ₂ [all data] = 0.1879 |

Table 6.15 Crystal structure information of (18C6)Na(TCNQ)₂·2H₂O in this study

6.3.22 Preparation of (18C6)K(TCNQ)_{2.5}

A solution of KTCNQ (0.0243g, 0.1mmol), TCNQ⁰ (0.0204g, 0.1mmol) and 18-crown-6 (0.0264g, 0.1mmol) in dry acetonitrile (50ml) was under refluxing for three hours, filtered whilst hot and then left to cool. The solvent was left to evaporate slowly over a period of several days and the solid which formed was then separated by filtration. The solid was washed with diethyl ether (50ml) and dried in vacuum to form a needle of bright black crystalline solid (0.04311g, 61%). MS (solution) (MeCN) (ESI⁺) m/z: 204.1 (TCNQ⁺). (ESI⁺) m/z: 287.2 (Crown + Na⁺). IR $\nu_{\max}/\text{cm}^{-1}$ 2899 (saturated CH stretch), 2209, 2196, 2176 (CN stretch), 1566 (C=C(CN)₂ stretch), 1522 (C=C ring stretch), 1341 (CH bend), 1159 (C-CN and C-C ring stretch), 961 (C-C ring stretch), 839, 700 (CH out of plane bend). Raman $\nu_{\max}/\text{cm}^{-1}$ 2203 (CN stretch), 1603 (C=C ring stretch), 1386 (C-CN stretch), 1204 (C=C-H bending). M.p. 256°C (dec.). Combustion Analysis: Calculated: C: 61.98%, H: 4.21%, N: 17.21%. Found: C: 61.84%, H: 4.00%, N: 17.08%.

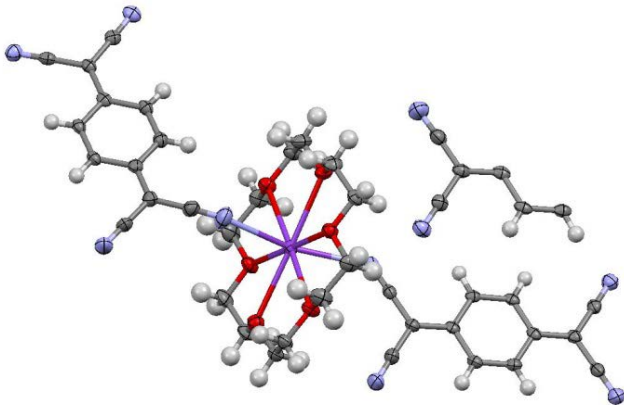
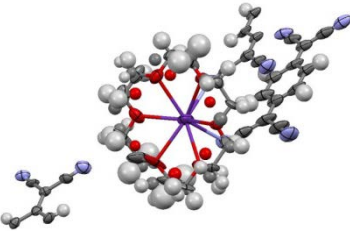
| | | |
|--|---|-----------------------------------|
|  | | |
| $\text{C}_{42}\text{H}_{34}\text{KN}_{10}\text{O}_6$ | $a = 8.1026(5) \text{ \AA}$ | $\alpha = 90^\circ$ |
| $M_r = 813.89$ | $b = 31.843(2) \text{ \AA}$ | $\beta = 100.894(2)^\circ$ |
| Monoclinic, $P2_1/c$ | $c = 16.2844(11) \text{ \AA}$ | $\gamma = 90^\circ$ |
| $T = 100(2) \text{ K}$ | $V = 4125.8(5) \text{ \AA}^3$ | $Z = 4$ |
| $\lambda = 0.71075 \text{ \AA, Kat}$ | $0.56 \times 0.06 \times 0.04 \text{ mm}^3$ | Needle; Black |
| $D_c = 1.310 \text{ Mg / m}^3$ | $\mu = 0.189 \text{ mm}^{-1}$ | Completeness = 96.3% |
| Independent reflections = 9114 [$R_{\text{int}} = 0.0453$] | $R_1 [I \geq 2\sigma(I)] = 0.0391$ | $wR_2 [\text{all data}] = 0.0993$ |

Table 6.16 Crystal structure information of (18C6)K(TCNQ)_{2.5} in this study

6.3.23 Preparation of (18C6)Rb(TCNQ)₂

A solution of Rb₂(TCNQ)₃ (0.0392g, 0.1mmol), TCNQ⁰ (0.0204g, 0.1mmol) and 18-crown-6 (0.0264g, 0.2mmol) in dry acetonitrile (50ml) was heated under reflux for three hours, filtered whilst hot and then left to cool. The solvent was left to evaporate slowly over a period of several days and the solid which formed was then separated by filtration. The solid was washed with diethyl ether (50ml) and dried in vacuum to form a needle of bright black crystalline solid (0.04311g, 61%). IR $\nu_{\max}/\text{cm}^{-1}$ 2851 (saturated CH stretch), 2209, 2196, 2171 (CN stretch), 1564 (C=C(CN)₂ stretch), 1505 (C=C ring stretch), 1353 (CH bend), 1154 (C-CN and C-C ring stretch), 962 (C-C ring stretch), 840, 700 (CH out of plane bend). Raman $\nu_{\max}/\text{cm}^{-1}$ 2205 (CN stretch), 1604 (C=C ring stretch), 1390 (C-CN stretch), 1203 (C=C-H bending). M.p. 240°C (lit⁶⁴. 235°C). Combustion data is awaited.

The R_{int} value of (18C6)Rb(TCNQ)₂ is not available, which probably caused by several reasons. The structure might be disordered which needs further analysis; the shape of the crystal which will affect the absorption of the X-ray; the symmetry interpretation of the product; the quality of the data or the systematic error. The crystal structure of this sample needs to be further analysed.

| | | |
|--|---|-------------------------------------|
|  | | |
| C ₃₆ H _{33.27} N ₈ O ₆ Rb | a = 8.1907(5) Å | α = 100.771(9)° |
| M _r = 759.44 | b = 12.8013(9) Å | β = 95.148(8)° |
| Triclinic, P-1 | c = 17.8935(13) Å | γ = 101.724(9)° |
| T = 100(2) K | V = 1788.7(2) Å ³ | Z = 2 |
| λ = 0.71075 Å, Kat | 0.04 × 0.02 × 0.02 mm ³ | Needle; Black |
| D _c = 1.410 Mg / m ³ | μ = 1.441 mm ⁻¹ | Completeness = 99.4% |
| Independent reflections = 8172 [R_{int} = N/A*] | R ₁ [$I \geq 2\sigma(I)$] = 0.1197 | wR ₂ [all data] = 0.3745 |

*N/A: not available

Table 6.17 Crystal structure information of (18C6)Rb(TCNQ)₂ in this study

6.3.24 Preparation of (18C6)Cs(TCNQ)₂

A solution of Cs₂(TCNQ)₃ (0.0439g, 0.1mmol), TCNQ⁰ (0.0204g, 0.1mmol) and 18-crown-6 (0.0529g, 0.2mmol) in dry acetonitrile (50ml) was heated under reflux for three hours, filtered whilst hot and then left to cool. The solvent was left to evaporate slowly over a period of several days and the solid which formed was then separated by filtration. The solid was washed with diethyl ether (50ml) and dried in vacuum to form a plate of metallic dark blue crystalline solid (0.01072g, 13%). MS (solution) (MeCN) (ESI⁻) m/z: 204.5 (TCNQ⁻). (ESI⁺) m/z: 287.5 (Crown + Na⁺). IR $\nu_{\max}/\text{cm}^{-1}$ 2900 (saturated CH stretch), 2209, 2196, 2170 (CN stretch), 1563 (C=C(CN)₂ stretch), 1505 (C=C ring stretch), 1327 (CH bend), 1105 (C-CN and C-C ring stretch), 961 (C-C ring stretch), 840, 699 (CH out of plane bend). Raman $\nu_{\max}/\text{cm}^{-1}$ 2197 (CN stretch), 1606 (C=C ring stretch), 1390, 1435 (C-CN stretch), 1198 (C=C-H bending). M.p. 308°C (dec.). Combustion data is awaited.

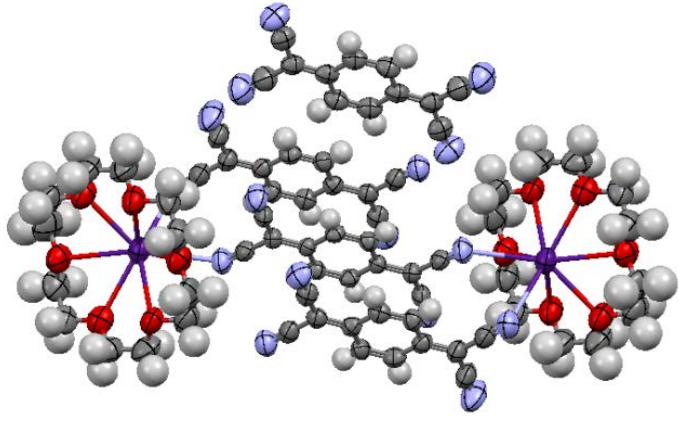
| | | |
|---|-------------------------------------|-------------------------------------|
|  | | |
| C _{35.97} H ₃₂ CsN ₈ O ₆ | a = 8.1734(5) Å | $\alpha = 97.124(6)^\circ$ |
| M _r = 805.30 | b = 12.9982(9) Å | $\beta = 96.993(6)^\circ$ |
| Triclinic, P-1 | c = 18.1214(13) Å | $\gamma = 100.605(6)^\circ$ |
| T = 100(2) K | V = 1857.0(2) Å ³ | Z = 2 |
| $\lambda = 0.71075$ Å, Ros | 0.05 × 0.04 × 0.02 mm ³ | Plate; Dark Blue |
| D _c = 1.051 Mg / m ³ | $\mu = 1.052$ mm ⁻¹ | Completeness = 99.6% |
| Independent reflections = 8489 [R _{int} = 0.1145] | R ₁ [I ≥ 2σ(I)] = 0.0568 | wR ₂ [all data] = 0.1258 |

Table 6.18 Crystal structure of (18C6)Cs(TCNQ)₂ in this study

6.3.25 Preparation of (B18C6)K(TCNQ)₂

A solution of KTCNQ (0.0243g, 0.1mmol), TCNQ⁰ (0.0204g, 0.1mmol) and benzo-18-crown-6 (0.0312g, 0.1mmol) in dry acetonitrile (50ml) was heated under reflux for three hours, filtered whilst hot and then left to cool. The solvent was left to evaporate slowly over a period of several days and the solid which formed was then separated by filtration. The solid was washed with diethyl ether (50ml) and dried in vacuum to form a needle of metallic dark blue crystalline solid (0.04326g, 57%). MS (solution) (MeCN) (ESI⁻) m/z: 204.1 (TCNQ⁻). (ESI⁺) m/z: 335.2 (Crown + Na⁺). IR $\nu_{\max}/\text{cm}^{-1}$ 3052, 2937 (saturated CH stretch), 2226, 2195, 2166 (CN stretch), 1559 (C=C(CN)₂ stretch), 1507 (C=C ring stretch), 1301 (CH bend), 1120 (C-CN and C-C ring stretch), 937 (C-C ring stretch), 830, 684 (CH out of plane bend). Raman $\nu_{\max}/\text{cm}^{-1}$ 2207 (CN stretch), 1606 (C=C ring stretch), 1390 (C-CN stretch), 1205 (C=C-H bending). M.p. 200°C (dec.). Combustion Analysis: Calculated: C: 63.40%, H: 3.99%, N: 14.78%. Found: C: 62.88%, H: 3.70%, N: 15.02%.

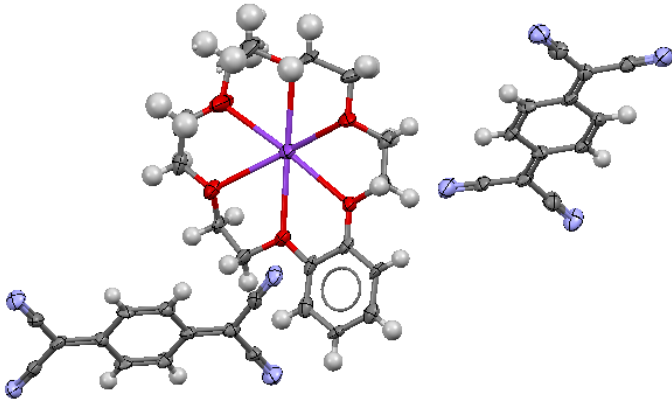
| | | |
|--|--|-----------------------------------|
|  | | |
| $\text{C}_{40}\text{H}_{30.06}\text{KN}_8\text{O}_6$ | $a = 6.4464(5) \text{ \AA}$ | $\alpha = 90^\circ$ |
| $M_r = 757.88$ | $b = 35.158(3) \text{ \AA}$ | $\beta = 99.822(2)^\circ$ |
| Monoclinic, $P2_1/m$ | $c = 8.0945(5) \text{ \AA}$ | $\gamma = 90^\circ$ |
| $T = 100(2) \text{ K}$ | $V = 1807.7(2) \text{ \AA}^3$ | $Z = 2$ |
| $\lambda = 0.71075 \text{ \AA, Kat}$ | $0.28 \times 0.06 \times 0.04 \text{ (mm}^3\text{)}$ | Plate; Dark Blue |
| $D_c = 1.392 \text{ Mg / m}^3$ | $\mu = 0.208 \text{ mm}^{-1}$ | Completeness = 98.3% |
| Independent reflections = 4182 [$R_{\text{int}} = 0.0573$] | $R_1 [I \geq 2\sigma(I)] = 0.0494$ | $wR_2 [\text{all data}] = 0.1461$ |

Table 6.19 Crystal structure information of (B18C6)K(TCNQ)₂ in this study

6.3.26 Preparation of (DB18C6)K(TCNQ)₂

A solution of KTCNQ (0.0243g, 0.1mmol), TCNQ⁰ (0.0204g, 0.1mmol) and dibenzo-18-crown-6 (0.0360g, 0.1mmol) in dry acetonitrile (50ml) was heated under reflux for three hours, filtered whilst hot and then left to cool. The solvent was left to evaporate slowly over a period of several days and the solid which formed was then separated by filtration. The solid was washed with diethyl ether (50ml) and dried in vacuum to form a block of black crystalline solid (0.0565g, 70%). MS (solution) (MeCN) (ESI⁺) m/z: 204.1 (TCNQ⁻). (ESI⁺) m/z: 383.2 (Crown + Na⁺). IR $\nu_{\max}/\text{cm}^{-1}$ 2968, 2935, 2887 (saturated CH stretch), 2214, 2189 (CN stretch), 1579 (C=C(CN)₂ stretch), 1528 (C=C ring stretch), 1379 (CH bend), 1161 (C-CN and C-C ring stretch), 948 (C-C ring stretch), 815, 709 (CH out of plane bend). Raman $\nu_{\max}/\text{cm}^{-1}$ 2204 (CN stretch), 1605 (C=C ring stretch), 1388 (C-CN stretch), 1205 (C=C-H bending). M.p. 220°C (lit⁶⁴. 224–225°C). Combustion data is awaited.

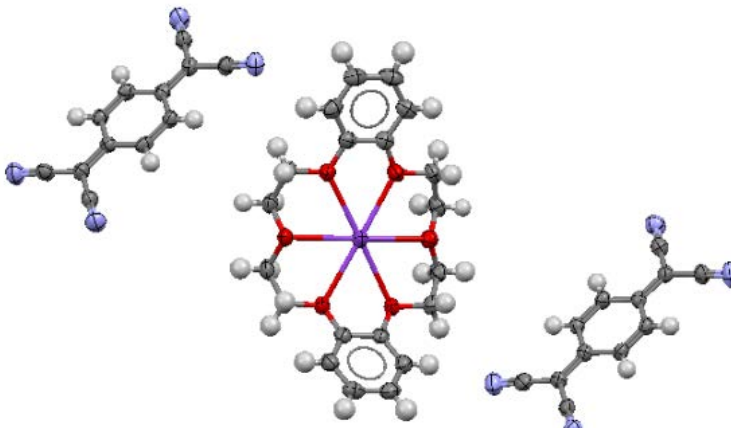
| | | |
|---|--|-----------------------------------|
|  | | |
| $\text{C}_{44}\text{H}_{32}\text{KN}_8\text{O}_6$ | $a = 7.8459(3) \text{ \AA}$ | $\alpha = 96.6200(10)^\circ$ |
| $M_r = 807.87$ | $b = 14.5336(4) \text{ \AA}$ | $\beta = 93.222(2)^\circ$ |
| Triclinic, P-1 | $c = 17.8334(4) \text{ \AA}$ | $\gamma = 101.779(2)^\circ$ |
| $T = 120(2) \text{ K}$ | $V = 1970.77(10) \text{ \AA}^3$ | $Z = 2$ |
| $\lambda = 0.71075 \text{ \AA}$, Ros | $0.32 \times 0.25 \times 0.03 \text{ (mm}^3\text{)}$ | Block; Black |
| $D_c = 1.361 \text{ Mg / m}^3$ | $\mu = 0.196 \text{ mm}^{-1}$ | Completeness = 98.7% |
| Independent reflections = 8916 [$R_{\text{int}} = 0.0769$] | $R_1 [I \geq 2\sigma(I)] = 0.0845$ | $wR_2 [\text{all data}] = 0.1855$ |

Table 6.20 Crystal structure information of (DB18C6)K(TCNQ)₂ in this study

6.3.27 Preparation of (DB18C6)RbTCNQ

A solution of $\text{Rb}_2(\text{TCNQ})_3$ (0.0784g, 0.1mmol), TCNQ^0 (0.0204g, 0.1mmol) and dibenzo-18-crown-6 (0.0720g, 0.2mmol) in dry acetonitrile (50ml) was heated under reflux for three hours, filtered whilst hot and then left to cool. The solvent was left to evaporate slowly over a period of several days and the solid which formed was then separated by filtration. The solid was washed with diethyl ether (50ml) and dried in vacuum to form a mixture of a plate of metallic dark violet and a plate of a bright yellow-green crystalline solid (0.0081g, 25%). The product of bright yellow-green was shown to be TCNQ^0 after by an X-ray crystallographic study. The dark violet solid had: MS (solution) (MeCN) (ESI⁻) m/z : 204.1 (TCNQ^-). (ESI⁺) m/z : 383.5 (Crown + Na^+). IR $\nu_{\text{max}}/\text{cm}^{-1}$ 2925, 2885, 2805 (saturated CH stretch), 2189, 2181, 2168, 2157 (CN stretch), 1582 ($\text{C}=\text{C}(\text{CN})_2$ stretch), 1503 ($\text{C}=\text{C}$ ring stretch), 1343 (CH bend), 1175 ($\text{C}-\text{CN}$ and $\text{C}-\text{C}$ ring stretch), 941 ($\text{C}-\text{C}$ ring stretch), 824, 751 (CH out of plane bend). Raman $\nu_{\text{max}}/\text{cm}^{-1}$ 2203 (CN stretch), 1603 ($\text{C}=\text{C}$ ring stretch), 1385 ($\text{C}-\text{CN}$ stretch), 1196 ($\text{C}=\text{C}-\text{H}$ bending). M.p. 226°C (lit.⁶⁴. 173-177 °C). Combustion Analysis: Calculated: C: 59.13%, H: 4.34%, N: 8.61%. Found: C: 59.95%, H: 4.91%, N: 11.94%.

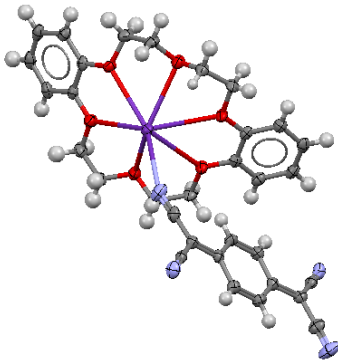
| | | |
|--|---|-----------------------------------|
|  | | |
| $\text{C}_{32}\text{H}_{27}\text{RbN}_4\text{O}_6$ | $a = 11.3645(8) \text{ \AA}$ | $\alpha = 90^\circ$ |
| $M_r = 649.04$ | $b = 9.1162(5) \text{ \AA}$ | $\beta = 100.490(1)^\circ$ |
| Monoclinic, $P2_1/n$ | $c = 28.758(2) \text{ \AA}$ | $\gamma = 90^\circ$ |
| $T = 100(2) \text{ K}$ | $V = 2929.6(3) \text{ \AA}^3$ | $Z = 4$ |
| $\lambda = 0.71075 \text{ \AA, Kat}$ | $0.10 \times 0.06 \times 0.02 \text{ mm}^3$ | Plate; Dark Violet |
| $D_c = 1.472 \text{ Mg / m}^3$ | $\mu = 1.742 \text{ mm}^{-1}$ | Completeness = 98.3% |
| Independent reflections = 6623 [$R_{\text{int}} = 0.0831$] | $R_1 [I \geq 2\sigma(I)] = 0.0349$ | $wR_2 [\text{all data}] = 0.0901$ |

Table 6.21 Crystal structure information of (DB18C6)RbTCNQ in this study

6.3.28 Preparation of (DC18C6)K(TCNQ)₃

A solution of KTCNQ (0.0243g, 0.1mmol), TCNQ⁰ (0.0204g, 0.1mmol) and dicyclohexano-18-crown-6 (0.0372g, 0.2mmol) in dry acetonitrile (50ml) was heated under reflux for three hours, filtered whilst hot and then left to cool. The solvent was left to evaporate slowly over a period of several days and the solid which formed was then separated by filtration. The solid was washed with diethyl ether (50ml) and dried in vacuum to form bright purple crystalline needles (0.0516g, 63%). MS (solution) (MeCN) (ESI⁻) m/z: 204.1 (TCNQ⁻). (ESI⁺) m/z: 395.2 (Crown + Na⁺). IR $\nu_{\max}/\text{cm}^{-1}$ 2932, 2883 (saturated CH stretch), 2222, 2201, 2174 (CN stretch), 1559 (C=C(CN)₂ stretch), 1507 (C=C ring stretch), 1330 (CH bend), 1125 (C-CN and C-C ring stretch), 950 (C-C ring stretch), 841, 749 (CH out of plane bend). Raman $\nu_{\max}/\text{cm}^{-1}$ 2203 (CN stretch), 1605 (C=C ring stretch), 1389 (C-CN stretch), 1195, 1204 (C=C-H bending). M.p. 228°C (dec.). Combustion Analysis: Calculated: C: 65.67%, H: 4.72%, N: 16.41%. Found: C: 65.85%, H: 4.79%, N: 16.66%.

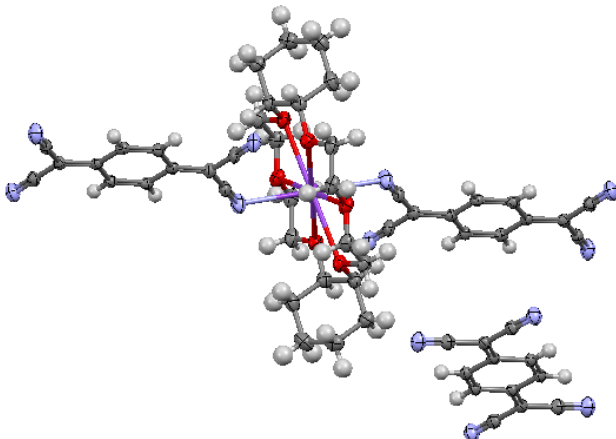
| | | |
|--|---|-----------------------------------|
|  | | |
| $\text{C}_{56}\text{H}_{48}\text{KN}_{12}\text{O}_6$ | $a = 7.9615(5) \text{ \AA}$ | $\alpha = 87.104(4)^\circ$ |
| $M_r = 1024.16$ | $b = 9.9749(7) \text{ \AA}$ | $\beta = 79.048(4)^\circ$ |
| Triclinic, P-1 | $c = 16.7923(11) \text{ \AA}$ | $\gamma = 80.132(4)^\circ$ |
| $T = 100(2) \text{ K}$ | $V = 1289.68(15) \text{ \AA}^3$ | $Z = 1$ |
| $\lambda = 0.71075 \text{ \AA, Kat}$ | $0.32 \times 0.11 \times 0.04 \text{ mm}^3$ | Needle; Bright Purple |
| $D_c = 1.319 \text{ Mg / m}^3$ | $\mu = 0.167 \text{ mm}^{-1}$ | Completeness = 99.8% |
| Independent reflections = 5895 [$R_{\text{int}} = 0.0298$] | $R_1 [I \geq 2\sigma(I)] = 0.0354$ | $wR_2 [\text{all data}] = 0.1006$ |

Table 6.22 Crystal structure information of (DC18C6)K(TCNQ)₃ in this study

6.3.29 Preparation of (DC18C6)Rb(TCNQ)₃

A solution of Rb₂(TCNQ)₃ (0.0784g, 0.1mmol), TCNQ⁰ (0.0204g, 0.1mmol) and dicyclohexano-18-crown-6 (0.0745g, 0.2mmol) in dry acetonitrile (50ml) was heated under reflux for three hours, filtered whilst hot and then left to cool. The solvent was left to evaporate slowly over a period of several days and the solid which formed was then separated by filtration. The solid was washed with diethyl ether (50ml) and dried in vacuum to form a plate of metallic dark violet crystalline solid (0.02745g, 51%). MS (solution) (MeCN) (ESI⁻) m/z: 204.1 (TCNQ⁻). (ESI⁺) m/z: 395.2 (Crown + Na⁺). IR $\nu_{\max}/\text{cm}^{-1}$ 2972, 2923, 2874 (saturated CH stretch), 2223, 2202, 2174, 2152 (CN stretch), 1541 (C=C(CN)₂ stretch), 1514 (C=C ring stretch), 1330 (CH bend), 1125 (C-CN and C-C ring stretch), 988 (C-C ring stretch), 858, 749 (CH out of plane bend). Raman $\nu_{\max}/\text{cm}^{-1}$ 2226 (CN stretch), 1601 (C=C ring stretch), 1388, 1451 (C-CN stretch), 1194, 1205 (C=C-H bending). M.p. 220°C (dec.). Combustion data is awaited.

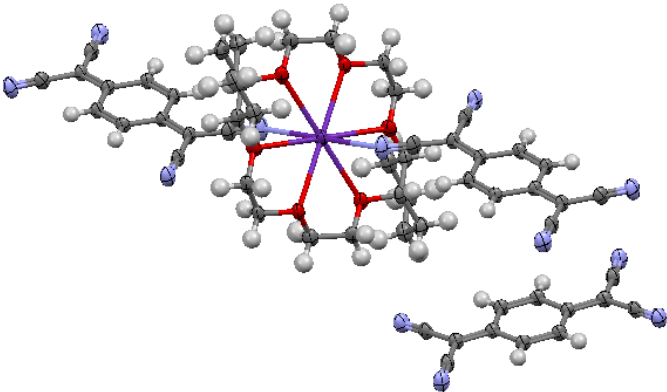
| | | |
|---|-------------------------------------|-------------------------------------|
|  | | |
| C ₅₆ H ₄₈ RbN ₁₂ O ₆ | a = 7.9703(5) Å | α = 87.019(5)° |
| M _r = 1070.53 | b = 9.9460(7) Å | β = 79.386(5)° |
| Triclinic, P-1 | c = 16.9055(11) Å | γ = 80.334(5)° |
| T = 100(2) K | V = 1298.21(15) Å ³ | Z = 1 |
| λ = 0.71075 Å, Ros | 0.07 × 0.06 × 0.02 mm ³ | Plate; Dark Violet |
| D _c = 1.369 Mg / m ³ | μ = 1.017 mm ⁻¹ | Completeness = 99.5% |
| Independent reflections = 5939 [R _{int} = 0.1672] | R ₁ [I ≥ 2σ(I)] = 0.0549 | wR ₂ [all data] = 0.1421 |

Table 6.23 Crystal structure information of (DC18C6)Rb(TCNQ)₃ in this study

6.3.30 Preparation of (DC18C6)Cs(TCNQ)₂

A solution of Cs₂(TCNQ)₃ (0.0878g, 0.1mmol), TCNQ⁰ (0.0204g, 0.1mmol) and dicyclohexano-18-crown-6 (0.0745g, 0.2mmol) in dry acetonitrile (50ml) was heated under reflux for three hours, filtered whilst hot and then left to cool. The solvent was left to evaporate slowly over a period of several days and the solid which formed was then separated by filtration. The solid was washed with diethyl ether (50ml) and dried in vacuum to form a plate of metallic dark blue crystalline solid (0.02613g, 57%). MS (solution) (MeCN) (ESI⁻) m/z: 204.1 (TCNQ⁻). (ESI⁺) m/z: 395.2 (Crown + Na⁺). IR $\nu_{\max}/\text{cm}^{-1}$ 3050, 2937 (saturated CH stretch), 2222, 2201, 2179, 2157 (CN stretch), 1542 (C=C(CN)₂ stretch), 1506 (C=C ring stretch), 1336 (CH bend), 1155 (C-CN and C-C ring stretch), 990 (C-C ring stretch), 862, 698 (CH out of plane bend). Raman $\nu_{\max}/\text{cm}^{-1}$ 2201 (CN stretch), 1605 (C=C ring stretch), 1390, 1430 (C-CN stretch), 1197 (C=C-H bending). M.p. 218°C (dec.). Combustion data is awaited.

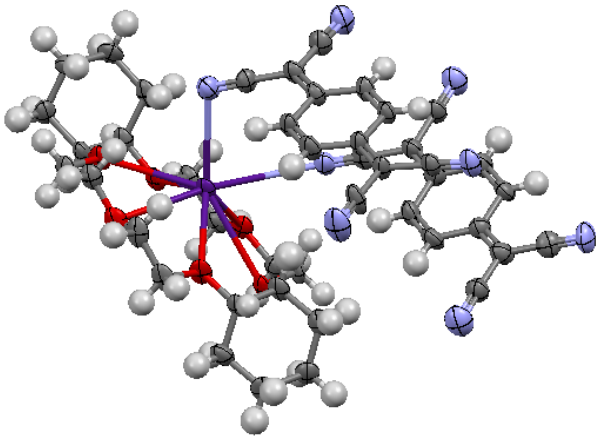
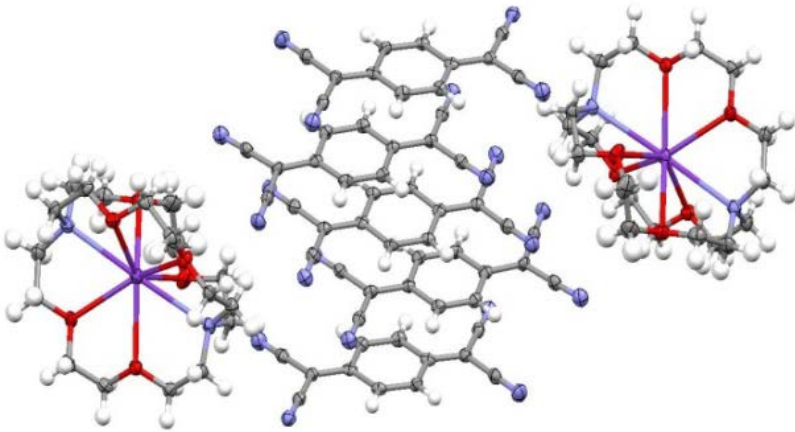
| | | |
|---|-------------------------------------|-------------------------------------|
|  | | |
| C ₄₄ H ₄₄ CsN ₈ O ₆ | a = 8.2698(5) Å | α = 90° |
| M _r = 913.78 | b = 13.2663(9) Å | β = 90° |
| Orthorhombic, P2 ₁ 2 ₁ 2 ₁ | c = 38.069(3) Å | γ = 90° |
| T = 100(2) K | V = 4176.5(5) Å ³ | Z = 4 |
| λ = 0.71075 Å, Ros | 0.07 × 0.03 × 0.02 mm ³ | Plate; Dark Blue |
| D _c = 1.453 Mg / m ³ | μ = 0.945 mm ⁻¹ | Completeness = 98.8% |
| Independent reflections = 9300 [R _{int} = 0.1716] | R ₁ [I ≥ 2σ(I)] = 0.0720 | wR ₂ [all data] = 0.1948 |

Table 6.24 Crystal structure information of (DC18C6)Cs(TCNQ)₂ in this study

6.3.31 Preparation of (C222)K(TCNQ)_{2.5}

A solution of KTCNQ (0.243g, 1mmol), TCNQ⁰ (0.204g, 1mmol) and 2.2.2-Cryptand (0.377g, 1mmol) in dry acetonitrile (50ml) was boiled for five minutes, filtered whilst hot and then left to cool. The solvent was left to evaporate slowly over a period of several days and the solid which formed was then separated by filtration. The solid was washed with diethyl ether (50ml) and dried in vacuum to a small bright black crystalline solid (0.4002g, 49%). MS (solution) (MeCN) (ESI⁻) m/z: 204.1 (TCNQ⁻). (ESI⁺) m/z: 399.2 (Crown + K⁺). IR $\nu_{\max}/\text{cm}^{-1}$ 2961, 2885, 2810 (saturated CH stretch), 2200, 2178, 2152 (CN stretch) (lit¹⁶⁵. 2177, 2156), 1557 (C=C(CN)₂ stretch), 1512 (C=C ring stretch), 1354 (CH bend), 1175 (C-CN and C-C ring stretch), 949 (C-C ring stretch), 834, 749 (CH out of plane bend). Raman $\nu_{\max}/\text{cm}^{-1}$ 2189 (CN stretch), 1600, 1614 (C=C ring stretch), 1389, 1434 (C-CN stretch), 1195 (C=C-H bending). M.p. 210°C (dec.). Combustion Analysis: Calculated: C: 62.25%, H: 5.01%, N: 18.15%. Found: C: 62.18%, H: 5.02%, N: 18.06%.



| | | |
|--|---|-----------------------------------|
| $\text{C}_{96}\text{H}_{92}\text{K}_2\text{N}_{24}\text{O}_{12}$ | $a = 8.049(8) \text{ \AA}$ | $\alpha = 90^\circ$ |
| $M_r = 1852.14$ | $b = 36.85(3) \text{ \AA}$ | $\beta = 98.002(14)^\circ$ |
| Monoclinic, $P2_1/n$ | $c = 15.941(13) \text{ \AA}$ | $\gamma = 90^\circ$ |
| $T = 100(2) \text{ K}$ | $V = 4682(7) \text{ \AA}^3$ | $Z = 2$ |
| $\lambda = 0.71075 \text{ \AA}$, Kat | $0.20 \times 0.20 \times 0.20 \text{ mm}^3$ | Plate; Dark Blue |
| $D_c = 1.314 \text{ Mg / m}^3$ | $\mu = 0.176 \text{ mm}^{-1}$ | Completeness = 92.3% |
| Independent reflections = 9830 [$R_{\text{int}} = 0.0630$] | $R_1 [I \geq 2\sigma(I)] = 0.0870$ | $wR_2 [\text{all data}] = 0.1924$ |

Table 6.25 Crystal structure information of (C222)K(TCNQ)_{2.5} in this study

6.3.32 Preparation of (C222)Rb(TCNQ)_{2.5}

A solution of Rb₂(TCNQ)₃ (0.0784g, 1mmol), TCNQ⁰ (0.408g, 2mmol) and 2.2.2-Cryptand (0.754g, 2mmol) in dry acetonitrile (50ml) was heated under reflux for three hours, filtered whilst hot and then left to cool. The solvent was left to evaporate slowly over a period of several days and the solid which formed was then separated by filtration. The solid was washed with diethyl ether (50ml) and dried in vacuum to form a plate of metallic dark blue crystalline solid (0.02859g, 59%). MS (solution) (MeCN) (ESI⁻) m/z: 204.1 (TCNQ⁻). (ESI⁺) m/z: 399.2 (Crown + K⁺). IR $\nu_{\text{max}}/\text{cm}^{-1}$ 3054, 2978, 2873 (saturated CH stretch), 2232, 2203, 2173 (CN stretch), 1560 (C=C(CN)₂ stretch), 1522 (C=C ring stretch), 1341 (CH bend), 1200 (C-CN and C-C ring stretch), 924 (C-C ring stretch), 847, 763 (CH out of plane bend). M.p. 300°C (dec.). Combustion data is awaited.

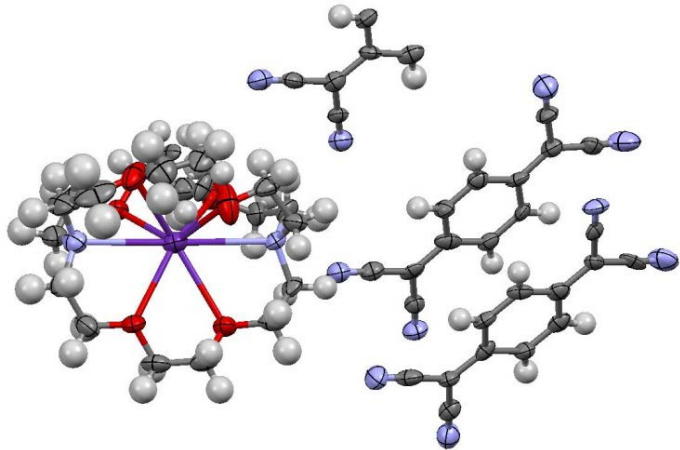
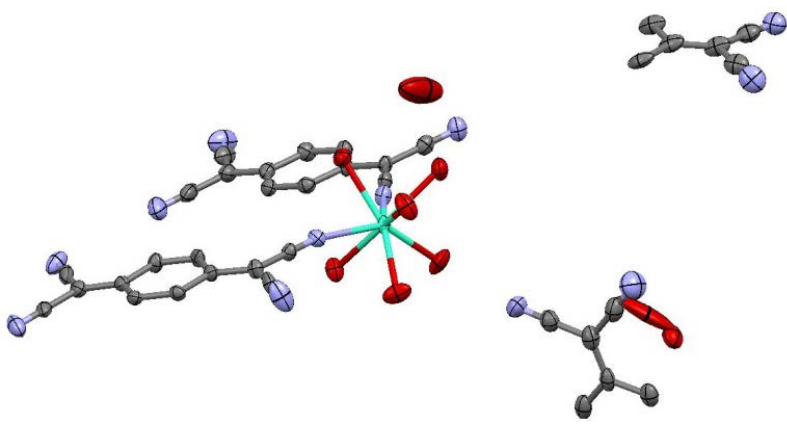
| | | |
|---|-------------------------------------|-------------------------------------|
|  | | |
| C ₄₈ H ₄₆ RbN ₁₂ O ₆ | a = 8.0182(5) Å | α = 90° |
| M _r = 972.44 | b = 36.908(3) Å | β = 97.938(3)° |
| Monoclinic, P2 ₁ /n | c = 15.7974(11) Å | γ = 90° |
| T = 100(2) K | V = 4630.2(6) Å ³ | Z = 4 |
| λ = 0.71075 Å, Ros | 0.09 × 0.06 × 0.20 mm ³ | Plate; Dark Blue |
| D _c = 1.395 Mg / m ³ | μ = 1.133 mm ⁻¹ | Completeness = 99.4% |
| Independent reflections = 10576 [R _{int} = 0.2504] | R ₁ [I ≥ 2σ(I)] = 0.1184 | wR ₂ [all data] = 0.3089 |

Table 6.26 Crystal structure information of (C222)Rb(TCNQ)_{2.5} in this study

6.3.33 Preparation of Tb(TCNQ)₃(H₂O)₆·3H₂O

Following the established procedures of Zhang et al.²³⁶, a suitable amount of LiTCNQ (0.124g, 0.6mmol) was dissolved in deionised water (20ml) at room temperature. Terbium(III) chloride (0.071g, 0.2mmol) was also dissolved in deionised water (20ml) at room temperature. These two separated solutions were then mixed in a suitable round bottom flask without any further heating or stirring. The solid which formed was filtered and was washed with dry diethyl ether. Then, drying the complex in vacuum afforded a bright blue powder of Tb(TCNQ)₃(H₂O)₆·3H₂O (0.061g, 41%). IR $\nu_{\text{max}}/\text{cm}^{-1}$ 2186, 2123 (CN stretch). Combustion data is awaited.



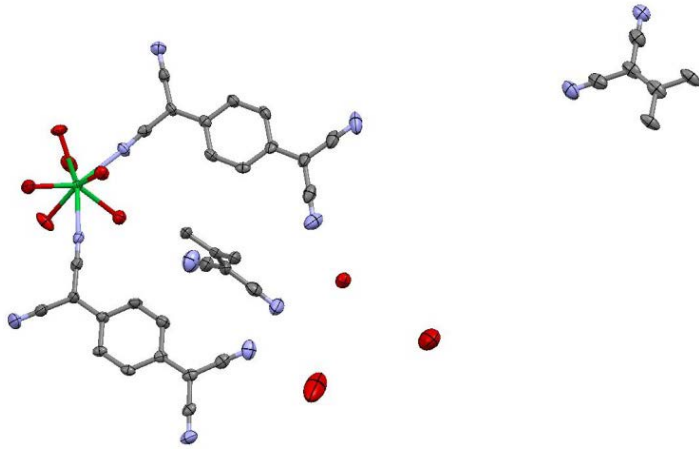
| | | |
|--|---|-----------------------------------|
| $\text{C}_{36}\text{H}_{30}\text{TbN}_{12}\text{O}_9$ | $a = 11.110(3) \text{ \AA}$ | $\alpha = 90^\circ$ |
| $M_r = 933.64$ | $b = 25.401(6) \text{ \AA}$ | $\beta = 107.180(4)^\circ$ |
| Monoclinic, $P2_1/n$ | $c = 15.210(4) \text{ \AA}$ | $\gamma = 90^\circ$ |
| $T = 100(2) \text{ K}$ | $V = 4100.8(18) \text{ \AA}^3$ | $Z = 4$ |
| $\lambda = 0.71075 \text{ \AA}$, Kat | $0.05 \times 0.01 \times 0.01 \text{ mm}^3$ | Block; Bright Blue |
| $D_c = 1.512 \text{ Mg / m}^3$ | $\mu = 1.791 \text{ mm}^{-1}$ | Completeness = 99.9% |
| Independent reflections = 9392 [$R_{\text{int}} = 0.0701$] | $R_1 [I \geq 2\sigma(I)] = 0.0536$ | $wR_2 [\text{all data}] = 0.1044$ |

Table 6.27 Crystal structure information of Tb(TCNQ)₃(H₂O)₆·3H₂O in this study

6.3.34 Preparation of Yb(TCNQ)₃(H₂O)₆·3H₂O

Following the established procedures of Zhang et al.²³⁶, a suitable amount of LiTCNQ (0.126g, 0.6mmol) was dissolved in deionised water (20ml) at room temperature. Ytterbium(III) chloride (0.062g, 0.2mmol) was then dissolved in deionised water (20ml)

at room temperature. These two solutions were then mixed in a suitable round bottom flask without any further heating or stirring. The solid which formed was filtered and was washed with dry diethyl ether. Then, drying the complex in vacuum afforded a bright blue powder of $\text{Yb}(\text{TCNQ})_3(\text{H}_2\text{O})_6 \cdot 3\text{H}_2\text{O}$ (0.065g, 40%). IR $\nu_{\text{max}}/\text{cm}^{-1}$ 2162, 2190 (CN stretch). Combustion data is awaited.



| | | |
|--|--|-----------------------------------|
| $\text{C}_{36}\text{H}_{30}\text{YbN}_{12}\text{O}_9$ | $a = 11.067(2) \text{ \AA}$ | $\alpha = 90^\circ$ |
| $M_r = 947.76$ | $b = 25.288(5) \text{ \AA}$ | $\beta = 107.063(6)^\circ$ |
| Monoclinic, $P2_1/n$ | $c = 15.120(3) \text{ \AA}$ | $\gamma = 90^\circ$ |
| $T = 100(2) \text{ K}$ | $V = 4045.3(14) \text{ \AA}^3$ | $Z = 4$ |
| $\lambda = 1.54187, \text{Dot}$ | $0.1 \times 0.09 \times 0.01 \text{ mm}^3$ | Sheet; Bright Blue |
| $D_c = 1.556 \text{ Mg / m}^3$ | $\mu = 4.852 \text{ mm}^{-1}$ | Completeness = 99.6% |
| Independent reflections = 7101 [$R_{\text{int}} = 0.0721$] | $R_1 [I \geq 2\sigma(I)] = 0.0505$ | $wR_2 [\text{all data}] = 0.1196$ |

Table 6.28 Crystal structure information of $\text{Yb}(\text{TCNQ})_3(\text{H}_2\text{O})_6 \cdot 3\text{H}_2\text{O}$ in this study

Appendix 1

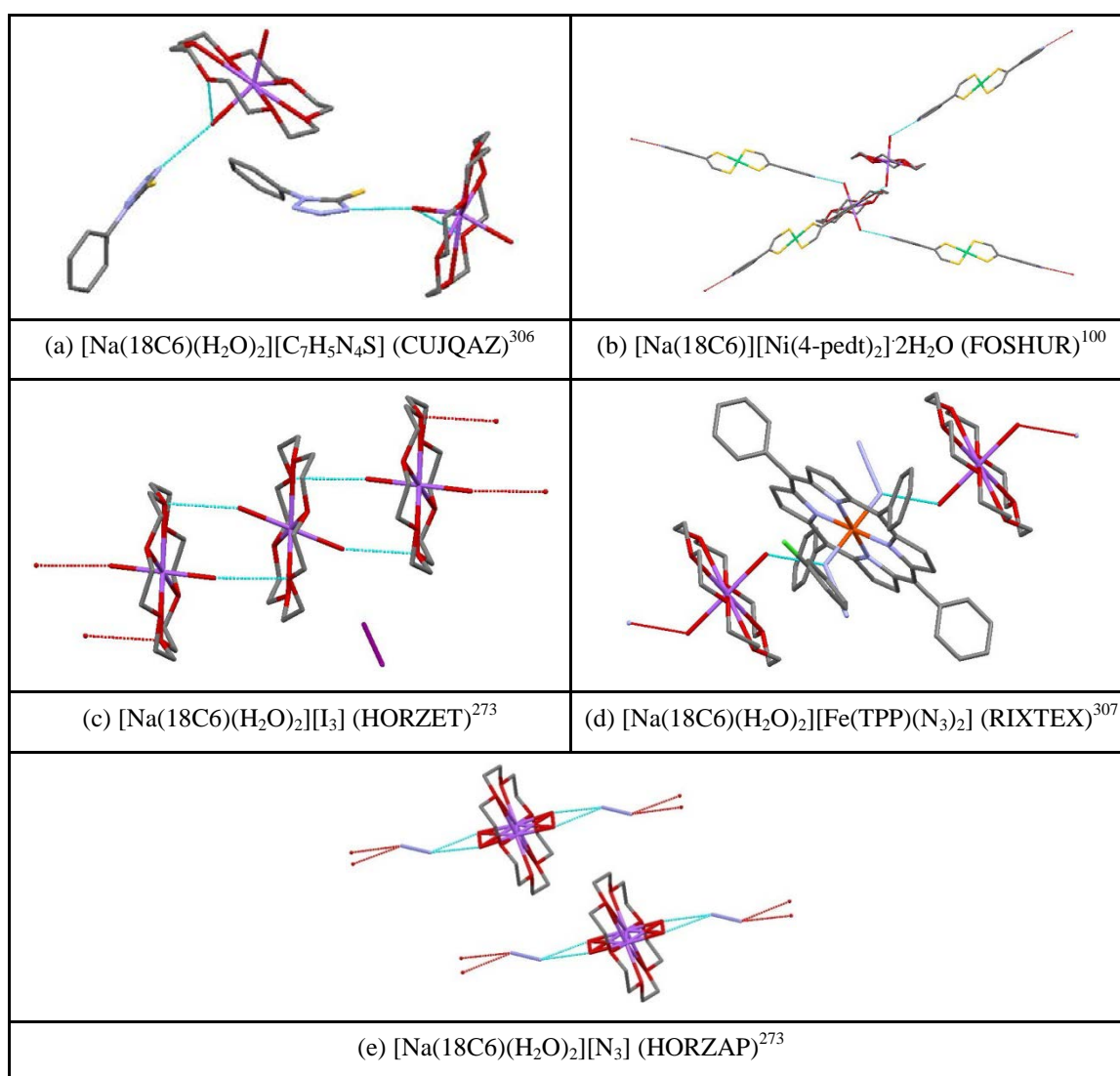


Figure A.1 Five examples of Na^+ ion coordination in crown ether complexes (hydrogen atoms are excluded)

There are not any chosen examples, showing the $\text{Na}^+ \cdots \text{H}_2\text{O} \cdots \text{Na}^+$ bridge coordination, which are listed in Figure A.1. In Figure A.1 (a), each Na^+ ion is not disordered with two H_2O molecules coordinated and an $\text{N} \cdots \text{H}$ hydrogen bond is formed between hydrogen atom from H_2O molecule and nitrogen atom from adjacent tetrazolate anion³⁰⁶; in Figure A.1 (b), each Na^+ ion is not disordered sitting in the cavity of crown ether ring with two H_2O molecules coordinated. $\text{N} \cdots \text{H}$ hydrogen bonds are formed between hydrogen atom from H_2O molecule and nitrogen atom from adjacent counter-anion. The distance of $\text{Na}^+ \cdots \text{H}_2\text{O}$ is 2.332 Å which is longer than the (18C6)Na(TCNQ)₂·2H₂O complex (2.138 Å)¹⁰⁰; in Figure A.1 (c), each Na^+ ion is not

Appendix 1

disordered sitting in the cavity of 18C6 unit with two H₂O molecules coordinated. There is no water-anion interaction but instead the hydrogen atom from H₂O molecule can bond to crown ether oxygen with further forming a linear H₂O \cdots Na⁺ \cdots H₂O interaction²⁷³; in Figure A.1 (d), each Na⁺ ion is not disordered sitting in the cavity of 18C6 with two H₂O molecules coordinated and an N \cdots H hydrogen bond is formed between hydrogen atom from H₂O molecule and nitrogen atom from adjacent counter-anion. The distance of Na⁺ \cdots H₂O is 2.329 Å which is longer than the (18C6)Na(TCNQ)₂·2H₂O complex (2.138 Å)³⁰⁷; in Figure A.1 (e), each Na⁺ ion is disordered in the cavity of crown ether ring with two H₂O molecules coordinated, which participate in forming the intramolecular hydrogens²⁷³.

Bibliography

- (1) Carroll, R. L.; Gorman, C. B. The Genesis of Molecular Electronics. *Angew. Chem. Int. Ed. (English)* **2002**, *41*, 4378-4400.
- (2) Krieger, Y. G. Molecular electronics: Current state and future trends. *J. Struct. Chem.* **1993**, *34*, 896-904.
- (3) Bergren, A. J.; McCreery, R. L. Analytical Chemistry in Molecular Electronics. *Annu. Rev. Anal. Chem.* **2011**, *4*, 173-195.
- (4) Blum, A. S.; Soto, C. M.; Sapsford, K. E.; Wilson, C. D.; Moore, M. H.; Ratna, B. R. Molecular electronics based nanosensors on a viral scaffold. *Biosens. Bioelectron.* **2011**, *26*, 2852-2857.
- (5) Ratner, M. A brief history of molecular electronics. *Nat Nano* **2013**, *8*, 378-381.
- (6) Tour, J. M. Molecular Electronics. Synthesis and Testing of Components. *Acc. Chem. Res.* **2000**, *33*, 791-804.
- (7) Heath, J. R.; Ratner, M. A. Molecular Electronics. *Phys. Today* **2003**, *56*, 43-49.
- (8) Ang, W. H.; Casini, A.; Sava, G.; Dyson, P. J. Organometallic ruthenium-based antitumor compounds with novel modes of action. *J. Organomet. Chem.* **2011**, *696*, 989-998.
- (9) Patra, M.; Gasser, G. Organometallic Compounds: An Opportunity for Chemical Biology? *ChemBioChem* **2012**, *13*, 1232-1252.
- (10) Noffke, A. L.; Habtemariam, A.; Pizarro, A. M.; Sadler, P. J. Designing organometallic compounds for catalysis and therapy. *Chem. Commun.* **2012**, *48*, 5219-5246.
- (11) Gasser, G.; Metzler-Nolte, N. The potential of organometallic complexes in medicinal chemistry. *Curr. Opin. Chem. Biol.* **2012**, *16*, 84-91.
- (12) Bulaevskiĭ, L. Peierls structure transition in quasi-one-dimensional crystals. *Phys. Usp.* **1975**, *18*, 131.
- (13) Fedutin, D. Thermoelectric Properties of Quasi-one-dimensional Platinum Complexes. *J. Exp. Theor. Phys.* **1973**, *17*, 214.
- (14) Chiang, C. K.; Fincher Jr, C.; Park, Y.; Heeger, A.; Shirakawa, H.; Louis, E.; Gau, S.; MacDiarmid, A. G. Electrical conductivity in doped polyacetylene. *Phys. Rev. Lett.* **1977**, *39*, 1098.
- (15) Bredas, J. L.; Street, G. B. Polarons, bipolarons, and solitons in conducting polymers. *Acc. Chem. Res.* **1985**, *18*, 309-315.
- (16) Tickle, I. J.; Prout, C. K. Molecular complexes. Part XVII. Crystal and molecular structure of perylene-7, 7, 8, 8-tetracyanoquinodimethane molecular complex. *J. Chem. Soc., Perkin Trans. 2* **1973**, 720-723.

Bibliography

- (17) Munnoch, P. J.; Wright, J. D. Crystal structure of the 1: 1 molecular complex of chrysene and tetrafluoro-p-benzoquinone (fluoranil). *J. Chem. Soc., Perkin Trans. 2* **1975**, 1071-1074.
- (18) Hunter, C. A.; Sanders, J. K. The nature of π - π interactions. *J. Am. Chem. Soc.* **1990**, *112*, 5525-5534.
- (19) Akamatu, H.; Inokuchi, H.; Matsunaga, Y. Electrical conductivity of the perylene-bromine complex. *Nature* **1954**, *173*, 168-169.
- (20) Underhill, A. E. Molecular metals and superconductors. *J. Mater. Chem.* **1992**, *2*, 1-11.
- (21) Acker, D.; Harder, R.; Hertler, W.; Mahler, W.; Melby, L.; Benson, R. E.; Mochel, W. 7, 7, 8, 8-Tetracyanoquinodimethane and its electrically conducting anion-radical derivatives. *J. Am. Chem. Soc.* **1960**, *82*, 6408-6409.
- (22) Ma, L.; Hu, P.; Kloc, C.; Sun, H.; Michel-Beyerle, M. E.; Gurzadyan, G. G. Ultrafast spectroscopic characterization of 7,7,8,8-tetracyanoquinodimethane (TCNQ) and its radical anion (TCNQ⁻). *Chem. Phys. Lett.* **2014**, *609*, 11-14.
- (23) Qu, X.; Lu, J.; Zhao, C.; Boas, J. F.; Moubaraki, B.; Murray, K. S.; Siriwardana, A.; Bond, A. M.; Martin, L. L. (Pro₂H⁺)₂(TCNQ⁻)₂·TCNQ: An Amino Acid Derived Semiconductor. *Angew. Chem.* **2011**, *123*, 1627-1630.
- (24) Klots, C. E.; Compton, R. N.; Raaen, V. F. Electronic and ionic properties of molecular TTF and TCNQ. *J. Chem. Phys.* **1974**, *60*, 1177-1178.
- (25) Milián, B.; Pou-Amérigo, R.; Viruela, R.; Ortí, E. On the electron affinity of TCNQ. *Chem. Phys. Lett.* **2004**, *391*, 148-151.
- (26) Jérôme, D. Organic Conductors: From Charge Density Wave TTF–TCNQ to Superconducting (TMTSF)₂PF₆. *Chem. Rev.* **2004**, *104*, 5565-5592.
- (27) Zhao, C.; Bond, A. M. Photoinduced Oxidation of Water to Oxygen in the Ionic Liquid BMIMBF₄ as the Counter Reaction in the Fabrication of Exceptionally Long Semiconducting Silver-Tetracyanoquinodimethane Nanowires. *J. Am. Chem. Soc.* **2009**, *131*, 4279-4287.
- (28) O'Mullane, A. P.; Fay, N.; Nafady, A.; Bond, A. M. Preparation of Metal–TCNQ Charge-Transfer Complexes on Conducting and Insulating Surfaces by Photocrystallization. *J. Am. Chem. Soc.* **2007**, *129*, 2066-2073.
- (29) Nafady, A.; Bond, A. M.; Bilyk, A.; Harris, A. R.; Bhatt, A. I.; O'Mullane, A. P.; De Marco, R. Tuning the Electrocrystallization Parameters of Semiconducting Co[TCNQ]²⁻ Based Materials To Yield either Single Nanowires or Crystalline Thin Films. *J. Am. Chem. Soc.* **2007**, *129*, 2369-2382.

- (30) Neufeld, A. K.; O'Mullane, A. P.; Bond, A. M. Control of Localized Nanorod Formation and Patterns of Semiconducting CuTCNQ Phase I Crystals by Scanning Electrochemical Microscopy. *J. Am. Chem. Soc.* **2005**, *127*, 13846-13853.
- (31) Miller, J. S. Four-Center Carbon–Carbon Bonding†. *Acc. Chem. Res.* **2007**, *40*, 189-196.
- (32) Huang, J.; Kingsbury, S.; Kertesz, M. Crystal packing of TCNQ anion π -radicals governed by intermolecular covalent π – π bonding: DFT calculations and statistical analysis of crystal structures. *PCCP* **2008**, *10*, 2625-2635.
- (33) Shi, X. Q.; Lin, C.; Minot, C.; Tseng, T.-C.; Tait, S. L.; Lin, N.; Zhang, R. Q.; Kern, K.; Cerdá, J. I.; Van Hove, M. A. Structural Analysis and Electronic Properties of Negatively Charged TCNQ: 2D Networks of (TCNQ)₂Mn Assembled on Cu(100). *J. Phys. Chem. C* **2010**, *114*, 17197-17204.
- (34) Jaeger, C. D.; Bard, A. J. Electrochemical behavior of donor-tetracyanoquinodimethane electrodes in aqueous media. *J. Am. Chem. Soc.* **1980**, *102*, 5435-5442.
- (35) Sugimoto, T.; Ueda, K.; Endo, S.; Toyota, N.; Tada, T.; Nishimura, K.-i.; Kohama, M.; Shiwaku, K.; Yamamoto, K.; Yamaguchi, T.; Suenaga, Y.; Munakata, M. 1:2 Dimethyl-substituted tetracyanoquinodimethane.: Its radical anion mixed salts: ferromagnetic behavior and high electrical conductivity at room temperature. *Chem. Phys. Lett.* **1998**, *288*, 767-775.
- (36) Grossel, M. C.; Evans, F. A.; Hriljac, J. A.; Prout, K.; Weston, S. C. Triplet excitons in isolated TCNQ^{•-} dimers (TCNQ= tetracyanoquinodimethane). *J. Chem. Soc., Chem. Commun.* **1990**, 1494-1495.
- (37) Lu, J.; Qu, X.; Peleckis, G.; Boas, J. F.; Bond, A. M.; Martin, L. L. Synthesis and structural characterization of a TCNQ based organic semi-conducting material with a 2: 5 stoichiometry. *J. Org. Chem.* **2011**, *76*, 10078-10082.
- (38) Toupet, L.; Karl, N. Non-Sinusoidal Structure of the 1:1 Complex of Phenothiazine and 7,7,8,8-Tetracyanoquinodimethane. *Acta Crystallogr. Sect. C.* **1995**, *51*, 249-251.
- (39) Kobayashi, H. Sinusoidal structure of the 1:1 complex of phenothiazine and 7,7,8,8-tetracyanoquinodimethane, PTZ-TCNQ. *Acta Crystallogr. Sect. B.* **1974**, *30*, 1010-1017.
- (40) Prout, C. K.; Tickle, I. J. Molecular complexes. Part XIV. Crystal and molecular structure of the π^* -electron-acceptor molecule 1, 2, 4, 5-tetracyanobenzene. *J. Chem. Soc., Perkin Trans. 2* **1973**, 520-523.
- (41) Dillon, R. J.; Bardeen, C. J. Time-Resolved Studies of Charge Recombination in the Pyrene/TCNQ Charge-Transfer Crystal: Evidence for Tunneling. *J. Phys. Chem. A* **2012**, *116*, 5145-5150.
- (42) Shimomura, S.; Kitagawa, S. Soft porous crystal meets TCNQ: charge transfer-type porous coordination polymers. *J. Mater. Chem.* **2011**, *21*, 5537-5546.

Bibliography

- (43) Liu, Y.; Zheng, N.; Li, H.; Yin, B. Supramolecular gels based on monopyrrolotetrathiafulvalene and its TCNQ charge-transfer complex. *Soft Matter* **2013**, *9*, 5261-5269.
- (44) Jono, R.; Fujisawa, J.-i.; Segawa, H.; Yamashita, K. Theoretical Study of the Surface Complex between TiO₂ and TCNQ Showing Interfacial Charge-Transfer Transitions. *J. Phys. Chem. Lett.* **2011**, *2*, 1167-1170.
- (45) Eldaroti, H. H.; Gadir, S. A.; Refat, A. A.; Adam, A. M. A. Charge transfer complexes of the donor acriflavine and the acceptors quinol, picric acid, TCNQ and DDQ: synthesis, spectroscopic characterizations and antimicrobial studies. *Int J Electrochem Sci* **2013**, *8*, 5774-5800.
- (46) Tsutsumi, J. y.; Matsui, H.; Yamada, T.; Kumai, R.; Hasegawa, T. Generation and Diffusion of Photocarriers in Molecular Donor–Acceptor Systems: Dependence on Charge-Transfer Gap Energy. *J. Phys. Chem. C* **2012**, *116*, 23957-23964.
- (47) Zhu, L.; Yi, Y.; Fonari, A.; Corbin, N. S.; Coropceanu, V.; Brédas, J.-L. Electronic Properties of Mixed-Stack Organic Charge-Transfer Crystals. *J. Phys. Chem. C* **2014**, *118*, 14150-14156.
- (48) Shaanan, B.; Shmueli, U.; Rabinovich, D. Structure and packing arrangement of molecular compounds. VII. 7, 7, 8, 8-Tetracyanoquinodimethane-naphthalene (1: 1). *Acta Crystallogr. Sect. B-Struct. Cryst. Cryst. Chem.* **1976**, *32*, 2574-2580.
- (49) Goetz, K. P.; Vermeulen, D.; Payne, M. E.; Kloc, C.; McNeil, L. E.; Jurchescu, O. D. Charge-transfer complexes: new perspectives on an old class of compounds. *J. Mater. Chem. C* **2014**, *2*, 3065-3076.
- (50) Dobrowolski, M. A.; Garbarino, G.; Mezouar, M.; Ciesielski, A.; Cyranski, M. K. Structural diversities of charge transfer organic complexes. Focus on benzenoid hydrocarbons and 7,7,8,8-tetracyanoquinodimethane. *CrystEngComm* **2014**, *16*, 415-429.
- (51) Wu, X.; Wang, M.; Du, M.; Lu, J.; Chen, J.; Khan, A.; Usman, R.; Wei, X.; Feng, Q.; Xu, C. Reversible Accommodation and Desorption of Aromatics on a Charge Transfer Cocrystal Involving an Anthracene Derivative and TCNQ. *Cryst. Growth Des.* **2015**, *15*, 434-441.
- (52) Song, J.; Ji, Z.; Nie, Q.; Hu, W. Facilely and efficiently tuning metal-organic nanostructures of a charge-transfer complex based on a water controlled nanoreaction and the chemistry of 7,7,8,8-tetracyanoquinodimethane (TCNQ). *Nanoscale* **2014**, *6*, 2573-2576.
- (53) Endres, H.: Salts of 7, 7, 8, 8-Tetracyano-p-quinodimethane with Simple and Complex Metal Cations. In *Extended linear chain compounds*; Springer, 1983; pp 263-317.
- (54) Endres, H. Salts of 7, 7, 8, 8-Tetracyano-p-quinodimethane with Simple and Complex Metal Cations. *Extended Linear Chain Compounds* **2012**, *3*, 263.

- (55) Grossel, M. C.; Duke, A. J.; Hibbert, D. B.; Lewis, I. K.; Seddon, E. A.; Horton, P. N.; Weston, S. C. An Investigation of the Factors that Influence the Decomposition of 7,7',8,8'-Tetracyanoquinodimethane (TCNQ) and Its Salts to, and Structural Characterization of, the α,α -Dicyano-p-toluoylecyanide Anion. *Chem. Mater.* **2000**, *12*, 2319-2323.
- (56) Hertler, W.; Hartzler, H.; Acker, D.; Benson, R. Substituted quinodimethans. III. Displacement reactions of 7, 7, 8, 8-tetracyanoquinodimethan. *J. Am. Chem. Soc.* **1962**, *84*, 3387-3393.
- (57) Miller, J. S.; Reis Jr, A. H.; Gebert, E.; Ritsko, J.; Salaneck, W.; Kovnat, L.; Cape, T. W.; Van Duyne, R. P. Synthesis and characterization of the metamagnetic 1: 1 1-D phase of the decamethylferrocenium 7, 7, 8, 8-tetracyano-p-quinodimethanide: $\text{Fe}[\text{C}_5(\text{CH}_3)_5]_2^+(\text{TCNQ})^-$. *J. Am. Chem. Soc.* **1979**, *101*, 7111-7113.
- (58) Suchanski, M. R.; Van Duyne, R. P. Resonance Raman spectroelectrochemistry. IV. The oxygen decay chemistry of the tetracyanoquinodimethane dianion. *J. Am. Chem. Soc.* **1976**, *98*, 250-252.
- (59) Abrahams, B. F.; Hudson, T. A.; Robson, R. A New Approach to TCNQ-Based Coordination Polymers via TCNQH_2 . *Cryst. Growth Des.* **2008**, *8*, 1123-1125.
- (60) Hudson, T. A.; Robson, R. A New Class of TCNQ Derivatives Easily Generated from TCNQH_2 Containing Discrete TCNQ^{2-} Anions and Noncoordinating Cations. *Cryst. Growth Des.* **2009**, *9*, 1658-1662.
- (61) Abrahams, B. F.; Elliott, R. W.; Hudson, T. A.; Robson, R. A New Class of Easily Generated TCNQ^{2-} -Based Coordination Polymers. *Cryst. Growth Des.* **2010**, *10*, 2860-2862.
- (62) Abrahams, B. F.; Elliott, R. W.; Hudson, T. A.; Robson, R. A new type of 3D $[(\text{M}^{\text{II}})_2(\text{TCNQ}^{-\text{II}})_3]^{2-}$ coordination network with spacious channels of hexagonal cross-section generated from TCNQH_2 . *CrystEngComm* **2012**, *14*, 351-354.
- (63) Tseng, T.-C.; Urban, C.; Wang, Y.; Otero, R.; Tait, S. L.; Alcamí, M.; Écija, D.; Trelka, M.; Gallego, J. M.; Lin, N.; Konuma, M.; Starke, U.; Nefedov, A.; Langner, A.; Wöll, C.; Herranz, M. Á.; Martín, F.; Martín, N.; Kern, K.; Miranda, R. Charge-transfer-induced structural rearrangements at both sides of organic/metal interfaces. *Nat Chem* **2010**, *2*, 374-379.
- (64) Morinaga, M.; Nogami, T.; Kanda, Y.; Matsumoto, T.; Matsuoka, K.; Mikawa, H. The Syntheses, Electrical Resistivities, and Electronic Absorption Spectra of Cation-TCNQ-Crown Ether Complexes. *Bull. Chem. Soc. Jpn.* **1980**, *53*, 1221-1227.
- (65) Afify, H.; Abdel-Kerim, F.; Aly, H.; Shabaka, A. The Electrical Conductance of Some Alkali-and Divalent Transition Metal TCNQ Salts. *Z. Naturforsch., Part A* **1978**, *33*, 344.
- (66) Bloor, D.; Kagawa, Y.; Szablewski, M.; Ravi, M.; Clark, S. J.; Cross, G. H.; Palsson, L.-O.; Beeby, A.; Parmer, C.; Rumbles, G. Matrix dependence of light emission from TCNQ adducts. *J. Mater. Chem.* **2001**, *11*, 3053-3062.

Bibliography

- (67) Cole, J. M.; Copley, R. C. B.; McIntyre, G. J.; Howard, J. A. K.; Szablewski, M.; Cross, G. H. Charge-density study of the nonlinear optical precursor DED-TCNQ at 20 K. *Phys. Rev. B, PRB* **2002**, *65*, 125107.
- (68) Grossel, M. C.; Weston, S. C. Synthesis of materials for molecular electronic applications. *Contemp. Org. Synth.*, **1994**, *1*, 367-386.
- (69) Blochwitz, J.; Fritz, T.; Pfeiffer, M.; Leo, K.; Alloway, D. M.; Lee, P. A.; Armstrong, N. R. Interface electronic structure of organic semiconductors with controlled doping levels. *Org. Electron.* **2001**, *2*, 97-104.
- (70) Wudl, F.; Smith, G.; Hufnagel, E. Bis-1, 3-dithiolium chloride: an unusually stable organic radical cation. *J. Chem. Soc.D: Chem.Comm.* **1970**, 1453-1454.
- (71) Hendon, C. H.; Tiana, D.; Walsh, A. Conductive metal-organic frameworks and networks: fact or fantasy? *PCCP* **2012**, *14*, 13120-13132.
- (72) Solovyeva, V.; Huth, M. Defect-induced shift of the Peierls transition in TTF-TCNQ thin films. *Synth. Met.* **2011**, *161*, 976-983.
- (73) Zhu, L.; Yi, Y.; Li, Y.; Kim, E.-G.; Coropceanu, V.; Brédas, J.-L. Prediction of Remarkable Ambipolar Charge-Transport Characteristics in Organic Mixed-Stack Charge-Transfer Crystals. *J. Am. Chem. Soc.* **2012**, *134*, 2340-2347.
- (74) Torrance, J. B. The difference between metallic and insulating salts of tetracyanoquinodimethone (TCNQ): how to design an organic metal. *Acc. Chem. Res.* **1979**, *12*, 79-86.
- (75) Jerome, D.; Schulz, H. Organic conductors and superconductors. *Adv. Phys.* **2002**, *51*, 293-479.
- (76) Kistenmacher, T. J.; Phillips, T. E.; Cowan, D. O. The crystal structure of the 1: 1 radical cation-radical anion salt of 2, 2'-bis-1, 3-dithiole (TTF) and 7, 7, 8, 8-tetracyanoquinodimethane (TCNQ). *Acta Crystallogr. Sect. B-Struct. Cryst. Cryst. Chem.* **1974**, *30*, 763-768.
- (77) Ferraris, J.; Cowan, D.; Walatka, V. t.; Perlstein, J. Electron transfer in a new highly conducting donor-acceptor complex. *J. Am. Chem. Soc.* **1973**, *95*, 948-949.
- (78) Tomkiewicz, Y.; Torrance, J.; Scott, B.; Green, D. Charge transfer equilibria in TTF-TCNQ solutions. *J. Chem. Phys.* **1974**, *60*, 5111-5112.
- (79) Odom, S. A.; Caruso, M. M.; Finke, A. D.; Prokup, A. M.; Ritchey, J. A.; Leonard, J. H.; White, S. R.; Sottos, N. R.; Moore, J. S. Restoration of Conductivity with TTF-TCNQ Charge-Transfer Salts. *Adv. Funct. Mater.* **2010**, *20*, 1721-1727.
- (80) Horton, P. N. An investigation of supramolecular interactions in some electronically active organic and organometallic materials. University of Southampton, 2001.

- (81) Blessing, R.; Coppens, P. On the crystallography of the TTF-TCNQ salt at reduced temperatures. *Solid State Commun.* **1974**, *15*, 215-221.
- (82) Schultz, A. J.; Stucky, G. D.; Blessing, R. H.; Coppens, P. The temperature dependence of the crystal and molecular structure of DELTA. 2, 2'-bi-1, 3-dithiole [TTF] 7, 7, 8, 8-tetracyano-p-quinodimethane [TCNQ]. *J. Am. Chem. Soc.* **1976**, *98*, 3194-3201.
- (83) Filhol, A.; Bravic, G.; Gaultier, J.; Chasseau, D.; Vettier, C. Room-and high-pressure neutron structure determination of tetrathiafulvalene-7, 7, 8, 8-tetracyano-p-quinodimethane (TTF-TCNQ). Thermal expansion and isothermal compressibility. *Acta Crystallogr. Sect. B-Struct. Cryst. Cryst. Chem.* **1981**, *37*, 1225-1235.
- (84) Phillips, T. E.; Kistenmacher, T. J.; Bloch, A. N.; Ferraris, J.; Cowan, O. The crystal and molecular structure of the organic conductor 4, 4', 5, 5'-tetramethyl-2, 2'-bis-1, 3-dithiolium 7, 7, 8, 8-tetracyano-p-quinodimethanide [TMTTF-TCNQ]. *Acta Crystallogr. Sect. B-Struct. Cryst. Cryst. Chem.* **1977**, *33*, 422-428.
- (85) Kistenmacher, T. J.; Phillips, T. E.; Cowan, D. O.; Ferraris, J. P.; Bloch, A. N.; Poehler, T. Crystal structure and diffuse X-ray scattering of the 1.3: 2 salt of 4, 4', 5, 5'-tetramethyl- $\Delta^{2,2'}$ -bis-1, 3-dithiole [TMTTF] and 7, 7, 8, 8-tetracyano-p-quinodimethane [TCNQ], a nonstoichiometric quasi one-dimensional organic conductor. *Acta Crystallogr. Sect. B-Struct. Cryst. Cryst. Chem.* **1976**, *32*, 539-547.
- (86) Kobayashi, H.; Nakayama, J. The Crystal Structure of the Charge-transfer Complex of Dibenzotetrathiafulvalene-Tetracyanoquinodimethane, DBTTF-TCNQ. *Bull. Chem. Soc. Jpn.* **1981**, *54*, 2408-2411.
- (87) Emge, T. J.; Wiygul, F. M.; Chappell, J. S.; Bloch, A. N.; Ferraris, J. P.; Cowan, D. O.; Kistenmacher, T. J. Crystal Structures for the Electron Donor Dibenzotetrathiafulvalene, DBTTF, and Its Mixed-stack Charge-transfer Salts with the Electron Acceptors 7, 7, 8, 8-tetracyano-p-quinodimethane, TCNQ, and 2, 5-difluoro-7, 7, 8, 8-tetracyano-p-quinodimethane, 2, 5-TCNQF₂. *Mol. Cryst. Liq. Cryst.* **1982**, *87*, 137-161.
- (88) Tomkiewicz, Y.; Taranko, A.; Schumaker, R. Hexamethylene-tetrathiafulvalenium tetracyanoquinodimethanide as a prototype of a quasi-one-dimensional organic conductor. *Phys. Rev. B, PRB* **1977**, *16*, 1380.
- (89) Bloch, A.; Cowan, D.; Bechgaard, K.; Pyle, R.; Banks, R.; Poehler, T. Low-temperature metallic behavior and resistance minimum in a new quasi one-dimensional organic conductor. *Phys. Rev. Lett.* **1975**, *34*, 1561.
- (90) Chasseau, D.; Gaultier, J.; Fabre, J.; Giral, L. Octaméthylène-3, 4; 3', 4'tétrathia-2, 2', 5, 5'fulvalène-tétracyano-7, 7, 8, 8 p-quinodiméthane (OMTTF-TCNQ). *Acta Crystallogr. Sect. B-Struct. Cryst. Cryst. Chem.* **1982**, *38*, 1632-1635.
- (91) Murata, K.; Fukumoto, Y.; Yokogawa, K.; Kang, W.; Takaoka, R.; Tada, R.; Hirayama, H.; Brooks, J. S.; Graf, D.; Yoshino, H. Magnetic-Field-Induced Phase Transition

Bibliography

and a Possible Quantum Hall Effect in the Quasi-One-Dimensional CDW Organic Conductor HMTSF-TCNQ. *J. Mod. Phys.* **2014**, *5*, 673-679.

(92) Yang, S.; Brooks, A. C.; Martin, L.; Day, P.; Pilkington, M.; Clegg, W.; Harrington, R. W.; Russo, L.; Wallis, J. D. New chiral organosulfur donors related to bis (ethylenedithio) tetrathiafulvalene. *Tetrahedron* **2010**, *66*, 6977-6989.

(93) Herranz, M. Á.; Sánchez, L.; Martín, N. Tetrathiafulvalene: A paradigmatic electron donor molecule. *Phosphorus, Sulfur, and Silicon and the Related Elements* **2005**, *180*, 1133-1148.

(94) Bendikov, M.; Wudl, F.; Perepichka, D. F. Tetrathiafulvalenes, oligoacenes, and their buckminsterfullerene derivatives: the brick and mortar of organic electronics. *Chem. Rev.* **2004**, *104*, 4891-4946.

(95) Yamamoto, H. M.; Hagiwara, M.; Kato, R. New phase of (BEDT-TTF)(TCNQ). *Synth. Met.* **2003**, *133–134*, 449-451.

(96) Mori, T.; Inokuchi, H. Crystal structure of the mixed-stacked salt of bis (ethylenedithio) tetrathiafulvalene (BEDT-TTF) and tetracyanoquinodimethane (TCNQ). *Bull. Chem. Soc. Jpn.* **1987**, *60*, 402-404.

(97) Mori, T.; Inokuchi, H. Structural and electrical properties of (BEDT-TTF)(TCNQ). *Solid State Commun.* **1986**, *59*, 355-359.

(98) Saito, G.; Hayashi, H.; Enoki, T.; Inokuchi, H. The Study of Charge Transfer Complexes of BEDT-TTF Derivatives. *Mol. Cryst. Liq. Cryst.* **1985**, *120*, 341-344.

(99) Avarvari, N.; Wallis, J. D. Strategies towards chiral molecular conductors. *J. Mater. Chem.* **2009**, *19*, 4061-4076.

(100) Rabaça, S.; Cerdeira, A. C.; Neves, A. I. S.; Dias, S. I. G.; Mézière, C.; Santos, I. C.; Pereira, L. C. J.; Fourmigué, M.; Henriques, R. T.; Almeida, M. Complexes based on asymmetrically substituted pyridine–dithiolenes ligands [M(4-pedt)₂] (M = Au, Cu, Ni; 4-pedt = 1-(pyridin-4-yl)-ethylene-1,2-dithiolate): Synthesis, structure and physical properties. *Polyhedron* **2009**, *28*, 1069-1078.

(101) Wallis, J. D.; Griffiths, J.-P. Substituted BEDT-TTF derivatives: synthesis, chirality, properties and potential applications. *J. Mater. Chem.* **2005**, *15*, 347-365.

(102) Yang, S.; Pop, F.; Melan, C.; Brooks, A. C.; Martin, L.; Horton, P.; Auban-Senzier, P.; Rikken, G. L. J. A.; Avarvari, N.; Wallis, J. D. Charge transfer complexes and radical cation salts of chiral methylated organosulfur donors. *CrystEngComm* **2014**, *16*, 3906-3916.

(103) Andersen, J. R.; Bechgaard, K.; Jacobsen, C.; Rindorf, G.; Soling, H.; Thorup, N. The crystal and molecular structure of the organic conductor 2, 3, 6, 7-tetramethyl-1, 4, 5, 8-tetraselenafulvalenium 2, 5-dimethyl-7, 7, 8, 8-tetracyano-p-quinodimethanide (TMTSF–DMTCNQ). *Acta Crystallogr. Sect. B-Struct. Cryst. Cryst. Chem.* **1978**, *34*, 1901-1905.

- (104) Andrieux, A.; Duroure, C.; Jérôme, D.; Bechgaard, K. The metallic state of the organic conductor TMTSF-DMTCNQ at low temperature under pressure. *Journal de Physique Lettres* **1979**, *40*, 381-383.
- (105) Soling, H.; Rindorf, G.; Thorup, N. The structure of dibenzo-1, 4, 5, 8-tetrathiafulvalenium 2, 5-dichloro-7, 7, 8, 8-tetracyano-p-quinodimethanide, DBTTF-TCNQCl₂, at 295 and 115 K. *Acta Crystallogr. Sect. B-Struct. Cryst. Cryst. Chem.* **1981**, *37*, 1716-1719.
- (106) Jacobsen, C.; Pedersen, H.; Mortensen, K.; Bechgaard, K. Dibenzo-TTF-dichloro-TCNQ: a quasi-one-dimensional magnetic semiconductor. *J. Phys. C: Solid St. Phys.* **1980**, *13*, 3411.
- (107) Grossel, M. C.; Weston, S. C. A Truly Isolated TCNQ^{•-} Dimer? *Chem. Mater.* **1996**, *8*, 977-980.
- (108) Bluemel, J.; Hebendanz, N.; Hudeczek, P.; Koehler, F. H.; Strauss, W. Synthesis and NMR spectroscopy of metallocenium ions. Support for a new ferromagnetic coupling mechanism in decamethylmetallocenium tetracyanoethenides. *J. Am. Chem. Soc.* **1992**, *114*, 4223-4230.
- (109) Schweizer, J.; Golhen, S.; Lelièvre-Berna, E.; Ouahab, L.; Pontillon, Y.; Ressouche, E. Magnetic interactions and spin densities in molecular compounds: an example. *Physica B: Condensed Matter* **2001**, *297*, 213-220.
- (110) Miller, J. S.; Epstein, A. J.; Reiff, W. M. Ferromagnetic molecular charge-transfer complexes. *Chem. Rev.* **1988**, *88*, 201-220.
- (111) Miller, J. S.; Epstein, A. J. Organic and organometallic molecular magnetic materials—designer magnets. *Angew. Chem. Int. Ed. (English)* **1994**, *33*, 385-415.
- (112) Miller, J. S.; Zhang, J. H.; Reiff, W. M.; Dixon, D. A.; Preston, L. D.; Reis, A. H.; Gebert, E.; Extine, M.; Troup, J.; et al. Characterization of the charge-transfer reaction between decamethylferrocene and 7,7,8,8-tetracyano-p-quinodimethane (1:1). The ⁵⁷Fe Moessbauer spectra and structures of the paramagnetic dimeric and the metamagnetic one-dimensional salts and the molecular and electronic structures of (TCNQ)ⁿ (n = 0, -1, -2). *J. Phys. Chem* **1987**, *91*, 4344-4360.
- (113) Lehn, J. M.: *Supramolecular Chemistry: Concepts and Perspectives*; Wiley, 1995.
- (114) Lawrence, D. S.; Jiang, T.; Levett, M. Self-Assembling Supramolecular Complexes. *Chem. Rev.* **1995**, *95*, 2229-2260.
- (115) Lehn, J.-M. Toward complex matter: Supramolecular chemistry and self-organization. *Proc. Natl. Acad. Sci. U.S.A.* **2002**, *99*, 4763-4768.
- (116) Beer, P. D.; Gale, P. A.; Smith, D. K.: *Supramolecular chemistry*; Oxford University Press, 1999.

Bibliography

- (117) Chang, S. K.; Van Engen, D.; Fan, E.; Hamilton, A. D. Hydrogen bonding and molecular recognition: synthetic, complexation, and structural studies on barbiturate binding to an artificial receptor. *J. Am. Chem. Soc.* **1991**, *113*, 7640-7645.
- (118) McGrath, J. M.; Pluth, M. D. Understanding the Effects of Preorganization, Rigidity, and Steric Interactions in Synthetic Barbiturate Receptors. *J. Org. Chem.* **2014**, *79*, 711-719.
- (119) Tron, A.; Thornton, P. J.; Rocher, M.; Jacquot de Rouville, H.-P.; Desvergne, J.-P.; Kauffmann, B.; Buffeteau, T.; Cavagnat, D.; Tucker, J. H. R.; McClenaghan, N. D. Formation of a Hydrogen-Bonded Barbiturate [2]-Rotaxane. *Org. Lett.* **2014**, *16*, 1358-1361.
- (120) Hänni, K. D.; Leigh, D. A. The application of CuAAC 'click' chemistry to catenane and rotaxane synthesis. *Chem. Soc. Rev.* **2010**, *39*, 1240-1251.
- (121) Grunder, S.; McGrier, P. L.; Whalley, A. C.; Boyle, M. M.; Stern, C.; Stoddart, J. F. A Water-Soluble pH-Triggered Molecular Switch. *J. Am. Chem. Soc.* **2013**, *135*, 17691-17694.
- (122) Barin, G.; Frasconi, M.; Dyar, S. M.; Iehl, J.; Buyukcakil, O.; Sarjeant, A. A.; Carmieli, R.; Coskun, A.; Wasielewski, M. R.; Stoddart, J. F. Redox-Controlled Selective Docking in a [2]Catenane Host. *J. Am. Chem. Soc.* **2013**, *135*, 2466-2469.
- (123) Wang, C.; Dyar, S. M.; Cao, D.; Fahrenbach, A. C.; Horwitz, N.; Colvin, M. T.; Carmieli, R.; Stern, C. L.; Dey, S. K.; Wasielewski, M. R.; Stoddart, J. F. Tetrathiafulvalene Hetero Radical Cation Dimerization in a Redox-Active [2]Catenane. *J. Am. Chem. Soc.* **2012**, *134*, 19136-19145.
- (124) Pedersen, C. J. Cyclic polyethers and their complexes with metal salts. *J. Am. Chem. Soc.* **1967**, *89*, 7017-7036.
- (125) Pedersen, C. J. Crystalline Salt Complexes of Macrocyclic Polyethers. *J. Am. Chem. Soc.* **1970**, *92*, 386-391.
- (126) Pedersen, C. J. The Discovery of Crown Ethers (Noble Lecture). *Angew. Chem. Int. Ed. (English)* **1988**, *27*, 1021-1027.
- (127) Pedersen, C. J.; Frensdorff, H. Macrocyclic polyethers and their complexes. *Angew. Chem. Int. Ed. (English)* **1972**, *11*, 16-25.
- (128) Cram, D. J. Preorganization—from solvents to spherands. *Angew. Chem. Int. Ed. (English)* **1986**, *25*, 1039-1057.
- (129) Hancock, R. D. Chelate ring size and metal ion selection. The basis of selectivity for metal ions in open-chain ligands and macrocycles. *J. Chem. Educ.* **1992**, *69*, 615.
- (130) Steed, J. W. First- and second-sphere coordination chemistry of alkali metal crown ether complexes. *Coord. Chem. Rev.* **2001**, *215*, 171-221.

- (131) Grossel, M. C.; Weston, S. C. Supramolecular control of molecular electronic behaviour of TCNQ⁻ salts. *J. Phys. Org. Chem.* **1992**, *5*, 533-539.
- (132) Grossel, M. C.; Weston, S. C. Thallium tetracyanoquinodimethanide (TCNQ) and its 18-crown-6 complex. *J. Chem. Soc., Chem. Commun.* **1992**, 1510-1512.
- (133) Gokel, G. W.; Leevy, W. M.; Weber, M. E. Crown ethers: sensors for ions and molecular scaffolds for materials and biological models. *Chem. Rev.* **2004**, *104*, 2723-2750.
- (134) Fabbrizzi, L.; Poggi, A. Sensors and switches from supramolecular chemistry. *Chem. Soc. Rev.* **1995**, *24*, 197-202.
- (135) McSkimming, G.; Tucker, J. H. R.; Bouas-Laurent, H.; Desvergne, J.-P.; Coles, S. J.; Hursthouse, M. B.; Light, M. E. Photoinduced Formation of a Cryptand from a Coronand: An Unexpected Switch in Cation Binding Affinity. *Chem. Eur. J.* **2002**, *8*, 3331-3342.
- (136) H. R. Tucker, J.; Bouas-Laurent, H.; Marsau, P.; W. Riley, S.; Desvergne, J.-P. A novel crown ether-cryptand photoswitch. *Chem. Commun.* **1997**, 1165-1166.
- (137) Nogami, T.; Morinaga, M.; Mikawa, H.; Nakano, H.; Horioka, M.; Horiuchi, H.; Tokonami, M. Crystal Structure of Potassium 2,2'-(2,5-Cyclohexadiene-1,4-diylidene)bis[propanedinitrile]-1,4,7,10,13,16-hexaoxacyclooctadecane, [K⁺("18-Crown-6")]TCNQ⁻. *Bull. Chem. Soc. Jpn.* **1990**, *63*, 2414-2416.
- (138) Braga, D.; Grepioni, F.; Desiraju, G. R. Crystal engineering and organometallic architecture. *Chem. Rev.* **1998**, *98*, 1375-1406.
- (139) Izatt, R. M.; Bradshaw, J. S.; Nielsen, S. A.; Lamb, J. D.; Christensen, J. J.; Sen, D. Thermodynamic and kinetic data for cation-macrocycle interaction. *Chem. Rev.* **1985**, *85*, 271-339.
- (140) Ganjali, M. R.; Rouhollahi, A.; Mardan, A. R.; Hamzeloo, M.; Mogimi, A.; Shamsipur, M. Lead Ion-Selective Electrode Based on 4'-Vinylbenzo-15-crown-5 Homopolymer. *Microchem. J.* **1998**, *60*, 122-133.
- (141) Brandel, J.; Sairenji, M.; Ichikawa, K.; Nabeshima, T. Remarkable Mg²⁺-selective emission of an azacrown receptor based on Ir(III) complex. *Chem. Commun.* **2010**, *46*, 3958-3960.
- (142) Liu, H.; Shao, X.-B.; Jia, M.-X.; Jiang, X.-K.; Li, Z.-T.; Chen, G.-J. Selective recognition of sodium cyanide and potassium cyanide by diaza-crown ether-capped Zn-porphyrin receptors in polar solvents. *Tetrahedron* **2005**, *61*, 8095-8100.
- (143) Hamidi, A. S.; Kazemi, S. Y.; Zolgharnein, J. Highly Efficient and Selective Transport of Cu (II) with a Cooperative Carrier Composed of Tetraaza-14-Crown-4 and Oleic Acid through a Bulk Liquid Membrane. *Sep. Sci. Technol.* **2009**, *45*, 58-65.
- (144) Li, M.-J.; Chu, B. W.-K.; Zhu, N.; Yam, V. W.-W. Synthesis, Structure, Photophysics, Electrochemistry, and Ion-Binding Studies of Ruthenium(II) 1,10-Phenanthroline

Bibliography

Complexes Containing Thia-, Seleno-, and Aza-Crown Pendants. *Inorg. Chem.* **2007**, *46*, 720-733.

(145) Suzuki, K.; Watanabe, K.; Matsumoto, Y.; Kobayashi, M.; Sato, S.; Siswanta, D.; Hisamoto, H. Design and synthesis of calcium and magnesium ionophores based on double-armed diazacrown ether compounds and their application to an ion sensing component for an ion-selective electrode. *Anal. Chem.* **1995**, *67*, 324-334.

(146) Rounaghi, G.; Popov, A. I. Complexing ability of some mixed sulfur-oxygen crown ethers in nonaqueous solvents. *J. Inorg. Nucl. Chem.* **1981**, *43*, 911-915.

(147) Izatt, R.; Terry, R.; Hansen, L.; Avondet, A.; Bradshaw, J.; Dalley, N.; Jensen, T.; Christensen, J.; Haymore, B. A calorimetric titration study of uni- and bivalent metal ion interaction with several thia derivatives of 9-crown-3, 12-crown-4, 15-crown-5, 18-crown-6, 24-crown-8, and with several oxathiapentadecanes in water or water-methanol solvents at 25°C**. *Inorg. Chim. Acta* **1978**, *30*, 1-8.

(148) Lamb, J.; Izatt, R.; Swain, C.; Christensen, J. A systematic study of the effect of macrocycle ring size and donor atom type on the log K, ΔH , and $T\Delta S$ of reactions at 25°C in methanol of mono- and divalent cations with crown ethers. *J. Am. Chem. Soc.* **1980**, *102*, 475-479.

(149) Craig, A. S.; Katak, R.; Matthews, R. C.; Parker, D.; Ferguson, G.; Lough, A.; Adams, H.; Bailey, N.; Schneider, H. Synthesis of 1, 10-dithia-4, 7, 13, 16-tetra-azacyclo-octadecane, 1-aza-4, 7-dithiacyclononane, and N, N'-1, 2-bis (1-aza-4, 7-dithia-cyclononyl) ethane. Structural and solution studies of their silver complexes. *J. Chem. Soc., Perkin Trans. 2* **1990**, 1523-1531.

(150) Wainwright, K. P. Synthetic and structural aspects of the chemistry of saturated polyaza macrocyclic ligands bearing pendant coordinating groups attached to nitrogen. *Coord. Chem. Rev.* **1997**, *166*, 35-90.

(151) Kimura, E. Macrocyclic polyamines with intelligent functions. *Tetrahedron* **1992**, *48*, 6175-6217.

(152) Liang, X.; Sadler, P. J. Cyclam complexes and their applications in medicine. *Chem. Soc. Rev.* **2004**, *33*, 246-266.

(153) Lehn, J. M. Supramolecular chemistry - scope and perspectives molecules, supermolecules, and molecular devices (Nobel Lecture). *Angew. Chem. Int. Ed. (English)* **1988**, *27*, 89-112.

(154) Lehn, J. M. Cryptates: the chemistry of macropolycyclic inclusion complexes. *Acc. Chem. Res.* **1978**, *11*, 49-57.

- (155) Graf, E.; Kintzinger, J. P.; Lehn, J. M.; LeMoigne, J. Molecular recognition. Selective ammonium cryptates of synthetic receptor molecules possessing a tetrahedral recognition site. *J. Am. Chem. Soc.* **1982**, *104*, 1672-1678.
- (156) Whitesides, G. M.; Grzybowski, B. Self-assembly at all scales. *Science* **2002**, *295*, 2418-2421.
- (157) Winfree, E.; Liu, F.; Wenzler, L. A.; Seeman, N. C. Design and self-assembly of two-dimensional DNA crystals. *Nature* **1998**, *394*, 539-544.
- (158) Pfeil, A.; Lehn, J.-M. Helicate self-organisation: positive cooperativity in the self-assembly of double-helical metal complexes. *J. Chem. Soc., Chem. Commun.* **1992**, 838-840.
- (159) Griffiths, K. E.; Stoddart, J. F. Template-directed synthesis of donor/acceptor [2] catenanes and [2] rotaxanes. *Pure Appl. Chem.* **2008**, *80*, 485-506.
- (160) Fyfe, M. C.; Stoddart, J. F. Synthetic supramolecular chemistry. *Acc. Chem. Res.* **1997**, *30*, 393-401.
- (161) Allwood, B. L.; Spencer, N.; Shahriari-Zavareh, H.; Stoddart, J. F.; Williams, D. J. Complexation of Paraquat by a bisparaphenylene-34-crown-10 derivative. *J. Chem. Soc., Chem. Commun.* **1987**, 1064-1066.
- (162) Ashton, P. R.; Slawin, A. M.; Spencer, N.; Stoddart, J. F.; Williams, D. J. Complex formation between bisparaphenylene-(3n+ 4)-crown-n ethers and the paraquat and diquat dications. *J. Chem. Soc., Chem. Commun.* **1987**, 1066-1069.
- (163) Deng, W.-Q.; Flood, A. H.; Stoddart, J. F.; Goddard, W. A. An electrochemical color-switchable RGB dye: tristable [2] catenane. *J. Am. Chem. Soc.* **2005**, *127*, 15994-15995.
- (164) Desiraju, G. R. Crystal Engineering: A Holistic View. *Angew. Chem. Int. Ed. (English)* **2007**, *46*, 8342-8356.
- (165) Desiraju, G. R. Supramolecular Synthons in Crystal Engineering - A New Organic Synthesis. *Angew. Chem. Int. Ed. (English)* **1995**, *34*, 2311-2327.
- (166) Desiraju, G. R.: *The crystal as a supramolecular entity*; John Wiley & Sons, 2008; Vol. 18.
- (167) Moulton, B.; Zaworotko, M. J. From molecules to crystal engineering: supramolecular isomerism and polymorphism in network solids. *Chem. Rev.* **2001**, *101*, 1629-1658.
- (168) Atkins, P.: Physical chemistry 4th ed. Cambridge University Press, Cambridge, 1990.
- (169) Kuhn, B.; Mohr, P.; Stahl, M. Intramolecular Hydrogen Bonding in Medicinal Chemistry. *J. Med. Chem.* **2010**, *53*, 2601-2611.
- (170) Takahashi, O.; Kohno, Y.; Nishio, M. Relevance of weak hydrogen bonds in the conformation of organic compounds and bioconjugates: evidence from recent experimental data and high-level *ab initio* MO calculations. *Chem. Rev.* **2010**, *110*, 6049-6076.

Bibliography

- (171) Desiraju, G. R. Reflections on the Hydrogen Bond in Crystal Engineering. *Cryst. Growth Des.* **2011**, *11*, 896-898.
- (172) Aakeröy, C. B.; Seddon, K. R. The hydrogen bond and crystal engineering. *Chem. Soc. Rev.* **1993**, *22*, 397-407.
- (173) Sherrington, D. C.; Taskinen, K. A. Self-assembly in synthetic macromolecular systems multiple hydrogen bonding interactions. *Chem. Soc. Rev.* **2001**, *30*, 83-93.
- (174) Nishio, M. The CH/ π hydrogen bond in chemistry. Conformation, supramolecules, optical resolution and interactions involving carbohydrates. *PCCP* **2011**, *13*, 13873-13900.
- (175) Gilman-Politi, R.; Harries, D. Unraveling the Molecular Mechanism of Enthalpy Driven Peptide Folding by Polyol Osmolytes. *J. Chem. Theory Comput.* **2011**, *7*, 3816-3828.
- (176) Hellgren, M.; Kaiser, C.; de Haij, S.; Norberg, Å.; Höög, J. O. A hydrogen-bonding network in mammalian sorbitol dehydrogenase stabilizes the tetrameric state and is essential for the catalytic power. *Cell. Mol. Life Sci.* **2007**, *64*, 3129-3138.
- (177) Fernández, A.; Rogale, K.; Scott, R.; Scheraga, H. A. Inhibitor design by wrapping packing defects in HIV-1 proteins. *Proc. Natl. Acad. Sci. U.S.A.* **2004**, *101*, 11640-11645.
- (178) Kitagawa, S.; Uemura, K. Dynamic porous properties of coordination polymers inspired by hydrogen bonds. *Chem. Soc. Rev.* **2005**, *34*, 109-119.
- (179) Wilson, C. C.; Shankland, N.; Florence, A. J. A single-crystal neutron diffraction study of the temperature dependence of hydrogen-atom disorder in benzoic acid dimers. *J. Chem. Soc., Faraday Trans.* **1996**, *92*, 5051-5057.
- (180) Szyc, Ł.; Guo, J.; Yang, M.; Dreyer, J.; Tolstoy, P. M.; Nibbering, E. T. J.; Czarnik-Matusiewicz, B.; Elsaesser, T.; Limbach, H.-H. The Hydrogen-Bonded 2-Pyridone Dimer Model System. 1. Combined NMR and FT-IR Spectroscopy Study. *J. Phys. Chem. A* **2010**, *114*, 7749-7760.
- (181) Yang, M.; Szyc, Ł.; Dreyer, J.; Nibbering, E. T. J.; Elsaesser, T. The Hydrogen-Bonded 2-Pyridone Dimer Model System. 2. Femtosecond Mid-Infrared Pump-Probe Study. *J. Phys. Chem. A* **2010**, *114*, 12195-12201.
- (182) Leiserowitz, L. Molecular packing modes. Carboxylic acids. *Acta Crystallogr. Sect. B-Struct. Cryst. Cryst. Chem.* **1976**, *32*, 775-802.
- (183) Leiserowitz, L.; Nader, F. The molecular packing modes and the hydrogen-bonding properties of amide: dicarboxylic acid complexes. *Acta Crystallogr. Sect. B-Struct. Cryst. Cryst. Chem.* **1977**, *33*, 2719-2733.
- (184) Beyer, T.; Price, S. L. Dimer or Catemer? Low-Energy Crystal Packings for Small Carboxylic Acids. *J. Phys. Chem. B* **2000**, *104*, 2647-2655.
- (185) Das, D.; Desiraju, G. R. Effects of the substituent on the formation of dimers and catemers in phenylpyruvic acids. *CrystEngComm* **2006**, *8*, 674-679.

- (186) Das, D.; Desiraju, G. R. Packing Modes in Some Mono- and Disubstituted Phenylpropionic Acids: Repeated Occurrence of the Rare syn,anti Catemer. *Chem. Asian. J.* **2006**, *1*, 231-244.
- (187) Wiechert, D.; Mootz, D.; Dahlems, T. The Formic Acid 1D Array with H Bonds All Reversed: Structure of a Cocrystal with Hydrogen Fluoride^{1,2}. *J. Am. Chem. Soc.* **1997**, *119*, 12665-12666.
- (188) Shionoya, M.; Tanaka, K. Artificial metallo-DNA: a bio-inspired approach to metal array programming. *Curr. Opin. Chem. Biol.* **2004**, *8*, 592-597.
- (189) Jorgensen, W. L.; Pranata, J. Importance of secondary interactions in triply hydrogen bonded complexes: guanine-cytosine vs uracil-2,6-diaminopyridine. *J. Am. Chem. Soc.* **1990**, *112*, 2008-2010.
- (190) Pranata, J.; Wierschke, S. G.; Jorgensen, W. L. OPLS potential functions for nucleotide bases. Relative association constants of hydrogen-bonded base pairs in chloroform. *J. Am. Chem. Soc.* **1991**, *113*, 2810-2819.
- (191) Sijbesma, R. P.; Beijer, F. H.; Brunsveld, L.; Folmer, B. J. B.; Hirschberg, J. H. K. K.; Lange, R. F. M.; Lowe, J. K. L.; Meijer, E. W. Reversible Polymers Formed from Self-Complementary Monomers Using Quadruple Hydrogen Bonding. *Science* **1997**, *278*, 1601-1604.
- (192) Sherrington, D. C.; Taskinen, K. A. Self-assembly in synthetic macromolecular systems via multiple hydrogen bonding interactions. *Chem. Soc. Rev.* **2001**, *30*, 83-93.
- (193) Shirotani, I.; Sakai, N. Physicochemical properties of alkali metal cation-TCNQ anion radical salts. *J. Solid State Chem.* **1976**, *18*, 17-25.
- (194) Fritchie, C. J.; Arthur, P. A refinement of the crystal structure of cesium tetracyanoquinodimethanide. *Acta Crystallographica* **1966**, *21*, 139-145.
- (195) Hoekstra, A.; Spoelder, T.; Vos, A. The crystal structure of rubidium-7,7,8,8-tetracyanoquinodimethane, Rb-TCNQ, at -160°C. *Acta Crystallogr. Sect. B.* **1972**, *28*, 14-25.
- (196) Konno, M.; Ishii, T.; Saito, Y. The crystal structures of the low- and high-temperature modifications of potassium 7,7,8,8-tetracyanoquinodimethanide. *Acta Crystallographica Section B* **1977**, *33*, 763-770.
- (197) Konno, M.; Saito, Y. The crystal structure of sodium 7,7,8,8-tetracyanoquinodimethanide. *Acta Crystallographica Section B* **1974**, *30*, 1294-1299.
- (198) Konno, M.; Saito, Y. The crystal structure of sodium 7,7,8,8-tetracyanoquinodimethanide at 80°C. *Acta Crystallographica Section B* **1975**, *31*, 2007-2012.
- (199) van Bodegom, B.; de Boer, J. L.; Vos, A. A new form of rubidium-7,7,8,8-tetracyanoquinodimethane. *Acta Crystallographica Section B* **1977**, *33*, 602-604.
- (200) van der Wal, R. J.; van Bodegom, B. 2:3 Complex of rubidium and 7,7,8,8-tetracyanoquinodimethane. *Acta Crystallographica Section B* **1978**, *34*, 1700-1702.

Bibliography

(201) van der Wal, R. J.; van Bodegom, B. The crystal structure of the 2:3 complex of rubidium and 7,7,8,8-tetracyanoquinodimethane, Rb_2TCNQ_3 , at 113 K. *Acta Crystallographica Section B* **1979**, *35*, 2003-2008.

(202) Sakai, N.; Shirotani, I.; Minomura, S. Electrical Conduction in TCNQ Anion Radical Salts. *Bull. Chem. Soc. Jpn.* **1972**, *45*, 3314-3320.

(203) Sakai, N.; Shirotani, I.; Minomura, S. Phase Transition of Alkali Metal Cation-TCNQ Anion Radical Simple Salts. *Bull. Chem. Soc. Jpn.* **1972**, *45*, 3321-3328.

(204) Vegter, J. G.; Hibma, T.; Kommandeur, J. New phase transitions in simple M-TCNQ-salts. *Chem. Phys. Lett.* **1969**, *3*, 427-429.

(205) Bailey, J. C.; Chesnut, D. B. ESR Study of Morpholinium TCNQ Complexes. *J. Chem. Phys.* **1969**, *51*, 5118-5128.

(206) Konno, M. t.; Saito, Y. The crystal structure of sodium 7, 7, 8, 8-tetracyanoquinodimethanide. *Acta Crystallogr. Sect. B-Struct. Cryst. Cryst. Chem.* **1974**, *30*, 1294-1299.

(207) Konno, M.; Saito, Y. The crystal structure of sodium 7, 7, 8, 8-tetracyanoquinodimethanide at 80°C. *Acta Crystallogr. Sect. B-Struct. Cryst. Cryst. Chem.* **1975**, *31*, 2007-2012.

(208) Konno, M.; Ishii, T.; Saito, Y. The crystal structures of the low-and high-temperature modifications of potassium 7, 7, 8, 8-tetracyanoquinodimethanide. *Acta Crystallogr. Sect. B-Struct. Cryst. Cryst. Chem.* **1977**, *33*, 763-770.

(209) van Bodegom, B.; De Boer, J.; Vos, A. A new form of rubidium-7, 7, 8, 8-tetracyanoquinodimethane. *Acta Crystallogr. Sect. B-Struct. Cryst. Cryst. Chem.* **1977**, *33*, 602-604.

(210) Shirotani, I.; Kobayashi, H. The Crystal Structure of Rb (TCNQ)-II. *Bull. Chem. Soc. Jpn.* **1973**, *46*, 2595-2596.

(211) Van Der Wal, R.; Van Bodegom, B. The crystal structure of the 2: 3 complex of rubidium and 7, 7, 8, 8-tetracyanoquinodimethane, Rb_2TCNQ_3 , at 113 K. *Acta Crystallogr. Sect. B-Struct. Cryst. Cryst. Chem.* **1979**, *35*, 2003-2008.

(212) Van Der Wal, R.; van Bodegom, B. 2: 3 Complex of rubidium and 7, 7, 8, 8-tetracyanoquinodimethane. *Acta Crystallogr. Sect. B-Struct. Cryst. Cryst. Chem.* **1978**, *34*, 1700-1702.

(213) Fritchie, C. J.; Arthur, P. A refinement of the crystal structure of cesium tetracyanoquinodimethanide. *Acta Crystallogr.* **1966**, *21*, 139-145.

(214) Barrie, P. J.; Groombridge, C. J.; Grossel, M. C.; Weston, S. C. Variable temperature MAS NMR studies of the phase transition in NaTCNQ . *J. Chem. Soc., Chem. Commun.* **1992**, 1216-1218.

- (215) Kobayashi, H. The crystal structure and the phase transition of ammonium 7, 7, 8, 8-tetracyanoquinodimethanide, NH_4TCNQ . *Acta Crystallogr. Sect. B-Struct. Cryst. Cryst. Chem.* **1978**, *34*, 2818-2825.
- (216) Richard, P.; Zanghi, J.-C.; Guedon, J.-F.; Hota, N. Structure cristalline du complexe de potassium avec le tetracyano-7, 7, 8, 8 quinodimethane. *Acta Crystallogr. Sect. B-Struct. Cryst. Cryst. Chem.* **1978**, *34*, 788-792.
- (217) Kotani, T.; Sorai, M.; Suga, H. Heat capacities of the electron acceptor 7, 7, 8, 8-tetracyano-quinodimethane (TCNQ) and its radical-ion salt $\text{NH}_4^+(\text{TCNQ})^-$ showing spin-Peierls transition. *J. Phys. Chem. Solids* **2009**, *70*, 1066-1073.
- (218) Li, Q.; Yan, P.; Hou, G.; Wang, Y.; Li, G. Three alkaline-earth metal complexes with 3D networks constructed from a 7, 7, 8, 8-tetracyanoquinodimethane ligand: synthesis, structure and electrochemical properties. *Dalton Trans.* **2013**, *42*, 7810-7815.
- (219) Heintz, R. A.; Zhao, H.; Ouyang, X.; Grandinetti, G.; Cowen, J.; Dunbar, K. R. New insight into the nature of $\text{Cu}(\text{TCNQ})$: solution routes to two distinct polymorphs and their relationship to crystalline films that display bistable switching behavior. *Inorg. Chem.* **1999**, *38*, 144-156.
- (220) Nafady, A.; Bond, A. M.; Bilyk, A.; Harris, A. R.; Bhatt, A. I.; O'Mullane, A. P.; De Marco, R. Tuning the electrocrystallization parameters of semiconducting $\text{Co}[\text{TCNQ}]_2$ -based materials to yield either single nanowires or crystalline thin films. *Journal of the American Chemical Society* **2007**, *129*, 2369-2382.
- (221) Nafady, A.; O'Mullane, A. P.; Bond, A. M.; Neufeld, A. K. Morphology Changes and Mechanistic Aspects of the Electrochemically-Induced Reversible Solid-Solid Transformation of Microcrystalline TCNQ into $\text{Co}[\text{TCNQ}]_2$ -Based Materials (TCNQ=7, 7, 8, 8-Tetracyanoquinodimethane). *Chem. Mater.* **2006**, *18*, 4375-4384.
- (222) Neufeld, A. K.; Madsen, I.; Bond, A. M.; Hogan, C. F. Phase, morphology, and particle size changes associated with the solid-solid electrochemical interconversion of TCNQ and semiconducting CuTCNQ (TCNQ= tetracyanoquinodimethane). *Chem. Mater.* **2003**, *15*, 3573-3585.
- (223) Shields, L. Crystal structure of AgTCNQ and contrasting magnetic properties of electrochemically synthesised AgTCNQ and CuTCNQ (7, 7, 8, 8-tetracyanoquinodimethane). *J. Chem. Soc. Faraday Trans.* **1985**, *81*, 1-9.
- (224) Xiao, K.; Tao, J.; Puretzky, A. A.; Ivanov, I. N.; Retterer, S. T.; Pennycook, S. J.; Geohegan, D. B. Selective Patterned Growth of Single-Crystal Ag-TCNQ Nanowires for Devices by Vapor-Solid Chemical Reaction. *Adv. Funct. Mater.* **2008**, *18*, 3043-3048.
- (225) O'Kane, S. A.; Clérac, R.; Zhao, H.; Ouyang, X.; Galán-Mascarós, J. R.; Heintz, R.; Dunbar, K. R. New Crystalline Polymers of $\text{Ag}(\text{TCNQ})$ and $\text{Ag}(\text{TCNQF}_4)$: Structures and Magnetic Properties. *J. Solid State Chem.* **2000**, *152*, 159-173.

Bibliography

- (226) Mukherjee, B.; Mukherjee, M.; Park, J.-e.; Pyo, S. High-Performance Molecular Memory Device Using Ag–TCNQ Crystals Grown by Solution Process. *J. Phys. Chem. C* **2009**, *114*, 567-571.
- (227) Nafady, A.; Bond, A. M.; Bilyk, A. Controllable Synthesis and Fabrication of Semiconducting Nanorod/Nanowire Bundles of Fe[TCNQ]₂(H₂O)₂ via Electrochemically Induced Solid-Solid Phase Transformation of TCNQ Microcrystals. *J. Phys. Chem. C* **2008**, *112*, 6700-6709.
- (228) Nafady, A.; Bond, A. M.; O'Mullane, A. P. Electrochemically-Induced TCNQ/Mn[TCNQ]₂(H₂O)₂ (TCNQ= 7, 7, 8, 8-Tetracyanoquinodimethane) Solid–Solid Interconversion: Two Voltammetrically Distinct Processes That Allow Selective Generation of Nanofiber or Nanorod Network Morphologies. *Inorg. Chem.* **2009**, *48*, 9258-9270.
- (229) Nafady, A.; Bond, A. M.; Qu, V.; Martin, L. L. Kinetic and thermodynamic interplay of cation ingress and egress at a TCNQ-modified electrode in contact with aqueous electrolyte mixtures containing Co(II) and Ni(II) cations. *J. Solid State Electrochem.* **2013**, *17*, 1609-1620.
- (230) Chris J. Jones: *d- and f-Block*; The Royal Society of Chemistry, 2001.
- (231) Ghosh, D. C.; Biswas, R. Theoretical calculation of absolute radii of atoms and ions. Part 1. The atomic radii. *Int. J. Mol. Sci.* **2002**, *3*, 87-113.
- (232) Arnaud-Neu, F. Solution chemistry of lanthanide macrocyclic complexes. *Chem. Soc. Rev.* **1994**, *23*, 235-241.
- (233) Lima, L. s. M.; Lecointre, A.; Morfin, J.-F. o.; De Blas, A.; Visvikis, D.; Charbonnière, L. c. J.; Platas-Iglesias, C.; Tripier, R. l. Positively charged lanthanide complexes with cyclen-based ligands: synthesis, solid-state and solution structure, and fluoride interaction. *Inorg. Chem.* **2011**, *50*, 12508-12521.
- (234) De Sa, G.; Malta, O.; de Mello Donegá, C.; Simas, A.; Longo, R.; Santa-Cruz, P.; Da Silva, E. Spectroscopic properties and design of highly luminescent lanthanide coordination complexes. *Coord. Chem. Rev.* **2000**, *196*, 165-195.
- (235) Ishikawa, N.; Iino, T.; Kaizu, Y. Interaction between f-electronic systems in dinuclear lanthanide complexes with phthalocyanines. *J. Am. Chem. Soc.* **2002**, *124*, 11440-11447.
- (236) Zhang, J.; Yan, P.; Li, G.; Hou, G.; Suda, M.; Einaga, Y. Systematic investigation of an array of TCNQ lanthanide complexes: synthesis, structure and magnetic properties. *Dalton Trans.* **2009**, 10466-10473.
- (237) Li, D.-P.; Wang, T.-W.; Li, C.-H.; Liu, D.-S.; Li, Y.-Z.; You, X.-Z. Single-ion magnets based on mononuclear lanthanide complexes with chiral Schiff base ligands [Ln(FTA)₃L](Ln= Sm, Eu, Gd, Tb and Dy). *Chem. Commun.* **2010**, *46*, 2929-2931.

- (238) Bünzli, J.-C. G.; Piguet, C. Lanthanide-containing molecular and supramolecular polymetallic functional assemblies. *Chem. Rev.* **2002**, *102*, 1897-1928.
- (239) Bünzli, J.-C. G.; Piguet, C. Taking advantage of luminescent lanthanide ions. *Chem. Soc. Rev.* **2005**, *34*, 1048-1077.
- (240) Bünzli, J.-C. G.; Comby, S.; Chauvin, A.-S.; Vandevyver, C. D. New opportunities for lanthanide luminescence. *J. Rare Earths* **2007**, *25*, 257-274.
- (241) Bünzli, J.-C. G. Benefiting from the unique properties of lanthanide ions. *Acc. Chem. Res.* **2006**, *39*, 53-61.
- (242) Cram, D. J. The design of molecular hosts, guests, and their complexes (Nobel lecture). *Angew. Chem. Int. Ed. (English)* **1988**, *27*, 1009-1020.
- (243) Zhang, J.-W.; Wang, Y.; Yan, P.-F.; Hou, G.-F.; Li, G.-M. Solvent-directed lanthanide 7,7,8,8-tetracyano-p-quinodimethane complexes: Syntheses, structures, magnetic and electrochemical properties. *Inorg. Chim. Acta* **2014**, *416*, 22-27.
- (244) Klanderman, B.; Hoesterey, D. Complex Radical-Ion Salts of TCNQ (Tetracyanoquinodimethane) with Cyanine Dye and Related Cations. *J. Chem. Phys.* **1969**, *51*, 377-382.
- (245) Shibaeva, R.; Atovmyan, L. The structure of conducting 7, 7, 8, 8-tetracyanoquinodimethane complexes. *J. Struct. Chem.* **1972**, *13*, 514-531.
- (246) Shibaeva, R.; Atovmyan, L.; Ponomarjev, V.; Philipenko, O.; Rozenberg, L. The crystal structure of the 1: 2 complex of 3, 3'-dimethylthiacyanine and 7, 7, 8, 8-tetracyanoquinodimethane, $(C_{17}H_{15}N_2S_2)^+(C_{12}H_4N_4)^-(C_{12}H_4N_4)$. *Tetrahedron Lett.* **1973**, *14*, 185-188.
- (247) Kaminskii, V.; Shibaeva, R. P.; Atovmyan, L. Crystal and molecular structure of a 1: 2 complex of 3, 3'-diethylthiacarbocyanin and 7, 7, 8, 8-tetracyanoquinodimethane $(C_{21}H_{21}N_2S_2)^+(C_{12}H_4N_4)^-(C_{12}H_4N_4)^0$. *J. Struct. Chem.* **1974**, *14*, 646-650.
- (248) Torrance, J.; Scott, B.; Welber, B.; Kaufman, F.; Seiden, P. Optical properties of the radical cation tetrathiafulvalenium (TTF^+) in its mixed-valence and monovalence halide salts. *Phys. Rev. B, PRB* **1979**, *19*, 730.
- (249) Torrance, J. FRAMEWORK FOR CLASSIFYING AND INTERPRETING THE PHYSICAL PROPERTIES OF CHARGE-TRANSFER SALTS OF TCNQ: THE UNIFYING FEATURE OF ORGANIC METALS*. *Ann. N.Y. Acad. Sci.* **1978**, *313*, 210-233.
- (250) Fadly, M.; El Gandoor, M.; Sawaby, A. Solid state properties and molecular structure of some divalent nd^{10} cation-TCNQ salts. *J. Mater. Sci.* **1992**, *27*, 1235-1239.
- (251) Fadly, M.; Shabaka, A. The electrical behaviour and conduction mechanism of some mixed transition metal TCNQ salts. *J. Mater. Sci.* **1988**, *23*, 4521-4524.
- (252) Owens, G. A. E.S.R. studies of TCNQ complex salts. University of Nottingham, 1978.

Bibliography

- (253) Symons, M. C.; Symons, M.: *Chemical and biochemical aspects of electron-spin resonance spectroscopy*; Van Nostrand Reinhold New York, 1978.
- (254) Eaton, G. R.; Eaton, S. S.; Barr, D. P.; Weber, R. T.: *Quantitative EPR*; Springer Science & Business Media, 2010.
- (255) Jones, M. T.; Chesnut, D. B. Triplet Spin Exchange in Some Ion Radical Salts. *J. Chem. Phys* **1963**, 38, 1311-1317.
- (256) Kepler, R. G. Magnetic Properties of a New Class of Highly Conductive Organic Solids. *J. Chem. Phys* **1963**, 39, 3528-3532.
- (257) Chesnut, D. B.; Arthur, P. Spin Correlation in Ion Radical Salts; The System $(\text{Cs}^+)_2(\text{TCNQ})_3$. *J. Chem. Phys* **1962**, 36, 2969-2975.
- (258) Hibma, T.; Kommandeur, J. Dynamics of triplet excitons in the simple tetracyanoquinodimethane (TCNQ) salts of rubidium, potassium, and tri-methyl-benzimidazol. *Phys. Rev. B, PRB* **1975**, 12, 2608.
- (259) Rembaum, A.; Hermann, A. M.; Stewart, F. E.; Gutmann, F. Electronic properties of some tetracyanoquinodimethane complexes. *J. Phys. Chem* **1969**, 73, 513-520.
- (260) Zhang, Z.; Zhao, H.; Matsushita, M. M.; Awaga, K.; Dunbar, K. R. A new metal-organic hybrid material with intrinsic resistance-based bistability: monitoring in situ room temperature switching behavior. *J. Mater. Chem. C* **2014**, 2, 399-404.
- (261) Acker, D. S.; Hertler, W. R. Substituted Quinodimethans. I. Preparation and Chemistry of 7,7,8,8-Tetracyanoquinodimethan. *J. Am. Chem. Soc.* **1962**, 84, 3370-3374.
- (262) Girlando, A.; Morelli, L.; Pecile, C. Infrared active fundamental vibrations of TCNQ and chloranil monovalent anions. *Chem. Phys. Lett.* **1973**, 22, 553-558.
- (263) Boyd, R. H.; Phillips, W. D. Solution Dimerization of the Tetracyanoquinodimethane Ion Radical. *J. Chem. Phys* **1965**, 43, 2927-2929.
- (264) Poonia, N. S. Coordination chemistry of sodium and potassium complexation with macrocyclic polyethers. *J. Am. Chem. Soc.* **1974**, 96, 1012-1019.
- (265) Dunitz, J.; Dobler, M.; Seiler, P.; Phizackerley, R. Crystal structure analyses of 1, 4, 7, 10, 13, 16-hexaoxacyclooctadecane and its complexes with alkali thiocyanates. *Acta Crystallogr. Sect. B-Struct. Cryst. Cryst. Chem.* **1974**, 30, 2733-2738.
- (266) Bandrauk, A.; Ishii, K.; Truong, K.; Aubin, M. Hydrogen bonding and properties of organic conductors. 2. Electronic properties and structure of $\text{M}_2(\text{TCNQ})_3$ and $\text{M}(\text{TCNQ})_2$ systems. *J. Chem. Phys* **1985**, 89, 1478-1485.
- (267) Grossel, M. C.; Evans, F. A.; Hriljac, J. A.; Morton, J. R.; Lepage, Y.; Preston, K. F.; Sutcliffe, L. H.; Williams, A. J. Isolated free-radical pairs in Rb^+ 18-crown-6 TCNQ^- single crystals (TCNQ = tetracyanoquinodimethane). *J. Chem. Soc., Chem. Commun.* **1990**, 439-441.

- (268) Hynes, R. C.; Morton, J. R.; Preston, K. F.; Williams, A. J.; Evans, F.; Grossel, M. C.; Sutcliffe, L. H.; Weston, S. C. Electron paramagnetic resonance study of isolated free radical pairs in M^+ 18-crown-6 TCNQ $^-$. (TCNQ = 7,7',8,8'-tetracyano-p-quinodimethane; $M = K, Rb$). *J. Chem. Soc., Faraday Trans.* **1991**, *87*, 2229-2233.
- (269) Bondi, A. van der Waals volumes and radii. *J. Phys. Chem. A* **1964**, *68*, 441-451.
- (270) Slater, J. C. Atomic Radii in Crystals. *J. Chem. Phys* **1964**, *41*, 3199-3204.
- (271) Takamatsu, N.; Akutagawa, T.; Hasegawa, T.; Nakamura, T.; Inabe, T.; Fujita, W.; Awaga, K. One-Dimensional Antiferromagnetic Chain in $[Ni(dmit)_2]^-$ Salts of $[K^+ \text{ or } Rb^+ (4, 13\text{-diaz-18-crown-6})]$ Supramolecular Cation. *Inorg. Chem.* **2000**, *39*, 870-871.
- (272) Grossel, M. C.; Evans, F. A.; Hriljac, J. A.; Morton, J. R.; LePage, Y.; Preston, K. F.; Sutcliffe, L. H.; Williams, A. J. Isolated free-radical pairs in Rb^+ 18-crown-6 TCNQ-single crystals (TCNQ= tetracyanoquinodimethane). *J. Chem. Soc., Chem. Commun.* **1990**, 439-441.
- (273) W. Steed, J.; C. Junk, P. Stabilisation of sodium complexes of 18-crown-6 by intramolecular hydrogen bonding \dagger . *J. Chem. Soc., Dalton Trans.* **1999**, 2141-2146.
- (274) Zhu, Y.; Dou, J.; Li, D.; Wang, D. Cation- π interactions. Synthesis and crystal structure of complexes $[K(B18-C-6)]NCS$ and $[K(DB18-C-6)]_2[Hg(SCN)_4]$. *INDIAN J CHEM, SEC A*. **2004**, *43*, 2126-2131.
- (275) ZHU, Y.-h.; DU, M.-x.; LI, D.-c.; WANG, D.-q.; DOU, J.-m. One-dimensional Chain Dibenzo-18-crown-6 Complex: $[K(DB18-C-6)]_2[Pt(SCN)_6] \cdot 2H_2O \cdot C_2H_4Cl_2$ Assembled by Cation- π Interactions. *CHEM. RES. CHINESE U.* **2005**, *21*, 123-126.
- (276) Chekhlov, A. Preparation and crystal structure of bis [(dibenzo-18-crown-6) potassium] bis (μ_2 -chloro)-tetrachlorodicuprate (II). *Russ. J. Gen. Chem.* **2009**, *79*, 1821-1824.
- (277) Fraser, M. E.; Fortier, S.; Markiewicz, M. K.; Rodrigue, A.; Bovenkamp, J. W. The crystal structures of the 1:1:1 complexes of dicyclohexano-18-crown-6 (isomer B) with potassium phenoxide and phenol and dicyclohexano-18-crown-6 (isomer A) with sodium phenoxide and phenol. *Can. J. Chem.* **1987**, *65*, 2558-2563.
- (278) Futamata, M.; Morioka, Y.; Nakagawa, I. Infrared and Raman spectra of alkali metal salts of TCNQ. *Spectrochimica Acta*. **1983**, *39*, 515-528.
- (279) Iqbal, Z.; Christoe, C.; Dawson, D. Infrared absorption and reflection studies of organic radical salt: K^+TCNQ^- . *J. Chem. Phys* **1975**, *63*, 4485-4489.
- (280) Bozio, R.; Pecile, C. Phase transitions of (1:1) alkaline salts of TCNQ as studied by vibronic intensity enhancement in the infrared spectra. *J. Chem. Phys* **1977**, *67*, 3864-3868.
- (281) Bozio, R.; Girlando, A.; Pecile, C. Vibrational analysis of spectra of quinonoid molecular ions. Part 3. \dagger - Vibrational spectra and assignment of 7,7,8,8-tetracyanoquinodimethane radical anion. *J. Chem. Phys, Faraday Transactions 2: Molecular and Chemical Physics* **1975**, *71*, 1237-1254.

Bibliography

- (282) Bandrauk, A.; Truong, K.; Carlone, C.; Jandl, S.; Ishii, K. Hydrogen bonding and properties of organic conductors. 2. Infrared and Raman spectra of some $M_2(TCNQ)_3$ and $M(TCNO)_2$ systems. *J. Chem. Phys.* **1985**, *89*, 434-442.
- (283) S.C.Weston. University of London, 1992.
- (284) El-Azhary, A. A.; Al-Kahtani, A. A. Experimental and Theoretical Study of the Vibrational Spectra of Free 12-Crown-4. *J. Phys. Chem. A* **2005**, *109*, 4505-4511.
- (285) Al-Rusaese, S.; Al-Kahtani, A. A.; El-Azhary, A. A. Experimental and Theoretical Study of the Vibrational Spectra of 12-Crown-4-Alkali Metal Cation Complexes. *J. Phys. Chem. A* **2006**, *110*, 8676-8687.
- (286) 15-Crown-5; SIGMA-ALDRICH, Ed., 2015.
- (287) Gorman, M. The evidence from infrared spectroscopy for hydrogen bonding: A case history of the correlation and interpretation of data. *J. Chem. Educ.* **1957**, *34*, 304.
- (288) Gokel, G. W.; Cram, D. J.; Liotta, C. L.; Harris, H. P.; Cook, F. L. Preparation and purification of 18-crown-6 [1,4,7,10,13,16-hexaoxacyclooctadecane]. *J. Org. Chem.* **1974**, *39*, 2445-2446.
- (289) Takenaka, T. Infrared and Raman Spectra of TCNQ and TCNQ- d_4 Crystals (Commemoration Issue Dedicated to Professor Rempei Gotoh On the Occasion of his Retirement). *Bull. Inst. Chem. Res., Kyoto Univ.*, **1969**, *47*, 14.
- (290) Pouretedal, H. R.; Semnani, A. Spectroscopic Study of the Interaction Between TCNQ and Cryptand 222 in Chloroform Solution. *Iran. J. Chem. Chem. Eng. Vol* **2005**, *24*.
- (291) Ramanathan, R.; Walia, S.; Kandjani, A. E.; Balendran, S.; Mohammadtaheri, M.; Bhargava, S. K.; Kalantar-Zadeh, K.; Bansal, V. Low-temperature fabrication of alkali metal-organic charge transfer complexes on cotton textile for optoelectronics and gas sensing. *Langmuir* **2014**, *31*, 1581-1587.
- (292) Faulques, E.; Leblanc, A.; Molinié, P.; Decoster, M.; Conan, F.; Guerchais, J. E.; Sala-Pala, J. Determination of charge transfer in molybdenum complexes of 7,7,8,8-tetracyano-p-quinodimethane with vibrational spectroscopy. *Spectrochim. Acta Mol. Biomol. Spectrosc.* **1995**, *51*, 805-819.
- (293) Ye, C.; Cao, G.; Fang, F.; Xu, H.; Xing, X.; Sun, D.; Chen, G. Morphology investigation of Ag(TCNQ) synthesized by the vapor-transport reaction method. *Micron* **2005**, *36*, 461-464.
- (294) Ozutsumi, K.; Natsuhara, M.; Ohtaki, H. An X-ray diffraction study on the structure of 18-crown-6 ether complexes with alkali metal ions in aqueous solution. *Bull. Chem. Soc. Jpn.* **1989**, *62*, 2807-2818.
- (295) Hong, C.; Yan, P.; Li, Q.; Hou, G.; Li, G. Synthesis, structure and electrochemical properties of TCNQ lanthanide complexes. *J. Organomet. Chem.* **2013**, *739*, 45-51.

- (296) Bruker AVII400 FT-NMR Spectrometer (400/1).
<http://www.southampton.ac.uk/nmr/instrumentation/avii400-1.page?> (accessed 01/10/2015).
- (297) Bruker AVIIHD400 FT-NMR Spectrometer (400/3).
<http://www.southampton.ac.uk/nmr/instrumentation/aviihd400-3.page?> (accessed 01/10/2015).
- (298) Paper and Thesis Information 2014.
<https://groupsite.soton.ac.uk/Research/Chemistry-Mass-Spectrometry/Documents/Forms/AllItems.aspx?RootFolder=%2FResearch%2FChemistry-Mass-Spectrometry%2FDocuments%2FPaper%20and%20Thesis%20Information%202014&FolderCTID=0x012000A7C927A84D981741B4321CC390138D5D&View={A1A895AD-5C9D-477B-B1B2-B916D521D548}> (accessed 01/10/2015).
- (299) Equipment.
http://www.southampton.ac.uk/sdc/small_mol_diffraction/equipment.page (accessed 01/10/2015).
- (300) Sheldrick, G. M. Crystal structure refinement with SHELXL. *Acta Crystallographica Section C: Structural Chemistry* **2015**, *71*, 3-8.
- (301) Dolomanov, O. V.; Bourhis, L. J.; Gildea, R. J.; Howard, J. A.; Puschmann, H. OLEX2: a complete structure solution, refinement and analysis program. *J. Appl. Crystallogr.* **2009**, *42*, 339-341.
- (302) Macrae, C. F.; Edgington, P. R.; McCabe, P.; Pidcock, E.; Shields, G. P.; Taylor, R.; Towler, M.; Streek, J. v. d. Mercury: visualization and analysis of crystal structures. *J. Appl. Crystallogr.* **2006**, *39*, 453-457.
- (303) Rigaku: *CrystalClear-SM Expert 3.1 b27*. 2013.
- (304) Rigaku: *CrystalClear-SM Expert 2.0 r13*. 2011.
- (305) Rigaku: *CrystalClear- SM Expert 2.1 b29*. 2013.
- (306) Jiménez-Sandoval, O.; Cea-Olivares, R.; Hernández-Ortega, S.; Silaghi-Dumitrescu, I. Structural studies of tetrazoles. Crystal and molecular structure and ab initio calculations of 1-phenyl-1H-tetrazole-5-thiolate, as its [diaqua(18-crown-6)sodium] salt: An anionic tetrazole free of direct metal interactions. *Heteroat. Chem* **1997**, *8*, 351-359.
- (307) Ellison, M. K.; Nasri, H.; Xia, Y. M.; Marchon, J.-C.; Schulz, C. E.; Debrunner, P. G.; Scheidt, W. R. Characterization of the Bis(azido)(meso-tetraphenylporphinato)ferrate(III) Anion. An Unusual Spin-Equilibrium System. *Inorg. Chem.* **1997**, *36*, 4804-4811.